Mechanics of Pneumatic Tire - Supporting Ground Interaction

by

FUMITOSHI ISHIKAWA

A Thesis submitted to the Faculty of Graduate Studies and Research in Partial Fulfillment of the Requirements for the Degree of Doctor of Philosophy

Department of Civil Engineering and Applied Mechanics
McGill University
Montreal, Quebec, Canada

August 1989

©

ACKNOWLEDGEMENTS

The author wishes to express his sincere gratitude and appreciation to his research director, Dr. R.N. Yong, William Scott Professor of Civil Engineering and Applied Mechanics, for his guidance, suggestions and constant encouragement throughout this research

This study was conducted under contract arrangement with Mobility Section of Defense Research Establishment (Ottawa) and McGill University/Prof. Yong. The research assistantship provided by the contract arrangements is highly appreciated

The author is very thankful to Dr. P Boonsinsuk, Mr. A Murcia and Mr. F. Caporsucio for their helpful discussions, helping in the computer programming, and their assistance with the experiments

The author is indebted to Prof D R. Axelrad, Dr. D.M. Xu and Prof. M. Fukue for their valuable suggestions and comments

The author appreciates his family,especially his parents, for their utmost sacrifice and encouragement in bringing the author to his present attainment Special thanks are given to Young Suk for her help ranging from the experiments to the arrangement of numerous data, including the measurements of some experimental results.

An acknowledgement is also due to Joan Armour for carefully typing the manuscript.

Last but not least, the author wishes to express his deep gratitude to the many other persons who helped make this study possible.

RESUME

Ce mémoire porte sur les études experimentales et analytiques relativement aux mécanismes d'interaction d'un pneu surmonté verticalement d'une charge et reposant sur une surface solide, i.e , base rigide, glaise et sable.

De nombreuses expériences furent menees dans differentes conditions afin de déterminer les interactions en termes de results, e.g. le déplacement de l'essieu, surface de contact, la distribution de la pression au point de contact, etc. Les résultats concernant la distribution de la pression demontrent l'importance de reconnaître le pneu comme étant un corps pneumatique afin d'enoncer une theorie rationnelle relativement a l'interaction entre pneu et point de contact La distribution de pression et l'aire de contact obtenues lors d'experiences sont egalement utilisées afin de valider une approche analytique (i e , première approche analytique présentée dans le memoire)

Une descripton hypothétique de la progression de la deformation du pneu fait l'objet d'une discussion basee sur les resultats des expériences

La discussion favorise une meilleure comprehension des mécanismes d'interactions et de la selection d'un outil de base analytique (ou numerique) en établissant les deux présentes methodes analytiques

Dans la partie analytique, les deux approches analytiques distinctes et bi-dimensionnelles (i.e , les premiere et deuxieme approches analytiques) sont etablies en prenant en consideration les conditions de deformations planes en determinant la longueur du point de contact et la pression exercee. Toutefois ce memoire se concentre surtout sur la premiere approche analytique tandis que la seconde ne fait l'objet que d'une etude complementaire.

Dans la premiere approche analytique, le véritable profil du point de contact est pris en considération, tandis que les théories actuelles (Hertz, Muskhelishvili, etc.) ignorent essentiellement la cinématique donc, le mode de distribution de pression des surfaces de contact.

Dans cette premiere approche analytique, les etapes sont les suivantes:

(1) Transformer un probleme d'interaction pneu-surface d'appui en un problème equivalent de deformation plane (-value); ceci est fait afin d'éviter que les facteurs complexes inherents au pneumatique ne soient pris en considération dans la formulation analytique;

(2) Determiner le module d'elasticite de la section déformee de la surface de contact en prenant en considération le profil du point de contact;

(3) Determiner la longueur du point de contact ainsi que la pression exercée en utilisant la methode d'ensemble des variables.

Les resultats analytiques sont en accord avec ceux obtenus lors des experiences; des efforts ont ete deployés afin de solutionner les problemes de glissement.

La seconde approche analytique, laquelle est une technique iterative combinant la methode incrementielle des elements finis et la méthode d'ensemble des variables, est etablie principalement afin de solutionner un probleme d'interaction entre un solide elastique et un demi plan elastique non-lineaire Deux differents types de problemes d'interaction sont resolus (i e , pneu/glaise et roue rigide/interactions surfaces enneigees Dans les deux cas, les resultats numeriques concernant la longueur du point de contact demontrent une correlation acceptable avec les résultats des experiences, alors que pour la roue rigide, les résultats obtenus relativement à l'enfoncement n'ont pas cette correlation

ABSTRACT

This dissertation is concerned with experimental and analytical studies of the mechanics of interaction where a pneumatic tire is loaded vertically on a supporting ground, i.e , rigid base, clay and sand

The numerous experiments were conducted under various conditions to characterize the interactions in terms of the experimental results, e.g. axle displacement, contact area, contact pressure, etc The results of pressure distribution indicate that recognizing a tire as a pneumatic body is crucial in establishing a rational theory for tire-supporting ground interaction problems. The pressure distribution and contact area obtained in the experiments are also utilized in validating an analytical approach (i e. First Analytical Approach) established in the dissertation.

A hypothetical description of the progress of tire deformation is discussed based on the experimental results The discussion helps in providing a better understanding of the mechanics of the interaction, and for selecting basic analytical and/or numerical tools in establishing the present analytical methods

In the analytical work, the two distinct analytical approaches (i e First and Second Analytical Approaches) are established under the plane strain condition in predicting contact length and pressure However, the first analytical approach is emphasized in this dissertation, while the second one is rather a complementary work

In the first analytical approach, the real contact profile is taken into account, while the existing contact theories (by Hertz, Muskhelishvili, etc) essentially ignore the real kinematics of contact surfaces on which the pattern of pressure distribution greatly depends. In this first analytical approach, the following steps are taken:

(1) transform a tire-supporting ground interaction problem into an equivalent free boundary (-value) problem of the deformed supporting ground; this is done so

that the complex factors inherent to pneumatic tires are not directly taken into the analytical formulation;

(2) determine the modulus of elasticity of the deformed supporting ground by taking into account the contact profile,

(3) find the contact length and pressure by means of the complex variable method.

The contact length and pressure analytically obtained are in close agreement with those obtained through experimentation. An attempt has also been made to solve the sliding interaction problems

The second analytical approach, which is an iterative technique combining the incremental finite element method and the complex variable method, is established fundamentally to solve an interaction problem between an elastic solid and a nonlinear elastic half-plane Two different types of interaction problems are solved, i.e. tire-clay and rigid wheel-snowpack interactions. Numerical results on contact length for both problems showed acceptable agreement with the experimental results, while those on sinkage obtained for the rigid wheel did not

TABLE OF CONTENTS

	Acknowledgements	i
	Resume	ii
	Abstract	iv
	Table of Contents	vi
	List of Figures	xii
	List of Tables	xx
	Notation	xxi
Chapter		
1	Introduction	1
	1.1 The Physical Problem	1
	1.2 Approaches to Interaction Problems	5
2.	A Brief Review of Contact Analyses Based on Analytical and Computational Methods: Contact Mechanics of Pneumatic Tires Interacting with a Rigid Base	8
	2.1 Introduction	8
	2.2 A Brief Review of Analytical Methods	9
	2.2.1 Introduction	9
	2.2.2 Analytical Methods for Three-Dimensional Contact Problems	14
	2.2.3 Analytical Methods for Two-Dimensional Contact Problems (Plane Strain Condition)	19
	2.2.4 Applicability of the Analytical Methods	
	2.2.5 Concluding Remarks on the Analytical Methods	28
	2.3 A Brief Review of Computational Methods	30
	2.4 Contact Problems Involving Pneumatic Bodies and Elastic Membranes	34
	2.5 Contact Mechanics of Pneumatic Tires Interacting with a Rigid Base	37

2.6 Conclusions and Selection of Analytical and/or Computational Methods as Fundamental Tools 51

3. Experiments on Tire-Supporting Ground Interaction Problems 57

3.1 Introduction 57

3.2 Experimental Program and Procedure for Tire-Rigid Base Interactions 63

3.2.1 Preliminaries 63
3.2.2 Experimental Procedure 65

3.3 Experimental Program and Procedure for Tire-Supporting Soil Interaction 70

3.3.1 Preliminaries 70
3.3.2 Experimental Procedure 74
3.3.3 Soils Used in the Study 75

3.4 Representative Contact Length, Contact Width and Contact Pressure Distribution 76

3.4.1 Representative Contact Length and Contact Width 76
3.4.2 Representative Contact Pressure Distribution 80

3.5 Discussions and Remarks on the Experimental Results of Tire-Rigid Base Interactions 85

3.5.1 Load-Axle Displacement Relationships 85
3.5.2 Contact Area-Load Relationships 87
3.5.3 Average (Ground) Contact Pressure-Inflation Pressure Relationships 88
3.5.4 Contact Pressure Distribution 90
3.5.5 Concluding Remarks on the Experimental Results on Tire-Rigid Base Interactions 97

3.5.5.1 Load-Axle Displacement and Contact Area-Load Relationships 98
3.5.5.2 Average (Ground) Contact Pressure-Inflation Pressure Relationships 99
3.5.5.3 Contact Pressure Distribution 100

3.6 Discussions and Remarks on the Experimental Results of Tire-Supporting Clay Interactions 104

3.6.1 Load-Axle Displacement Relationships 105

3.6.2 Contact Area - Load Relationships 111
3.6.3 Average Contact Pressure-Load Relationships 114
3.6.4 Contact Pressure Distribution Along Tire-Supporting Clay Interface 120

3.7 Discussions and Remarks on the Experimental Results of Tire-Supporting Sand Interactions 129

3.7.1 Axle Displacement Characteristics of Tire on Sand 129
3.7.2 Contact Pressure Distributions at the Tire-Sand Interface 130

3.8 Summary and Remarks on the Experimental Results of Tire-Soil Interactions 135

4. First Analytical Approach for Sliding Interaction Problems: Application to a Pneumatic Tire-Supporting Clay and a Pneumatic Tire-Rigid Base Interaction Problem 137

4.1 Introduction 137

4.2 Complex Variable Analysis for a Sliding Contact Problem Between a Solid with a Smooth Profile and a Half-Plane 139

4.2.1 Preliminary 139
4.2.2 Stresses and Rotations in a Half-Plane Represented by a Complex Function 142
4.2.3 Transformation of a Sliding Contact Problem into a Riemann-Hilbert Problem 158
4.2.4 General Solution to the Riemann-Hilbert and the Sliding Contact Problems 163
4.2.5 Summary 167

4.3 Free Boundary Problems Equivalent to Tire-Clay and Tire-Rigid Base Interaction Problems; A Question to Solutions Obtained by the Existing Analytical Methods for a Certain Class of Contact Problems 169

4.3.1 Preliminary 169
4.3.2 A Free Boundary Problem Equivalent to a Tire-Clay Interaction Problem 177
4.3.3 A Free Boundary Problem Equivalent to a Rigid Base Interaction Problem 180
4.3.4 A Comparison of Solutions Obtained by the Existing Analytical Methods and the Proposed Present Analytical Approach for a Certain Class of Contact Problems (Figs. 4.4a and 4.4b) 183
4.3.5 Summary 194

4.4 On Elasticities of Nearly Rigid Base and Supporting Clay Contacting with a Pneumatic Tire 198

4.4.1 Introduction 198
4.4.2 A Definition and a General Derivation of Elastic Modulus for Deformed Half-Plane 199
4.4.3 Development of Elastic Moduli of Nearly Rigid Base for Two Distinct Contact Profiles 203
4.4.4 Development of Elastic Moduli of Supporting Clay for Two Distinct Contact Problems 210

4.5 Scheme of the Present Analytical Approach with a Flow Diagram 215

4.6 Discussions and Remarks on the Experimental and Analytical Results for the Tire-Clay and Tire-Rigid Base Interaction Problems 218

4.6.1 Introduction 218
4.6.2 The Interaction Problems Solved by the Present Analytical Approach and the Presumptions Imposed on the Problems 218
4.6.3 Discussions and Remarks on the Experimental and Analytical Results for the Selected Problems 224

5. Second Analytical Approach: Application to Tire-Supporting Clay and Rigid Wheel-Supporting Snowpack Interaction Problems 273

5.1 Introduction 273

5.2 Method of Analysis 274

5.3 Applications to Interaction Problems 284

5.3.1 A Tire-Supporting Clay Interaction Problem 284
5.3.2 A Rigid Wheel-Supporting Snowpack Interaction Problem 293

5.4 Comments on the Formulation and Results of Numerical Analysis 302

6. Summary, Concluding Remarks, Contributions and Recommendations for Future Work 304

6.1 Summary 304

6.2 Concluding Remarks 307

6.3 Contributions 312

6.3.1 Experiments 312
6.3.2 Theories 313

6.3.3 Findings During the Development of the Analytical Approaches 314

6.4 Recommendations for Future Work 315

References 317

Appendix A 329

1. Preliminaries: Airy Stress Function 329
2. Complex Representation of Airy Stress Function 331
3. Complex Representation of Stresses and Displacement 333
4. Boundary Conditions Where Traction Force and/or Displacements are Given a Priori 338
5. On the Expression of $U,_1 + U,_2$ (Eqs. A.16, A.17) 338
6. General Formulation and Propositions for the Half-Plane 340
7. Transformation of the General Formulae for the Half-Plane 340
8. A Definition of Riemann-Hilbert (Boundary) Problem 353
9. A Transformation of Contact Problem to a Riemann-Hilbert Problem 354
   - 9.1 Development of the Riemann-Hilbert Problem for the Sliding Contact Problem 355
   - 9.2 The General Solution to the Riemann-Hilbert Problem Governing the Contact Problem 362
   - 9.3 Contact Pressure and Contact Area 366
   - 9.4 Contacting Pressure and Contact Length for a Contacting Body with Three Different Profiles 371

Appendix B 373

I. A Brief Review of Two- and Three-Dimensional Contact Problems 373

Analytical Methods for Three-Dimensional Contact Problems 373

Method 1 (Three-Dimensional Hertz Theory) 373
Method 2 (Hankel Transform) 375

Analytical Methods for Two-Dimensional Contact Problems 382

Method 3 (Two-Dimensional Hertz Theory) 382
Method 4 (Singular Integral Equations) 385
Method 5 (Integral Equation with Pi-Kernel: refer to Chapter 2) 20
Method 6 (Fourier Transform) 387

Method 7 (Complex Variable Method) 394

II. A Link Between the Complex Variable Method (Method 7) and the Singular Integral Equation Approach (Methods 4,5,& 6) 399

III. Two Computational Methods Formulating Contact Problems 402

Method 1: Finite Element Method 402
Method 2: Variational Inequalities 406

Appendix C: Experimental Results on Tire-Rigid Base Interactions 418

Appendix D: Experimental Results on Tire-Clay Interactions 544

Appendix E: Experimental Results on Tire-Sand Interactions 608

LIST OF FIGURES

Fig. No.		Page
1.1	A Pneumatic Tire Interacting with a Deformable (or Non-Deformable) Supporting Ground	4
1.2	Organization of the Dissertation	6
2.1	Five Typical Contact Problems	10
2.2	Contact Problems Between a Punch with Sharp Edges and an Elastic Half-Plane	25
2.3	An Inflated Rectangular Membrane Contacting with a Rigid Smooth Indentor	35
2.4	Contact Problem for Two Parallel Membranes Subjected to Transverse Pressures	35
2.5a,b	A Large Tire Used for 200 Ton Dump Trucks	39
2.6	A Buffed Tire Fixed in Rectangular Coordinate System	41
2.7	A Cross Section of Loaded Tire in y-z Plane	41
2.8	A Receding and an Advancing Contact Resulting From a Tire-Rigid Base Contact	42
2.9	A Slice of Cross Section of Carcass Along y-z Plane	45
2.10	A Ring-Shaped Cross Section of a Carcass	45
2.11	Progress of Deformations of a Carcass Leading to a Hypothetical Instability Mode	46
2.12	Hypothetical Load-Displacement Curves (at Datum Points) for a Carcass	48
2.13	Hypothetical Configurations and Contact Pressure Distributions for a Highly Idealized 2-D Spring Model of Carcass Before and After a Snap-Through Type Instability	50
2.14	Idealized and Realistic Contact Problems	52

2.15	A Quarter of a Discretized Elastic Cylinder Under a Uniform Load	53
3.1	Full-Size Truck Tires Used in the Study	58
3.2a	GOODYEAR 7.00-16LT (treaded)	61
3.2b	MICHELIN 7.00R-16XCL (treaded)	61
3.2c	MICHELIN 11.00R 16XL (treaded & buffed)	62
3.2d	MICHELIN 12.5R 16.5XLM (treaded & buffed)	62
3.3	Test Set-Up for Load-Displacement Relationship	64
3.4	Test Set-Up for Measuring Contact Pressure Distribution (i.e. Steel Plate Housing Pressure Transducers)	64
3.5a	Steel Plate Housing Pressure Transducers for GOODYEAR 7.00-16LT	66
3.5b	Steel Plate Housing Pressure Transducers for MICHELIN 7.00R-16XCL	67
3.5c	Steel Plate Housing Pressure Transducers for MICHELIN 11.00R-16XL	68
3.5d	Steel Plate Housing Pressure Transducers for MICHELIN 12.5R-16.5XLM	69
3.6	Test Set-Up for Tire-Soil Interaction	71
3.7	Soil Bin and Pressure Transducers Embedded in Soil Surface	72
3.8	Spraying Paint Along Contact Boundary	73
3.9	Plane View of Contact Surface	73
3.10	Three Typical Shapes of Contact Surfaces Obtained in the Present Experiments	78
3.11	Real Elliptic-Type Contact Surface and Its Corresponding Representative Contact Surface	81
3.12	Contact Pressure Distribution on a Contact Surface	81

3.13	Contact Pressure Distributions Along y- and x-Axes Based on the Pressure Distribution Given in Fig. 3.12	82
3.14	A Representative Contact Pressure Distribution Interpreted on a Representative Contact Surface	83
4.1	An Elastic Solid Sliding Quasi-Statically Over an Elastic Half-Plane	141
4.2	Kinematics of Contact Profile	170
4.3	An Approximated Deformed Configuration and a Contact Profile	170
4.4a	A Contact Between an Elastic Solid S_2 and a Rigid Half-Plane S_1	175
4.4b	A Contact Between a Rigid Solid S_2 and an Elastic Half-Plane S_1	175
4.5a	An Interaction Between a Pneumatic Tire and a Supporting Clay	178
4.5b	A Tire Deformed Under Contact Pressure	178
4.5c	A Supporting Clay Deformed Under Contact Pressure	178
4.6a	An Interaction Between a Pneumatic Tire and a Rigid Base	181
4.6b	A Deformed Tire Under Contact Pressure	181
4.6c	An Undeformed Rigid Base Under Contact Pressure	181
4.7	An Interaction Between a Pneumatic Tire and a Nearly Rigid Base	184
4.8a	A Contact Problem Simulating the Real One Shown in Fig. 4.4a	187
4.8b	A Contact Problem Simulating the Real One Shown in Fig. 4.4b	187
4.9	A Pattern of Contact Pressure Distributions for the Contact Problem (Fig. 4.8a) Obtained by the Present Analyticval Approach (Section 4.3.3)	190

4.10	A Pattern of Contact Pressure Distributions Either Obtained by the Present Analytical Approach (Section 4.3.2) for the Contact Problem (i.e. Fig. 4.8b) or Obtained by the Existing Analtyical Methods for the Contact Problems (i.e. Figs. 4.8a,b)	190
4.11	A Deformed Half-Plane Due to an Interaction with a Pneumatic Tire	200
4.12	An Idealized Relationship Between Average Contact Pressure and Contact Measure Obtained in Experiments for Tire-Rigid Base Interactions	204
4.13	An Idealized Relationship Between Nominal Contact Area and Load Obtained in Experiments for Tire-Rigid Base Interactions	204
4.14	An Idealized Relationship Between Average Contact Pressure and Contact Measure Obtained in Experiments for Tire-Supporting Clay Interactions	211
4.15	Flow Diagram of the Present Analytical Approach	217
4.16a-d	Average Contact Pressure - Contact Measure Relationships for GOODYEAR 7.00-16LT (treaded and buffed)	225
4.17a-d	Average Contact Pressure - Contact Measure Relationships for MICHELIN 7.00-16XCL (treaded and buffed)	229
4.18a-d	Average Contact Pressure - Contact Measure Relationships for MICHELIN 11.00R-16XL (treaded and buffed)	233
4.19a-d	Average Contact Pressure - Contact Measure Relationships for MICHELIN 12.5R-16.5XLM (treaded and buffed)	237
4.20a,b	Comparisons Between Experimental and Frictionless Analytical Solutions for GOODYEAR 7.00-16LT (buffed) on Clay	242
4.21a,b	Comparisons Between Experimental and Frictionless Analytical Solutions for MICHELIN 7.00R-16XCL (buffed) on Clay	244

4.22a,b	Comparison Between Experimental and Frictionless Analytical Solutions for MICHELIN 11.00R-16XL (buffed) on Clay	246
4.23a,b	Comparison Between Experimental and Frictionless Analytical Solutions for MICHELIN 12.5R-16.5XLM (buffed) on Clay	248
4.24a-j	Comparison Between Experimental and Frictionless Analytical Solutions for GOODYEAR 7.00-16Lt (buffed) on Rigid Surface	250
4.25a-c	Comparison Between Experimental and Frictionless Analytical Solutions for MICHELIN 7.00R-16XCL (buffed) on Rigid Surface	260
4.26a-c	Comparison Between Experimental and Frictionless Analytical Solutions for MICHELIN 11.00R-16XL (buffed) on Rigid Surface	263
4.27a-c	Comparison Between Experimental and Frictionless Analytical Solutions for MICHELIN 12.5R-16.5XLM (buffed) on Rigid Surface	266
4.28a-c	Comparison Between Frictionless and Frictional Analytical Solutions on Rigid Surface	269
5.1	Nonlinear Contact Problem Between a Linear Elastic Solid and a Nonlinear Elastic Half-Plane	275
5.2	Contact Pressure Induced by a Contact Between a Linear Elastic Solid and a Nonlinear Elastic Half-Plane	275
5.3	Flow Diagram of Numerical Iteration	277
5.4	Finite Element Discretization (i.e. C.S.T. Elements) of Nonlinear Elastic Half-Plane and Boundary Conditions	281
5.5	Deformed Configuration of Discretized Half-Plane Due to Pressure	282
5.6	Approach Between Plates and an Elastic Cylinder	282
5.7	Stress-Strain Curves of Kaolinite Clay Under Plane-Strain Triaxial Tests (Boonsinuk [13])	287
5.8	Small Tires Studied by P. Boonsinsuk [13]	288

5.9a-f	Comparison Between Experimental and Predicted Values of Half Contact Length for Clay	290
5.10	Stress-Strain Curves of 2 and 4 Day Snow Obtained by Confined Compression Tests (Metaxas [82])	294
5.11	Test Apparatus Used for Plate Penetration (Metaxas [82])	295
5.12a	Rigid Wheel and Snowpack Before Making Contact	296
5.12b	Rigid Wheel and Snowpack Before Making Contact	296
5.13a	Comparison Between Experimental and Predicted Values of Sinkage for a Rigid Wheel on a Snowpack Aged for 2 Days	298
5.13b	Comparison Between Experimental and Predicted Values of Sinkage for a Rigid Wheel on a Snowpack Aged for 4 Days	299
5.14a	Comparison Between Experimental and Predicted Values of Half Contact Length for a Rigid Wheel on a Snowpack Aged for 2 Days	300
5.14b	Comparison Between Experimental and Predicted Values of Half Contact Length for a Rigid Wheel on a Snowpack Aged for 4 Days	301
A.1	Notations Used for a Boundary on an Arc	337
A.2	An Elastic Lower Half-Plane	341
A.3	Multiply-Connected Infinite Region	342
A.4	Two Connected Regions for Defining Analytic Continuation	347
A.5	Two Connected Regions Symmetric with Respect to x-axis for Defining Schwartz Principle	347
A.6	Union of Simple, Non-Intersecting Arcs and Contours in Complex Plane	351
A.7	Limit Point on an Arc	351
A.8	An Elastic Solid Contacting with an Elastic Half-Plane Under a Vertical Loading	356

B.1	A Contact Problem Between Two Linearly Elastic Solids with Various Supports	405
B.2	A Linearly Elastic Solid in Contact with a Rigid Frictionless Foundation	407
C.1a-i	Load-Axle Displacement Relationship on Rigid Base	418
C.2a-h	Gross Contact Area - Load Relationship on Rigid Base	438
C.3a-h	Gross Contact Area - Inflation Pressure Relationship on Rigid Base	446
C.4a-d	Average Ground Contact Pressure - Inflation Pressure Relationship on Rigid Base	454
C.5a-f	Pressure Transducer Readings Within the Footprint of GOODYEAR 7.00-16LT (treaded)	462
C.6a-n/3	Pressure Readings and/or Pressure Distribution Within and/or Across the Footprint of GOODYEAR 7.00-16LT (buffed)	468
C.7a-p	Pressure Transducer Readings Within the Footprint of MICHELIN 7.00R-16XCL (treaded)	492
C.8a/1-b/4	Pressure Readings and/or Pressure Distribution Within and/or Across the Footprint of MICHELIN 7.00R-16XCL (buffed)	507
C.9a-f	Pressure Transducer Readings Within the Footprint of MICHELIN 11.00R-16XL (treaded)	514
C.10a/1-b/3	Contact Pressure Distribution Within the Footprint of MICHELIN 11.00R-16XL (buffed)	520
C.11a-c	Pressure Transducer Readings Within the Footprint of MICHELIN 12.5R-16.5XLM (treaded)	525
C.12a-i/2	Pressure Readings and/or Pressure Distribution Within and/or Across the Footprint of MICHELIN 12.5R-16.5XLM (buffed)	528
C.13	Description of Soil Stress Pressure Transducer	543
D.1	Stress-Strain Curves of Kaolinite Clay Under Plane Strain Triaxial Tests	544
D.2a-d	Load - Axle Displacement Relationships	545

D.3a-d	Contact Area - Axle Load Relationships	553
D.4a-d	Load - Contact Length Relationships	557
D.5a-d	Average Contact Pressure - Axle Load Relationships	561
D.6a-D.9c	Isobars (or Profiles) of Pressure Distribution Within the Footprint of GOODYEAR 7.00-16LT (treaded or buffed) in Clay	566
D.10a-D.13b	Isobars (or Profiles) of Pressure Distribution Within the Footprint of MICHELIN 7.00R-16XCL (treaded or buffed) in Clay	576
D.14a-D.17b	Isobars (or Profiles) of Pressure Distribution Within the Footprint of MICHELIN 11.00R-16XL (treaded or buffed) in Clay	586
D.18-D.21b	Isobars (or Profiles) of Pressure Distribution Within the Footprint of MICHELIN 12.5R-16.5XLM	594
D.22a-d	Variation of Contact Pressure (at Center) With Wheel Load	603
D.23	Descriptions of Soil Stress Gauge	607
E.1	Stress-Strain Relationship of Silica Sand (Triaxial Test)	608
E.2a-d	Load-Displacement Relationship for Each Tire on Sand	609
E.3a-E.6b	Isobars (or Profiles) of Pressure Distribution Within the Footprint of GOODYEAR 7.00-16LT (treaded or buffed) in Sand	614
E.7a-E.10b	Isobars (or Profiles) of Pressure Distribution Within the Footprint of MICHELIN 7.00R-16XCL (treaded or buffed) in Sand	622
E.11a-E.14b	Isobars (or Profiles) of Pressure Distribution Within the Footprint of MICHELIN 11.0R-16XL (treaded of buffed) in Sand	630
E.15a-E.18b	Isobars (or Profiles)ution Within the Footprint of MICHELIN 12.5R-16.5XLM (treaded or buffed) in Sand	638

LIST OF TABLES

Table No.		Page
2.1	Applicability of the Analytical Methods (2-D and 3-d)	28
3.1	Detailed Information on Tested Tires	59
4.1a	Buffed Tire-Clay Interaction Problems Solved by the Analytical Approach	219
4.1b	Buffed Tire - Rigid Base Interaction Problems Solved by the Analytical Approach	220
4.1c	Buffed Tire - Rigid Base Interaction Problems Solved by the Analytical Approach	221
5.1	Data on Contact Surface for Clay	289
5.2a,b	Specifications of Rigid Wheel and Snow Bin	296
C.1a	Comparison of Axle Displacement (Load = 3.0 kN, Inflation Pressure = 103.5 kPa)	427
C.1b	Measure of Carcass Stiffness for Each Tire Based on Carcass Stiffness of Treaded GOODYEAR 7.00-16LT (Inflation Pressure = 310.5 kPa) as One Unit	428
C.2a-h	Data on Contact Area for Each Tire on Rigid Surface	429
C.3	Ratio of Lug (or Rib) to Gross (or Total) Contact Area	437
C.4	Test Conditions Imposed in Pressure Distribution Determination	458
D.1a-h	Data on Contact Area	549
D.2	Test Conditions Imposed in Determination of Contact Pressure Distribution for Tire-Clay Interaction	565
E.1	Data on Contact Area in Sand	613

NOTATION

a	half contact length
a.e.	almost everywhere
A	(measured) nominal contact area
A_m	$2R^*B$, maximum contact area potentially might occur for each tire, R^* = representative (or idealized) radius of tire, B = representative contact width
$b = \|b_{ij}\|$	determinant of covariant metric tensor b
$\underline{b}_i$, $\underline{b}^i$	covariant and contravariant base vectors of the complex coordinates z^i, respectively
b_{ij}, b^{ij}	covariant and contravariant metric tensors, respectively
B^{ij}	cofactor of b_{ij}
$C^n(E)$	space of n-times continuously differentiable functions on a set (or domain) E
$\mathbb{C}$	complex plane
D_2^*	Laplacian operator, i.e. $D_2^*(\cdot) = b^{ij}(\cdot)_{,ij}$
D^i	displacements ($= u + iv$, $i^2 = -1$)
D_x, D_y, D_z	partial derivative operators with respect to x, y and z
$\underline{e}_i$	unit base vector
$\underset{\sim}{e}$	engineering strain tensor
E	modulus of elasticity
E^*	elastic measure
E'	$E/(1 - \nu^2)$

G	shear modulus
$h(t)$	function describing contact profile
$H^m(D)$	Hilbert space of integer order (or Hilbertian – Sobolev space)
$H^s(D)$	Hilbert space of real order, $s \in [0, \infty)$ (or Fractional Sobolev space)
$H_o^m(D)$	$\{u \in H^m(D)$: u and all its distributional derivatives up to m-1 are zero on the boundary of the domain D$\}$
$H^{-s}(D)$	negative Sobolev spaces = dual of $H_o^s(D)$
$Im\{\ \}$	imaginary part of $\{\ \}$
k	constant coefficient of friction
K	$\begin{cases} 3-4\nu \text{ (plane strain condition)} \\ (3-\nu)/(1+\nu) \text{ (plane stress condition)} \end{cases}$
L^*	biharmonic operator in cylindrical coordinates
$L^p(E)$	Lebesgue space, $p \in [0, \infty]$
$\underline{n}$	unit outward normal vector
$p_n(x)$	Polynomial of degree n
P	vertical load per unit width
$P(t)$	contact pressure
P^{mn}	stress components referred to the complex variable
$\underline{r}$	position vector
R	radius of cylinder or arbitrary positive real value
$\mathbb{R}$	$\mathbb{R}^1$
$\mathbb{R}^n$	n-dimensional Euclidian space
$\mathbb{R}^+$	set of all positive real numbers
R^*	representative radius of tire

$\mathrm{Re}\{\ \}$	real part of $\{\ \}$
S	space of rapidly decreasing test function
S'	dual space of S
T	tangential load
T_{ij}, T^{ij}	components of Cauchy stress tensor
$\underset{\sim}{T}$	Cauchy stress tensor
$T(t)$	contact shear stress
$u = u_1$	horizontal displacement
$u^m = u_m$	components of displacement vector, m = 1,2
$v = u_2$	vertical displacement
W	vertical load or axle load (i.e. force or force per unit width)
x	$= x_1$
x_i	Cartesian coordinate $(x_1, x_2) = (x,y)$
X	horizontal component of resultant force
y	$= x_2$
y^1	Cartesian coordinate
Y	vertical component of resultant force
z	complex variable = x + iy, $i^2 = -1$, ; $\bar{z} = x - iy$
z^i	complex coordinates, $(z^1, z^2, z^3) = (z, \bar{z}, y^3)$
$\delta^i_j = \delta_{ij}$	Kronecker's delta
$\varepsilon^{mn}, \varepsilon_{mn}$	ε-systems
	contact measure = A/Am
ϵ	"belongs to"
	small arbitrary positive real value

ν	Poisson's ratio
ν'	$\nu/(1-\nu)$
ρ	mass density
σ	average contact pressure
Φ	sectionally holomorphic function (i.e. standard defining function)
$\|\cdot\|$	Euclidian norm
$\|\cdot\|_V$	norm on a linear space V, e.g., $\|\cdot\|_{L2}$
$\subset$, $\supset$	inclusion signs
$\cap$	intersection
$\cup$	union

CHAPTER 1

INTRODUCTION

1.1 The Physical Problem

The purpose of this dissertation is to study quasi-static (sliding and/or non-sliding) interaction problems, experimentally (i.e. non-sliding) and theoretically (i.e. sliding and non-sliding), which occur between various types of pneumatic tires (or rigid wheel) and supporting ground such as rigid base, clay, sand and snow in order to support studies on mobility of wheeled vehicles (referred to as as simply vehicles hereafter). Such interaction problems may also be referred to as contact problems unless any confusion arises. The studies of the present interaction problems are focussed on determining quantities such as contact area (or contact length) and (patterns of) contact pressure distributions.

The basic motivations in carrying out the present research will be stated in the following: The mobility of all types of vehicles is naturally influenced, to a greater or lesser extent, by the mechanism of interactions which depend on factors such as type of tire, magnitude of load, inflation pressure, type of supporting ground (e.g. soil) interacting with a tire, relative deformability between a tire and the supporting ground (e.g. soil), velocity of vehicles, friction, tread pattern, etc. This suggests that it is not proper to establish a rational theory on any mobility problems without careful consideration of the interadtion mechanism which is extremely

complicated due to the structure of pneumatic tires. The interaction problems, involving pneumatic tires would, in general, exhibit quite different "pictures" on contact areas, contact profiles, and patterns of contact pressure distributions in particular, compared with what one expects from an intuition or an understanding of the various well-known contact theories in relation to contact problems between two linearly elastic solids. This is attributed to the differences of kinematics of surfaces between pneumatic tires and elastic solids - where every pneumatic tire could be regarded as a toroidal shell-like-tensioned stiff membrane. This makes the present interaction problems one of the most difficult contact problems regardless of whether the problem is static or not.

It may be noted here that due to the tires being such complicated structures, highly complex deformed configurations would be exhibited near and at the contact po · n during a loading sequence. This could possibly lead the loaded tire to an unstable deformed configuration influencing the contact pressure distribution, which will be discussed further in Chapter 2.

We can find several studies of the interaction problems involving pneumatic tires, e.g. Hiroma et al [49], Padovan et al [107] and Kabe et al [57]. In these studies each pneumatic tire is modelled by either an elastic continuum or elastic springs; the interaction problem was then solved numerically (i.e. finite element method). However, such models are obviously too simple to represent real interaction problems, hence obtaining erroneous results particularly with regard to patterns of contact pressure distributions since

pneumatic tires cannot be represented by elastic solids. In order to overcome such difficulties in modelling the pneumatic tires a simple analytical approach is developed in Chapter 4 for the present interaction problems involving the various pneumatic tires. Another method, an iterative method which is derived based on combining the complex variable method and the incremental finite element method. will also be introduced in Chapter 5, while it was initially developed for solving interaction problems between linear and nonlinear elastic solids (Yong et al [146,147]).

It is noted here that the interaction problems involving a pneumatic tire, in fact, involve two different types of contact problems simultaneously occurring at contact portions "A" and "B", as shown in Fig. 1.1. This makes the present interaction problems even more difficult and far more complex than the others even after idealization. A radial pressure along the rim is initially uniform, but it will change as the axle load is applied. The radial pressure at the contact portion "A" will increase, as the magnitude of axle load increases, while the radial pressure at the rest of the portion will decrease. These types of problems resemble inclusion problems. This is one of the major obstacles in establishing some computational methods as well as the analytical methods for interaction problems involving pneumatic tires. A little more discussion on these two types of contacts is given in Section 2.5.

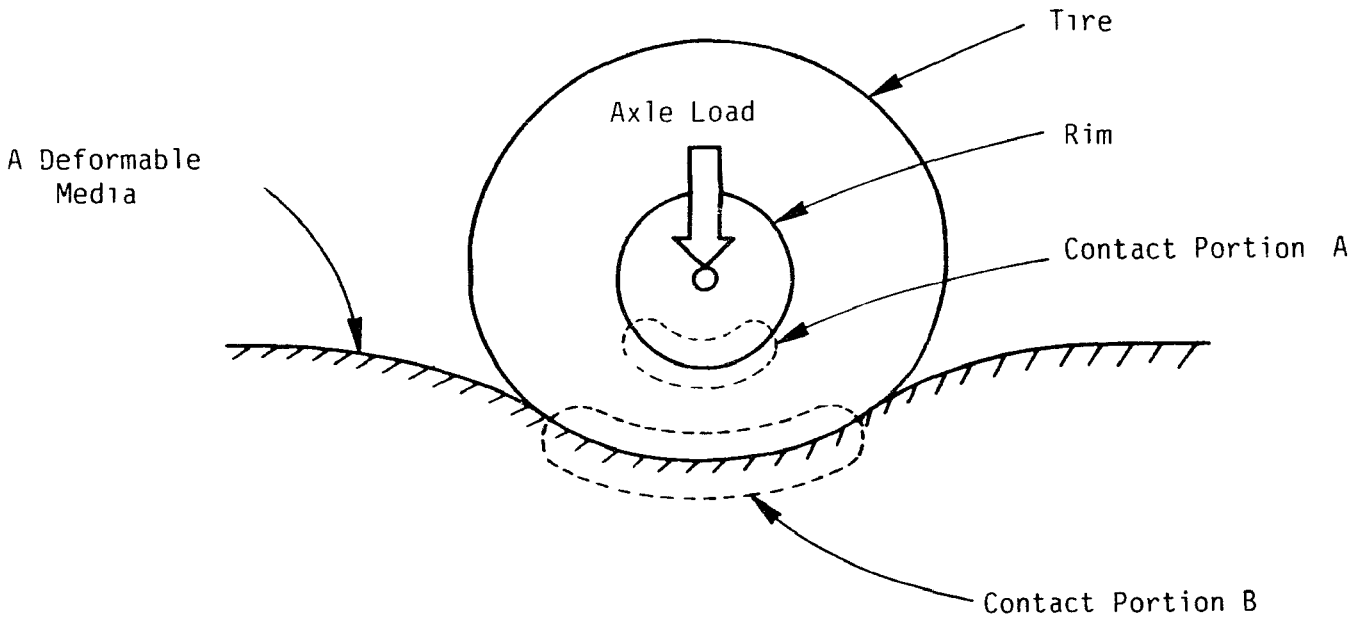


Fig. 1.1 A Pneumatic Tire Interacting with a Deformable (or Non-Deformable) Supporting Ground

1.2 Approaches to Interaction Problems

Our primary problems emphasized in this dissertation are the interaction problems involving pneumatic tires contacting with either a supporting clay or a (flat) rigid base (Chapter 4), although we also consider the contact problems occurring between a pneumatic tire and a supporting clay, and a rigid wheel and a supporting snowpack as secondary problems (Chapter 5). Hereafter the interaction problems refer to those involving (pneumatic) tires unless otherwise stated. Those present problems will be highly idealized in two-dimensional plane strain problems. In solving such problems, an analytical approach (Chapter 4) and an iterative method (Chapter 5), which is obtained by combining an analytical technique with a numerical technique, are developed.

This dissertation consists of six chapters and is organized in the following manner, as can also be seen from Fig. 1.2.

In Chapter 2 we will review several analytical and computational methods for various contact problems, most of which were developed in solving contact problems between two linearly elastic solids. In the area of contact problems such as those involving either a pneumatic body or transversely loaded membranes only a few computational methods have been developed. Considering both the review and the contact mechanism which is influenced by deformation of tires, we select the analytical and the numerical methods which are the basic tools in developing the two methods (Chapters 4 and 5) for the present interaction problems.

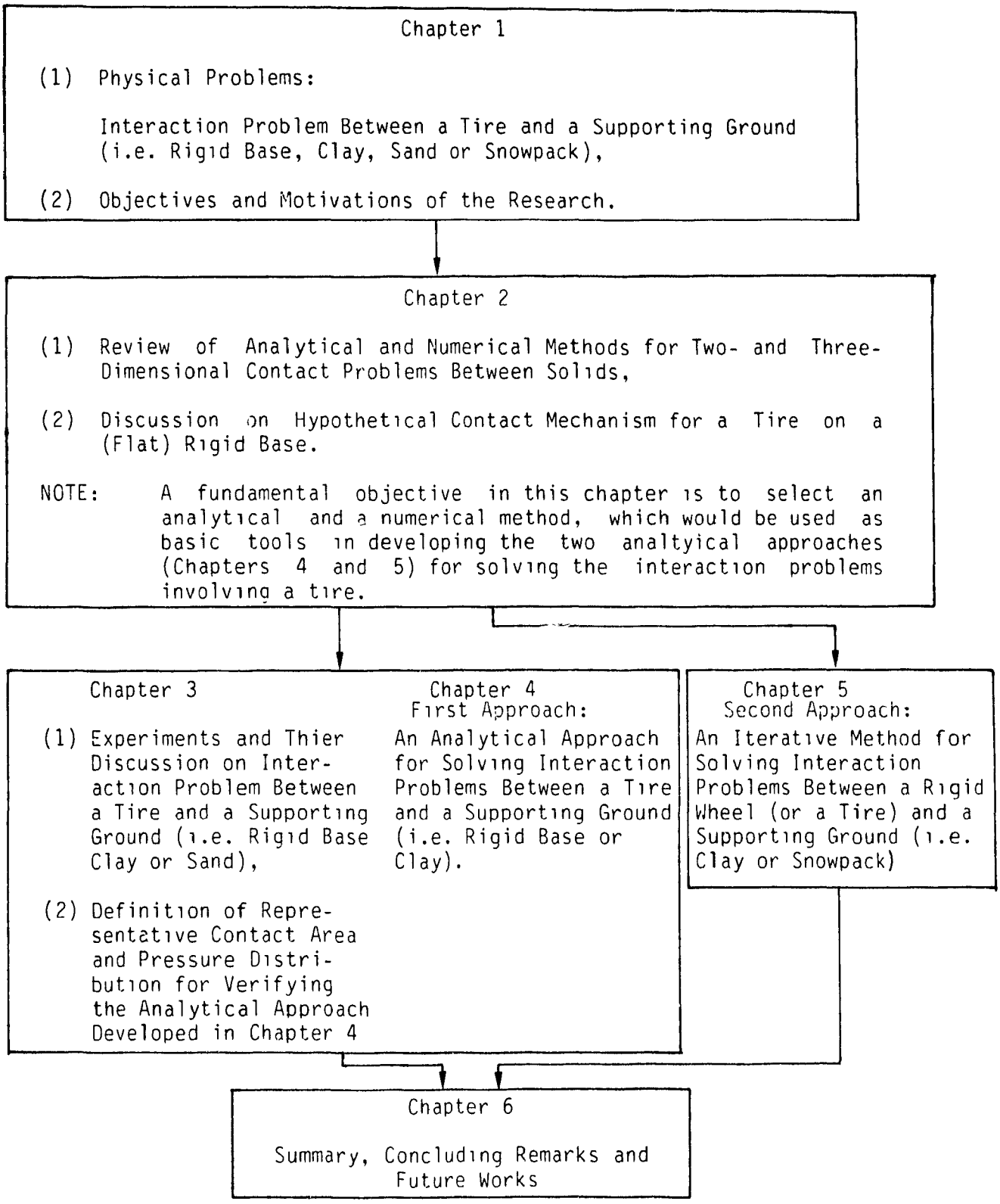


Fig. 1.2 Organization of the Dissertation

The numerous experiments on the interaction problems between various tires and a supporting ground (rigid base, clay or sand) were conducted under plane strain conditions to determining quantitatively contact area, shapes of contact surfaces, contact profiles and contact pressure distributions. In Chapter 3, the techniques used in these experiments are explained. The experimental results are also discussed extensively for characterizing the interaction problems. Besides the represenative contact area (i.e. length) and contact pressure are defined in order to verify the two-dimensional analytical approach developed in Chapter 4.

In Chapter 4 the analytical approach to the interaction problems, such as both tire-rigid base and tire-supporting clay interaction problems will be introduced. The approach is developed based on a fundamental mathematical tool, the complex variable method of which is selected from the various analytical methods reviewed in Chapter 2.

In Chapter 5 another method will be introduced, primarily for solving interaction problems between linear and nonlinear elastic solids (Yong, et al [146,147]. The method is an iterative method which is derived by combining the incremental finite element method with the complex variable method, assuming that the load increments are so small that the complex variable method, applied in linear elasticity problems, is also accepted in handling large deformations occurring in the supporting snowpack (or supporting clay). Then the iterative method was applied to the interaction problems (i.e. a tire-supporting clay and a rigid wheel-supporting snow). In Chapter 6, the summary, concluding remarks, contributions and future works are described.

CHAPTER 2

A BRIEF REVIEW OF CONTACT ANALYSES BASED ON ANALYTICAL AND COMPUTATIONAL METHODS: CONTACT MECHANICS OF PNEUMATIC TIRES INTERACTING WITH A RIGID BASE

2.1 Introduction

The purpose of this chapter is to select fundamental analytical and/or numerical tools which will aid in developing the analytical approaches introduced in Chapters 4 and 5 for the present interaction problems by reviewing the various analytical and computational contact analyses with consideration given to the mechanics of a (pneumatic) tire interacting with a rigid half-space.

We will review seven analytical methods (sections 2.2.2, 2.2.3 and 2.2.4), two for three-dimensional and five for two-dimensional contact problems. In section 2.3, a brief review of computational contact analyses will be given, while contact problems involving elastic membranes (e.g. pneumatic bodies) are also shown to be solved by the computational methods given in section 2.4.

In section 2.5 the contact mechanics of a pneumatic tire will be discussed paying particular attention to the process of deformations of a tire membrane at contact surface. In the final section (section 2.6) the analytical and computational methods will be selected as fundamental tools for the contact analyses which will be developed in Chapters 4 and 5.

2.2 A Brief Review of Analytical Methods

2.2.1 Introduction

Since Hertz established an analytical method for a three-dimensional frictionless contact problem in 1881 (e.g. Love [75]), which is often referred to as the Hertz theory of contact, an enormous amount of analytical methods for various types of contact problems between two elastic "solids", including inclusion problems, have been studied and developed over the century. Various work on this subject can be found in Lubkin [76], Kalker [58], Johnson [56], Lur'e [77], Gladwell [41], Muskhelishvili [86] and Galin [36]. However, often many of the analytical methods are closely related to one another when one looks at the mathematical tools used. Most contact problems virtually lead to one or more integral equations, depending on conditions and/or idealizations of the given contact problems. For this reason we will limit our review of the analytical methods to some typical ones for both two- and three-dimensional contact problems although the review will emphasize the two-dimensional contact analyses since the present contact analyses (Chapters 4 and 5) are developed under the plane strain condition. We will review only two analytical methods for the three-dimensional contact problems and five analytical methods for the two-dimensional contact problems by considering the following basic factors. Prior to those factors being mentioned, however, five typical contact problems shown in Fig. 2.1 are considered first. The two contacting solids, where S_2 and S_1 are referred to as the upper and lower solids respectively, could be subjected either to a normal load (W), a tangential load (T) or a

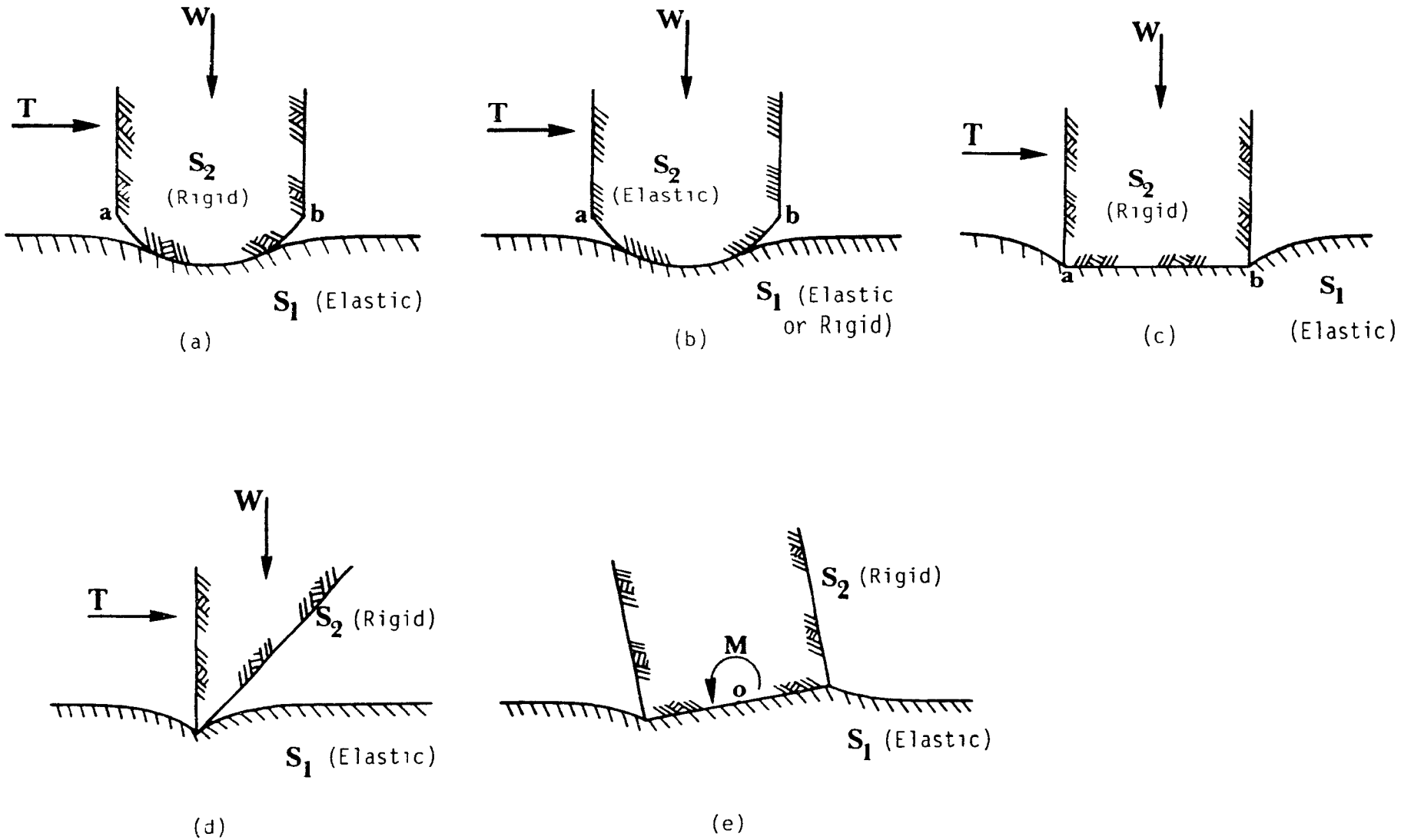


Fig. 2.1 Five Typical Contact Problems

moment (M), and a combined load otherwise. The points "a" and "b" in Fig. 2.1(a),(b) denote the edges of the solids S_2. It is noted that, although all the lower solids S_1 in Fig. 2.1 are shown to be half-spaces (-planes), it will be seen later that their profiles can be more general to some analytical methods.

Now the factors and conditions, influencing the development of analytical methods will be described as follows:

1. geometric conditions (profiles of two contacting solids)
   (i) smoothness of contact surface
   - parabolic, flat, half-space (-plane), wedge-shaped, etc.,
   (ii) symmetricity of solids,
   (iii) whether a solid is finite or not (if the solid is infinite, it is a half-space (-plane));
2. material conditions
   (i) either one or both of them is elastic (see e.g. Fig. 2.1(a), (b)),
   (ii) if a solid is elastic, it is linearly elastic, homogeneous and isotropic;
3. contact surface is either (i) frictionless (or unbonded), (ii) completely adhesive (or bonded), or (iii) (uniformly) limiting frictional;
4. a type of load applied quasi-statically is either (i) vertical load (W), (ii) tangential load (T), (iii) moment (M), or (iv) a combination of all of them, W, T and M.

There is one more thing which should be mentioned regarding the contact condition (or the smoothness of contact ends). That is, if the edges "a" and "b" of an upper solid shown in Fig. 2.1 (a),(b) are in contact with an elastic half-space, the contact is called "complete", and "incomplete" otherwise. Accordingly, the contact shown in Fig. 2.1(c) is complete.

We will now briefly describe two different ways of classifying types of contact problems based on the different criterions, of which one is due to the applicability of the Hertz theory (see section 2.2.2) and inclusions of contact surfaces at different levels of loads is the other. First, the classification due to the Hertz theory will be described so that all problems are classified as either "Hertzian" or "non-Hertzian" contact.

A. HERTZIAN AND NON-HERTZIAN CONTACT PROBLEMS

1. Hertzian contact problems are problems to which the Hertz theory is applicable. Roughly speaking, by considering the above factors, the contact problems should satisfy the following conditions: (i) profiles of contacting solids are basically parabolic approximated by the second degree polynomials (although one solid could be a half-space), (ii) either one or both of the contacting solids is elastic, (iii) frictionless, (iv) normal load, (v) incomplete contact.
2. Non-Hertzian contact problems are merely problems which are not Hertzian contact problems.

For example, the contact problems shown in Fig. 2.1 (a), (b), of which contacts are incomplete, without tangential load are Hertzian, and the rest of the problems in Fig. 2.1 are non-Hertzian. It is noted, however, that in order to obtain better solutions by the Hertz theory, all contact problems should be elastically and geometrically similar due to the development of the Hertz theory.

The next classification of contact problems is due to Dundurs [22] and Dundurs and Stippes [23], which depends on inclusions of contact surfaces at different levels of load, and each state of contact is called either "receding", "stationary" or "advancing". The definitions of these contacts will be simply given below.

B. RECEDING, STATIONARY AND ADVANCING CONTACTS

1. A state of contact surfaces is called "receding" if a contact surface at the current load is contained in the contact surface at the previous load.
2. A state of contact surfaces is called "stationary" when a contact surface does not change as the level of load changes.
3. A state of contact surfaces is called "advancing" if a contact surface at the current load is not contained in the contact surface at the previous load.

For example, all Hertzian contacts are advancing, while the contact shown in Fig. 2.1(c) is stationary. The classification given above is based on changes of contact surfaces and depends very much on factors such as profiles of solids and types of loads.

In the following three sections (2.2.2, 2.2.3 and 2.2.4), ideas and features of the seven different analytical methods for two- and three-dimensional contact problems will be briefly described with consideration of the factors and the two different types of classifications of contact problems. Applicability of the analytical methods will be clarified in a table (Table 2.1) shown in section 2.2.4. It is noted that details of the methods, with the exception of method 5, can be found in Appendix B. In the last section (2.2.5) a conclusion regarding the analytical methods will be given.

2.2.2 Analytical Methods for Three-Dimensional Contact Problems

Method 1 (Three-Dimensional Hertz Theory)

a. This method is based on the following results:

(i) A relationship between a normal pressure applied on an elastic-half space and its responses (i.e. vertical displacements), i.e. the displacement at a point of surface $z = 0$ is given by

$$w(x,y,0) = (1-\nu)g/2\pi G \qquad (2.1)$$

where G, ν are the shear modulus and the Poisson's ratio of the elastic half space, respectively, and g is a Newtonian potential (see Eq. B.2 in Appendix B).

(ii) A geometric result at a contact surface due to vertical displacements $\bar{w}_i$ (i=1,2) of the two solids being pressed each other. That is described by,

$$\bar{w}_1 + \bar{w}_2 = H - d(z_2, d_1) \qquad (2.2)$$

where $\bar{w}_1$, $\bar{w}_2$ are the displacements of the solids S_2 and S_1 respectively, H the approach and $d(z_2, z_1)$ is a distance function describing the distance between the surfaces of the two "undeformed" solids.

The two results (i) and (ii) stated above with the assumption that two solids are approximated by two elastic half-spaces leads to an integral equation (Eq. B.4)

$$g(x,y,0) = \iint_S \frac{p(r,s)}{\tilde{R}}\, dr\, ds = \{H - d(z_2,z_1)\}/\tilde{M} \qquad (2.3)$$

where $p(r,s)$ is a pressure distribution; $\tilde{M}$ stands for material constants; $\tilde{R} = \{(x-r) + (y-s)^2\}^{1/2}$, (Eq. B.4).

Since the right hand term in Eq. 2.3 is a quadratic function (due to an assumption on profiles of solids), it was solved for the pressure by means of a potential of ellipsoid (see Love [75]).

b. Comments on Method 1

1. The expression for the displacement at the surface in Eq. 2.1 (or Eq. B.1 in Appendix B) is due to normal stress, and is obtained from the Boussinesq-Cerruti potentials by neglecting shear stresses at the surface of the half-space, thus requiring only one potential, a Newtonian potential as shown in Eq. 2.3 and Eq. B.2 (Appendix B). For this reason the Hertz theory is naturally limited to frictionless contact problems.

2. While Hertz established a contact theory in which he assumed profiles of contacting solids as being described by quadratic functions, it was shown by Ahmadi, Keer and Mura [4] that the basic idea can be extended in solving non-Hertzian contact problems. This would be carried out so long as the right hand side in Eq. 2.3 (or Eq. B.2) results in a function under a condition that the function of pressure distribution is absolutely integrable almost everywhere in the contact surface S. This implies that the Hertz theory is not supposed to be modified (or extended) to solving the contact problems shown in Fig. 2.1 (c), (d), where the sharp portions of the rigid solids S_2 are in contact with the half-spaces.

Method 2 (Axisymmetric Hankel Transform Method)

This method was first investigated by Harding and Sneddon [48] (and Sneddon [122]) to solve axisymmetric problems in elasticity, as well as frictionless axisymmetric contact problems between a rigid punch and a half-space. The extension of this method was carried out by Gladwell [38,39,41], and allows the contact problems to be in the frictional and adhesive states.

The steps of the method by Harding and Sneddon [48] will be summarized in the following (refer to Appendix B):

a. Steps

1. Displacement solutions, expressed in terms of potentials (or Papkovich-Neuber solution), are transformed into polar coordinates (Eq. B.11).

2. Introduction of a new function F (Eq. B.12), which is derived from the two harmonic functions, will reduce a problem to solving a fourth order differential equation as given in Eq. B.15 to

$$L^*(F) = 0 \tag{2.4}$$

where L^* stands for a biharmonic operator (in cylindrical coordinates and is symmetric with respect to z) and the function F is called the displacement potential, which in the end describes displacements (Eq. B.14) and stress fields.

3. Since the differential equation in Eq. 2.4 is defined in a half-space for axisymmetric problems, the Hankel transform may be the best analytical tool for solving the equation.

4. Application of the Hankel transform to Eq. 2.4 (or Eq. B.17 where n=0 for axisymmetric problems) leads to an ordinary differential equation (shown in Eq. B.18), i.e.

$$D^*(H) = 0 \tag{2.5}$$

where D^* represents a linear ordinary differential operator of the fourth order, and H ($=G_o$) is the Hankel transform of F ($=F_o$) (Eq. B.19) expressed as

$$H = HK[F] \tag{2.6}$$

in which HK stands for the Hankel transform of order zero (or Fourier-Bessel transform), and H is the image of the Hankel transform.

5. The general solution F is then obtained by inverting the Hankel transform of Eq. 2.6, after the general solution H ($= G_o$) (Eq. B.21) of the ordinary differential equation in Eq. 2.5 is

substituted into the left hand side of Eq. 2.6. This is shown to be

$$F = HK^{-1}\,[HK[F]] = HK^{-1}[H] \qquad (2.7)$$

where HK^{-1} is the inversion of the Hankel transform.

6. Substitution of F as obtained in Eq. 2.7 into Eq. B.14c leads to the expression of the displacement shown in Eq. B.23. In the same way, the stresses can also be found as shown in Eqs. B.24 and B.25. Once the coefficients A, B, C and D in Eq. B.26, which is the general solution of Eq. 2.5, are determined from the given boundary conditions, it means that an axisymmetric contact problem is solved. Determination of such coefficients requires us, in the end, to solve a pair of integral equations as given in Eq. B.31(a), (b) and seek one coefficient D, which depends on the displacement boundary condition (in Example Problem) given in Eq. B.22a.

b. Comments on Method 2

1. Solving an axisymmetric contact problem by this method is equivalent to solving a mixed boundary-value problem (see Method 2 in Appendix B or Eqs. B.22(a), (b), (c) given in Example Problem).

2. The conditions required for the function F(r,z) and its Hankel transform H(t,z) must satisfy the following conditions:

(i) $L^*(F) = 0$ in Eq. 2.4 implies that

$F(r,z) \in C^n (E_r \times E_z)$, $n \geq 4$, where $E_r = [0, \infty)_r$ and

$E_z = [0, \infty)$.

(ii) Equation 2.7 by means of the Hankel transform holds only if

(1) $F \in L^1(E_r)$ for each fixed $z > 0$ (note that L^1 is a Lebesque space) and

(2) $F \in C(E_r)$ almost everywhere (i.e. Fourier-Bessel integral theorem). It is noted that the Hankel transform is a unitary operator on $L^2(E_r)$, i.e.

(a) $HK: L^2(E_r) \to L^2(E_t)$ and (b) $\| HK(h) \|_{L^2} = \| h \|_{L^2}$

where $\| \cdot \|_{L^2}$ denotes the L^2 - norm on $E = [0, \infty)$.

(iii) Since the general solution F is expressed as shown in Eq. 2.7, the image of the Hankel transform H, which is, in this case, the general solution of Eq. 2.5, must satisfy all the conditions in (i) and (ii) given above. That requires H(t.z) to be such that

$$H(t,z) \in C^n(E_r \times E_z),\ n \geq 4, \text{ and } H \in L^1(E_t)$$

for a fixed $z > 0$ in order that the expressions of displacements and stresses given in Eqs. B.23, B.24 and B.25 are defined.

2.2.3 Analytical Methods for Two-Dimensional Contact Problems (Plane Strain Condition)

Method 3 (Two-Dimensional Hertz Theory)

The basic assumptions and/or conditions, required for this two-dimensional (2-D hereafter) Hertz theory, are the same as those considered in the three-dimensional (3-D hereafter) Hertz theory. The 2-D Hertz theory is, however, less straightforward compared with the

3-D Hertz theory, because of the indeterminancy of vertical displacements in the half-plane. This is one of the inherent inadequacies for plane elasticity. Some more details on this method can be found in Appendix B.

Method 4 (Singular Integral Equations)

Method 4 (e.g. Muskhelishvili [86,87] and Johnson [55]) reduces a contact problem occurring on an elastic half-plane, into the form of a singular integral equation (abbreviated as SIE hereafter), which can be solved provided that a slope of the deformed contact surface is known a priori. Such an SIE can be obtained from the expression(s) of the vertical (boundary) displacement field of the half-plane subjected to stress(es) distributed over a finite portion.

In Appendix B, only two types of SIEs are considered for which one solves a frictionless contact problem (Eq. B.45) and the other a (limiting) frictional contact problem (Eq. B.47). Since such SIEs are easily transformed to Riemann-Hilbert problems which are derived on the basis of the complex variable method, they can be solved by the approach (complex variable method) considered in Method 7. A link between the SIEs and complex variable method for contact problems is described further in (II) of Appendix B.

Method 5 (Integral Equation with π-Kernel)

This method, considered by Popov (e.g., Gradwell [31]) solves a frictionless contract problem where a vertical displacement field

$v^*(x)$ is prescribed over the contact surface L as

$$v^*(x) = f(x) + d^* , \qquad x \text{ on } L \tag{2.8}$$

where d* is a known constant.

Then he derived the following integral equation

$$-\frac{2(1-\nu^2)}{\pi E} \int_L p(t) \log |x-t| \, dt = f(x) + c^*, \quad x \text{ on } L \tag{2.9}$$

by considering Eq. 2.8 and Eq. B.35 (Appendix B). In Eq. 2.9, "c*" is an indeterminant constant, and Popov calls the kernel log |x-t| the π-kernel, while the integration is seen to be a surface potential in two-dimensional Euclidian space with the density p(x). After taking a derivative with respect to x, this method is deduced to the previous Method 4, in which a frictionless contact problem is reduced to the singular integral equation given in Eq. B.45.

One difference between the two methods (Method 4 and 5) is that Method 4 requires only a slope of displacement while Method 5 requires the displacement field (which may be a part from a constant term). It should, however, be noted that since the constant c* in Eq. 2.9 is indeterminant, so is the general solution p(x). The solution is then obtained after neglecting this constant, and has a square singularity at the contact ends. Physically, this implies that every contact is a complete one, i.e. for example the edges "a", "b" of the punch shown in Fig. 2.1(a) are in contact with the half-plane under a normal load. Besides in Method 5, a solid S_2 contacting with a half-plane is restricted to being rigid, while it is not necessary in Method 4.

This concludes that Method 4 is applicable to a wider class of contact problems as compared to Method 5.

Method 6 (Fourier Transform)

This method (see Gladwell [41]) is straightforward as shown in Appendix B, once the Popkovich-Neuber potentials are defined by means of conjugate Fourier transform in Eqs. B.49. These potentials are also harmonic functions because there is no body forces present. It is applicable to frictionless contact problems, where mixed boundary conditions with prescribed displacement (or slope) at the contact surface are given.

As shown in Appendix B, the problem is finally reduced to a singular integral equation with an unknown pressure (Eq. B.59), which is the same as shown in Methods 4 and 5. The singular integral equation, hence, can be solved by inverting the Hilbert transform.

Since the Fourier transform is exclusively used in this method, it may be helpful to consider what types of functions are allowed in the operations - such as inversion, differentiabilities, etc. As shown in the end of Method 6 given in Appendix B, it would be sufficient to consider the function spaces such as L^1 and L^2, so long as frictionless contact problems are concerned so that pressures would be in a space of either L^1, L^2 or $L^1 \cap L^2$.

Method 7 (Complex Variable Method)

This method, which is based on the theory of complex variables,

was first introduced in a (plane) elasticity problem by G.V. Kolosov in 1909 (see Muskhelishvili [86]), and is largely attributed to the work by Muskhelishvili [86,87]. It is applicable to a wide class of complicated elasticity problems due to the intrinsic character of holomorphic functions used in this method. A particular feature of the method is its ability to reduce a contact problem to a Riemann-Hilbert problem (i.e. a pair of equations governing contact problems), from which one obtains a sectionally holomorphic function (e.g. a holomorphic function being discontinuous across the contact surface). It defines contact stresses and slopes of contact surfaces as shown in Eqs. B.68, B.69 and B.76a,b (i.e. Eqs. A.60 and A.61). More details of the method can be found in Appendices A, B (Method 7) and Chapter 4. The initial development of the theory given in Appendix A, which is fully devoted to this method [86], may be elementary and quite lengthy. However, it is an ingeneous approach that Muskelishvili chose in relating mathematics and physical matters. For example, he does not take the usual approach in solving a biharmonic equation (Eq. A.4b). He fully uses the characteristics of holomorphic functions instead, and hence obtains a (holomorphic) solution (Eq. A.15) represented by two holomorphic functions. In his approach, however, it is not required that the solution is assumed to be holomorphic, a priori.

Some comments on the method will be given in the following:

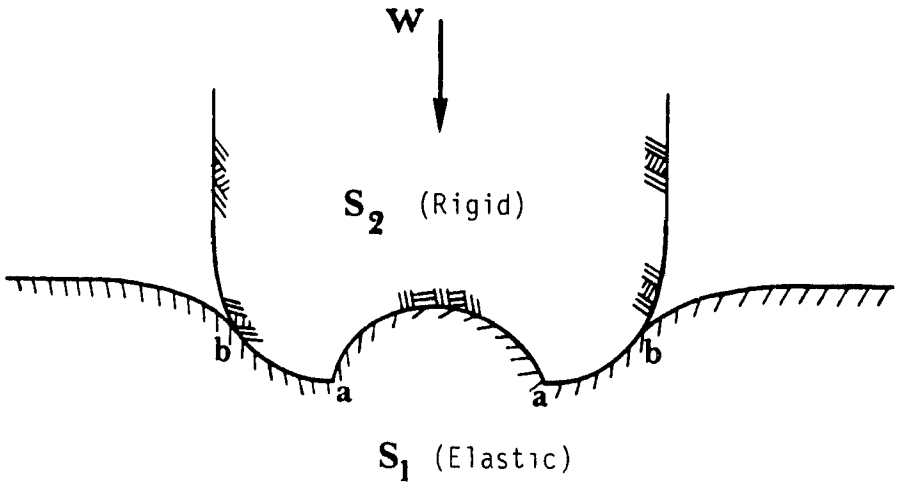
1. A sectionally holomorphic function (or complex potential), satisfying a Riemann-Hilbert problem for a contact problem, always exists if each function of contact stresses have a compact

support in the real axis (i.e. closure of the domain where stresses are not zero is bounded in the real axis). This condition is physically required. Besides if the contact stresses are Holder continuous (Eq. A.55), then the Plemelj formuale (Eqs. A.57 and A.58), which are essential to the method, are defined.

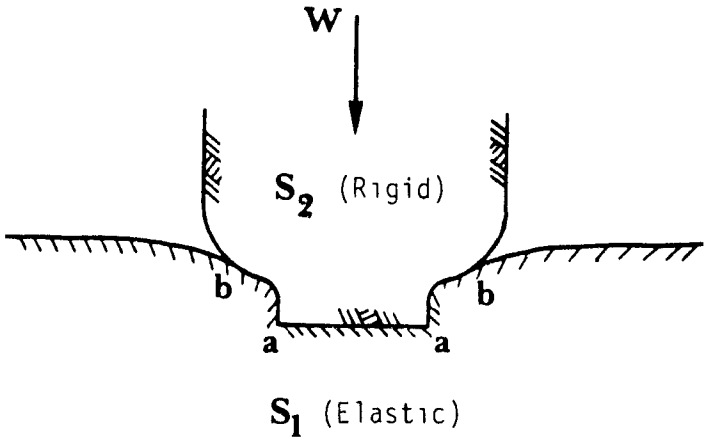
2. The definition of the contact stresses (Eqs. A.62 or Eqs. B.76) is really the "loose" definition of hyperfunctions of one variable, as also discussed in Appendix B, where the space of hyperfunctions is larger than the space of Schwartz distributions. The hyperfunctions are also sometimes referred to as Sato distributions due to the name of the founder, M. Sato. More details on the theory of hyperfunctions can be found in some books, e.g. Kaneko [60], Morimoto [85], Imai [53], Kashiwara, Kawai and Kimura [61].

   According to the theory of hyperfunctions, the assumption of the Holder continuity on contact stresses can be discarded. If contact stresses are in the space of hyperfunctions with a compact support, then the Plemelj formalae still hold. This result is useful in solving the contact problems such as those shown in Figs. 2.2 a,b. Since the profile of each (idealized) punch is not smooth at the corners "a" with possibly right angle, the stresses would also be discontinuous (i.e. unbounded) at "a", hence no longer Hölder continuous.

3. As shown in (II), Appendix B, the Riemann-Hilbert problem for a



(a)



(b)

Fig. 2.2 Contact Problems Between a Punch with Sharp Edges and an Elastic Half-Plane

contact problem is equivalent to the singular integral equation shown previously in Methods 4, 5 and 6, when a contacting solid S_2 is rigid, in particular.

4. Since the complex variable method is applicable for a contact problem where two contacting solids are deformable, we will be able to derive a singular integral equation for the contact problem from the Riemann-Hilbert (contact) problem by tracing backward the steps taken in (II), Appendix B.

2.2.4 Applicability of the Analytical Methods

The limitations to each method reviewed in the previous sections 2.2.2 & 2.2.3 are described in Table 2.1. Contact problems considered here are mainly those shown in Fig. 2.1 with consideration of the factors shown in section 2.2.1. The notations and/or abbreviations used in Table 2.1 will be explained in the following.

Dimension of Problems

(i) 3-D (Axisymm) = three-dimensional (axisymmetric)

(ii) 2-D = two-dimensional

Types of Analytical Methods

(i) Each number represents the number of the method, e.g. 1, 2,... 5,...are respectively Method 1, Method 2,...,Method 5,...

(ii) The brackets show the abbreviation of each method.

Profiles of Solids

For 2-D and 3-D problems,

(i) Half = half-space (or -plane for 2-D solid),

(ii) Flat = a solid with a flat surface (Fig. 2.1 c)

For 2-D and/or 3-D problems,

(iii) H_1 = a quadratic function (Hertz) in 2-D and 3-D,

(iv) H_2 = flat, parabolic, spherical and conical (Sneddon).

For 2-D problems,

(v) $P_n = A\ x^n$, n = positive integers (A = a constant),

(vi) ALL = (i), (ii) and (v), shown above, are all included.

Deformability of Solids

(i) S_{ij}^{ER} = a solid S_i is elastic and a solid S_j is rigid (i,j=1 or 2)

S_{ii}^{EE} = both solids S_i and S_j are elastic (i,j=1 or 2).

(ii) ALL = all kinds of combinations in (i).

Types of Contact Surface

FL = frictionless,

AD = (completely) adhesive,

LF = limiting frictional.

Types of Loads

W = vertical load

T = horizontal (or tangential) force

M = moment (Fig. 2.1 c)

ALL = W, T, M

Dimension	Types of Analytical	Profile of Solids		Deformability of Solids	Types of Contact Surfaces	Types of Loads
		S_1	S_2			
3-D	1 (3-D Hertz)	Half H_1	Half H_1	ALL	FL	W
3-D (axisymm)	2 (Hankel Trans)	Half	Flat H_2	S_{12}^{ER}	FL	W
2-D	3 (2-D Hertz)	Half H_1	Half H_1	ALL	FL	W
	4 (S.I. Eq.)	Half	ALL	S_{12}^{ER}	FL,LF	W,T
	5 (I.E.:Pi-Kernel)	Half	ALL	S_{12}^{ER}	FL	W
	6 (Fourier)	Half	ALL	S_{12}^{ER}	FL	W
	7 (Complex V.M.)	ALL	ALL	ALL	ALL	ALL

TABLE 2.1 Applicability of the Analytical Methods (2-D and 3-D)

2.2.5 Concluding Remarks on the Analytical Methods

Although the methods reviewed in the previous two sections (2.2.2 and 2.2.3), do not cover many other important methods (which may be possibly superior in some aspects to those reviewed here), each method and its concept is still (practically) important even after many types of numerical methods have been developed, and some of them have been extensively and profoundly studied by many researchers in the various fields. Particular reasons why the previous seven methods are

selected for review are such that; (a) each method is an initial development and has different approaches (at least they appear so), (b) to study connections between a contact problem and the main mathematical tools used, and (c) to find out the differences, advantages and disadvantages (from the mathematical point of view, in particular) for all the methods.

In the following some points regarding the methods and/or comparisons between them will be given by referring to the comments given in the review of each method and Table 2.1.

1. Methods 2,4,5 and 6 may be considered to be the analytical tools for mixed boundary-value problems rather than solving contact problems, since these methods require an input of either a profile of a punch or a deformed profile and/or a slope of deformed surface. All contact problems, especially two elastic solids in contact, should rather be categorized as free boundary (-value) problems (e.g. Duvaut and Lions [24], Lions [73]), where boundary-values such as contact pressures and slopes are sought.
2. Differences between Methods 1 and 2 are clear from Table 2.1. Either one of the methods may be chosen depending on problems. For example if a contact problem occurs between two deformable solids whose (undeformed) profiles are approximated by second order polynomials, then Method 1 may be chosen. If a contact profile is initially known and is not suitably approximated by a second order polynomial, then Method 2 will be chosen.

3. All the analytical methods in 2-D problems are essentially identical, except for Method 3 (2-D Hertz theory), provided there is no friction at the contact surface. Differences between these methods are summarized as follows:

(i) In Method 4, the Fredholm singular integral equation of the first kind (abbreviated as SIE.1, and SIE.2 for the second kind) will be obtained for frictionless contact problems, and the SIE.2 for the frictional (in limiting friction) contact problems.

(ii) Methods 5 and 6, which are applicable to frictionless problems only, are reduced to SIE.1.

(iii) As shown in (II), Appendix B, a SIE.2 (Method 4) can be transformed to a Riemann-Hilbert problem, and hence the converse, i.e. from a Riemann-Hilbert problem to an SIE.2 (or 1), should also hold.

(iv) In Table 2.1, it is clear, in the 2-D contact problems, that Method 7 (CVM) is superior to all other methods. It is also interesting to note that if the Riemann-Hilbert problems are transformed to SIE.2 by means of Plemelj formulae, then whichever problems can be solved by Method 7 can also be solved by Method 4. Functions, which define contact stresses by virtue of sectionally holomorphic functions, happen to be a loose definition of hyperfunctions (i.e. Sato distributions).

2.3 A Brief Review of Computational Methods

In boundary-value problems in solid mechanics, the computational methods such as the finite element method (e.g., displacement, hybid

and mixed) (see Gallagher [37], Zienkiewicz [153], Oden [89,101] Ciarlet [18] and Strang and Fix [127]) and the boundary element method based on the boundary integral equation (see Cruse and Rizzo [20], and Brebbia [14]) changed the approach in analyzing problems in continuum mechanics, and have also been proven to be powerful tools in solving (elliptic) problems in various fields of engineering and science. They have also been applied to the particular problems in elasticity, such as contact problems, which are not considered to be boundary-value problems but are rather categorized in the field of free boundary (-value) problems (see Duvaut and Lions [24]). There are basically two different approaches for solving contact problems by means of the above methods; the first approach seeks the solution iteratively by trial and error, while the second one reduces the contact problem to a special class of mathematical programming problems.

The first one, which employs the finite element methods, can be traced back to the work by Wilson and Parsons [137], who suggested a method for solving a frictionless contact problem between two elastic solids by using the displacement finite element method. Ohte [104] extended this method to a frictional contact problem where the irreversibility of the stick-slip phenomenon was modelled. Chan and Tuba [16] used a similar technique in studying the effects of clearance, load and friction on turbine blade fastenings. Gaertner [35] was able to model the frictional problem by forcing the strain variables to the appropriate values according to the contact

conditions on the interface. Tsuta and Yamaji [134] also proposed a method applicable to the frictional contact problem by considering non-linearities, which arise from variation of the contact surface and irreversible frictional effects resulting from stick-slip phenomenon, based on load incremental theory. Later Okamoto and Nakazawa [105] extended this method for the faster convergence (see III in Appendix B).

In all the foregoing studies the approaches are based on the standard displacement finite element methods. Other finite element methods such as the hybrid and the mixed finite element methods are found to be superior to the displacement finite element methods when particular problems in structures and solid mechanics are concerned, e.g. stress concentration, plates and shells, etc. However, we can find only a little work regarding the analyses of contact problems due to the lengthy complicated algebraic formulations and some mathematical difficulties such as existence and stability of solutions. The difference between the hybrid and the mixed finite element methods, which are quite similar in the way that functionals in both methods, depend on the field variables of both displacements and stresses. These can be drawn as follows: the hybid methods are special cases of the mixed methods obtained by taking continuity across interelement boundaries as constraints and using the method of Lagrange multipliers to enforce the constraints in an average variational sense e.g. Pian [110], Pian et al [112], Oden [94]. Pian and Kubomura [111] proposed an incremental variational formulation based on the assumed hybrid method for a frictional contact problem by

taking into account contact reactions as the additional field variables so as to satisfy the continuity of stresses across the contact surface. The method based on the mixed method was considered by Tseng and Olson [135] who retained the stress variable at the contact surface with forced boundary conditions and the displacement variable with natural boundary conditions. Anderson [5] and Anderson, Fredriksson and Persson [6] applied the boundary element method to a frictional contact problem, and solved it iteratively by trial and error.

Another approach which reduces the contact problem to a mathematical programming problem, is formulated by either direct consideration of contact criteria (e.g. Corney and Serieg [19], Chand, Haug and Rim [17]) or as a variational inequality (e.g. Oden and Kikuchi [96], Oden [94], Kikuchi [65,66], Oden, Kukuchi and Song [97]). Solutions are obtained by using a quadratic programming method (e.g., Corney and Seireg [19], Chand, Haug and Rim [17]), or a penalty method (e.g. Oden and Kikuchi [96], Oden [94]). The principle of variational inequalities (see, III in Appendix B, Duvant and Lions [24], Oden and Kikuchi [96] and Panagiotopoulos [109]) is useful in investigating the mathematical properties of the solution, such as existence, uniqueness and regularity. It is noted here about a well-known fact that if the Coulomb's law of friction is applied to a contact problem involving elastic solids, then the normal contact stress is ill-defined (e.g. Duvaut and Lions [24]). This led to the series of studies on the friction law, e.g., Oden and Pires [99,100]. Rabier, Martins and Oden [114] and Kikuchi [64].

2.4 Contact Problems Involving Pneumatic Bodies and Elastic Membranes

There are relatively few works on this class of contact problems, where contacting bodies are not elastic solids but membrane types (e.g. thin membrane, pneumatic bodies, beam, plates, shells, etc.). This type of contact problem is also often referred to as an obstacle problem, where a membrane comes into contact with a rigid body with arbitrary shape. Some interesting analyses on this class of contact problem were carried out by Feng [27], Feng and Huang [28,29], Feng and Yang [30], John [54], Naumann [88], Oden and Kubitza [98], Kikuchi [66], Ohtake, Oden and Kikuchi [103], Endo, Oden, Becker and Miller [25], Oden and Kikuchi [95].

Particular attention is paid to the series of work done by Feng [27], Feng et al [28,29,30], Oden and Kikuchi [95], and Endo et al [25], since their studies are closely connected to the analysis of the present interaction problems involving pneumatic tires in contact with another solid (i.e. either elastic or rigid).

Feng and Huang [29] described the analysis of a nonaxisymmetric frictionless contact problem between an inflated highly deformable membrane and a rigid punch as shown in Fig. 2.3.

The idea of this analysis is summarized as follows: First the total potential energy for the deformed configuration is defined. This is a function of the unknown spatial coordinates y_i (i=1,2,3). The total potential energy is minimized subject to inequality constraints of the geometrical contact condition which is reduced to an equality constraint through the use of a slack variable. The

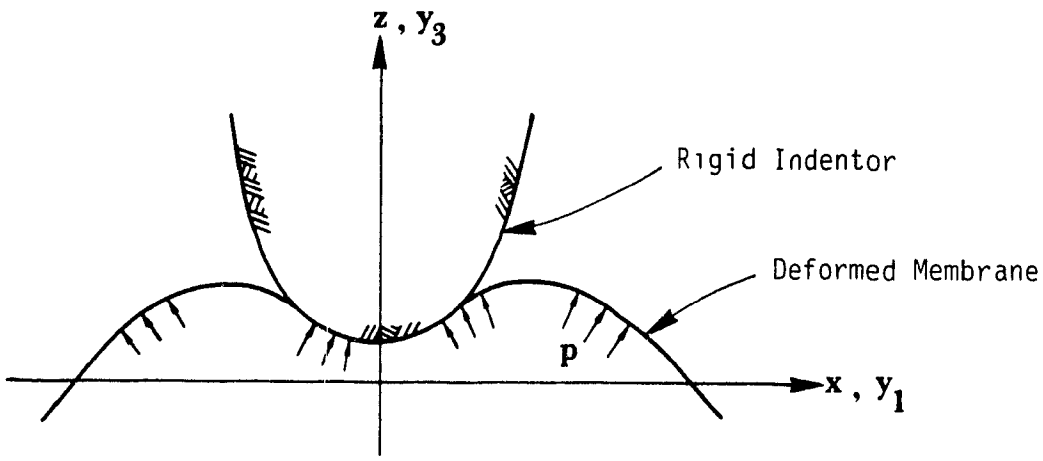


Fig. 2.3 An Inflated Rectangular Membrane Contacting with a Rigid Smooth Indentor

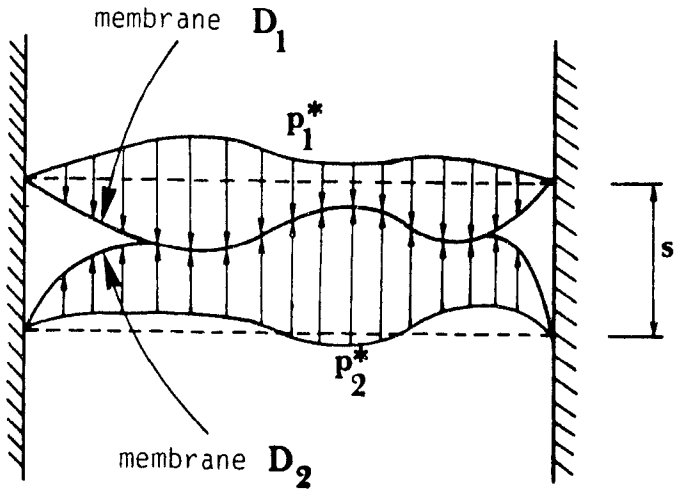


Fig. 2.4 Contact Problem for Two Parallel Membranes Subjected to Transverse Pressures

unknown spacial coordinates containing coefficients and the slack variable that minimize the total potential energy for an equilibrium state are then determined by applying the Fletcher and Powell's iterative descent method.

Oden and Kikuchi [95] formulated a variational inequality for a contact problem for two parallel linearly elastic membranes subjected to transverse pressures as shown in Fig. 2.4.

The basic form of the variational formulation is the same as that for the two solid elastic membranes in contacts such as in Eq. B.130 and B.131, except for some minor details. The variational inequality for this problem is

$$\sum_{i=1}^{2} a_i(u^i, v^i) \geq \sum_{i=1}^{2} f_i(v^i - u^i) \text{ , for all } v^i \text{ in } K \qquad (2.10)$$

where

$$a_i(u^i, v^i - u^i) = \int_{D_i} t_i \text{ grad } u^i \cdot \text{grad } (v^i - u^i)\, dV;$$

D_i are the membranes "i", i=1,2; "grad" is the gradient operator; t_i are the tension forces in the membrane D_i; $f_i(v^1 - u^i) = \int_{D_i} p_1^* (v^i - u^i)\, dV$; p_1^* are the transverse pressures; the constraint set K for the contact condition is given as

$$K = \{ (v^1, v^2) \in H_0^1(D_1) \times H_0^1(D_2) : v^1 + s \geq v^2$$

almost everywhere in $D_1 \cap D_2$, the contact surface $\}$ $\qquad (2.11)$

In the constraint set K, the (standard) Sobolev space $H^1(D)$ (Refs. [1],[68],[90],[101],[128],[152]) is replaced by $H_0^1(D)$ since the norm of grad v, i.e. $|v|_1 = \int_D |\text{grad } v|^2 \, dV$, can be defined only on $H^1(D)$; $|v|$ is the semi-norm on $H_0^1(D)$.

The left hand terms of Eq. 2.10, $a(u,v) = \sum_{i=1}^{2} a_i (u^i, v^i)$, are the continuous, coersive bilinear form on $H_0^1(D_1) \times H_0^1(D_2)$, hence there is a unique solution u^i in K.

Endo et al [25] considered a class of contact problems where an incompressible, finite elastic solid, including plates, shells, etc., come into contact with a frictionless rigid half-space. The finite element method, based on the Lagrange multiplier and the exterior penalty method, was constructed under a highly nonlinear contact constraint. The system of highly nonlinear equations, which includes the equation of contact constraint, was solved by developing the Riks-type algorithm, since the application of the method of incremental loading accumulates considerable errors. The method developed is also applicable to a large deformation of a (thick) shell as well as a contact problem where the shell comes into contact with the rigid half space due to the inflation pressure.

2.5 Contact Mechanics of Pneumatic Tires Interacting With a Rigid Base

In what follows the characteristics of pneumatic tires, which will greatly influence the results (i.e. contact area, contact stress, etc.) of interaction problems involving pneumatic tires, will be studied on the basis of the numerous experimental results, obtained

for the present studies (refer to Chapter 3 and Appendices C, D and E). Particular attention will then be paid to the role of carcasses (i.e. shape, stiffness, etc.) during the loading process, where deformations at the end will naturally influence contact mechanics of tires due to practical loads (e.g. weight of vehicle) applied and/or inflation pressure, regardless of the size and stiffness of the tires.

A tire, such as that shown in Fig. 2.5, is also under consideration. This tire is for 200-ton dump trucks which are mainly operated in mining areas, and is 3.6 meters in diameter, 1.1 meters width and a weight of 3.5 tons.

Most pneumatic tires, which are considered to be toroidal shell-shaped stiff membranes tensioned due to inflation pressures, are, in general, highly deformable relative to the magnitudes of certain axle loads applied in practice. This is because carcasses of tires are not made very stiff, except those shown in Fig. 2.5, and as such bending moments occurring in the tires at contact surfaces do not damage the carcasses so long as they have reasonable inflation pressures, tensioning (or stiffening) carcasses, and loadings do not exceed certain magnitudes.However, when a tire comes into contact with another solid, then the the carcass at the contact portion would probably exhibit a sort of instability, which is directly related to the progress of contact area and changes in contact stress distributions. Such instability phenomena will be discussed later where a pneumatic tire comes into contact with a rigid base.

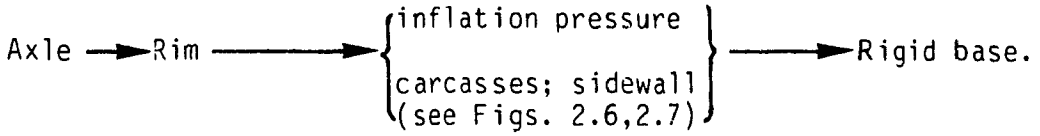


(a) (b)

Fig. 2.5a,b A Large Tire Used for 200 Ton Dump Trucks

First, a global view of a tire-rigid base contact is considered from the point of view of the mechanism of how an applied load is transmitted from the axle of the tire to the rigid base. Figure 2.6 gives a rough sketch of an unloaded pneumatic tire fixed in the rectangular Cartesian coordinate system, where the origin "o" coincides with the center of mass gravity of the tire. Figure 2.7 gives a cross section (in the y-z plane) of a loaded tire where W and p denote a (vertical) load and an inflation pressure, respectively.

As can be seen from Fig. 2.7, the applied load will be clearly transmitted to the rigid base in the following order:



It is also noted that the transmission of load described above would naturally lead to two types of contact problems, as shown in Fig. 2.8, which was also mentioned in Chapter 1. One occurs between the rim and the sidewall of the carcass, a (receding type) contact with the contact arc "b". This may also be perceived to be a special type of inclusion problem. The other occurs between the crown and the rigid base, with contact length "L", which is an advancing contact. This advancing contact problem is the one which is the main interest for the mobility problems, and was investigated in this dissertation.

The receding contact between the rim and the sidewall is described as follows: If there is no load being applied on the axle, then the rim and the sidewall, under initially stressed

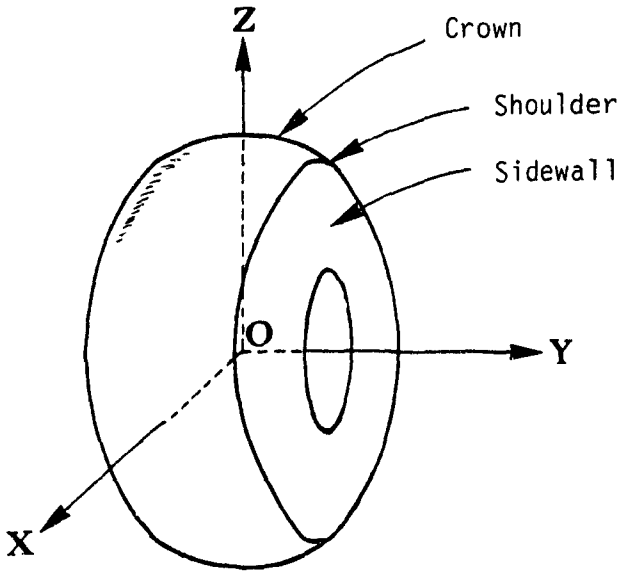


Fig. 2.6 A Buffed Tire Fixed in Rectangular Coordinate System

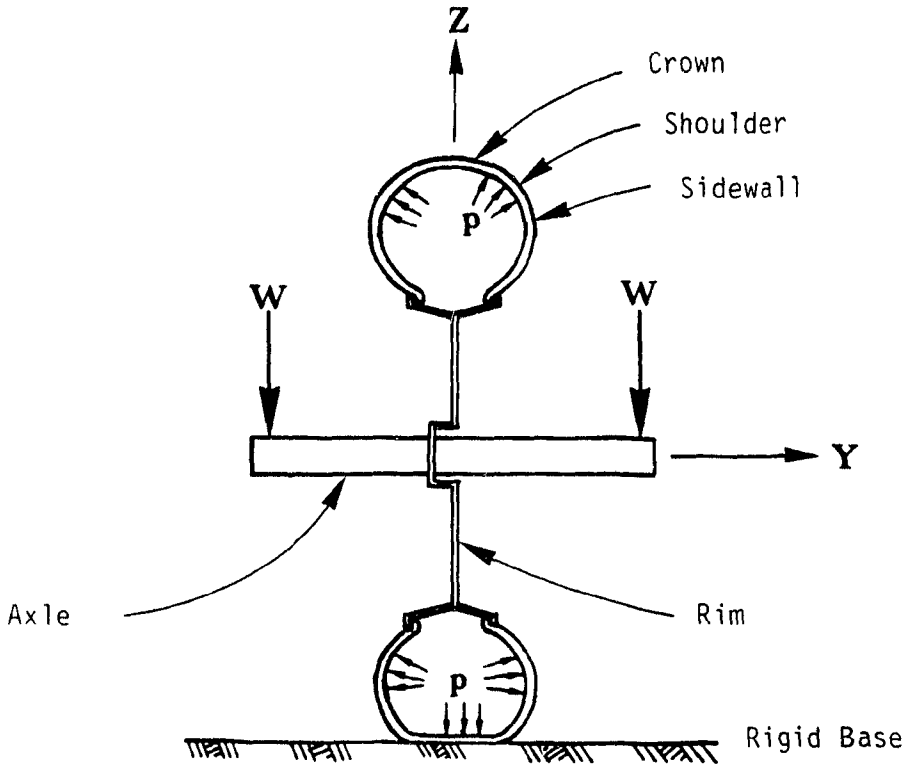


Fig. 2.7 A Cross Section of Loaded Tire in y-z Plane

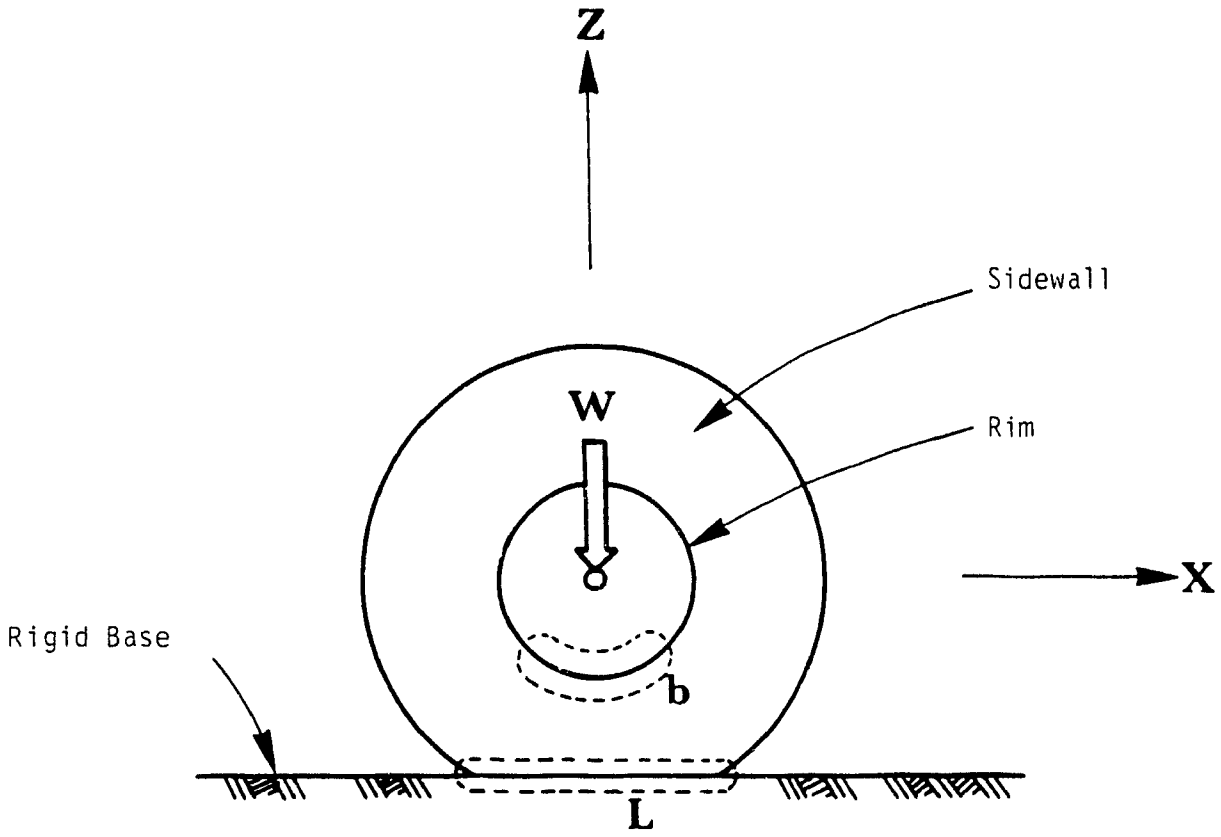


Fig. 2.8 A Receding and an Advancing Contact Resulting From a Tire-Rigid Base Contact

condition along the boundary, are completely in contact so that the arc "b" represents the whole boundary, i.e. a circumference of the rim and the sidewall. However, once the load is applied, only a part of the boundary is a significant contact (although it is likely that the whole boundary is still completely in contact due to the initial stress along the circumference of the rim), and the contact portion transmits the applied load. This results in a receding contact or an inclusion problem between the rim and the sidewall. Although such a contact will not be considered herein, it may be treated as a special case of 2-D inclusion problems (e.g. Gladwell [41] pp. 404-421) where a rigid material (i.e. a rim) is perfectly fitted into the hole of an infinitely large rubber-like-membrane (e.g. sidewall) which is subjected to tension forces at infinity.

Now we will focus our particular attention on the characteristics of deformations of a carcass, transmitting an applied load through a rim onto a rigid base, which would be strongly related to contact pressure distributions. We will limit our discussion to only a cross section (cut along the y-z plane) of the carcass in contact with the rigid base, as shown in Fig. 2.7. The cross-section (cut along the x-z plane) of the carcass, forming a ring-shaped stiff membrane, is not expected to directly influence the contact pressure distributions relative to the x-z plane, because of the ring shape, stiffness (in bending along the y-z plane), etc. and only a small partial load will be transmitted through this cross section. This is obvious since the applied load is directly transmitted through the rim to sidewall of carcass. Accordingly, we will only consider a mechanism of a slice of

the cross section along the y-z plane under the inflation pressure "p " and the load "W" (not total), carried by the carcass as shown in Fig. 2.9.

Such a slice is considered to consist of two types of shallow shells, i.e. shallow arches in this case, sidewall and crown, as shown in Fig. 2.11(a), although there are tires whose cross sections of carcasses are more like open rings as shown in Fig. 2.10.

Deformation characteristics of such ring-shaped carcasses, however, can be regarded as a special cases of the one shown in Fig. 2.11(a). During the loading process, it is assumed that the top portion of the sidewalls (contacting with the rim) are fixed by a "sort" of hinge, as shown in Fig. 2.11(a), in such a way that the top portions will remain fixed against loads applied through the rigid base. The loads W_1 and W_2 in Fig. 2.11(b) and (c) are thus considered to be reaction.

We will then consider the deformation characteristics of sidewall and crown walls separately, even though they cannot be separated for the overall deformation characteristics of the carcass. Applying the first load W_1, sufficiently small, to the unloaded carcass, an arbitrary datum point of side walls will be displaced laterally by "u_1", while the center of the crown at contact will move upward by "v_1" as shown in Fig. 2.11(b). Each displacement is considered to take the maximum in its direction. The displacements, u_1 and v_1, corresponding to the initial load W_1 are also plotted in Fig. 2.12(a), (b) where the load-displacement curves are hypothetic. We will see a

the cross section along the y-z plane under the inflation pressure "p " and the load "W" (not total), carried by the carcass as shown in Fig. 2.9.

Such a slice is considered to consist of two types of shallow shells, i.e. shallow arches in this case, sidewall and crown, as shown in Fig. 2.11(a), although there are tires whose cross sections of carcasses are more like open rings as shown in Fig. 2.10.

Deformation characteristics of such ring-shaped carcasses, however, can be regarded as a special cases of the one shown in Fig. 2.11(a). During the loading process, it is assumed that the top portion of the sidewalls (contacting with the rim) are fixed by a "sort" of hinge, as shown in Fig. 2.11(a), in such a way that the top portions will remain fixed against loads applied through the rigid base. The loads W_1 and W_2 in Fig. 2.11(b) and (c) are thus considered to be reaction.

We will then consider the deformation characteristics of sidewall and crown walls separately, even though they cannot be separated for the overall deformation characteristics of the carcass. Applying the first load W_1, sufficiently small, to the unloaded carcass, an arbitrary datum point of side walls will be displaced laterally by "u_1", while the center of the crown at contact will move upward by "v_1" as shown in Fig. 2.11(b). Each displacement is considered to take the maximum in its direction. The displacements, u_1 and v_1, corresponding to the initial load W_1 are also plotted in Fig. 2.12(a), (b) where the load-displacement curves are hypothetic. We will see a

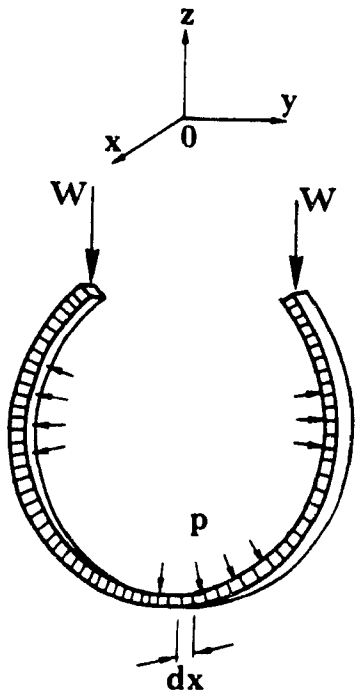


Fig. 2.9 A Slice of Cross Section of Carcass Along y-z Plane

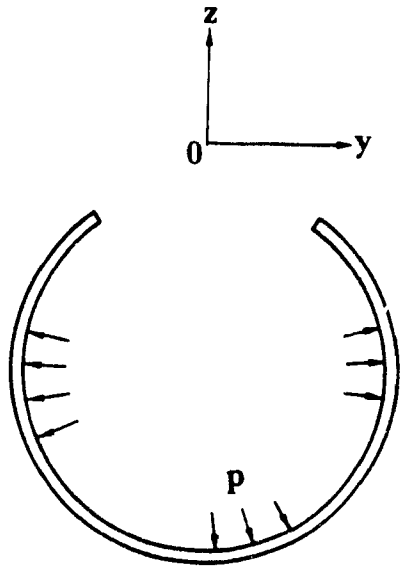


Fig. 2.10 A Ring-Shaped Cross Section of a Carcass

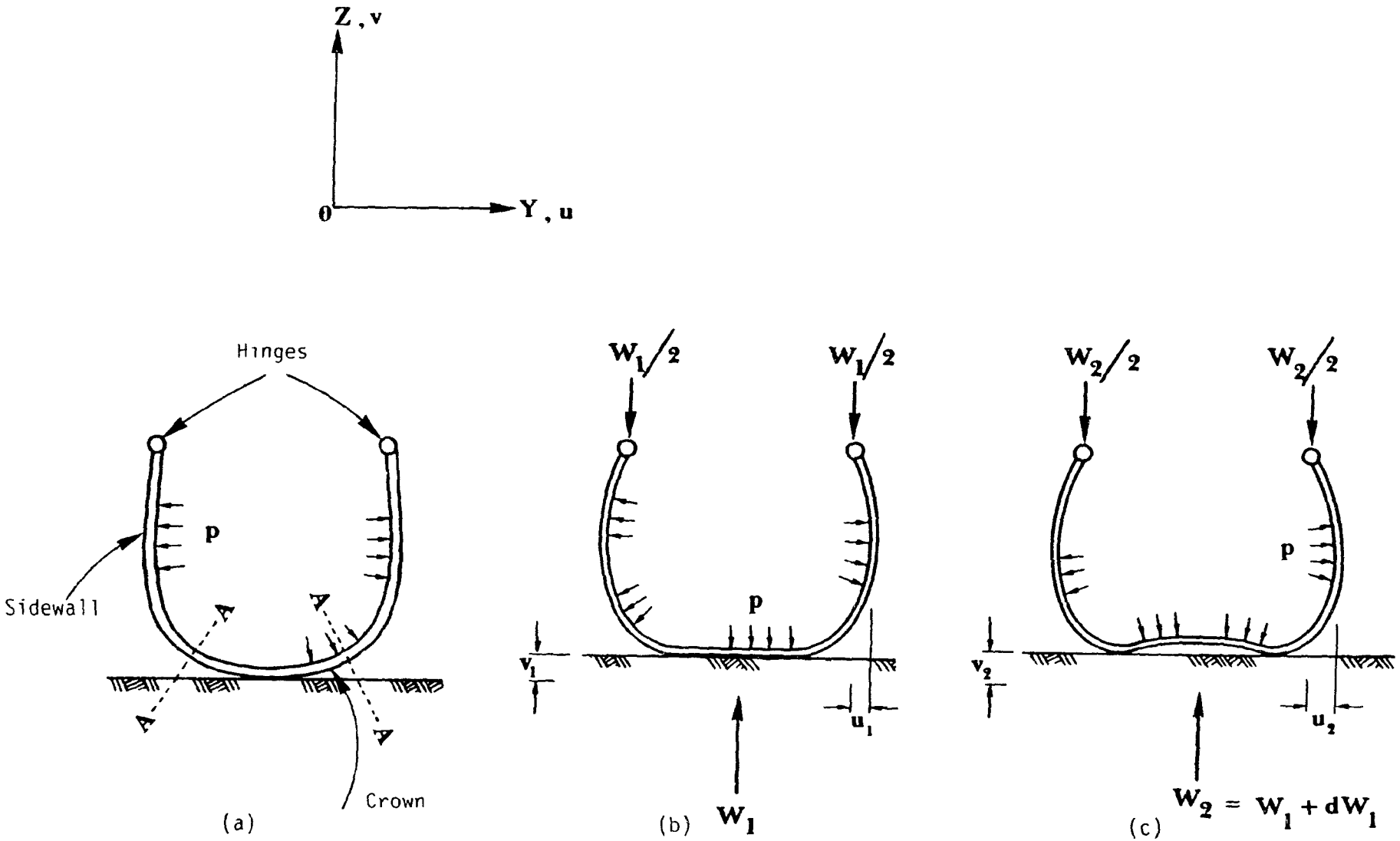
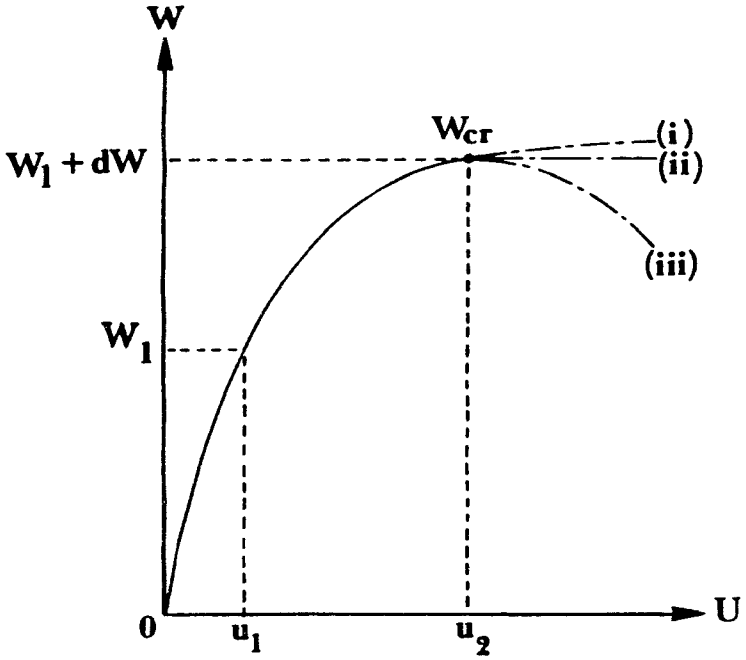


Fig. 2.11 Progress of Deformations of a Carcass Leading to a Hypothetical Instability Mode

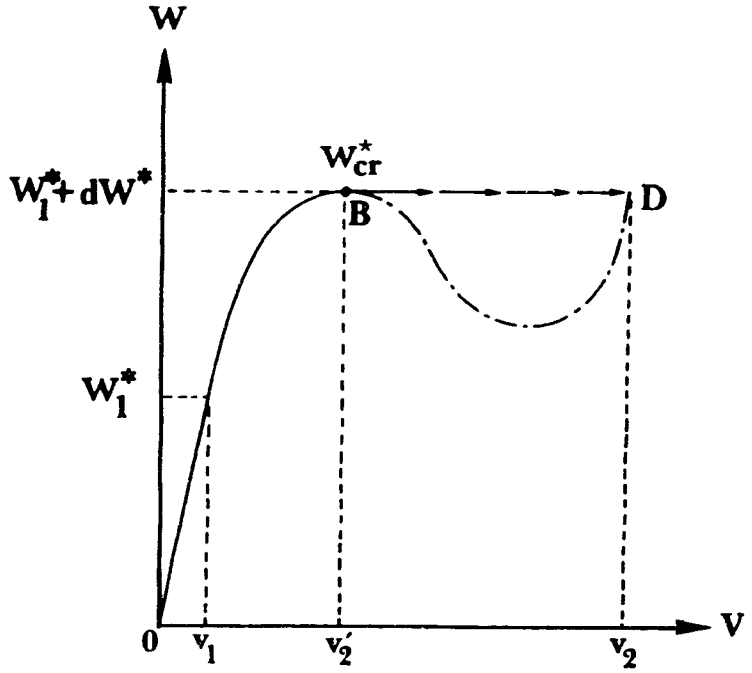
sort of verification later (Chapter 3) about these curves considering the three different types of experimental results, i.e. (1) changes in pressure near the center of contact surface, (2) relationships between average pressure and inflation pressure, (3) large lateral displacements of sidewall as load increase.

Next we will treat separately, the deformation characteristics in the sidewalls and the crown produced from load increment. First it is assumed that the side walls are subjected to a load increment, dW, large enough that the total load, W_1 + dW, reaches a point (e.g. a critical or a limit point), W_{cr}, where the application of further loads would possibly cause large lateral displacements in the sidewalls due to an instability condition as shown in Fig. 2.11(c). Such an unstable condition may exhibit one of the following three different types of deformation characteristics (shown in Fig. 2.12(a)): a large lateral displacement, u, starts with either (i) little increase or (ii) no increase in loading: otherwise (iii) the sidewalls (i.e. shallow arches) lose the capability of carrying any further loads after the load $W_{cr} = W_1 + dW$, and if this phenomenon occurs, it is considered to be a "flattening instability".

Next, deformation characteristics of the crown will be considered, in the same way, for the mode caused by a load increment. If a sufficiently large increment load dW* (not necessarily equal to the increment dW for the sidewalls) is applied to the carcass at the deformed state (Fig. 2.11(b)) so that the total load, W_1^* + dW*, reaches a critical point, then a sudden jump in the vertical



(a) Lateral Displacements of Sidewall Leading to a Flattering-Type Instability Mode



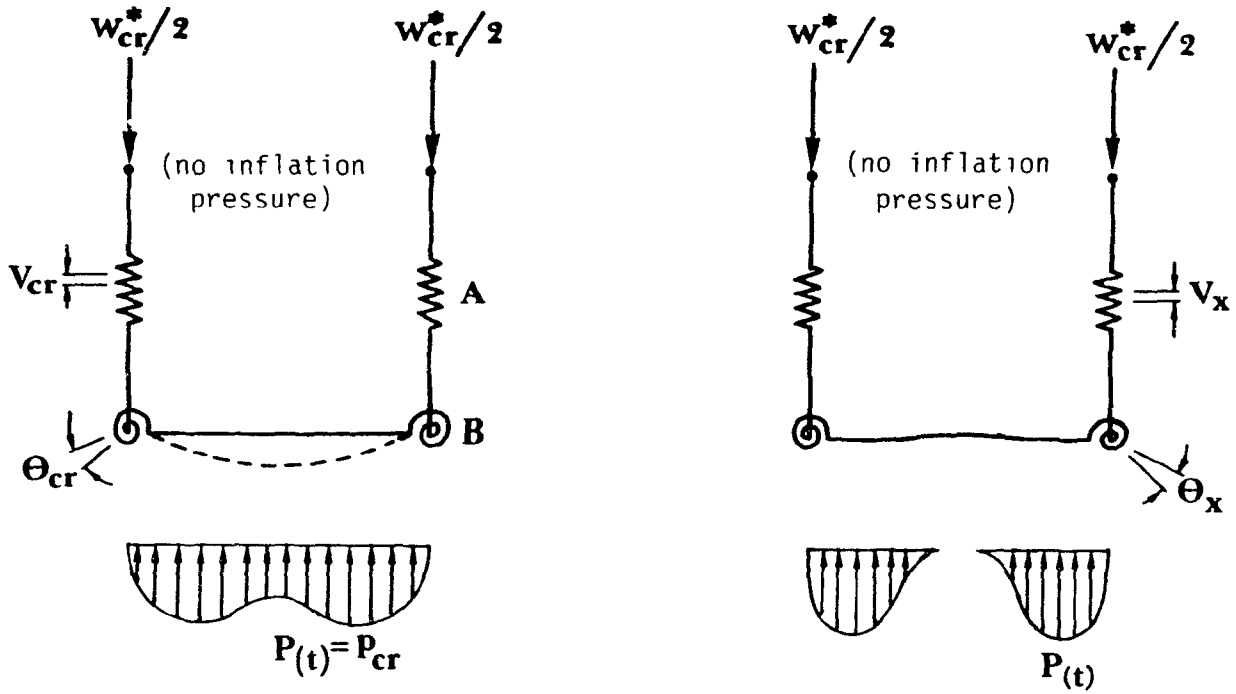
(b) Vertical Displacements of Crown Leading to a Snap-Through Type Instability Mode

Fig. 2.12 Hypothetical Load-Displacement Curves (at Datum Points) for a Carcass

displacements at the crown would occur, as shown in Fig. 2.12(b), from v_2' corresponding to the point B (or W_{cr}*) to v_2 corresponding to D, a new equilibrium point. This causes the crown to deform upward, although there may not be any "gap" at the crown in contact as shown in Fig. 2.11(c). Such a phenomenon, jumping from one stable equilibrium configuration to another, is generally called "snap-through" (or oil-canning) buckling. If such a deformation mode occurs at the crown in contact, then the pressure near the center of the contact portion will certainly decrease. The physical event occurring in the crown can also be interpreted in the following way. Assume a simple spring model of carcass (Fig. 2.13(a)) in which the (modelled) crown is in contact, producing contact pressure distribution P(t) at a position t. The model of the carcass consists of three parts; a spring A simulating a nonlinear stiffness of the sidewall, a spring B for the joint (or the shoulder) between the sidewall and the crown. Hence it is conceivable that a snap-through type instability of the crown in contact will take place as soon as the contact pressure, as a transverse load, reaches the critical value p_{cr} (Fig. 2.13(a)). Therefore, deformations in the springs A and B jump from (v_{cr}, ϕ_{cr}) to (v_x, ϕ_x) after buckling as shown in Fig. 2.13 (a), (b).

Two things related to the snap-through type instability of the crown will be noted.

The first one is that this would always happen to a crown in contact, regardless of inflation pressure, so long as the carcass is stiff enough in bending, and a pneumatic tire is able to sustain a



(a) At Critical Configuration (b) After Buckling

Fig. 2.13 Hypothetical Configurations and Contact Pressure Distributions for a Highly Idealized 2-D Spring Model of Carcass Before and After a Snap-Through Type Instability

critical load. Another one is that contact pressure at a particular cross section, where a snap-through type instability occurred, will possibly be reduced no matter whether or not there is an obvious gap (shown in Fig. 2.11(c)) between the deformed carcass and other media such as a rigid base and a supporting soil. This hypothsis can also be extended to a real tire - soft soil interaction, partly because a portion near the center of the contact surface would be almost flat for the equilibrium, regardless how soft the soil is, whenever the magnitude of axle load applied is large in the practical sense.

2.6 Conclusions and Selection of Analytical and/or Computational Methods as Fundamental Tools

We have reviewed the various analytical and computational analyses for certain types of contact problems such as those between two linear solids, or those involving elastic membranes. In the analytical methods, the complex variable method (i.e. Method 7 in section 2.2.3) is shown to be superior over the other methods, while it is also obvious that the computational methods would be better compared with an analytical method for most of the contact problems. However, there arises at least one difficulty, apart from the friction which was discussed in section 2.3, when the computational method (the finite element method) is applied to contact problems such as those shown in Fig. 2.14(a), (b) and (c). We can illustate this problem by considering two idealized contact problems as shown in Fig. 2.14(a) and (b). One is that of an elastic cylinder pressed onto a rigid base

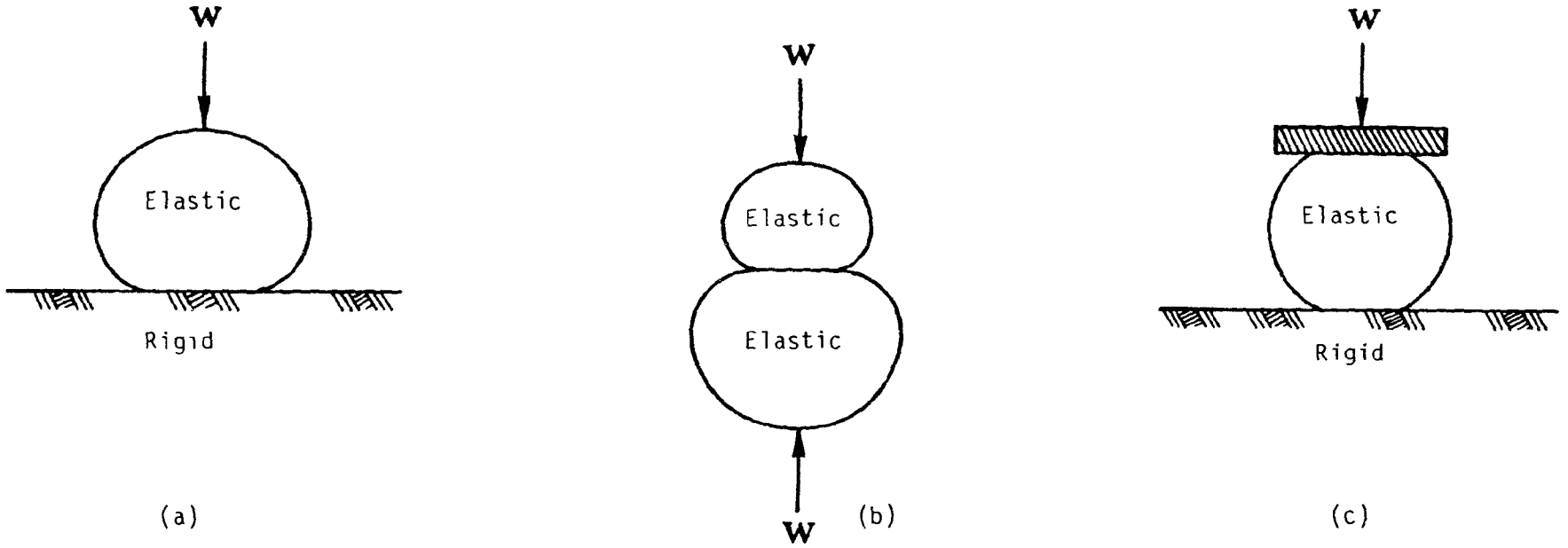


Fig. 2.14 Idealized and Realistic Contact Problems

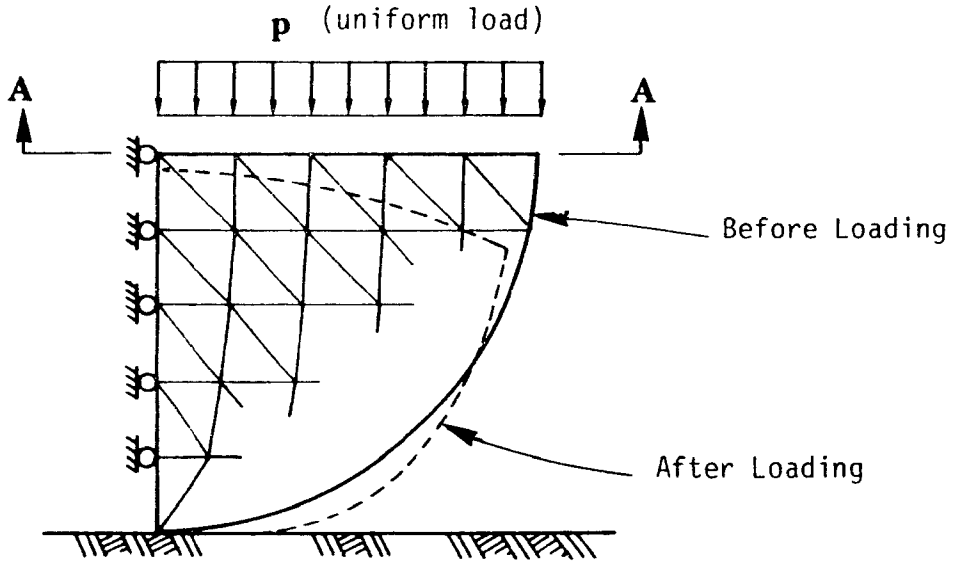


Fig. 2.15 A Quarter of a Discretized Elastic Cylinder Under a Uniform Load

due to a point load W (Fig. 2.14(a)). The other is where two elastic cylinders are being pressed together by the point loads (Fig. 2.14(b)). The point loads in Fig. 2.14(a),(b), however, should be interpreted in such a way that the load is really transmitted to an elastic cylinder(s) through a rigid plate as shown in Fig. 2.14(c). Such a contact problem is often solved by applying a "uniform" pressure on the cross section A-A shown in Fig. 2.15, when the finite element method is employed as an analytical tool.

Application of the uniform load at the cross-section will produce erroneous solutions since the pressure distribution at the cross-section A-A for the real problem shown in Fig. 2.14(c) is not uniform. We only know from the simple contact problem (Fig. 2.14(c)) that the vertical displacements at the cross-section A-A are uniform. Hence, the contact problem shown cannot be simulated by the discretized one given in Fig. 2.15.

There are far greater difficulties when considering contact problems involving pneumatic tires. One such difficulty has been described in Chapter 1 and in section 2.5. That is, that an interaction involving a pneumatic tire inherently contains two different types of contact problems. These must be solved simultaneously as shown in Fig. 2.8. Also, large deformations near contact surface may possibly lead the carcass at the contact portion to an unstable configuration. These two problems must be at least considered in the solution method. Complex material properties of the highly deformable carcass, which is neither isotropic nor homogeneous,

must also be taken into account. Further, if a media contacting with the tire is highly deformable material, such as clay, the problem becomes then far more complicated. Considering all of these difficulties, one realizes that it is nearly impossible to solve such complex (three-dimensional) contact problems with the present knowledge of contact analyses, mechanics, mathematics and numerical analyses.

In the development of the analytical approach given in Chapter 4 we will consider such problems, i.e. tire-supporting clay and tire-rigid base interaction problems. We then employ the complex variable method (i.e. Method 7 in section 2.2.3) as a basic mathematical tool in developing an analytical approach by taking into account the contact profiles. The main reason for selecting the complex variable method as a fundamental analytical tool is that it has a greater flexibility in approximating the boundaries of contacting bodies, including contact profiles, when compared with the other methods (sections 2.2.3, 2.2.4 and 2.2.5). Besides, the way the contact stresses are derived from the complex variable method has a significant relationship to the foundation of mathematics, i.e. the relationship between the definition of contact stresses in terms of the sesctionally holomorphic function and the definition of hyperfunctions (section 2.2.3 and Appendix B). From the point of view of the theory of hyperfunctions, contact stresses are shown to exist in a large class of functions.

In another interaction problem, i.e. a rigid wheel-supporting

snow (or supporting clay), considered in Chapter 5, we will select the complex variable method and the incremental finite element method for the analytical and computational methods, respectively. The contact analysis is an iterative method which is developed by combining the complex variable method with the incremental finite element method with the assumption that load increments are sufficiently small so that the complex variable method, which is applicable to linear elasticity problems only, is naturally accepted in handling large deformations occurring in supporting clay (or snowpack). One of the reasons that the complex variable method is selected as an analytical tool is the reduction of computational effort required in the several iterations at every load increment, while the other reasons are the same as those stated for the analytical approach in Chapter 4.

CHAPTER 3

EXPERIMENTS ON TIRE-SUPPORTING GROUND INTERACTION PROBLEMS

3.1 Introduction

This chapter presents the results of the laboratory investigation conducted to study the response of four full-size truck tires when being loaded quasi-statically and vertically on a ground which is either an undeformable rigid base or deformable soils. Two different soil types were used in the study, i.e. kaolinite clay and silica sand. The overall objective was to study the contact characteristics between the tires and the ground (i.e. rigid base, clay or sand) in terms of vertical axle displacement, contact area and contact pressures, which would reflect the influences of tire carcass stiffness, tread, inflation pressure and wheel (or axle) load. Such studies will contribute to the understanding of the load-carrying capability of each tire on the various different grounds. Moreover, the experimental results such as contact area and contact pressure distribution will be used in validating the analytical approach, which will be developed in the following Chapter 4. All the knowledge gained in the experiments will be helpful in predicting the performance of the tires in off-road vehicle mobility.

The four tires were different in dimension, configuration, carcass stiffness, tread, etc. (Table 3.1, Fig. 3.1). Each originally-treaded tire had a counterpart produced by buffing all treads from a new treaded tire (Figs. 3.1 and 3.2), resulting in a smooth treadless tire. By testing both treaded and buffed tires under

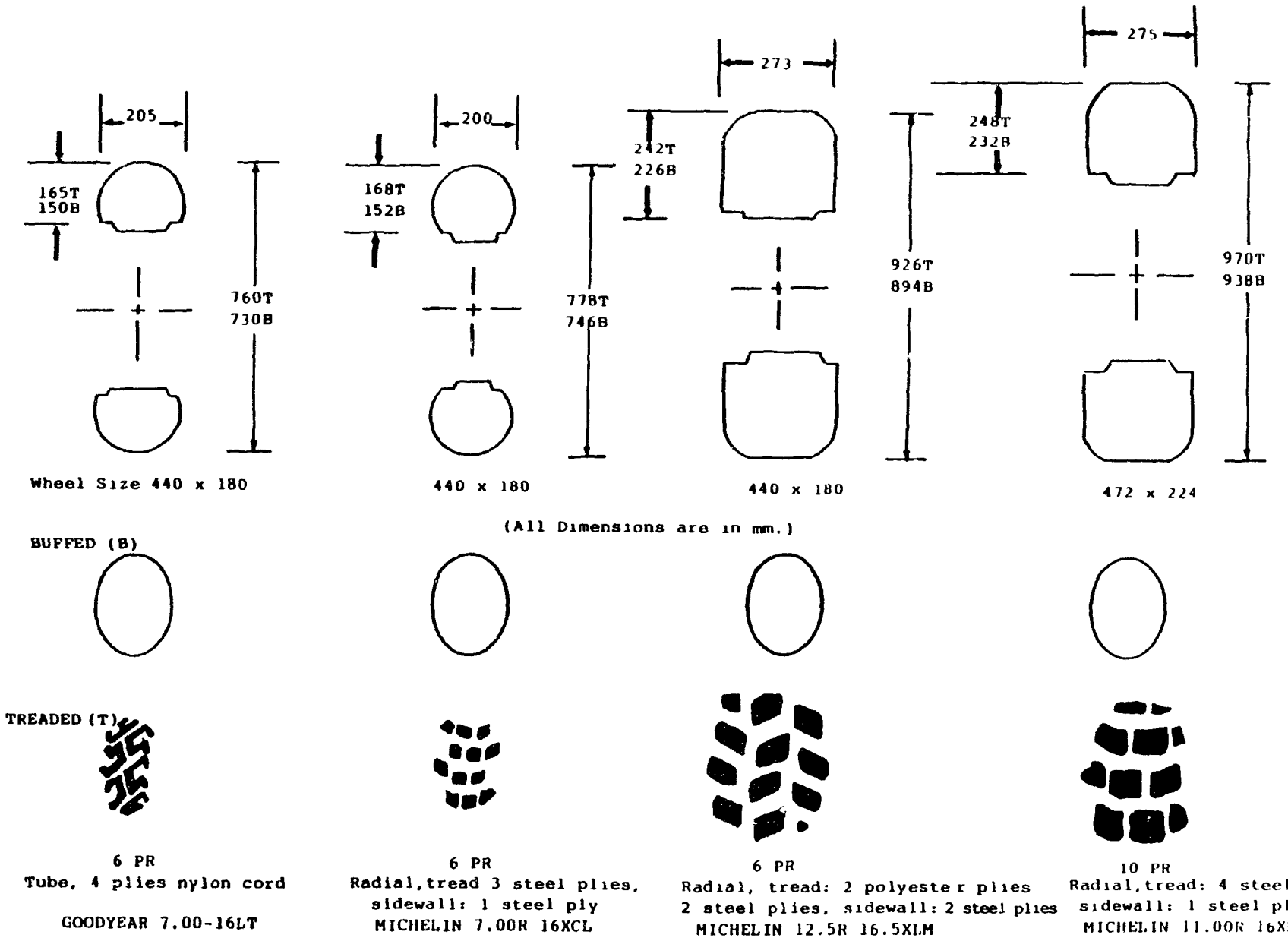


Fig. 3.1 Full-Size Truck Tires Used in the Study

TIRE	PLY ARRANGEMENT	MAXIMUM LOAD	NO. OF TIRES TESTED
GOODYEAR 7.00-16LT (tube type)	4 plies nylon cord	Single 8.036 kN at 310.5 kPa Dual 7.054 kN at 310.5 kPa	2 (treaded and buffed)
MICHELIN 7.00R-16XCL (tube type)	radial Tread: 3 steel plies Sidewall: 1 steel ply	Single 8.371 kN at 310.5 kPa Dual 7.879 kN at 310.5 kPa	2 (treaded and buffed)
MICHELIN 11.00R-16XCL (tubeless)	radial Tread: 4 steel plies Sidewall: 1 steel ply	Single 20.179 kN at 552 kPa Dual 20.179 kN at 552 kPa	2 (treaded and buffed)
MICHELIN 12.5R-16.5XLM	radial Tread: 2 polyester plies 2 steel plies Sidewall: 2 polyester plies	Single 13.549 kN at 241.5 kPa Dual 12.879 kN at 241.5 kPa	2 (treaded and buffed) 1 (treaded): split rim used on axle displacement (rigid base)

TABLE 3.1 Detailed Information on Tested Tires

the same conditions, the influences on the presence of tread can be identified. The buffed tire represents the worst-case scenario of a treaded tire being heavily used such that its treads are worn out. Each tire was subjected to vertical loadings quasi-statically at various inflation pressures for obtaining axle displacement, contact area and contact pressures at several locations. The details of each tire are shown in Table 3.1, Fig. 3.1 and Fig. 3.2. The tires tested were:

(a) GOODYEAR 7.00-16LT (treaded and buffed)

(b) MICHELIN 7.00R-16XCL (treaded and buffed)

(c) MICHELIN 11.00R-16XL (treaded and buffed)

(d) MICHELIN 12.5R-16.5XLM (treaded and buffed).

The tire dimensions and tread patterns are shown schematically in Fig. 3.1 while photographs of the tires are displayed in Figs. 3.2a-d. It should be noted that the former two tires, listed in (a) and (b) above, are much smaller than the latter two tires, listed in (c) and (d). Hence the results obtained for those two different tire groups cannot be compared directly.

The experimental programs and procedures for the tire-rigid base and the tire-soil (clay or sand) will be described in sections 3.2 and 3.3. The representative contact length, width and pressure will be defined in section 3.4 for the verificiation of the first analytical approach proposed in Chapter 4. The discussions and the remarks on the experimental results for the individual interaction problem will be stated in sections 3.5, 3.6 and 3.7. All the necessary experimental results regarding axle displacement, contact area and



Fig 3.2 a GOODYEAR 7.00-16LT
(treaded)

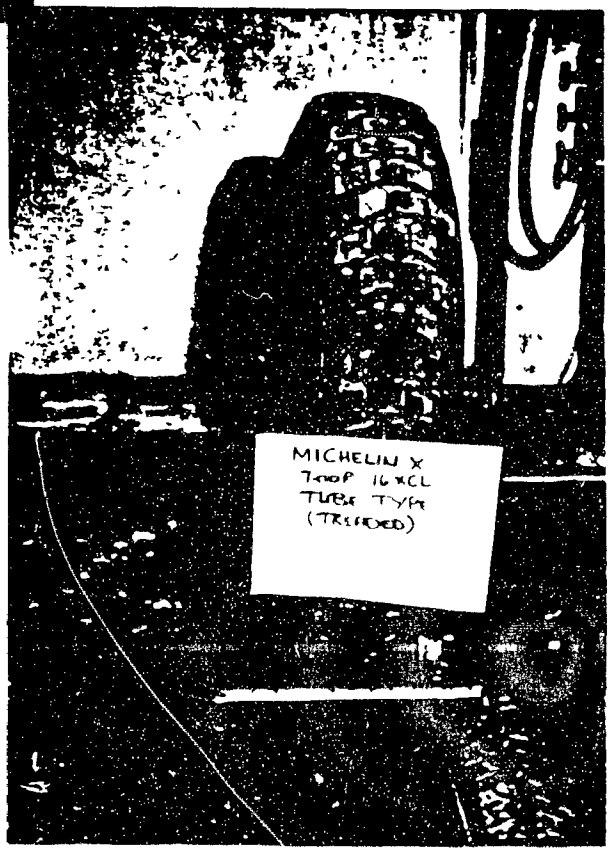


Fig. 3.2b MICHELIN 7.00R 16XCL
(treaded)

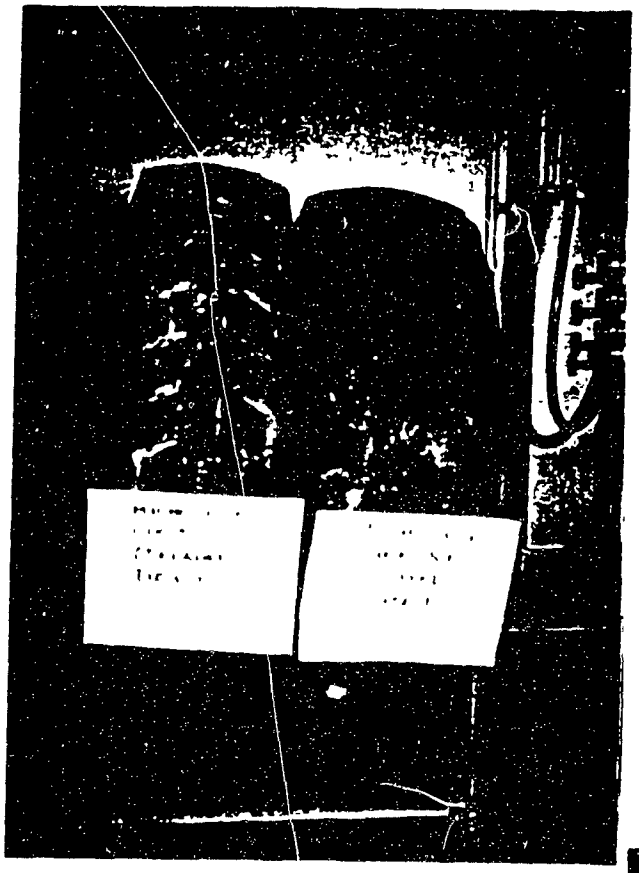


Fig. 3.2c MICHELIN 11.00R 16XL
(treaded & buffed)

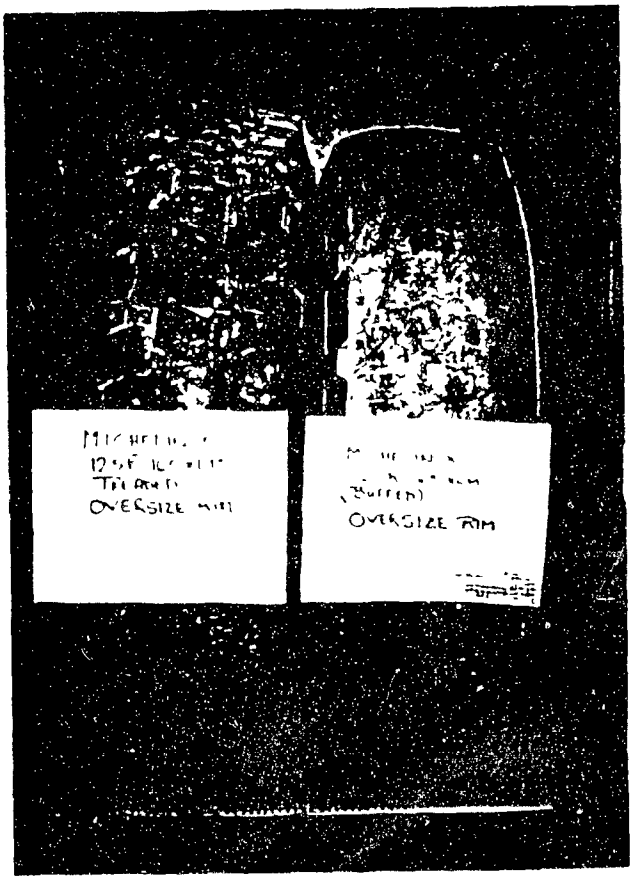


Fig. 3.2 d MICHELIN 12.5R 16.5XLM
(treaded & buffed)

contact pressure can be given in Appendices C, D and E for the tire-rigid base, the tire-clay and the tire-sand interactions, respectively. In section 3.8, the summary and remarks of the experimental results on the tire-soil interactions will be stated.

3.2 Experimental Program and Procedure for Tire-Rigid Base Interactions

3.2.1 Preliminaries

The experimental program can be divided into two main categories, namely:

(a) determination of load-axle displacement-contact area relationships,

(b) measurement of contact pressure.

The reference supporting ground, which each tire comes into contact with, is a rigid and horizontal surface.

In the experiment, each tire was loaded vertically through its wheel which was connected to a rigid steel frame (Fig. 3.3). The tire with the steel frame was assembled in an Instron loading machine which provides a constant rate of vertical loading (Fig. 3.3). In each determination of load-displacement relationship, the tire was inflated to a specified inflation pressure and loaded under a constant rate until the load reached the rated maximum value using the appropriate inflation pressure. The contact area between a loaded tire and the rigid base was measured by the footprint of the tire as recommended by ASTM F870-84.

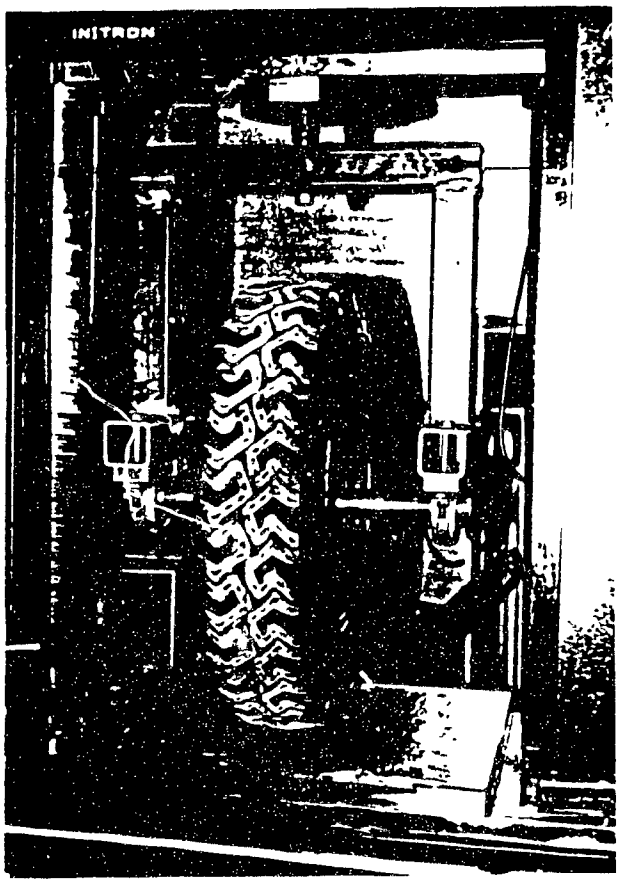


Fig 3.3 Test Set-Up for Load-Displacement Relationship

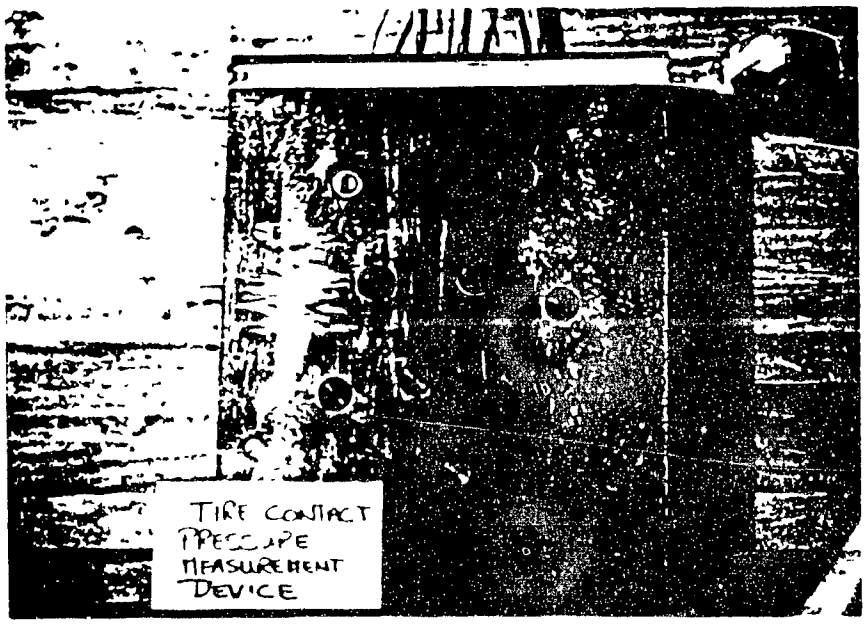


Fig. 3.4 Test Set-Up for Measuring Contact Pressure Distribution (i.e Steel Plate Housing Pressure Transducers)

The contact pressure exerted by each tire onto a rigid base was measured by a set of pressure transducers (Fig. C.13). The position of each transducer was arranged according to the tread pattern of the tire (Fig. 3.1 and Fig. 3.2), as exemplified in Fig. 3.4. All pressure transducers were mounted on a rigid steel plate specially prepared for each treaded pattern as displayed in Figs. 3.5a-d.

3.2.2 Experimental Procedure

For each tire-rigid base interaction, the experiment was carried out in the following steps:

STEP 1 Inflate each tire to the required pressure; there are 3 different inflation pressures for each tire; there are 8 tires to be tested (4 treaded tires and 4 corresponding buffed tires).

STEP 2 Cover the pressure transducers embedded in a rigid aluminum plate (Fig. 3.4) by a paper. The paper must be thin enough that the position of the transducers, if in contact, will come out clearly on the paper after removing the load.

STEP 3 Spray paint on a portion of the tire surface that will come into contact with the rigid aluminum plate.

STEP 4 Apply a load using the Instron machine, i.e. there are 5 different loads to be applied for each tire with the same inflation pressure.

STEP 5 Take readings of the pressure transducers, while axle displacements are measured simultaneously by the chart recorder.

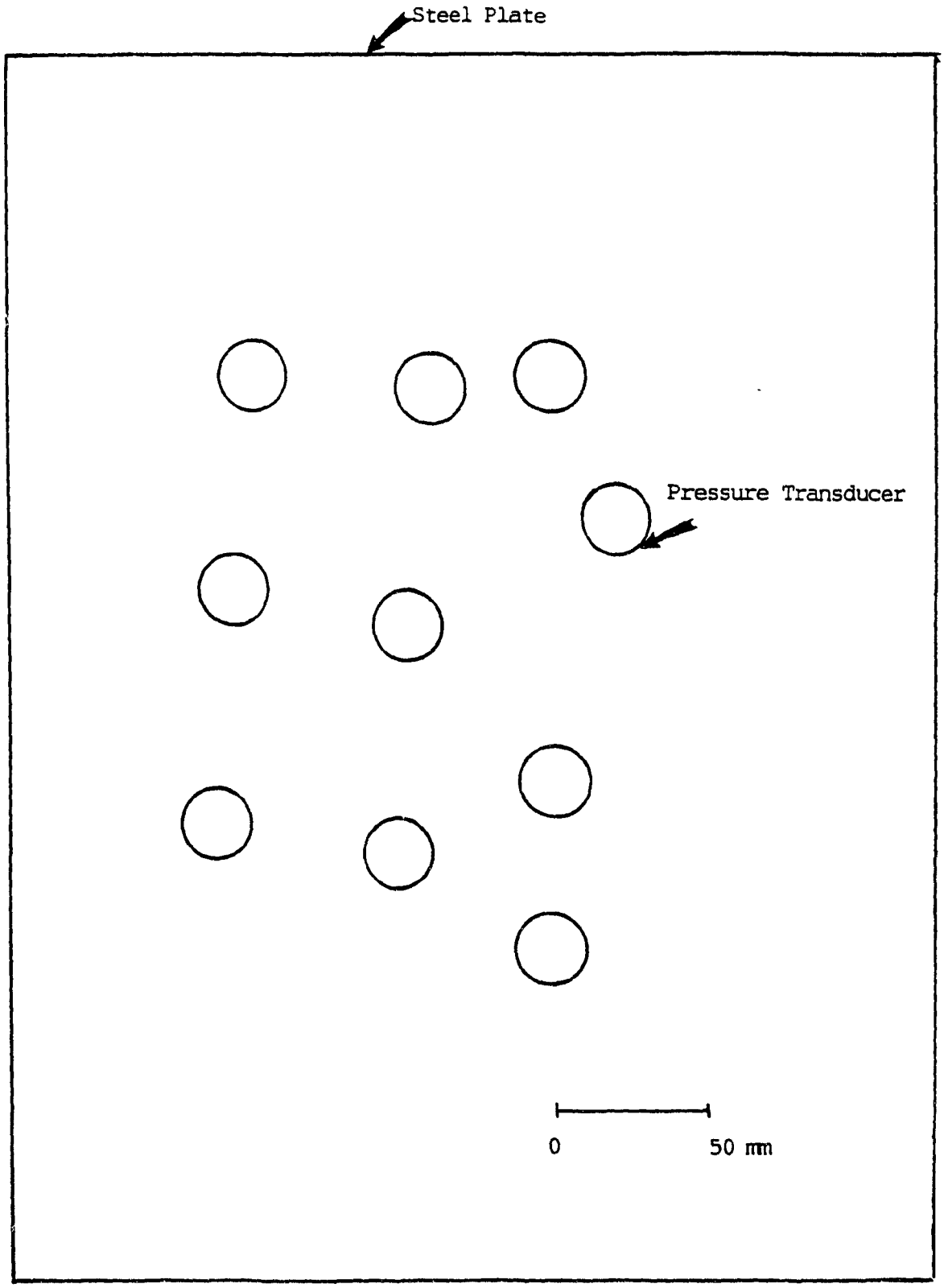


Fig. 3.5a Steel Plate Housing Pressure Transducers for GOODYEAR 7.00-16LT

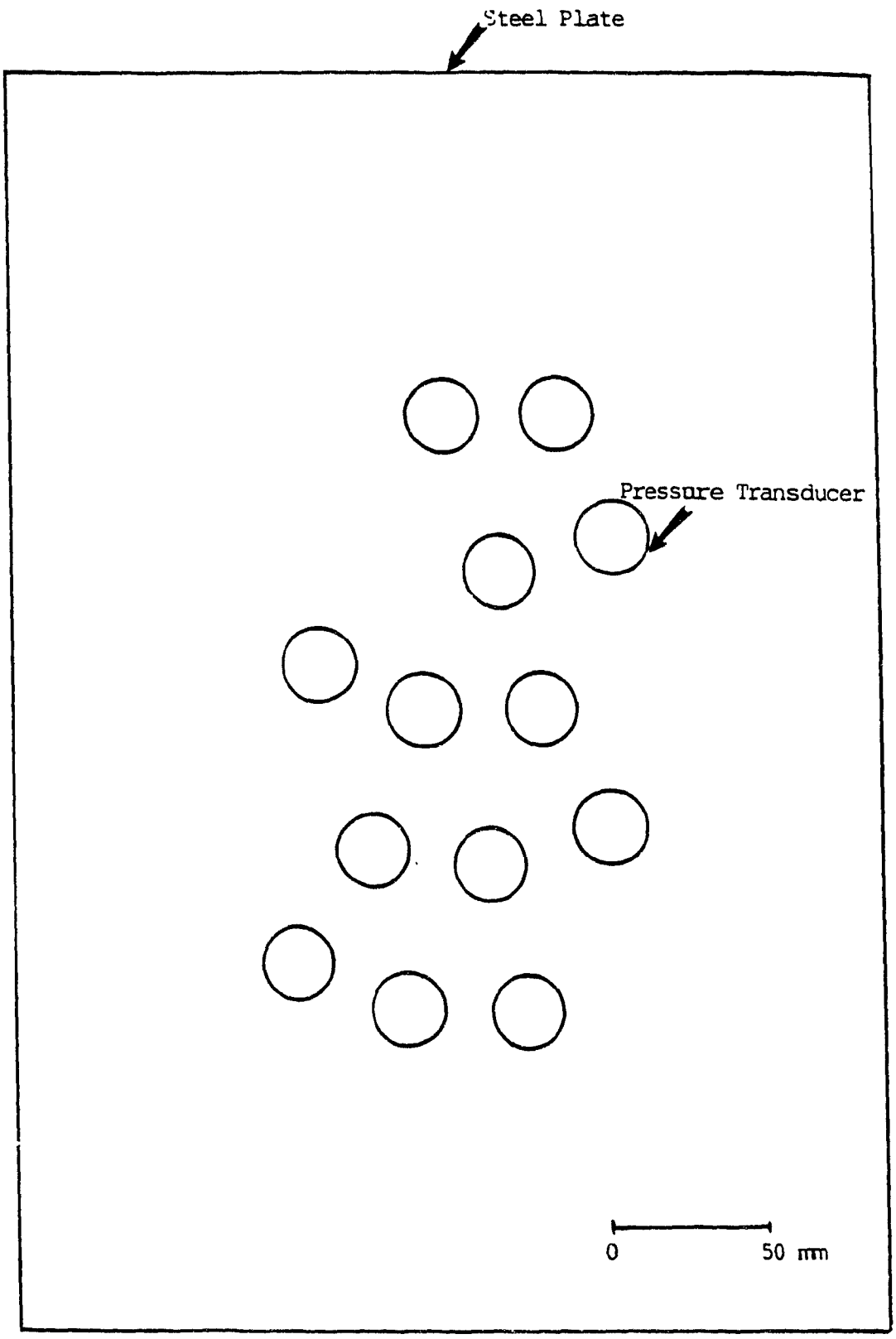


Fig. 3.5b Steel Plate Housing Pressure Transducers for MICHELIN 7.00R-16XCL

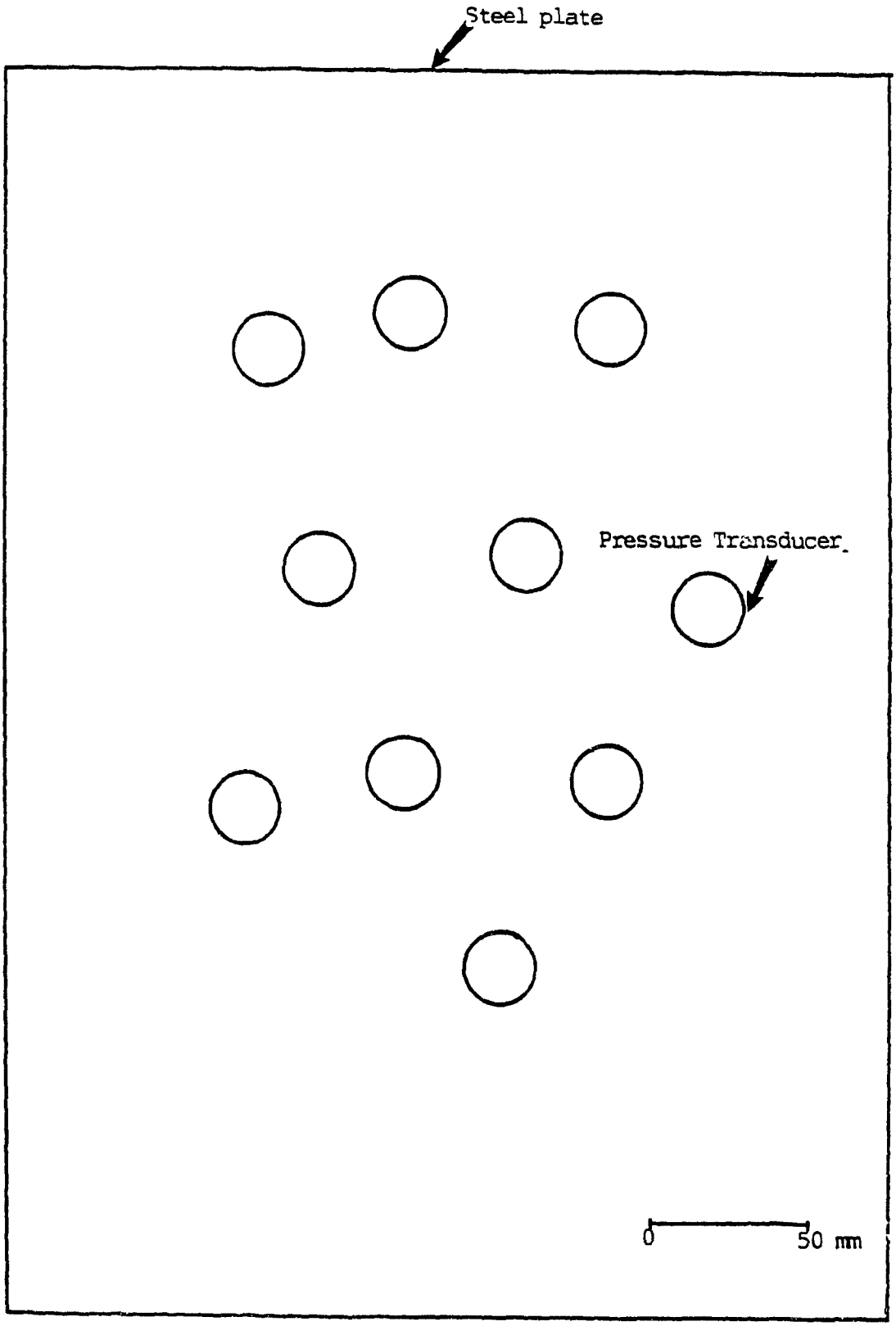


Fig. 3.5c Steel Plate Housing Pressure Transducers for MICHELIN 11.00R-16XL

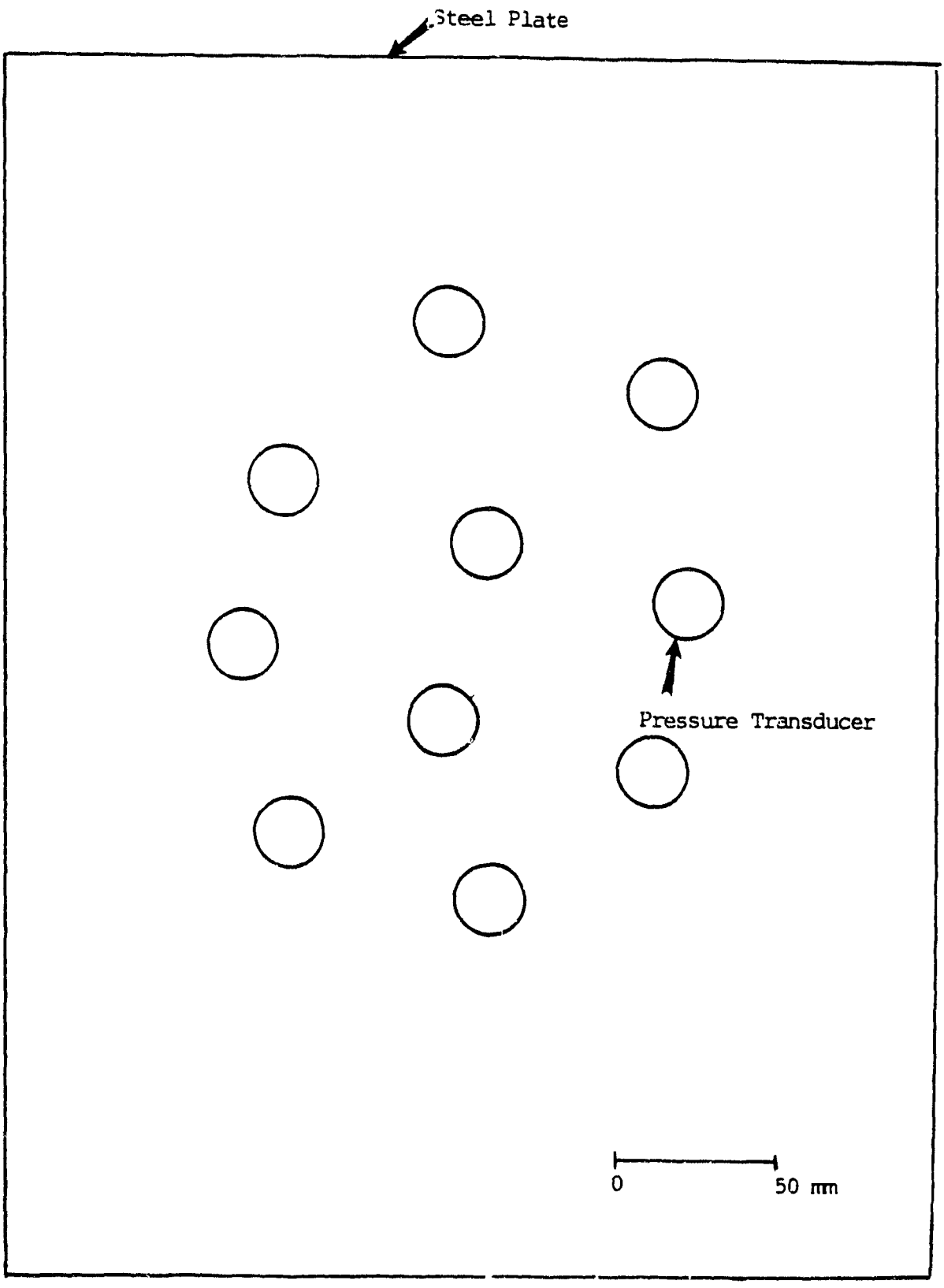


Fig. 3.5d Steel Plate Housing Pressure Transducers for MICHELIN 12.5R-16.5XLM

STEP 6 Release the load.

STEP 7 Remove the paper on which both contact surface and position of the pressure transducers are printed by the paint.

The above process, STEP 1 through STEP 7, was then repeated 3 times for every interaction in order to obtain accurate measurements, especially for pressure distribution patterns.

The results obtained from the experiments on the tire-rigid base interactions will be discussed in the subsequent section 3.4.

3.3 Experimental Program and Procedure for Tire-Supporting Soil Interactions

3.3.1 Preliminaries

The basic work involved in the experiments of tire-soil interactions is the same as that for the tire-rigid base interaction - to seek axle displacement, contact area and contact pressure.

The tire-soil contact area was measured by loading the tire stationally onto the soil (Fig. 3.6). The soil was contained in a soil bin, 0.56 m wide by 1.22 m deep by 9.17 m long (Fig. 3.7). The width of the soil bin was slightly larger than the width of the tire in order to promote a plane strain condition for simplifying the analysis of tire-soil interaction. The contact area was determined by spraying paint all along the contact boundary of the tire-clay interaction (Fig. 3.8). A photograph of the contact surface was then taken after lifting the tire from the soil (Fig. 3.9), enabling accurate measurement of the contact area (in horizontal projection).

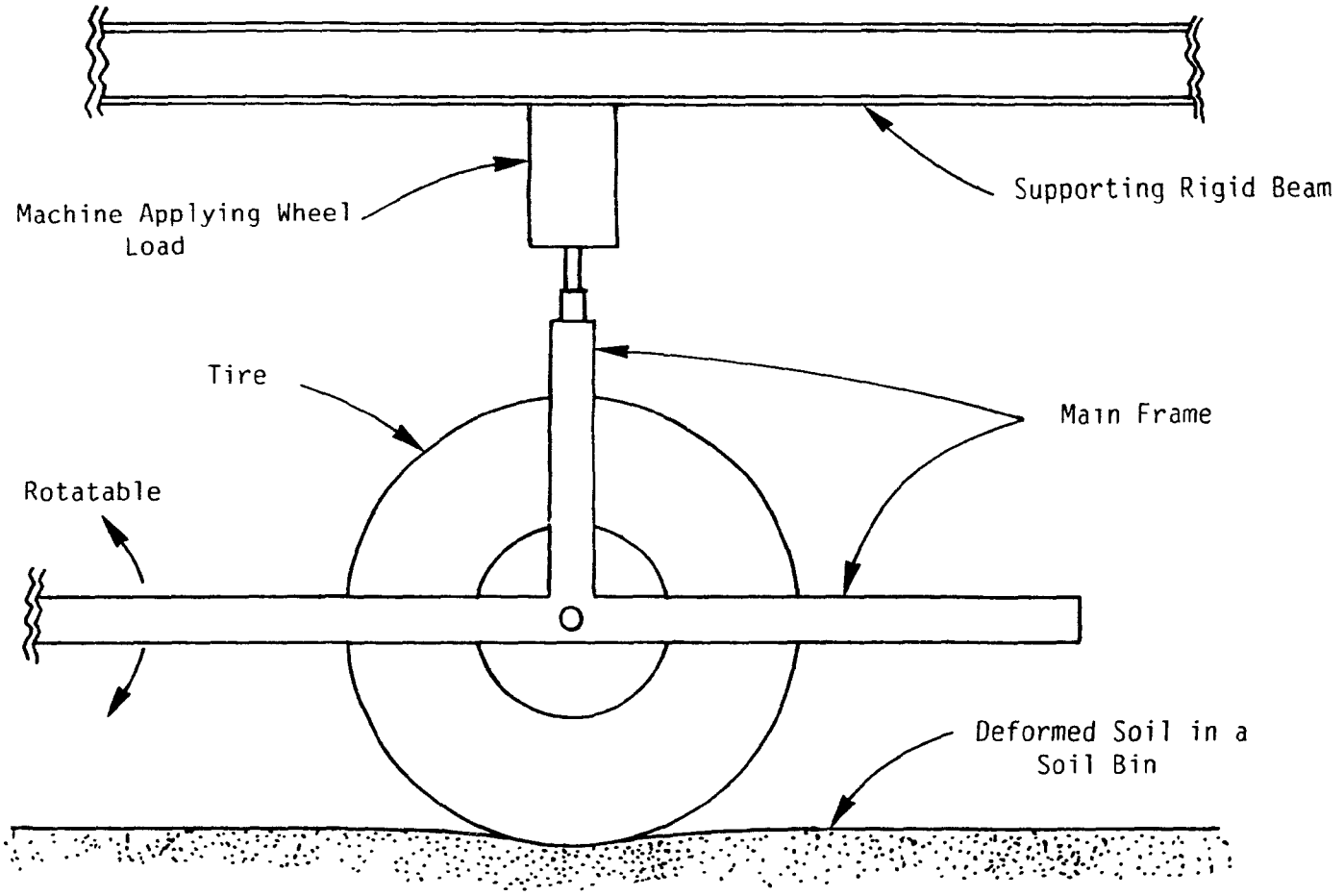


Fig. 3.6 Test Set-Up for Tire-Soil Interaction

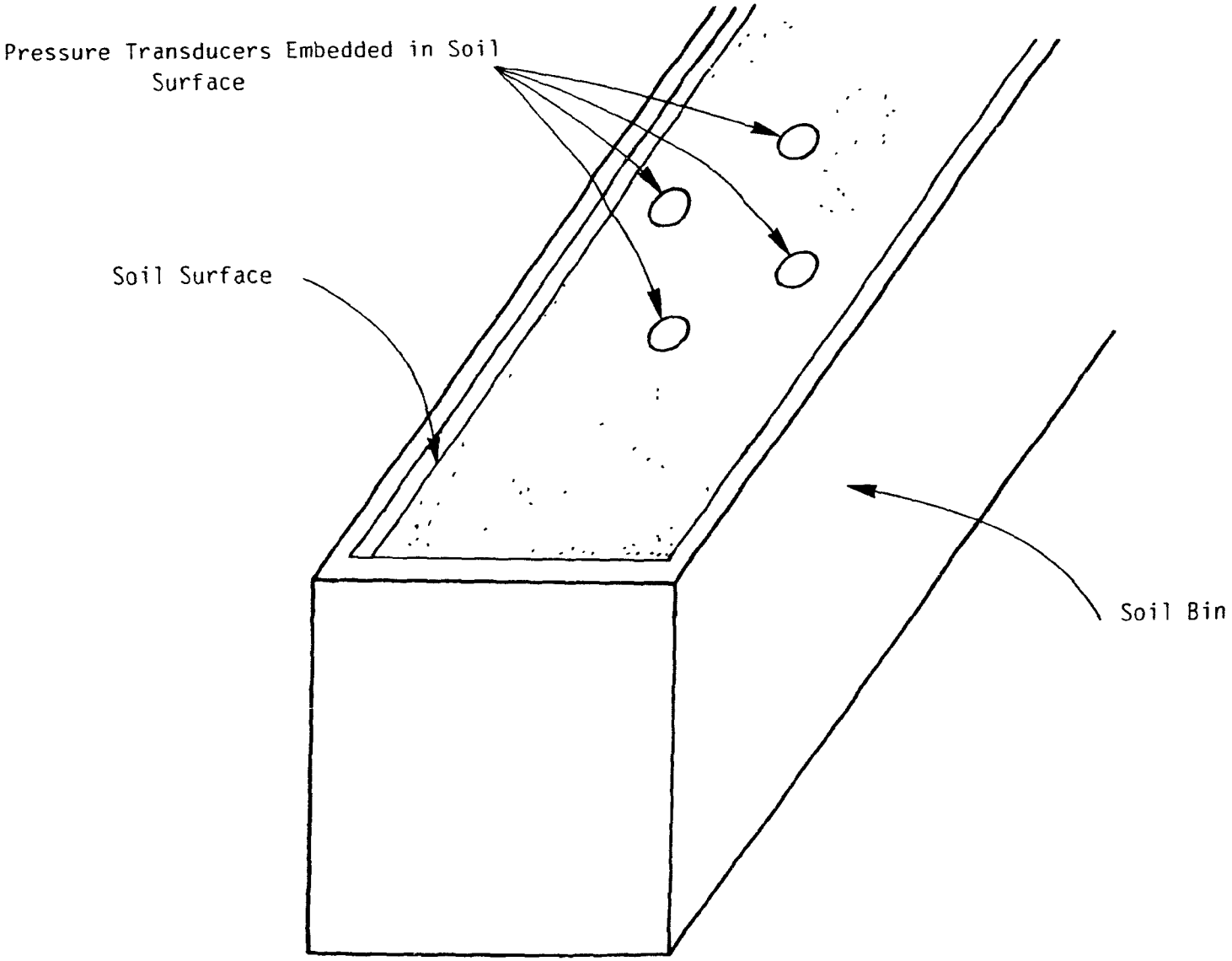


Fig. 3.7 Soil Bin and Pressure Transducers Embedded in Soil Surface

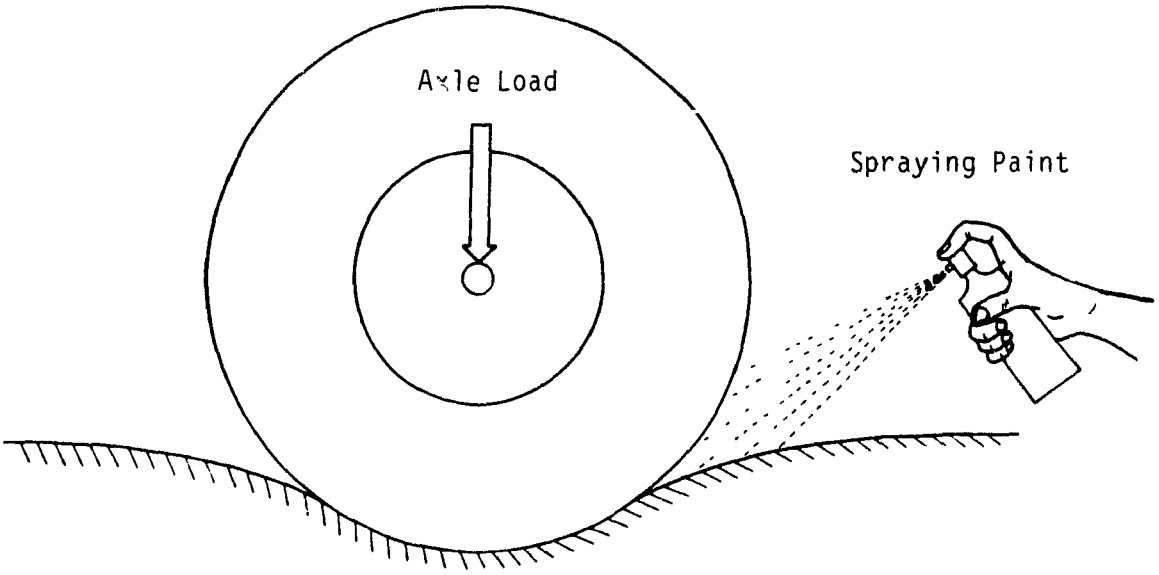


Fig. 3.8 Spraying Paint Along Contact Boundary

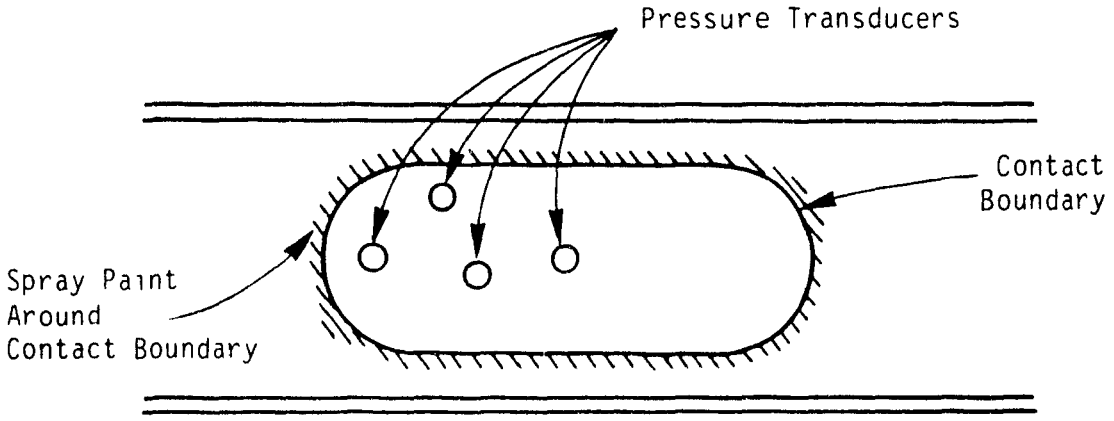


Fig. 3.9 Plane View of Contact Surface

The contact pressure distribution was monitored by embedding four pressure transducers (Fig. C.23) in the soil as shown in Fig. 3.7. The pressure transducers were continuously monitored until the tire was loaded to the designated load and the readings were unchanged.

3.3.2 Experimental Procedure

STEP 1 Locate each pressure transducer at the appropriate position on the soil (Fig. 3.7)

STEP 2 Inflate the tire to the required pressure; 2 different inflation pressures for 8 tires.

STEP 3 Apply the load slowly onto the rigid steel frame (Fig. 3.6); there are 3 to 4 loads for each tire under the same inflation pressure.

STEP 4 Spray paint along the contact boundary (Fig. 3.8).

STEP 5 Take a reading of the pressure transducer and measure the axle displacement.

STEP 6 Unload and take a photograph of the contact surface (Fig. 3.9).

STEP 7 Measure (vertical) displacements of soil surface at several positions, although the measurements will be influenced by the effect of rebound.

STEP 8 Level the soil surface.

The above process, STEP 1 through STEP 8, was repeated 2 to 3 times for every tire-soil interaction under the same conditions, e.g. intensities of load and inflation pressure, while changing the locations of the four pressure transducers. This was especially

important to obtain accurate (patterns of) contact pressure distributions.

3.3.3 Soils Used in the Study

Two different types of soil were employed in the experiment, Flat D kaolinite clay and No. 16 silica sand.

The index properties of the kaolinite clay are:

liquid limit 54.5 %

plastic limit 37.5 %

specific gravity 2.62.

The kaolinite clay was prepared at a water content of 43.1% which was found to have good workability. The clay was compacted uniformly into the soil bin at a density of 900 kg per cubic meter (average) which was found to vary slightly within the soil bin. The stress-strain curves of the kaolinite clay under plane-strain triaxial conditions are given in Fig. C.1.

The silica sand was uniformly graded and dry. It was deposited in layers into the soil bin to achieve a uniform density of 1475 kg per cubic meter. The stress-strain relationships of the sand obtained from triaxial tests under plane strain condition resembling the soil-bin situation are illustrated in Fig. E.1.

Hereafter the kaolinite clay and the silica sand used in the experiments will often be referred to as the clay and the sand respectively. Discussions and remarks on the experimental results for the tire-clay and tire-sand interactions will be given in the subsequent sections 3.5 and 3.6.

3.4 Representative Contact Length, Contact Width and Contact Pressure Distribution

One of the main purposes for this dissertation is to develop analytical approaches for solving tire-supporting ground (i.e. rigid base, clay) interaction problems, of which each can be categorized as a three-dimensional contact problem between a pneumatic body with stiff membrane and a half-space. However, because of numerous complexities lying in the real tire-supporting ground interaction problems, the original interaction problem is reduced to a two-dimensional contact problem by imposing the plane strain condition.

For two-dimensional contact analysis, it is necessary to represent a real contact surface by an idealized rectangular surface which defines the representative contact length and contact width. The real contact pressure distribution must also be defined by one for the corresponding rectangular contact surface. In the computation, it is particularly important to define a good representative contact width.

In section 3.4.1, the representative contact length and contact width are defined for a tire on clay and rigid base. The representative contact pressure distribution is then defined in section 3.4.2.

3.4.1 Representative Contact Length and Contact Width

In the experiments, shapes of contact surfaces vary depending on types of tires, intensities of loadings, inflation pressures, tread, etc. Three typical contact surfaces observed in the experiments are

shown in Figs. 3.10a-c. The definitions of the representative contact length and contact width are described for the three different cases in the following, depending on the available information regarding real contact surfaces.

Case 1

The definition for this case is that all the information on contact surfaces are given in advance. Then the definition is given as follows:

(i) Let the representative contact length be equal to the length of contact surfaces (e.g. Figs. 3.10a-c) along the y-axis (i.e. longitudinal direction) which is in the direction that a tire travels,

(ii) Then the representative contact width can be defined by dividing the contact area by the representative contact length.

This definition was used to define the representative contact length and contact width for the experimental results for the tire-supporting ground (i.e. rigid base, soils). Hereafter the "representative" could be sometimes dropped out.

Case 2 (Tire-Clay Interactions)

In the experimental results on the tire-clay interactions, the representative contact width obtained in the experiments were kept within bounds of 70 to 90 percent of the nominal widths of the tires, according to Table D.1a-h, even though the load was so small compared with its peak loading applied in each experiment or the self-weight of

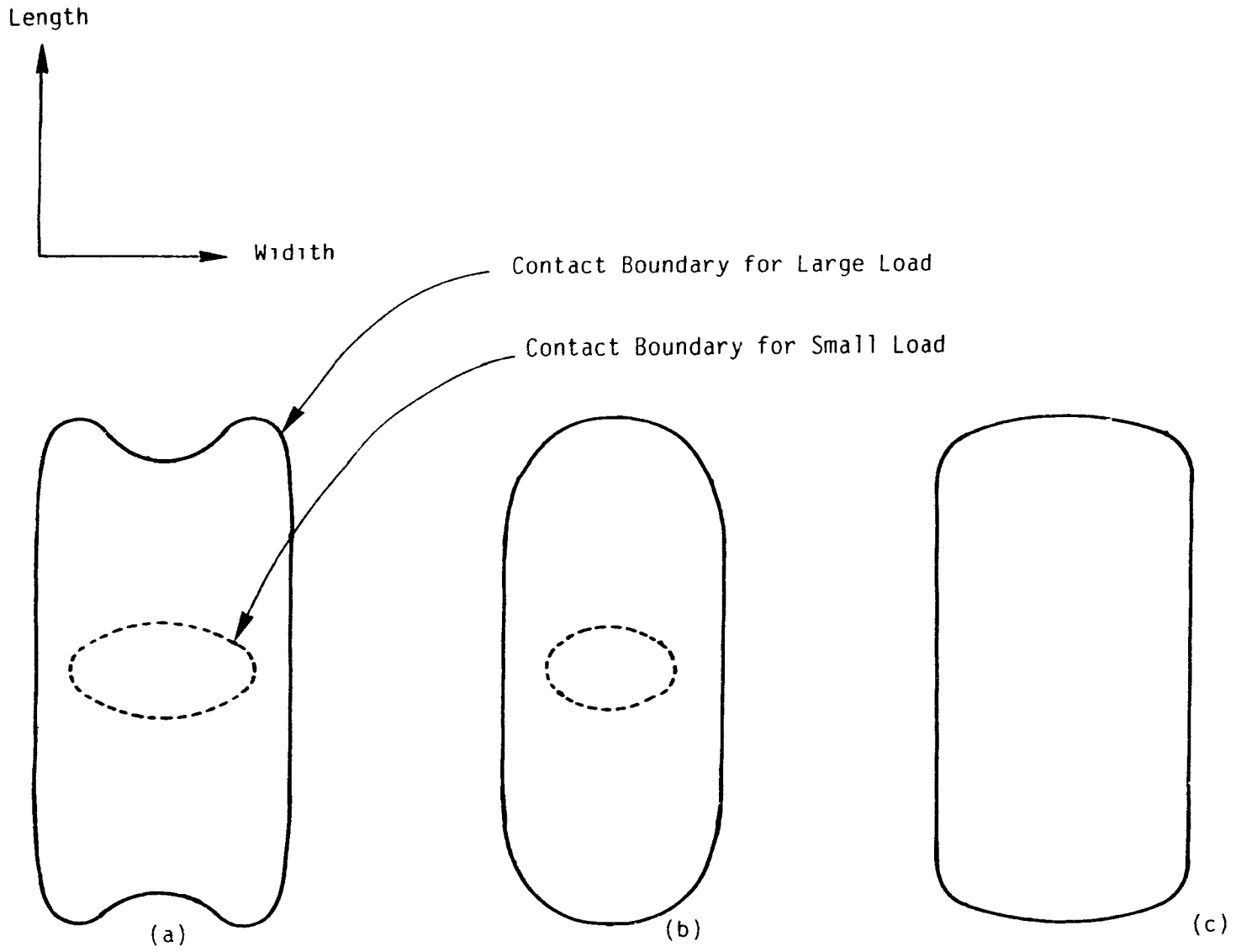


Fig. 3.10 Three Typical Shapes of Contact Surfaces Obtained in the Present Experiments

vehicle. One may then set a constant contact width be about 75 percent of nominal width of each tire regardless of magnitude of loading. The contact length could be obtained by (i) dividing contact area by the contact width if the contact area is available, or (ii) applying the analytical approach (Chapters 4 and 5), both of which would produce the "rough" approximation of the representative contact length.

Case 3 (Tire-Rigid Base Interactions)

In the case of the tire-rigid base interactions, however, the representative contact width kept on changing as shown in Table C.2a-h, unlike that of tire-clay interactions, until the axle load reached its peak value applied in the experiment. Accordingly, it is not possible to set a constant contact width for various loadings. For the tire-rigid base interaction problems, there will be two alternatives depending on the situation:

(i) If the load is above a certain level (i.e. at least near the peak load applied), the contact width can be represented by a constant as in Case 2 for the tire-clay interactions since the contact width ranges from 60 to 80 percent of the nominal tire width (Table C.2a-h).

(ii) The representative contact width is given by a polynomial, which is a function of load, upon the information on contact surface by carrying out a few simple laboratory tests. This approach can, of course, be applied in representing the contact width for the tire-clay interactions; besides the

approach is used in developing the analytical approach presented in Chapter 5.

If the load-contact area relationships are known, the contact length can be obtained by dividing the contact area by the contact width defined above.

It is noted that the importance of obtaining a better definition for a real contact surface also lies in a possibility of which realistic results in the three-dimension could be approximately reproduced from the analytical solution for a given interaction problem.

3.4.2 Representative Contact Pressure Distribution

A typical contact pressure distribution on the elliptic-type contact surface, observed in the experiment, will be considered (Figs. 3.11 and 3.12). A represenative contact pressure distribution can then be defined from the real one (Fig. 3.12), as shown in Fig. 3.14, in the following way. Hereafter the real contact pressure will be denoted by "p", while the representative contact pressure on a corresponding rectangular surface will be denoted by "p*".

A contact pressure at a cross section x' - x' (along the transverse plane) shown in Figs. 3.12 and 3.13 will be considered.

(i) Integrate the contact pressure $p(x,y^*)$ along x'-x' plane. Put the integration as $P^*(y^*)$, i.e.

$$P^*(y^*) = \int_{x'-x'} p(x,y^*)\, dx$$

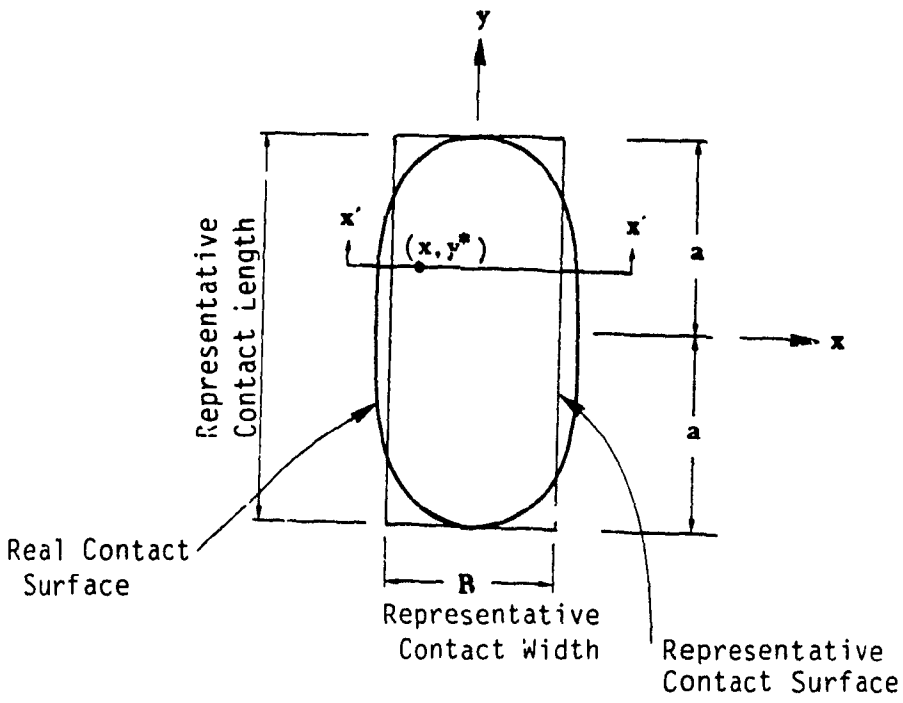


Fig. 3.11 Real Elliptic-Type Contact Surface and Its Corresponding Representative Contact Surface

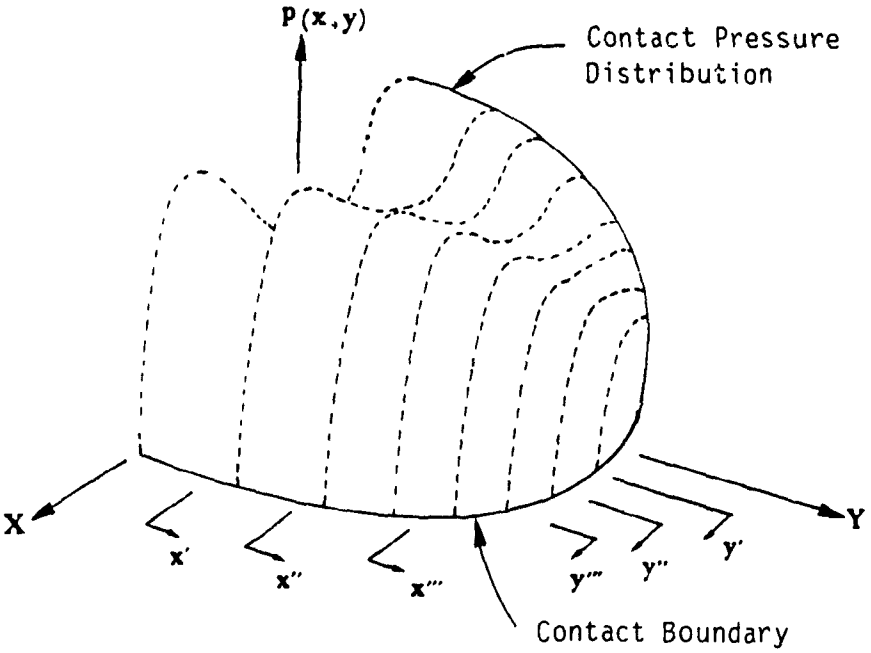


Fig. 3.12 Contact Pressure Distribution on a Contact Surface

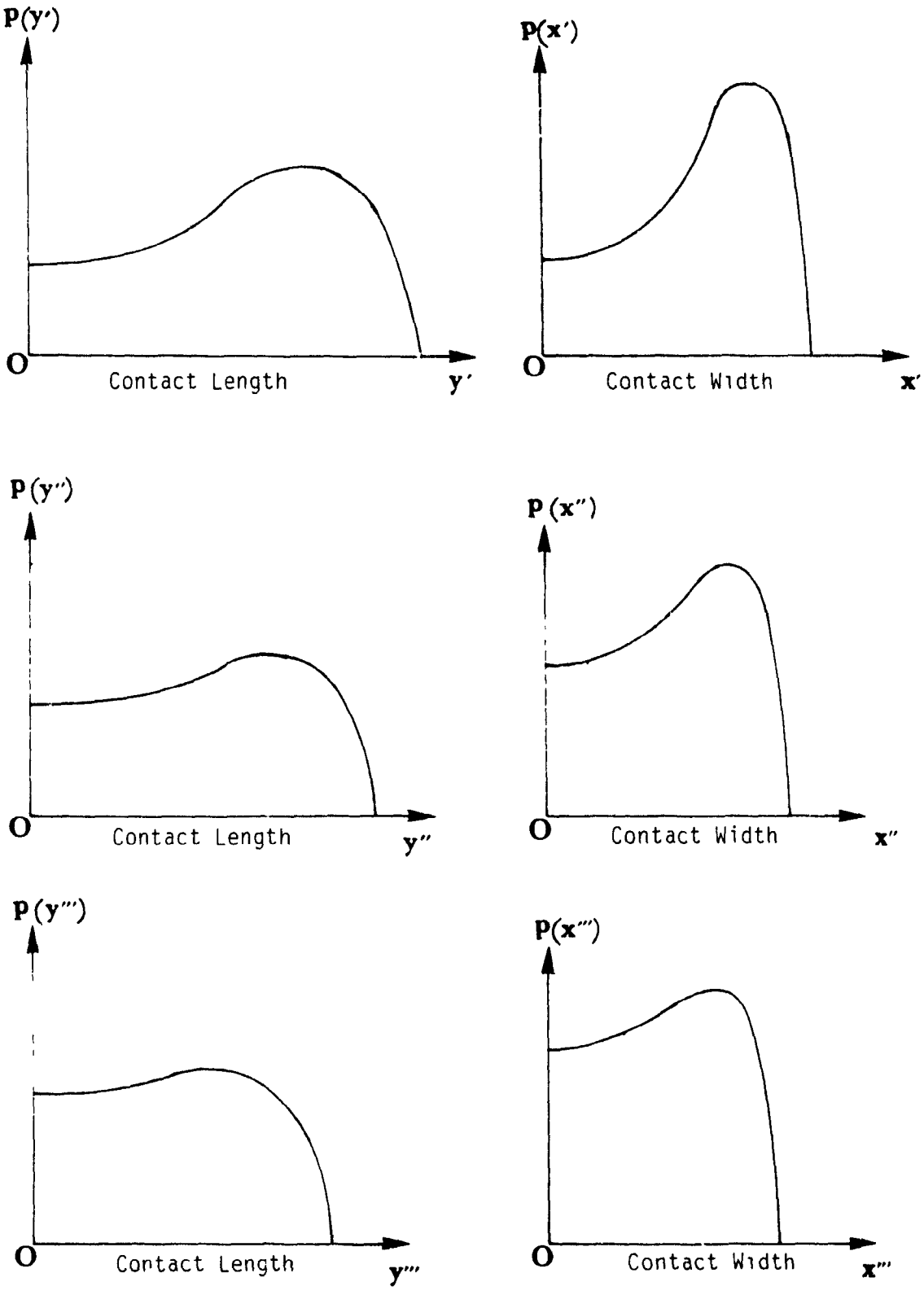


Fig. 3.13 Contact Pressure Distributions Along y- and x-Axes Based on the Pressure Distribution Given in Fig. 3.12

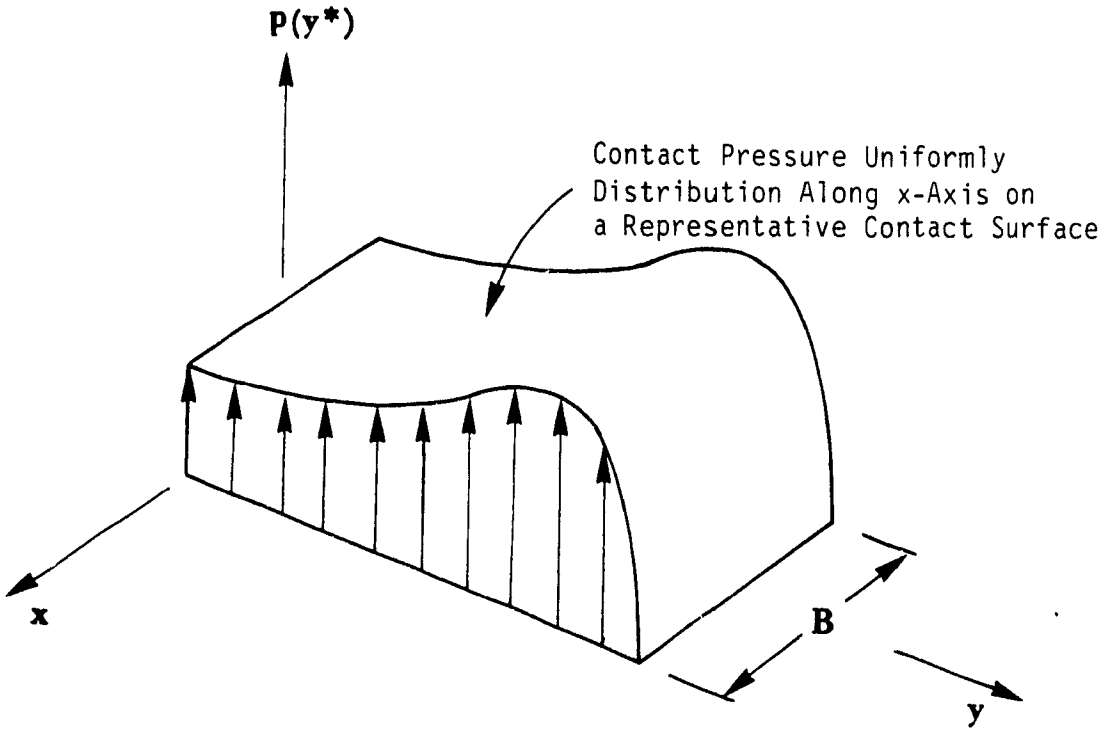


Fig. 3.14 A Representative Contact Pressure Distribution Interpreted on a Representative Contact Surface

(ii) Define p* by dividing P*(y*) by the representative contact width, B, i.e.

$$p^*(y^*) = P^*(y^*)/B$$

This pressure is uniform across x'-x' at y = y*.

One can approximate the representative pressure, p*(y), shown in Fig. 3.14 along the longitudinal plane (i.e. y-axis) by repeating the above process at the different cross sections x" - x", x"' - x"' and so on.

These representative contact surfaces (section 3.4.1) and the contact pressure distributions will help in validating the two-dimensional analytical approaches, while the analytical solutions could also be used in reproducing the actual ones reasonably well, provided that both the basic shape of the contact surface and the pattern of pressure distributions are known a priori by conducting a simple laboratory test.

3.5 Discussions and Remarks on the Experimental Results of Tire-Rigid Base Interactions

Discussions and remarks on the experiments of the tire-rigid base interactions will be given based on the experimental data such as axle displacement, contact area and contact pressure. The axle displacement is also equivalent to the "approach" between the axle and the surface of rigid base. The results such as axle displacement, contact area, average (ground) contact pressure (i.e. load/contact area) and the contact pressure distribution, which will be considered in the subsequent sections, would be influenced by various factors such as geometry of tire, construction, tread (i.e. physical and geometrical properties of lugs, tread pattern, etc.), carcass stiffness (after inflation), and the intensities of both load and inflation pressure, all of which are considered to be intrinsic factors. All the results required for the discussions are provided in Appendix C.

3.5.1 Load-Axle Displacement Relationships

The load-axle displacement relationships according to the procedure described in section 3.2 are presented in Figs. C.1a-h for nine tires (Table 3.1) in the following order: GOODYEAR 7.00-16LT (treaded and buffed), MICHELIN 7.00R 16XCL (treaded and buffed), MICHELIN 11.00R 16XL (treaded and buffed), MICHELIN 12.5R 16.5XLM (treaded and buffed) with a single rim; besides MICHELIN 12.5R 16.5XLM (treaded) with a split rim was tested only to obtain axle displacement

on a rigid base. Figures C.1a-i show that the relationships between wheel (or axle) loads and axle displacements in general, appear to be almost linear. Buffing the tire, which eliminates the contribution of tread to the load-carrying capacity of the tire, resulted in lower tire stiffness, except in MICHELIN 7.00R 16XCL (Figs. C.1c and C.1d). The maximum reduction in tire stiffness due to buffing occurred in the GOODYEAR 7.00-16LT (Figs. C.1a, b and Tables C.1a, b). This could be expected due to the tread pattern (Figs. 3.1 and 3.2), showing that the number of lugs (or ribs) in contact would be lower than those of other tires (i.e. all MICHELIN tires) if the gross (or total) contact areas for the four treaded tires are the same. This can also be deduced from the ratio of lug (or rib) area to total (or gross) contact area (Table C.3 or Tables C.2a-h).

The difference between bias and radial tire cord arrangements in the load-carrying can be observed by comparing GOODYEAR 7.00-16LT (bias) and MICHELIN 7.00R 16XCL (radial). Both tires had similar load range and inflation pressures (Table 3.1). The tire dimensions are also agreeable (Fig. 3.1). When compared at the same maximum load of 8.0 kN at the inflation pressure of 310.5 kPa, the axle deflection of the bias-ply treaded tire was 23.5 mm (15.7%, Fig. C.1a) while that of the radial-ply treaded tire was 28.6 mm (18.8%, Fig. C.1c). The percentage of axle displacement was calculated based on the undeformed carcass height of the buffed tire as shown in Fig. 3.1. This confirms the common observation that a radial-ply tire deflects more than a comparable bias-ply tire.

Stiffness of tires can be compared on the same reference level of load and inflation pressure. Thus all tire deflections at the same load of 3.0 kN and the same inflation pressure of 103.5 kPa are obtained from the load-displacement relationships as listed in Table C.1a for direct comparison. For example, the stiffest tire is MICHELIN 11.00R 16X (treaded) among all tires when compared in terms of percent tire deflection.

3.5.2 Contact Area - Load Relationships

The contact area was measured by the footprint of the tire loaded vertically on a rigid surface as shown in Figure 3.3. Both total or gross contact area and lug (or rib) area were measured from the tire print. The measured gross contact area for all tires studied (except MICHELIN 12.5R 16.5XLM with split rim) are compiled in Tables C.2a-C.2h, following the order given in section 3.4.1.

The gross contact area for each tire is plotted as a function of wheel (or axle) load and presented in Figs. C.2a-h. The contact areas increase almost linearly for most cases as the load increases.

The effects of removing treads from the tires on the contact area development are not necessarily to increase gross contact area of the treaded tire, using similar load and inflation pressures. At low axle (or wheel) load and low inflation pressure, the contact area of the buffed tire is larger than that of its counterpart treaded tire. However, this is reversed when either the load or the inflation pressure is raised. Such a development can be observed even when the inflation pressure is kept constant as the load changes.

3.5.3 Average (Ground) Contact Pressure - Inflation Pressure Relationships

The average (ground) contact pressure can be calculated by dividing the load with the corresponding contact area. The average contact pressure and the inflation pressure relationships for each tire (both treaded and buffed) are depicted in Figs. C.4a - C.4d and correspond to Figs. C.3a - C.3h. The relationships show the influences of both inflation pressure and stiffness of carcass on the development of contact area.

The average contact pressure is, in general, expected to be equal or higher than the inflation pressure, due to the stiffness of the carcass, if the carcass is perfectly in contact with the rigid base. For all full-size tires studied, the average contact pressure is higher, as expected, than the inflation pressure when the inflation pressure is low (Figs. C.4a - C.4d). The average contact pressure is, however, lower than the inflation pressure when the latter is relatively high. Such trends also resulted in the treaded tires even if the actual lug area was considered instead of the gross contact area used in calculating the average (ground) contact pressure as shown in the figures.

Of all the tires tested, a notable difference between treaded and buffed tires is that the average contact pressures for the treaded tires, except MICHELIN 11.00R 16XL, are always higher than those for the buffed tires when considering the case of the lowest inflation pressure, while the average contact pressures for the treaded tires are lower than those for the buffed tires at the highest inflation

pressures for all the tires. The higher average contact pressures at the lowest inflation pressures (except MICHELIN 1.00R 16XL) for the treaded tires, when compared with those for the buffed tires, are attributed to the treads stiffening carcass.

The fact observed in the results (i.e. the average contact pressure is lower than the inflation pressure when the latter is relatively high) can be partly explained in the following, since it is unlikely to happen if only perfect contact is concerned.

First, considering the extreme case where the stiffness of a membrane is negligibly low, then the contact pressure must be approximately equal to the inflation pressure. It is physically impossible that average contact pressure (i.e. load/contact area) is lower than the inflation pressure, unless, for example, the volume of the tire increases, so long as the carcass portion within the contact boundary (generally referred to as contact surface) is perfectly in contact with the rigid base. It was observed that there was little change in the volume since the inflation pressure, which was being recorded during the loading, showed negligibly small change. This implies that the portion within the contact boundary, which is observable, could have had one of the following situations (see Figs. 2.11c and 2.13b in section 2.5): (i) there were some gaps between the carcass (within the boundary) and the rigid surface, or (ii) some portions of the carcass in contact were (at least) being forced upward without creating any gaps within the contact boundary, thus resulting in the average contact pressures which are lower than the inflation pressure

at the highest inflation pressures (Figs. C.4a-d).

These phenomena are directly linked to both the carcass stiffness and the lateral displacements of the sidewall, as was discussed rather hypothetically in section 2.5 (see Figs. 2.11, 2.12 and 2.13). As the load increases, the lateral displacements of the sidewall become larger, and this would lead the contacting carcass to deform upward (but not necessarily with the gap), such as those shown in Figs. 2.11c and 2.13b, so long as the crown and the shoulder (see Figs. 2.6, 2.7) have certain stiffness (i.e. not like a thin membrane with negligible stiffness).

3.5.4 Contact Pressure Distribution

Following the test arrangement for measuring contact pressure underneath a tire as described in section 3.2, all treaded and buffed tires (a total of eight tires) were subjected to (contact) pressure determination. Of all the experiments on pressure distributions under the condition of 3 inflation pressures and 5 loads, a list of test conditions (i.e. inflation pressure, load) is given in Table C.4. For treaded tires the measured contact pressures at the specific locations within the contact surfaces (or footprints) are illustrated in Figs. C.5, C.7, C.9 and C.11 as listed in Table C.4. For buffed tires, and contours representing equal pressure intensities (i.e. isobars) within the contact surfaces are shown in Figs. C.6, C.8, C.10 and C.12. The contour lines are drawn approximately under the assumption that the contact pressures are symmetrically distributed within the contact patch. Such an assumption made it possible to draw when the pressure

transducer readings were insufficient. The pressure distribution approximated was verified by integrating it over the contact surface since such an integration will provide the reaction force, which must be equal, in magnitude, to the applied load for a static equilibrium of the two contacting bodies. According to the calculation for checking the accuracy of pressure distribution drawn, error of each pressure distribution was shown to stay within five to ten percent. Such small errors support that the readings of pressure transducers and the pressure distribution drawn are sufficiently reliable. The average contact pressures for the buffed tires are listed in Table C.4 and are also shown in the pressure distribution diagrams (Figs. C.5, C.7, C.9, and C.11). For the treaded tires, the average contact pressures are given in Table C.4 based on both gross and lug areas and in Figs. C.5, C.7, C.9 and C.11 based on lug areas.

In the following (A, B, C, D), the features regarding the contact pressures such as patterns of pressure distributions and changes of pressure intensities as load changes will be specially concerned for each tire.

(A) GOODYEAR 7.00-16LT

In the treated GOODYEAR 7.00-16LT, three inflation pressures (34.5, 103.5 and 310.5 kPa) were considered, each being tested with two wheel loads (Table C.4). Because of the non-symmetrical tread pattern of the tire, the contact pressure measured by the non-symmetrical locations of the pressure transducers (Fig. 3.5a) varied widely (Figs. C.5a-f). It should be noted that the tread pattern of

GOODYEAR 7.00-16LT is repetitive, but not symmetrical, with respect to the longitudinal plane of the tire (Figs. 3.1, 3.2a and C.5a). Thus the contact pressures measured should not be expected to distribute symmetrically across the footprint (i.e. contact) surface. The results of the contact pressures measured lead to the following observations:

a. In general, the measured contact pressures are higher along the periphery of the footprint than around its center. Of the six conditions tested, only two (Figs. C.5a and C.5e) that were loaded with lower wheel loads exhibited slightly higher pressures near the center of the footprint than its periphery. This could be attributed to the effect of stiffness of sidewall (and treads), which sustained the lateral displacements of the sidewall relatively smaller at the lower loads.

b. The measured contact pressures were generally observed to be lower than the average (ground) contact pressures which were calculated based on the lug areas (Figs. C.5a-C.5f). This may have happened partly because of difficulties arising in the experiments in positioning the pressure transducers right beneath the treads.

c. The measured contact pressures were higher than the inflation pressure when the latter were low. This was reversed when the inflation pressure was higher, following the results presented in Fig. C.4a.

For the buffed counterpart, GOODYEAR 7.00-16LT (buffed), contact (ground) pressures were similarly measured and the results were

plotted as pressure contours in Figs. C.6a-n, following the results given in Table C.4. Cross sections showing the pressure distribution profiles across the footprint are illustrated, while profiles of the calculated wheel load (per unit length) distributed along the longitudinal footprint are given, whenever appropriate (see an example in Fig. C.6c/2).

From the pressure distributions obtained for the buffed GOODYEAR 7.00-16LT (Figs. C.6a-n), the following observations can be made:

a. The average contact pressure based on the gross contact area was always higher than the pressure close to the center of the footprint. The difference was more pronounced when the inflation pressure was low (i.e. 34.5 kPa in Fig. C.6a-e), attributed to the carcass stiffness.

b. The pressure intensifies along the periphery of the footprint and could be considerably higher than the average contact pressure, particularly when the inflation pressure was low and the wheel load was relatively high. The pressure around the center of the contact area was normally less than the inflation pressure.

c. The pattern of wheel load distribution (per unit length) would be similar to those of the pressure distributions defined based on the interpretation (section 3.4) since the real shape of contact surface is close to the idealized rectangular contact surface. This implies that any results produced by using the idealized pressure distribution would be quite realistic.

d. The pressures underneath the sidewalls were particularly higher

than those at any other part within the contact surface. This can be deduced from the load-transfer mechanism, discussed in section 2.5.

(B) MICHELIN 7.00R 16XCL

The pressure transducer readings are presented with respect to their locations in the contact surface (Figs. C.7a-p) for the treaded MICHELIN 7.00R 16XCL. Contours of equal contact pressures are plotted for the buffed contour part (Figs. C.8a-b).

From inspection of the contact pressures measured underneath the treads, the pressures around the center of the footprint were generally higher than those measured near the periphery of the footprint. Such results are contrary to those observed in GOODYEAR 7.00-16LT addressed in (A). Since the two tires, GOODYEAR 7.00-16LT and MICHELIN 7.00R 16XCL are similar in general characteristics (i.e. dimensions and ply rating - Table 3.1 and Fig. 3.1), the difference in the contact pressure is likely due to the following reasons:

a. The tread pattern of the MICHELIN 7.00R 16XCL lacks the stiff shoulder ribs found in GOODYEAR 7.00-16LT.

b. The ratio of lug area to gross contact area of MICHELIN 7.00R 16XCL is lower than that of GOODYEAR 7.00-16LT (Tables C.2a & b, and C.3).

c. The stiffness of treads relative to the stiffness of the sidewall for MICHELIN 7.00R 16XCL (radial ply) is higher than that for GOODYEAR 7.00-16LT (bias ply) (see ply arrangement in Table 3.1). The pressure distributions with the footprints of the buffed

MICHELIN tire are illustrated in Figs. C.8a and b for the inflation pressure 103.5 kPa and 310.5 kPa, respectively. The maximum wheel loads applied were sufficiently large to fully develop contact areas. For both inflation pressures, the highest contact pressures appeared underneath the sidewalls, and the contact pressures were higher around the periphery of the footprint and at the center. Unlike the inflation pressure of 103.5 kPa (and all the results in GOODYEAR), the contact pressure reached peak value at the center of the footprint and diminished towards the edges, considering the mid-longitudinal plane (Figs. C.8b/1-2).

(C) MICHELIN 11.00R 16XL

The pressure transducer readings underneath the treads are illustrated in Figs. C.9a-f with different test conditions as illustrated in Table C.4. Contours of equal pressures drawn for the buffed tire are shown in Figs. C.10a and b.

The majority of the contact pressures measured underneath the treads of the MICHELIN were higher than the average contact pressures and the inflation pressures (Figs. C.9a-f). At the inflation pressures of 34.5 kPa and 207 kPa, the pressures measured near the edges of the footprint were higher than those around the center (Figs. C.9a-d). This was not found in the contact pressures exerted by the higher inflation pressure of 414 kPa (Figs. C.9e and f). Without the contribution of the treads in supporting the wheel load, the sidewall of the buffed tire imposed the higher contact pressures around the

periphery of the footprints (Figs. C.10a and b). The contact pressures around the center of the footprints were lower than the corresponding inflation pressures.

(D) MICHELIN 12.5R 16.5XLM

Similar to other tires tested in this study, various wheel loads and inflation pressures were employed for MICHELIN 12.5R 16.5 XLM as listed in Table C.4.

The contact pressure measured underneath the treads varied widely from one tread to another (Figs. C.11a-c). Like other treaded tires, definite pressure distribution patterns could not be established. Equal-pressure contours were drawn for the counterpart buffed tire (Figs. C.12a-i). When the inflation pressure was low (103.5 kPa), the contact pressures underneath the sidewalls were higher than others within the contact surfaces (Figs. C.12c and d). The contact pressures were higher than both the inflation pressures used and the average contact pressures. As the inflation pressure was higher (i.e. 207 kPa), the highest contact pressures were found near the center of the contact surfaces (Figs. C.12g-i). Thus the contact pressure distribution was parabolic-shaped, instead of saddle-shaped as found when the inflation pressure was low. It should be noted that the parabolic-type distribution for the contact pressure was observed only in the buffed tire, MICHELIN 12.5R 16.5XLM. This could possibly have happened partly because of the differences in materials of sidewalls between MICHELIN 12.5R 16.5XLM and the other tires. As shown in Table

3.1, the sidewalls of MICHELIN 12.5R 16.5XLM are constructed by using two polyester plies while those of the other two MICHELIN tires (i.e. 7.00R 16XCL, 11.00R 16XL) are constructed by using one steel ply.

Considering only the three MICHELIN tires with the conditions of the ply arrangement of both sidewalls and treads in Table 3.1, it is clear that the stiffer sidewalls of the two MICHELIN tires (i.e. 7.00R 16XCL and 11.00R 16XL) will carry relatively higher loads compared with those of the MICHELIN 12.5R 16.5XLM, thus resulting in higher pressure distributions underneath the sidewalls and the saddle-shaped pressures for the former two MICHELIN tires. When comparing the shapes of contact surfaces of MICHELIN 12.5R 16.5XLM with those of the other tires, it is observed that the shapes of the MICHELIN 12.5R 16.5XLM remained more elliptic compared with the others. This implies that the load transfer mechanism of MICHELIN 12.5R 16XLM is quite different as compared with the others, due to the effects of sidewall stiffnesses, influencing lateral deformation of sidewall as discussed in section 2.5, so long as applied loads for this MICHELIN tire are limited to the present range. Influences on the lower stiffness of the sidewall of the MICHELIN 12.5R 16.5XLM, which is due to material such as polyester, can be found in the resulting lower average contact pressure at the lowest inflation pressure (shown in Fig. C.4d).

3.5.5 Concluding Remarks on the Experimental Results of Tire-Rigid Base Interactions

Load-carrying capability of each tire can be partly characterized by considering the relationships such as load-(axle) displacement

load-contact area, and measured contact pressure (underneath the tread for each treaded tire), change in contact pressure around the center of the contract surface, and the shape of the contact surface. Summary and remarks on overall characteristics of the tire-rigid base interactions are given in the following based on the discussion of the results stated in sections 3.5.1-3.5.4.

3.5.5.1 Load- Axle Displacement and Contact Area-Load Relationships

Both relationships, load- axle displacement and contact area, represent the overall stiffness of each tire in terms of axle displacement and contact area.

In the previous sections 3.5.1 and 3.5.2, load- axle displacement and contact area-load relationships appeared to be almost linear for all the tires (treaded and buffed) and for all the inflation pressures, while contact area is gross (or total) contact area. The effect of tread of GOODYEAR 7.00-16LT was the highest for load-displacement relationship. The difference between GOODYEAR 7.00-16LT and the other tires - partly due to cord arrangement (bias, radial), tread pattern and area of lug. The stiffest tire is MICHELIN 11.00R 16XL (treaded) amongst all tires when compared in terms of percentage deflection.

The effects of removing treads from tires on the contact area development are not necessarily to increase gross contact area of the treaded tires, using similar load and inflation pressures. At low wheel (or axle) load and low inflation pressure, the contact area of the buffed tire is larger than that of its counterpart treaded tire.

However, this is reversed when either the load or the inflation pressure is raised. Such a development can be observed even when the inflation pressure is kept constant as the load changes.

It is noted that the linearity of load-displacement relationship may not generally imply the linearity of contact area-load relationship when a body interacting with tires is (linearly) elastic.

3.5.5.2 Average (Ground) Contact Pressure-Inflation Pressure Relationships

The relationships show the influences of both inflation pressure and stiffness of carcass on the development of contact area.

Of all the tires tested, a notable difference between treaded and buffed tires is that the average contact pressures (based on gross contact area) for the treaded tires are always higher than those for the buffed tires when considering the case of the lowest inflation pressures (except MICHELIN 11.00R 16XL), while the average contact pressures for the treaded tires are lower than those for the buffed tires at the highest inflation pressure for all the tires. The higher average contact pressures at the lowest inflation pressures (except MICHELIN 11.00R 16XL) for the treaded tires, when compared with those for the buffed tires, are attributed to the treads stiffening the tires.

Another important tendency in the results is that, for all tires (treaded and buffed), the average contact pressure at the lower inflation pressure is higher than the inflation pressure. The average contact pressure is, however, lower than the inflation pressure when

the latter is relatively high for all the tires. However, the result of which the average contact pressure is lower than the inflation pressure is unlikely to occur if the contact is perfect while the carcass stiffness contributed to the carrying load. Such a question was considered previously in sections 2.5 and 3.5.3.

3.5.5.3 Contact Pressure Distribution

Features of contact pressure distribution, change of contact pressure around the center of the contact surface (with change of load) and shape of contact surface are briefly stated below in (1), (2) and (3), respectively, for the set (i.e. treaded and buffed) of each tire.

GOODYEAR 7.00-16LT

(1) For both treaded and buffed tires, the measured contact pressure was higher along the periphery of the contact surface than around its center regardless of the inflation pressure. The highest pressure was, in general, observed underneath the sidewall.

(2) The pressure around the center changed little even if the load increased for both the tires (i.e. treaded and buffed).

(3) The shapes of the contact surfaces for both the tires were almost rectangular regardless of inflation pressures and loads.

MICHELIN 7.00R 16XCL

(1) The pressure distributions for the treaded tire were substantially different from those for the buffed one. The

higher pressure was generally observed around the center of the contact surface rather than along the periphery for almost all the inflation pressures for the treaded one, while they tended to distribute uniformly as the load increased. On the other hand, the pressure distributions for all the buffed tires were similar to those observed in GOODYEAR 7.00-16LT, although the pressure around the center was not necessarily the lowest.

(2) For all inflation pressures, the contact pressure around the center for the treaded tire started to decrease with the increase in load.

(3) The shapes of all the contact surfaces produced for the treaded tire were seen to be more elliptical, while those for the buffed tire were clearly rectangular.

MICHELIN 11.00R 16XL

(1) For the treaded tire, the lower pressure was observed around the center rather than along the periphery except for the lower inflation pressures (34.5 kPa and 207 kPa). Then the higher pressure appeared to be around the center for the highest inflation pressure (414 kPa). For the buffed counterpart, the higher pressure appeared along the periphery and the highest pressure was detected underneath the sidewall.

(2) The pressure generally dropped as the load increased for the treaded tire.

(3) The shapes of contact surfaces under all the conditions were almost elliptic for both the treaded and buffed tires.

MICHELIN 12.5R 16.5XLM

(1) Among all the inflation pressures (34.5 kPa, 103.5 kPa and 207 kPa), the higher pressure appeared around the center for the two higher inflation pressures, for the treaded tire, while it did not happen for the lowest inflation pressure, 34.5 kPa. For the buffed tire, the higher pressure was shown underneath the sidewall while the pressure around the center was not so low either, for the lower inflation pressure 103.5 kPa. But when the inflation pressure was doubled to 207 kPa, the pressure distribution clearly changed to a parabolic type, i.e. the highest pressure occurred around the center.

(2) For the buffed tire, the pressure around the center did not change for the lower inflation pressure (103.5 kPa) as the load increased. But for the higher inflation pressure (207 kPa), the pressure around the center increased moderately as the load increased, and it had little change at the higher load.

(3) The shapes of contact surfaces were elliptical for both the treaded and buffed tires under all the inflation pressures and loadings.

In the summary of the contact pressure distributions given above, the following are cited for the treaded tires and their counterparts, separately:

Treaded Tires

a. Increase in the inflation pressure (i.e. stiffening carcass) for both MICHELIN 11.00R 16XL and MICHELIN 12.5R 16.5XLM changed the

position, where the higher contact pressures occurred, from the portion underneath the sidewall and/or periphery to the center of contact surface. However, this did not happen to the rest of the tires.

b. The shape of contact surface for GOODYEAR 7.00-16LT was rectangular while those for all the MICHELIN tires were more like elliptic, regardless of the inflation pressures and the loads.

Buffed Tires

a. All the pressure distributions drawn were different although the distributions for GOODYEAR 7.00-16LT and MICHELIN 11.00R 16XL were slightly similar.

b. Overall results on pressure distributions clearly indicated that the sidewalls can carry a higher load, more than any other part of the tire carcass within the contact surface, except probably the MICHELIN 12.5R 16.5XLM.

c. The shapes of contact surface for GOODYEAR 7.00-16LT and MICHELIN 7.00R 16XCL were rectangular while the two other tires remained elliptic.

For all the treaded tires and their counterparts, the contact pressure around the center either ceased to increase or dropped down as the load became higher. When the contact pressure distribution is only concerned for the tire tests, carcass construction, material used for carcass and wearing of treads (which depends much on the pressure distribution) seems to be more dominant factors compared with inflation pressure and load applied.

3.6 Discussions and Remarks on the Experimental Results of Tire-Supporting Clay Interactions

In the tire-rigid base interactions, change of carcass stiffness clearly influenced all the results, while the carcass stiffness (i.e. slope of load-axle displacement on rigid base), in general, highly depends on both the strain of tire membrane due to inflation pressure and the rigidity of lugs due to the existence of tread (Table C.1b). However, in the case of tire-clay interactions, tread pattern, geometry and rigidity of lug would become more significant factors since lugs penetrate into the clay surface as the tire comes into contact with the supporting clay. Accordingly all such factors, where rigidity of the lug contributes to contact characteristics as well as to carcass stiffness, should be considered as intrinsic factors although it is too complex to take each factor into account for the analysis of tire-clay interactions.

Therefore, the effects of inflation pressure and the existence of tread will be considered in the following discussions, particularly for axle displacement (Figs. D.2a-d) and contact area (Tables D.1a-h; Figs. D.3a-d) given in the first two sections, 3.6.1 and 3.6.2, respectively. The discussions on average contact pressure (Tables D.1a-h; Figs. D.5a-d) and contact pressure distribution (Figs. D.6-D.21) over the contact surface (or footprint) will be described in sections 3.6.3 and 3.6.4, respectively. The importance which should be kept in mind is that the carcass stiffness, which seemed to be the dominant factor for tires on rigid base, is no longer the dominant

factor for tires on clay. In sections 3.6.1 and 3.6.2, the influence of inflation and tread on the axle displacement and contact area will be emphasized for each tire.

3.6.1 Load-Axle Displacement Relationships

GOODYEAR 7.00-16LT

Inflation pressures of both the treaded and the buffed tires were 34.5 kPa and 310.5 kPa. The range of axle loads for both the tires (i.e. treaded and buffed) with the low inflation pressure (34.5 kPa) was approximately 1.5 kN and 4.0 kN, while that for both the tires with high inflation pressure (310.5 kN) was approximately 1.6 kN and 5.1 kN.

(i) Influence of Inflation Pressure

Here the stiffness change of the tire (either treaded or buffed) depends only on the inflation pressures. Hence the influence of the stiffness change will be individually observed for the treaded and buffed tires.

The axle displacements for the treaded tire with the low inflation pressure (34.5 kPa) were much larger than those for the high inflation pressure (310.5 kPa), while the results were reversed in the case of the buffed tire although the difference was relatively small. The influence of the two quite different inflation pressures on the axle displacements became apparent for the treaded tire as the load increased. These results imply that the relative stiffness between the treaded tire and the supporting clay changed drastically

when the inflation pressure increased, while that between the buffed tire and the supporting clay changed little. In other words, the change of inflation pressure for the treaded tire would be quite significant in the results unlike that for the counterpart, the buffed tire. This can be seen from the slope (i.e. load vs axle displacement relationship) of the treaded tire with the low inflation pressure (34.5 kPa) which happened to be the most moderate, and its axle displacement became the largest when the load reached the highest.

(ii) Influence of Tread

The stiffness change of the tires (treaded and buffed), whose inflation pressures were kept constant at either 34.5 kPa or 310.5 kPa, is controlled by whether or not the tire is treaded. The axle displacements of both the treaded and the buffed tires will be compared under the same inflation pressure (and the same loading).

For the low inflation pressure 34.5 kPa, the axle displacements of the treaded tire were lower than those of the buffed one when the loading range was low. But the situation was reversed as the load increased. In the case of high inflation pressure 310.5 kPa, the axle displacements of the buffed tire were clearly higher than those of the treaded one for all the loadings. It is also noted that their slopes were almost the same. The results stated above therefore imply that the influence due to buffing the treads, which means the reduction of carcass stiffness, was clearly observed at the inflation pressure of 310.5 kPa, while it was less at the inflation pressure of 34.5 kPa. It should be mentioned that the results of the axle displacements for

the tires (i.e. treaded and buffed) at the low inflation pressure (34.5 kPa) suggests that a softer (or buffed) tire would not necessarily produce the higher axle displacement. This could be partly due to the relative stiffness between the tire and the supporting ground (or clay).

MICHELIN 7.00R 16XCL

The inflation pressures were the same as those used for the GOODYEAR 7.00-16LT, i.e. 34.5 kPa and 310.5 kPa.

(i) Influence of Inflation Pressure

The axle displacement for the treaded tire with the inflation pressure of 310.5 kPa was slightly larger than that with the inflation pressure of 34.5 kPa, while it was reversed for the buffed tire. Such results contrast to those obtained for the treaded GOODYEAR 7.00-16LT. The results here imply that the change in the stiffness due to the inflation pressures did not influence so much the axle displacement as compared to the treaded GOODYEAR 7.00-16LT.

(ii) Influence of Tread

The axle displacement of the buffed tire under an inflation pressure (i.e. 34.5 kPa or 310.5 kPa) is almost twice as large as that of the treaded tire. These results suggest that buffing this tire would significantly reduce the carcass stiffness, resulting in large axle displacements in the wide range of inflation pressure. In other words, the influence of tread is important, at least, between the inflation pressure of 34.5 kPa and 310.5 kPa, while it did not happen

for the GOODYEAR 7.00-16LT.

From the above notable results of the axle displacements for both the tires (i.e. GOODYEAR 7.00-16LT, MICHELIN 7.00R-16XCL), one can deduce the following:

(1) A softer tire (i.e. a tire with a lower inflation pressure or a buffed tire) on clay-like-material would not necessarily produce the larger axle displacement as compared with its counterpart, a stiffer tire. This may be partly due to the relative stiffness between the tire and the clay-like-material, and the range of loading,

(2) The axle displacements resulting from changing the inflation pressure will imply the following. The range of the inflation pressure, influencing the axle displacements, is possibly narrower for the treaded GOODYEAR 7.00-16LT as compared with that for the treaded MICHELIN 7.00R-16XCL. However, there seems little difference in such results in the case of the buffed tires. In other words, for example, for the treaded MICHELIN 7.00R-16XCL the change in carcass stiffness due to the inflation pressures within the range of 34.5 kPa and 310.5 kPa is not so significant for the clay used for the experiments, although the inflation pressures within the same range would have greatly influenced the results for the treaded GOODYEAR 7.00-16LT (at the higher loadings in particular).

(3) Reduction of the carcass stiffness by buffing the treads clearly increased all the axle displacements but that for the GOODYEAR

7.00-16LT at the lower inflation pressure of 34.5 kPa.

MICHELIN 11.00R-16XL

Inflation pressures used for this tire were 34.5 kPa and 207 kPa. The range of the wheel load was between 2 kN and 5.5 kN.

The axle displacements for all cases were approximately the same under the load applied. There are at least two reasons for such results. First, the carcass is so stiff that buffing treads would not influence it so much. This may be partly due to the highest ply rating. Secondly, the wheel load was not sufficiently high for obtaining better comparisons in the axle displacements while this tire is capable of carrying much higher loads compared with any other tires employed in the present experiments.

MICHELIN 12.5R-16.5XLM

Inflation pressures were the same as those used for the MICHELIN 11.0R-16XL. The range of load for the inflation pressure of 34.5 kPa was between 1.7 kN and 3.5 kN while for the inflation pressure of 207 kPa, it was between 1.7 kN and 5.4 kN.

For the treaded tire, the low inflation pressure of 34.5 kPa clearly produced the higher axle displacements, which became even more evident as the load increased, than those of 207 kPa. It is also interesting to note that the difference between the axle displacements for the two different inflation pressures (i.e. 34.5 kPa and 207 kPa) for this treaded tire-clay contact is almost the same as that obtained for the treaded tire-rigid base. Considering this fact and the characteristic that the axle displaced linearly on the rigid base

under the application of loading, it is possible to conclude that the clay surface contacting with this treaded tire could have displaced linearly, at least, within the range of applied load (i.e. between 1.7 kN and 3.5 kN). Similar results were obtained for the treaded tire GOODYEAR 7.00-16LT.

In buffed form, however, the axle displacement for the lower inflation pressure became higher than that for the higher inflation pressure only after the applied load reached a certain level (i.e. about 2.3 kN).

The axle displacement for each experiment was controlled mainly by the inflation pressure, the tread of the tire, the deformability of the supporting clay and the load. The inflation pressure and the condition of the tread (i.e. either treaded or buffed) changed and determined the stiffness of the tire, while the condition of the supporting clay remained unchanged throughout the experiments. As shown in Figs. D.2a-d, the results on both the magnitude and the change of the axle displacements appeared to be quite random, and thereby it is hard to draw a particular conclusion. The change of inflation pressure and the condition of the tread significantly influenced the results on the axle displacements for most of the cases with the exception of the MICHELIN 11.00R-16XL. This must have occurred due to the stiffness of the MICHELIN 11.0R-16XL, which was extremely high relative to that of the supporting clay. The influence of the load was, for example, observed in the results of the buffed MICHELIN 12.5R-16.5XLM, in particular.

It should be noted that a softer tire, which would imply a buffed tire with lower inflation pressure, does not necessarily produce a larger axle displacement on clay than a stiffer one. Therefore, the magnitude of the axle displacement would depend on the relative stiffness between a tire and a supporting clay, and the applied load.

3.6.2 Contact Area-Axle Load Relationships

GOODYEAR 7.00-16LT

The contact area for the buffed tire (i.e. both the lower and higher inflation pressures) became larger with the increase of load, when compared with that for the treaded tire, as shown in Fig. D.3a. The curves of contact area-wheel load relationship in the lower range of load (i.e. in between the two loads, zero and the lowest loading among those at which the contact areas were measured) were predicted and drawn, as shown in Figs. D.3a-d, on the basis of the experimental results. Such a prediction would be useful to see the overall relationship for the contact area-load. It is then observed that all the relationships (Fig. D.3a) between contact area and load were clearly nonlinear. It should also be noted that the results for contact area-load shown in Fig. D.3a reflect on the results of axle displacements (Fig. D.2a). For example, in the case of the treaded tire, the contact area for the inflation pressure 34.5 kPa was very close to that for the inflation pressure 310.5 kPa. Such a result was also observed for the axle displacement in place of the contact area, as shown in Fig. D.2a.

MICHELIN 7.00r-16XCL

The results obtained (Fig. D.3b) for this tire were similar to those obtained for the GOODYEAR 7.00-16LT. This is, that the contact area for the buffed tire was clearly higher for each inflation pressure than that for the treaded one. However, the effect of buffing treads of MICHELIN 7.00R-16XCL resulting in lower carcass stiffness, was significantly higher than that of the GOODYEAR 7.00-16LT. Each relationship of contact area and load was closer to linear when compared with that for the GOODYEAR 7.00-16LT.

Some comparison between the results obtained for the tires, GOODYEAR 7.00-16LT and MICHELIN 7.00R-16XCL, can be made in the following, since the nominal size of both tires is approximately equal (Fig. 3.1).

(1) For the MICHELIN 7.00R-16XCL tire, the contact area for the buffed form with the lower inflation pressure of 34.5 kPa was much larger (i.e. in fact, the largest amongst the results for this tire) than that for the treaded one with the same inflation pressure, which happened to be the smallest. Such results were obtained in spite of the experimental results for axle displacement and contact area on the rigid base (Figs. C.1c-d and Figs. C.2c-d) where the existence of tread was insignificant for the lower inflation pressure in particular.

(2) The contact area for the buffed MICHELIN 7.00R-16XCL with the lower inflation pressure was the largest when compared with the others, while the rest of the contact area for both GOODYEAR

7.00-16LT and MICHELIN 7.00R-16XCL was almost the same (Figs. D.3a-b).

It is evident from the comparisons stated in (1) and (2) that the influence of tread is more remarkable for the interaction of tire-supporting clay than the inflation pressure which was clearly dominant in the case of the interaction of tire on rigid base.

MICHELIN 11.0R-16XL

The contact area of this tire on clay appeared to vary slightly with respect to changes in load, inflation pressure and the presence of tread (Fig. D.3c). While the contact area of the buffed tire became higher as the load increased, such a small difference in all the results was like that shown in the GOODYEAR 7.00-16LT.

The influence of tread was particularly seen at the higher inflation pressure of 207 kPa. However, there could have been obvious influences on the contact area due to the lower and higher inflation pressures in the lower range of loading rather than tread if the predicted curves of contact area-load were correct (Fig. D.3c). In the case of the results (Figs. D.3a-b) shown previously for the two smaller tires, such influences of inflation pressure in the lower loading were not seen, except the contact area obtained for the treaded MICHELIN 7.00R-16XCL.

MICHELIN 12.5R-16.5XLM

The relationships of contact area-load (Fig. D.3d) for this tire

greatly contrasted with those obtained for the last three tires in point of role of inflation pressure. The notable results on contact area can be drawn in following: Firstly, the influence of tread on contact area was much smaller as compared with those shown for the other tires (Figs. D.3a-c), and that was particularly evident when considering MICHELIN 12.5R-16.5XLM with the higher inflation pressure in both the treaded and buffed forms. Unlike the results obtained in the three other tires, the contact area for the lower inflation pressure 34.5 kPa (i.e. both treaded and buffed tires) was larger than that for the higher inflation pressure. Secondly, the contact area-load relationships for the lower inflation pressure were also quite linear with the increase of load for both the treaded and buffed tires.

3.6.3 Average Contact Pressure-Axle Load Relationships

The relationships of load-average contact pressure on clay appeared to vary randomly as shown in Figs. D.5a-d. However, some comments regarding the average contact pressure can be immediately stated as follows:

(i) The average contact pressures clearly depended on the load, unlike those obtained on the rigid base (Tables C.2a-h).

(ii) In the case of larger tires such as MICHELIN 11.00R-16XL and MICHELIN 12.5R-16XLM, most of the average contact pressures did not exceed the inflation pressures.

(iii) A stiffer tire does not necessarily produce the higher average contact pressure unlike what have been obtained on

the rigid base; in other words, the tendancy of the results for each tire on clay was usually completely different from those observed in the tire-rigid base contact.

One important thing which should be emphasized here is, that the carcass stiffness of each tire (i.e. slope of load-axle displacement on rigid base as shown in Figs. C.1a-h) is not only the dominant factor for the average contact pressure on clay, as stated above in (iii). There are many other factors, influencing all the results on clay. In the following studies regarding the average contact pressure, only three factors will be concerned such as carcass stiffness, size of tire and tread, i.e. physical and geometrical properties of lugs (or ribs) and tread pattern. On the rigid base the existence of tread largely contributes to the carcass stiffness. In tire-supporting clay interaction, however, it could also have contributed directly to carrying the axle load since the penetration of tread into the supporting clay would help the tire to resist sliding on the curved contact surface.

Prior to the studies of the average contact pressure, the influence of tread on the carcass stiffness will be simply reviewed from Figs. C.1a-h and Table C.1b. Buffing the tire, GOODYEAR 7.00-16LT, clearly showed the largest decrease in the carcass stiffness at both the lower and the higher inflation pressures amongst all four types of tires used in the present experiments. In the case of the three MICHELIN tires, the difference in the carcass stiffnesses for the treaded and the buffed tires was relatively small, particularly at

the higher inflation pressure (Table C.1b). Also, it should be noted that the carcass stiffness of the smaller tires (i.e. GOODYEAR 7.00-16LT and MICHELIN 7.00R-16XCL) at the higher inflation pressures were slightly larger than those of the larger ones (i.e. MICHELIN 11.00R-16XL and MICHELIN 12.5R-16XLM), due to the larger inflation pressure for the smaller tires, regardless of the tread; nevertheless the situation was reversed when the lower inflation pressure was considered.

The average contact pressures at both the lower and the higher inflation pressures for each buffed tire such as GOODYEAR 7.00-16LT, MICHELIN 7.00R-16XCL and MICHELIN 11.00R-16XL were nearly identical, despite the large difference in carcass stiffness for the lower and the higher inflation pressures as shown in Table C.1b. Such a result implies that the carcass stiffness is not a significant factor on the average contact pressure (as well as axle displacement on clay) for the three buffed tires, while obviously there would have been no influence from tread and size of tire either. In the case of the treaded tires, since there was a distinct difference in the average contact pressure at the lower and the higher inflation pressures for each tire, except MICHELIN 11.0R-16XL, a little more detail about the results will be given for each tire in the following.

GOODYEAR 7.00-16LT

For the GOODYEAR 7.00-16LT, the average contact pressure of the treaded tire at the lower inflation pressure was almost the same as

that obtained for the buffed tire at the lower and the higher inflation pressures, while the one for the treaded tire at the higher inflation pressure became notably higher as the load increased (Fig. D.5a).

These results imply that the presence of tread for the lower inflation pressure has little importance on the results; yet, the tread could be an important factor only when the inflation pressure is at least higher than 310.5 kPa.

MICHELIN 7.00R-16XCL

As stated previously (Fig. D.5b), the average contact pressures at the lower and the higher inflation pressures for the buffed tire were almost identical. In the treaded tire, the results were highly sensitive to the change of inflation pressure, and they were much higher than those obtained for the buffed tire. Also, the average contact pressure of the treaded tire at the lower inflation pressure was higher than that for the higher inflation pressure. These results suggest that, in the case of the MICHELIN 7.00R-16XCL, the presence of tread, i.e. the physical and the geometrical properties of lugs, seemed to have become more dominant factors when compared with the carcass stiffness. It should be noted that the gap between the average contact pressures for the treaded and the buffed tires tended to become narrower as the inflation pressure became higher, as shown in Fig. D.5b. Such a result implies that the two factors, the tread and the carcass stiffness, would be equally important at the higher inflation pressure.

MICHELIN 11.0R-16XL

All the average contact pressures of the MICHELIN 11.00R-16XL tested under all conditions were almost identical (Fig. D.5c). Such a result was the exception among the results obtained for all the tires. There could have been little influence on the results from the physical property of the tread and the inflation pressure. The result may have been obtained partly due to factors such as the size of the tire, which is much larger, the size of the tread and the distance between the lugs.

MICHELIN 12.5R-16.5XLM

At the higher inflation pressure, the carcass stiffness was observed to be clearly the dominant factor, thereby resulting in nearly identical average contact pressure (Fig. D.5d). On the contrary, there was a visible difference in the average contact pressure at the lower inflation pressure for the treaded and the buffed tires. Such results are attributed to both the carcass stiffness and the tread. For the buffed tire, however, the smaller difference was seen in the average contact pressures at the lower and the higher inflation pressures, as compared with the results obtained for the treaded tire. In the case of the buffed tire, the average contact pressure at the lower inflation pressure could become closer to the one at the higher inflation pressure, if the present lower inflation pressure, 34.5 kPa, is even lowered, as what had happened to the average contact pressures obtained for the buffed tires of GOODYEAR 7.00-16LT, MICHELIN 7.00R-16XCL and MICHELIN 11.00R-16XL.

CONCLUDING REMARKS ON AVERAGE CONTACT PRESSURE ON CLAY

The variation of average contact pressure on clay for each different tire was discussed by considering factors such as carcass stiffness, the existence of tread and the size of tire. The influences of these factors were then studied for each interaction when the tire is either treaded or buffed. The concluding remarks can be stated as follows:

(1) The carcass stiffness is an important factor, but not a dominant factor as it was for the tire-rigid base interaction, i.e. the stiffer tire did not produce the higher average contact pressure,

(2) Among the four different types of tires, the change in inflation pressure for all the buffed tires, with the exception of MICHELIN 12.5R-16.5XLM, influenced very little the average contact pressure; in the case of the buffed MICHELIN 12.5R-16.5XLM, the gap between the average contact pressures for the lower and the higher inflation pressure would possibly become narrower if the higher inflation pressure were increased, thus implying that both the carcass stiffness and the size of tire could be negligible for every buffed tire whose inflation pressure is at a certain level,

(3) The tread tended to become either a non-negligible or a dominant factor when the inflation pressure was raised,

(4) The average contact pressures for the group of smaller tires (i.e. GOODYEAR 7.00-16LT and MICHELIN 7.00R-16XCL) were shown to be larger than those for the group of larger tires (i.e. MICHELIN

11.00R-16XL and MICHELIN 12.5R-16.5XLM),

(5) The treaded, smaller tires at higher inflation pressure clearly showed the higher average contact pressures,

(6) The average contact pressures for the smaller tires, such as the treaded and buffed GOODYEAR 7.00-16LT and the treaded MICHELIN 7.00R-16XCL at the lower inflation pressure exceeded their own lower inflation pressure as the load increased.

3.6.4 Contact Pressure Distribution Along Tire-Supporting Clay Interface

The contact pressures at selected points across the tire-supporting clay were measured by soil stress gauges (Fig. D.23). Due to the limited number of soil stress gauges available (a maximum of 4 gauges) the data obtained were interpreted by assuming that the contact pressures were symmetrically distributed across the tire-clay contact surface. Thus contours of equal contact pressures (i.e. isobars) could be drawn, similar to the technique used in determining the contact pressure distribution along the tire-rigid base contact surface. The tires used in this test series and the test conditions imposed are listed in Table D.2, together with the figure numbers showing corresponding contours and profiles of contact pressures of the tires. In general, two inflation pressures were applied in both treaded and buffed tires. A high inflation pressure was chosen such that the tire deflection was small when measured on a rigid base, while a low inflation pressure was selected to produce the opposite

effect. The wheel load applied was adjusted so that the tire sank sufficiently deep into the clay, simulating an actual operation mode.

Because of the size of the soil stress gauge (2 inches in diameter) in comparison with the lug sizes with small openings (Fig. 3.1), the contact pressures were measured directly under the lugs (or ribs) in treaded tires. For simplicity, the contours of contact pressures were drawn over the entire contact surface, not only over the lug or rib surface. Thus, if the contact pressure shown was integrated over the entire contact surface, the resulting force would undoubtedly be higher than the applied load. A correction could be made by introducing the ratio of the lug (or rib) area to the total (or gross) contact area as shown in Table C.3 (or Tables C.2a-h).

GOODYEAR 7.00-16LT

The footprints of the treaded tire GOODYEAR 7.00-16LT were roughly rectangular due to the strong ribs (Figs. D.6a and D.7a) unlike those of the buffed counterpart which were more or less eliptical (Figs. D.8a and D.9a). Using the low inflation pressure of 34.5 kPa in the treaded tire, the contact pressure intensified near the periphery of the contact area and dropped at the center (Figs. D.6a and b). The average contact pressure of 48.8 kPa was obviously less than the maximum value of 70 kPa measured underneath the tread (Fig. D.6b), while the central region of the contact area experienced approximately the same contact pressure as the applied inflation pressure. This might be attributed to the possibility that the tire deflects around its center. Such a result would be chiefly related to

the relativity between the bending stiffness of tire membrane and the deformability of the supporting clay, and could have occurred due to the increasing stiffness of clay as the applied load was raised. The causes regarding such pressure, which were also observed in most of the tire-rigid base interactions, were discussed in greater detail in the previous section. The high contact pressure around the periphery of the contact area was probably caused by the strong ribs and the stiffness of the circumference (in the vertical longitudinal plane).

When the inflation pressure was high in the treaded GOODYEAR 7.00-16LT (i.e. 310.5 kPa), the contact pressures were high and concentrated around the central region (Figs. D.7a and 7b), unlike the contact pressure distribution observed in the same tire using lower inflation pressure (Figs. D.6a and b). Since the tire deflection should be low, the tire should considerably deform the supporting clay, particularly at its center. The clay therefore underwent high deformation, leading to high resisting stress (Fig. D.1).

Similar pressure distribution patterns were exhibited by the buffed tire GOODYEAR 7.00-16LT (Figs. D.8a-c and D.9a-c). The effects of inflation pressure on the pressure concentration were comparable to those observed in the treaded counterpart (Figs. D.6a-b and D.7a-b). The fact that the contact pressure underneath the buffed tire could be higher than the inflation pressure indicated the contribution of the carcass stiffness. Without the presence of strong ribs, the high intensity of contact pressure around the periphery of the contact area was not as discernable as that found in the treaded tire.

MICHELIN 7.00R-16XCL

The test conditions imposed on MICHELIN 7.00R-16XCL are listed in Table D.2 while the pressure distributions across the footprints are illustrated in Figs. D.10-D.13. The contact pressures measured underneath the lugs of the treaded tire were noticeably higher than the calculated average contact pressure, because of the difference in the contact area considered. With a low inflation pressure of 34.5 kPa, the contact pressures intensified near the periphery of the contact area (Figs. D.10a-c), accompanied by a sharp drop at the central region. When compared with the same tire inflated to a higher pressure (310.5 kPa) in Figs. D.11a-c, the contact pressures measured around the center of their contact surfaces were lower. This should be attributed to the higher tire deflection in the treaded tire with the low inflation pressure. The maximum contact pressures measured in both test conditions were approximately in the same range of 150-160 kPa. The pressure distributions observed in the treaded tire MICHELIN 7.00R-16XCL were similar to those found in the treaded tire GOODYEAR 7.00-16LT (Figs. D.6, D.7, D.10 and D.11).

When the buffed tire was inflated at a low pressure of 34.5 kPa, the maximum contact pressure was measured to be approximately the same as the inflation pressure (Figs. D.12a and b). The contact pressures measured around the central area were, however, lower than the inflation pressure. It was likely that the tire deflection in the supporting clay was quite high. By increasing the inflation pressure to 310.5 kPa in the buffed tire, all contact pressures measured were much lower than the inflation pressure (Figs. D.13a and b), the

maximum value being about 45 kPa. Furthermore, the contact pressures underneath the buffed tire were also lower than those measured beneath the treaded tire (Figs. D.10 and D.11). Evidently the lugs of the treaded tire caused stress concentration in the clay underneath.

MICHELIN 11.00R-16XL

The wheel loads and inflation pressures used in determining the contact pressures at the tire-clay interfaces of the tire MICHELIN 11.00R-16XL are shown in Table D.2 while the contours and profiles of the contact pressure distribution are depicted in Figs. D.14-D.17. Using the low inflation pressure of 34.5 kPa, the contact pressure of the button-treaded tire was high at the center of the contact area and decreased towards the periphery (Figs. D.14a and b). All the contact pressures measured were higher than the inflation pressure applied (i.e. 34.5 kPa). Without the saddle-shaped pressure distribution found in the previous two tires (i.e. GOODYEAR 7.00-16LT and MICHELIN 7.00-16XCL), it is likely that the treaded MICHELIN 11.00R-16XL did not deflect significantly in clay even though the inflation pressure applied (34.5 kPa) was very low when compared with the recommended value (550 kPa or 80 psi as shown in Table 3.1). This should be attributed to the highest ply rating of MICHELIN 11.00R-16XL (Table 3.1), which indicated high carcass stiffness. Similar pressure distribution was displayed by the same tire when a higher inflation pressure of 207 kPa was applied (Figs. D.15a and b). The maximum contact pressure (about 100 kPa in Fig. D.15a) was however higher than that measured in the softer tire (about 80 kPa in Fig. D.14a).

After removing the tread in MICHELIN 11.00R-16XL, the pressure distributior that exhibited high intensity near the periphery of the contact area could be observed as illustrated in Figs. D.16 and D.17. When the low inflation pressure value of 34.5 kPa was used, the contact pressure reached a maximum of about 55 kPa and concentrated closed to the longitudinal edge of the contact area (Figs. D.16a and b). The contact pressure at the center of the contact area was about 25 kPa which was less than the inflation pressure (34.5 kPa), possibly indicating high tire deflection. Increasing the inflation pressure to 207 kPa, the high intensity of the contact pressure moved closer to the center of the contact area (Figs. D.17a and b). However, the resulting maximum pressure (about 33 kPa) was less than that generated by the lower inflation pressure of 34.5 kPa. This likely reflects the high carcass stiffness of MICHELIN 11.00R-16XL which should contribute substantially to resist the wheel load, particularly in the vertical longitudinal plane in the case of low inflation pressure. The tire behaved like a flexible foundation with strong stiffening structures at its edge. When the inflation pressure was increased the tire deflected less causing the tire carcass in all directions to contribute more to resisting the wheel load.

MICHELIN 12.5R-16.5XLM

The test conditions adopted for determining the contact pressures of the tire-clay interfaces of MICHELIN 12.5R-16.5XLM are given in Table D.2. The contours of equal contact pressures and the corresponding profiles are illustrated graphically in Figs. D.18-D.21.

In the treaded tire, the saddle-shaped pressure distribution pattern was obtained in both low and high inflation pressures (Figs. D.18a and b, D.19a-c). In the case of low inflation pressure (i.e. 34.5 kPa), the maximum contact pressure (about 45 kPa) was slightly higher than the applied inflation pressure (Figs. D.18a and b). By contrast, the contact pressures were significantly less than the inflation pressure of 207 kPa in the other treaded tire (Figs. D.19a-c). Such behaviour should be attributed to the combined influences of inflation pressure, carcass stiffness and tread.

Without tread, the buffed tire MICHELIN 12.5R-16.5XLM displayed a parabolic-like distribution pattern in the measured contact pressures (Figs. D.20 and D.21). It is likely that there was an insignificant amount of tire deflection occurring even though a low inflation pressure of 34.5 kPa was introduced. The contribution of the button lugs in the treaded tire to resisting the wheel load seemed to be the major factor governing the difference in the pressure distribution observed in the treaded and buffed tires.

Effect of Wheel Load on Pressure at Center of Contact Surface for Clay

An additional series of experiments was performed to investigate the effect of wheel load on the contact pressure at the tire-clay interface. For direct comparison among the tires studied only the contact pressure at the center of the contact area was measured for every tire to provide the basis of the contact pressure - wheel load relationship. It should be recalled that the contact pressure at the center of the contact surface is not necessarily the highest; the

contact pressure distributions were mostly saddle-shaped. For the same tire inflated at a specific inflation pressure, the variation of the referenced contact pressure with wheel load should be indicative of the changes in the contact pressures at other points in the contact surface.

The relationships of the referenced contact pressure and wheel load for all tires studied are shown in Figs. D.22a-d. In the treaded GOODYEAR 7.00-16LT, the contact pressure measured at the center of the tire-clay interface decreased with increasing wheel load (Fig. D.22a). The high inflation pressure of 310.5 kPa generated higher contact pressure than the low inflation pressure of 34.5 kPa, indicating the influence of tire flexibility and sinkage. Similarly, as the wheel load increased, both tire flexibility and sinkage increased leading to the saddle-shaped pressure distribution (Figs. D.6 and D.7). In addition, the actual contact area of the treaded tire increased as the tire sinkage increased since the clay was squeezed into the grooves and touched the tire carcass.

Without tread, the high inflation pressure of 310.5 kPa caused the contact pressure to drop with increasing wheel load in agreement with the treaded tire. However, the soft buffed tire (34.5 kPa inflation pressure) demonstrated only a slight variation in the contact pressure resulting from higher tire sinkage (Fig. D.2a) and contact area (Fig. D.3a).

The 'stiff' and 'soft' conditions of the buffed tire MICHELIN 7.00R-16XCL behaved differently as shown in Fig. D.22b. The 'soft'

condition induced by the low inflation pressure of 34.5 kPa led to lower contact pressure when the wheel load was higher. This was opposite to the behaviour of the 'stiff' condition produced by the high inflation pressure of 310.5 kPa, probably because the increase in tire sinkage affected the contact pressure more than the increase in contact area. In MICHELIN 11.00R-16XL, only the treaded tire exhibited an increase in the contact pressure following an increase in wheel load (Fig. D.22c). However, the contact pressure under the treaded tire with the low inflation pressure of 34.5 kPa was reduced after the wheel load was increased to more than 3.2 kN. Unlike other tires tested, the contact pressure of MICHELIN 12.5R-16.5XLM measured at the center of the tire-clay interface varied from about 20 kPa to about 150 kPa, covering a wider range (Fig. D.22d). The contact pressure changed slightly with increasing wheel load. The effects of tread in MICHELIN 12.5R-16.5XLM on contact pressure appeared to contradict those observed in other tires since the treaded tire generated less contact pressure than the buffed tire using similar inflation pressure and wheel load. This could be explained by the difference in the pressure distribution between the treaded and buffed tires. In the treaded tire, the pressure distribution exhibited a saddle-shaped pattern (Figs. D.18 and D.19) while the buffed tire showed a parabolic-like pressure distribution. Thus the contact pressure at the center of the contact surface in the treaded tire was not the highest, unlike that of the buffed tire. It can be noticed that a wide variation existed in all tires such that conclusive trends could hardly be established to cover all factors involved.

3.7 Discussion and Remarks on the Experimental Results of Tire-Supporting Sand Interactions

3.7.1 Axle Displacement Characteristics of Tires on Sand

Similar to the study of axle displacements of tires on clay (Section 3.6), all the tires used in this research were loaded statically on the No. 16 silica sand contained in the soil bin in order to measure the resulting axle displacements. For selected wheel loads and inflation pressures, contact areas were measured together with contact pressures following the procedures described in Section 3.3. The use of sand made it possible to compare the performances of tires under two different types of supporting ground, i.e. cohesive clay and cohesionless sand.

The wheel load-axle displacement relationships of the tires studied are presented in Figs. E.2a-d. All tires shared similar behaviour. The axle displacement increased as higher wheel load was applied and the axle displacement of the tire was significantly higher when the inflation pressure was decreased. In comparison, the axle displacement of the treaded tire was lower than that of the buffed tire using the same inflation pressure and wheel load. The contact pressure underneath the lug should be higher than the contact pressure underneath the buffed tire because of the lower actual contact area. In consequence, the strain (or displacement) underneath the lug should be higher (Fig. E.1). The behaviour of the tire resting on sand should be better understood from the measurement of contact pressure distribution presented in the next section.

3.7.2 Contact Pressure Distribution at the Tire-Sand Interface

Following the procedures described in Section 3.3, the contact pressure distributions across the contact area between tire and sand were determined for all the tires studied. Each tire was tested by using two inflation pressures to produce a 'stiff' tire (i.e. high inflation pressure and low tire deflection) and a 'soft' tire (i.e. low inflation pressure and high tire deflection).

GOODYEAR 7.00-16LT

The test conditions imposed on the tire GOODYEAR 7.00-16LT are listed in Table E.1 which includes the width and the length of a rectangular representative contact area for the actual contact area. The contact pressure distributions for both treaded and buffed conditions are illustrated in Figs. E.3-E.6. Using the same wheel load of 3.548 kN in the treaded tire, the resulting contact area of the 'stiff' tire (310.5 kPa inflation pressure) was about 20% less than that of the 'soft' tire (34.5 kPa inflation pressure) as shown in Table E.1. In consequence, the maximum contact pressure measured underneath the soft tire (190 kPa, Figs. E.3a and b) was less than that generated by the stiff tire (280 kPa, Figs. E.4a and b). The decrease in the tire-sand contact area caused by nigher inflation pressure coincided with the response of the axle displacement displayed in Fig. E.2a. Evidently the carcass stiffness contributed to such behaviour of the tire resting on sand. It was likely that the stiff tire could develop high contact pressure in sand because of its high stiffness and the high load resistance of sand. Since the

strength of the sand depended considerably on the applied normal stress (Fig. E.1), higher resistance to the applied wheel load could be generated by the sand due to high contact pressure. In the soft tire, high contact pressure would deflect the tire carcass leading to an increase in contact area. Without tire deflection, high contact pressure could be generated at the tire-sand interface because of the dependence of the sand strength on confining pressures. Such behaviour was similar to the case of tire-clay interaction (Section 3.6), although the clay was less compressible and its strength was less dependent on the confining pressures (Fig. D.1).

In the treaded tire, it is noticeable that the highest contact pressure concentrated close to the sides of the tire in both inflation pressures (Figs. E.3 and E.4). As with the same tire conditions in clay, the contact pressure in clay intensified close to the longitudinal edge of the contact area (Figs. D.6 and D.7). The presence of stiff side-ribs in GOODYEAR 7.00-16LT and the sand characteristics should be the major contributing factors. Buffing the tread caused the contact area configuration to change from the rectangular-like shape observed in the treaded tire to the elipse-like shape exhibited by the buffed tire (Figs. E.5 and E.6). In the soft tire with the low inflation pressure of 34.5 kPa, high contact pressure centered around the longitudinal edge of the contact surface (Figs. E.5a and b), reflecting high tire deflection. The stiff buffed tire with the high inflation pressure of 310.5 kPa behaved similar to the treaded tire in that the contact pressure intensified near the

sides of the tire. Thus the saddle-shaped pressure profile in the transverse direction of the contact area was more noticeable in the stiff tire.

The average ground contact pressure calculated for the treaded tire was about one-third to one-fourth of the maximum contact pressure measured (Figs. E.3 and E.4). However, the average contact pressure was about half of the maximum contact pressure measured in the buffed tire (Figs. E.5 and E.6). Thus the contact pressure was more uniformly distributed in the buffed tire due to the absence of tread.

MICHELIN 7.00R-16XCL

The applied wheel load and the inflation pressure used in the experiment are listed in Table E.1. The contact area decreases as inflation pressure increases. This results in a lower contact pressure in the soft tire (with a low inflation pressure of 34.5 kPa), comparing Figs. E.7 and E.8. A high intensity of contact pressure was observed to be concentrated along the sides of the contact surface at both inflation pressures. The maximum contact pressure was more than twice the contact pressure at the center of the contact surface, resulting in sharp peaks in the saddle-shaped pressure distribution pattern (Figs. E.7b and E.8b).

A similar pressure distribution was exhibited by the buffed tire using both low and high inflation pressures (Figs. E.9 and E.10). The maximum contact pressure of the soft tire, about 130 kPa (Figs. E.9a and b), was higher than that of the stiff tire (about 104 kPa - Figs. E.10a and b). This may be attributed to the high carcass stiffness at

low inflation pressure, as with the treaded tire using the same inflation pressure.

MICHELIN 11.0R-16XL

The test conditions imposed on the tire MICHELIN 11.00R-16XL are shown in Table E.1. The contact area of the soft tire with the low inflation pressure of 34.5 kPa was higher than the stiff tire with the high inflation pressure of 207 kPa (Table E.1). In effect, the maximum contact pressure measured in the soft tire (220 kPa, Figs. E.11a and b) was lower than that developed by the stiff tire (280 kPa, Figs. E.12a and b). In the soft tire, the contact pressure intensified near the periphery of the contact surface (Figs. E.11a and b), reflecting the contribution of tire carcass to resisting the wheel load when the tire deflection was high. The high intensity of the contact pressure measured in the stiff treaded tire centered around the sides of the tire, resulting in sharp peaks in the saddle-shaped pressure distribution pattern (Figs. E.12a and b). The average contact pressures calculated for both tires were about one-fifth of their maximum values.

Without tread, the contact pressure was highest in the soft buffed tire with the low inflation pressure of 34.5 kPa (Figs. E.13 and E.14). This could be attributed to high carcass stiffness and tire deflection when the inflation pressure was low. Although the pressure distribution was saddle-shaped, the difference between the peak and the central values was small (Figs. E.13a and b, E.14a and

b). The average contact pressure was about half of the contact pressure at the center of the contact area.

MICHELIN 121.5R-16.5XLM

Table E.1 lists the test conditions employed in determining the contact pressure distribution at the tire-sand interface of the tire MICHELIN 12.5R-16.5XLM. In the treaded tire, the pressure distribution pattern was similar in both low and high inflation pressure (Figs. E.15 and E.16). When the inflation pressure was low, the peak values of the saddle-shaped pressure distribution pattern were significantly higher than the central values (Figs. E.13a and b). Such a difference was much less in the treaded tire using the high inflation pressure of 207 kPa (Figs. E.16a-c). Since the contact area of the soft tire was slightly higher than that of the stiff tire (Table E.1), the maximum contact pressure measured in the former was approximately half that of the latter.

A similar pressure distribution pattern was found in the buffed tire employing both low and high inflation pressures (Figs. E.17 and E.18). In the soft tire, the effect of high carcass stiffness and high tire deflection was more pronounced (Figs. E.17a and b). The stiff tire produced much less contact area than the soft tire (Table E.1), leading to a much higher contact pressure (Figs. E.18a and b). The contribution of the tire carcass stiffness to resisting the applied wheel load was less significant in the stiff tire.

3.8 Summary and Remarks on the Experimental Results of Tire-Soil Interations

From the study of the interactions between pneumatic tires and soils (clay and sand) under static conditions, the following conclusions can be made:

a. The contact pressure distribution across the tire-soil contact area is highly irregular, particularly in treaded tires. However, an approximate outline of contact pressure distribution can be drawn by assuming that the contact pressure is symmetrically distributed with respect to the longitudinal axis of the tire-soil contact area.

b. In general, the contact pressure distribution at the tire-soil interface is saddle-shaped where the peak value occurs near the periphery of the contact area. The differences between the peak value and the central value of the contact pressure intensity is dependent primarily on inflation pressure, load, tire carcass stiffness, tread, and soil type.

c. When the inflation pressure is sufficiently low to cause significant tire deflection in soil, the tire carcass stiffness contributes considerably to resisting the applied wheel load.

d. The effects of tread on the intensity and the distribution of contact pressure at the contact area are not significant in soft clay. The presence of tread normally intensifies the contact pressure at the tire-sand interface when

compared to a smooth tire surface.

e. In sand, the contact area is generally reduced when the inflation pressure is increased due to the high rate of strength increment with increasing strain (i.e. high stiffness) in sand.

f. Because of the complex interaction between tire and soil, it is difficult to predict the contact pressure distribution of the tire-soil interface. The major factors contributing to the development of contact area and contact pressure are tire-soil relative stiffness, inflation pressure, carcass stiffness, tread, soil characteristics and wheel load. Tire construction in terms of bias-ply or radial-ply arrangement cannot be deduced from observations of contact pressure distribution.

CHAPTER 4

FIRST ANALYTICAL APPROACH FOR SLIDING INTERACTION PROBLEMS: APPLICATION TO A PNEUMATIC TIRE - SUPPORTING CLAY AND A PNEUMATIC TIRE - RIGID BASE INTERACTION PROBLEMS

4.1 Introduction

In Chapter 2 one sees how complex an interaction problem becomes when it involves a pneumatic tire as an interacting body, where the tire is an inflated one, consisting of a rim (metal) and a toroidal (stiff) shell-shaped membrane (orthotropic and highly deformable material). In this chapter a two-dimensional analytical approach is developed to solve such interaction problems, i.e. tire-supporting clay and tire-rigid base interactions, where a tire is subjected to either a static vertical axle load or an inclined axle load so that a tire slides quasi-statically over another body.

The present analytical approach is developed in Sections 4.3 and 4.4, while Section 4.2 gives a little more elaborate review of the complex variable method in deriving useful equations which are necessary for the present analytical approach. A scheme for the analytical approach with the flow diagram is then given in section 4.5. In the final section 4.6 various interaction problems for tire-supporting clay and tire-rigid base interactions will be solved using the present approach.

A basic idea for the present analytical approach is to transform an original tire-supporting clay into an equivalent free boundary problem (section 4.3) by considering contact profiles in order that

complicated physical and geometrical properties of a tire will not directly come into an analysis. Then such a free boundary problem can be solved by virtue of the complex variable-based contact analysis (Method 7 in section 4.2), which is basically developed for a contact problem between two linearly elastic solids, provided that an elastic modulus of deformed supporting clay is obtained in conjunction with some experimental data on tire-clay interactions (section 4.4).

In the case of tire-rigid base interaction problems, the same analytical approach can be applied by assuming that a rigid base is deformable. In other words, the original rigid base, interacting with a tire, is simulated by a "nearly" rigid base (section 4.3) whose elastic modulus with a corresponding contact profile is also obtained (section 4.4).

In both cases, the supporting clay and nearly rigid base are assumed to be elastic, homogeneous and istropic.

The reasons for choosing the complex variable method, reviewed in Chapter 2, as the basic mathematical tool which plays an important role in the present analytical approach, are restated as follows:

(i) any complicated contact profiles can be approximated by polynomials,

(ii) the authors feel that seeking a sectionally holomorphic function (or a complex potential) obtained from a Riemann-Hilbert problem governing a contact problem, which will finally give a contact pressure distribution and contact

area (i.e. contact length), is easier than the equivalent singular integral equation, and

(iii) such a sectionally holomorphic function, which will be called a standard defining function in the theory of hyperfunctions (or Sato distributions) [53,60,61,85], can represent a wider class of contact pressure distributions due to its relation to the definition of hyperfunction although this property of the function will be of little interest in the present interaction problems. Besides, the foundation of hyperfunctions was well established in the application.

4.2 Complex Variable Analysis for a Sliding Contact Problem Between a Solid with a Smooth Profile and a Half-Plane

4.2.1 Preliminary

Our main purpose in this section is to obtain closed form solutions (refer to Appendix A) for a force equilibrium equation, contact pressure distribution and contact area for a sliding contact problem between a linearly elastic solid and a half-plane by virtue of the complex variable method (details given in section 9 of Appendix A). The force equilibrium equation so obtained is then, as explained at step 3 in the introduction and more details in section 4.4, employed to define a formula of elastic modulus for the half-plane at each deformed state which is given by a function of load, slope of contact profile, Poisson's ratio and an elasticity measure whose definition is given in section 4.4.

Muskhelishvili [86] showed a way of solving a sliding contact problem, where a rigid solid is assumed to slide quasi-statically on a linearly elastic half-plane, based on the complex variable method. His approach will be applied to a contact problem, as shown in Fig. 4.1, where a linearly elastic solid S_2 slides over the half-plane which is either rigid or linearly elastic. We will then show the complete solutions for this problem, in a case where the undeformed profile of a solid S_2 is approximated by a polynomial of the second and the fourth order, at the end of this chapter. More details of this method are also given in section 9 of Appendix A, and the complete solutions of the problem, where the undeformed profile of solid S_2 is given by a polynomial of the second and/or the fourth order, can be found in section 9.4 of Appendix A. The results so obtained can certainly be applied to a case where the solid S_2 is rigid and the half-plane S_1 is linearly elastic.

This section (details given in Appendix A), consists of three subsections as follows:

Section 4.2.2 - stresses and rotations in a deformed half-plane can be represented by a complex function, so-called sectionally holomorphic function, defined in entire complex domain except on an interval of the real axis, with the assumption that there are no body forces present.

Section 4.2.3 - the sliding contact problem is then transformed into a problem called the Riemann-Hilbert problem whose solution happens to be sectionally holomorphic.

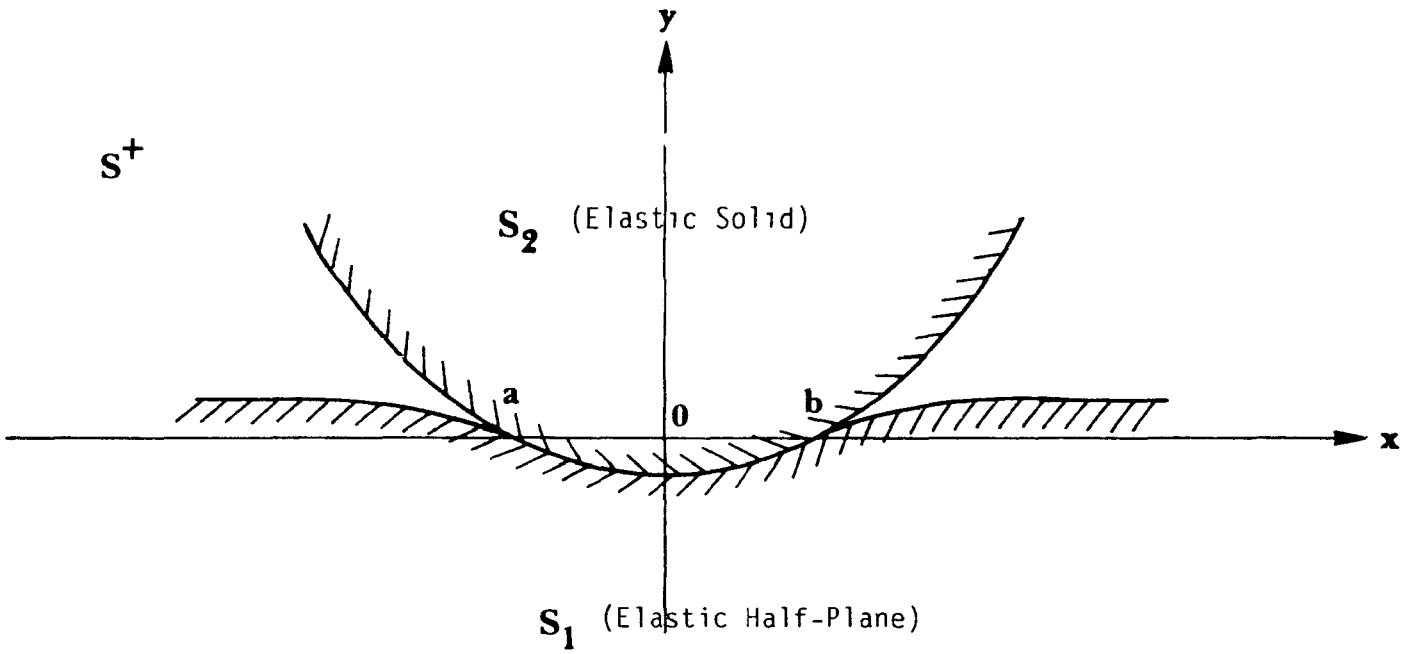


Fig. 4.1 An Elastic Solid Sliding Quasi-Statically Over an Elastic Half-Plane

Section 4.2.4 - the general solution of the Riemann-Hilbert problem is simply stated, from which various sliding contact problems can be solved provided that the material constants, coefficient of friction and undeformed profiles of contacting solids are given a priori.

We will first introduce the notations used in Fig. 4.1. Let $L = (a,b)$ and the arc $\overset{\frown}{ab}$ be, respectively, the nominal contact surface, being an open interval on the real axis, and the true contacting surface, being a boundary of contacting solids S_2 and S_1. The notations S^+ and S^- are respectively, the upper and the lower half-planes of the complex plane, i.e.

$$S^+ = \{x + iy : y > 0\} \text{ and } S^- = \{x + iy : y < 0\}$$

All the materials and the results related to the development of the analytical approach are compactly described while referring to Appendix A.

4.2.2 Stresses and Rotations in a Half-Plane Represented by a Complex Function

In this subsection we define a complex function, so-called sectionally holomorphic function (or sometimes also called complex potential), which can represent stresses and rotations in a deformed half-plane S^-. Before defining such a function, we will first simply show that stresses and displacements in an arbitrary simply-connected open domain R can be determined by virtue of two holomorphic functions. There are basically two ways of developing these two

functions: One is due to the stress formulation in elasticity problems (i.e. stresses unknown) considering the translational equilibrium equation and the Beltrami-Michel stress compatibility equations, while the other is due to the displacement formulation (i.e. displacements unknown) considering the Navier space equilibrium equations and the stress-displacement equations [34,78].

By choosing the way based on the stress formulation, we will review two distinct approaches in establishing the relationships between stresses (or displacement) and two holomorphic functions for the arbitrary open domain R. The first approach, described in (A), is largely attributed to the work done by Muskhelishvili [86], as shown in Appendix A, while the second one in (B) is developed by virtue of the tensor analysis employed in the theory of complex variables which is applied for linear elasticity problems by Green and Zerna [45] and for finite elasticity problems by Green and Shield [44] and Adkins, Green and Shield [2].

(A) The First Approach Determining the Relationships Between Stresses (or Displacements) and Two Holomorphic Functions

In a two-dimensional elasticity problem where no body forces are present, the introduction of an Airy stress function is reduced to a problem of seeking a biharmonic function (i.e. Airy stress function) for a deformed, simply-connected smooth open domain R with an arbitrary profile, as shown in standard text and reference books [34,45,46,78,129] on linear elasticity or in Appendix A. Referring to Appendix A, it is shown in Eq. A.4b as,

$$D^4 U(X) = D^2(D^2U(X)) = 0 \qquad X = (x,y) \in R \tag{4.1}$$

where D^2 is the Laplacian operator under the rectangular Cartesian coordinate system, i.e. $D^2 = \partial/\partial x + \partial/\partial y$; the function $U(x,y)$ is the biharmonic function; $(\underline{\cdot})$ denotes a vector quantity; the symbol "$\in$" means "belongs to" so that "$X \in R$" means "a point $X = (x,y)$ belongs to the open domain R".

The solution of Eq. 4.1 is shown to be

$$U(x,y) = x\Gamma(x,y) + y\boldsymbol{\theta}(x,y) + \Lambda(x,y) \tag{4.2}$$

where Γ, $\boldsymbol{\theta}$ and Λ are harmonic functions in R, i.e. $D^2\Gamma = D^2\boldsymbol{\theta} = D^2\Lambda = 0$

The solution U can then be represented in terms of complex functions as follows. First putting $D^2 U = P$, then there is a holomorphic function $f(z)$,

$$f(z) = P + iQ \qquad (i = \sqrt{-1}) \quad z \in R \tag{4.3}$$

where z is a complex variable, i.e. $z = x + i\,y$ and Q is a harmonic conjugate of P.

Next let $\phi(z)$ be another holomorphic function such that

$$f(z) = 4\, d\phi(z)/dz = 4\phi'(z).$$

One then obtains,

$$\phi(z) = \frac{1}{4} \int^z f(z)\, dz = p + i\,q \qquad z \in R \tag{4.4}$$

Since $\phi(z)$ is holomorphic, p and q are also harmonic in R, one obtains the following results by considering the Cauchy-Riemann equations.

$$\left.\begin{aligned} D^2 p = D^2 q = 0 \qquad & X \in R \\ \text{and} \quad \frac{\partial p}{\partial x} = \frac{\partial q}{\partial y} = \frac{1}{4} D^2 U = \frac{P}{4} \qquad & X \in R \end{aligned}\right\} \tag{4.5}$$

since

$$\frac{d\phi}{dz} = \phi'(z) = \frac{\partial p}{\partial x} + i \frac{\partial q}{\partial x} = \frac{1}{4} f(z) \tag{4.6}$$

We then can define another harmonic function p_1 by

$$p_1 = U - xp - yq \tag{4.7}$$

such that

$$D^2 p_1 = D^2 (U - xp - yq) = 0$$

hence obtaining the biharmonic function

$$U = xp + yq + p_1 \tag{4.8}$$

Now, if we put q_1 to be a harmonic conjugate of p_1, then one obtains another holomorphic function ψ as

$$\psi = p_1 + i q_1 \tag{4.9}$$

We finally obtain the biharmonic function U by means of two holomorphic functions $\phi(z)$ and $\psi(z)$ by considering Eq. 4.8 as follows:

$$U = \mathrm{Re}\,[\bar{z}\phi(z) + \psi(z)] \qquad z \in R \tag{4.10}$$

or

$$2U = \bar{z}\phi(z) + z\bar{\phi}(\bar{z}) + \psi(z) + \bar{\psi}(\bar{z}) \qquad z \in R \tag{4.11}$$

where Re [ ] stands for the real part of functions in [ ]; $\bar{z}$ is the complex conjugate of z, i.e. $\bar{z} = x - i\,y$, and $\bar{\phi}(\bar{z})$ (or $\bar{\psi}(\bar{z})$) is the conjugate function of $\phi(z)$ (or $\psi(z)$), i.e. $\bar{\Phi}(\bar{z}) = \overline{\Phi(z)}$ since for an arbitrary complex function $G(z) = u(x, y) + i\,v(x, y)$, it is defined that $\bar{G}(z) = \overline{G(\bar{z})} = u(x, -y) - i\,v(x, -y)$.

Now considering the stress-strain relationship in Eq. A.3 (Appendix A), one obtains displacements as

$$u = \frac{1}{E'}\left\{4p - (1+\nu')\frac{\partial U}{\partial x}\right\} \tag{4.12a}$$

and

$$v = \frac{1}{E'}\left\{4q - (1+\nu')\frac{\partial U}{\partial y}\right\} \tag{4.12b}$$

where

$$E' = \frac{E}{1-\nu^2}, \qquad \nu' = \frac{\nu}{1-\nu} \qquad \begin{pmatrix} E = \text{elastic modulus} \\ \nu = \text{Poisson's ratio} \end{pmatrix}$$

Hence one obtains the following:

$$E' = (u + i\,v) = 4\phi(z) - (1+\nu')\left(\frac{\partial U}{\partial x} + i\,\frac{\partial U}{\partial y}\right) \qquad (4.13)$$

Introducing complex conjugates z, $\bar{z}$ as independent variables one finds the following relationships for the partial differentiations between the rectangular coordinates (x, y) and the complex conjugate coordinates $(z, \bar{z})$,

$$\frac{\partial}{\partial x} + i\,\frac{\partial}{\partial y} = 2\,\frac{\partial}{\partial \bar{z}}\,, \quad \frac{\partial}{\partial x} - i\,\frac{\partial}{\partial y} = 2\,\frac{\partial}{\partial z} \qquad (4.14)$$

Then in Eq. 4.13

$$\begin{aligned}\frac{\partial U}{\partial x} + i\,\frac{\partial U}{\partial y} = 2\,\frac{\partial U}{\partial \bar{z}} &= \frac{\partial}{\partial \bar{z}}\{\bar{z}\phi(z) + z\bar{\phi}(\bar{z}) + \psi(z) + \bar{\psi}(\bar{z})\} \\ &= \phi(z) + \overline{\phi'}(\bar{z}) + \overline{\psi'}(\bar{z}) \\ &= \phi(z) + \overline{\phi'(z)} + \overline{\psi'(z)} \end{aligned} \qquad (4.15)$$

Substituting Eq. 4.15 into Eq. 4.13,

$$2G(u + i\,v) = K\phi(z) - z\overline{\phi'(z)} - \overline{\psi'(z)} \qquad z \in \mathbf{R} \qquad (4.16)$$

where G is the shear modulus and $K = 3-4\nu$.

Equation 4.16 for displacements can be found in Eq. A.19. The stresses can also be found in a similar way by considering Eqs. 4.14, 4.15 and Eq. A.4a (Appendix A). One finally can find the

relationships between stresses and two holomorphic functions as follows:

$$T_{xx} + T_{yy} = 2\{\phi'(z) + \overline{\phi'(z)}\} = 4 \text{ Re } \{\phi(z)\} \quad z \varepsilon R \quad (4.17)$$

$$T_{yy} - T_{xx} - 2i\, T_{xy} = 2\,\{z\phi''(z) + \psi''(z)\} \quad z \in R \quad (4.18)$$

which are the same as those in Eqs. A.16" and A.17" (Appendix A).

(B) The Second Approach Determining the Relationships Between Stresses (or Displacements) and Two Holomorphic Functions (Based on the Complex Coordinate System)

Here the relationships between stresses (and displacements) and two holomorphic functions will be developed on the basis of the complex coordinates by virtue to tensor transformation, which will be rather useful for finite deformation problems.

We will initially consider the three-dimensional case for the sake of generalization since there is no particular difficulty compared with the two-dimensional case. Let us suppose every point in the deformed solid is defined by a set of Cartesian coordinates y^i = (i=1,2,3) with its corresponding complex conjugate coordinates $(z, \bar{z})$ and z^3 such that

$$z = y^1 + i\, y^2, \quad \bar{z} = y^1 - i\, y^2 \qquad (4.19)$$

and taking z^3 -axis to be parallel to the y^3 -axis so that $z^3 = 0$ corresponds to the plane $y^3 = 0$, i.e. $z^3 = y^3$.

Considering the contravariant tensor transformation of y^i , one sees that

$$z^1 = \frac{\partial z}{\partial y^m} y^m = \frac{\partial z}{\partial y} y^1 + \frac{\partial z}{\partial y^2} y^2 + \frac{\partial z}{\partial y^3} y^3 = y^1 + i\, y^2 = z$$

$$z^2 = \frac{\partial z}{\partial y^m} y^m = y^1 - y^2 = z \qquad (4.20a)$$

$$z^3 = \frac{\partial z^3}{\partial y^m} y^m = y^3$$

Accordingly, the complex conjugate coordinates $(z, \bar{z})$ with z^3 will be denoted by the coordinates z^i $(i=1,2,3)$ called complex coordinates so that

$$(z^1, z^2, z^3) = (z, \bar{z}, y^3) \qquad (4.20b)$$

Putting $\underline{b}_i$ and $\underline{b}^j$ to be the covariant and contravariant base vectors of the complex coordinates z^i , then the position vector $\underline{r}$ of a point of the deformed solid is written as

$$\underline{r} = z^1 \underline{b}_i = z_i \underline{b}^i \qquad (4.21)$$

where

$$\underline{b}_i = \left(\frac{\partial y^1}{\partial z^i}, \frac{\partial y^2}{\partial z^i}, \frac{\partial y^3}{\partial z^i}\right) \qquad (4.22)$$

and

$$\underline{b}^j = b^{jm}\,\underline{b}_m \qquad (b^{jm} = \text{contravariant metric tensor}) \tag{4.23}$$

The repeated indices such as "ı" in Eq. 4.21 and "m" in Eq. 4.23 will be summed on 1 and 2 unless stated otherwise.

Since the coordinates y^i can be expressed in terms of the coordinate z^i such as

$$y^1 = \frac{1}{2}(z^1+z^2),\quad y^2 = -\frac{i}{2}(z^1-z^2),\quad y^3 = z^3 \tag{4.24}$$

the base vector $\underline{b}_j$ will be obtained as follows,

$$\underline{b}_1 = (\tfrac{1}{2}, -\tfrac{i}{2}, 0),\ \underline{b}_2 = (\tfrac{1}{2}, \tfrac{i}{2}, 0),\ \underline{b}_3 = (0, 0, 1) \tag{4.25}$$

Hence the covariant metric tensor b_{ij} is defined as

$$b_{ij} = \underline{b}_i \cdot \underline{b}_j = \frac{\partial y^m}{\partial z^i}\frac{\partial y^m}{\partial z^j} = \begin{pmatrix} 0 & 1/2 & 0 \\ 1/2 & 0 & 0 \\ 0 & 0 & 1 \end{pmatrix} \tag{4.26a}$$

and the contravariant metric tensor b^{ij} is determined, by using the results of b_{ij}, as

$$b^{ij} = B^{ij}/b = \begin{pmatrix} 0 & 2 & 0 \\ 2 & 0 & 0 \\ 0 & 0 & 1 \end{pmatrix} \tag{4.26b}$$

where B^{ij} is the co-factor of b_{ij} and b is the determinant of b_{ij}, i.e. $b = |b_{ij}| = -1/4$, $(b)^{1/2} = 1/2$, $i = (-1)^{1/2}$.

Based on the materials obtained above for the complex coordinate system z^i, we will obtain an equation which turns out to be the biharmonic equation obtained in Eq. 4.10 in Cartesian coordinate system y^i. We now define the stress components referred to the complex coordinates z^i in the deformed solid by P^{mn}, and the corresponding stress components referred to the coordinates y^i by T^{ij}. Then by using the contravariant transformation: $y^i \to z^i$,

$$P^{mn} = \frac{\partial z^m}{\partial y^i} \frac{\partial z^n}{\partial y^j} T^{ij} \quad (T^{ij} = T_{ij}) \tag{4.27}$$

where T^{ij} are the components of Cauchy stress; $(T^{11}, T^{12}, T^{22}) = (T_{xx}, T_{xy}, T_{yy})$. Thus the stresses are such that

$$\underset{\sim}{P} = \underset{\sim}{I} \quad (\sim \text{ denotes second order tensors}) \tag{4.28a}$$

or in components

$$P^{mn}\, \underline{b}_m \otimes \underline{b}_n = T^{mn}\, \underline{e}_m \otimes \underline{e}_n \quad (\underline{e}_i = \text{unit base vectors}) \tag{4.28b}$$

Considering the plane strain condition, $T^{3j} = T^{j3} = 0$ $(j=1,2)$, one obtains the following relationships,

$$\begin{aligned} P^{11} &= (T^{11} - T^{22}) + 2i\, T^{12} \\ P^{22} &= (T^{11} - T^{22}) - 2i\, T^{12} = \overline{P^{11}} \\ P^{12} &= P^{21} = T^{11} + T^{22} \\ P^{33} &= T^{33} \end{aligned} \tag{4.29}$$

where $\overline{(\cdot)}$ merely denotes the complex conjugate of $(\cdot)$.

In the plane strain condition the stress P^{ij} can also be defined by means of the Airy stress function U in the same form used for

defining the stress T^{ij} in y^i coordinates (see refs. [44,45, 133]) as,

$$P^{ij} = (\epsilon^{jm}\,\epsilon^{in}\,U)_{;mn} \equiv \epsilon^{jm}\epsilon^{in}\,U_{,mn} \tag{4.30}$$

where ; and , respectively denote covariant and partial differentiations with respect to the coordinates z^i ; $\epsilon^{mn}\sqrt{b} =$

$$\epsilon_{mn}/\sqrt{b} = \begin{cases} 1 & \text{if } m = 1,\ n = 2 \\ -1 & \text{if } m = 2,\ n = 1 \\ 0 & \text{otherwise} \end{cases}$$

and $\epsilon_{mj}\epsilon^{mi} = \delta^i_j$ (the Kronecker delta)

In Eq. 4.30 the covariant differentiation is, however, replaced by partial differentiation due to the obvious reason that the metric tensor b in Eq. 4.27 is constant.

Following the contravariant tensor transformation in Eq. 4.28, one derives the equilibrium equations and stress compatibility equations defined for the stresses in the complex coordinates z^i .

It can be seen that the stress defined by means of an Airy stress function U in Eq. 4.30, satisfies the following translational equilibrium equation.

$$\text{Div}\ \underset{\sim}{P} = \underline{0} \tag{4.31a}$$

where Div is the divergence operator ; $\text{Div} = (\underline{b}^i \frac{\partial}{\partial z^i})\cdot$, and $\underset{\sim}{P} = P^{ij}\ \underline{b}_i \otimes \underline{b}_j$, or writing in components,

$$P^{ij}_{,i} = 0 \tag{4.31b}$$

hence substitution of the stresses in Eq. 4.30 into Eq. 4.31 gives,

$$\varepsilon^{jk}\,\varepsilon^{il}\,U_{,ikl} = 0 \tag{4.32}$$

Further the stress in Eq. 4.30 must also satisfy the following equation, which is equivalent to the two-dimensional Beltrami-Michell compatibility equation in Cartesian coordinate y^i .

$$D_*^2\;\; P^{m\cdot}_{\cdot m} = 0 \qquad \text{(sum on m)} \tag{4.33}$$

where D_*^2 is the Laplacian operator given as $D_*^2(\cdot) = b^{ij}(\cdot)_{,ij}$ and $P^{m\cdot}_{\cdot m}$ is a mixed component stress of P^{ij}.

Using Eq. 4.30

$$P^{m\cdot}_{\cdot m} = b_{mn}\,P^{mn} = b_{mn}\,\varepsilon^{ni}\varepsilon^{mj}\,U_{,ij}\ , \tag{4.34}$$

hence Eq. 4.33 leads to

$$D_*^2\;\; P^{m\cdot}_{\cdot m} = b^{ij}\,b^{kl}\,U_{,ijkl} = 0 \tag{4.35}$$

Considering the symmetry of b^{ij}, Eq. 4.35 yields

$$b^{ij}b^{kl}\,U_{,ijkl} = 4\,b^{12}\,b^{12}\,U_{,1122} = 0 \tag{4.36}$$

Therefore, the problem is reduced, as shown previously in (A), to finding the Airy stress function (i.e. the biharmonic function) U,

$$U_{,1122} \equiv \frac{\partial^4 U}{(\partial z^1)^2(\partial z^2)^2} = \frac{\partial^4 U}{\partial z \partial z\ \partial z \partial z} = 0 \tag{4.37}$$

or, since $b^{12} = 2$ in Eq. 4.27, Eq. 4.36 becomes

$$D_*^4 U \equiv D_*^2 (D_*^2 U) = 0 \tag{4.38}$$

where $$D_*^4 = 16 \frac{\partial^4}{(\partial z^1)^2 (\partial z^2)^2} = \frac{\partial^4}{(\partial y^1)^4} + 2 \frac{\partial^4}{(\partial y^1)^2 (\partial y^2)^2} + \frac{\partial^4}{(\partial y^2)^4}$$

The solution to Eq. 4.37 (or 4.38) is given in Eq. 4.10 of (A) (see Appendix A).

$$2U = \bar{z}\phi(z) + z\bar{\phi}(\bar{z}) + \psi(z) + \bar{\psi}(\bar{z})$$

or

$$2U = z^2\phi(z^1) + z^1\bar{\phi}(z^2) + \psi(z^1) + \bar{\psi}(z^2) \tag{4.39}$$

This solution can also be obtained by the direct integration of Eq. 4.38 by assuming that the solution is holomorphic, a priori [86]. This assumption, however, can be avoided by the approach taken by Muskhelishvili [86] (Appendix A).

Using the solution in Eq. 4.11 and Eq. 4.30, the stress P^{ij} can be expressed as,

$$\begin{aligned} P^{11} &= -4U_{,22} = -2(z^1\bar{\phi}_{,22} + \bar{\psi}_{,22}) \\ P^{22} &= -4U_{,11} = -2(z^2\phi_{,11} + \psi_{,11}) \\ P^{12} &= 4U_{,12} = 2(\phi_{,1} + \psi_{,2}) \end{aligned} \tag{4.40}$$

where $\phi_{,1} = \phi'(z) = d\phi(z)/dz$ and $\bar{\phi}_{,2} = \bar{\phi}' = d\bar{\phi}(\bar{z})/d\bar{z}$, etc.

Considering the results obtained in Eqs. 4.29 and 4.40, the stresses can be shown, by using the variables z and $\bar{z}$, as follows

$$P^{11} = (T^{11} - T^{22}) + 2i\,T^{12} = -2[z\bar{\phi}''(\bar{z}) + \bar{\psi}''(\bar{z})]$$
$$P^{12} = T^{11} + T^{22} = 2[\phi'(z) + \bar{\phi}'(\bar{z})] \qquad (4.41)$$
$$(P^{12}-P^{11})/2 = T^{22} - i\,T^{12} = \phi'(z) + \bar{\phi}'(\bar{z}) + z\bar{\phi}''(\bar{z}) + \bar{\psi}''(\bar{z})$$

The expressions of stresses are seen to be the same as those in Eqs. A.41 and A.42.

The displacements can also be found in a similar manner. First we define the displacement components in the complex coordinates z^i by D^i, and the corresponding displacement components in the coordinates y^i by u^i. Since both displacements are related by the contravariant tensor transformation which is described as

$$D^i = \frac{\partial z^i}{\partial y^m}\, u^m \quad (u^m = u_m \text{ or } u^1 = u \text{ and } u^2 = v) \qquad (4.42)$$

the displacements D^i are defined by

$$D^1 = u^1 + i\,u^2, \quad D^2 = D^1 = u^1 - i\,u^2 \qquad (4.43)$$

Further, the relationship between stress and displacement in the complex coordinates z^i can also be written by virtue of the transformation in Eq. 4.28 as,

$$P^{1j} = G(b^{im} D^j_{,m} + b^{jn} D^i_{,n}) + \frac{2\nu G}{1-2\nu}\, b^{ij}\, D^m_{,m} \qquad (4.44)$$

After a little algebraic work and taking into account Eqs. 4.40 and 4.44, one can find the displacements, which are expressed by two holomorphic functions as

$$2G(u^1 + i\,u^2) = (3-4\nu)\,\phi(z) - z\overline{\phi}'(\overline{z}) - \overline{\psi}'(\overline{z}) \qquad (4.45)$$

which is the same as that in Eq. A.19 (Appendix A).

(C) Development of a Sectionally Holomorphic Function Representing Stresses and Rotations

The stresses and displacements in an arbitrary simply-connected domain were defined in terms of two holomorphic functions from two different approaches based on two different coordinates, the Cartesian coordinates and the complex coordinates as shown respectively in the subsections (A) and (B). The stresses are defined in Eqs. 4.17, 4.18 appeared in (A), and in Eqs. 4.41 in (B), while the displacements are defined in Eq. 4.16 in (A), and Eq. 4.45 in (B). In order to consider contact problems, no matter what type they are, it is required to extend a holomorphic function defined in a half-plane into another half-plane, say the lower half-plane S^- into the upper half-plane S^+. The details of this extension (i.e. analytical continuations) can be found in section 7 of Appendix A which appears to be somewhat different from what will be shown in the following; yet both are essentially equivalent.

If $\phi(z)$ is holomorphic for $z \in S^-$, then $\overline{\phi}(z) = \overline{\phi(\overline{z})}$ is holomorphic for $z \in S^+$ since $z \in S^+$, $\overline{z} \in S^-$. Now we consider Eq. A.25 expressing resultant forces, i.e.

$$X + iY = -\,i\left[\phi(z) + z\overline{\phi}'(\overline{z}) + \overline{\psi}'(\overline{z})\right]_A^B$$

and try to extend $\phi(z)$ to the whole complex plane by putting

$$\phi(z) = - z\overline{\phi}'(z) - \overline{\psi}'(z) \qquad z \in S^+ \qquad (4.46)$$

This implies that we are trying to extend $\phi(z)$, which is initially defined to be holomorphic in S^-, to the upper half-plane S^+ so that the functions $\phi(z)$ are an analytical continuation of each other through the unloaded parts of the boundary (i.e. outside of portion [A,B]) where the resultant forces X + i Y = 0. For an arbitrary point z in S^-, Eq. 4.46 can be written as

$$\left.\begin{aligned} \phi(\bar{z}) &= - \bar{z}\overline{\phi}'(\bar{z}) - \overline{\psi}'(\bar{z}) \qquad z \in S^- \\ \text{or} \qquad \overline{\psi}'(\bar{z}) &= - \phi(\bar{z}) - z\overline{\psi}'(\bar{z}) \qquad z \in S^- \end{aligned}\right\} \qquad (4.47)$$

Differentiating Eq. 4.47 with respect to $\bar{z}$,

$$\overline{\psi}''(\bar{z}) = - \phi'(\bar{z}) - \overline{\phi}'(\bar{z}) - \bar{z}\overline{\phi}''(\bar{z}) \qquad z \in S^- \qquad (4.48)$$

Putting $\Phi(z) = \phi'(z)$ and substituting Eqs. 4.47 and 4.48 into Eqs. 4.41 and 4.45, one obtains for $z \in S^-$

$$T_{11} + T_{22} = 2[\Phi(z) + \bar{\Phi}(z)] \qquad (4.49a)$$

$$(T_{11} - T_{22}) + 2i\, T_{12} = 2[\phi(\bar{z}) + \bar{\phi}(\bar{z}) + (\bar{z}-z)\overline{\Phi}'(\bar{z})] \qquad (4.49b)$$

or

$$(T_{22} - T_{11}) + 2i\, T_{12} = 2[(\bar{z}-z)\Phi'(z) - \phi(z) - \bar{\phi}(z)] \qquad (4.49c)$$

$$T_{22} - i\, T_{12} = \phi(z) - \phi(\bar{z}) + (z-\bar{z})\, \overline{\Phi}'(\bar{z}) \tag{4.49d}$$

$$2G(u_1 + i\, u_2) = K\phi(z) + \phi(\bar{z}) + (\bar{z}-z)\, \overline{\Phi}'(\bar{z}) \tag{4.49e}$$

where $T_{11} = T_{xx}$, $T_{12} = T_{xy}$ and $T_{22} = T_{yy}$; $u_1 = u$, $u_2 = v$; $K = 3 - 4\nu$ for the plane strain condition.

We can also obtain the rotations along the surface by taking derivatives with respect to x_1,

$$2G(u_{1,1} + i\, u_{2,1}) = K\Phi(z) + \Phi(\bar{z}) + (\bar{z}-z)\, \overline{\Phi}'(\bar{z}) \tag{4.50}$$

All the above equations (4.49 and 4.50) are obtained regardless of whether the analytic continuation is carried out either from the upper half-plane or from the lower half-plane. It is noted that displacements in Eq. 4.49e are not bounded at infinity (Eq. A.39), hence they will not be considered in the analysis. This is an inherent problem in the theory of plane elasticity.

4.2.3 Transformation of a Sliding Contact Problem into a Riemann-Hilbert Problem

The contact problem under consideration is subjected to the following conditions:

(1) Stresses and rotations in the half-plane vanish at infinity.

(2) An external force exerted by the solid S_1 (or S_2) to another solid S_2 (or S_1) is known a priori.

(3) The slope of the true contact surface, the arc ab, is small enough on the interval L such that the true surface is represented by the interval L = (a,b).

The details of the transformation of contact problems can also be seen in section 9 of Appendix A.

Let $\Phi_1(z)$ and $\Phi_2(z)$ be sectionally holomorphic functions in the solids S_1 and S_2 respectively, except at the segment L = (a,b) (i.e. the line of discontinuity) of the real axis.

If, under condition (3), contact stresses and rotations are representable on the segment L = (a,b), then the stresses T_{yy} and T_{xy} at a boundary for the solids S_1 and S_2 on the real axis are expressed by using Eq. 4.9 as

$$\left.\begin{aligned} &\text{for } S_1 \quad T_{yy}^{(1)} - i\, T_{xy}^{(1)} = \Phi_1(t) - \Phi_1(t) , \qquad t \in L \\ \text{and} \\ &\text{for } S_2 \quad T_{yy}^{(2)} - i\, T_{xy}^{(2)} = \Phi_2^{+}(t) - \Phi_2^{-}(t) , \qquad t \in L \end{aligned}\right\} \tag{4.51}$$

where $\Phi_1^{+}(t)$ and $\Phi_i^{-}(t)$ are limited functions of $\Phi(z)$ such that

$$\Phi_1^{+}(t) = \lim_{z \to t} \Phi_i(z) \quad (z \in S^{+}) \text{ and } \Phi_1(t) = \lim_{z \to t} \Phi_i(z) \quad (z \in S^{-});$$

the superscripts (1) and (2) denote the quantities for the solids S_1 and S_2.

It is noted that such limiting functions are considered to be hyperfunctions (e.g. Imai [53], Kaneko [60], Kashiwara et al [61] and

Morimoto [85]) while the sectionally holomorphic functions are called standard defining functions.

Since the contacting elastic solids S_1 and S_2 are in a state of static equilibrium, the magnitudes of the normal and the shear stresses at the contact surface L must be equal and opposite for each elastic solid, i.e., stresses at the contact surface are equal, but are acting in opposite directions. Considering Eqs. 4.11a and 4.11b, one observes that $\Phi_1(z) + \Phi_2(z)$ is homomorphic in the entire complex plane since $\Phi_1(z) + \Phi_2(z)$ is continuous across the real line. Furthermore, imposing $\Phi_1(z)$ and $\Phi_2(z)$ be vanished at infinity leads to the following:

$$\Phi_1(z) + \Phi_2(z) = 0 \qquad z \in \mathbb{C}$$

or

$$\Phi_1(z) = -\Phi_2(z) \qquad z \in \mathbb{C} \tag{4.52}$$

The above results imply that the contact problem was reduced to finding the one sectionally holomorphic function either $\Phi_1(z)$ or $\Phi_2(z)$.

It is ready to transform the quasi-statically sliding contact problem, where the solid S_2 slides slowly over the half-plane S_1 under the condition of limiting friction along the surface of the half-plane. The contact stresses such as shear and normal stresses are denoted by T(t) and P(t) respectively. (i.e. $T_{(t)} = T_{xy}$ and $P_{(t)} = T_{yy}$)

are assumed to be related pointwise by

$$T(t) = k\, P(t) \qquad t \in L \tag{4.53}$$

where k is a constant coefficient of friction.

Let $f_1(t)$ and $f_2(t)$ be smooth functions describing undeformed profiles of the solids S_1 and S_2 respectively. It will be seen later that the first derivative of the function f_2 should be at least Hölder continuous (e.g., Muskhelishvili [86]); however, such a continuity is not necessary in the space of hyperfunctions (e.g. Kaneko [60]). After an application of vertical loading, the following relationship holds at the contact surface,

$$f_1(t) + v^{(1)-}_{(t)} = f_2(t) + v^{(2)+}_{(t)} \qquad t \in L$$

or

$$v^{(1)-}_{(t)} - v^{(2)+}_{(t)} = f_2(t) - f_1(t) = f_{(t)} \qquad t \in L \tag{4.54}$$

where the superscripts "-" and "+" denote the limiting of the functions $v^{(i)}$ (i=1,2) on L; f(t) may be called the "distance function".

Differentiating Eq. 4.54

$$v^{(1)}_{(t)} - v^{(2)}_{(t)} = f(t)_{,t} \equiv f' \tag{4.55}$$

provided that the limits and the differentiations of the vertical displacements $v^{(i)}_{(t)}$ (i=1,2) are interchangeable. We will further

discuss Eq. 4.54 in section 4.3. Considering Eqs. 4.53 and 4.55 and the rotations in Eq. 4.50, one obtains the following equation (Eq. A.83 in Appendix A).

$$\Phi^{+}(t) = q\,\Phi^{-}(t) + f_o \qquad t \in L \tag{4.56a}$$

where

$$q = -e^{i2\pi\alpha} \tag{4.57a}$$

$$\alpha = \frac{1}{\pi} \tan^{-1}\left[k\,\frac{G_1(K_2-1) - G_2(K_2-1)}{G_1(K_2+1) + G_2(K_1+1)}\right] \tag{4.57b}$$

$$f_o = 4i\,f'(t)\,\frac{G_1G_2\,(1+ik)\,\exp(i\pi\alpha)\,\cos\pi\alpha}{G_1(K_2+1) + G_2(K_1+1)} \tag{4.57c}$$

G_i = Shear moduli, $K_i = 3-4\nu_i$ $(i = 1,2)$. (4.57d)

The Rieman-Hilbert problem in Eq. 4.56a was obtained by considering the slope of displacements at the contact surface L. Next considering that the surface outside of the contact is free from any stresses or loads, then another Riemann-Hilbert problem can be obtained from Eq. A.60 as shown in Eq. A.83b, i.e.

$$\Phi^{+}(t) - \Phi^{-}(t) = 0 \qquad \text{not on } L \tag{4.56b}$$

Solving a contact problem between two solids is then equivalent to solving the system of two equations (Eqs. 4.56a,b) for a sectionally holomorphic function $\Phi(z)$, which is discontinuous only along the contact surface.

4.2.4 General Solutions to the Riemann-Hilbert and the Sliding Contact Problems:

The details of analysis of the Riemann-Hilbert problem in Eq. 4.56 are rendered in Section 9 of Appendix A and only the solution of Eq. 4.56 (Eq. A.103) is stated here as

$$\phi(z) = \frac{2M(1+ik)\exp(i\pi\alpha)\cos\pi\alpha}{\pi(z-a)^{\gamma}(b-z)^{1-\gamma}} \int_a^b \frac{(t-a)^{\gamma}(b-t)^{1-\gamma} f'(t)}{t-z}\, dt + \frac{P(1+ik)\exp(i\pi\alpha)}{2(z-a)^{\gamma}(b-z)^{1-\gamma}} \qquad z \in \mathbb{C}\backslash L \tag{4.58}$$

where $\gamma = \frac{1}{2} + \alpha$, (4.59a)

α is given in Eq. 4.57b, (4.59b)

$$M = \frac{G_1 G_2}{G_1(K_2+1) + G_2(K_1+1)}\,, \tag{4.59c}$$

and P is the vertical load, which is a force per unit width.

Using Eqs. 4.49d, 4.53 and 4.58, the contact stresses are obtained as

$$P(t_o) + i\,T(t_o) = \phi^{+}(t_o) - \phi^{-}(t_o) \qquad t_o \in L \tag{4.60}$$

Then the pressure $P(t_o)$ is given by

$$P(t_o) = -4M\bar{f}'(t_o)\sin\pi\alpha\cos\pi\alpha + 4M\cos^2\pi\alpha\, X^{+}(t_o) \int_a^b \frac{f'(t)\,dt}{X^{+}(t)(t-t_o)} + P\cos\pi\alpha\,\frac{X^{+}(t_o)}{\pi} \tag{4.61}$$

where α and M are given in Eqs. 4.57b and 4.59c respectively, and

$$X^{+}(t_o) = X(t_o) = (t_o-a)^{\gamma}\ (b-t_o)^{1-\gamma} \tag{4.62}$$

In Eq. 4.61 what remains to be worked out is the calculation of the integration on L = (a,b), assuming that the function f(t) (i.e. $f_2(t)$-$f_1(t)$) is given. If the profiles of the undeformed solids S_1 and S_2 are described by the functions $f_1(t)$ and $f_2(t)$ which are even functions, then one can safely set the contact surface L = (a,b) ≈ (-a,a) so long as the coefficient of friction k is less than unity. Then Eq. 4.62 is

$$X(t_o) = (a + t_o)^{\gamma}\ (a-t_o)^{1-\gamma} \tag{4.63}$$

Describing the solid S_1 as the half-plane and the solid S_2 with the smooth profile respectively, by setting f_1 = 0 and f_2 = summation of the two polynomials, say g_1 and g_2, then one obtains a distance function f(t) defined in Eq. 4.54

$$f = f_o - f_1 = f_2 = q_1 + q_2 \tag{4.64}$$

where g_1 and g_2 are given by

$$q_1(t) = d_1 \frac{t^2}{R} \tag{4.65a}$$

and

$$q_2(t) = d_2 \frac{t^4}{R^3} \tag{4.65b}$$

(d_1, d_2 and R are arbitrary values for now).

Their derivatives are

$$f' = q_1' - q_2' \tag{4.66}$$

where $$q_1' = D_1 \frac{t}{R} = 2d_1 \frac{t}{R} \quad (\text{i.e. } D_1 = 2d_1) \tag{4.67a}$$

and $$q_2' = D_2 \frac{t^3}{R} = 4d_2 \frac{t^3}{R} \quad (\text{i.e. } D_2 = 4d_2) \tag{4.67b}$$

Considering Eqs. 4.63 and 4.66 in the integration of Eq. 4.61, the pressure is eventually obtained in an equation (Eq. A.124) as,

$$P(t) = \frac{4M \cos^3 \pi\alpha}{R}(a+t)^{1-\gamma} (a-t)^{\gamma} \{D_1+D_2 \frac{a^2}{R^2} (1+C_2+ \frac{t^2}{a^2})\} \tag{4.68}$$

where α, M, D_1 and D_2 are given by Eqs. 4.57b, 4.59c, 4.67a and 4.67b, respectively: the coefficient C_2 is given in Eq. A.115 as

$$C_2 = 2\gamma(\gamma-1) \quad . \quad (\gamma = \frac{1}{2} + \alpha) \tag{4.69}$$

The contact area L = (-a,a) is also obtained, by imposing the condition that the pressure P(t) is zero at t = $\pm$ a, hence obtaining the following force equilibrium equation (Eq. A.127)

$$V_4(1+C_2+C_4)a^4 + V_2(1+C_2)a^2 - P = 0 \tag{4.70}$$

where $$V_2 = (4D_1 M \pi \cos^2 \pi\alpha) R^{-1} \tag{4.71a}$$

$$V_4 = (4D_2 M \pi \cos^2 \pi\alpha) R^{-3} \tag{4.71b}$$

$$C_4 = \frac{2}{3}\gamma(\gamma-1)(\gamma^2-\gamma+1) \qquad (4.71c)$$

(C_4 is given in Eq.A.115).

Therefore, half of the contact area is obtained by

$$a = \left(\frac{Y}{2}\right)^{1/2}\left[-1 + \left\{1+4P\,\frac{V_4(1+C_2+C_4)}{\{(V_2(1+C_2)\}^2}\right\}^{1/2}\right]^{1/2} \qquad (4.72)$$

where $Y = V_2(1+C_2)/V_4(1+C_2+C_4)$.

Hence once the material properties, coefficient of friction, and the distance function f(t) in Eq. 4.64 are given, the contact area and the pressure are obtained by using Eqs. 4.72 and 4.68. In section 9.3 of Appendix A, we obtained the formulae of contact pressure distributions and contact area for the solid S_2 whose (undeformed) profile is prescribed by the three different functions as given in Eqs. A.131a, A.134a and A.137a. If the body S_2 is an elastic solid with a circular shape then solutions are easily obtained by approximating its profile using an equation given in either Eq. A.131a or A.134a. However, if the body S_2 is not solid (e.g. pneumatic tires), one would hardly obtain solutions which are close enough to the real ones, no matter how well we approximate the (undeformed) profile of the pneumatic body. This problem, which arises from the lack of consideration of kinematics of contact profiles in the analytical formulation, will be solved by considering equivalent contact problems discussed in the following section 4.3.

4.2.5 Summary

In the previous sections an analytical method (i.e. the complex variable method), which solves the sliding contact problems where a linearly elastic solid S_2 slides quasi-statically over an elastic half-plane S_2, was briefly described while referring to the detailed analysis given in Appendix A. The idea of the analytical method is based on transformation of a sliding contact problen into a corresponding Riemann-Hilbert problem, by virtue of the complex variable method, which will be solved by finding a sectionally holomorphic function under the given conditions (e.g. material properties, undeformed shapes of contacting solids, friction, etc.). We will summarize in the following how the analytical method is derived:

(1) Airy stress function U is represented by two complex functions holomorphic in an arbitrary elastic domain R (Eqs. 4.10, 4.11 or 4.39),

(2) Stresses and displacements are then defined in terms of the two holomorphic functions (Eqs. 4.16, 4.17, 4.18 or Eqs. 4.41, 4.45),

(3) Next the arbitrary elastic domain R is considered to occupy the lower half-plane then stresses, displacements and rotations are defined by means of one complex function holomorphic in the entire complex plane except the loaded segments on the real axis (Eqs. 4.49 and 4.50),

(4) In section 4.2.3 a sliding contact problem is transformed into a Riemann-Hilbert problem (Eq. 4.56a,b) by considering Eq. 4.50, the relationship between normal and shear stresses (Eq. 4.53) and

the slope of the distance function (Eq. 4.55),

(5) The general solution of the Riemann-Hilbert problem is obtained in Eq. 4.58 by imposing a condition that the sectionally holomorphic function vanishes at infinity, hence obtaining the pressure in the form given in Eq. 4.61,

(6) For a contact between a solid S_2 with the profile given by a polynomial function in the second and fourth order and a half-plane S_1, one can obtain complete solutions of contact pressure (Eq. 4.68), the force equilibrium (Eq. 4.70) and contact area (Eq. 4.72) after carrying out lengthy algebraic work for the integration in Eq. 4.61, which is partly shown in Section 9.3 of Appendix A.

4.3 Free Boundary Problems Equivalent to Tire-Clay and Tire-Rigid Base Interaction Problems; A Question to Solutions Obtained by the Existing Analytical Methods for a Certain Class of Contact Problems

4.3.1 Preliminary

Since pneumatic tires are not solid continua, the complex variable-based-contact analysis presented in the previous section 4.2 cannot be directly applied to our present interaction problems. The complex variable-based-contact analysis is, nevertheless, useful and used to be a basic tool for the present interaction problems, which will be solved after transforming to the equivalent free boundary problems, with consideration of contact profiles and the elastic modulus of deformed solids (i.e. supporting clay and nearly rigid base) discussed and defined later in section 4.4.

In order to obtain such free boundary problems, we shall first re-consider the treatment of compatibility on the contact surface (Eq. 4.54) used in the complex variable-based-contact analysis. Refer to Figs. 4.2 and 4.3 where P denotes the axle load per unit width. Both figures represent the same contact problems between a solid S_2 with undeformed profile $f_2(t)$ and a half-plane S_1 with undeformed profile $f_1(t) = 0$, while showing mathematically different aspects on contact. It is noted that the real axis in Fig. 4.3 is in a geometrically approximated deformed state.

Figure 4.2 shows that the material points "p" and "q" (at $t = t_0$) of the free surfaces of the solids S_2 and S_1 respectively will

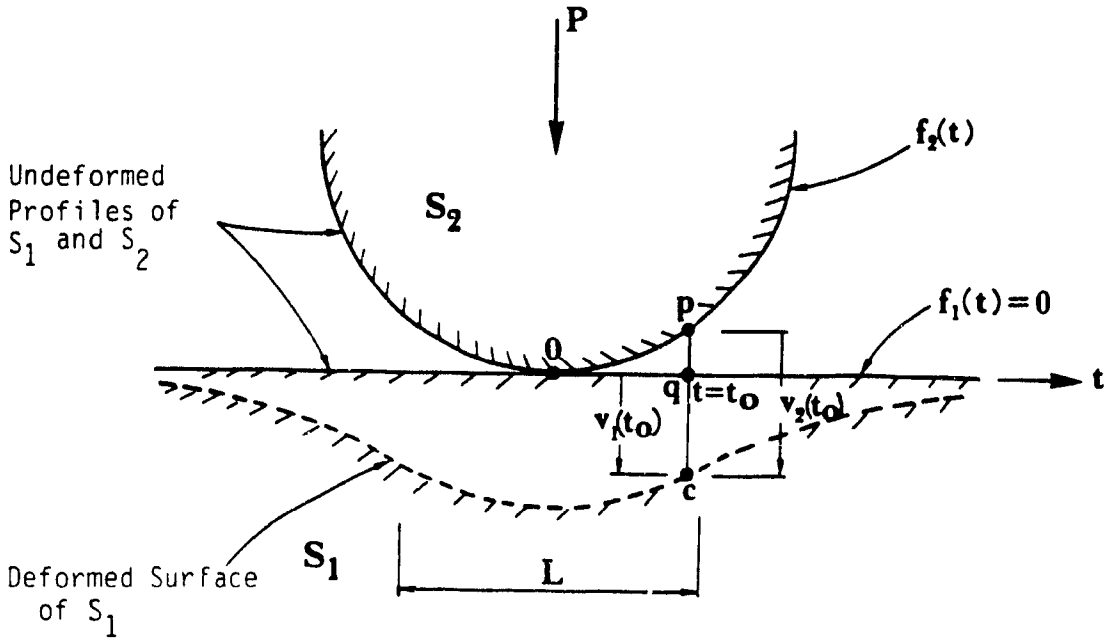


Fig. 4.2 Kinematics of Contact Profile

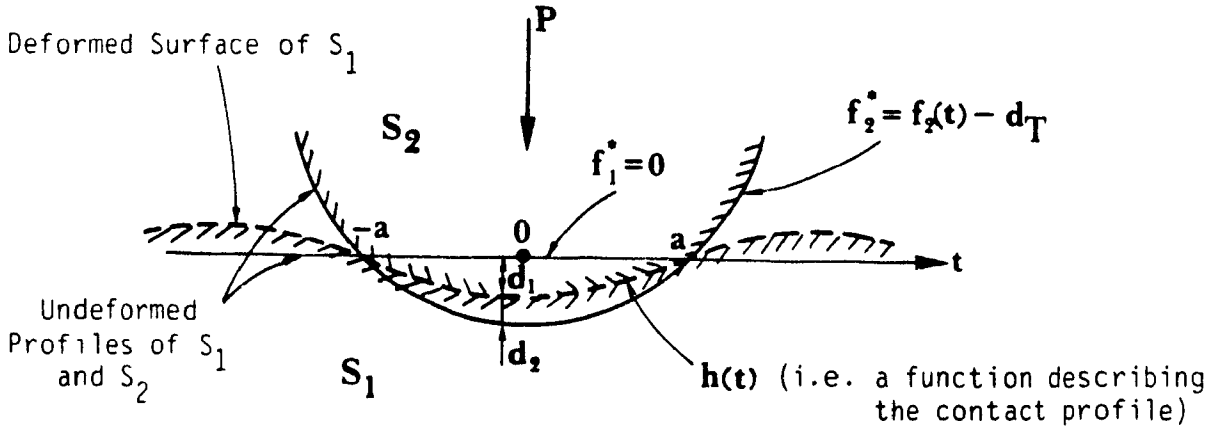


Fig. 4.3 An Approximated Deformed Configuration and a Contact Profile

displace vertically, assuming that horizontal displacements are negligible, and occupy the same point "c" (at $t = t_o$) due to the contact of surfaces upon application of vertical load. The vertical displacements of profiles of S_1 and S_2 are denoted by $v_1(t)$ and $v_2(t)$. It is then clearly seen from the geometries of undeformed and deformed solid surfaces that Eq. 4.54 holds on the contact surface L as

$$v_1(t) + f_1(t) = v_2(t) + f_2(t) \tag{4.75}$$

or

$$f(t) = v_1(t) - v_2(t) = f_2(t) - f_1(t) = f_2(t) \tag{4.76}$$

where $f_1(t) = 0$ and $f(t)$ is called distance function in Eq. 4.54.

The function $f(t)$ in Eq. 4.76 (or Eq. 4.54), whose slope $f'(t)$ comes into the complex variable-based-contact analysis, simply describes the distance between the surfaces of two undeformed solids, hence is called the distance function in Eq. 4.54. The distance function $f(t)$ may also be considered as a "relative approach" between the two undeformed surfaces. In Fig. 4.3, the real axis t, translated in parallel by the magnitude C, is that of a Cartesian coordinate system in deformed state, so that the function $f_1^*(t) = f_1(t) = 0$ while the function $f_2^*(t)$ describes the profile of the undeformed solid S_2, penetrating into the half-plane S_1 by the magnitude, $d_T + C$, $(d_T > 0)$. The value d_T is the approach of two solids so that $f_2^*(t) = f_2(t) - d_T$.

The function $h(t)$ in the deformed state defines the contact profile such that the vertical surface deformation of S_1, $v_1(t)$, is

given by $v_1(t) = h(t) - C$ on L while the functions $d_1(t)$ and $d_2(t)$ represent the approaches of solids S_1 and S_2, respectively, with respect to the displaced real axis shown in Fig. 4.3. Accordingly, the approach d_T is obtained by the summation of $d_1(t)$ and $d_2(t)$ at the origin (i.e. $t = 0$). We then obtain the following simple relationship on the nominal contact surface L of the real axis (refer to Fig. 4.3). Since $f(t) = f_2(t)$

$$f(t) + d_1(t) + d_2(t) = d_T \qquad t \in L \quad (4.77a)$$

or from Eq. 4.76

$$v_1(t) - v_2(t) + d_1(t) + d_2(t) = d_T \qquad t \in L \quad (4.77b)$$

Since $d_1(t) = -h(t)$ on L, Eq. 4.77a (or Eq. 4.77b) can also be written as,

$$f(t) = f_2(t) = v_1(t) - v_2(t) = d_T + h(t) - d_2(t) \quad t \in L \quad (4.78)$$

Moreover since $f^*(t) = f_2^*(t) - f_1^*(t) = f_2(t) - d_T$,

$$f^*(t) = h(t) - d_2(t) \qquad (h(t) = -d_1(t))\ t \in L \quad (4.79)$$

Differentiating Eqs. 4.78 and 4.79 with respect to t, one obtains,

$$v_1'(t) - v_2'(t) = f'(t) = (f^*(t))' \qquad t \in L \quad (4.80a)$$

$$= h'(t) - d_2'(t) \qquad t \in L \quad (4.80b)$$

$$= -(d_1'(t) + d_2'(t)) \qquad t \in L \quad (4.80c)$$

where $(\cdot)'$ denotes derivative with respect to t, i.e. $(\cdot)' = d(\cdot)/dt$.

In the foregoing study on the contact between two solids (Figs. 4.2, 4.3), the relationship between the undeformed profiles of solids (i.e. $f_1(t)$, $f_2(t)$), the vertical displacements (i.e. $v_1(t)$, $v_2(t)$), the approaches of each solid (i.e. $d_1(t)$, $d_2(t)$) and the contact profile h(t) were described. Particular attention is paid to a slope of vertical displacements (Eqs. 4.55, 4.80a), since it comes directly into the complex variable-based-contact analysis shown in the previous section and Appendix A. As shown in Eq. 4.80a (or Eq. 4.55), the slope of the surface displacements is equal to that of distance function f(t) (Eqs. 4.54, 4.78) which depends only on the undeformed profiles of the contacting solids. The slope is also given by the derivative of the approaches $d_1(t)$ (=-h(t)) and $d_2(t)$ as shown in Eqs. 4.80b,c. Although the slopes of both $d_1(t)$ and $d_2(t)$ must be uniquely expressed at each load for the compabibility at contact surface, the slope of the difference between $v_1(t)$ and $v_2(t)$ can be given by the slope of arbitrary approaches $d_1(t)$ and $d_2(t)$ as long as the summation of two approaches remain unchanged. These show that the slope, given by the vertical displacements $v_1(t)$ and $v_2(t)$, depends only on undeformed profiles of solids, and has no connection with the contact profile which must be taken into account in the contact analysis. Hence the solutions, patterns of pressure distributions in particular, which are obtained from the complex variable-based-contact analysis or other theories (e.g. Hertz theory), would not be reliable since these methods need only the slop of distance function f(t) (Eqs. 4.58, 4.61)

without considering contact profiles.

We will next consider two contact problems (Figs. 4.4a,b) of which two are contacting solids which are elastically and geometrically very different. The first contact problem shown in Fig. 4.4a is that where the upper solid S_2 is circular-shaped and elastic while the lower solid S_1 is the rigid half-plane. The second one is that where the half-plane S_1 is elastic and the circular-shaped solid S_2 is rigid, as shown in Fig. 4.4b. It is assumed that the circular shape of the two upper solids in Figs. 4.4a,b are the same.

For the first contact problem in Fig. 4.4a one obtains, by Eq. 4.80 (or Eq. 4.76) on the contact surface L*,

$$F_1(t) = f'(t) = -d_2'(t) \qquad t \in L^* \tag{4.81a}$$

and for the second contact in Fig. 4.4b on the contact surface L**

$$F_2(t) = f^{*\prime}(t) = h'(t) \qquad t \in L^{**} \tag{4.81b}$$

where $f^*(t)$ denotes the undeformed profile of S_2.

Then if L* is contained in L**, one clearly sees that

$$F_1(t) = F_2(t) \qquad t \in L^* \tag{4.82}$$

Furthermore, if the loads for both problems are equal (i.e. P* = P**), and the properties of linearly elastic materials for both the solid S_2 in Fig. 4.4a and the half-plane S_1 in Fig. 4.4b are identical, then one obtains the result from the complex variable-based-contact

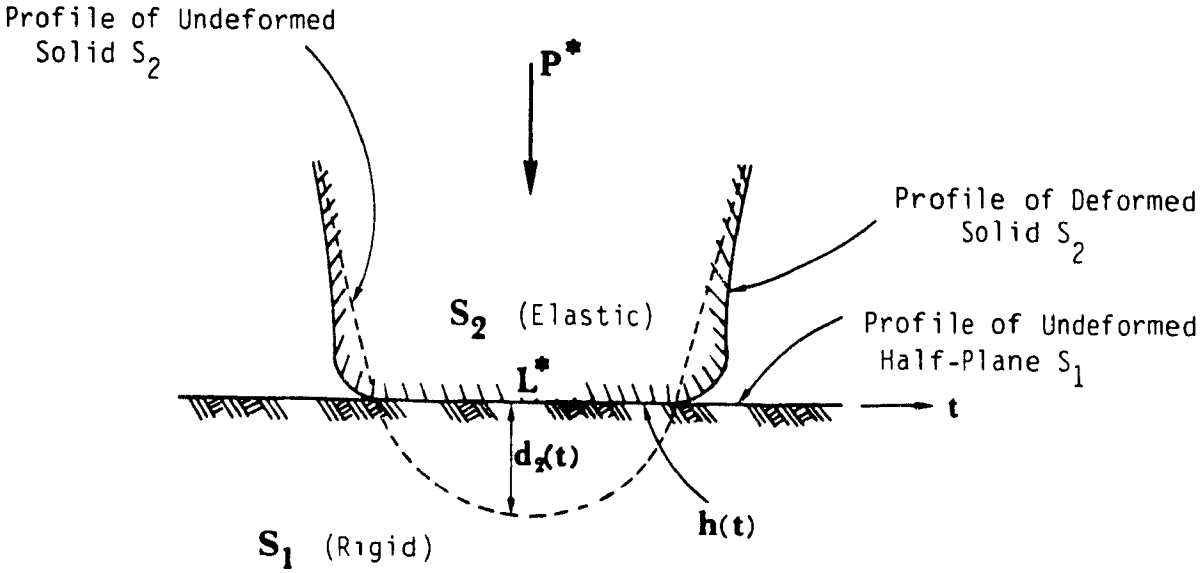


Fig. 4.4a A Contact Between an Elastic Solid S_2 and a Rigid Half-Plane S_1

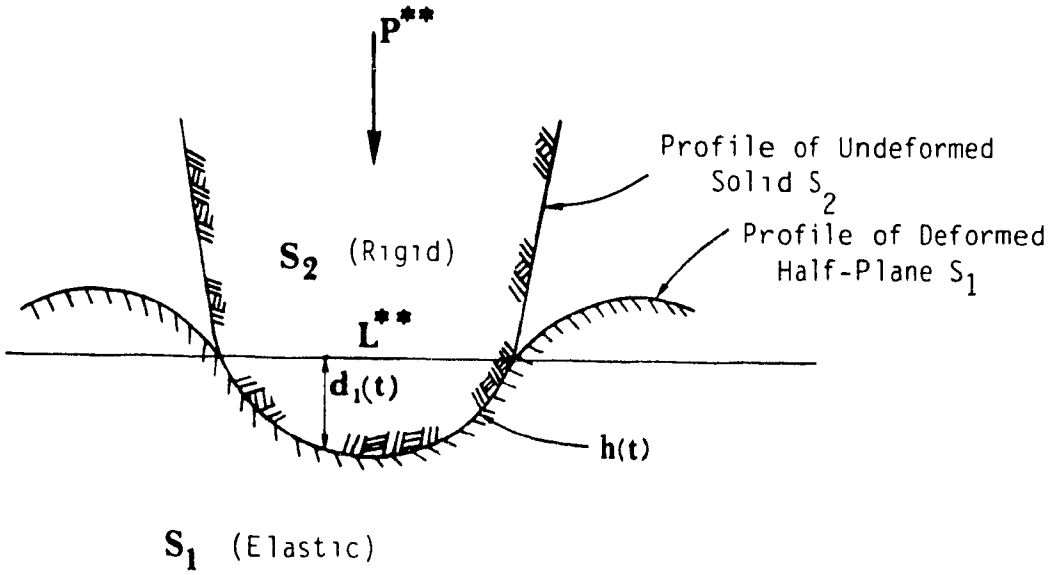


Fig. 4.4b A Contact Between a Rigid Solid S_2 and an Elastic Half-Plane S_1

analysis that the contact areas (i.e. contact lengths) for both cases are the same, i.e. $L^* = L^{**} = L$. Accordingly, one can also obtain the identical contact pressure distributions on L for the both cases by virtue of th analytical method. Thus this example problem shows that the contact problem in Fig. 4.4a is considered to be "mathematically" identical to that in Fig. 4.4b, according to this analytical method or the Hertz theory, since tne difference in contact profiles for the two problems does not come into the analytical formulation. These two contact problems will be re-considered in section 4.3.4, and we also raise a question about solutions obtained by the widely accepted analytical methods, for contact problems like those given in Fig. 4.4a.

It was demonstrated above that even if the two contact problems are different, the analytical methods will produce the same solutions since they are incapable of considering real contact profiles.

Hence, in order to overcome the difficulties considered above, and to avoid taking into account complex physical and geometrical characteristics of pneumatic tires, first the present interaction problems will be transformed into the equivalent free boundary problems by taking account of the contact profile h(t), which will be shown in the following sections 4.3.2 and 4.3.3. Then the free boundary problems will be solved by virtue of the complex variable-based-contact analysis, once the elastic modulus of the deformed half-plane (i.e. supporting clay or nearly rigid base) is determined in the way discussed in section 4.4. Such elastic modulus is defined by a function depending on a slope of contact profile, characteristics of

an interaction between a tire and a half-plane, and Poisson's ratio of half-plane.

4.3.2 A Free Boundary Problem Equivalent to a Tire-Clay Interaction Problem

A free boundary problem, equivalent to a tire-clay interaction problem as shown in Fig. 4.5a, will be derived by considering the deformed profile of the supporting clay contacting with the tire. The real axes t' and t, which are parallel to each other, denote respectively those at undeformed and deformed states, as was explained in the preliminary of section 4.3.1, while the translation is chosen in such a way that the real axis t is set to contain contact ends. In Fig. 4.5a the function $d_1(t)$ represents the approach of clay along (nominal) contact surface L, while the function $d_2(t)$ is that for the surface of a pneumatic tire. The two interacting bodies in Fig. 4.5a can be separated into two self-equilibrating bodies, without changing the deformed profiles, such as those in Fig. 4.5b and Fig. 4.5c, if the pressure P*(t) (normal to the deformed surfaces), exerted from the interaction, is being applied on each deformed surface L* of the tire and clay, holding the contact profile h(t). Such pressure P*(t) and surface L* are respectively true contact pressure and true contact surface. Then solving the original interaction problem in Fig. 4.5a is equivalent to solving a problem, defined by either the deformed tire in Fig. 4.5b or the deformed clay in Fig. 4.5c, for the unknown (contact) pressure P*(t) over the unknown (contact) surface L*. The problem, which is transformed from the original interaction problem,

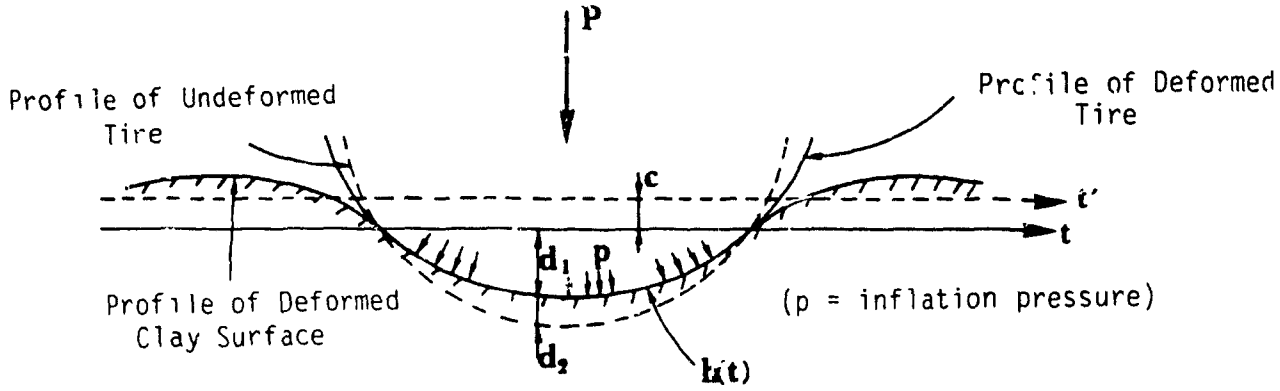


Fig. 4.5a An Interaction Between a Pneumatic Tire and a Supporting Clay

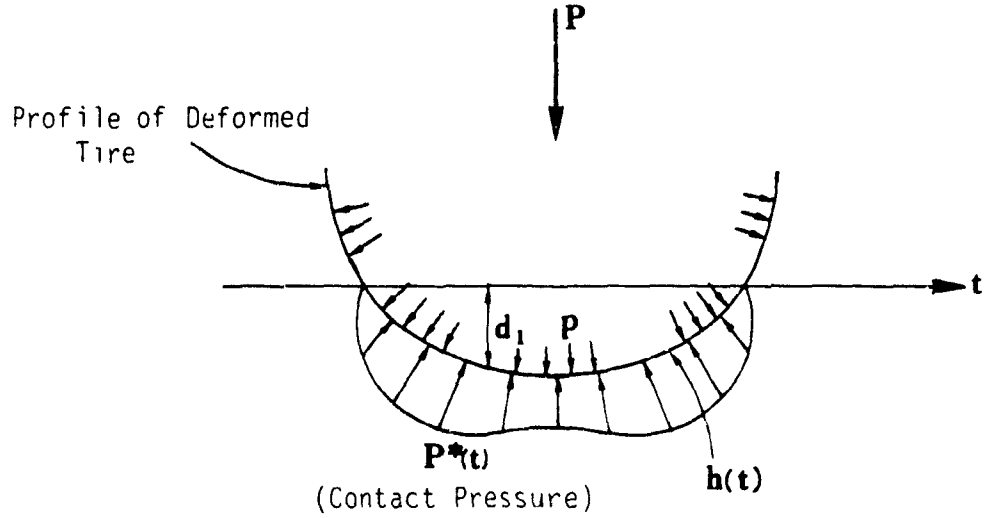


Fig. 4.5b A Tire Deformed Under Contact Fressure

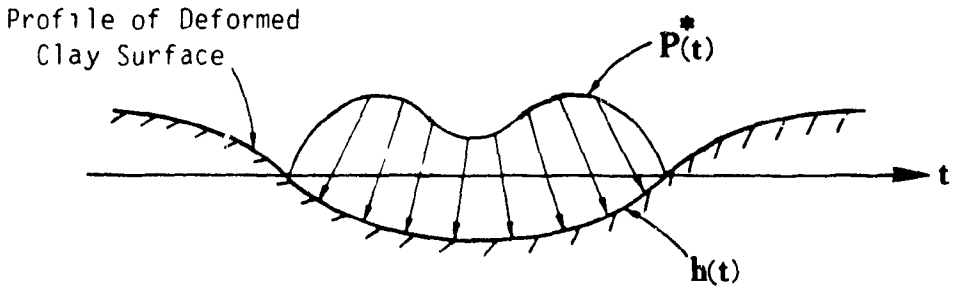


Fig. 4.5c A Supporting Clay Deformed Under Contact Pressure

is now termed as the free boundary problems equivalent to the tire-clay interaction problem.

In the following contact analysis, however, the true contact surface L^* will be represented by the nominal one L, i.e. $L^* \simeq L$, since the slope of the contact surface of the tire-clay interactions are observed in the experiments to be small enough for most cases. The contact pressure $P^*(t)$ is also replaced by the one denoted by $P(t)$, which is the pressure projected on the nominal contact surface.

Since the tire is a pneumatic and complex body, it is natural to consider the free boundary problem defined in Fig. 4.5c to obtain the contact pressure $P(t)$ and the contact area L. We assume that the deformation of the clay surface, after making contact with the tire, is given by the function $v_1(t)$ on L as shown in Fig. 4.5c i.e.

$$v_1(t) \simeq h(t) - C \qquad t \in L \tag{4.83}$$

where C represents the parallel translation of the real axis.

Since the tire is not directly considered in the analysis, the displacements $v_2(t)$, $d_2(t)$ will be neglected. Then the substitution of Eq. 4.83 into Eq. 4.78 leads to

$$f(t) = v_1(t) = h(t) - C \quad t \in L \tag{4.84}$$

Differentiating Eq. 4.84 with respect to t, one then obtains

$$f'(t) = v_1'(t) = h'(t) \ (\equiv - d_1'(t)) \quad t \in L \tag{4.85}$$

We then can solve the free boundary problem of deformed supporting clay (Fig. 4.5c) which is equivalent to the tire-clay interaction problem, by means of the complex variable-based-contact analysis (without considering the pneumatic tires in the contact analysis directly) after obtaining the elastic modulus of deformed supporting clay, which is governed by slope of contact profile, load, Poisson's ratio and elastic measure (section 4.4). The elastic measure, which is obtained from experiments of tire-clay interactions, is a measure of elasticity of two deformable bodies in contact. In addition, the slope of the deformed surface of clay is a measure of the deformabilities for the tire-clay interaction. Hence, the characteristics of tires, contacting with supporting clay, will be implicitly counted in the elastic modulus defined for the supporting clay. Further details on the definitions of the elastic modulus and elastic measure of clay are given in section 4.4.

4.3.3 A Free Boundary Problem Equivalent to a Tire-Rigid Base Interaction Problem

A free boundary problem equivalent to a tire-rigid base interaction problem as shown in Fig. 4.6a cannot be defined in a straightforward manner such as that defined for the tire-clay interaction problem.

First the two interacting bodies (Fig. 4.6a) for the tire-rigid base interaction problem will be separated into two self-equilibrating bodies, such as the deformed tire in Fig. 4.6b and the (undeformed)

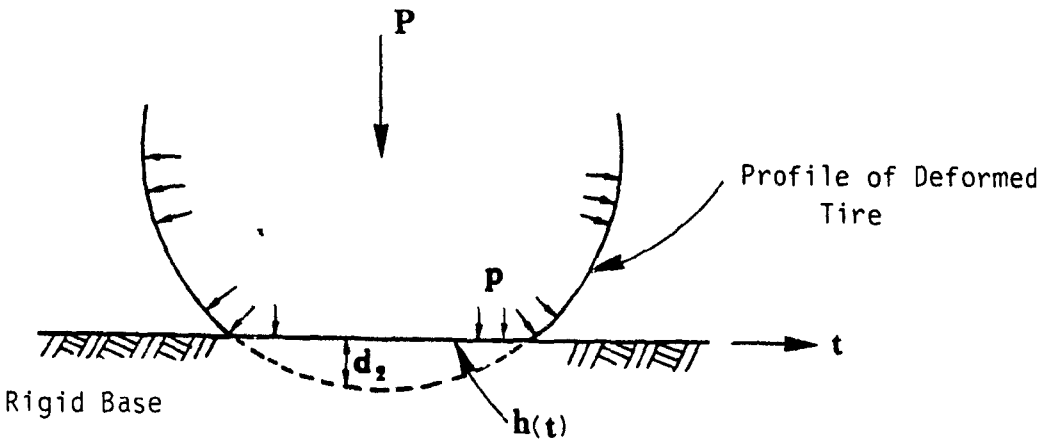


Fig. 4.6a An Interaction Between a Pneumatic Tire and a Rigid Base

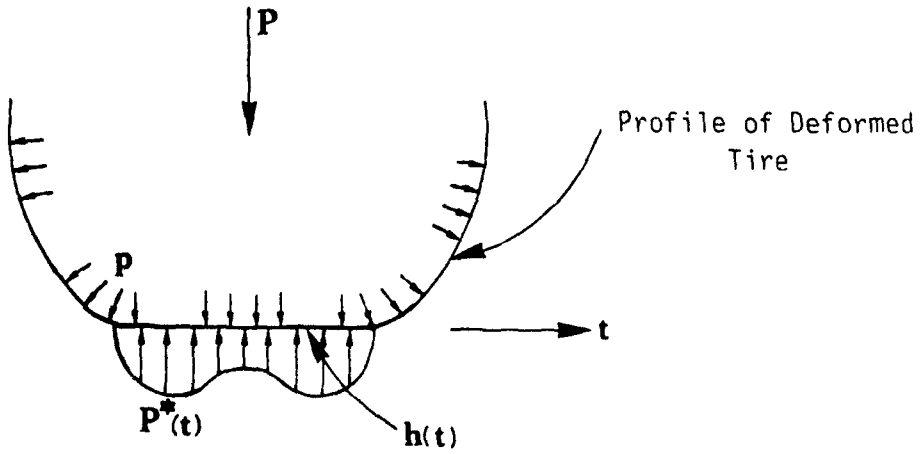


Fig. 4.6b A Deformed Tire Under Contact Pressure

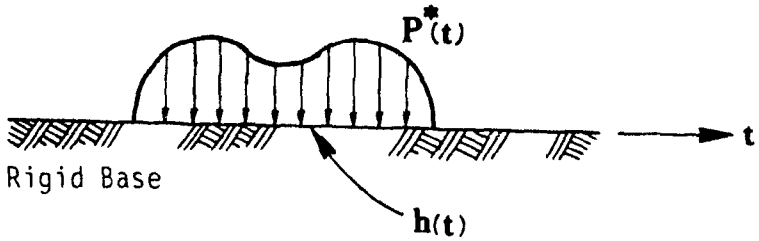


Fig. 4.6c An Undeformed Rigid Base Under Contact Pressure

rigid base in Fig. 4.6c, in which both of them are under contact pressure P(t) on the contact surface L. Although these two bodies, seeking unknown contact pressure and contact area with the given slope of the contact profile can be interpreted as free boundary problems equivalent to the tire-rigid base interaction problem, it is not possible to solve this problem by means of the present analytical approach, which was considered for tire-supporting clay interactions, since the elastic modulus cannot be defined for undeformable bodies (compared with tires) such as rigid base (section 4.4). This difficulty is overcome only if the present interaction problem is replaced by another problem with some assumptions. One could obtain two such problems, which might well represent the present interaction problem, with the following assumptions:

(1) tire is an elastic solid, or

(2) rigid base is replaced by a highly stiff deformable elastic solid.

The assumption given in (1) is essentially equivalent to assuming tires discretized by elastic springs (or finite elements) [49,57,107], which are radially distributed. Application of any analytical or numerical methods, established based on the assumption (1), to the present interaction problems would produce unacceptable erroneous results, especially for the pattern of pressure distributions. Such errors occur due to ignoring the fact that the kinematics of tire membranes cannot be approximated by those of elastic solids, and due to possible instabilities occurring in the tire membrane on the

contact portion as discussed in Chapters 2 and 3.

We will consider assumption (2), by replacing the rigid base S_1 by a deformable solid S_1^* (or nearly rigid base) so that any complex properties of pneumatic tires do not come into the contact analysis of the tire-nearly rigid base interaction problem, as was done previously for the tire-clay interaction problem. Such an interaction problem is shown in Fig. 4.7 where the contact profile h(t) is approximated by an appropriate polynomial $p_n(t)$ (n = even and $n \geq 4$) in such a way that its slope $h'(t) = p_n'(t)$ is set to be very small compared with unity, especially near the center of the contact surface according to the experimental results. The change of its slope is also small (i.e. no sudden change in slope), thus assuring that the approach $d_1(t)$ in Fig. 4.7 is much smaller than that of $d_2(t)$ of the tire. Hence, such a half-plane S_1^* is expected to approximate mathematically the rigid base. Then this free boundary problem will be solved in exactly the same way as that of the tire-clay interaction problem, after obtained elastic modulus of the deformable half-plane S_1^* which simulates the rigid base. Such elastic modulus will hereafter be called the elastic modulus of nearly rigid base S_1 (Section 4.4).

4.3.4 A Comparison of Solutions Obtained by the Existing Analytical Methods and the Proposed Present Analytical Approach for a Certain Class of Contact Problems (Figs. 4.4a and 4.4b)

In section 4.3.1, two entirely different contact problems, as shown in Figs. 4.4a and 4.4b, were considered, concluding that the two

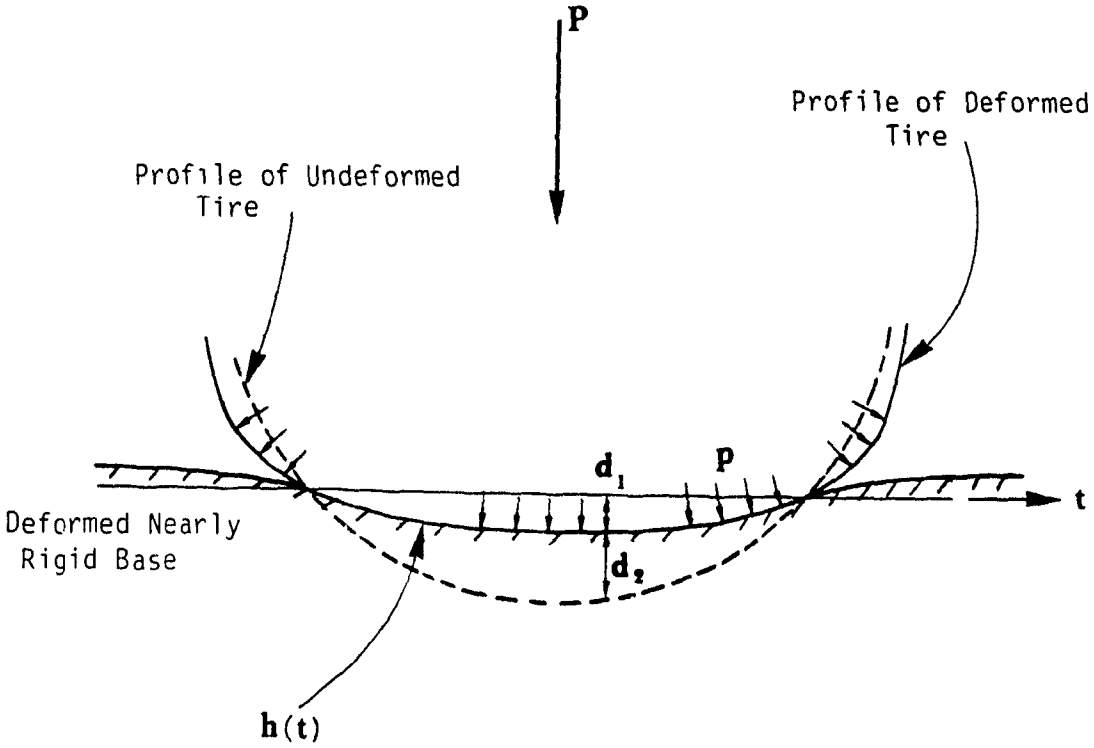


Fig. 4.7 An Interaction Between a Pneumatic Tire and a Nearly Rigid Base

problems are "mathematically" identical (i.e. give the same solutions), according to the existing analytical methods such as the complex variable-based-contact analysis and the Hertz theory, so long as the material properties of the linearly elastic solid S_2 in Fig. 4.4a and the linearly elastic half-plane S_1 in Fig. 4.4b are identical. This is clear from the following equation (Eq. A.132 in Appendix A) for the contact pressure distribution obtained by the existing analysis methods for two elastic solids in contact. If the undeformed profiles of the solids S_1 and S_2 are respectively given by $f_1(t) = 0$ and $f_2(t) = t^2/2R$ the contact pressure is shown to be

$$P(t) = \frac{4M}{R} (a^2-t^2)^{1/2} \qquad t \in L \qquad (4.86a)$$

where $M = \dfrac{G_1G_2}{\{G_1(K_2+1) + G_2(K_1+1)\}}$; $K_i = 3-4\nu_i$;

$G_i = \dfrac{E_i}{2(1+\ _i)}$; E_i = elastic modulus;

ν_i = Poisson's ratio (i=1,2) and "a" is a half of the contact length; R is radius of the cylinder if S_2 is to approximate an elastic cylinder,

The pressure distribution in Eq. 4.86a is also given by

$$P(t) = \frac{N}{2R} (a^2 - t^2)^{1/2} \qquad t \in L \qquad (4.86b)$$

where $N = \dfrac{E_1E_2}{E_2(1-\nu_1^2) + E_1(1-\nu_2^2)}$

or

$$P(t) = \frac{2P}{\pi a^2}\,(a^2 - t^2)^{1/2} \qquad t \in L \qquad (4.86c)$$

where P is the applied force per unit width.

Equations 4.86a,b,c show that even interchanging the material properties of the two elastic solids in contact, the results of contact pressure distributions (and contact area) obtained by Eq. 4.86 (and Eq. A.133) remain the same regardless of the differences in undeformed profiles and material properties for the two contacting solids. In other words, the results analytically obtained are not altered by the difference of two contact profiles due to the interchange of material properties.

Now we will compare and discuss the solutions (i.e. contact pressure distributions) obtained by virtue of both the existing analytical methods (i.e., Hertz theory, the complex variable-based contact analysis in section 4.2 and Appendix A, etc.) and the present analytical approach proposed in sections 4.3.2 and 4.3.3 the contact problems in Figs. 4.4a,b, which are elastically and geometrically very different. These contact problems are, however, simulated by those shown in Figs. 4.8a,b, respectively. This simulation is especially important for the problem in Fig. 4.4a, as was considered for the tire-rigid base interaction problem in section 4.3.3. A major difference in the solutions are attributed to contact profiles which are taken into account in the present analytical approach, and are not in the existing analytical methods.

The half-plane S_1^A in Fig. 4.8a (or the solid S_2^A in Fig. 4.8b)

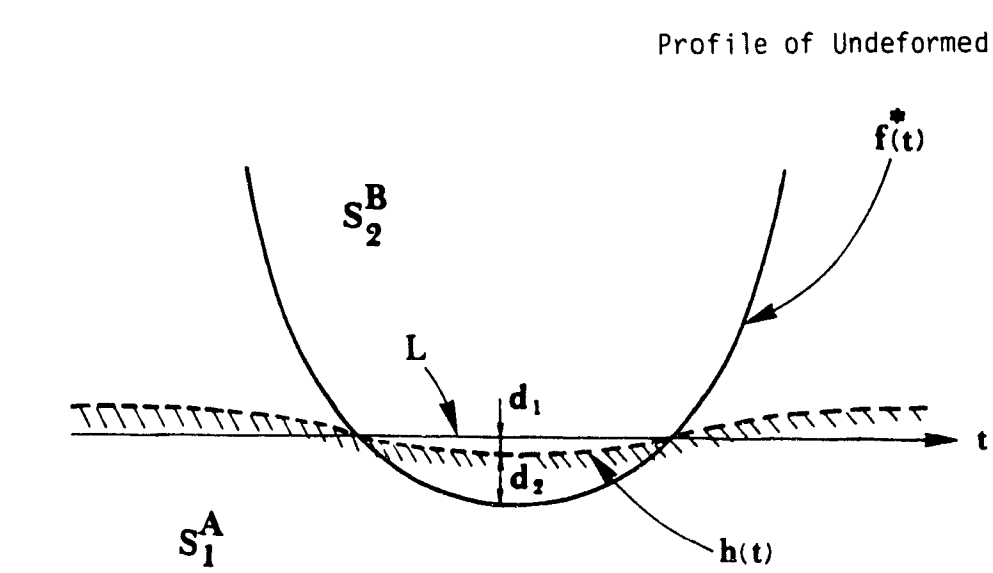


Fig. 4.8a A Contact Problem Simulating the Real One Shown in Fig. 4.4a

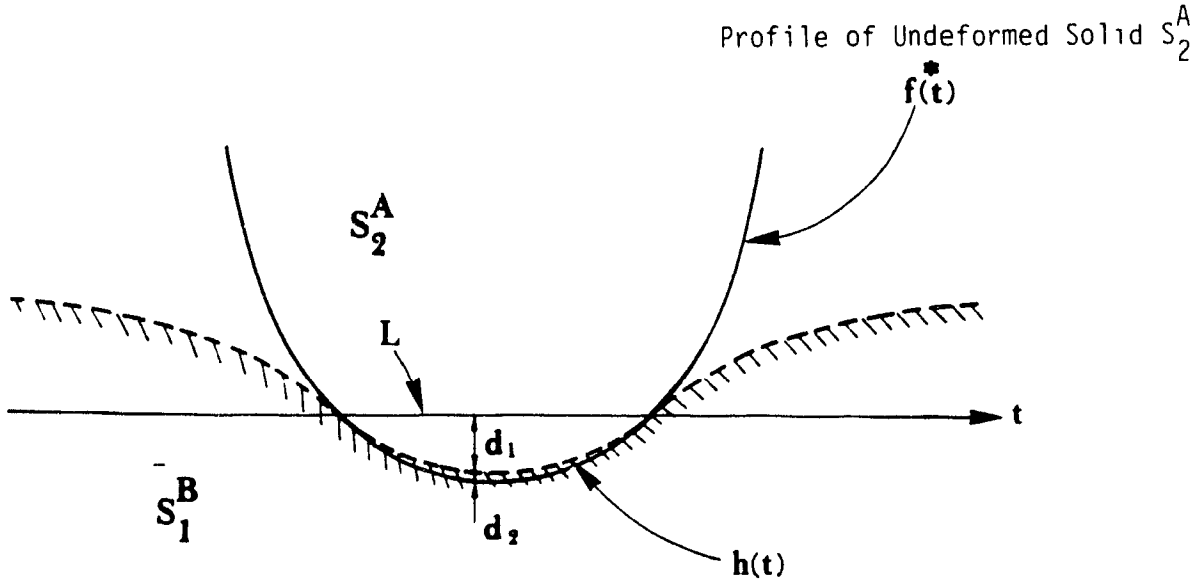


Fig. 4.8b A Contact Problem Simulating the Real One Shown in Fig. 4.4b

indicates that the original elastic half-plane S_1 in Fig. 4.4a (or S_2 in Fig. 4.4b) is now occupied by an elastic material denoted by E^A for simulation, while the solid S_2^B in Fig. 4.8a (or the half-plane S_1^B in Fig. 4.8b) indicates that the solid S_2 (or S_1 in Fig. 4.4a) is occupied by another elastically dissimilar material denoted by E^B. The elastic material E^A is now assumed to be so stiff, relative to E^B, that the contact profile h(t) and the undeformed profile f*(t) given by a second order polynomial (for the time being) for the solids S_2^B, S_2^A have the following relationships, (Fig. 4.8a and 4.8b):

(1) for the contact problem shown in Fig. 4.8a,

$$|h(t)| << |f^*(t)| \qquad t \in L \tag{4.87a}$$

and their slopes are,

$$|h'(t)| << |f^{*\prime}(t)| \qquad t \in L \tag{4.87b}$$

and also

$$h'(t) = f^{*\prime}(t) = 0 \quad \text{at } t = 0 \tag{4.87c}$$

(2) for the contact problem shown in Fig. 4.8b,

$$|h(t)| \simeq |f^*(t)| \qquad t \in L \tag{4.88a}$$

and their slopes are also,

$$|h'(t)| \simeq |f^{*\prime}(t)| \qquad t \in L \tag{4.88b}$$

and also

$$h'(t) = f^{*\prime}(t) = 0 \quad \text{at } t = 0 \tag{4.88c}$$

It is then acceptable to assume that the contact profile h(t) in Fig. 4.8a can be approximated by an appropriate polynomial of the degree n, denoted by $p_n(t)$ (e.g. n = even and $n \geq 4$), such that slope $h'(t) = p'_n(t)$ is particularly small in the vicinity of the center of the contact surface as compared with that given by $f^*(t)$, and the change of its slope is also small, while the contact profile h(t) in Fig. 4.8b is also approximated by a polynomial with the same order of $f^*(t)$ (second order polynomial). Now by applying the present analytical approach (sections 4.3.2 and 4.3.3) to the contact problem shown in Fig. 4.8a, a pattern of contact pressure distribution shown by a solid line in Fig. 4.9 would be obtained, while the application of the present analytical approach to the contact problem in Fig. 4.8b gives the contact pressure shown distribution in Fig. 4.10.

Next it is seen in the following examples that the application of the existing analytical methods, such as complex variable-based-contact analysis and the Hertz theory, to the two distinct contact problems shown in Fig. 4.8a and 4.8b will give the identical contact pressure distributions as expected from Eq. 4.86, and as shown in Fig. 4.10 - which is also obtained by the present analytical approach. If the elastic half-plane S_1^A in Fig. 4.8a becomes stiffer than at present, then the slope of the contact profile will decrease, hence requiring that the degree of polynomial approximating the contact profile be higher. This will induce another contact pressure distribution by virtue of the present analytical approach, such as that shown by a dotted line in Fig. 4.9, where the maximum contact

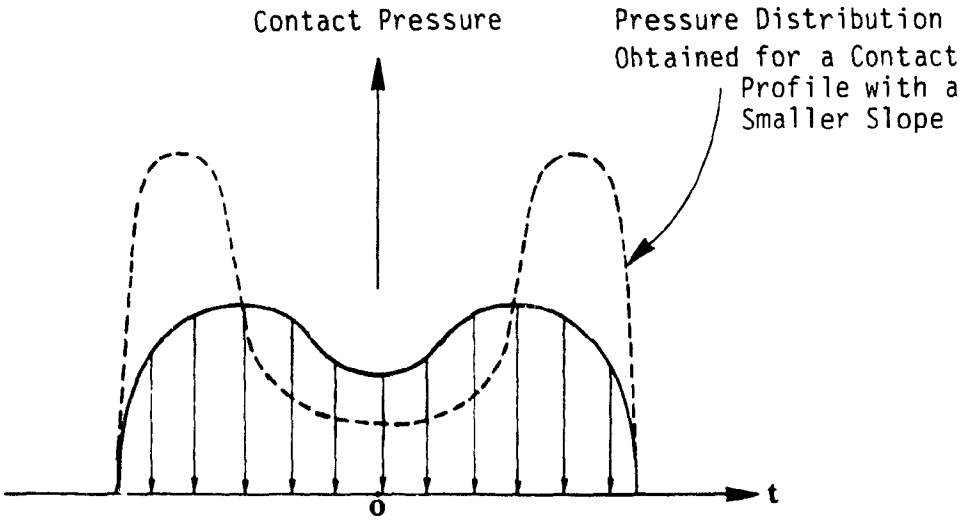


Fig. 4.9 A Pattern of Contact Pressure Distributions for the Contact Problem (Fig. 4.8a) Obtained by the Present Analytical Approach (Section 4.3.3)

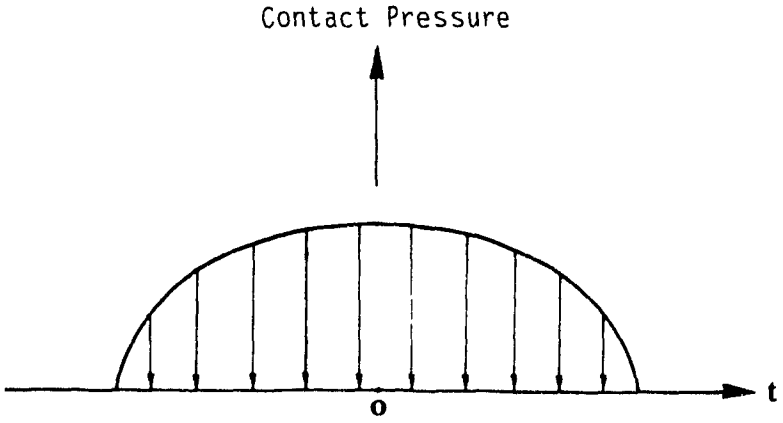


Fig. 4.10 A Pattern of Contact Pressure Distributions Either Obtained by the Present Analytical Approach (Section 4.3.2) for the Contact Problem (i.e. Fig. 4.8b) or Obtained by the Existing Analytical Methods for the Contact Problems (i.e. Figs. 4.8a,b)

pressures near the contact ends rise even more and their positions will also move nearer to the contact ends. Accordingly the contrasting patterns of contact pressure distributions for the contact problem (Fig. 4.8a) obtained by the present and the existing analytical methods will differ even further as the elastic half-plane S_2^A in Fig. 4.8a becomes stiffer as compared with S_2^B. Hence the solutions for the contact problem (Fig. 4.8a), which is to simulate the original one (Fig. 4.4a), obtained from the two distinct analytical methods will never become closer. These solutions (expected) with the experimental results (Chapter 3) suggest that the existing analytical methods, which are unable to consider real contact profiles, would be inappropriate in solving contact problems such as those shown in Figs. 4.4a and 4.8a where deformations occur only (or mostly) in the solid S_2 (which is often idealized to represent a finite solid, e.g., cylinders, punches, etc.), resulting contact profiles being (nearly) flat. This is partly due to the fact that the existing analytical methods were developed under the consideration that a half-plane will deform after contacting with the other solid.

We will close this section by giving solutions (i.e. contact pressure distributions) to the two original contact problems given in Fig. 4.4a and 4.4b, which are approximated by solving the contact problems in Fig. 4.8a and 4.8b, by means of the existing analtyical methods and the present analytical approach.

Solutions Obtained by the Existing Analytical Methods:

These solutions are simply deduced from Eq. 4.86b.

(1) The Contact Problem (Fig. 4.4a):

Assuming that the elastic modulus E_1^A of S_2^A in Fig. 4.8a is much greater than that of E_2^B of S_2^B, i.e. $E_2^B << E_1^A$ so that, $E_2^B(1-\nu_1^2)/E_1^A$ in Eq. 4.86b is negligible compared with the term $(1-\nu_2^2)$, then Eq. 4.86b gives

$$P_{(t)}^{(1)} = \frac{E_2^B}{2R(1-\nu_2^2)} (a^2-t^2)^{1/2} \qquad t \in L \qquad (4.89a)$$

(2) The Contact Problem (Fig. 4.4b):

Similarly, in Fig. 4.8b, $E_1^B << E_2^A$ such that $E_1^B/E_2^A \simeq 0$.

$$P_{(t)}^{(2)} = \frac{E_1^B}{2R(1-\nu_1^2)} (a^2 - t^2)^{1/2} \qquad t \in L \qquad (4.89b)$$

Since the material properties in both S_2^B and S_1^B are identical (i.e. E^B), $E_2^B = E_1^B$ and $\nu_1 = \nu_2$. Hence the contact pressures given by Eqs. 4.89a and 4.89b are identical, i.e. $P_{(t)}^{(1)} = P_{(t)}^{(2)}$ on L. A pattern of these pressure distributions is described in Fig. 4.10, which has been generally accepted.

Solutions Obtained by the Present Analytical Approach:

(1) The Contact Problem (Fig. 4.4a)

Suppose that a contact profile h(t) in Fig. 4.8a simulating the original problem in Fig. 4.4a is approximated by a fourth degree polynomial. The polynomial is given by $p_4(t) = t^4/3r^3$ in Eq. A.137a (Appendix A), where r is an appropriate positive constant value, such that the contact profile h(t) is set as

$$h(t) = p_4(t) = t^4/3r^3 - d_A \tag{4.90}$$

where d_A (>0) is an approach of the half-plane S_1^A, i.e. $d_A = d_1(0)$. The contact pressures for frictionless problems given by Eq. A.138 as

$$P_{(t)}^{(3)} = \frac{16M}{3r}\left(\frac{a}{r}\right)^2 \left(1+C_2 + \frac{t^2}{a^2}\right)(a^2 - t^2)^{1/2} \tag{4.91}$$

where $$M = \frac{E_2}{8(1-\nu_2^2)}$$

and the constant C_2 (Eq. A.115) for frictionless problems is given by, $C_2 = -1/2$.

Here E_2 in Eq. 4.91 must be interpreted in the sense of elastic modulus defined at the end of section 4.3.2 (and in section 4.4).

Rewriting $P_{(t)}^{(3)}$ in Eq. 4.91,

$$P_{(t)}^{(3)} = \frac{2E_2}{3r(1-\nu_2^2)}\left(\frac{a}{r}\right)^2\left(\frac{1}{2} + \frac{t^2}{a^2}\right)(a^2 - t^2)^{1/2} \tag{4.92a}$$

or

$$P_{(t)}^{(3)} = \frac{E_2}{3r^3(1-\nu_2^2)}(a^2 + 2t^2)(a^2 - t^2)^{1/2} \tag{4.92b}$$

A pattern of the contact pressure given by Eq. 4.92 (or Eq. 4.91) is shown in Fig. 4.9.

(2) The Contact Problem (Fig. 4.4b)

For this case a polynomial for the contact profile h(t) is simply set $h(t) = f^*(t)$, thus obtaining the contact pressure distribution $P_{(t)}^{(4)}$ which is identical to that given by Eqs. 4.89a and 4.89b.

i.e.,

$$\text{i.e.} \quad P^{(4)}_{(t)} = P^{(1)}_{(t)} = P^{(2)}_{(t)} \tag{4.93}$$

In the present analytical approach, patterns of contact pressure distributions will change depending on contact problems, hence depending on (approximated) contact profiles, while they will only depend on undeformed profiles of contacting solids in the existing analytical methods. In our experiments of various tire-rigid base interactions, we have found similar contact pressure distributions such as those shown in Fig. 4.9; the contact pressures are higher near the edge of the contact surface rather than the centers as shown in Fig. 4.9. Such experimental results were also reported by Kabe and Akasaka [57] (see comments of Fig. 7 in their paper).

4.3.5 Summary

We will summarize each section of section 4.3 in the following:

Section 4.3.1

The complex variable-based contact analysis (hereinafter often referred to as the analytical method), which does not take into account the contact profiles (Eq. 4.80), could produce acceptable solutions for contact problems such as

(i) Hertzian contact problem between two elastically and geometrically similar cylinders or

(ii) a contact problem between an elastic (or rigid) cylinder and an elastic half-plane where the resulting contact profile can be approximated by polynomials which would include a term of

the second degree function.

However, since tires are pneumatic bodies which means that there is no elasticity, Poisson's ratio etc., there is no way to apply any existing analytical methods directly to the present interaction problems. In order to overcome such difficulties, we will develop an analytical approach, which enables consideration of the contact profiles, on the basis of the complex variable-based contact analysis as an analytical tool. We will show our present analytical approaches in sections 4.3.2 and 4.3.3 that the present interaction problems are first transformed to equivalent free boundary problems by considering contact profiles, and then they will be solved by virtue of the analytical method after obtaining the elastic moduli in deformed states which are functions of the slope of contact profiles, characteristics of interactions, Poisson's ratios and loadings.

The two contrasting contact problems are also illustrated in Figs. 4.4a and 4.4b, since both problems are mathematically identical, according to the analytical methods (including the Hertz theory), even though the contact profiles are entirely different. The solutions obtained by such existing analytical methods for problems like those in Fig. 4.4a are questioned in section 4.3.4 when compared to those obtained by the present analytical approaches shown in sections 4.3.2 and 4.3.3, and the experimental results (Chapter 3).

Section 4.3.2

Our present analytical approach for the tire-supporting clay interaction problems is introduced. The analytical approach first

transforms an original interaction problem into an equivalent free boundary problem by taking account of contact profile (i.e. slope of contact profile), and then the free boundary problem will be solved by means of the complex variable-based contact analysis after obtaining the elastic modulus of deformed clay which will be defined in a subsequent section 4.4. This approach may also be conceived of as an inverse problem in elasticity that given a slope of contact profile $h(t)$ at a deformed state, corresponding to an axle load P, first obtain the elastic modulus (section 4.4) and then obtain contact area and contact pressure distribution by using the analytical method as a tool. In this way, one can avoid the direct consideration of the complexities of pneumatic tires in a formulation of contact analysis.

Section 4.3.3

The tire-rigid base interaction problems are also transformed into free boundary problems, but not in the same manner as that used for the tire-clay interactions since a rigid base, which may be occupied by materials like steel, concrete, rock or hard soil, is, in general, treated as undeformable, i.e. $h(t) = h'(t) = 0$, when in contact with a pneumatic tire, regardless of the magnitude of loading. One way of deriving such a free boundary problem is to replace a rigid base by a deformable half-plane so that the contact profile $h(t)$ is represented by a polynomial function of degree n, $p_n(t)$ (n = even and $n \geq 4$) where its slope $h'(t) = p_n'(t)$ is sufficiently small. Then the free boundary problem will be solved in the same manner as that for the tire-clay interaction problems (section 4.3.2),

after obtaining the elastic modulus for this deformable half-plane.

Section 4.3.4

A question regarding the solutions (i.e. contact pressure distributions) for contact problems such as the one illustrated in Fig. 4.4a (section 4.3.1), which are obtained by applying the existing analytical methods (e.g. the complex variable-based-contact analysis and the Hertz theory), is raised when compared with those obtained by applying our present analytical approach (sections 4.3.2 and 4.3.3). The contact problems in Figs. 4.4a and 4.4b are simulated respectively by those given in Figs. 4.8a and 4.8b. It is shown in Figs. 4.9 and 4.10 that although the solutions for the problems in Fig. 4.8b obtained by both the existing and the present methods are identical, the solutions for the problem in Fig. 4.8a, simulating the contact problem in Fig. 4.4a, which are between an elastic solid and a rigid half-plane, obtained by both methods are completely different. This happens since the existing analytical methods do not depend on contact profile, and depend only on the undeformed profiles of contacting solids in the formulation of contact problems, while the present analytical approaches proposed in sections 4.3.2 and 4.3.3 take into account contact profiles. The contact problems in Figs. 4.8a and 4.8b (or Figs. 4.4a and 4.4b) are mathematically equivalent, although not physically, according to the existing analytical methods, while they are not equivalent by the present analytical approach under the consideration of contact profiles.

The pattern of contact pressure distributions shown in Fig. 4.9,

which can be obtained by the present analytical approach was generally observed by our numerous experiments (tire-clay and tire-rigid base interactions) and also by other researchers (e.g. Kabe and Akasaka [57]).

4.4 On Elasticities of Nearly Rigid Base and Supporting Clay Contacting With a Pneumatic Tire

4.4.1 Introduction

In previous sections (4.3.2 and 4.3.3) it was shown that the present interaction problems will be solved approximately by transforming them into equivalent two-dimensional free boundary problems by taking account of contact profiles h(t) depending on loads. Hence, after obtaining the elastic modulus of deformed supporting clay (or nearly rigid base) contacting with a tire, one can obtain solutions (i.e. contact pressures and contact area) for a free boundary problem, which is equivalent to the given interaction problem, by virtue of the complex variable-based contact analysis under plane strain condition.

In order to obtain such an elastic modulus, this section is subdivided as follows. In the following section 4.4.2 a definition of elastic modulus and a general derivation of elastic modulus will be given. In sections 4.4.3 and 4.4.4, elastic moduli of deformed half-planes, which are occupied by nearly rigid base and supporting clay, will be found, and then their explicit forms will be derived for the two given contact profiles for each half-plane. The results given in sections 4.4.3 and 4.4.4 will be used in the subsequent sections (4.5 and 4.6) for solving the tire-supporting clay and tire-rigid base interaction problems in the present studies.

4.4.2 A Definition and a General Derivation of Elastic Modulus for Deformed Half-Plane

A. A Definition of Elastic Modulus for Deformed Half-Plane with a Contact Profile

The following conditions are given to deformed half-planes:

(1) the half-planes do not yield,

(2) the Poisson's ratios remain constant during loading,

(3) approximate slopes of contact profiles h(t) are available and they can be approximated by polynomials.

Figure 4.11 shows a deformed half-plane which resulted from pressures along the contact surface exerted by a pneumatic tire subjected to an axle load per unit width P. Then for a given load P and a corresponding contact profile h(t), a force equilibrium equation for the tire-supporting ground interaction can be derived, for example, as shown in Eq. 4.70 (i.e. Eq. A.127, Appendix A). Such a force equilibrium can be represented by a function of elastic modulus E, Poisson's ratio ν, half of the contact length a, coefficient of friction k, and slope of contact profile h'(t) in an implicit manner for the deformed half-plane, i.e.

$$P = W/B = f_1 (E, \nu, a, k; h'(t)) \qquad (4.94)$$

where W is the (total) axle load and B is its corresponding representative (i.e. idealized) contact width stated in section 4.3.

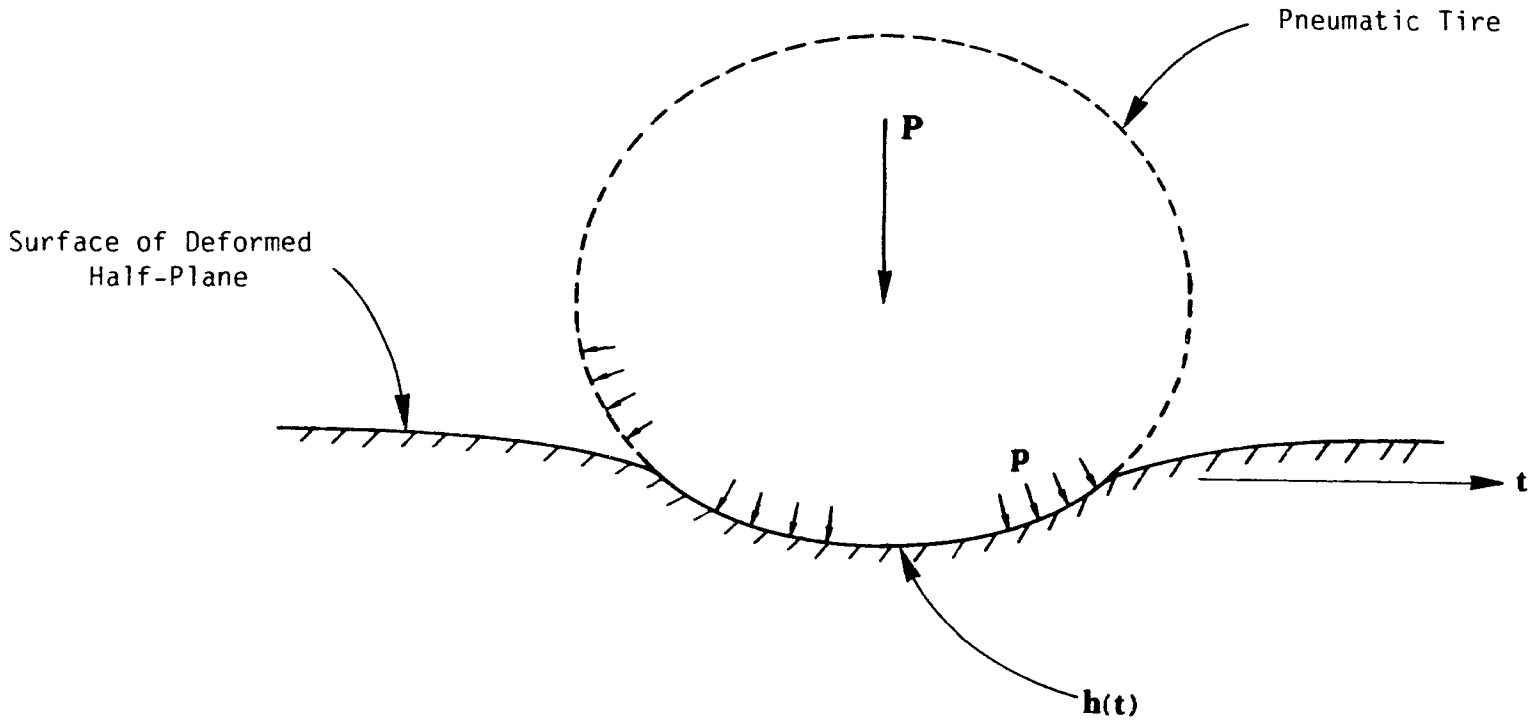


Fig. 4.11 A Deformed Half-Plane Due to an Interaction with a Pneumatic Tire

The elastic modulus E for the deformed half-plane must be defined so as to satisfy the force equilibrium equation for a given contact profile, which is derived from the complex variable-based contact analysis (section 4.2). Then such an elastic modulus E may be obtained by inverting Eq. 4.94 as,

$$E = f_2(w,B,\nu,a,k,h'(t)) \tag{4.95}$$

The elastic modulus E in Eq. 4.95, however, will be derived through consideration of the characteristics of two interacting bodies rather than directly inverting Eq. 4.94. Such characterization of two interacting bodies shown next, will exhibit clear distinctions between two different interactions such as tire-rigid base and tire-supporting clay interactions (sections 4.4.3 and 4.4.4).

B. A General Derivation of Elastic Modulus of Deformed Half-Plane with a Contact Profile

In the following it is briefly shown that the elastic modulus E of a deformed, nearly rigid base with

(1) For each h'(t) corresponding to an axle load W, one can analytically find a force equilibrium equation such as shown in Eq. 4.70 or Eq. 4.95 in compact form. From this force equilibrium equation one can derive the following equation,

$$\sigma = E^0(E,\nu,k,h'(t))\epsilon \tag{4.96a}$$

or simply

$$\sigma = E^0 \epsilon \tag{4.96b}$$

where σ = W/A and ϵ = A/Am; A = nominal contact area corresponding to axle load W; Am = 2R*B (R* = representative radius of pneumatic tire, B = representative contact width). The notations σ and ϵ will hereafter be called the average contact pressure and contact measure respectively.

(2) An equation similar to Eq. 4.96 can also be obtained from experiments of tire-clay and tire-rigid base interactions as follows

$$\sigma = E^* \epsilon \tag{4.97}$$

in which E* will be evaluated from the σ - ϵ relationship. The notation E* shows a characteristic of deformabilities of interacting bodies, and is hereafter called elastic measure for advancing contacts.

Equating Eq. 4.96 and 4.97, one obtains

$$E^0(E,\nu,k,h'(t)) = E^* \tag{4.98}$$

hence the elastic modulus E can be defined as

$$E = g(E^*,\nu,k,h'(t)) \tag{4.99}$$

Therefore, after obtaining E* in Eq. 4.97 from a few experiments, the elastic modulus E will be obtained from Eq. 4.99.

It is noted that the σ - ϵ relationships, which will be obtained from W-A relationships in experiments, characterize each interaction

for two contacting bodies more clearly than the W-A relationship, which can be seen later in interactions of tire-rigid base and tire-supporting clay (Sections 4.4.3 and 4.4.4).

4.4.3 Development of Elastic Moduli of Nearly Rigid Base for Two Distinct Contact Profiles

A. Elastic Measure E* for Tire-Rigid Base Interactions

We will briefly show how an elastic measure E* for a tire-rigid base interaction can be found as a function of axle load W. The idealized relationships between average contact pressure σ(= W/A) and contact measure ε(= A/Am) are observed to be those shown in Fig. 4.12 for all the experiments on tire-rigid base interactions. In the experiments as described in Chapter 3, four different tires with three inflation pressure are considered. The average contact pressure remains approximately constant as shown in Fig. 4.12 where ε_o denotes the maximum contact measure corresponding to the maximum loading W_o .

Hence, from Eq. 4.97

$$\sigma = E^* \varepsilon = N \quad \text{(constant)} \quad \varepsilon > 0 \qquad (4.100)$$

Next we will consider the relationships between load W and contact area A.

We then obtain the idealized relationships such as those shown in Fig. 4.13 for all the experiments. W-A relationships are approximately

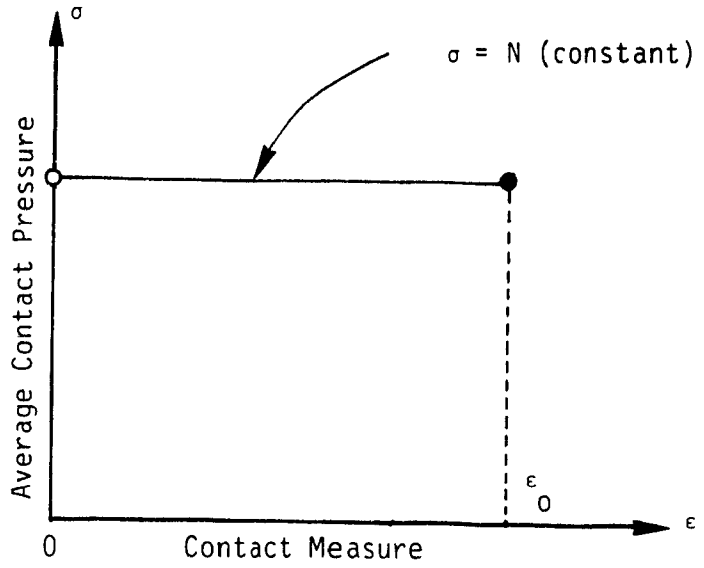


Fig. 4.12 An Idealized Relationship Between Average Contact Pressure and Contact Measure Obtained in Experiments for Tire-Rigd Base Interactions

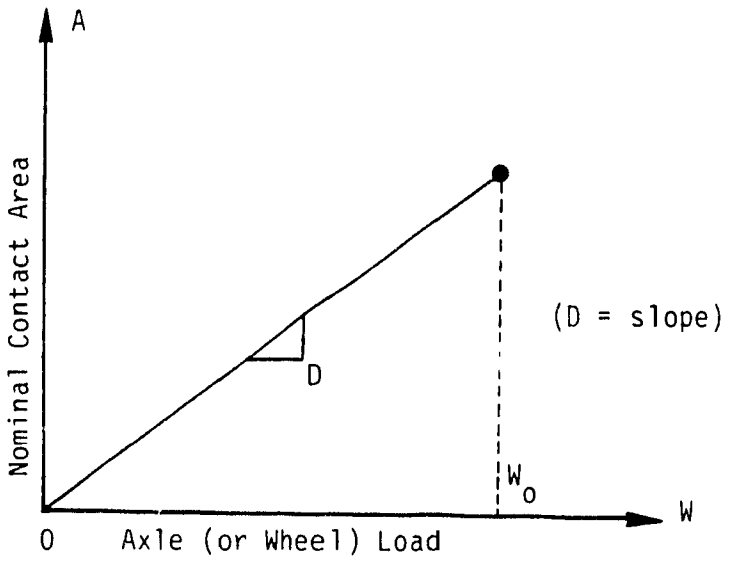


Fig. 4.13 An Idealized Relationship Between Nominal Contact Area and Load Obtained in Experiments for Tire-Rigid Base Interactions

linear with slopes D.

Then it is simply expressed as.

$$A = DW \qquad W > 0 \qquad (4.101a)$$

or

$$\frac{W}{A} = \frac{1}{D} \qquad W > 0 \qquad (4.101b)$$

where D is the slope of the graph for a W-A relationship.

Since $\sigma = W/A$ in Eq. 4.100, one finds the following relationships from Eq. 4.100 and Eq. 4.101b,

$$N = \frac{1}{D} \qquad (4.102a)$$

or

$$ND = 1 \qquad (4.102b)$$

Equations 4.101 and 4.102 will also give,

$$W = NA \qquad (4.103)$$

Hence, the elastic measure E* can be expressed as a function of axle loading W (or corresponding contact area) by considering Eqs. 4.100, 4.101, 4.102, and 4.103 as follows

$$E^* = \frac{\sigma}{\varepsilon} = N\frac{Am}{A} = \frac{N^2 Am}{W} \qquad W > 0 \qquad (4.104a)$$

or

$$E^* = \frac{WAm}{A^2} = \frac{Am}{D^2 W} \qquad W > 0 \qquad (4.104b)$$

B.1 Elastic Modulus of Nearly Rigid Base with a Contact Profile Approximated by a Polynomial Including Two Terms of Second and Fourth Degree Functions

We will derive the elastic modulus E of nearly rigid base for a contact profile, denoted as $h_1(t)$, which is given by the type of function in Eq. A.134a (Appendix A) so that its slope (Eq. A.134b) is given by

$$h_1'(t) = \frac{t}{R} + \frac{25}{32}\frac{t^3}{R^3} \qquad (4.105)$$

where R is an arbitrary positive constant for the moment. It is noted that the function in Eq. A.134a can approximate a profile of a cylinder much better than that in Eq. A.131a, if R describes its radius.

As described in B of section 4.4.2, we will first derive the force equilibrium equation for the given (slope of) contact profile h'(t) in Eq. 4.105, and then it is rewritten in the form of Eq. 4.96a. Then elastic modulus E will be derived by the approach shown in B of section 4.4.2 by using the elastic measure E* given in Eq. 4.104.

The force equilibrium for $h_1'(t)$ in Eq. 4.105 is given as follows (refer Eq. 4.70) for frictionless problem,

$$V_4(1+C_2+C_4)a^4 + V_2(1+C_2)a^2 - P = 0 \qquad (4.106)$$

where

$$V_2 = 4D_1M\pi/R = \frac{\pi E}{(2R(1-\nu^2)} \quad , \qquad (4.107a)$$

$$V_4 = 4D_2M\pi/R^3 = (\frac{5}{8})^2 \frac{\pi E}{R^3(1-\nu^2)} \quad , \qquad (4.107b)$$

$$a = \text{half of contact length} \quad , \tag{4.107c}$$

$$P = \text{axle load per unit width} \quad . \tag{4.107d}$$

Equation 4.106 can also be written as,

$$P = \frac{\pi E}{R(1-\nu^2)} \left\{ \left(\frac{5}{8R}\right)^2 (1+C_2+C_4)a^4 + \frac{1}{2} (1+C_2)a^2 \right\} \tag{4.108}$$

where for the frictionless problem, $C_2 = -1/2$ and $C_4 = -1/8$ (see Eq. A.115, Appendix A).

If B were to denote an idealized contact width although it is not necessarily known for the moment, then the contact area A and the potential maximum contact area Am will be respectivelly expressed as $A = 2aB$ and $Am = 2R^*B$ for a large load. Then the equation corresponding to Eq. 4.96a will be induced from Eq. 4.108 as follows:

$$\sigma = (E_1^0 + E_2^0)\varepsilon \tag{4.109}$$

where

$$E_1^0 = \frac{\pi E}{8(1-\nu^2)} \tag{4.110a}$$

$$E_2^0 = \frac{75\ \pi E}{1024(1-\nu^2)} \left(\frac{A}{Am}\right)^2 \tag{4.110b}$$

Next equating Eq. 4.100 and Eq. 4.109 with the consideration of Eq. 4.104, then one obtains an equation equivalent to that given in Eq. 4.98 as

$$E^* = E_1^0 + E_2^0 \tag{4.111}$$

Accordingly the elastic modulus E of a nearly rigid base corresponding to the contact profile in Eq. 4.105 is given by

$$E(W) = \frac{1024\ N^2\ Am^3\ (1-\nu^2)}{\pi W(128Am + 75\ D^2\ W^2)} \qquad W > 0 \qquad (4.112a)$$

where N and D are constants given in Eq. 4.100 and Eq. 4.101 respectively; ν = Poisson's ratio; W = axle load; Am = 2R*B.

Considering the relationship of N and D given in Eq. 4.102, the elastic modulus in Eq. 4.112a is given as

$$E(W) = \frac{1024\ N^4\ Am^3\ (1-\nu^2)}{\pi W(128\ N^2\ Am^2 + 75\ W^2)} \qquad W > 0 \qquad (4.112b)$$

or since N = 1/D in Eq. 4.102a, Eq. 4.112b is also expressed as

$$E(W) = \frac{1024\ Am^3\ (1-\nu^2)}{\pi W\ D^2(128\ Am^2 + 75\ D^2\ W^2)} \qquad W > 0 \qquad (4.112c)$$

Equations 4.112(a,b,c), obtained above, are the final forms for elastic modulus of a nearly rigid base in a deformed state. It should be mentioned that the elastic modulus (Eqs. 4.112a,b,c) depends on neither representative contact length "a" nor on contact width "B", but on the axle load only. It is achieved by transforming the force equilibrium equation (Eq. 4.106) into the equivalent form of the equation (Eq. 4.109), which is then compared with Eq. 4.100.

If we consider Eq. 4.103 for Eq. 4.112, one obtains the elastic modulus as a function of contact area A,

$$E_{(A)} = \frac{1024\ N\ Am^3\ (1-\nu^2)}{\pi A(128Am^2 + 75\ A^2)} \qquad A > 0 \qquad (4.113)$$

B.2 Elastic Modulus of Nearly Rigid Base with a Contact Profile Approximated by a Fourth Degree Polynomial (Eq. A.137a)

The elastic modulus for the nearly rigid base, whose contact profile is denoted as h (t) is given by a type of function in Eq. A.166a, and will be derived in exactly the same manner as was done in B.1 (section 4.4.3). The slope of contact profile will be given as

$$h'_2(t) = \frac{4}{3}\frac{t^3}{R^3} \qquad (4.114)$$

Then the corresponding force equilibrium is given as

$$V'_4\ (1 + C_2 + C_4)a^4 - P = 0 \qquad (4.115)$$

where for frictionless problems $C_2 = -1/2$, $C_4 = -1/8$ and

$$V'_4 = \frac{16M\pi}{3R^3} = \frac{2\pi E}{3R^3(1-\nu^2)}$$

Then for the above force equilibrium equation, one obtains the following equation

$$\sigma = E^0\ \epsilon \qquad (4.116)$$

where

$$E^0 = \frac{\pi E}{8(1-\nu^2)}\ \left(\frac{A}{Am}\right)^2 \qquad (4.117)$$

Then, as was done previously, equating Eq. 4.100 and Eq. 4.116, one obtains

$$E^* = E^0 \tag{4.118}$$

Accordingly, considering Eq. 4.104, the elastic modulus of a nearly rigid base for the contact profile given by Eq. 4.114 is obtained as

$$E_{(W)} = \frac{8(1-\nu^2)}{\pi D^4} \left(\frac{Am}{W}\right)^3 \qquad W > 0 \tag{4.119}$$

where Am = 2R*B and D = 1/N in Eq. 4.102.

The elastic modulus in Eq. 4.119 is also expressed as a function of contact area A, by considering Eqs. 4.101, 4.102 and 4.103, as

$$E_{(A)} = \frac{8(1-\nu^2)}{\pi D} \left(\frac{Am}{A}\right)^3 \qquad A > 0 \tag{4.120}$$

4.4.4 Development of Elastic Moduli of Supporting Clay for Two Distinct Contact Profiles

In this section the ideas employed in section 4.4.3 will be applied in determining the elastic modulus of clay in the deformed state. The elastic moduli of supporting clay for the two given contact profiles, which are considered in the previous section 4.4.3, will again be derived explicitly.

A. Elastic Measure E* for Tire-Clay Interactions

The elastic measure E* for tire-clay interactions can be obtained from the idealized relationships between average contact pressure (i.e. $\sigma = W/A$) and contact measure (i.e. $\varepsilon = A/Am$), which are based on experimental data, as shown in Fig. 4.14.

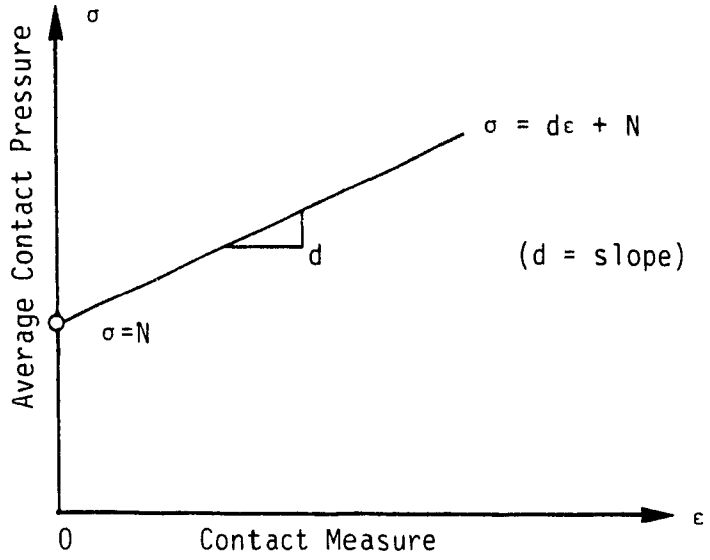


Fig. 4.14 An Idealized Relationship Between Average Contact Pressure and Contact Measure Obtained in Experiments for Tire-Supporting Clay Interactions

We may first decompose the average contact pressure σ as

$$\sigma = \sigma_1 + \sigma_2 = E^* \varepsilon \qquad \varepsilon > 0 \tag{4.121}$$

where $\sigma_1 = W_1/A$ and $\sigma_2 = W_2/A$ (i.e. $W = W_1 + W_2$).

Since the average contact pressure is approximated by a linear function as shown in Fig. 4.14,

$$\sigma = d\varepsilon + N \tag{4.122}$$

where d is the slope of σ and N is the approximated value shown in Fig. 4.14, one can put σ_1 and σ_2 in Eq. 4.121 as

$$\sigma_1 = N = E_1^* \varepsilon \tag{4.123a}$$

and

$$\sigma_2 = d\varepsilon = E_2^* \varepsilon \ . \tag{4.123b}$$

Substituting Eqs. 4.123 into Eq. 4.121,

$$\sigma = \sigma_1 + \sigma_2 = E^*\varepsilon = (E_1^* + E_2^*)\varepsilon \tag{4.124}$$

then the elastic measures E_1^* and E_2^* in components are obtained as

$$E_1^* = \frac{N^2 Am}{W_1} \tag{4.125a}$$

where the force W_1 is derived from Eq. 4.122 and Eq. 4.123 as

$$W_1 = \sigma_1 A = \frac{N\,Am}{2d} \left\{ - N + \left(N^2 + \frac{4Wd}{Am} \right)^{1/2} \right\} \tag{4.125b}$$

and

$$E_2^* = d \tag{4.125c}$$

It is however, noted that the elastic measure E_1^* in Eq. 4.125a will be set zero in the following derivation of elastic modulus since the values of N ($= \sigma_1$), which are obtained from the idealized relationships as shown in Fig. 4.14 are, in general, observed to be zero or negligibly small in the present experimental data on tire-supporting clay interactions. Therefore, the elastic measure E_2^* in Eq. 4.125c will be considered for the development of elastic modulus of supporting clay interacting with tires, i.e. Eq. 4.121 is now set

$$\sigma = \sigma_2 = E^*\varepsilon \tag{4.126}$$

where $E^* = E_2^* = d$, (4.127a)

and $\sigma = W/A$ and $\varepsilon = A/Am$ (4.127b)

B.1 Elastic Modulus of Supporting Clay with a Contact Profile Approximated by a Polynomial Including Two Terms of Second and Fourth Degree Functions

Considering Eq. 4.109 and Eq. 4.126, one deduces that for the type of contact profile in Eq. A.134a (or Eq. 4.105)

$$E^* = E_1^0 + E_2^0 \tag{4.128}$$

where E^*, E_1^0, and E_2^0 are respectively given in Eqs. 4.126, 4.110a and 4.110b.

Then the elastic modulus of supporting clay with the contact profile in Eq. A.134a (or Eq. 4.105) is given as

$$E_{(W)} = \frac{1024\ d^2 Am\ (1-\nu^2)}{\pi(128\ d\ Am + 75W)} \qquad W > 0 \qquad (4.129)$$

Expressing the elastic modulus as a function of contact area A by considering Eq. 4.126,

$$E_{(A)} = \frac{1024\ d\ Am^2\ (1-\nu^2)}{\pi(128\ Am^2 + 75\ A^2)} \qquad A > 0 \qquad (4.130)$$

B.2 Elastic Modulus of Supporting Clay with a Contact Profile Approximated by a Fourth Degree Polynomial (Eq. A.137a)

For a contact profile given by Eq. A.137a (or Eq. 4.114), one can obtain the following equation, by equating Eq. 4.116 and Eq. 4.126,

$$E^* = E^0 \qquad (4.131)$$

where E^* and E^0 are respectively given in Eq. 4.127 (or Eq. 4.125c) and Eq. 4.117, i.e.

$$d = \frac{E}{8(1-\nu^2)} \left(\frac{A}{Am}\right)^2 \qquad (4.132)$$

where $A^2 = WAm/d$.

Hence, the elastic modulus of supporting clay with the contact profile Eq. A.116a will be given as

$$E_{(W)} = \frac{8\, d^2\, Am\, (1-\nu^2)}{\pi W} \qquad W > 0 \qquad (4.133)$$

Expressing the elastic modulus in terms of contact area A,

$$E_{(A)} = \frac{8\, d\, Am^2\, (1-\nu^2)}{\pi A^2} \qquad A > 0 \qquad (4.134)$$

4.5 Scheme of the Present Analytical Approach with a Flow Diagram

The scheme of the present analytical approach to the interaction problems will be summarized in a step by step fashion in the following, by referring to the flow diagram of the approach shown in Fig. 4.15.

Step 1

(1.1) Choose one of the present interaction problems; an interaction problem of either tire-clay or tire-rigid base.

Step 2

(2.1) A free boundary problem is derived, which is equivalent to

(i) tire-clay interaction (section 4.3.2)

(ii) tire-rigid base interaction (section 4.3.3)

(2.2) An appropriate contact profile will be selected. Two functions given in Eqs. A.134a and A.137a, which are of the second and the fourth degree polynomial functions respectively, are considered to approximate contact

profiles. It is noted that the use of Eq. A.166a is adequate for both interactions since the slope of its function is very small required for both interactions.

(2.3) Derive the formulae of (vertical) force equilibrium equation, contact pressure and contact area for the given contract profile by means of the complex variable-based contact analysis (section 4.2 and Appendix A). These formulae are given in section 9.4 of Appendix A, and the corresponding force equilibrium equations are also given in Eqs. 4.106 and 4.115.

Step 3

Each step is clear from section 4.4 for obtaining the elastic modulus $E = f(E^*(W), \nu; h'(t))$ where an appropriate value for the Poisson's ratio ν should be given.

Step 4

(4.1) Choose which one of the following problems is to be determined, either

(i) quasi-static sliding interaction problem (frictional)

or

(ii) static interaction problem (frictionless).

(4.2) Calculate contact pressure and contact area using the formulae determined in step 2.3 (or section 9.4 of Appendix A).

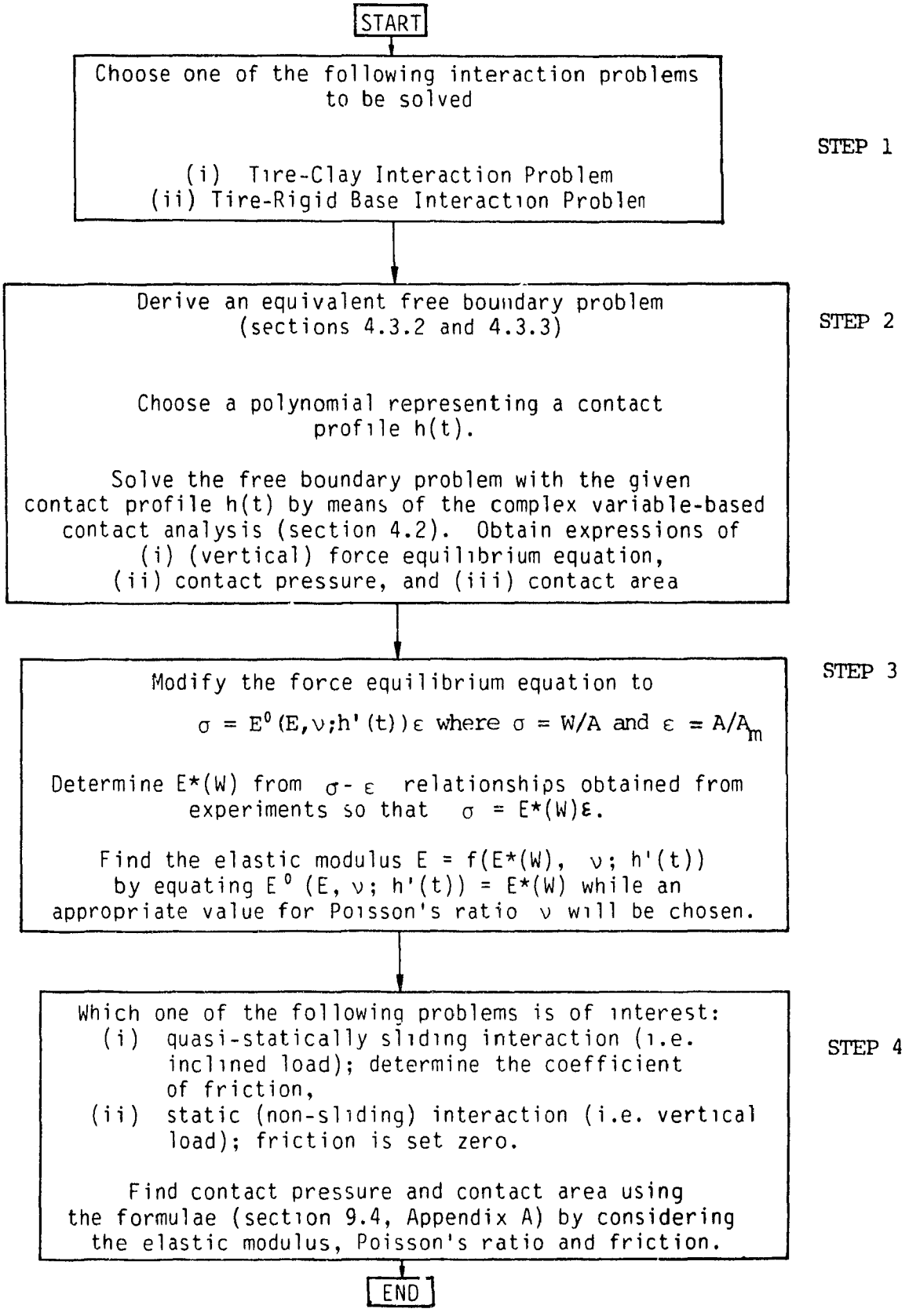


Fig. 4.15 Flow Diagram of the Present Analytical Approach

4.6 Discussions and Remarks on the Experimental and Analytical Results for the Tire-Clay and Tire-Rigid Base Interaction Problems

4.6.1 Introduction

The various interaction problems, selected from the interactions carried out in the experiments (Chapter 3), are solved for contact pressure distribution and contact area (i.e. contact length) by means of the analytical approach proposed in sections 4.3 and 4.4 for the tire-clay and tire-rigid base interactions, respectively. The scheme of the analytical approach is shown in section 4.5 with a flow diagram in Fig. 4.15. The results obtained analytically are then plotted together with the experimental results, chiefly in validating the present analytical approach. In section 4.6.2, the interaction problems and the presumptions imposed on the problems are stated. In section 4.6.3 the analytical and experimental results are compared and discussed.

4.6.2 The Interaction Problems Solved by the Present Analytical Approach and the Presumptions Imposed on the Problems

Two different types of interaction problems are considered; one is the buffed tire-clay interaction (Table 4.1a) and the other is the buffed tire-rigid base interaction (Table 4.1b.c). Hereafter the buffed tire is simply written as tire unless stated otherwise. The tire-sand interaction was avoided because of the behaviour of incohesive silica sand is fundamentally different from that of an

Types of Tires	Inflation Pressure (kPa)	Axle Load W (kN)	Radius of Tire R (m)	Representative Contact Width B (m)	Potential Maximum Contact Area, Am (m^2)
GOODYEAR 7.00-16LT	34.5	4.007	0.37	0.194	0.152
(BUFFED)	310.5	3.473	0.37	0.181	0.152
MICHELIN 7.00R-16XCL	34.5	3.584	0.376	0.217	0.138
(BUFFED)	310.5	3.584	0.376	0.212	0.138
MICHELIN 11.00R-16XL	34.5	3.206	0.461	0.244	0.232
(BUFFED)	207.	3.423	0.461	0.262	0.232
MICHELIN 12.5R-16.5XLM	34.5	3.206	0.44	0.241	0.219
(BUFFED)	207.	3.423	0.44	0.232	0.219

Table 4.1a Buffed Tire-Clay Interaction Problems Solved by the Analytical Approach

Types of Tires	Inflation Pressure (kPa)	Axle Load W (kN)	Representative Contact Width B (m)
GOODYEAR 7.00-16LT (BUFFED)	34.5	1.067	0.095
		1.423	0.113
		1.779	0.125
	103.5	2.669	0.104
		3.558	0.124
		4.448	0.136
	310.5	2.669	0.083
		4.003	0.08
		5.338	0.095
		6.672	0.108

Note 1: Radius of Tire (R) = 0.37 m

Note 2: Potential Maximum Contact Area (Am) = 0.152 m

Table 4.1b Buffed Tire-Rigid Base Interaction Problems Solved by the Analytical Approach

Types of Tires	Inflation Pressure (kPa)	Axle Load W (kN)	Radius of Tire R (m)	Representative Contact Width B (m)	Potential Maximum Contact Area, Am (m^2)
MICHELIN 7.00R-16XCL (BUFFED)	34.5	1.067	0.376	0.103	0.138
	103.5	2.846	0.376	0.109	0.138
	310.5	8.006	0.376	0.149	0.138
MICHELIN 11.00R-16XL (BUFFED)	34.5	1.868	0.461	0.103	0.232
	207.	6.405	0.461	0.137	0.232
	414.	13.344	0.461	0.152	0.232
MICHELIN 12.5R-16.5XLM (BUFFED)	34.5	1.423	0.44	0.16	0.219
	103.5	3.558	0.44	0.155	0.219
	207.	4.003	0.44	0.123	0.219

Table 4.1c Buffed Tire-Rigid Base Interaction Problems Solved by the Proposed Analytical Approach

elastic material.

The tire-clay and tire-rigid base interaction problems were selected from those which were carried out in the experiments (Chapter 3) so that the analytical solutions can be compared with those obtained in the experimentsl.

Five presumptions required for the present analytical approach are described in the following regarding Poisson's ratio, friction, contact profile, representative contact width and modulus of elasticity.

(1) Poisson's Ratio

The Poisson's ratios of both the supporting clay and "nearly" rigid base are assumed to take 0.35 for all the interaction problems. It is worthwhile to note from a practical point of view that changing the Poisson's ratio has very little influence on the analytical solutions such as contact pressure distribution and contact length.

(2) Friction at Contact Surface

The friction at the contact surface is considered to be zero for all the interaction problems given in Tables 4.1a,b. But the frictional problems were also considered for the tire-rigid base interactions in Table 4.1c by assuming that the friction be 0.37. It is also noted that there are no significant differences in the analytical results, at least, if the friction is set less than unity.

(3) Contact Profiles

The contact profiles observed in the experiments for the tire-clay interactions could be reasonably approximated by either one of

the two different forms given in Eqs. A.134a and A.137b. Their slopes are given by Eq. 4.105 (or Eq. A.134b) and Eq. 4.114 (or Eq. A.137b). These functions are also assumed to be independent of loading.

Furthermore, the real value "R" in the equations is set at a (nominal) radius of each tire in the present composition although such an assumption is not necessary so long as the function approximates a contact profile. As discussed previously, Eq. A.134a can well approximate an "arc-shaped" contact profile, which could result from an interaction between a solid cylinder and a soft supporting clay, provided that the solid cylinder is relatively stiffer than the clay and the load is under the certain magnitude, not to cause a "flat-shaped" contact profile.

In the present contact analysis, however, all the contact profiles observed between each tire and the supporting clay are approximated by the single equation Eq. A.137a. This presumed all the contact profiles are flat-shaped, regardless of the type of tire, inflation pressure and loading. Such a function given by Eq. A.137a is reasonably accurate in approximating the real ones according to the amount of experimental data on contact profiles. Besides the contact profiles obtained in most of the experiments showed little difference in their slopes, which are given by Eq. A.137b (or Eq. 4.114).

In the case of the tire-rigid base interaction problems, the contact profiles are assumed to take a form given by Eq. A.137a chiefly because the equation can well approximate a flat-shaped contact profile.

(4) Representative Contact Width

The definitions of the representative contact width were given for three different cases in section 3.4 of which the representative contact surfaces and contact pressure distribution were defined in order to make possible comparison of the two-dimensional analytical solution with the experimental results.

In general, since neither the representative contact width nor the contact area-load relationship is available for an arbitrary load, one would need to consider either Case 2 or Case 3 to define contact width, depending on problems, rather than Case 1 which can be used only when all the necessary information on contact surface is available. In the present computation, Case 1 is used for the definition of contact width, since the information on all the contact surfaces was available (Tables C.2 and D.1) and the main objective of the computation is to validate the proposed analytical approach.

(5) Modulus of Elasticity for Supporting Clay and Nearly Rigid Base

A modulus of elasticity for clay or rigid base is obtained according to the two contact profiles (Eqs. A.134a and A.137a) for all four different tires regardless of inflation pressures and loading. For obtaining modulus of elasticity for clay, the uniform (i.e. average) contact stress-contact measures in Figs. 4.16-4.19 are used.

4.6.3 Discussions and Remarks on the Experimental and Analytical Results for the Selected Problems

All the analytical and experimental results on the tire-clay and tire-rigid base interaction problems (Tables 4.1a,b and c) were

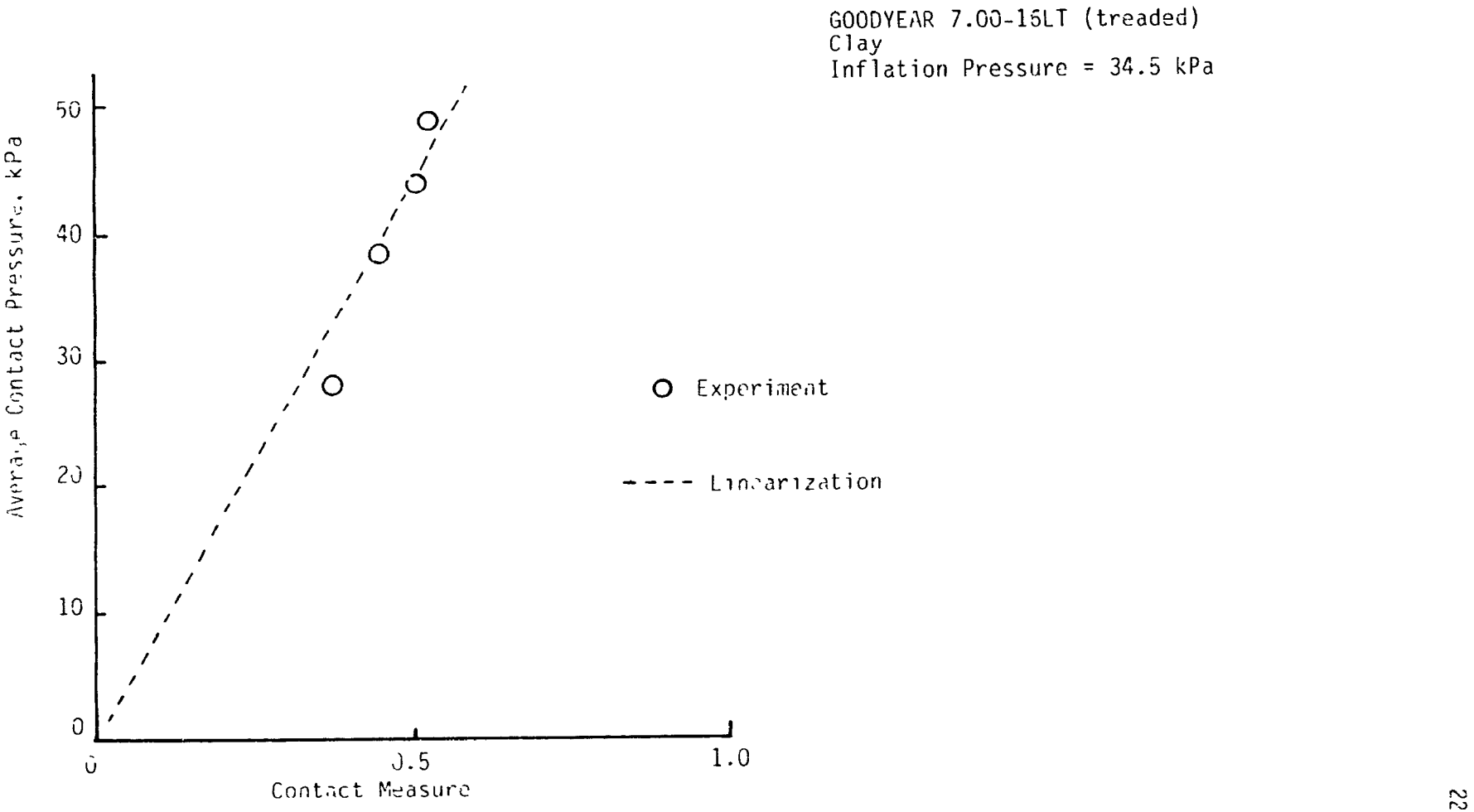


Fig. 4.16a Average Contact Pressure - Contact Measure Relationship for GOODYEAR 7.00-16LT (treaded)

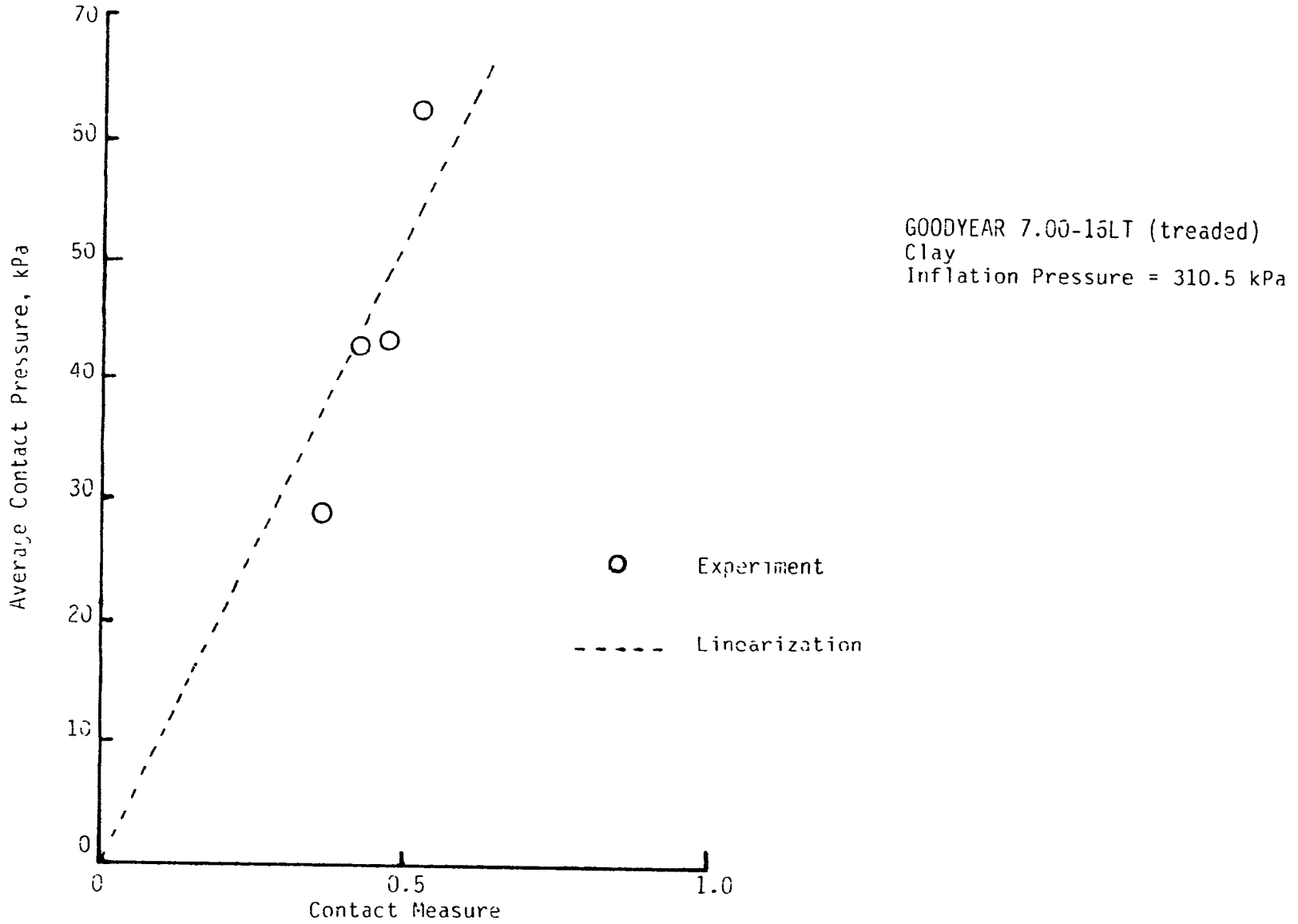


Fig. 4.16b Average Contact Pressure - Contact Measure Relationship for GOODYEAR 7.00-16LT (treaded)

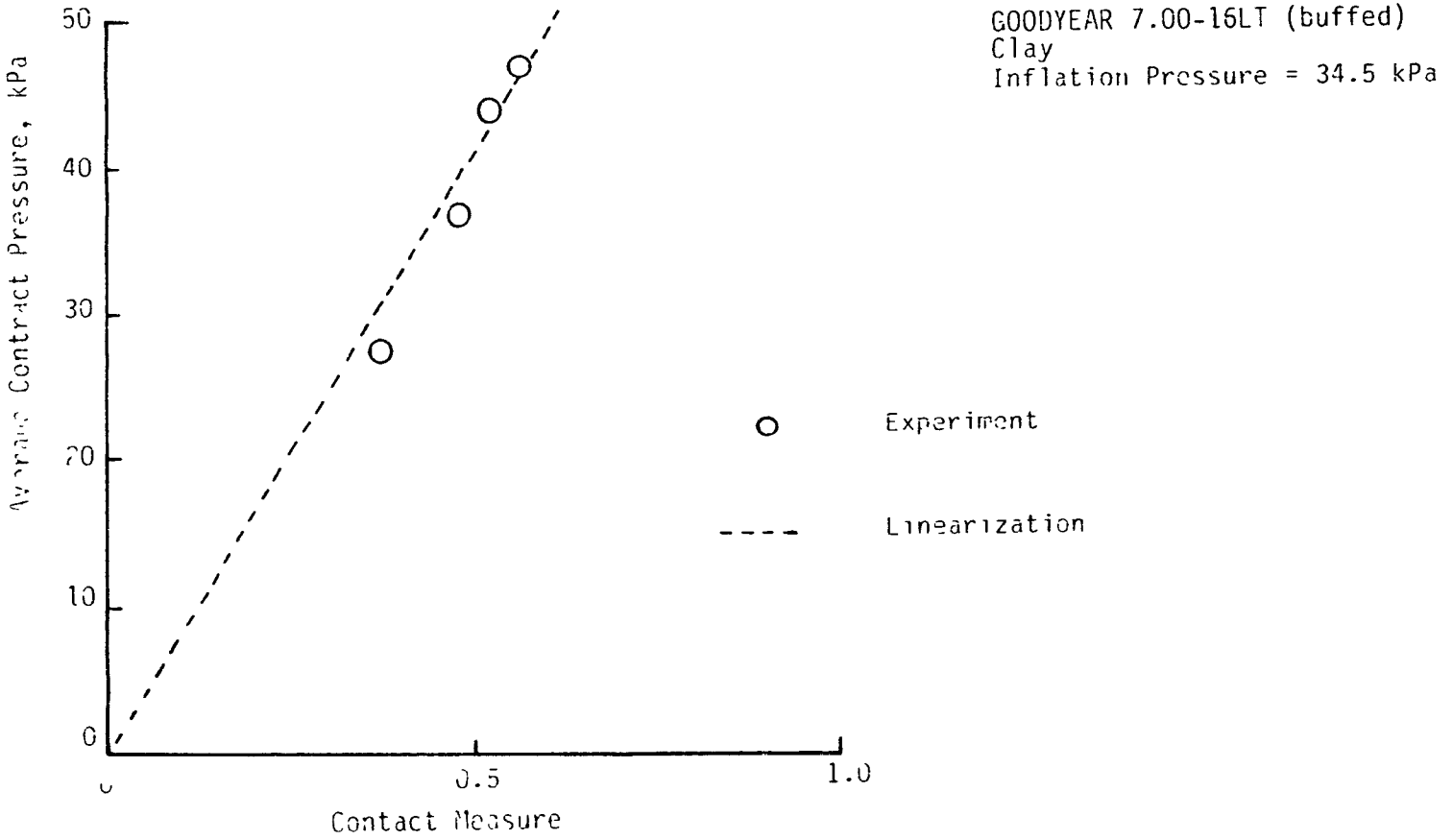


Fig. 4.16c Average Contact Pressure - Contact Measure Relationship for GOODYEAR 7.00-16LT (buffed)

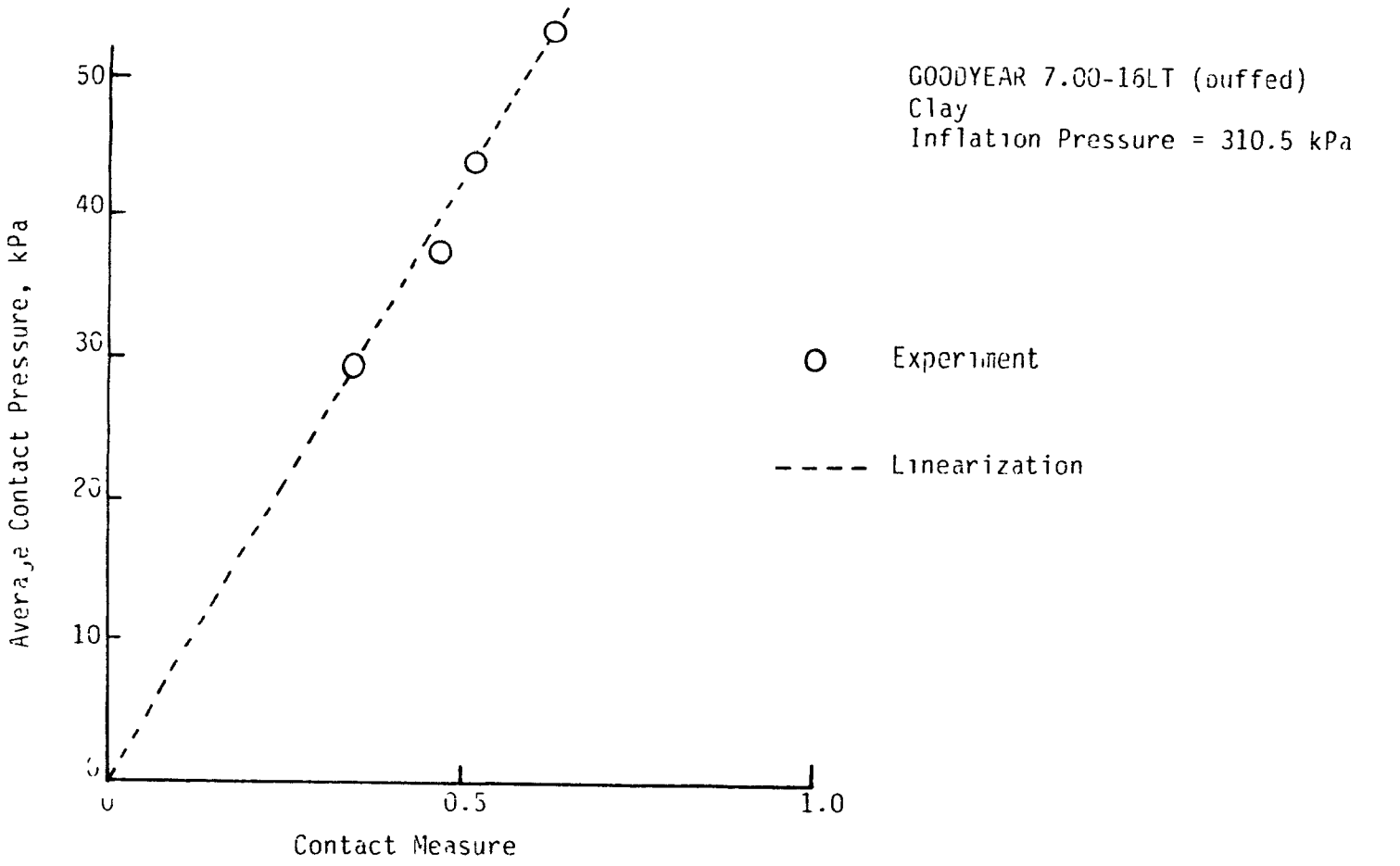


Fig. 4.16d Average Contact Pressure - Contact Measure Relationship for GOODYEAR 7.00-16LT (buffed)

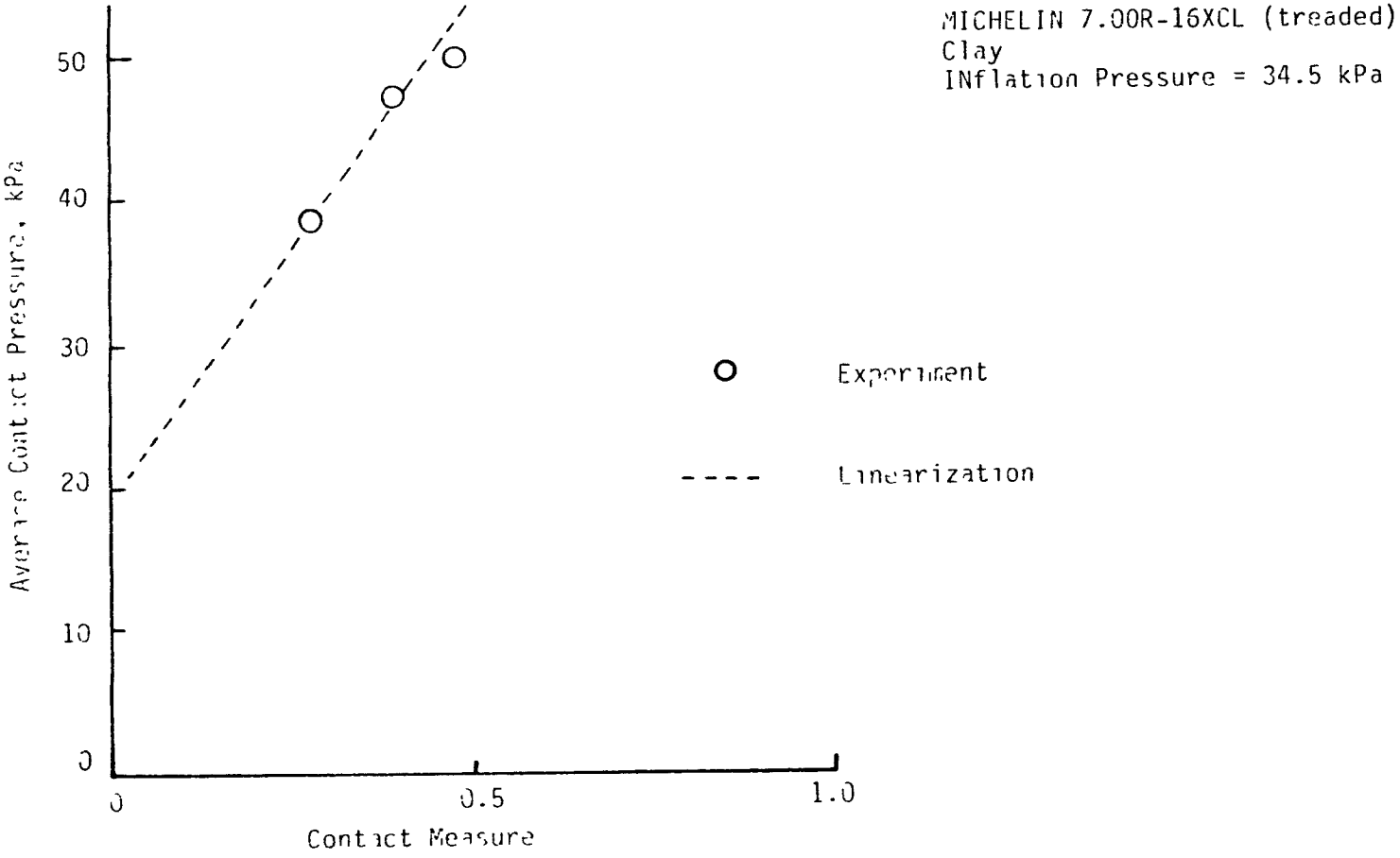


Fig. 4.17a Average Contact Pressure - Contact Measure Relationship for MICHELIN 7.00R-16XCL (treaded)

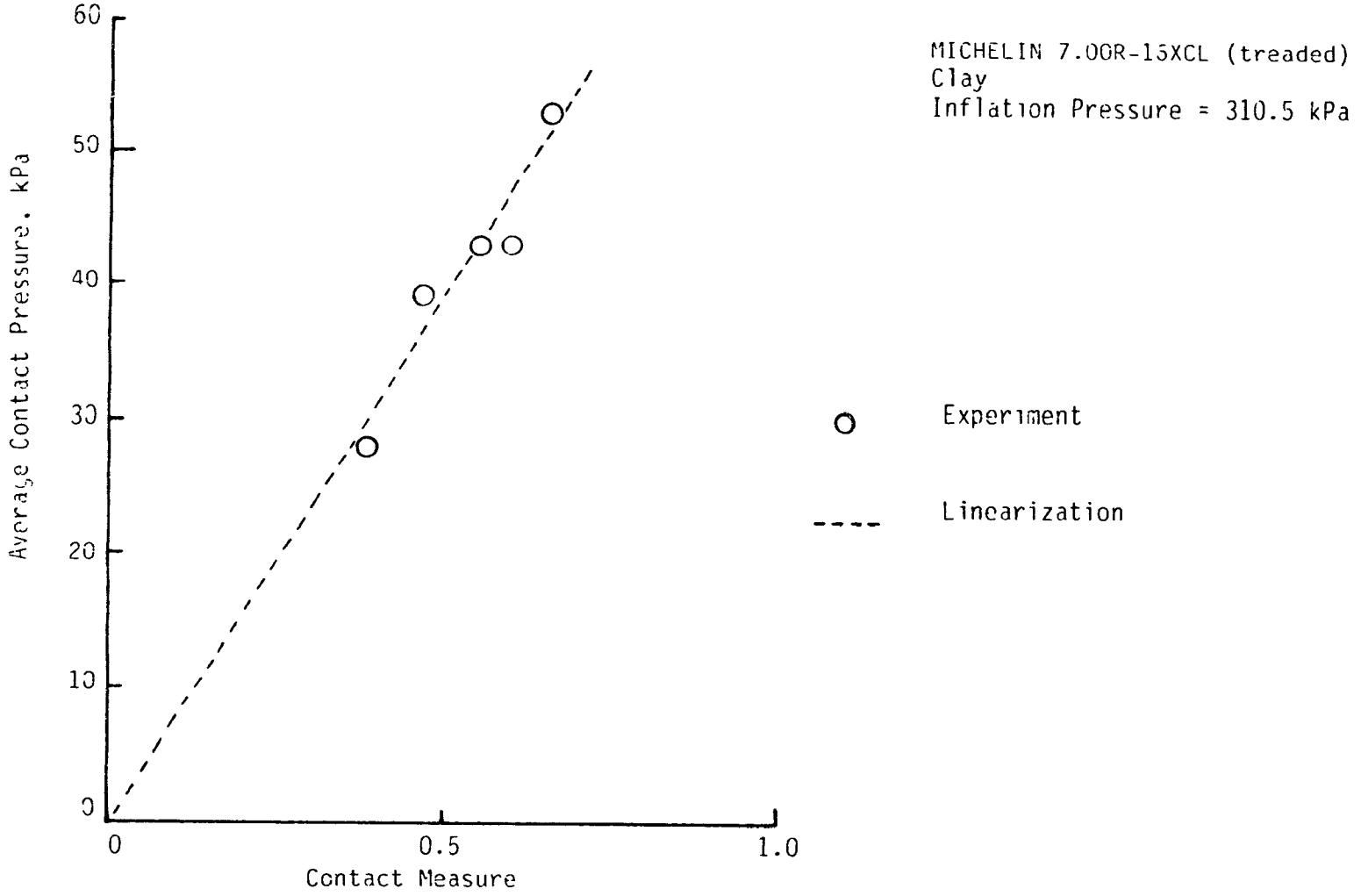


Fig. 4.17b Average Contact Pressure - Contact Measure Relationship for MICHELIN 7.00R-16XCL (treaded)

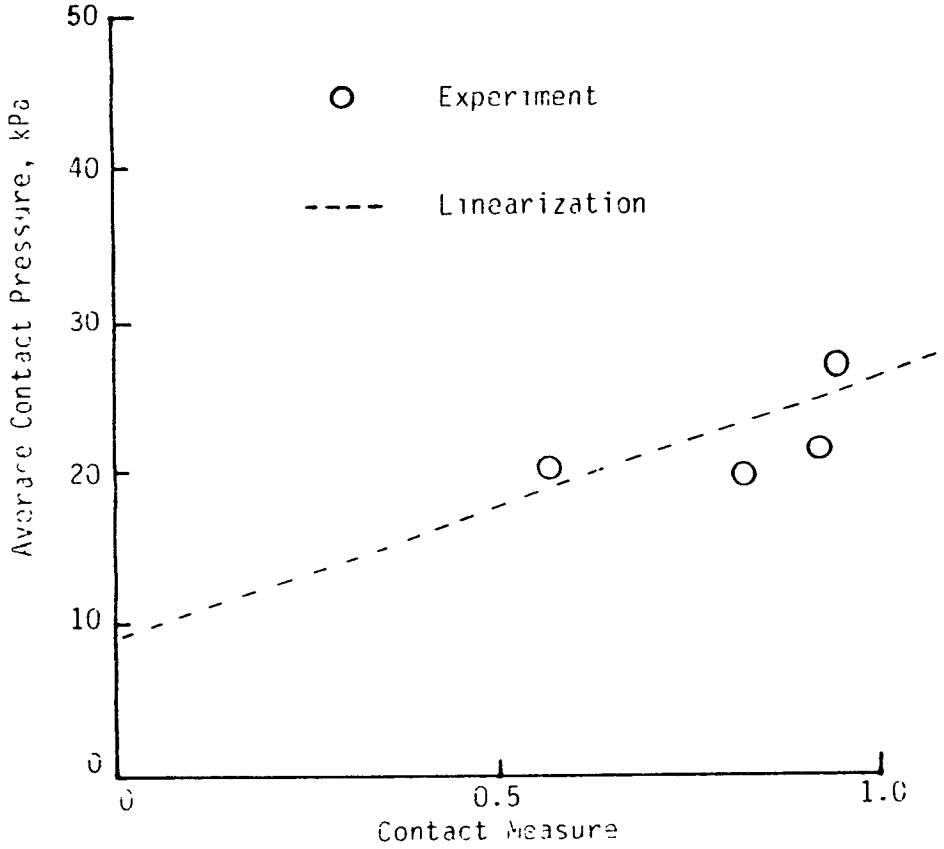


Fig. 4.17c Average Contact Pressure - Contact Measure Relationship for MICHELIN 7.00R-16XCL (buffed)

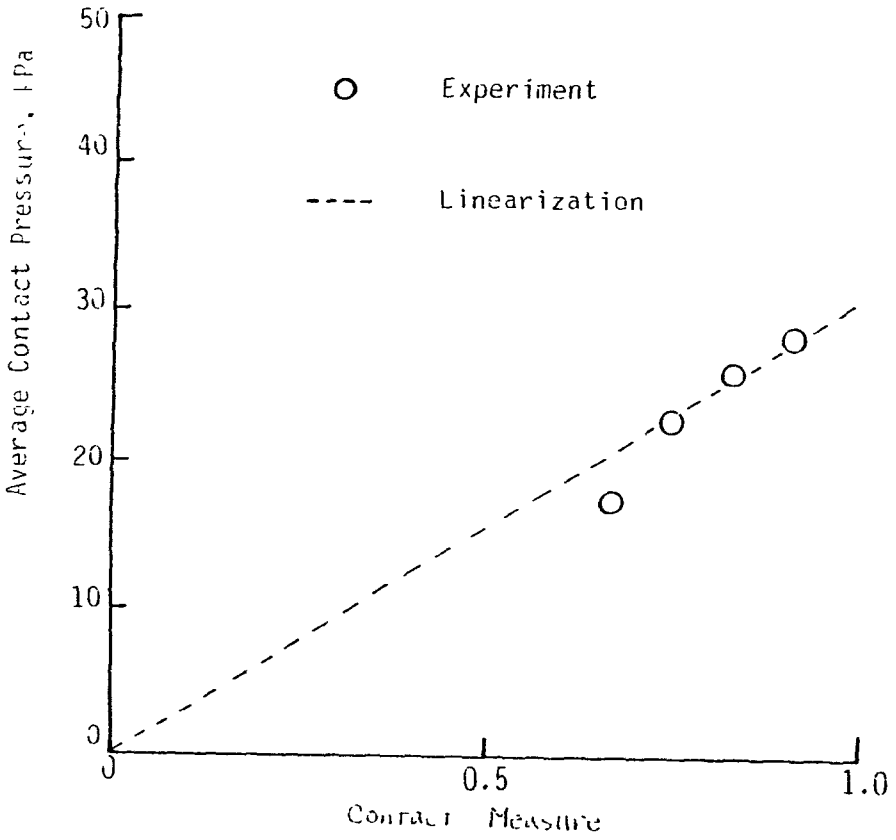


Fig. 4.17d Average Contact Pressure - Contact Measure Relationship for MICHELIN 7.00R-16XCL (buffed)

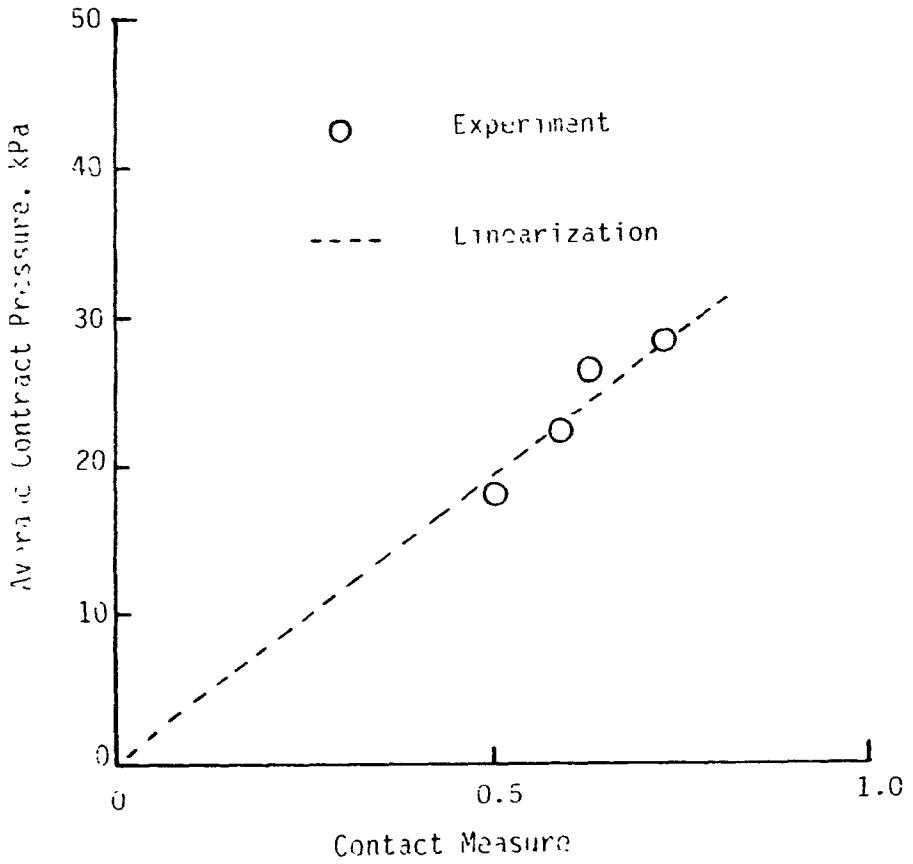


Fig. 4.18a Average Contact Pressure - Contact Measure Relationship for MICHELIN 11.00R-16XL (treaded)

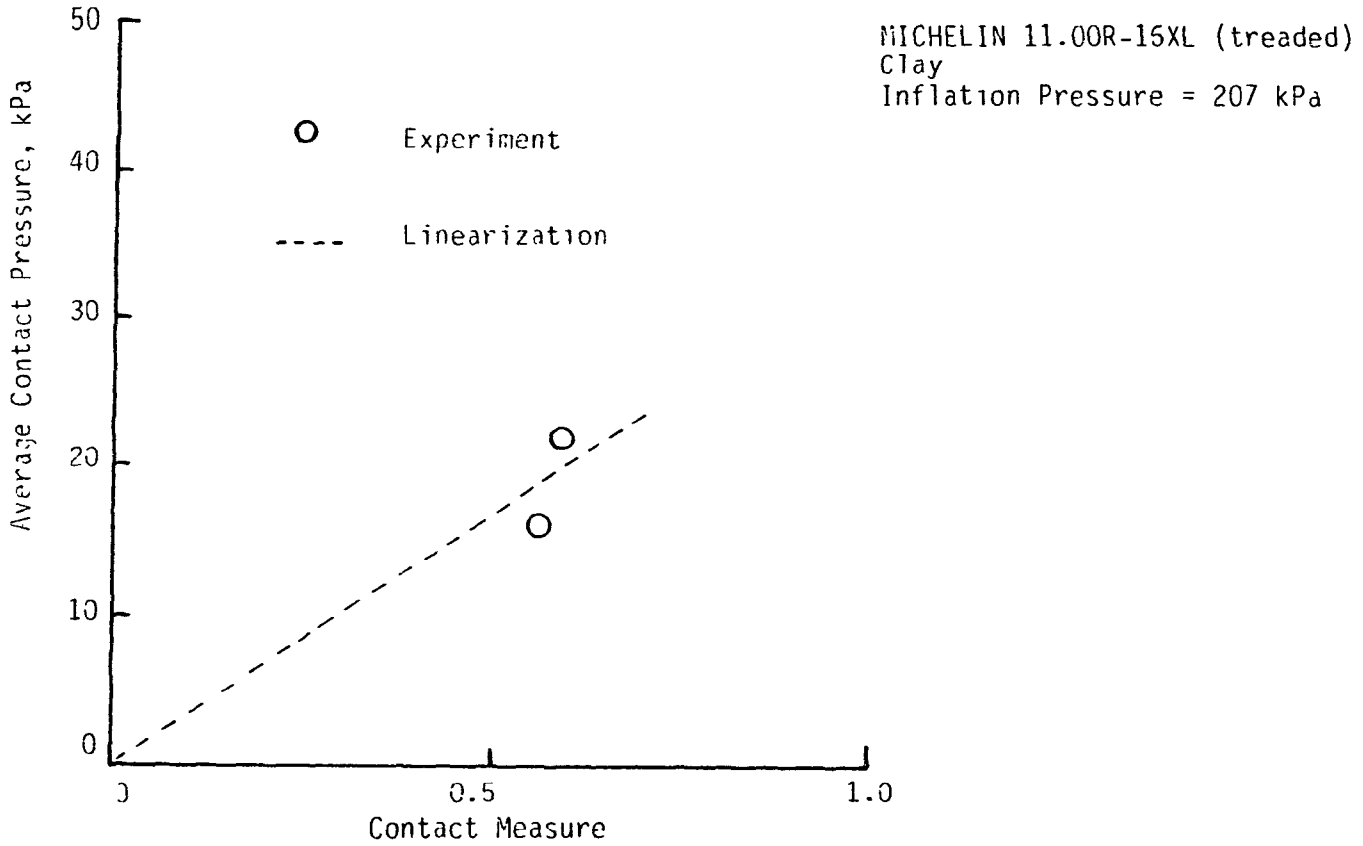


Fig. 4.18b Average Contact Pressure - Contact Measure Relationship for MICHELIN 11.00R-16XL (treaded)

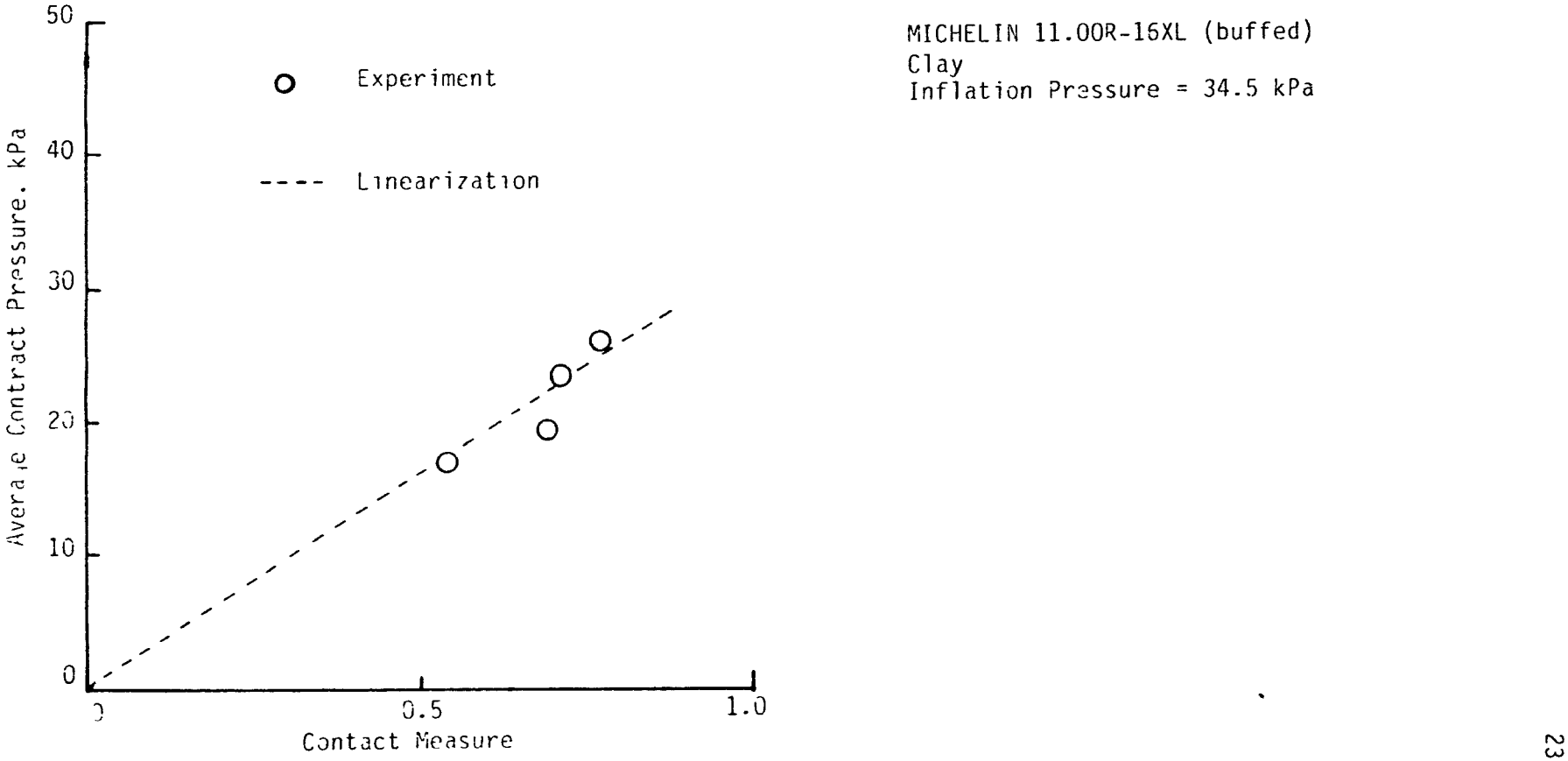


Fig. 4.18c Average Contact Pressure - Contact Measure Relationship for MICHELIN 11.00R-16XL (buffed)

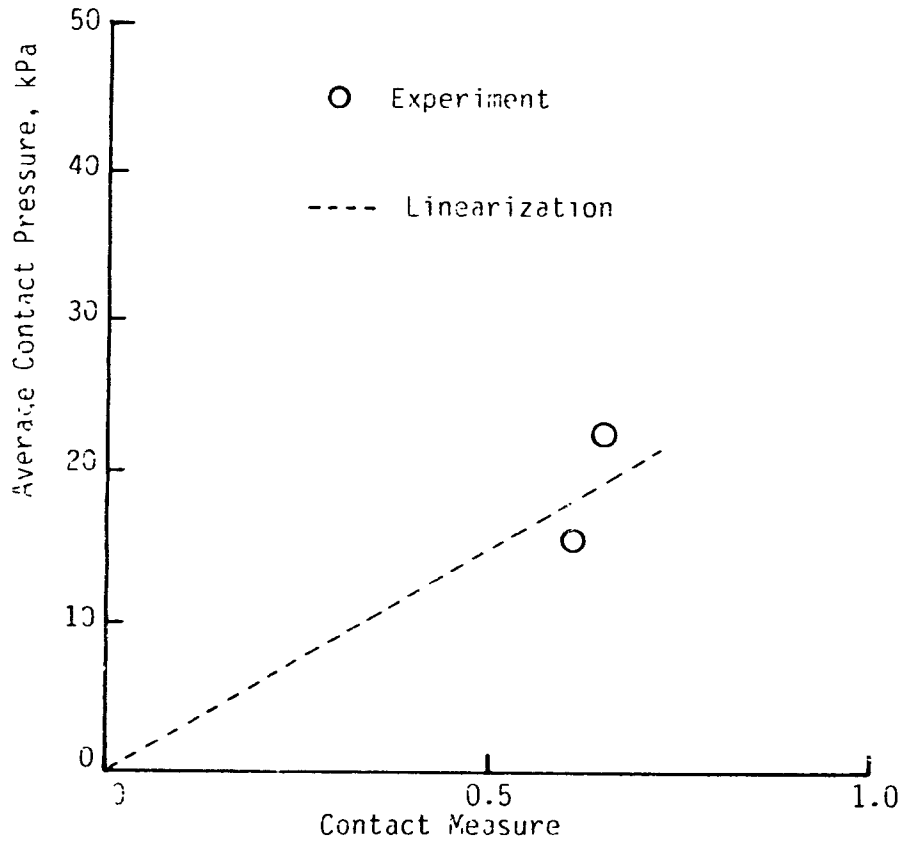
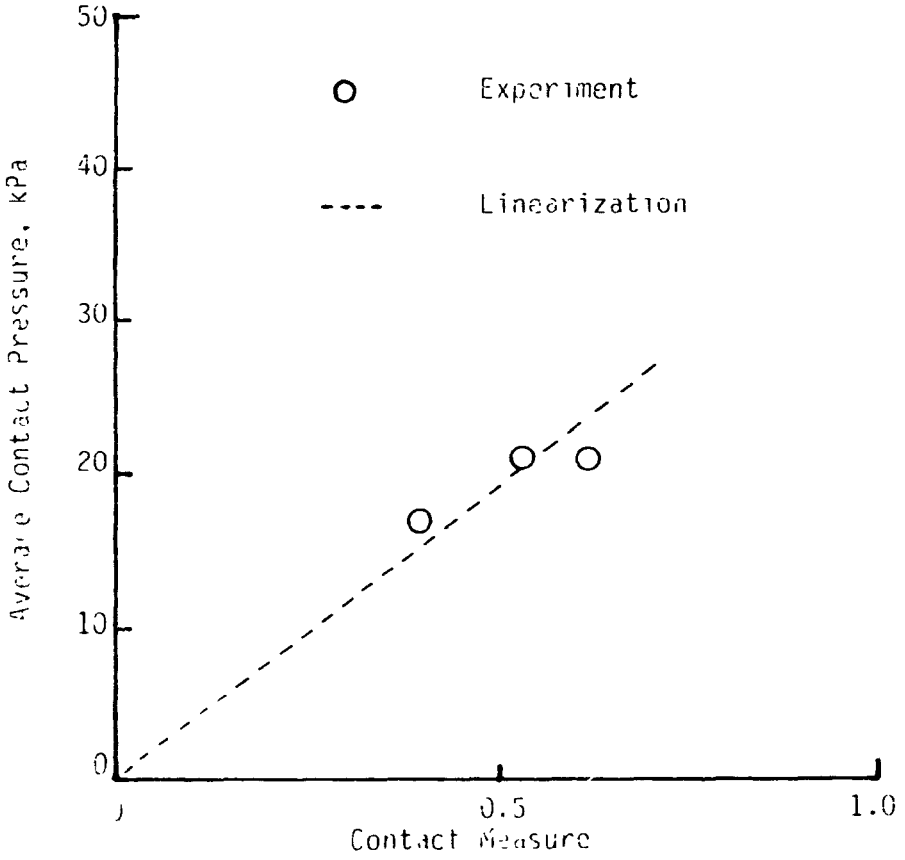


Fig. 4.18d Average Contact Pressure - Contact Measure Relationship for MICHELIN 11.00R-16XL (buffed)



MICHELIN 12.5R-16.5XLM (treaded)
Clay
Inflation Pressure = 34.5 kPa

Fig. 4.19a Average Contact Pressure - Contact Measure Relationship for MICHELIN 12.5R-16.5XLM (treaded)

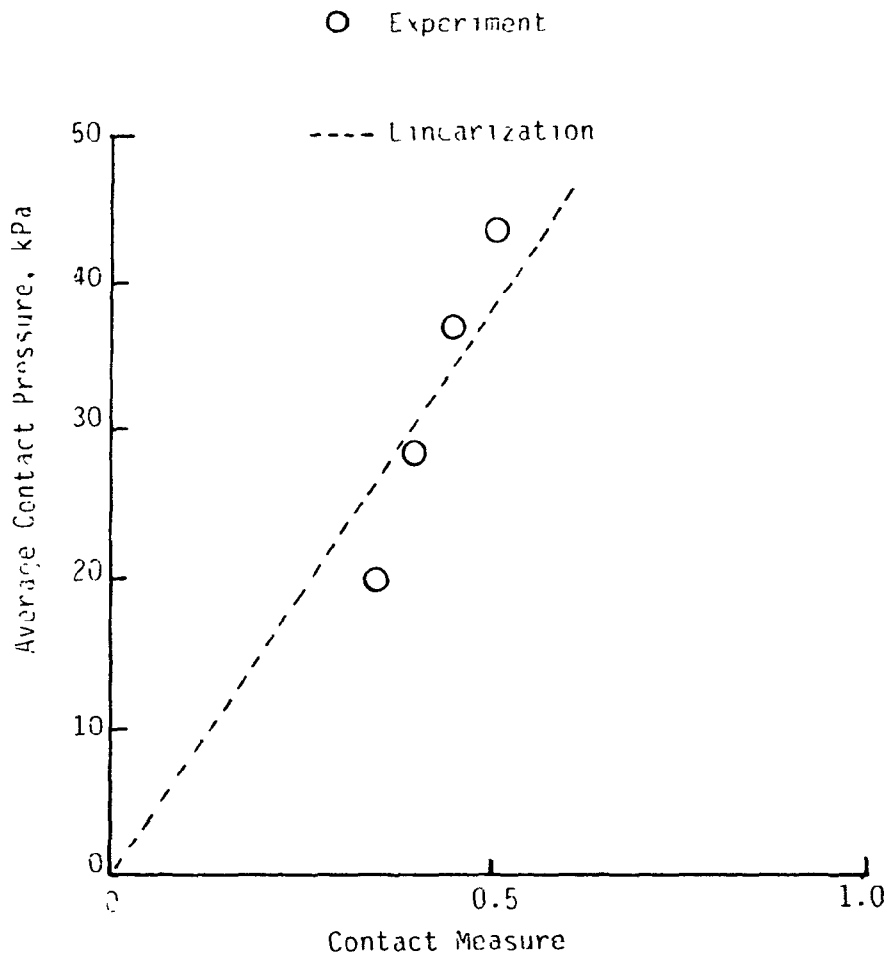


Fig. 4.19b Average Contact Pressure - Contact Measured Relationship for MICHELIN 12.5R-16.5XLM (treaded)

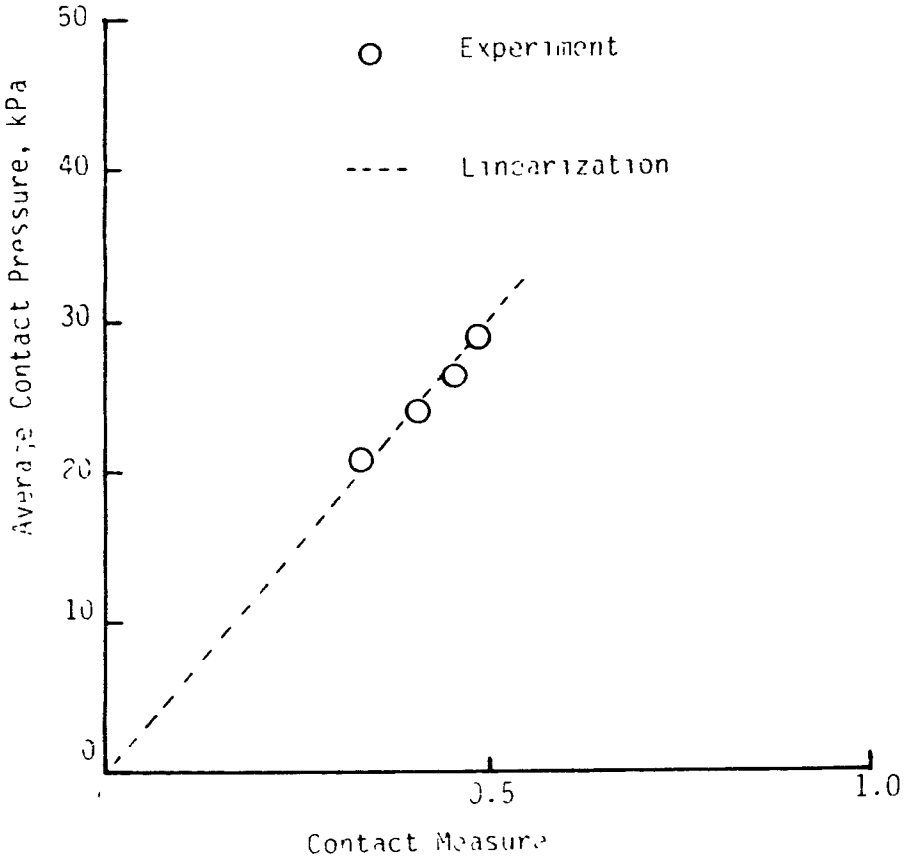


Fig. 4.19c Average Contact Pressure - Contact Measure Relationship for MICHELIN 12.5R-16.5XLM (buffed)

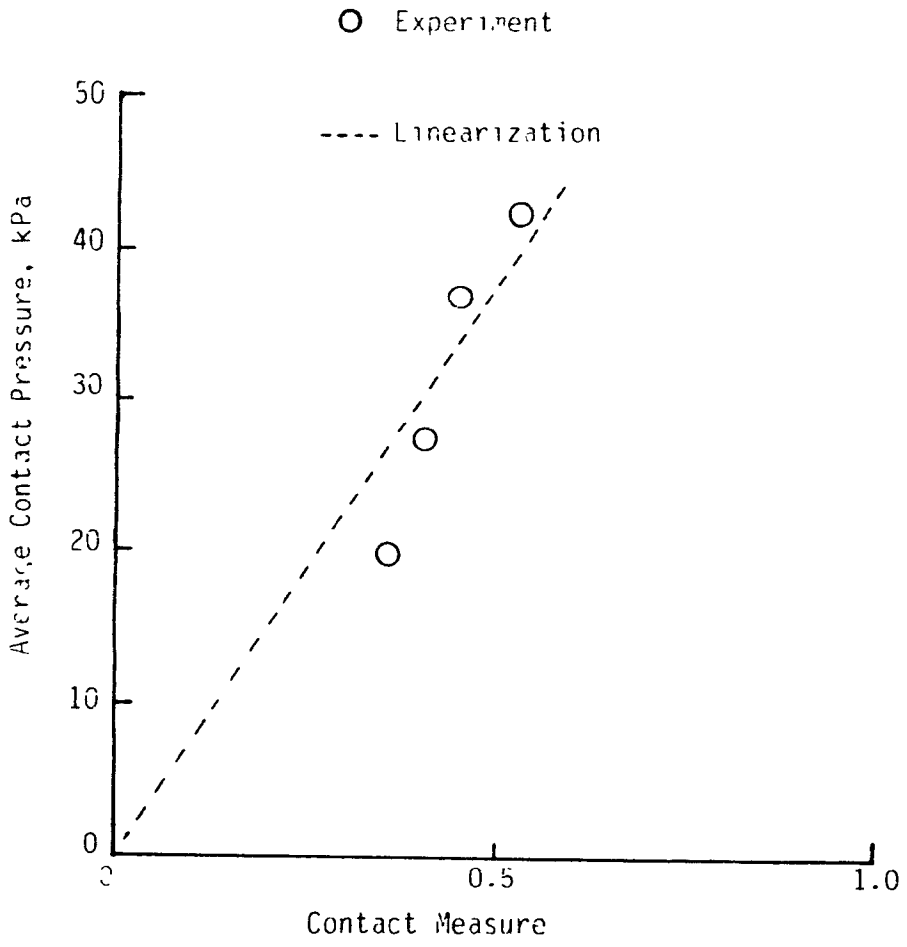


Fig. 4.19d Average Contact Pressure - Contact Measure Relationship for MICHELIN 12.5R-16.5XLM (buffed)

plotted in Figs. 4.20-4.28. Figures 4.20-4.23 show the results of the tire-clay interactions while Figs. 4.24-4.28 show the results of the tire-rigid base interactions. The analytical results for the frictionless and frictional cases are respectively shown in Figs. 4.20-4.27 and Fig. 4.28. In all these figures "Prediction 1" stands for the solution obtained based on the flat-shaped contact profile (Eq. A.137a), while "Prediction 2" stands for the solution obtained by assuming the contact profile to be arc-shaped (Eq. A.134a).

Tire-Clay Interactions

As shown in Figs. 4.20-4.23, all the experimental results agree quite well with the analytical solution, "Prediction 2", except the interactions involving the buffed tire MICHELIN 12.5R 16.5XLM, in spite of rough approximation in contact profile. The experimental results here mean the representative contact length and contact pressure distribution obtained from the experiments by means of the definitions given in section 3.4. In the case of MICHELIN 12.5R 16.5XLM, the representative contact pressure distributions obtained in the experiments agreed with "Prediction 1", which was obtained under the assumption of contact profile being arc-shaped.

These results are conjuctured from the discussion on the experimental results in Chapter 3, i.e. pressure distributions are saddle-shaped for the tires, GOODYEAR 7.00-16LT, MICHELIN 7.00R-16XCL, MICHELIN 11.00R-16XL while the tire MICHELIN 12.5R-16.5XLM produced parabolic pressure distributions.

GOODYEAR 7.00-16LT (buffed)
Clay
Inflation Pressure = 34.5 kPa
Wheel Load = 4.007 kN
Average Contact Pressure = 47 kPa
Contact Length = 442 mm
Contact Width = 192 mm

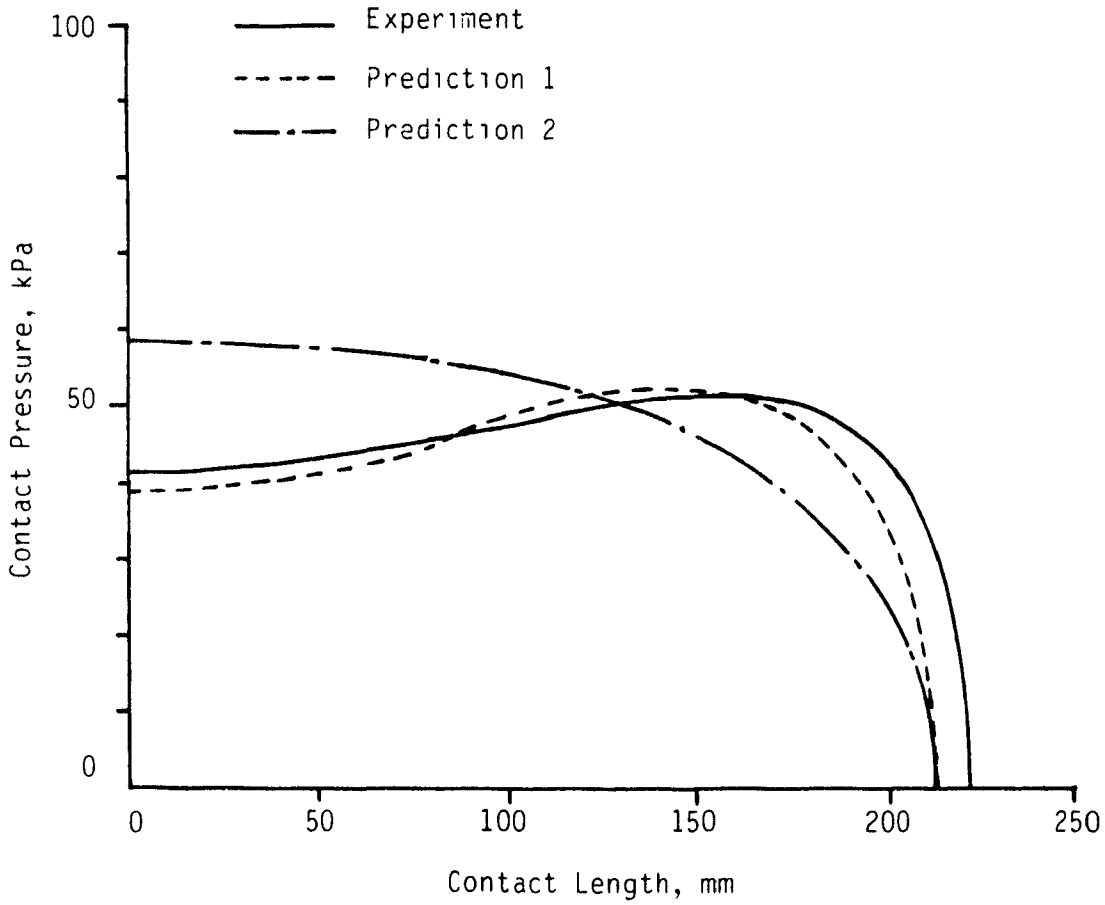


Fig. 4.20a Comparison Between Experimental and Frictionless Analytical Solutions on Clay

GOODYEAR 7.00-16LT (buffed)
Clay
Inflation Pressure = 310.5 kPa
Wheel Load = 3.474 kN
Average Contact Pressure = 44 kPa
Contact Length = 436 mm
Contact Width = 181 mm

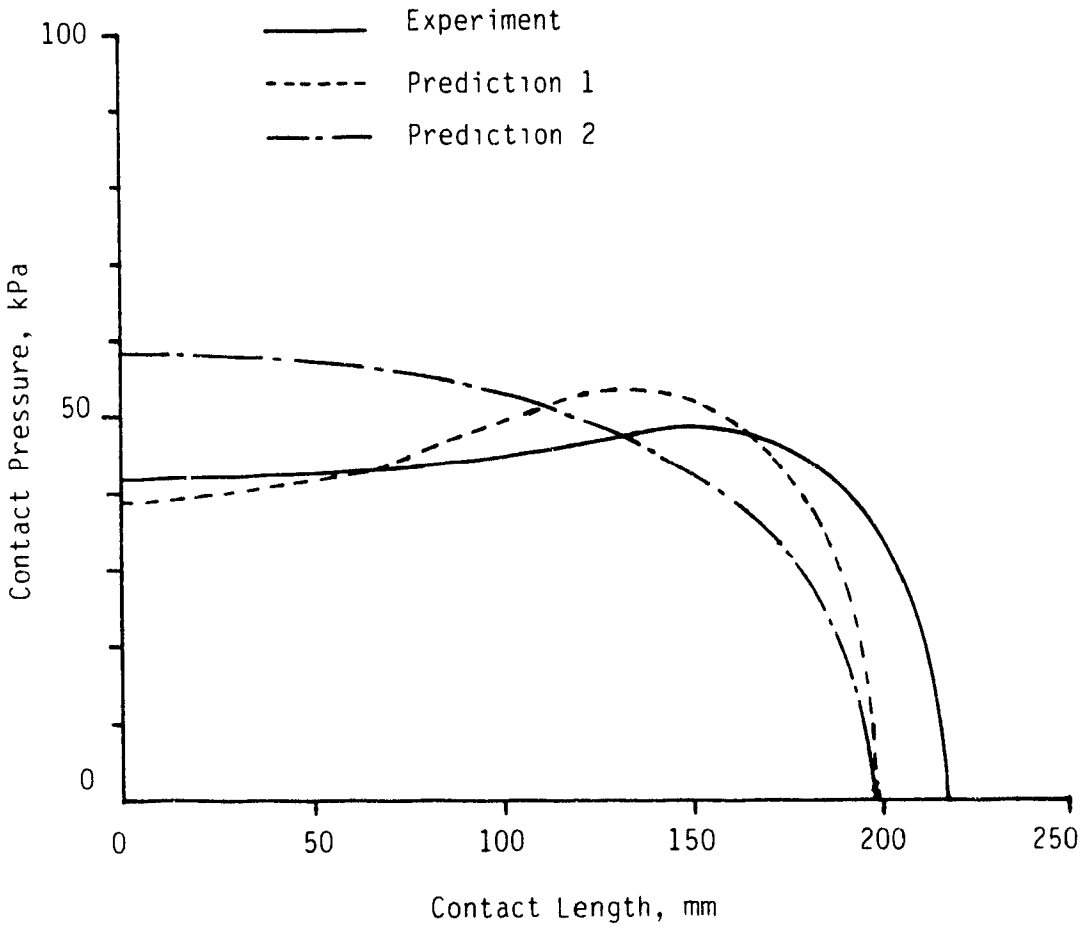


Fig. 4.20b Comparison Between Experimental and Frictionless Analytical Solutions on Clay

MICHELIN 7.00R-16XCL (buffed)
Clay
Inflation Pressure = 34.5 kPa
Wheel Load = 3.584 kN
Average Contact Pressure = 27.3 kPa
Contact Length = 608 mm
Contact Width = 217 mm

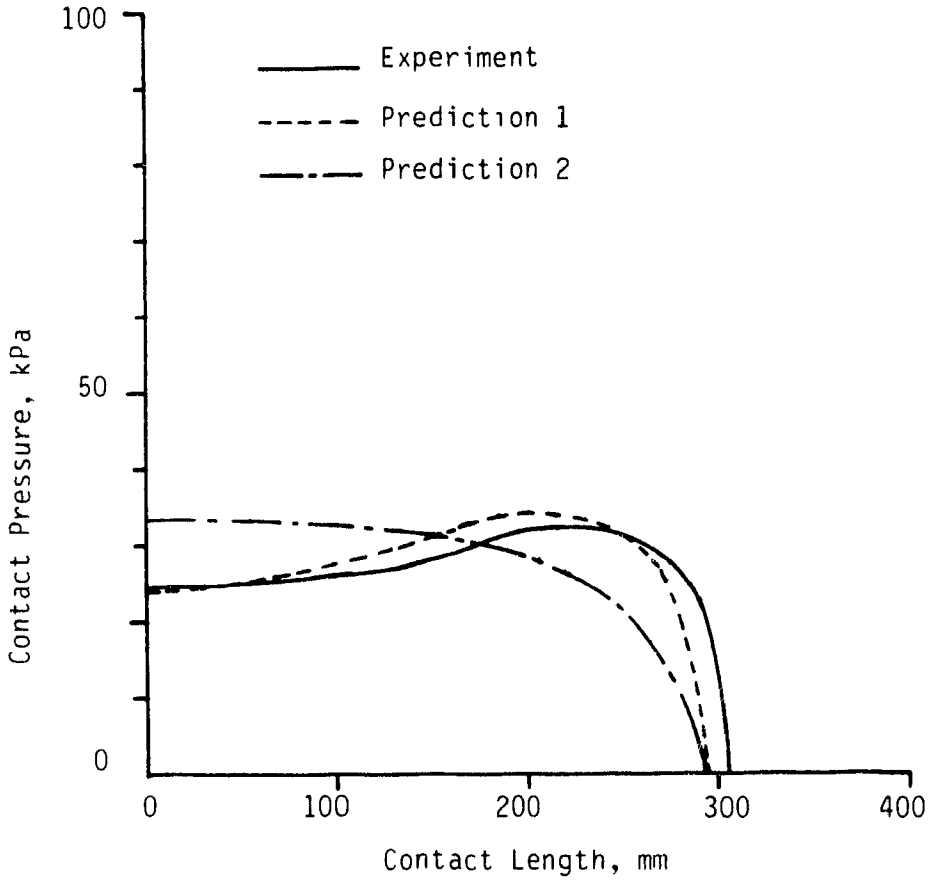


Fig. 4.21a Comparison Between Experimental and Frictionless Analytical Solutions on Clay

MICHELIN 7.00R-16XCL (buffed)
Clay
Inflation Pressure = 310.5 kPa
Wheel Load = 3.584 kN
Average Contact Pressure = 28.4 kPa
Contact Length = 596 mm
Contact Width = 212 mm

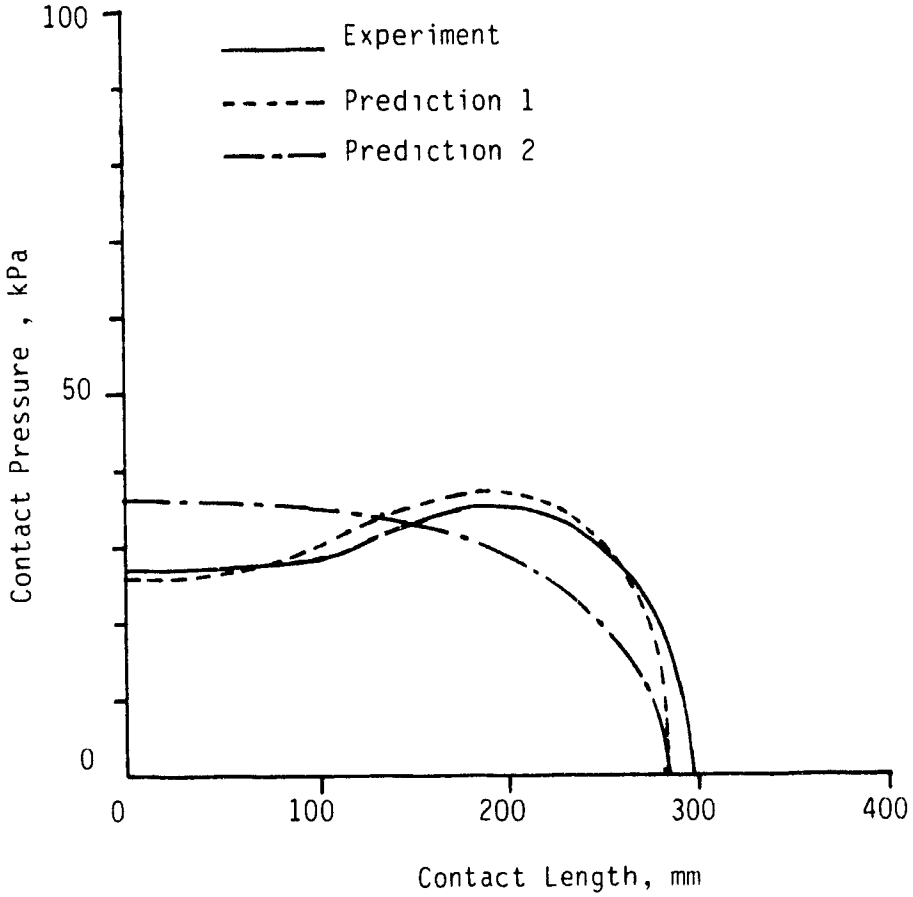


Fig. 4.21b Comparison Between Experimental and Frictionless Analytical Solutions on Clay

MICHELIN 11.00R-16XL (buffed)
Clay
Inflation Pressure = 34.5 kPa
Wheel Load =3.206 kN
Average Contact Pressure = 19.5 kPa
Contact Length = 626 mm
Contact Width = 262 mm

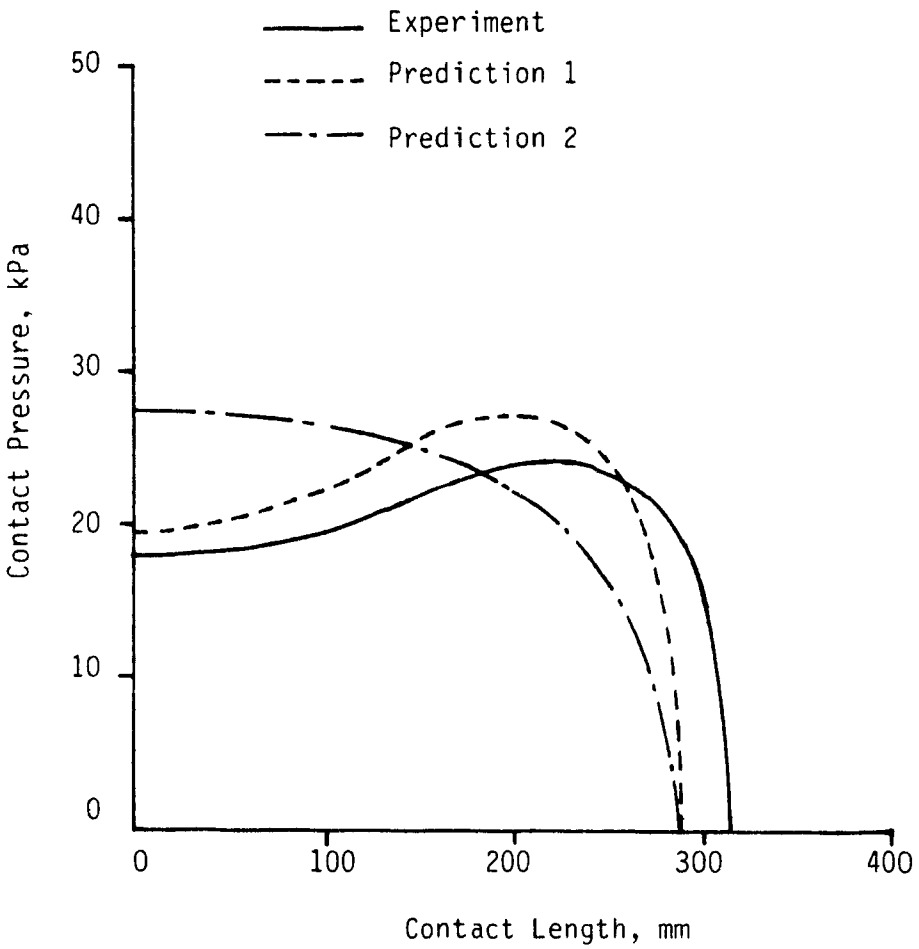


Fig. 4.22a Comparison Between Experimental and Frictionless Analytical Solutions on Clay

MICHELIN 11.00R-16XL (buffed)
Clay
Inflation Pressure = 207 kPa
Wheel Load = 3.423 kN
Average Contact Pressure = 22.4 kPa
Contact Length = 604 mm
Contact Width = 254 mm

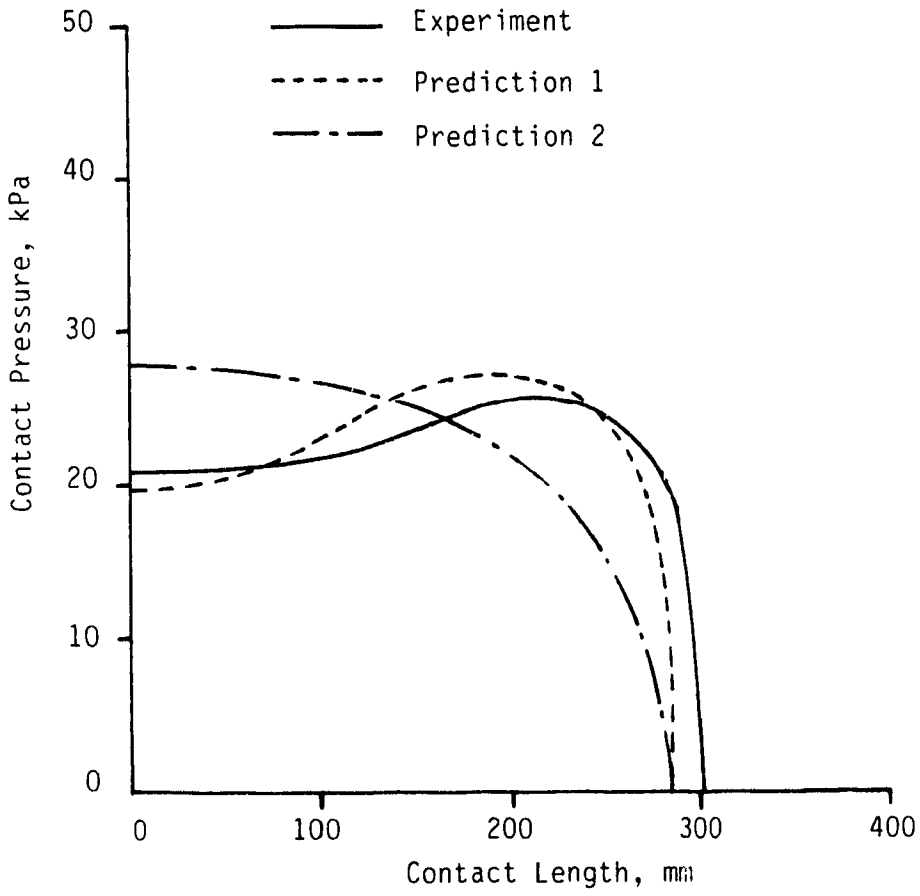


Fig. 4.22b Comparison Between Experimental and Frictionless Analytical Solutions on Clay

MICHELIN 12.5R-16.5XLM (buffed)
Clay
Inflation Pressure = 34.5 kPa
Wheel Load = 3.474 kN
Average Contact Pressure = 28.84 kPa
Contact Length = 500 mm
Contact Width = 241 mm

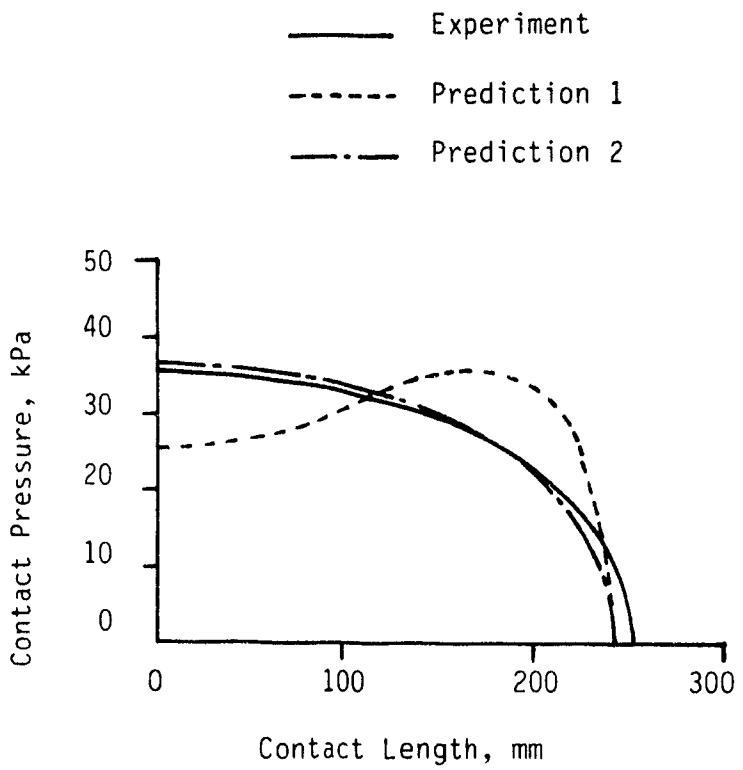


Fig. 4.23a Comparison Between Experimental and Frictionless Analytical Solutions on Clay

MICHELIN 12.5R-16.5XLM (buffed)
Clay
Inflation Pressure = 207 kPa
Wheel Load = 4.096 kN
Average Contact Pressure = 36.98 kPa
Contact Length = 472 mm
Contact Width = 234 mm

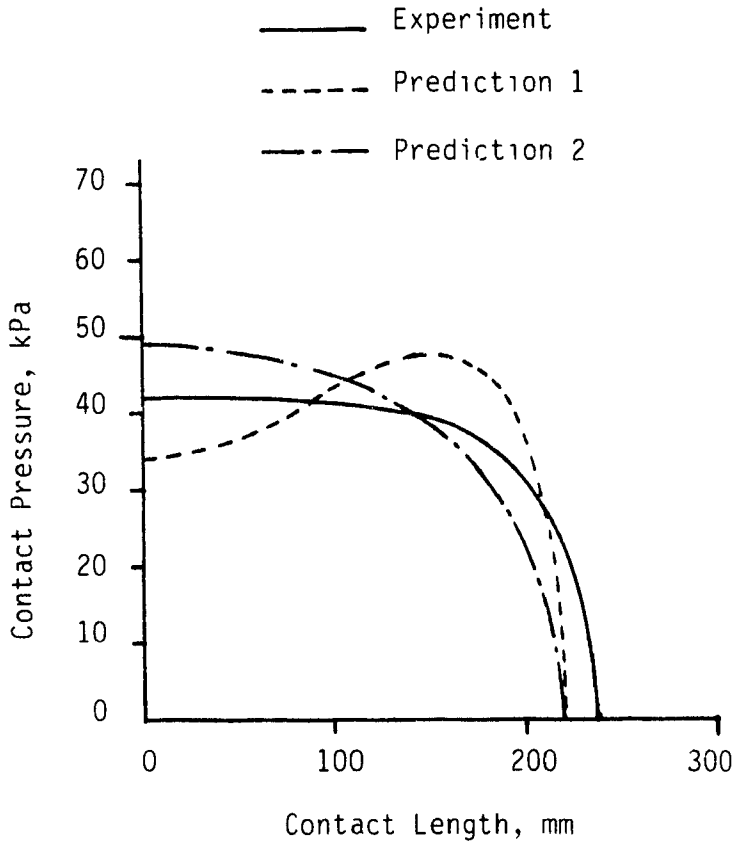


Fig. 4.23b Comparison Between Experimental and Frictionless Analytical Solutions on Clay

GOODYEAR 7.00-16LT (buffed)
Rigid Surface
Inflation Pressure = 34.5 kPa
Wheel Load = 1.067 kN
Average Contact Pressure = 48.7 kPa
Contact Length = 232 mm
Contact Width = 95 mm

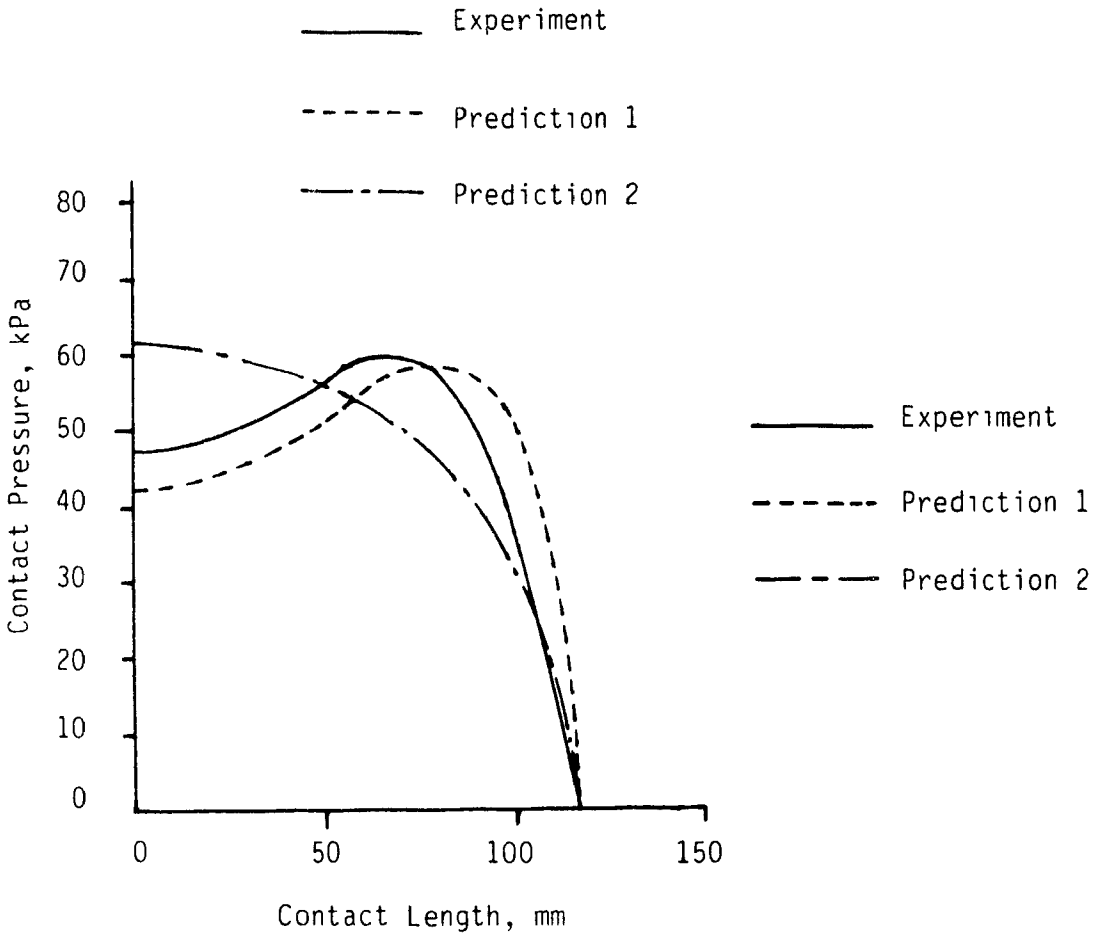


Fig. 4.24a Comparison Between Experimental and Frictionless Analytical Solutions on Rigid Surface

GOODYEAR 7.00-16LT (buffed)
Rigid Surface
Inflation Pressure = 34.5 kPa
Wheel Load = 1.423 kN
Average Contact Pressure = 48.7 kPa
Contact Length = 258 mm
Contact Width = 113 mm

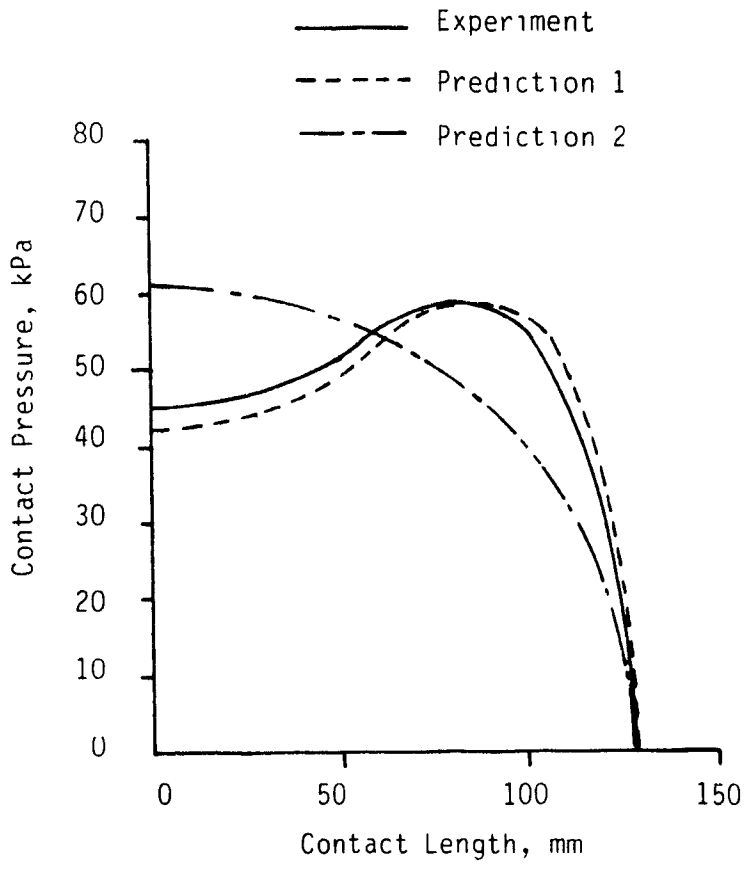


Fig. 4.24b Comparison Between Experimental and Frictionless Analytical Solutions on Rigid Surface

GOODYEAR 7.00-16LT (buffed)
Rigid Surface
Inflation Pressure = 34.5 kPa
Wheel Load = 1.779 kN
Average Contact Pressure = 48.7 kPa
Contact Length = 292 mm
Contact Width = 125 mm

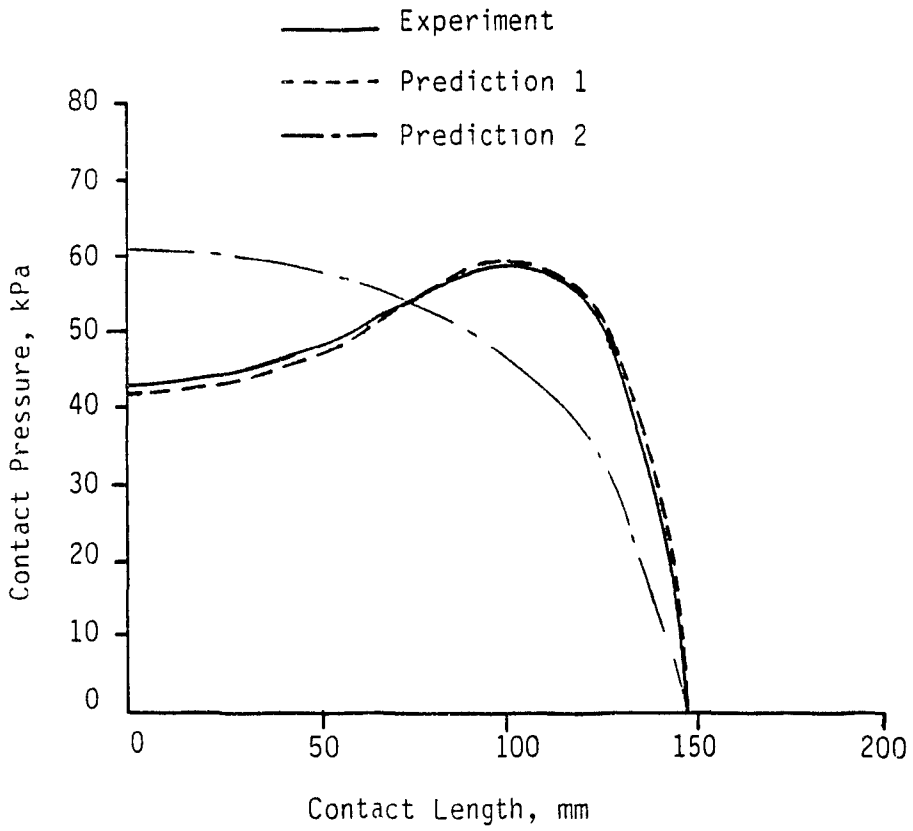


Fig. 4.24c Comparison Between Experimental and Frictionless Analytical Solutions on Rigid Surface

GOODYEAR 7.00-16LT (buffed)
Rigid Surface
Inflation Pressure = 103.5 kPa
Wheel Load = 2.669 kN
Average Contact Pressure = 110.8 kPa
Contact Length = 232 mm
Contact Width = 104 mm

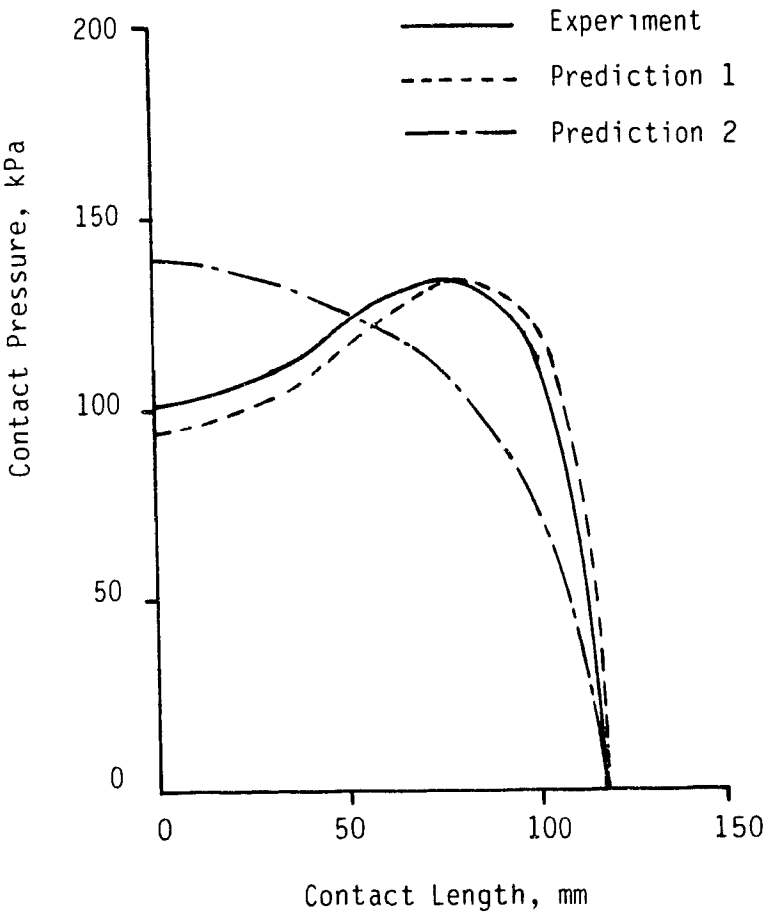


Fig. 4.24d Comparison Between Experimental and Frictionless Analytical Solutions on Rigid Surface

GOODYEAR 7.00-16LT (buffed)
Rigid Surface
Inflation Pressure = 103.5 kPa
Wheel Load = 3.558 kN
Average Contact Pressure = 110.8 kPa
Contact Length 260 mm
Contact Width = 124 mm

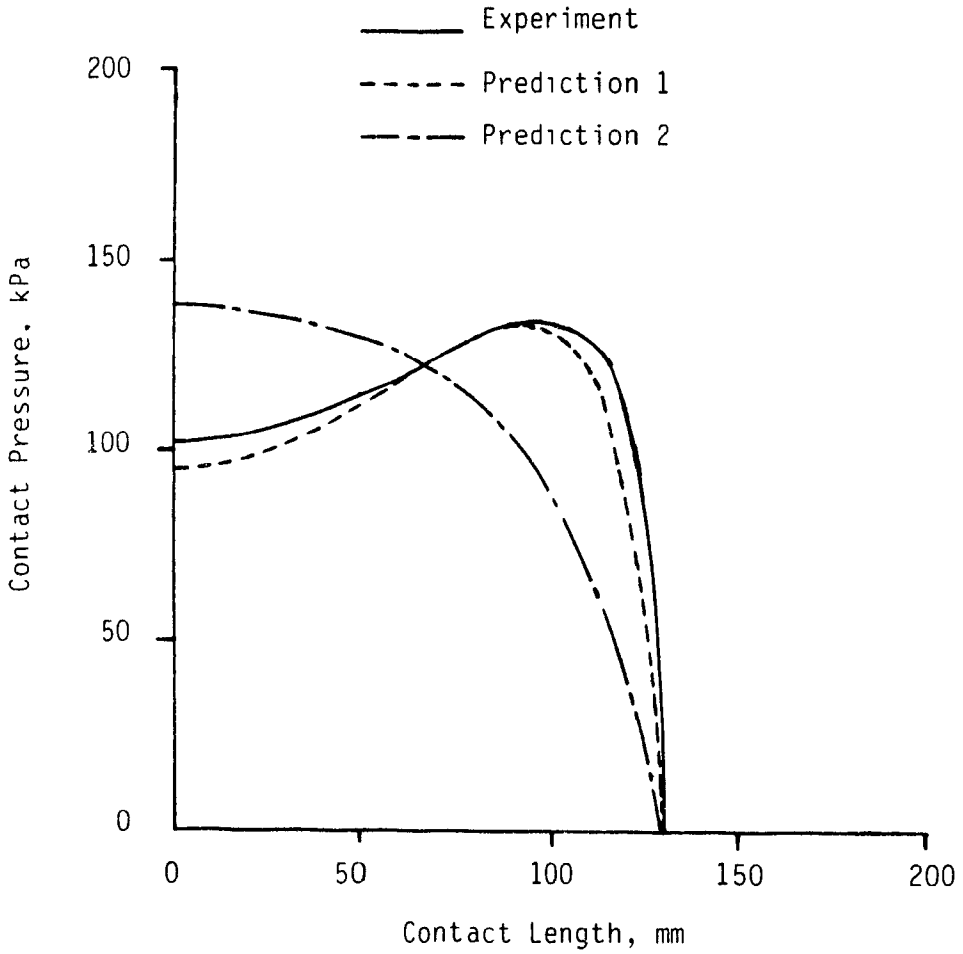


Fig. 4.24e Comparison Between Experimental and Frictionless Analtyical Solutions on Rigid Surface

GOODYEAR 7.00-16LT (buffed)
Rigid Surface
Inflation Pressure = 103.5 kPa
Wheel Load = 4.448 kN
Average Contact Pressure = 110.8 kPa
Contact Length = 295 mm
Contact Width = 136 mm

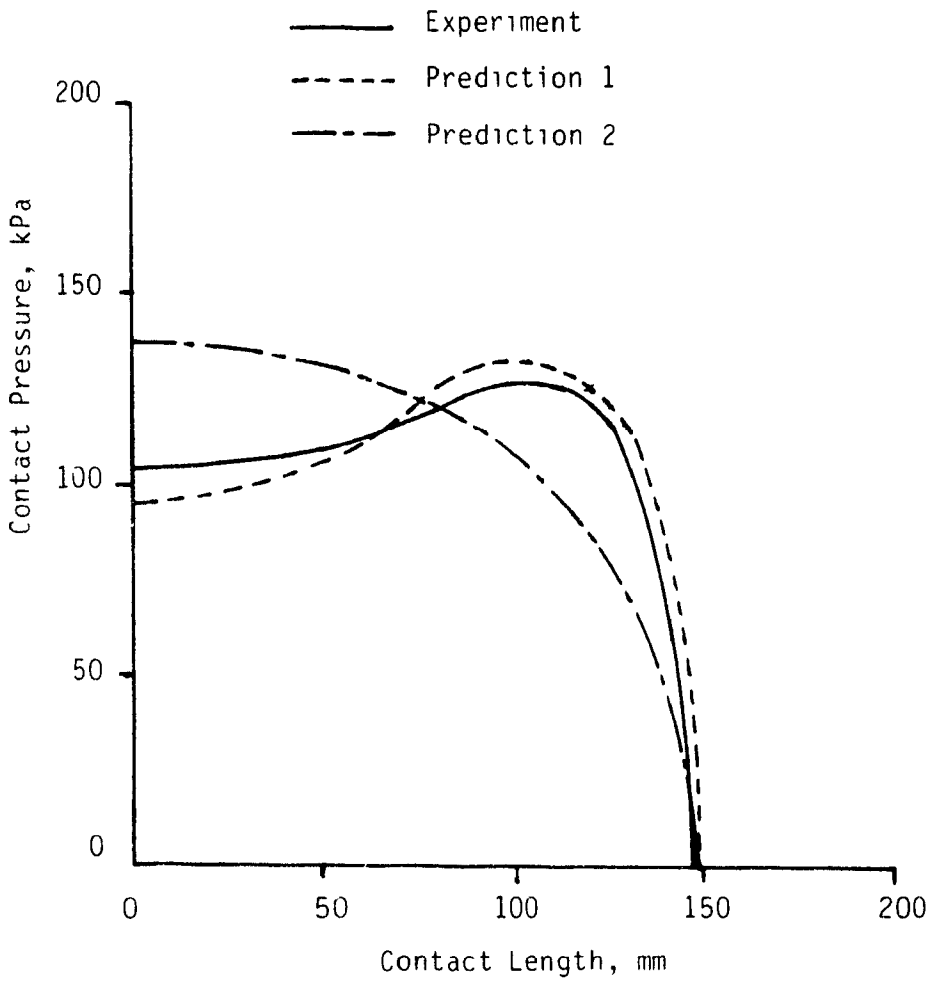


Fig. 4.24f Comparison Between Experimental and Frictionless Analytical Solutions on Rigid Surface

GOODYEAR 7.00-16LT (buffed)
Rigid Surface
Inflation Pressure = 310.5 kPa
Wheel Load = 2.669 kN
Average Contact Pressure = 246.5 kPa
Contact Length = 130 mm
Contact Width = 83 mm

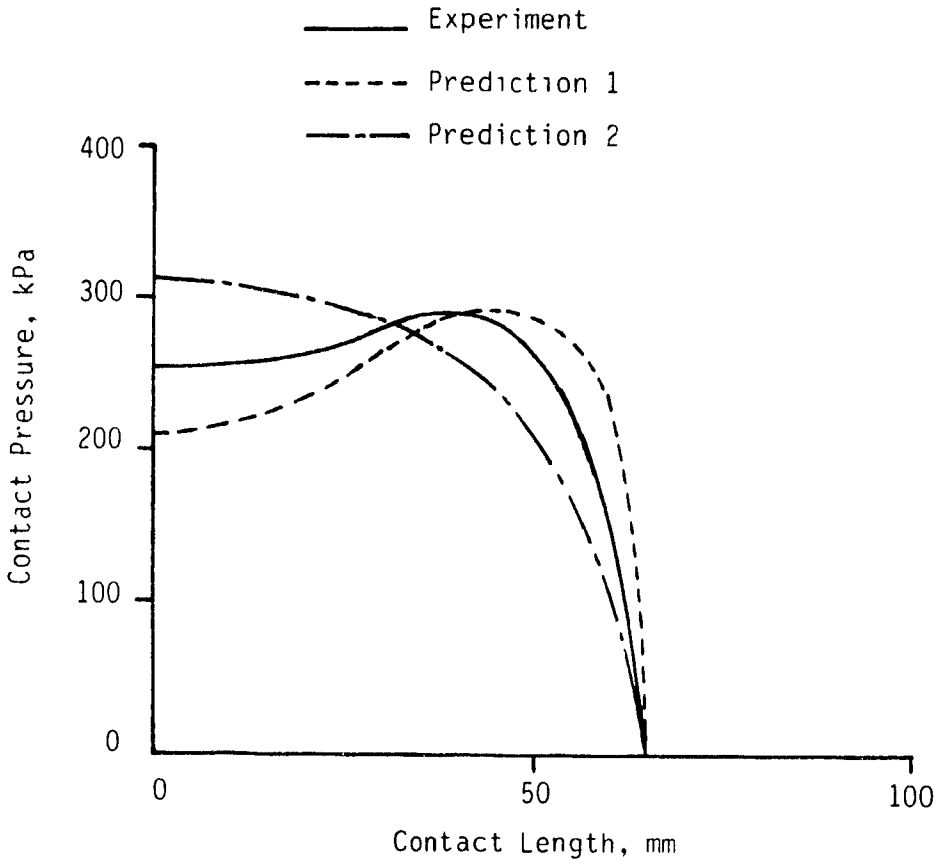


Fig. 4.24g Comparison Between Experimental and Frictionless Analytical Solutions on Rigid Surface

GOODYEAR 7.00-16LT (buffed)
Rigid Surface
Inflation Pressure = 310.5 kPa
Wheel Load = 4.003 kN
Average Contact Pressure = 246.5 kPa
Contact Length = 202 mm
Contact Width = 80 mm

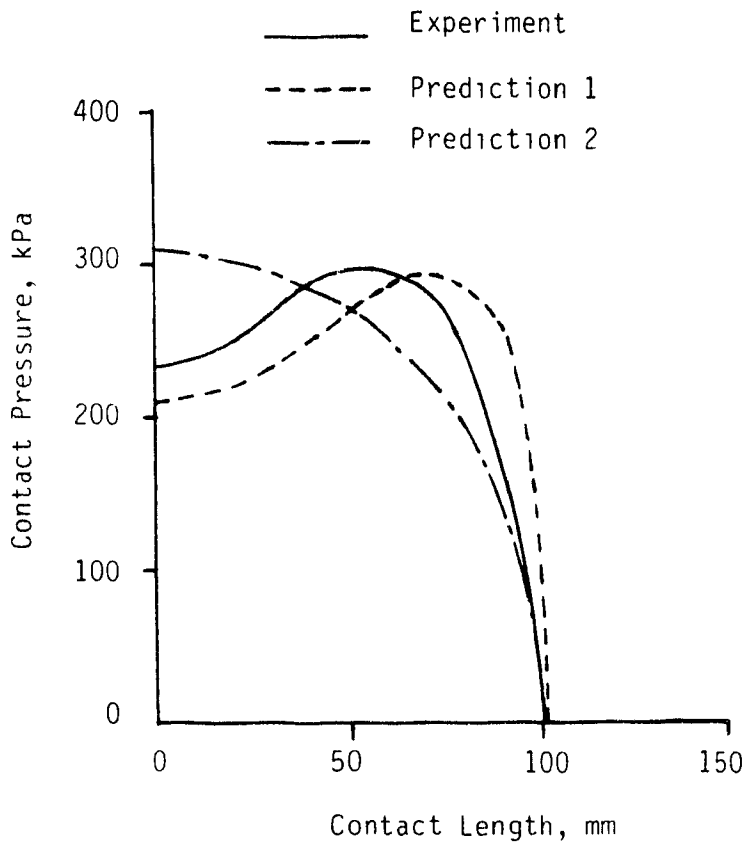


Fig. 4.24h Comparison Between Experimental and Frictionless Analytical Solutions on Rigid Surface

GOODYEAR 7.00-16LT (buffed)
Rigid Surface
Inflation Pressure = 310.5 kPa
Wheel Load = 5.338 kN
Average Contact Pressure = 246.5 kPa
Contact Length = 228 mm
Contact Width = 95 mm

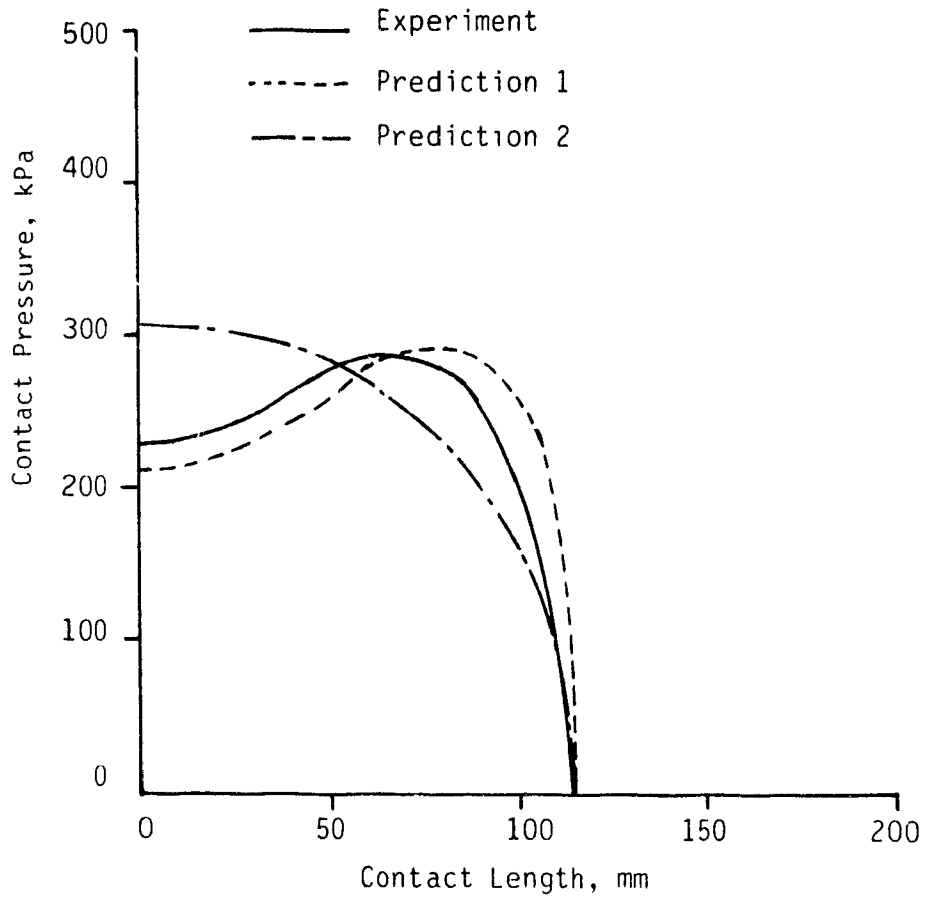


Fig. 4.24i Comparison Between Experimental and Frictionless Analytical Solutions on Rigid Surface

GOODYEAR 7.00-16LT (buffed)
Rigid Surface
Inflation Pressure = 310.5 kPa
Wheel Load = 6.672 kN
Average Contact Pressure = 246.5 kPa
Contact Length = 250 mm
Contact Width = 108 mm

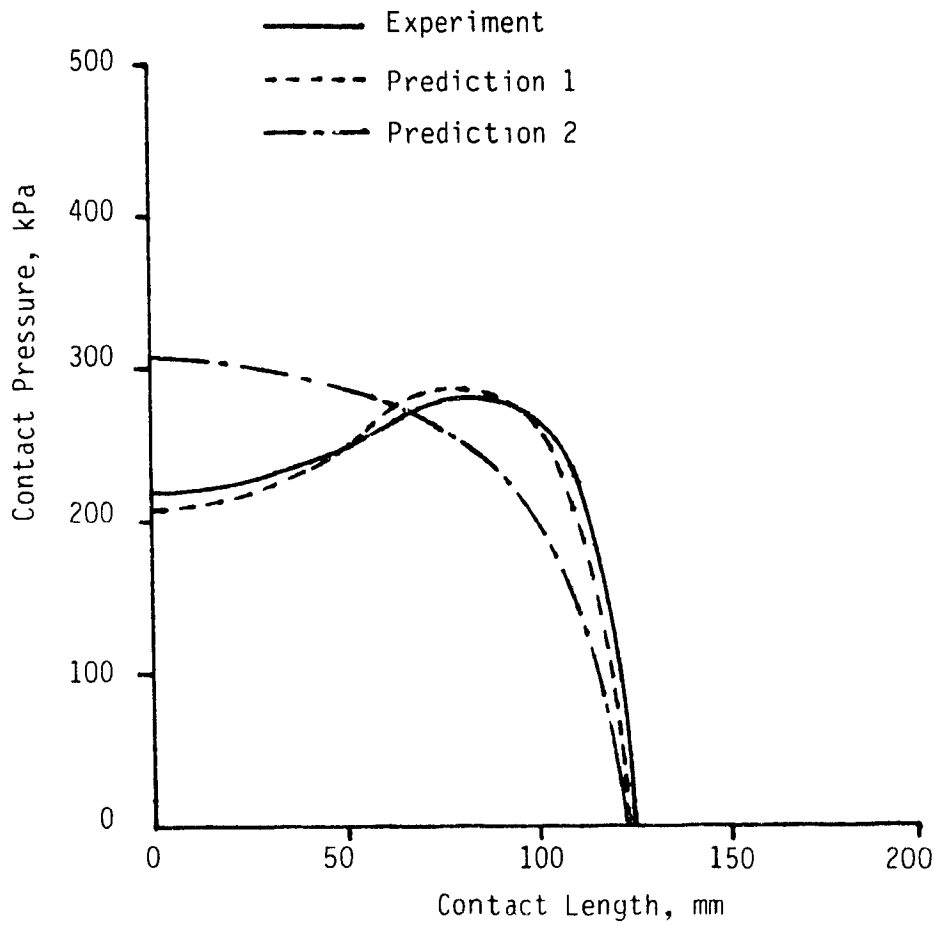


Fig. 4.24j Comparison Between Experimental and Frictionless Analytical Solutions on Rigid Surface

MICHELIN 7.00R-16XCL (buffed)
Rigid Surface
Inflation Pressure = 34.5 kPa
Wheel Load = 1.067 kN
Average Contact Pressure = 55.0 kPa
Contact Length = 188 mm
Contact Width = 103 mm

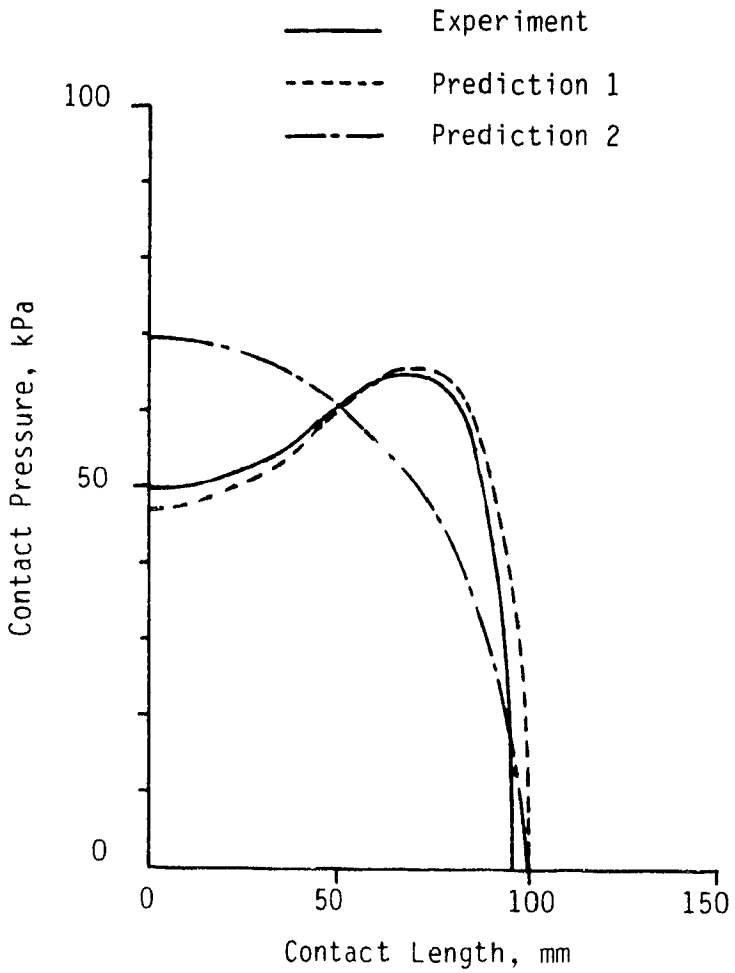


Fig. 4.25a Comparison Between Experimental and Frictionless Analytical Solutions on Rigid Surface

MICHELIN 7.00R-16XCL (buffed)
Rigid Surface
Inflation Pressure = 103.5 kPa
Wheel Load = 2.847 kN
Average Contact Pressure = 105.2 kPa
Contact Length = 217 mm
Contact Width = 124 mm

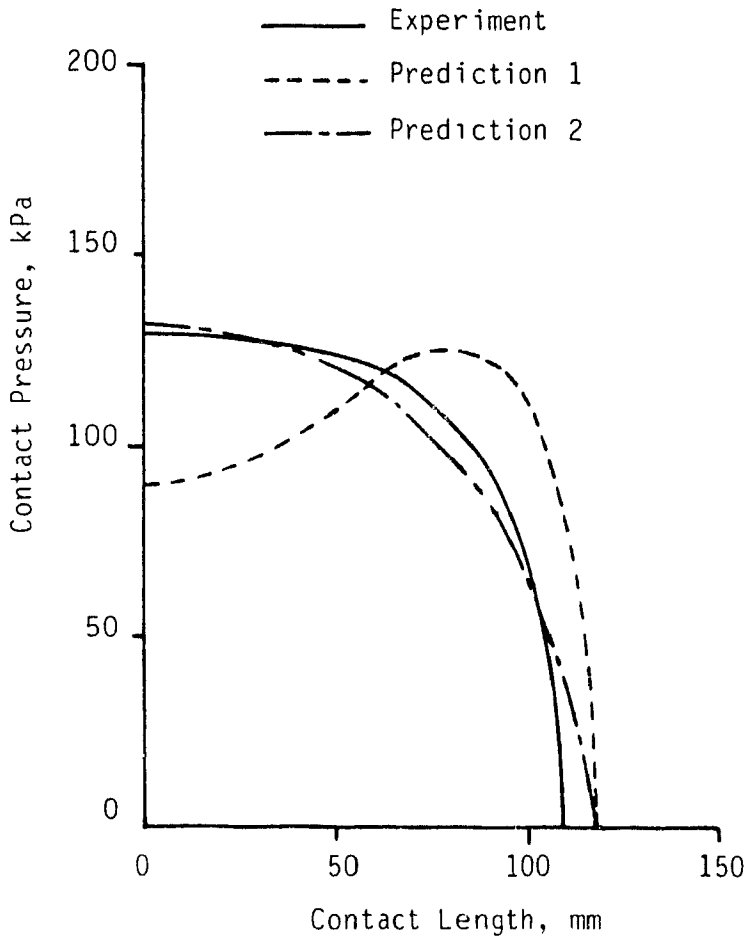


Fig. 4.25b Comparison Between Experimental and Frictionless Analytical Solutions on Rigid Surface

MICHELIN 7.00R-16XCL (buffed)
Rigid Surface
Inflation Pressure = 310.5 kPa
Wheel Load = 8.007 kN
Average Contact Pressure = 275.5 kPa
Contact Length = 223 mm
Contact Width = 130 mm

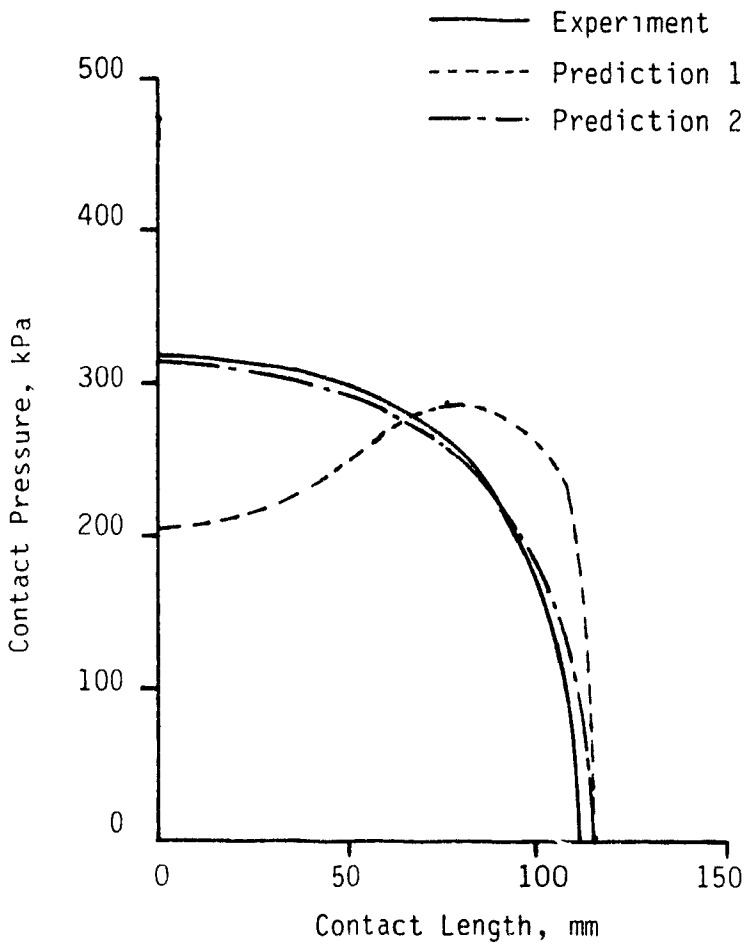


Fig. 4.25c Comparison Between Experimental and Frictionless Analytical Solutions on Rigid Surface

MICHELIN 11.00R-16XL (buffed)
Rigid Surface
Inflation Pressure = 34.5 kPa
Wheel Load = 1.868 kN
Average Contact Pressure = 76.0 kPa
Contact Length = 240 mm
Contact Width = 103 mm

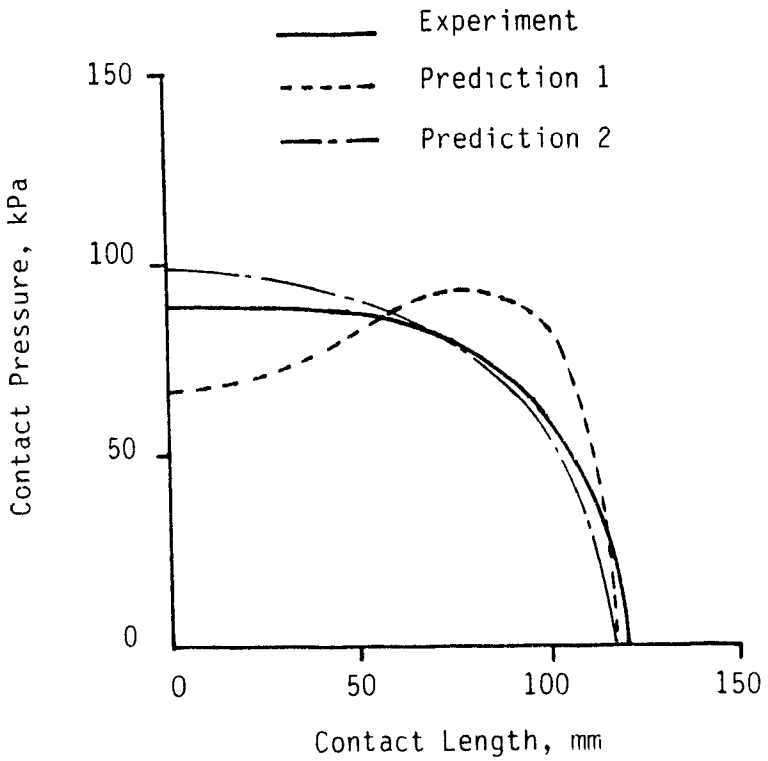


Fig. 4.26a Comparison Between Experimental and Frictionless Analytical Solutions on Rigid Surface

MICHELIN 11.00R-16XL (buffed)
Rigid Surface
Inflation Pressure = 207 kPa
Wheel Load = 6.405 kN
Average Contact Perssure = 222 kPa
Contact Length = 235 mm
Contact Width = 122 mm

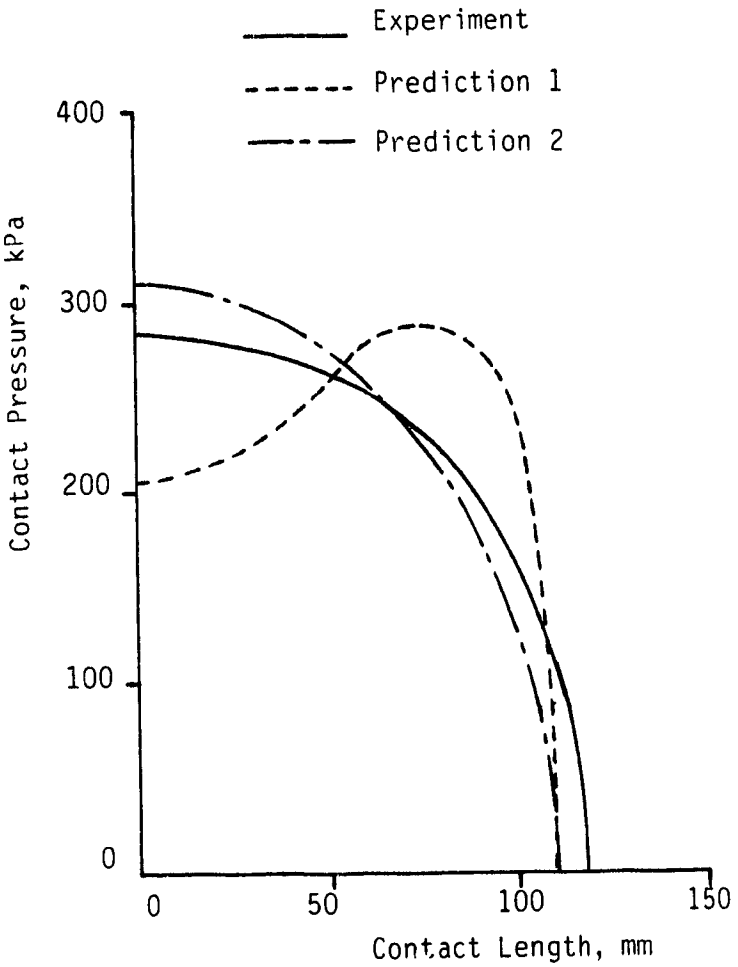


Fig. 4.26b Comparison Between Experimental and Frictionless Analytical Solutions on Rigid Surface

MICHELIN 11.00R-16XL (buffed)
Rigid Surface
Inflation Pressure = 414 kPa
Wheel Load = 13.34 kN
Average Contact Pressure = 345 kPa
Contact Length = 255 mm
Contact Width = 152 mm

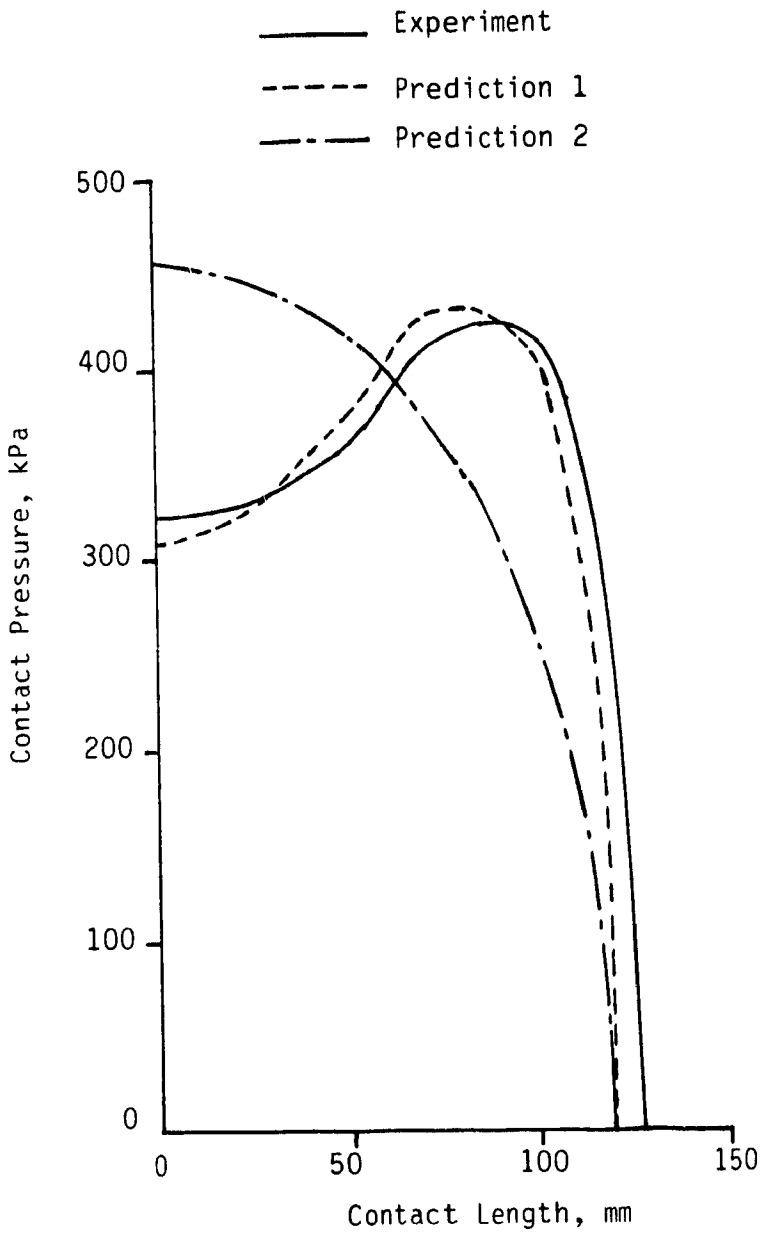


Fig. 2.26c Comparison Between Experimental and Frictionless Analytical Solutions on Rigid Surface

MICHELIN 12.5R-16.5XLM (buffed)
Rigid Surface
Inflation Pressure = 34.5 kPa
Wheel Load = 1.423 kN
Average Contact Pressure = 35 kPa
Contact Length = 254 mm
Contact Width = 160 mm

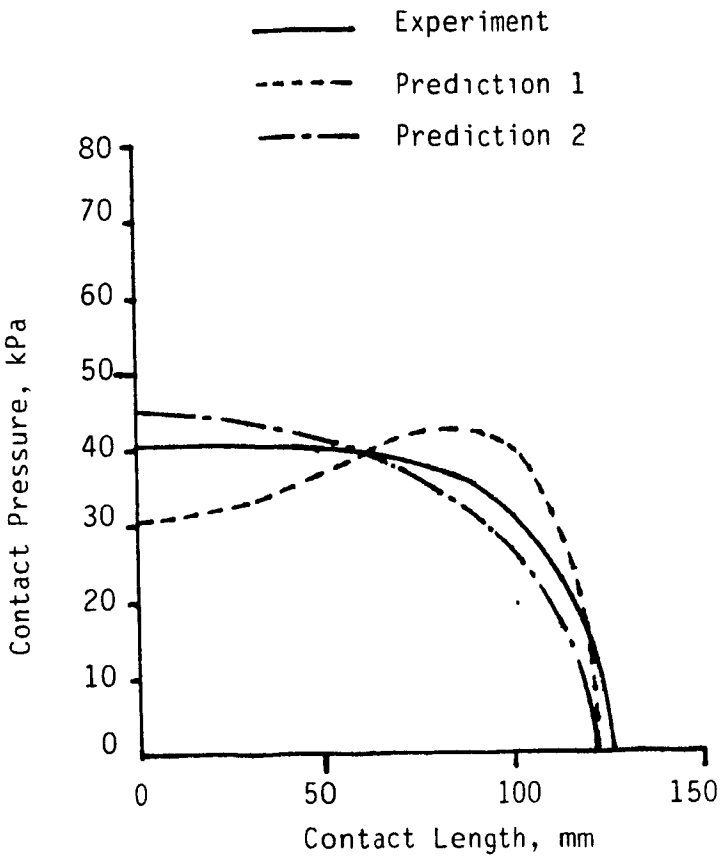


Fig. 4.27a Comparison Between Experimental and Frictionless Analytical Solutions on Rigid Surface

MICHELIN 12.5R-16.5XLM (buffed)
Rigid Surface
Inflation Pressure = 103.5 kPa
Wheel Load = 3.558 kN
Average Contact Pressure = 87.04 kPa
Contact Length = 264 mm
Contact Width = 155 mm

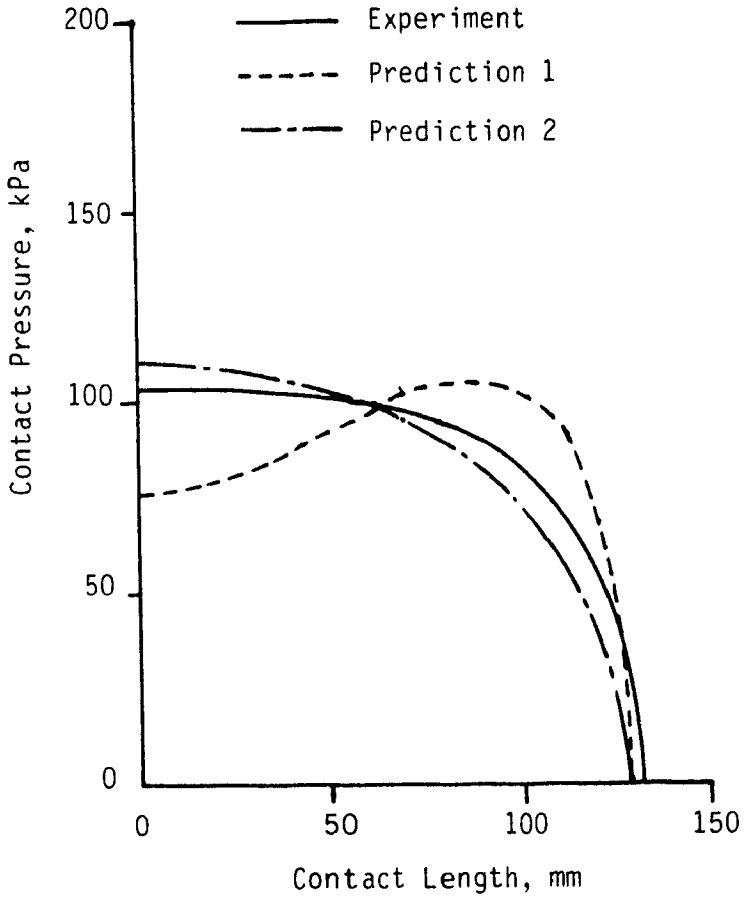


Fig. 4.27b Comparison Between Experimental and Frictionless Analytical Solutions on Rigid Surface

MICHELIN 12.5R-16.5XLM (buffed)
Rigid Surface
Inflation Pressure = 207 kPa
Wheel Load = 4.003 kN
Average Contact Pressure = 158 kPa
Contact Length = 208 mm
Contact Width = 123 mm

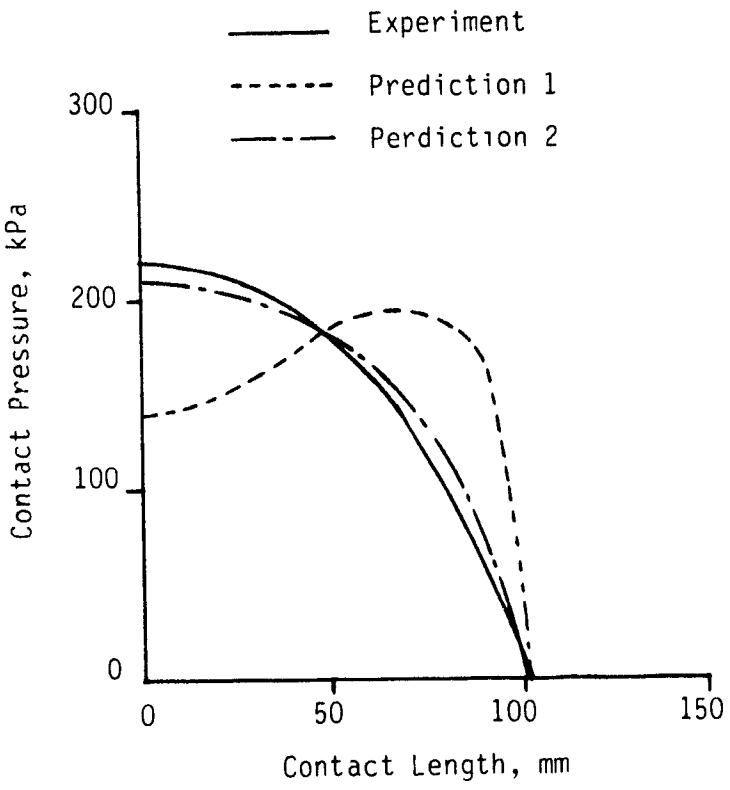


Fig. 4.27c Comparison Between Experimental and Frictionless Analytical Solutions on Rigid Surface

GOODYEAR 7.00-16LT (buffed)
Rigid Surface
Inflation Pressure = 34.5 kPa
Wheel Load = 1.779 kN
Average Contact Pressure = 48.7 kPa
Contact Length = 292 mm
Contact Width = 125 mm

Prediction 1 without Friction

Prediction 1 with Friction = 0.37

Prediction 2 without Friction

Prediction 2 with Friction = 0.37

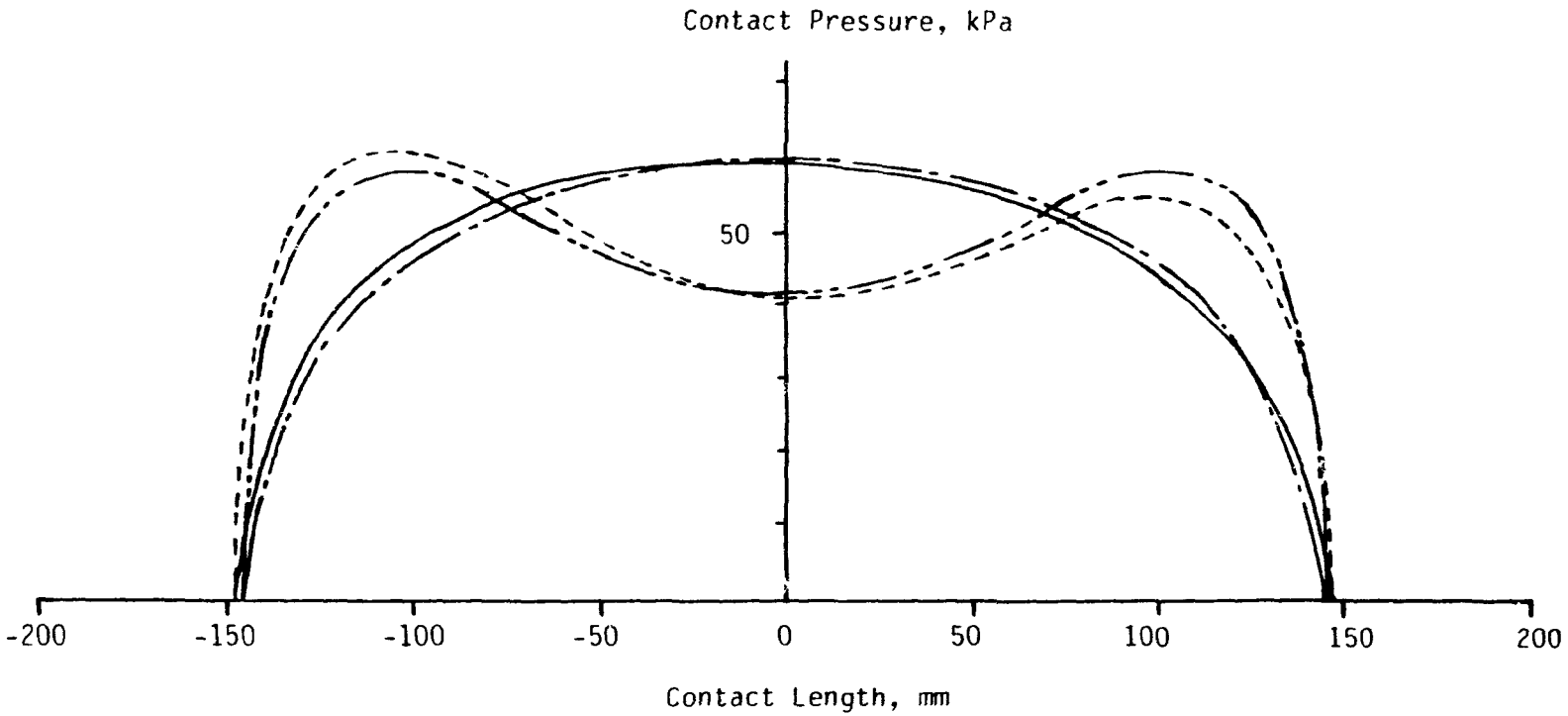


Fig. 4.28a Comparison Between Frictionless and Frictional Analytical Solutions on Rigid Surface

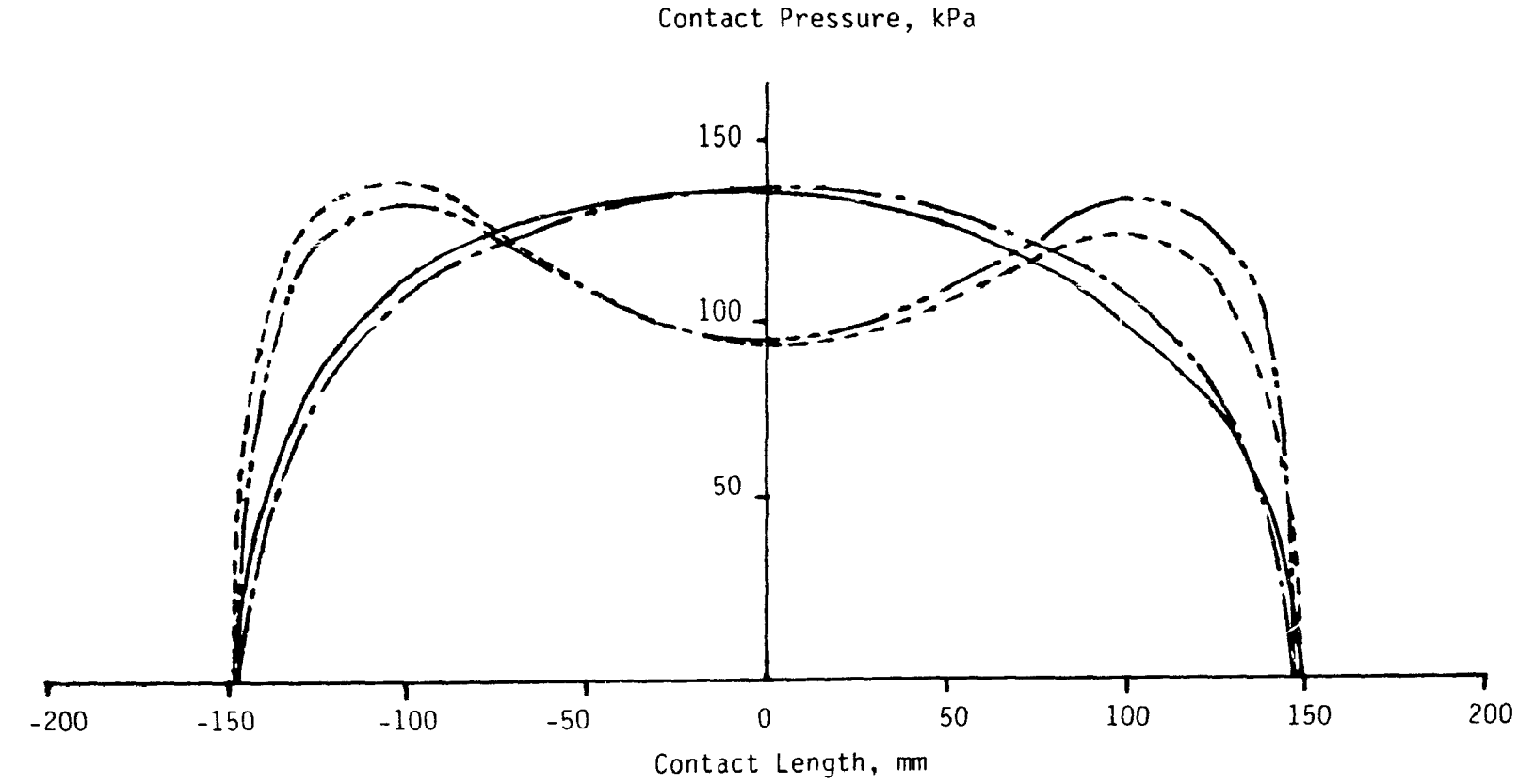


Fig. 4.28b Comparison Between Frictionless and Frictional Analytical Solutions on Rigid Surface

Prediction 1 without Friction

Prediction 1 with Friction = 0.37

Prediction 2 without Friction

Prediction 2 with Friction = 0.37

GOODYEAR 7.00-16LT (buffed)
Rigid Surface
Inflation Pressure = 310.5 kPa
Wheel Load = 4.003 kN
Average Contact Pressure = 246.5 kPa
Contact Length = 202 mm
Contact Width = 80 mm

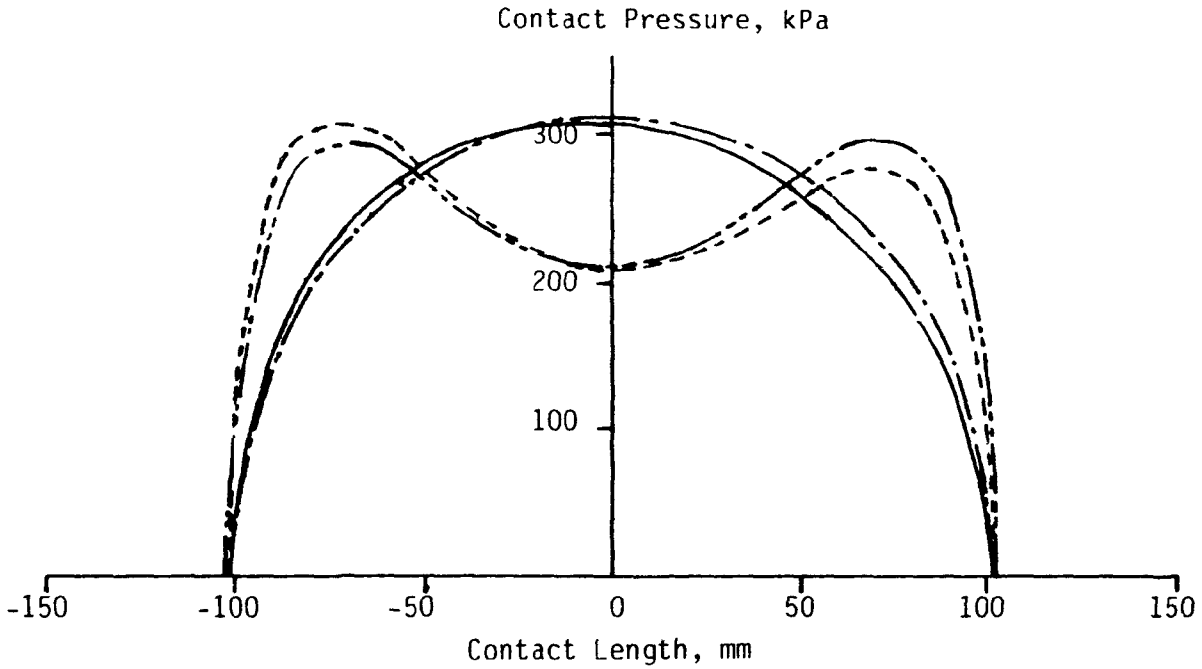


Fig. 4.28c Comparison Between Frictionless and Frictional Analytical Solutions on Rigid Surface

Tire-Rigid Base Interactions

For these interactions, the experimental and analytical results on pressure distribution, shown in Figs. 4.24-4.27, are quite similar to those obtained for the tire-clay interaction problems (Figs. 4.20-4.23). One notable difference is that, in the case of tire-rigid base interaction, the contact length is exactly the same as that obtained from the experiment for each interaction problem.

CHAPTER 5

SECOND ANALYTICAL APPROACH: APPLICATIONS TO TIRE-SUPPORTING CLAY AND RIGID WHEEL-SUPPORTING SNOWPACK INTERACTION PROBLEMS

5.1 Introduction

This chapter presents the second analytical approach - an iterative method - for solving static interaction problems such as tires-supporting clay and rigid wheels-supporting snowpack interactions (refer to Yong and Ishikawa [146]; Yong, Ishikawa and Fukue [147]). The tires considered here are assumed to be "elastic solids", for the moment. The iterative method for the second analytical approach will be developed based on two separate analtyical tools such as the complex variable method considered in Chapter 4 and the incremental finite element method based on the updated Lagrangian description [7,79.115]. These two methods are combined into an iterative scheme in such a way that a given interaction will be solved incrementally. Because of using the complex variable method, which was the fundamental mathematical tool employed in the first analytical approach in Chapter 4, the iterative method can be modified to solve a sliding interaction problem involving a tire as a "pneumatic body", rather than an elastic solid, if required.

The following reasons are cited for invoking the present iterative method:

(1) The complex variable method applied in two-dimensional elasticity problems can approximate complicated profiles of contacting

solids. An application of such an analytical method will simplify computational algorithms, thus greatly reducing computational efforts.

(2) The idea of load increments makes it possible to apply the complex variable method to the iterative scheme solving the present interaction problems, which are also the finite deformation problems since the contacting bodies such as clay and snow are highly deformable.

In deriving an iterative scheme in the following section 5.2, both supporting clay and supporting snowpack are assumed to be nonlinear half-planes while a tire is assumed to be a cylindrical solid, which is defined to be either linearly elastic or rigid. A frictionless contact between these two solids - a cylindrical solid and a half-plane is called a nonlinear frictionless contact problem in the following.

5.2 Method of Analysis

A nonlinear frictionless contact problem between a cylindrical solid (S_2) and a half-plane (S_1) will be considered in the following, as shown in Fig. 5.1. The nonlinear contact analysis for soliving such a problem is performed using an iterative technique which requires the use of a combination of a numerical and an analytical method - the incremental finite element method based on the updated Lagrangian formulation and the complex variable metnod applicable to linear contact problems. In implementing the iteration procedure for

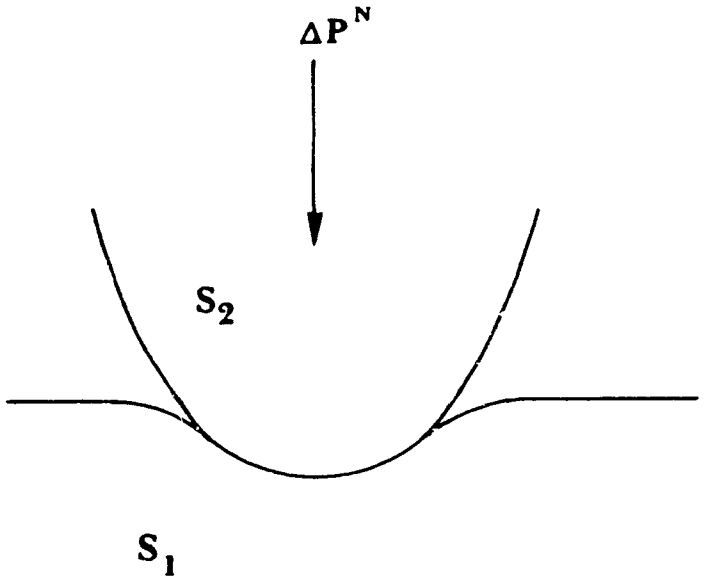


Fig. 5.1 Nonlinear Contact Problem Between a Linear Solid and a Nonlinear Half-Plane

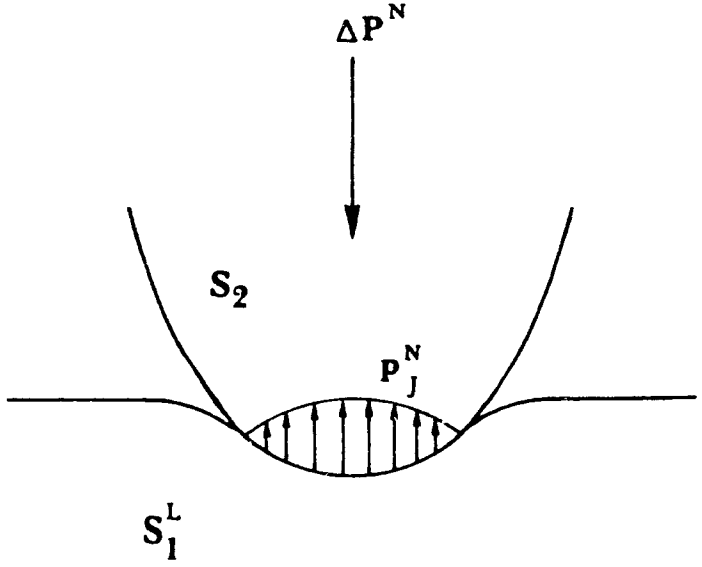


Fig. 5.2 Contact Pressure Induced by a Contact Between a Linear Solid and a Linear Half-Plane

solving the problem at hand, the following assumptions are made:

(1) the linear-cylindrical solid S_2 and the nonlinear half-plane S_1 are considered to be homogeneous and isotropic,

(2) the parabolic cylinder S_2 is approximated by a second degree polynomial as shown in function f_2 given as $f_2(x) = x^2/2R$ where R is the radius of the cylinder,

(3) the incremental loading is sufficiently small so that the deformation of the cylinder and the nonlinear half-plane are also small - to satisfy linear theory requirements in application of the complex variable method as well as the finite element method at each load incremental step,

(4) the contact pressure, which is obtained by solving a linear contact problem (Fig. 5.2) between a cylinder S_2 and a linear half-plane denoted by S_1^L whose modulus of elasticity is not known a priori, will simulate the contact pressures of the nonlinear contact problems shown in Fig. 5.3,

(5) Poisson's ratio ν_2 and modulus of elasticity E_2 at every load increment are known values of the cylinder S_2, as well as Poisson's ratio ν_1 of S_1^L, while E_1 of S_1^L is not known initially and is assumed to change at each iteration of every load increment.

ITERATION PROCEDURE AT Nth LOAD INCREMENT

The iteration process shown in the flow diagram (Fig. 5.3) consists of the following steps:

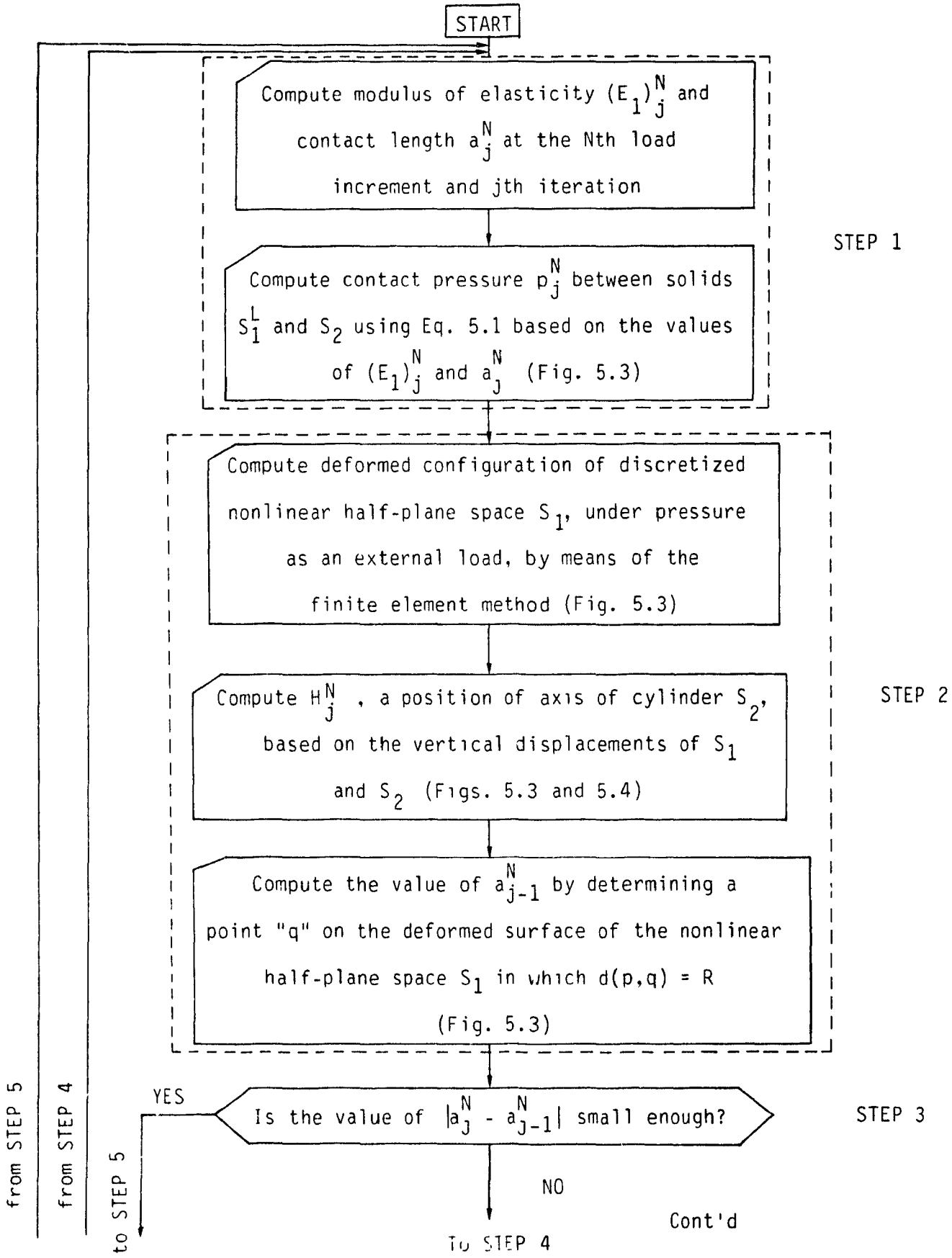


Fig. 5.3 Flow Diagram of Numerical Iteration

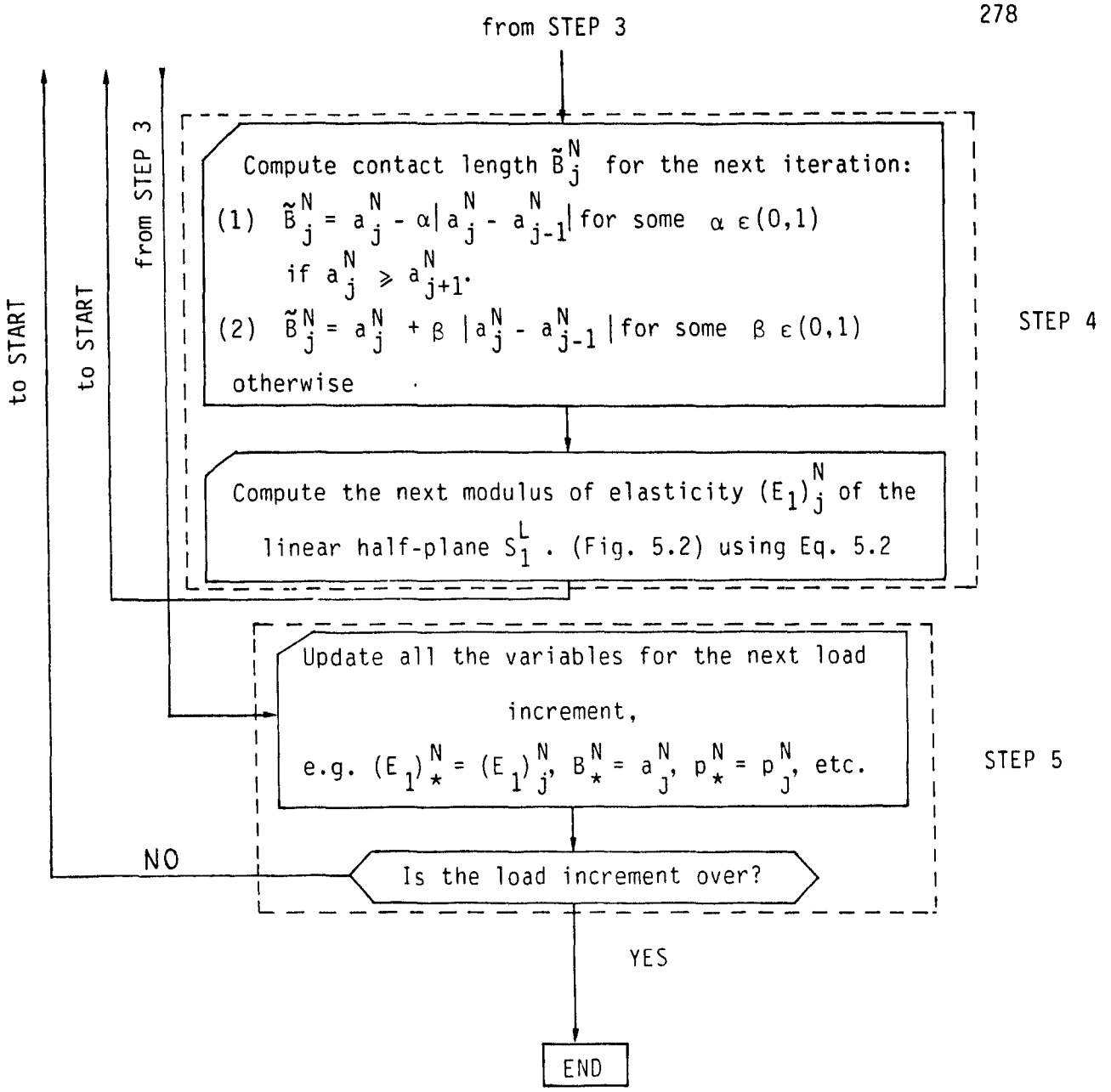


Fig. 5.3 Flow Diagram of Numerical Iteration

Step 1

Consider the linear contact problem shown in Fig. 5.2.

(a) Define $(E_1)_j^N$ an elasticity tensor of order four at Nth load increment and at jth iteration, in one of the following manners:

(i) $(E_1)_j^N$ = an initial elasticity coefficient $(E_1)_{initial}$ of the nonlinear half-plane S_1 of N = 1 and j = 1,

(ii) $(E_1)_j^N = (E_1)_*^{N-1}$, elasticity coefficient at the final iteration in the previous increment N-1, if N > 2 and j = 1,

(iii) $(E_1)_j^N = (\tilde{E}_1)_j^N$, elasticity coefficient computed on the basis of the (nominal) contact length, obtained at the end of each iteration process, when $N \geq 1$ and $j \geq 2$. Note that the roles of the elasticity coefficients $(E_1)_*^{N-1}$ and $(\tilde{E}_1)_j^N$ will be more evident at the end of steps 4 and 5.

(b) compute the contact pressure $p_j(x)$ by solving the linear contact problem in Fig. 5.2 using the following relationship:

$$p(x) = \frac{4(a^2-x^2)^{\frac{1}{2}}\, G_1 G_2}{R\,\{G_1(1+K_2) + G_2(1+K_1)\}} \tag{5.1}$$

where a = half of contact length,

G_m = shear modulus for a solid S_m,

$$K_m = \begin{cases} (3-4\nu_m)/(1+\nu_m) & \text{(plane stress)} \\ 3-4\nu_m & \text{(plane strain)} \end{cases}$$

(m = 1 and 2 for the solids S_1 and S_2 respectively).

using the elasticity coefficient $(E_1)_j^N$ obtained in (a) above. Under assumptions (2) and (3), the half of the

contact length "a" is obtained as

$$a^2 = \frac{PR}{2}\left(\frac{1+K_1}{G_1} + \frac{1+K_2}{G_2}\right) \tag{5.2}$$

in which $(E_1)^N = (E)_{initial}$ and "a" will be denoted by $a_j^N = B_{initial}$, $a_j^N = \tilde{B}_*^{N-1}$ or $a_j^N = B_j^N$ where B_*^{N-1} and B_j^N will also be defined in steps 4 and 5; P the force per unit width

Step 2

(a) Apply the pressure p_j obtained in Step 1 onto the nonlinear half-plane space S_1 which is discretized by the finite elements as shown in Fig. 5.4 and 5.5. Perform the nonlinear analysis using the incremental finite element method to determine the stresses as well as the deformed configuration of S_1.

(b) Determine $H_j^N = R - (DY_j^N + d^N)$ where H_j^N is the distance between the axis of the cylinder S_2 and the undeformed surface (or the X-axis of the reference frame) of the half-plane S_1 as shown in Fig. 5.5. Note that R is the radius of the cylinder, DY_j^N is the vertical displacement at the center of the free surface of the discretized nonlinear half-plane S_1 at the jth iteration in the Nth load increment, and d^N is the vertical displacement of the cylinder S_2 subjected to the incremental load p_j^N as shown in Fig. 5.6.

Making an additional assumption that the vertical displacement d^N (i.e. the approach of the two rigid plates) in Fig. 5.6 simulates the vertical displacement of the axis of the cylinder S_2 in Fig. 5.1, the analytical solution of the displacement d^N

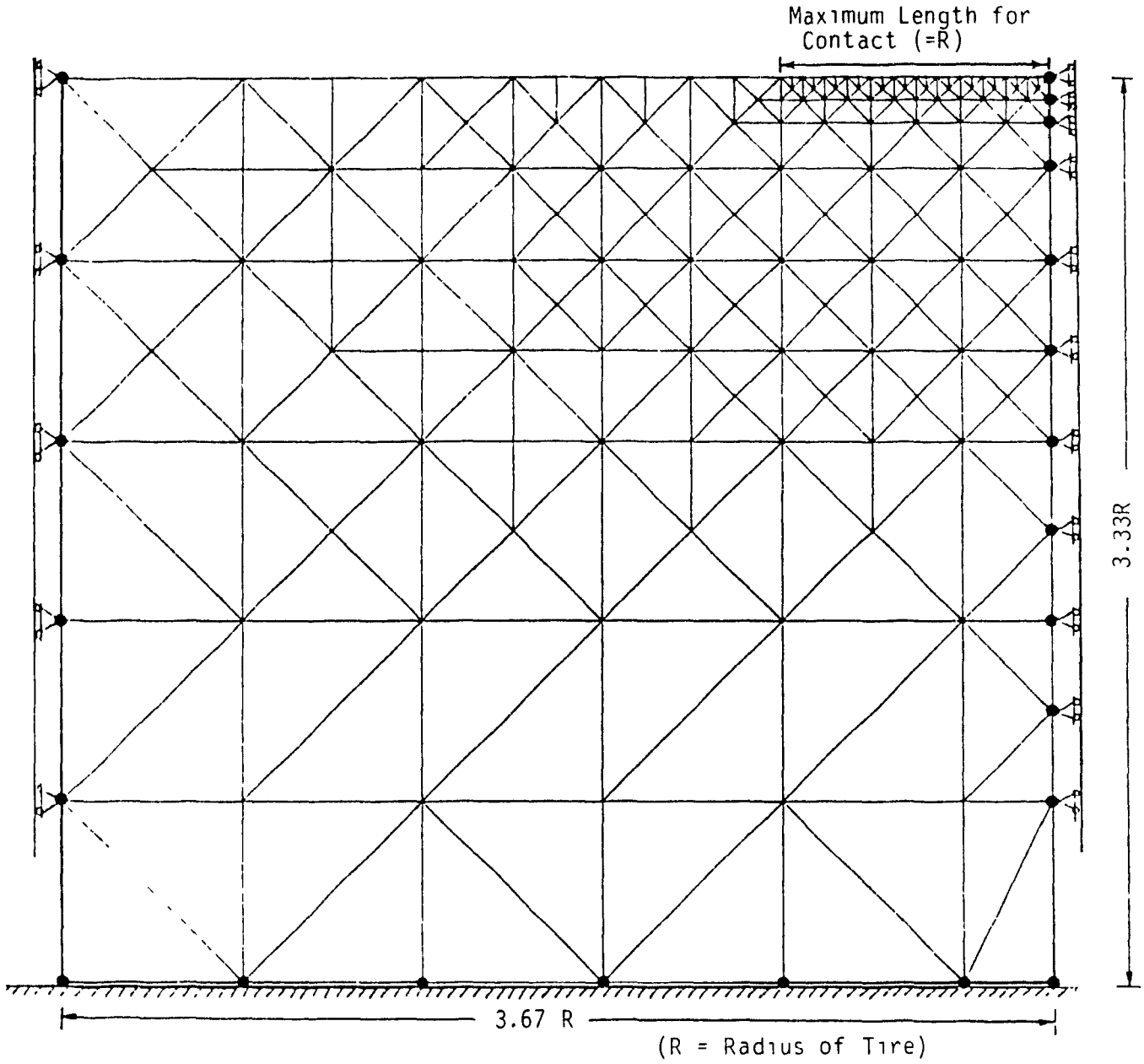


Fig. 5.4 Finite Element Discretization (i.e. C.S.T. Elements) of Nonlinear Elastic Half-Plane and Boundary Conditions

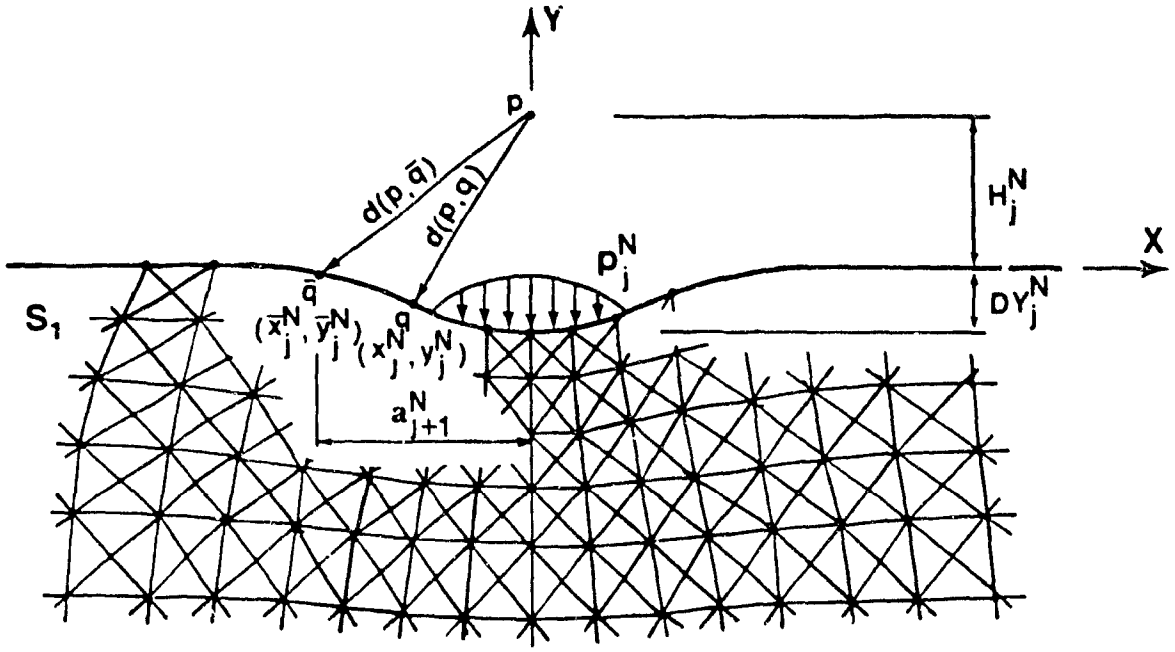


Fig. 5.5 Deformed Configuration of Discretized Half-Plane Due to Pressure

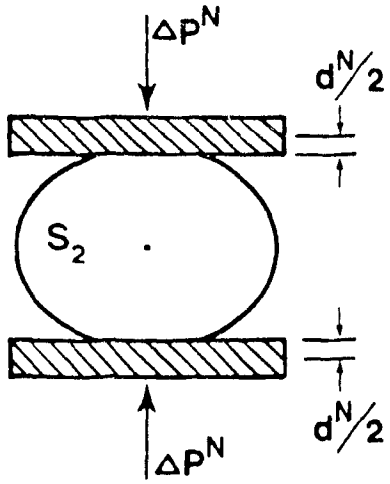


Fig. 5.6 Approach Between Plates and an Elastic Cylinder

can be obtained e.g. refer to Eq. 8.4.36 given by Gladwell [41: pp. 394-403]. After neglecting the higher order term in the equation, it can be shown as

$$d^N = \frac{2\Delta P^N}{\pi} \frac{1-\nu_2}{G_2} \log \{\frac{8\pi RG_2}{\Delta P^N(1-\nu_2)} - \frac{1}{2}\} + \frac{9}{16} \frac{\Delta P^N}{\pi R} \frac{(1-\nu_2)}{G_2} \quad (5.3)$$

where ν_2, G_2 and R are respectively the Poisson's ratio, shear modulus and radius of the cylinder S_2.

While the analytical solution given in Eq. 5.3 is used to obtain the vertical displacement d^N of the S_2 in Fig. 5.6, d^N can also be obtained accurately from experiments. The load-displacement curves are relatively linear in the case of tires acting on a rigid surface according to Boonsinsuk [13] and our experiments shown in Figs. C.1a-i.

(c) Let a point, p, in Fig. 5.5 be the position of the axis at the current deformed configuration of the cylinder. Determine a position q on the deformed surface of the half-plane at the current state where the distance between the two points p and q, denoted by d(p,q), is equal to the radius R of the cylinder as shown in Fig. 5.5.

(d) Define a^N_{j+1} as a distance between q, where d(p,q) = R and Y-axis of the reference frame.

Step 3

Let $s = |a^N_j - a^N_{j+1}|$ and choose a reasonably small number $\varepsilon > 0$.

(1) if $s \leq \varepsilon$, go to Step 5

(2) if $s > \epsilon$, go to Step 4.

Step 4

(a) Calculate $\tilde{B}_j^N$ for the next iteration

(i) If $a_j^N \geq a_{j+1}^N$, $\tilde{B}_j^N = a_j^N - \alpha|a_j^N - a_{j-1}^N|$. (5.4a)

(ii) If $a_j^N < a_{J+1}^N$, $\tilde{B}_j^N = a_j^N + \beta|a_j^N - a_{j-1}^N|$. (5.4b)

where α and β are real values such that $0 < \alpha, \beta < 1$.

(b) Calculate $(E_1)_j^N$ for the next iteration by substituting one of the $\tilde{B}_j^N$ obtained in Eq. 5.4a or Eq. 5.4b into Eq. 5.2 in Step 1.
Go to Step 1 for the next iteration.

Step 5

Update all the variables necessary to use the next load incrment.

i.e. $(E_1)_\star^N = (E_1)_j^N$, $B_\star^N = a_j^N$, $p_\star^N = p_j^N$, etc.

Go to Step 1 for the next load increment.

Step 1 through Step 5 need to be repeated until the total load is applied onto the cylinder.

5.3 Application to Interaction Problems

5.3.1 A Tire-Supporting Clay Interaction Problem

It is first noted here that an interaction problem between a pneumatic tire and a supporting clay was considered by the 2-D Hertz theory directly under the assumption that tires are linearly elastic

"solids" with Poisson's ratio 0.499 (e.g., Yong et al [140]). In obtaining the modulus of elasticity of the tire, i.e. the tire is assumed to be linearly elastic, it is observed by Boonsinsuk [13] that the relationship between the contact area and the applied load is approximately linear for a tire with a smooth surface (i.e. without treads) and nonlinear for a tire with treads, regardless of whether the relationship between vertical displacement and applied load is linear (or not). These results lead to the production of lienar and nonlinear moduli of elasticity respectively. Ignoring the nonlinearities of tire elasticity, which depends in part on tread patterns, rigidity of treads and tire carcass, inflation pressure, etc. might lead to unacceptable errors in computational output.

Now, if the tire is considered to be a nonlinearly elastic cylindrical solid, one needs to find the modulus of elasticity of tire at each load incremental step [146]. Such a nonlinear elastic modulus, E_{non}, of each cylindrical solid is determined in the simple form as

$$E_{non} = C \frac{W}{Ba^2} \tag{5.5}$$

where C is a known constant value depending on the radius of the tire and assumed Poisson's ratio of tire, W the applied load, B is contact width and a is half of contact length. The contact length and width are expressed in the simple parabolic estimate as,

$$a^2 = A_o + A_1 W + A_2 W^2 \tag{5.6a}$$

$$B = B_o + B_1 W + B_2 W^2 \tag{5.6b}$$

where A_o, A_1, A_2, B_o, B_1 and B_2 are constants obtained by normal equations for A's and B's based on the two N sets of experimental data (W_i, a_1) and (W_1, B_i), i=1,2,....,N. W_i, a_1 and B_1 are respectively the loads, the idealized half of contact lengths and contact width obtained from the experiments in tire-rigid surface contacts [13]. The load denoted by W in Eqs. 5.5, 5.6a and 5.6b is an applied load for a nonlinear contact problem between a tire and supporting clay. The clay considered [13] is the same as that used in Chapter 3.

Thus, at each incremental loading one solves the contact problem between the tire with the elastic modulus E_{non} for the corresponding load W and the nonlinear half-plane of clay by means of the iterative method described previously and shown in Fig. 5.3.

In the example problems, the interactions between pneumatic tires and clay studied by Boonsinuk [13] are considered here. The clay used in his study was kaolinite clay, which was also used in the present study (Chapter 3). The clay was characterized by the stress-strain relationship (Fig. 5.7). The pneumatic tires were very small as shown in Fig. 5.8. The data on the tire-clay interaction is provided in Table 5.1. The contact length was then computed by the second analytical approach for the various problems. The comparisons of contact length obtained numerically and experimentally for each problem are shown in Figs. 5.9a-f. They show a reasonable agreement.

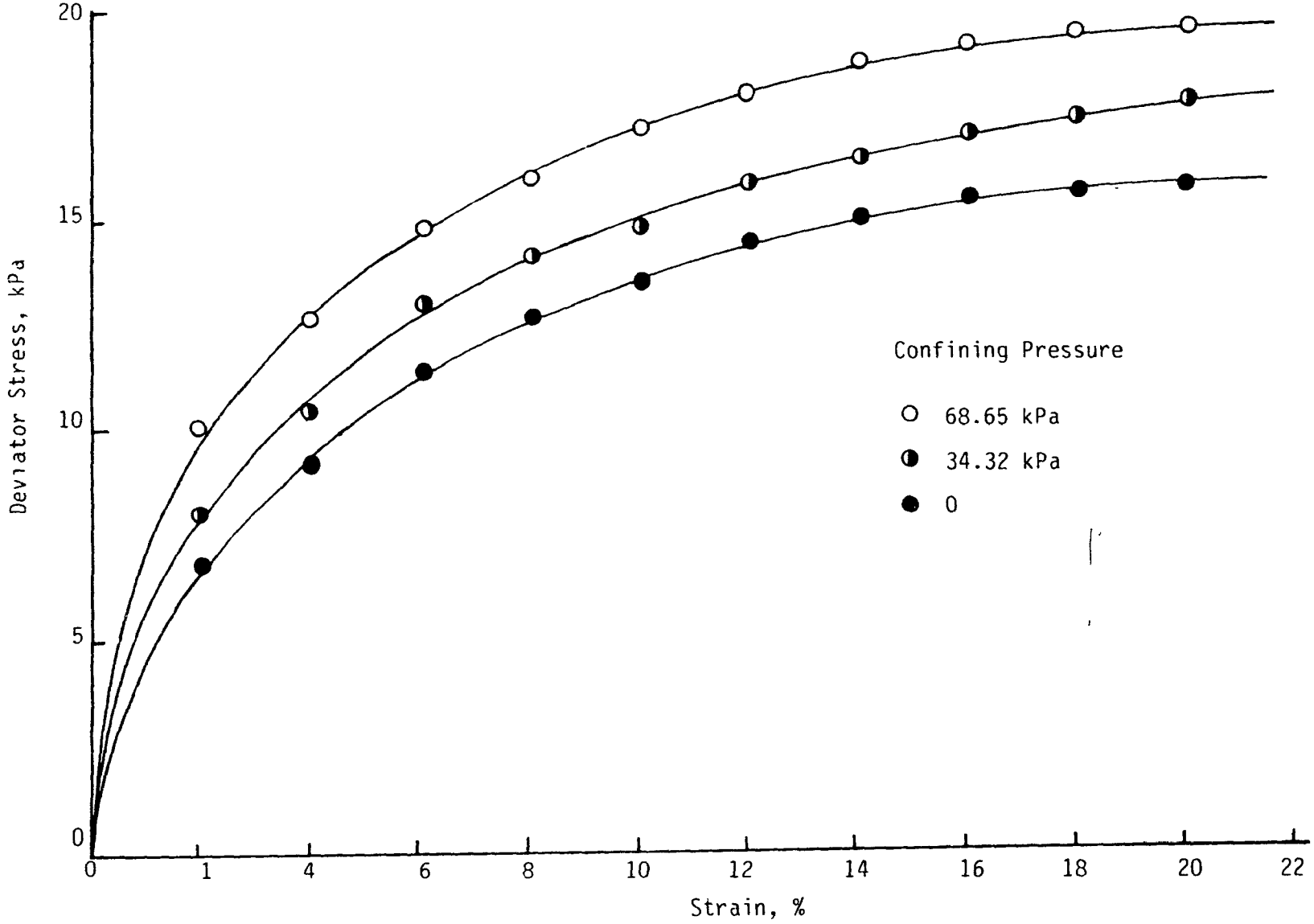


Fig. 5.7 Stress-Strain Curves of Kaolinite Clay Obtained by Plane Strain Triaxial Tests (Boonsinsuk [13])

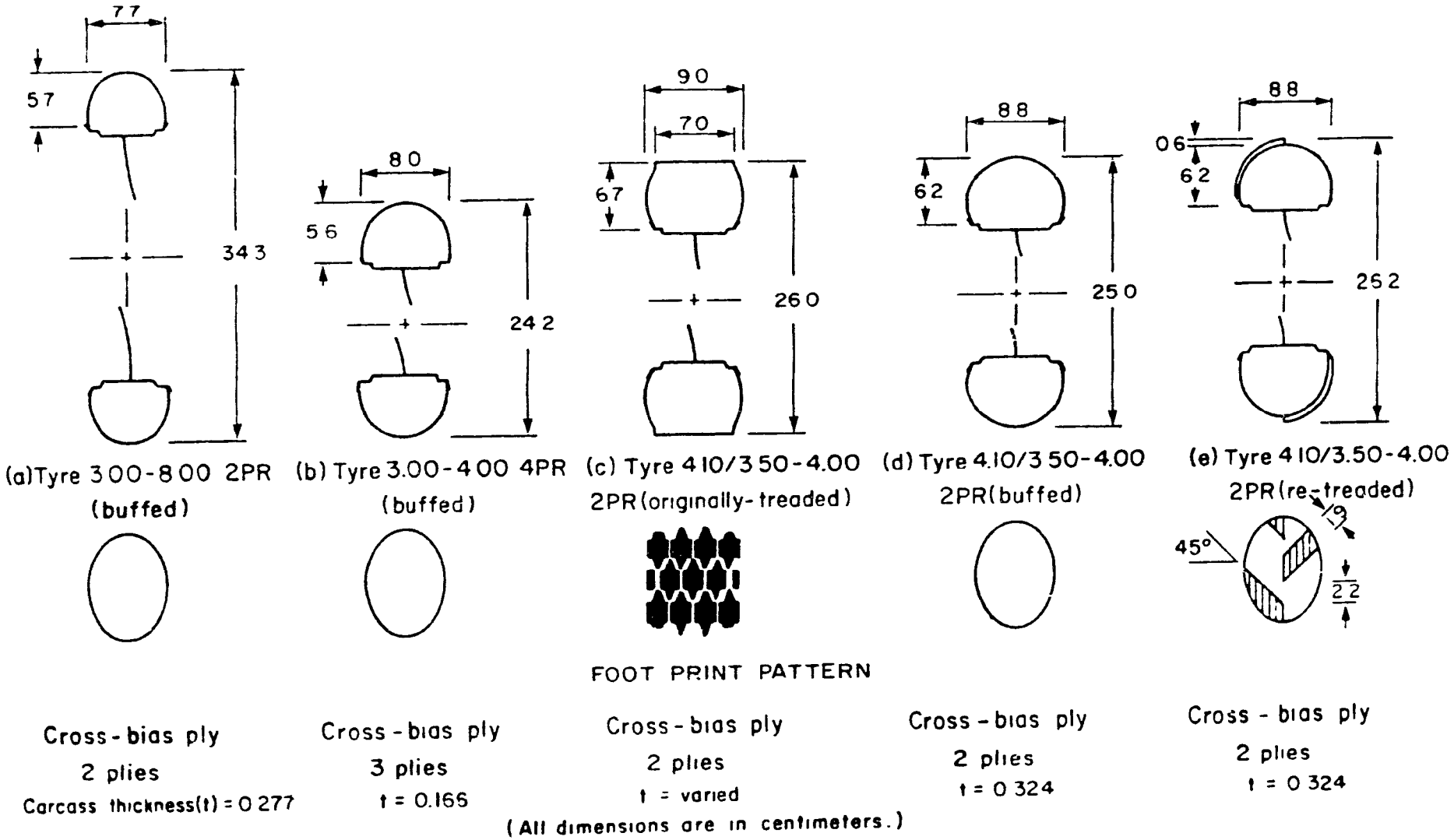
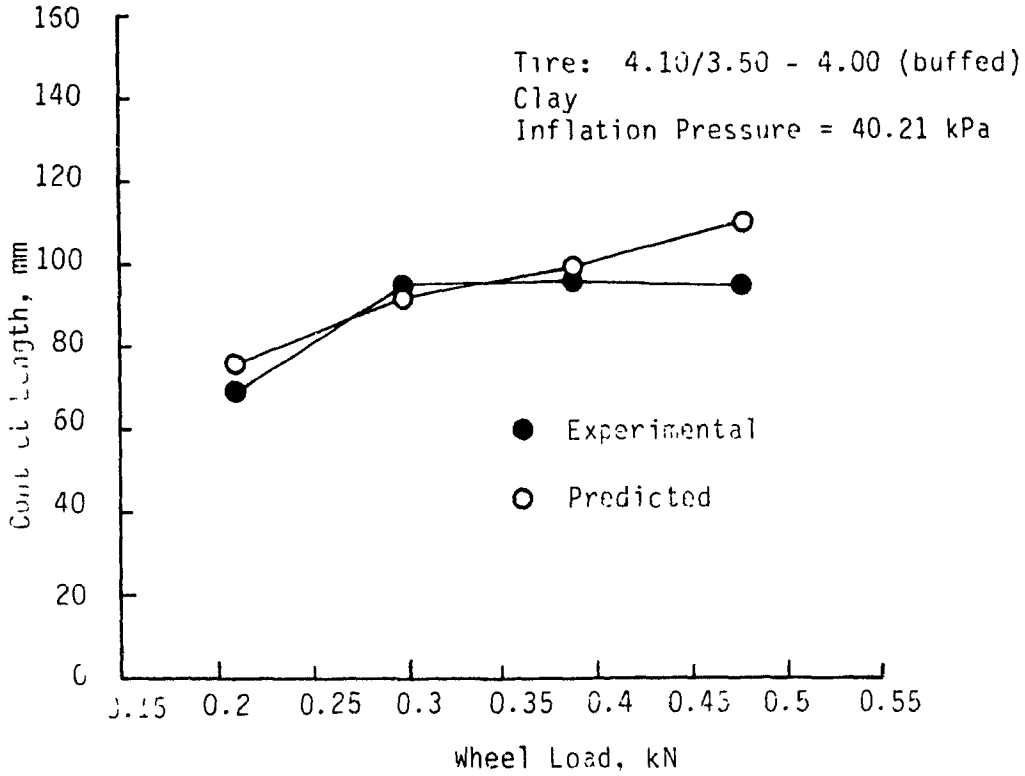


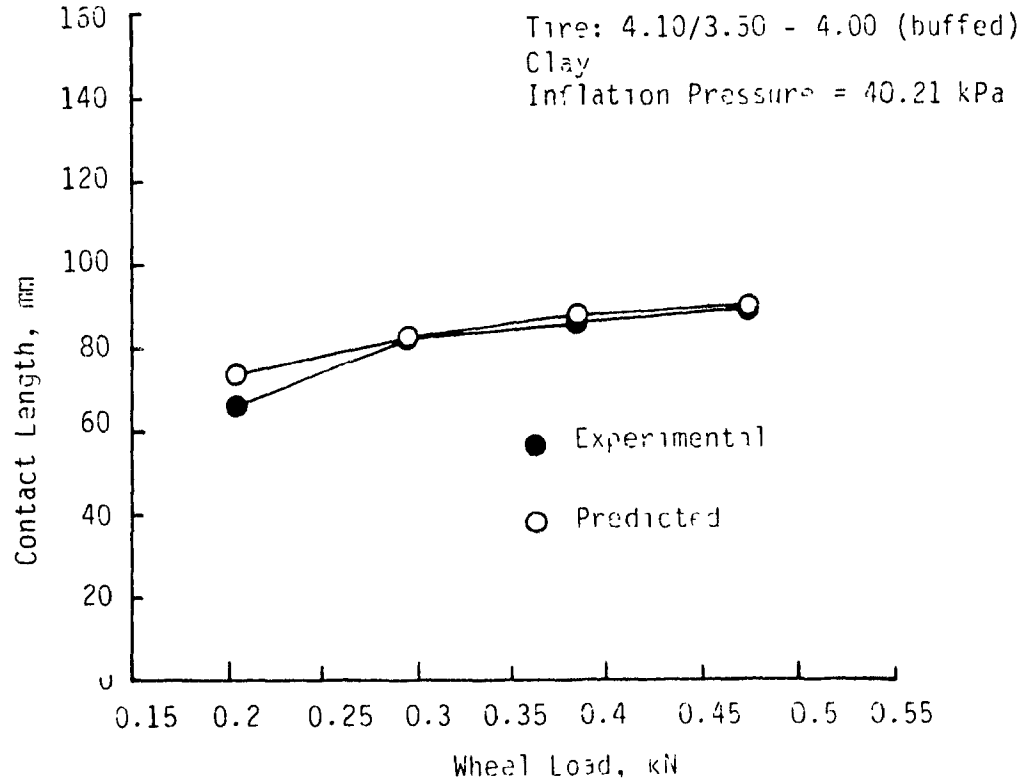
Fig. 5.8 Small Tires Studied by P. Boonsinsuk [13]

	Load (N)	Measured Contact Area (mm^2)	Representative Contact Surface	
			Length (mm)	Width (mm)
4.10/3.50 - 4.00 2PR (buffed) Inf. Press. = 40.21 kPa Radius = 115 mm	209.87 298.12 388.34 476.60	3800.0 5220.0 6140.0 7120.0	69.0 95.0 96.0 95.0	55.1 54.9 64.0 74.9
4.10/3.50 - 4.00 2PR (treaded) Inf. Press. = 40.21 kPa Radius = 125 mm	203.98 293.22 382.45 471.70	3960.0 5120.0 5380.0 5560.0	66.0 82.0 86.0 89.0	60.0 62.4 62.2 62.5
3.00 - 8.00 2PR (buffed) Inf. Press. = 20.59 kPa Radius = 165 mm	205.94 295.18 384.42 473.66	4580.0 6300.0 8400.0 9380.0	88.0 105.0 120.0 125.0	52.0 60.0 70.0 75.0
3.00 - 8.00 2PR (buffed) Inf. Press. = 40.21 kPa Radius = 165 mm	205.94 295.18 384.42 473.66	3750.0 4500.0 6440.0 7260.0	75.0 85.0 117.0 123.0	50.0 52.9 55.0 59.0
3.00 - 4.00 4PR (buffed) Inf. Press. = 20.59 kPa Radius = 110 mm	200.06 290.28 378.54 467.78	4390.0 5100.0 6200.0 6620.0	77.0 88.0 100.0 105.0	57.0 58.0 62.0 63.0
3.00 - 4.00 4PR (buffed) Inf. Press. = 40.21 kPa Radius = 110 mm	200.06 290.28 378.54 467.78	3500.0 4120.0 4670.0 5390.0	70.0 75.0 82.0 93.0	50.0 54.9 57.0 58.0

Table 5.1 Data on Contact Surface for Clay
(Boonsinsuk [13])

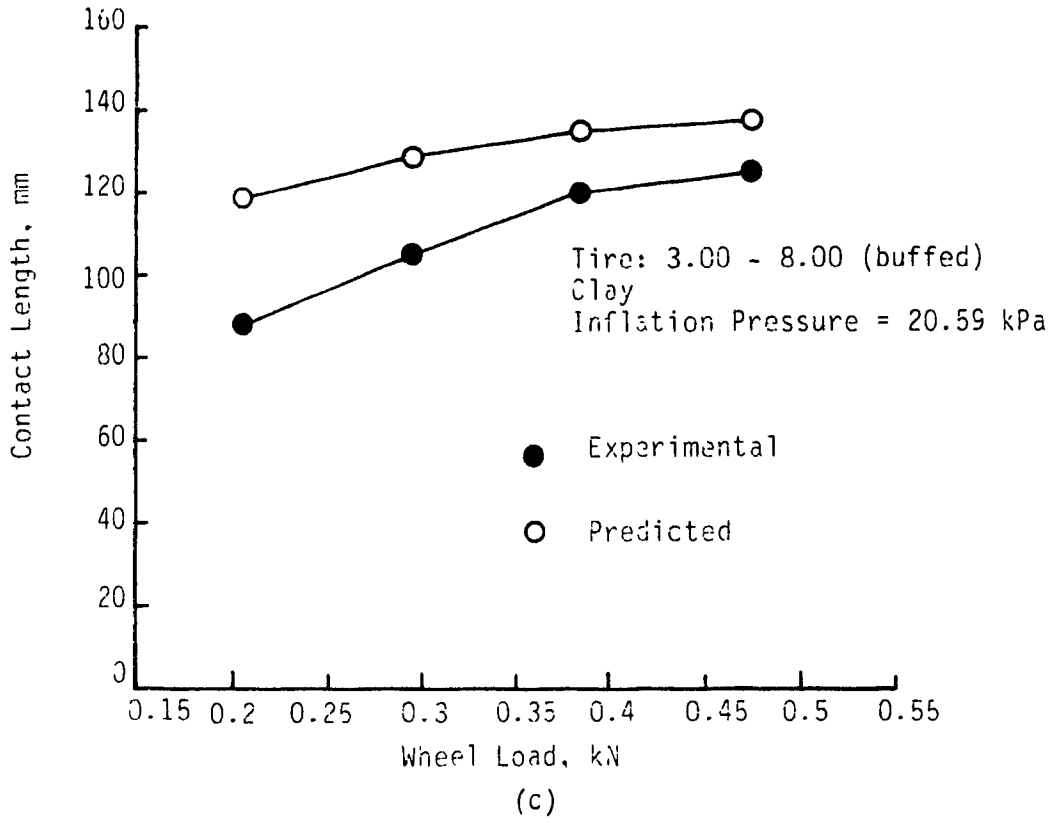


(a)



(b)

Fig. 5.9 Comparison Between Experimental and Predicted Values of Half Contact Length for Clay



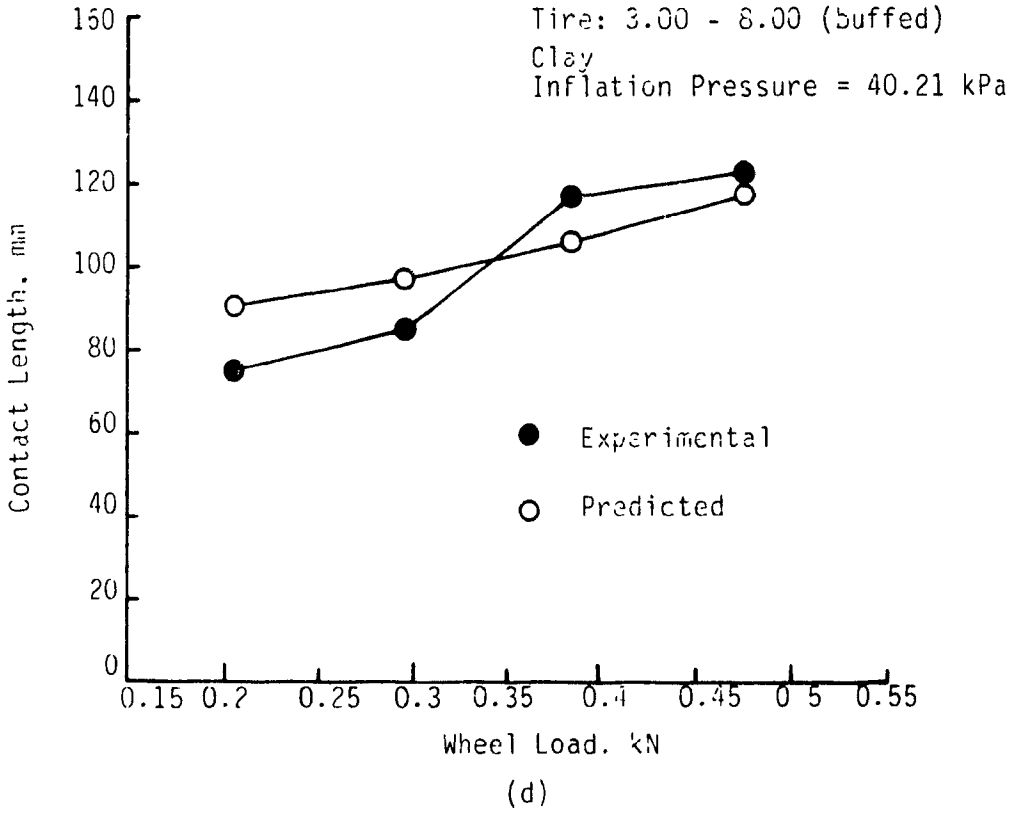
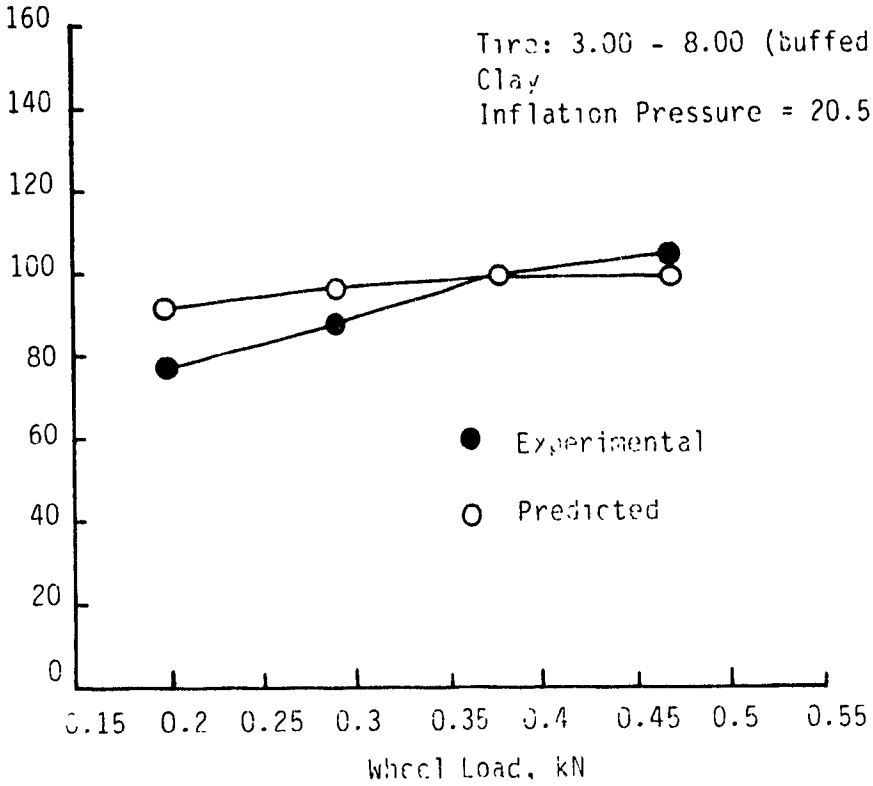
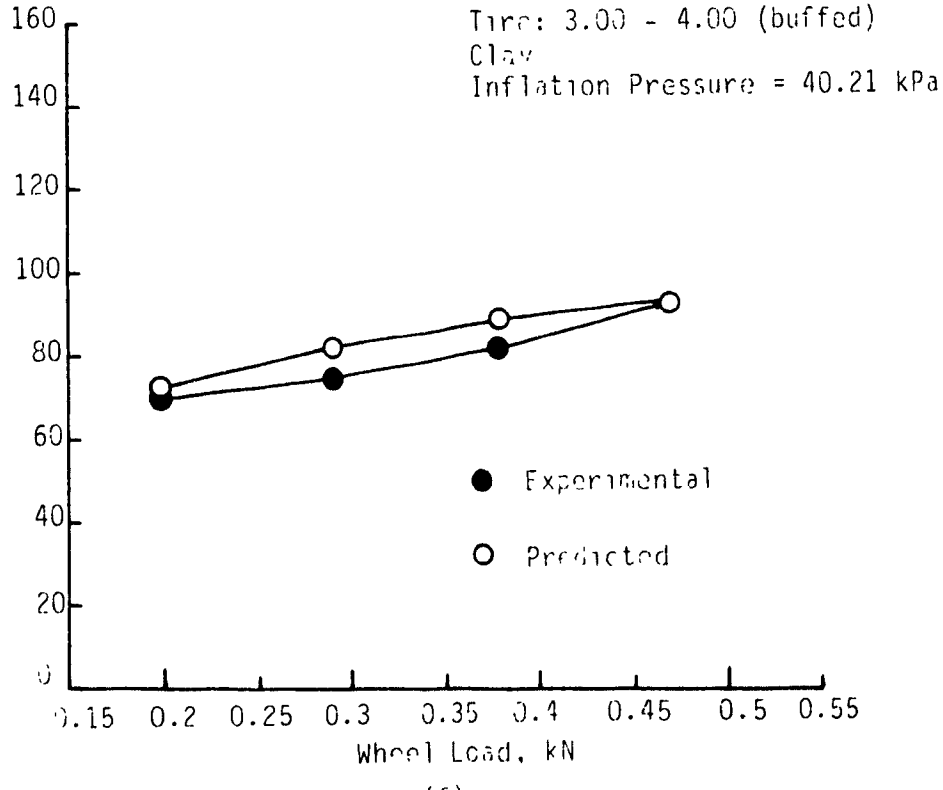


Fig. 5.9 Comparison Between Experimental and Predicted Values of Half Contact Length for Clay



(e)



(f)

Fig. 5.9 Comparison Between Experimental and Predicted Values of Half Contact Length for Clay

5.3.2 A Rigid Wheel - Supporting Snowpack Interaction Problem

In the case of a rigid wheel-snowpack interaction problem, we assume that the snow is a continuous elastic solid. It is furthermore assumed that Poisson's ratio is zero for all loadings, under the adiabatic condition. It is noted that a pneumatic tire can be considered as a rigid wheel if the tire is relatively stiff compared with the snow, e.g., the inflation of the tire must be high relative to the magnitude of loading; the snow is fresh. Such a condition is important for a pneumatic tire so that a contact profile at an equilibrium configuration keeps the original curvature.

Two sets of experiments on rigid wheel-snowpack interaction were conducted for different ages of snow. The snow considered was artifical snow, which was made in the cold room by crushing ice with a pulverizer. The age of the snow chosen was 2 and 4 days and the stress-strain relationship (Fig. 5.10), which is used in the computation, was obtained from the confined compression tests by Metaxas [82]. More details concerning the properties of the artificial snow can be found in the previous work, Yong, et al [145, 149], Fukue [33] and Metaxas [82]. For the experiments on the rigid wheel-snowpack interactions, the apparatus shown in Fig. 5.11 was used under the plane strain condition. The load was applied on the rigid wheel, whose specifications are given in Table 5.2, under a deformation rate of 0.584 mm/sec for both experiments (Figs. 5.12a,b). The cold room temperature was kept constant at 10 $\pm$ 3 degrees Celsius. The computations for obtaining contact length and sinkage were carried

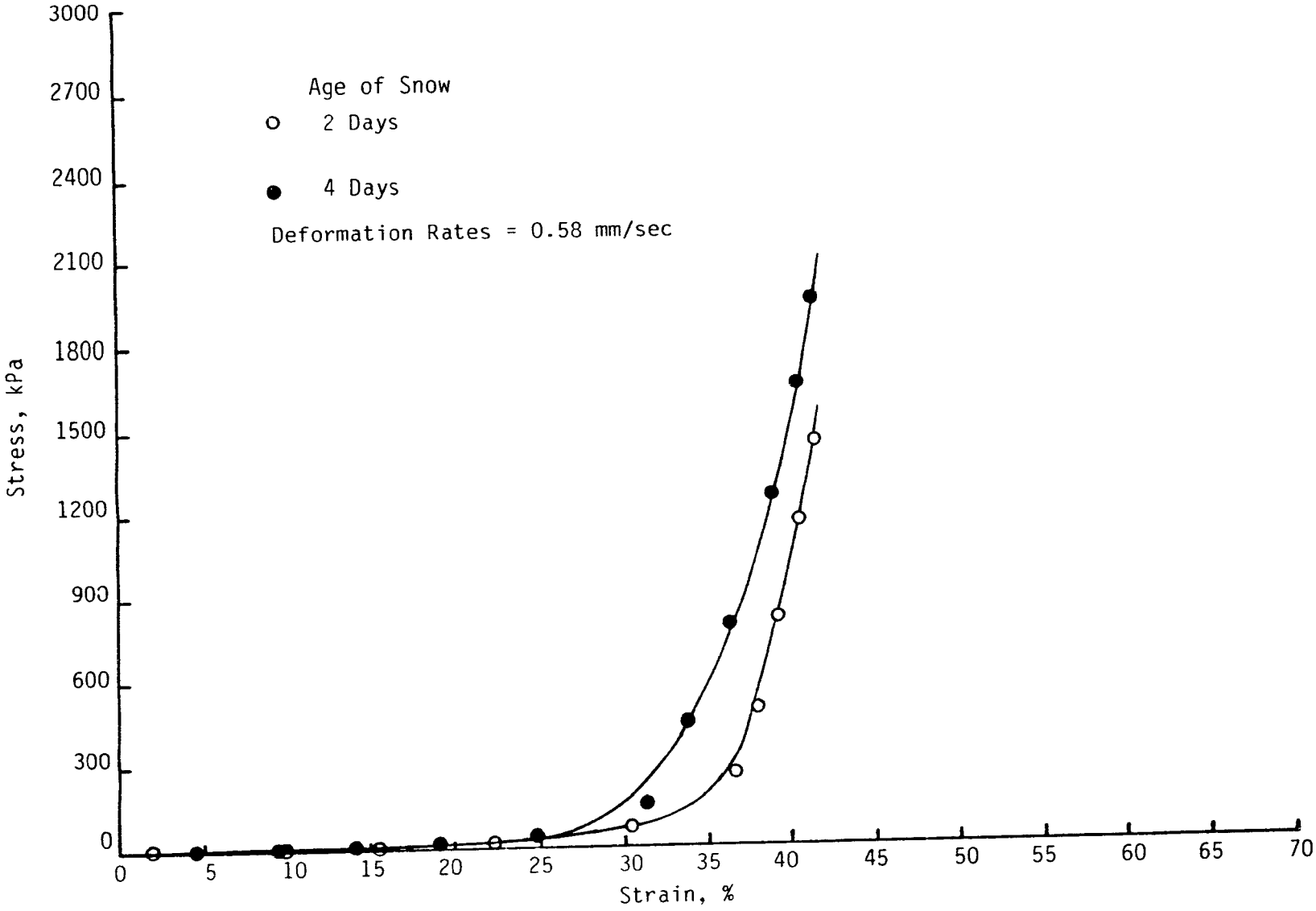
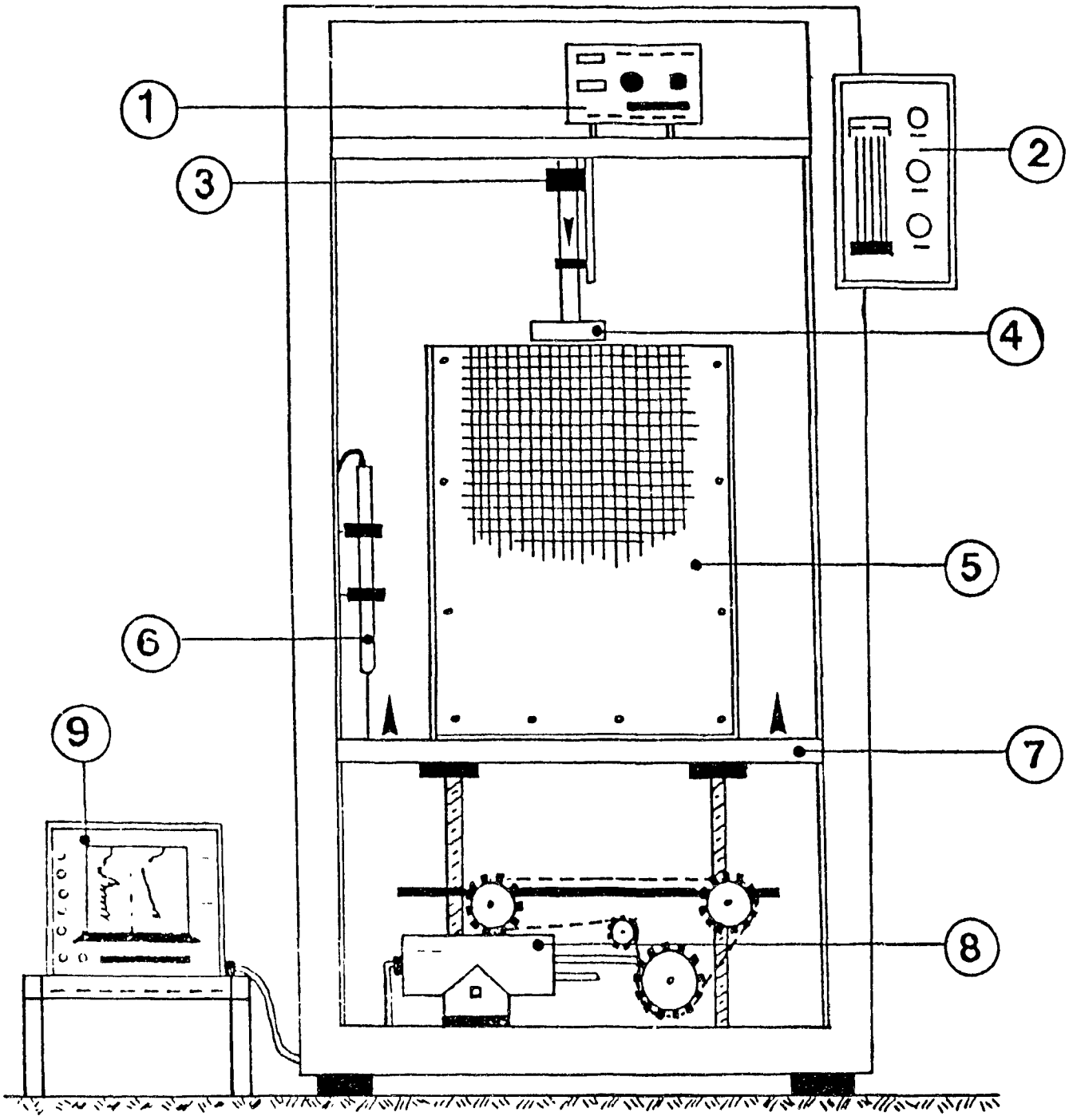


Fig. 5.10 Stress-Strain Curves of 2 and 4 Day Snow Obtained by Confined Compression Tests (Metaxas [82])



– Compression and Torque Loading Machine –

1. Torque or Penetration switch box
2. speed control unit
3. Load cell
4. Trafficability Tool
5. deep snow box
6. displacement transducer
7. moving platform
8. driving system
9. recording system

Fig. 5.11 Test Apparatus Used for Plate Penetration (Metaxas [82])

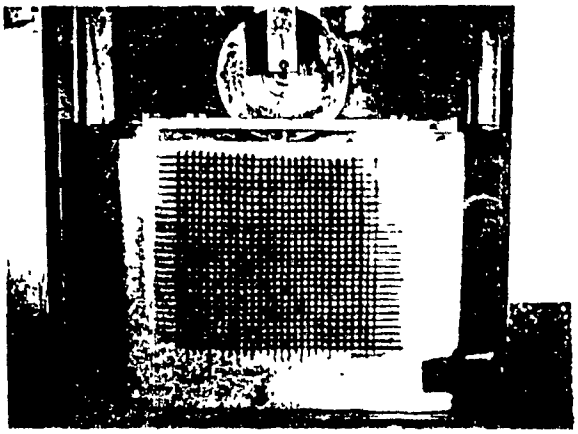


Fig. 5.12a Rigid Wheel and Snowpack Before Making Contact

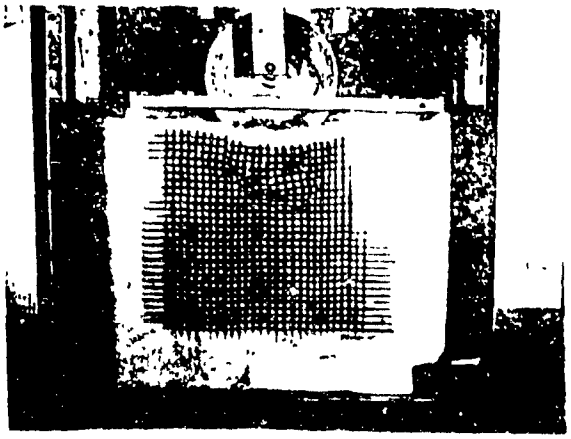


Fig. 5.12b Rigid Wheel and Snowpack Before Making Contact

	Rigid Wheel (Aluminum)
Radius	115 mm
Width	70.6 mm
Weight	2.3 kg

(a) Size and Weight of Rigid Wheel

	Snow Bin
Height	533 mm
Width	750 mm
Depth	75 mm

(b) Size of Snow Bin

Table 5.2 Specifications of Rigid Wheel and Snow Bin

out using those data.

Comparisons between the experimental and the numerical results with regard to sinkages of the wheel and nominal contact lengths are shown in Figs. 5.13 and 5.14 respectively. As can be seen in the figures, the numerical results for the contact lengths agree reasonably well with the experimental values (Fig. 5.14), while there are large discrepancies for sinkages (Fig. 5.13). It is noted that the results obtained for the tire-supporting clay interaction problems are better than those obtained for the rigid wheel-supporting snowpack interaction problems.

The results obtained in the rigid wheel-supporting snowpack interaction problems, could have been greatly influenced by many factors attributed to the complicated properties and behaviour of snow. The mechanical properties of snow depend on the factors, such as snow type including bonding strength, strain rate and temperature. At constant temperature, the mechanical properties of snow are strongly influenced by the strain rate or loading rate [33]. Therefore, difficulty arises when stress-strain-strain rate relationships at different positions (i.e. depth) are taken into account. In addition, snow behaves like a brittle material when the loading rate applied is relatively high. For this range in loading rate, local or micro-fractures of materials should be considered as well as high local deformation rate near the contact surface [33]. Under the loading condition as shown in Fig. 5.9, the actual relative deformation rate of snowpack is different at each position in the snowpack. The evaluation of relative strain rate at any point is

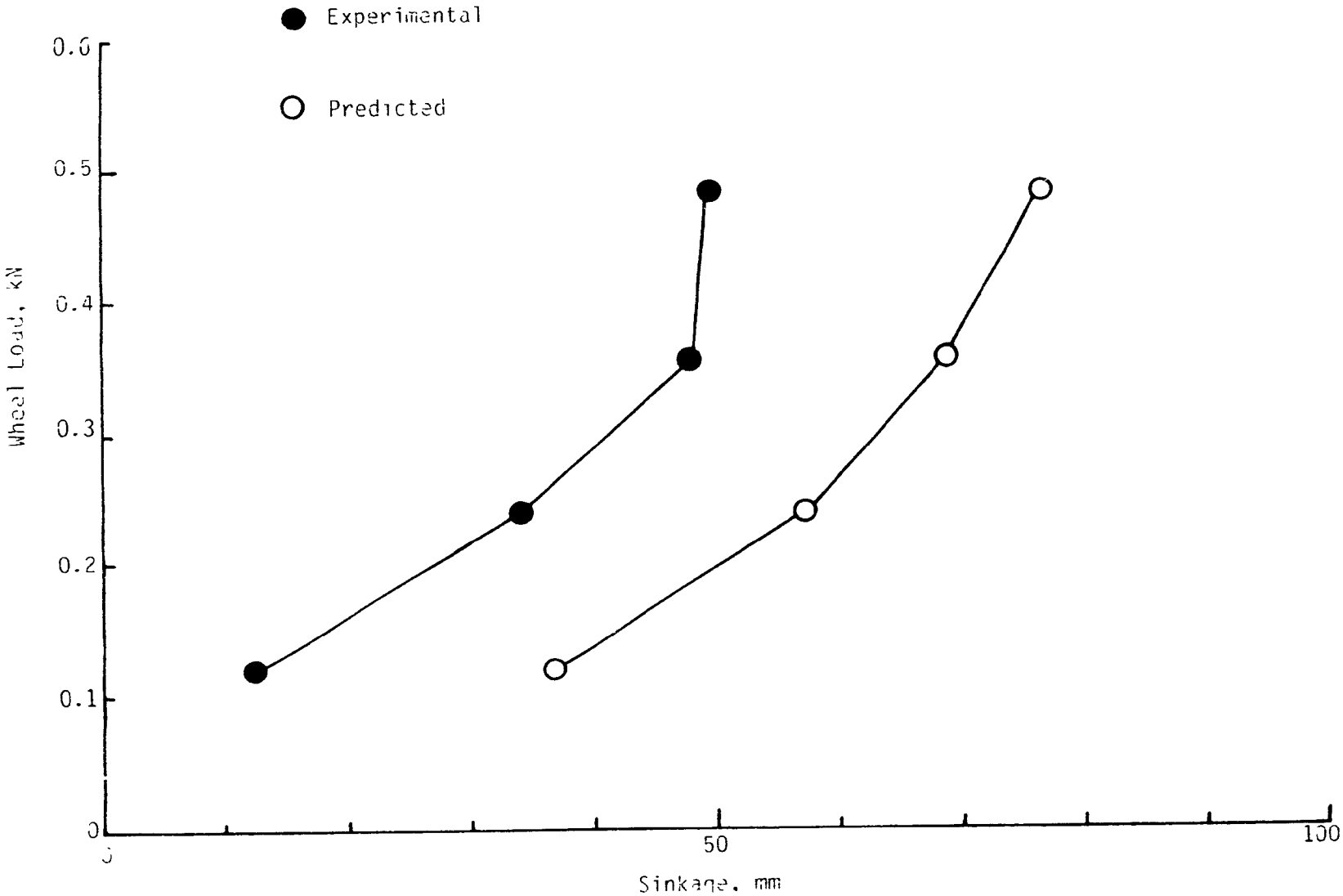


Fig. 5.13a Comparison Between Experimental and Predicted Values of Sinkage For a Rigid Wheel on a Snowpack Aged for 2 Days

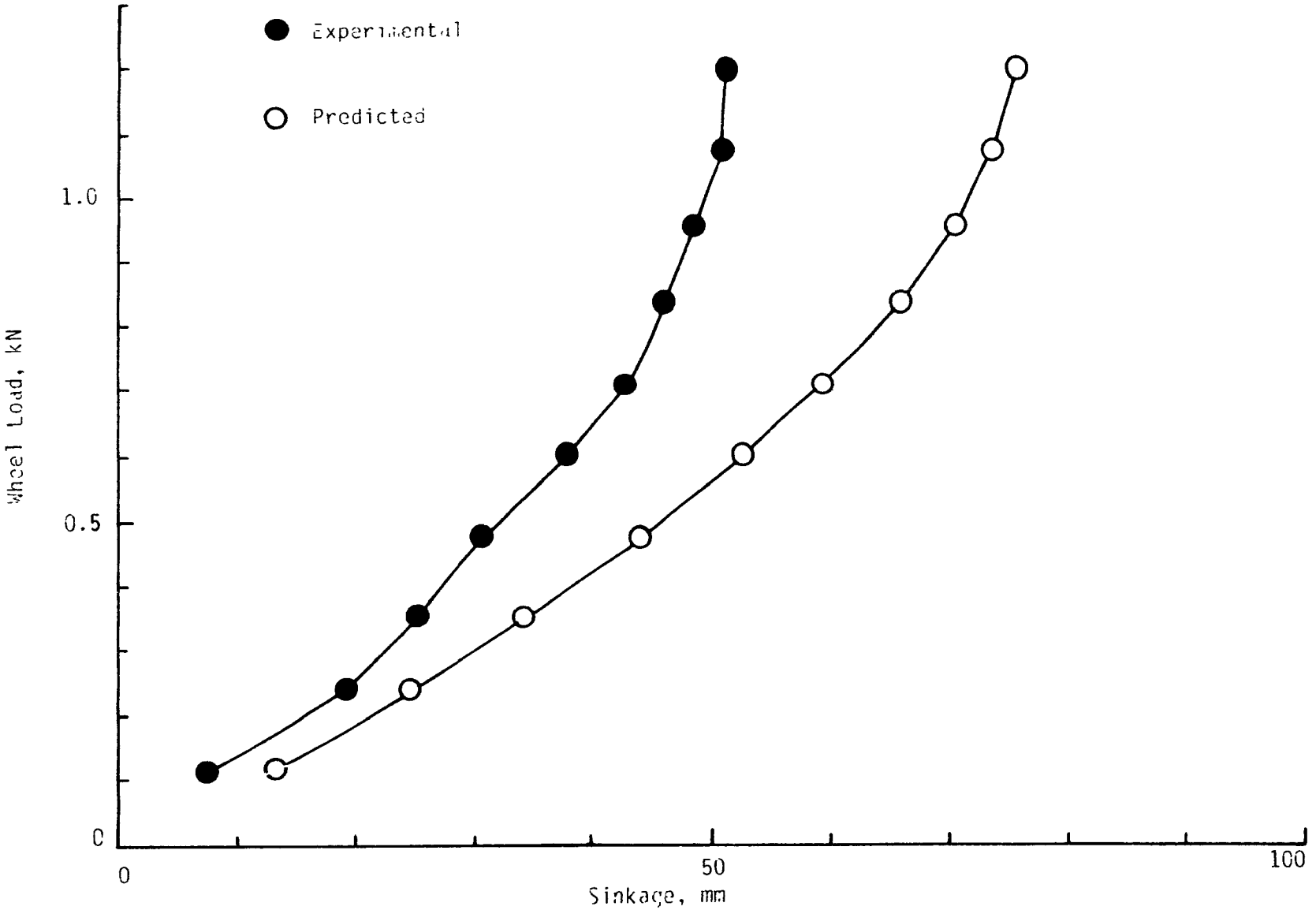


Fig. 5.13b Comparison Between Experimental and Predicted Values of Sinkage for a Rigid Wheel on a Snowpack Aged for 4 Days

Fig 5.11a

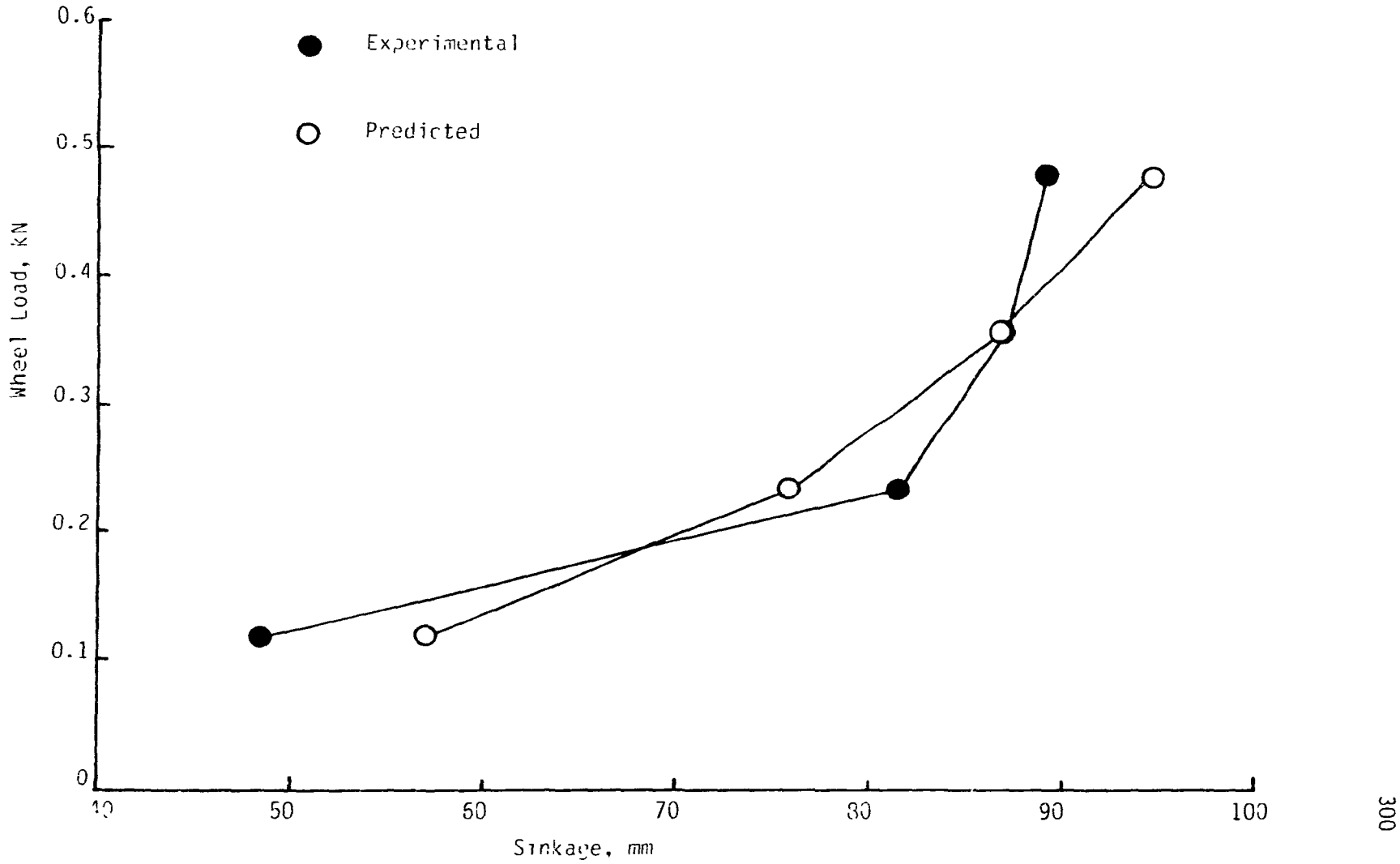


Fig. 5.14a Comparison Between Experimental and Predicted Values of Half Contact Length for a Rigid Wheel on a Snowpack Aged for 2 Days

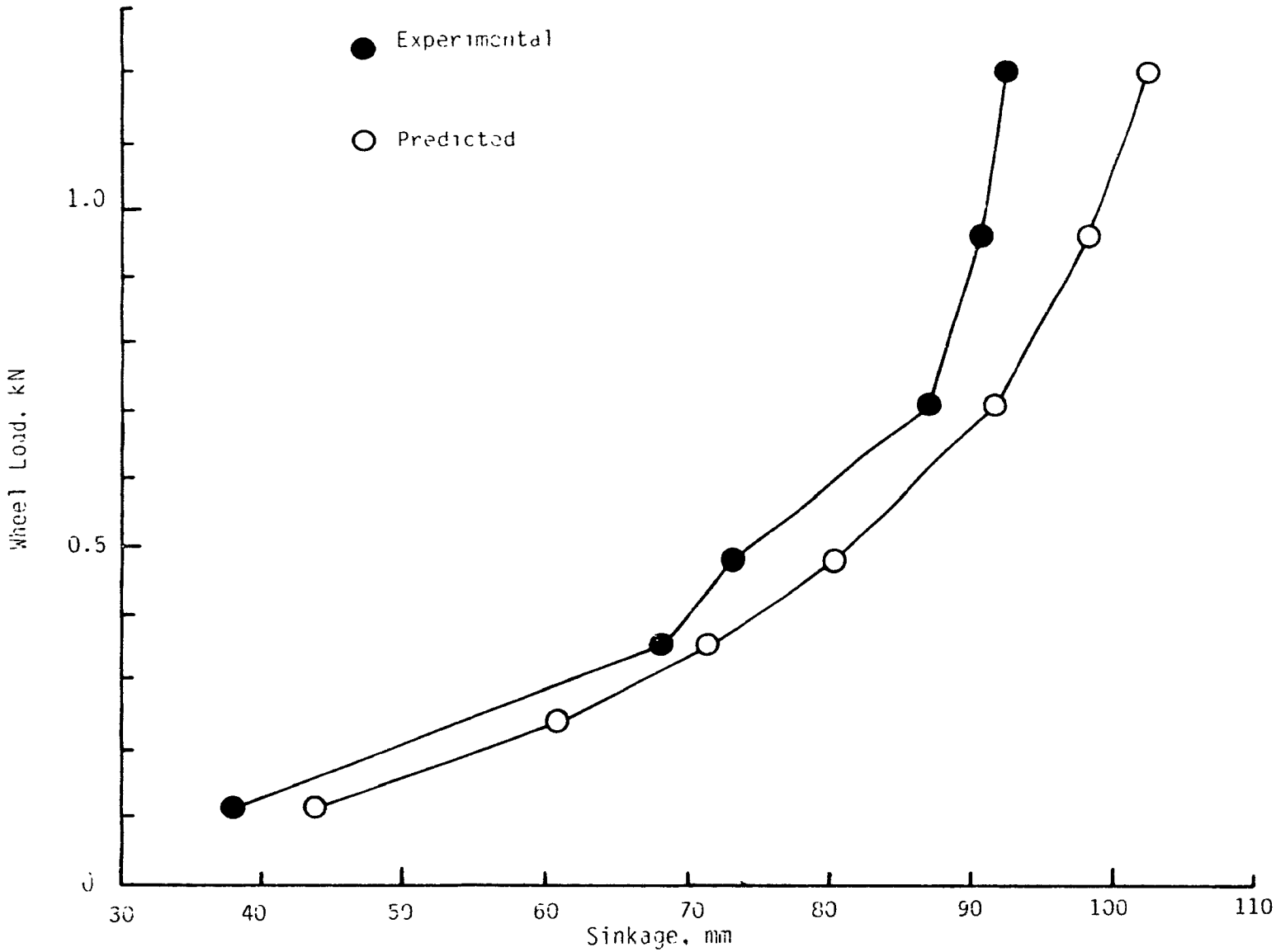


Fig. 5.14b Comparison Between Experimental and Predicted Values of Half Contact Length for a Rigid Wheel on a Snowpack Aged for 4 Days

extremely difficult because of the ductile-brittle transformation with respect to the rate effect and because of the viscous behaviour in ductile performance.

Considerable errors in predicting sinkage, observed in Fig. 5.10a and 5.10b, may have been partly attributed to the lack of consideration of the complicated mechanical behaviour of snow, as discussed above. Therefore, it is necessary to establish more rational constitutive equations of snow, a highly compressible material with sensitivity to deformation rate and temperature, for solving problems in snow mechanics.

5.4 Comments on the Formulation and Results of Numerical Analysis

The computer program of the finite element method, developed in the Geotechnical Research Center at McGill University, was modified and combined with the results obtained from the complex variable method in order to develop the present iterative method. The elements used for the nonlinar finite element analysis are the constant strain triangular elements.

In most of the numerical results the number of iterations required to obtain the contact lengths with reasonable accuracy are about two to four times, although numerical solutions would be oscillatory.

The following comments on the assumptions made for the two example problems can be stated:

(1) For the tire-clay interactions, a tire was assumed to be an

elastic solid. Such an assumption would have produced the unacceptable (pattern) of pressure distribution due to the erroneous contact profile. However, the contact length can be well approximated so long as the proper constitutive relationship for the supporting ground is available. This is because the contact length, which can be obtained analytically and numerically, depends on the total load (or force equilibrium equation) rather than pressure distribution, while the approximation of the pressure distribution depends entirely on the contact profile.

(2) The tire was assumed to be rigid for snowpack. But, from a practical point of view, no pneumatic tire can be assumed to be rigid no matter how soft the supporting ground is relative to the deformability of the tire. This is rather obvious considering that at an equilibrium position the tire would deform making the contact profile be rather flat, at least, around the center of the contact surface above a certain load.

This second analytical approach, which was initially established for a contact problem between a linear and a nonlinear elastic solid [146], should be modified, when solving an interaction problem involving a pneumatic body, to obtain the correct pattern of pressure distribution. In order to obtain such a modification, the contact profile should be taken into account directly, avoiding the complex properties of the tire, as was considered in Chapter 4.

CHAPTER 6

SUMMARY, CONCLUDING REMARKS AND RECOMMENDATIONS FOR FUTURE WORK

6.1 Summary

We have chiefly studied the numerous tire-supporting ground (i.e. rigid base, clay and sand) interaction problems, experimentally and analytically. The experiments on the tire-supporting ground interaction problems, where a tire was subjected to a vertical loading, were conducted under various inflation pressures, loading and tread conditions (i.e. treaded or buffed) by employing the four full-scale truck tires. The experimental results such as axle displacement, contact area and contact pressure were analyzed to characterize the interaction problems. The experimental results were also used to validate the first analytical approach developed in Chapter 4. Two different analytical approaches were proposed in Chapters 4 and 5 under the plane strain condition for solving the present interaction problems involving a tire as a contacting pneumatic body. The present dissertation, however, put greater emphasis on the first analytical approach developed in Chapter 4, rather than that given in Chapter 5.

In Chapter 2, we reviewed several analytical and numerical methods for contact problems, and the contact mechanism for a tire on a rigid base was also discussed. The main purpose of the work in this

chapter was to select an analytical and/or a numerical method as fundamental tools for establishing the two analytical approaches. Some well-known analytical and numerical methods for contact problems were reviewed in order to find out their applicability to the contact problems by studying the basic mathematical tools used in the methods. Those studies showed that some analytical methods are essentially equivalent to others; the method governing a contact problem by a singular integral equation is transfored to another method, based on the complex variable method, which governs a contact problem by a Riemann-Hilbert problem (section (II) in Appendix B). Besides, the discussions of contact mechanism of a tire on a rigid base also suggests how complex a contact problem would become when it involves a physically and geometrically complicated pneumatic body like a tire, and what kind of studies would be required in order to solve the present interaction problems. Consequently, we selected the complex variable method and finite element method as fundamental analytical and numerical tools for developing the two analytical approaches presented in Chapters 4 and 5.

Chapter 3 presented the procedure for the experiments on each interact and the discussions on characterizing the pneumatic tire-supporting ground (i.e. rigid base, clay and sand) interactions by means of the results, such as axle displacement, contact area and contact pressure distribution. The experiments were conducted under "nearly" plane strain conditions so that the results were also used to verify the two-dimensional analytical approach developed in Chapter 4.

In doing so, however, the real contact surface was defined by a representative rectangular contact surface, hence defining a representative contact length and width. The real contact pressure distribution on the real contact surface was also defined by one on the representative surface. Such quantities defined can be used to measure the accuracy of the first two-dimensional analytical approach in Chapter 4. Those quantities on a representative surface are hereafter called the experimental-based results (or quantities).

In Chapter 4, the first analytical approach was developed on the basis of the complex variable method selected in Chapter 2, by considering the contact profile, under an assumption that the supporting ground is elastic. The concept of this approach is to transform a real interaction problem to an equivalent free boundary (-value) problem, which takes into account the contact profile, in order to avoid the physical and geometrical complexities of a tire coming into a contact analysis directly. Then such a free boundary problem is solved for contact pressure and contact length by virtue of the complex variable method, after obtaining the corresponding elastic modulus of either the deformed supporting clay or the rigid base. The various buffed tire-supporting ground (i.e. rigid base or clay) interaction problems were solved, and compared with the experimental-based results which were derived from the real experimental results on the basis of the representative surface defined in Chapter 3. The comparisons between the analytical and experimental-based results showed quite good agreement despite several severe assumptions imposed

on the analytical approach. Besides a question was raised on some analytical methods, including the complex variable method applied to a contact problem between two elastic solids, which was reviewed in Chapter 2 (or Appendices A and B), although this is not a major subject in this dissertation.

The second analytical approach, established in Chapter 5, is an iterative method which combines two methods - the complex variable method and the incremental finite element method. The idea of load increments makes it possible to apply the complex variable method to an iterative scheme solving an interaction problem, which involves a supporting ground being finitely deformable. The supporting grounds considered in this chapter were clay and snowpack.

6.2 Concluding Remarks

A. Experimental Results (Chapter 3)

In the experiments, four different full-scale truck treaded tires were employed and each of them was accompanied by a buffed form. Each tire (i.e. treaded and buffed) was loaded slowly and vertically onto a supporting ground (i.e. rigid base, kaolinite clay or silica sand) under nearly plane strain conditions, while the inflation pressure and axle load varied for each experiment along with the tread condition (i.e. treaded or buffed).

Overall experimental results obtained by means of the three different supporting grounds were shown to be remarkably similar, with a few exceptions, regardless of the types of tires, the tread

condition, inflation pressure and load. They can be summarized as follows:

(1) Load-Axle Displacement relationships were quite linear,

(2) Load-Contact Area relationships were linear on a rigid base, while they tended to be nonlinear,

(3) Pressure distribution along the longitudinal direction (or the transverse direction) was mostly saddle-shaped,

(4) Pressure intensity around the center of the contact surface ceased to increase above a certain loading intensity,

(5) High pressure beneath the sidewalls was observed, suggesting that they carried the majority of the applied load.

Several facts, mainly regarding the load-carrying capability, can also be deduced from the relationships between the average contact pressure (i.e. load/contact area) and the inflation pressure together with the remarks in (3), (4) and (5) stated above. They can be simply summarized in the following, depending on the supporting ground, i.e. rigid base, clay and sand.

Tire On Rigid Base

The average contact pressure remained almost constant for each inflation pressure used, regardless of the intensity of the loading and the tread condition (i.e. treaded or buffed). The average contact pressures were higher than the inflation pressure used in each experiment when the latter pressure was low; however, this relationship tended to reverse as the inflation pressure increased. Hence the load-carrying capability is clearly attributed to the

carcass stiffness at the lower inflation pressures. At the higher inflation pressures, one could expect a pneumatic tire to behave more like an elastic solid. However, while raising the inflation pressure increases the carcass stiffness due to the tension increase in the carcass membrane, it also causes the non-negligible change in shape (cross-section) of sidewalls by increasing their curvatures. Such a change in shape of sidewalls would decrease the contribution of carcass in carrying the load since the highly curved sidewalls due to higher inflation pressure would not sustain the higher loading in proportion to the higher loading at lower inflation pressures. This would have been a major reason that, at higher inflation pressure, the average contact pressure became lower than the inflation pressure.

The remark given in (4) above can be explained as follows. As the deformation of the sidewalls due to the larger loading would start to create the non-negligible transverse shear deformation in the carcass (a portion of the crown) in contact so that the contact pressure around the center of the contact surface ceases to increase even if the load increases.

Tire on Clay and Sand

In clay the average contact pressure remained almost always lower than the inflation pressure, unlike the previous case for the tires on the rigid base, regardless of the type of tire, the inflation pressure, the load and the tread condition (i.e. treaded or buffed). Such results were obtained because the deformations occurred not only

in the tire but also in the clay. Similar relationships between the average contact pressure and the inflation pressure were also observed for the tires on sand. In the case of the deformable supporting ground like the clay and the sand, the load-carrying capability for the tire would be higher.

B. The First Analytical Approach (Chapter 4)

The analytical approach was established in Chapter 4 on the basis of the complex variable method by taking into account the contact profile.

Particular features of this approach are enumerated as follows:

(1) Complex physical and geometrical properties of a tire are not required directly in the analysis of interaction problems. However, the characteristics of each tire come in as a result of elastic measure E* which is required to evaluate the corresponding elastic modulus,

(2) Contact profiles are approximated by a polynomial function. A careful selection of order of polynomial is necessary to have a correct pattern of contact pressure distribution,

(3) A few experiments on tire-supporting clay (or rigid base) interaction are necessary to be carried out to obtain a relationship between average contact pressures and contact measure (section 4.4.3). From this relationship the elastic measure E* can be evaluated.

Most of the complexities in solving interaction problems involving a pneumatic tire, come from the structure of the tire. The

analytical approach, however, solves such interaction problems by avoiding all these complexities since the original interaction problem is first transformed into an equivalent free boundary problem. As shown in section 4.6, the comparisons between the analytical and experimental results for the various interaction problems show good agreement, demonstrating the acceptability of the present analytical approach.

C. The Second Analytical Approach (Chapter 5)

The second analytical approach is an iterative method developed by combining the complex variable method with the incremental finite element method. This approach is applicable to interaction problems involving tires which are assumed to be either elastic cylinders or rigid wheels. Solutions obtained by the approach are influenced by the following factors:

(1) an approach which simulates an axle displacement of the tire due to load increment,

(2) elastic modulus of each tire continuum, which depends on contact width, contact length and load. These values are obtained by experiments on a real tire-rigid base interaction,

(3) convergence of computed contact lengths,

(4) constitutive relationships of elastic half-planes, i.e. supporting clay and snowpacks.

For both interaction problems of tire-supporting clay and rigid wheel-supporting snowpack, we have obtained reasonably accurate

contact lengths. Errors in sinkage obtained numerically and experimentally for rigid wheel-supporting snowpack interactions are unacceptably large, partly due to the use of simple constitutive relationships for snow.

6.3 Contributions

6.3.1 Experiments

(1) The characteristics of the interactions, which depend on load, inflation pressure, tread (pattern), construction of tire, supporting ground (rigid base, clay and snad), are described in terms of the experimental results such as: (i) Load-Axle Displacement relationship, (ii) Load-Contact Area relationship, (iii) Shape of Contact Surface, (iv) Average Contact Pressure-Inflation Pressure relationship, (v) Contact Pressure Distribution, etc.

(2) The discussion of a hypothetical description on the progress of tire deformation due to the contact with the rigid base helps in understanding the fundamental mechanics of the tire-supporting ground interaction; the discussion is an outcome based on the experimental results such as pattern of pressure distribution, change of pressure intensity around the center of contact surface with the increase of loading and the average contact pressure-inflation pressure relationship on a rigid base under the consideration of the unstable motion of the tire carcass.

(3) An implication of saddle-shaped pressure distribution obtained in the experiments shows that it is important that one treat a

pneumatic tire as a pneumatic body in practice; realizing this fact, which is related to the contact profile, is crucial in establishing a rational theory on the tire-supporting ground interaction when a pattern of pressure distribution is concerned in particular.

6.3.2 Theories

First Analytical Approach

(1) Transformation of tire-supporting ground into an equivalent free boundary (-value) problem of the deformed supporting ground makes the original problem more tractable since the complex physical and geometrical factors of the tire do not directly come into the analytical formulation.

(2) Elasticity of the deformed supporting ground due to a contact with other medium (e.g. tire, solid, plate, etc.) is defined by taking into account both the deformed surface profile (i.e. contact profile) via the force equilibrium equation and the average contact pressure-contact measure relationship in the experiments; hence the influences on the physical and the geometrical factors of the other medium, including a pneumatic body like a tire, implicitly come into the analytical approach.

(3) Introduction of the elastic measure, which can be approximately obtained from the average contact pressure - inflation pressure relationship, makes simplification possible in obtaining the elasticity of the deformed supporting ground.

(4) Consideration of the contact profile in the analysis made

possible in obtaining the pattern of pressure distributions (i.e. saddle-shaped) which is agreeable with those obtained in the experiments.

Second Analytical Approach

(1) A simple iterative technique, which combines the incremental finite element method and the complex variable method, was established for solving a nonlinear contact problem between a linearly elastic solid and a nonlinearly elastic solid, not necessarily a half-plane.

(2) Computational efforts are greatly reduced due to the employment of an analytical technique, the complex variable method, which contribute in simplifying the computer algorithm and reducing the number of numerical iterations required for a higher accuracy.

(3) Acceptable contact lengths for the tire-clay interactions were obtained under an assumption that a pneumatic tire is nearly incompressible elastic solid; it is possible to obtain an acceptable contact length from a theoretical point of view while the pressure distribution pattern would not necessarily be acceptable to an interaction problem, especially that involving a pneumatic body.

6.3.3 Findings During the Development of the Analytical Approaches

(1) In the formulation of this approach, the real contact profile is taken into account; it is shown, however, that the existing contact theories (e.g., Hertz, Muskhelishvili, etc.), which are widely applied in solving a contact problem between two linearly elastic solids, essentially neglect the contact profile; instead

a function, expressing the distance between the profiles of the two undeformed solids, only comes into such contact theories, thus ignoring the real kinematics of a contact profile where the pattern of contact pressure greatly depends on.

(2) Most of the (singular) integral equations, governing contact problems, can be transformed into the Riemann-Hilbert problems by means of Plemelj formulae, and vice versa.

(3) The definition of contact stresses (i.e., pressure and shear) derived by a sectionally holomorphic function (i.e. standard defining function) can be considered as a general function known as a hyperfunction (i.e. Sato distribution).

(4) Contact stresses, induced at a surface of discontinuity, can be viewed equivalently to vortex and line source in the fluid mechanics from the point of view of the theory of hyperfunctions (refer to the end of Method 7 in Appendix B).

(5) Theorems used for the contact theory established by Muskhelishvili (Appendix A) can be relaxed by means of the hyperfunction.

6.4 Recommendations For Future Work

A. The First Analytical Approach

(1) Since the contact profile takes an important role in this first approach, a rational method of selecting the order of polynomial, which approximates a contact profile, should be further studied.

(2) When a higher order of polynomial function is selected for a contact profile, extremely complicated and lengthy algebraic

works are required in evaluating the integration (e.g. Eq. A.132). In order to overcome this difficulty, a systematic numerical approach can be developed for evaluating integrations.

(3) Since contact pressure near the center of the contact surface does not increase (rather decreases) above a certain axle loading, one can study the correlation between the contact pressure at the center, inflation pressure and axle load. This would also help in choosing the type of contact profile influencing contact pressure distribution.

B. The Second Analytical Approach

(1) Since axle displacements influence the approximated contact lengths, we may use those obtained in the experiments for higher accuracy.

(2) In order that this second approach be applicable to a real pneumatic tire, the first analytical approach, which takes into account the contact profile, will be considered for improving the second approach.

REFERENCES

1. Adams, R.A., "Sobolev Spaces", Academic Press, 1975.

2. Adkins, J.E., Green, A.E. and Shield, P.T.. "Finite Plane Strain", Phil. Trans. Roy. Soc. (London), A231, 181-213, 1953.

3. Agmon, S., "Lecture on Elliptic Boundary-Value Problems", D. Van Nostrand, 1965.

4. Ahmadi, N., Keer, L.M. and Mura, T., "Non-Hertzian Contact Stress Analysis for an Elastic Half Space - Normal and Sliding Contact", Int. J. Solids Structures, Vol. 19, No. 4, 357-373, 1983.

5. Anderson, T., "The Boundary Element Method Applied to Two-Dimensional Contact Problems with Friction", in Boundary Element Methods, ed. by Brebbia, C.A., Springer-Verlag. 239-258, 1981.

6. Anderson, T., Fredricksson, B. and Persson, B.G.A., "The Boundary Element Method Applied to Two-Dimensional Contact Problems", New Developments in Boundary Element Methods, ed. by Brebbia, C.A., CML Plublications, Southampton/U.K., 247-263, 1980.

7. Atluri, S.N., "On the Hybrid Stress Finite Element Model for Incremental Analysis of Large Deflection Problem", Int. J. Sol. Struct., Vol. 9, No. 10, 1177-1191, 1973.

8. Atluri, S.N. and Murakawa, H., "New General and Complementary Theorems, Finite Strain, Rate Sensitive Inelasticity and Finite Elements: Some Computational Studies", in Nonlinear Finite Element Analysis in Structural Mechanics, Proc. of Europe - U.S. Workshop, Ruhr Univ., Bochum, Germany, July 28-31, (ed. by Wunderlich, Stein, Bathe), 1980.

9. Aubin, J.-P., "Approximation of Elliptic Boundary - Value Problems", John Wiley and Sons, 1972.

10. Aubin, J.-P., "Applied Functional Analysis", John Wiley and Sons, 1979.

11. Ball, J.M., "Convexity Conditions and Existence Theorems in Nonlinear Elasticity", Arch. Ratl. Mech. Anal., 63, 337-403, 1977.

12. Batchelor, G.K., "Introduction to Fluid Dynamics", Cambridge Univ. Press, 1967.

13. Boonsinsuk, P., "Analysis and Prediction of Tyre-Soil Interaction and Mobility Performance", Ph.D. Thesis, McGill University, 1978.

14. Brebbia, C.A., "The Boundary Element Method for Engineers", Pretech Press, London, 1978.

15. Carroll, R.W., "Abstract Methods in Partial Differential Equations", Harper and Row Pub., 1969.

16. Chan, A.K. and Tuba, I.S., "A Finite Element Method for Contact Problems - Part I. Theory and Applications", Int. J. Mech. Sci., Vol. 13, 615-625, 1971.

17. Chand, R., Haug, E.J. and Rim, K., "Analysis of Unbonded Contact Problems by Means of Quadratic Programming", J. Optimization Theory and Applications, 20, 171-189, 1976.

18. Cirlet, P.G., "The Finite Element Method for Elliptic Problems", North-Holland, 1978.

19. Corney, T.F. and Seireg, A., "A Mathematical Programming Method for Design of Elastic Bodies in Contact", J. Appl. Mech., 387-392, June, 1971.

20. Cruse, T.A. and Rizzo, F.J. "Boundary Integral Equation Method: Computational Applied Mechanis", AMD-Vol. 11, ASME, New York, 1975.

21. Dacorogna, B., "Weak Continuity and Weak Lower Semicontinuity of Nonlinear Functionals", Lecture Note in Mathematics, Vol. 932, Springer-Verlag, Berlin, 1982.

22. Dundurs, J., "Properties of Elastic Bodies in Contact", de Pater, A.D. and Kalker, J.J. (Eds), The Mechanics of the Contact Between Deformable Bodies, Delft University Press, 54-66, 1975.

23. Dundurs, J. and Stippes, M., "Role of Elastic Contacts in Certain Contact Problems", J. Appl. Mech., 37, 965-970, 1970.

24. Duvaut, G. and Lions, J.L., "Inequalities in Mechanics and Physics", Springer-Verlag, Berlin/New York, 1976.

25. Endo, T., Oden, J.T., Becker, E.B. and Miller, T., "A Numerical Analysis of Contact and Limit-Point Behavior in a Class of Problems of Finite Elastic Deformation", Computers and Structures, Vol. 18, No. 5, 899-910, 1984.

26. Fattah, E.A., "Prediction of Moving Rigid Wheel Performance and Associated Subsoil Response Behavior", Ph.D. Thesis, McGill University, 1976.

27. Feng, W.W., "Identation of a Plane Membrane with a Rigid Paraboloid", Proc. of Int. Conf. on Computational Mechanics (ed. by Yagawa, G. & Atluri, S.N.), May 1986, Tokyo; Springer-Verlag.

28. Feng, W.W. and Huang, P., "On the General Contact Problem of an Inflated Nonlinear Plane Membrane", Int. J. Solids Structures, Vol. 11, 437-448, 1974.

29. Feng, W.W. and Huag, P., "On the Inflation of a Plane Nonlinear Membrane", J. Appl. Mech., 41, Trans. ASME, 96, Series E., 767-771, 1974.

30. Feng, W.W. and Yang, W.H., "On the Contact Problem of an Inflated Spherical Nonlinear Membrane", J. Appl. Mech., 40, Trans. ASME, 95, Series E, 209-214, 1973.

31. Fichera, G., "Existence Theorems In Elasticity", Handbuch der Physik, IV/2, Springer-Verlag, Berlin, 1972.

32. Friedman, A., "Variational Principles and Free Boundary-Value Problems", John Wiley and Sons, 1982.

33. Fukue, M., "Mechanical Performance of Snow Under Loading", Tokai Univ. Press., 1979.

34. Fung, Y.C., "Foundations of Solid Mechanics", Prentice-Hall, Englewood Cliffs, 1965.

35. Gaertner, R., "Investigation of Plane Elastic Contact Allowing for Friction", Comp. Struct., 7, 59-63, 1977.

36. Galin, L.A., "Contact Problems in the Theory of Elasticity", Moscow (1953), English translation, Sneddon, I.N. (Ed.), North Carolina State College, 1961.

37. Gallagher, R.H., "Finite Element Analysis: Fundamentals", Prentice-Hall, 1975.

38. Gladwell, G.M.L., "The Calculation of Mechanical Impedances Relating to an Indenter Vibrating on the Surface of a Semi-Infinite Elastic Body", J. Sound and Vibration, Vol. 8, 215-228, 1968.

39. Gladwell, G.M.L., "A Contact Problem for a Circular Cylindrical Punch in Adhesive Contact With an Elastic Half-Space: The Case of Rocking, and Translation Parallel to the Plane", Int. J. Eng. Sci., Vol. 7, 295-307, 1969.

40. Gladwell, G.M.L., "On Some Unbonded Contact Problems in Plane Elasticity Theory", J. Appl. Mech., Vol. 43, 263-267, 1976.

41. Gladwell, G.M.L., "Contact Problems in the Classical Theory of Elasticity", Sijthoff and Noordhoff International Pub., The Netherlands, 1980.

42. Goodman, L.E., "Contact Stress Analysis of Normally Loaded Rough Spheres", J. Appl. Mech., 515-522, Sept. 1962.

43. Green, A.E. and Adkins, J.E., "Large Elastic Deformations and Nonlinear Continuum Mechanics", Oxford Univ. Press, 1960.

44. Green, A.E. and Shield, R.T., "Finite Elastic Deformation of Incompressible Isotropic Bodies", Proc. Roy. Soc. (London), A202, 407-419, 1950.

45. Green, A.E. and Zerna, W., "Theoretical Elasticity", Clarendon, Oxford, 1954.

46. Gurtin, M. E., "The Linear Theory of Elasticity", Handbuch der Phisik (S. Flugge, Chief Editor), Vol. VIa/2, Springer-Verlag, Berlin, pp. 1-273, 1972.

47. Hanyga, A., "Mathematical Theory of Nonlinear Elasticity", Ellis Horwood Ltd. Pub., 1985.

48. Harding, J.W. and Sneddon, I.N., "The Elastic Stresses Produced by the Indentation of the Plane Surface of a Semi-Infinite Elastic Solid by a Rigid Punch", Cambridge Philosophical Society, Proceedings, Vol. 41, 16-26, 1945.

49. Hiroma, T., Ohta, Y. and Suyama, K., "Analysis of the Soil Deformation Beneath a Wheel by the Finite Element Method (II) - Elastic Soil Deformation Beneath an Elastic Wheel", (in Japanese), Trans. J.A.M.E., 47(2), 201-209, 1985.

50. Hlavacek, I. and Necas, J., "On Inequalities of Korn's Type", Arch. Ratl. Mech. Anal., 36, 304-334, 1970.

51. Hormander, L., "Linear Partial Differential Operators", Springer-Verlag, Berlin/New York, 1969.

52. Horrigmoe, G. and Bergan, P.G., "Incremental Variational Principles and Finite Element for Nonlinear Problems", Comp. Meth. Appl. Mech. and Struct., 7, 201-217, 1976.

53. Imai, I., "Theory of Applied Hyperfunctions (Sato Distributions)", (in Japanese), Vols. 1,2, Saiensu-sha, 1980.

54. John, O., "On Signorini Problems for von Karman Equations", Aplikace Mat., 22, 52-68, 1977.

55. Johnson, K.L., "Non-Hertzian Contact of Elastic Spheres", The Mechanics of the Contact Between Deformable Bodies, Proc. of the Symposium of the International Union of Theoretical and Applied Mechanics (ed. by de Pater, A.D. and Kalker, J.J.), Delft Univ. Press, 1975.

56. Johnson, K.L., "Contact Mechanics", Cambridge Univ. Press, 1985.

57. Kabe, K. and Akasaka, T., "Deformation and Cord Tension of a Radial Tire in Contact with the Road", The General Problem of Rolling Contact (ed. by Browne, A.L. and Tsai, N.T.), AMD-Vol. 40, The American Society of Mechanical Engineers, 1980.

58. Kalker, J.J., "Aspects of Contact Mechanics", de Pater, A.D. and Kalker, J.J. (Eds.), The Mechanics of the Contact Between Deformable Bodies, Delft Univ. Press, 1-25, 1975.

59. Kalker, J.J. and Van Randen, Y., "A Minimum Principle for Frictionless Elastic Contact with Application to Non-Hertzian Contact Problem", J. of Engrg. Math., Vol. 6, No. 2, 1972.

60. Kaneko, A., "Introduction to Hyperfunctions (i.e. Sato Distributions)", (in Japanese), Vols. 1, 2, Tokyo Daigaku Shuppan, 1980.

61. Kashiwara, M., Kawai, T. and Kimura, T., "Foundation of Algebraic Analysis", (in Japanese), Kinokuniya-shoten, Tokyo, 1980.

62. Kato, T., "Topological Analysis - Theory and Applications", (in Japanese), Kyoritsu-shuppan, 1957.

63. Kellog, O.D., "Foundations of Potential Theory", Springer, 1929.

64. Kikuchi, N., "Contact Problems in Elastostatics", Finite Elements: Special Problems in Solid Mechanics, Vol. 5, Ed. by Oden, J.T. and Carey, G.F., Prentice-Hall, 158-210, 1984.

65. Kikuchi, N., "A Class of Rigid Punch Problems Involving Forces and Moments by Reciprocal Variational Inequalities", J. Struct. Mech., 7(3), 273-295, 1979.

66. Kikuchi, N., "Beam Contact Problems Using Variational Inequalities", (in Japanese), Trans. of JSCE, NO. 294, Feb. 1980.

67. Knowles, J.K. and Sternberg, E., "On a Class of Conservation Laws in Linearlized and Finite Elastostatics", Arch. Ratl. Mech. Anal., 44, 1972.

68. Kufner, J., John, O. and Fucik, S., "Function Spaces", Noordhoff International Pub., Leyden, 1977.

69. Kuroda, N., "Functional Analysis", (in Japanese), Kyoritsu-shuppan, Tokyo, 1980.

70. Le Tallec, P., "Existence and Characterization of Hydrostatic Pressure in Finite Deformations of Incompressible Bodies", J. Elasticity, 11, 341-358, 1981.

71. Lee, B.C. and Kwak, B.M., "A Computational Method for Elastic-Plastic Contact Problems", Computers and Structures, Vol. 18, No. 5, 757-765, 1984.

72. Lighthill, M.J., "Introduction to Fourier Analysis and Generalized Functions", Cambridge Univ. Press. 1949.

73. Lions, J.L., "On Free Surface Problems", in Computational Mechanics, Lecture Notes in Mathematics, No. 461, ed. by Oden, J.T., Springer-Verlag, Berlin, 129-148, 1975.

74. Lions, J.L. and Magenes, E., "Non-Homogeneous Boundary-Value Problems and Applications", Vols. 1,2,3, Springer-Verlag, New York, 1969.

75. Love, A.E.H., "A Treatise on the Mathematical Theory of Elasticity", 4th Edition, Dover Pub., New York, 1944.

76. Lubkin, J.L., "Contact Problems", Handbook of Engineering Mechanics, ed. by Flugge, W., McGraw-Hill, New York, 1962.

77. Lur'e, A.I., "Three Dimensional Problems of the Theory of Elasticity", Moscow (1955), Translated from the original Russian by McVean, D.B., and Edited by Radok, J.R.M., Interscience Pub., New York, 1964.

78. Malvern, L.E., "Introduction to the Mechanics of a Continuous Medium", Prentice-Hall, Englewood Cliffs, 1969.

79. Marcal, P.V., "Large Strains, Large Displacement Analysis", Lectures of Finite Element Methods in Continuum Mechanics (ed. by Oden, J.T., de Arantes, E.R. and Olivria), 535-543, The Univ. of Alabama in Huntsville Press, 1973.

80. Marsden, J.E. and Hughes, T.J.R., "Mathematical Foundation of Elasticity", Prentice-Hall, Englewood Cliffs, 1983.

81. McMeeking, R.M. and Rice, J.R., "Finite Element Formulations for Problems of Large Elasto-Plastic Deformation", Int. J. Solids Struct., 11, 601-616, 1975.

82. Metaxas, I.J., "Snow Mechanics: Mechanical Properties Energy Analysis", A Masters Thesis, McGill Univ., 1984.

83. Mindlin, R.D., "Compliance of Elastic Bodies in Contact", J. Appl. Mech., 16, 256-268, 1949.

84. Mizohata, S., "Theory of Partial Differential Equations", (in Japanese), Iwanami-shoten, 1965.

85. Morimoto, M., "Introduction to Sato Distributions (i.e. Hyperfunctions", (in Japanese), Kyoritsu-shuppan, 1976.

86. Muskhelishvili, N.I., "Some Basic Problems of the Mathematical Theory of Elasticity", 3rd Edition, Moscow (1949), English translation, Radok, J.R.M. (Ed.), Noordhoff, Groningen, 1963.

87. Muskhelishvili, N.I., "Singular Integral Equations", 2nd Edition, Moscow (1946), English translation, Radok, J.R.M. (Ed.), Noordhoff, Groningen, 1958.

88. Naumann, J., "On Some Unilateral Boundary Value Problems in Nonlinear Plate Theory", Beitrage zur Analysis, 10, 119-134, 1977.

89. Oden, J.T., "Finite Elements of Nonlinear Continua", McGraw-Hill, New York, 1972.

90. Oden, J.T., "Applied Functional Analysis", Prentice-Hall, Englewood Cliffs, 1979.

91. Oden, J.T., "Analysis of a Class of Problems with Friction by Finite Element Methods", The Mathematics of Finite Elements and Applications IV (ed. by Whiteman, J.R.), Academic Press, 1982.

92. Oden, J.T., "Qualitative Methods in Nonlinear Mechanics", Prentice-Hall, Englewood Cliffs, 1986.

93. Oden, J.T., "Existence Theorems for a Class of Problems in Nonlinear Elasticity", J. Math. Anal. Appl., 69, 51-83, 1979.

94. Oden, J.T., "Mixed Finite Element Approximation via Interior and Exterior Penalties for Contact Problems in Elasticity", Hybrid and Mixed Finite Element Methods, ed. by Atluri, S.N., Gallagher, R.H. and Zienkiewicz, O.C., John Wiley and Sons, 1983.

95. Oden, J.T. and Kikuchi, N., "Finite Element Methods for Certain Free Boundary-Value Problems in Mechanics", Moving Boundary Problems (ed. by Wilson, D.G., Solomon, A.D. and Boggs, P.T.), Academic Press, New York, 1977.

96. Oden, J.T. and Kikuchi, N., "Finite Element Methods for Constrained Problems in Elasticity", Int. J. Num. Meth. Engrg., Vol. 18, 701-725, 1982.

97. Oden, J.T., Kikuchi, N. and Song, Y.J., "Reduced Integration and Exterior Penalty Methods for Finite Element Approximations of Contact Problems in Incompressible Elasticity", TICOM Report 80-2, The Univ. of Texas at Austin, 1980.

98. Oden, J.T., and Kubitza, W.K., "Numerical Analysis of Nonlinear Pneumatic Structures", Proc. Int. Colloq. Pneumatic Structures. 82-107, Stuttgart, 1967.

99. Oden, J.T. and Pires, E.B., "Nonlocal and Nonlinear Friction Laws and Variational Principles for Contact Problems in Elasticity", J. Appl. Mech., Vol. 50, 67-76, 1983.

100. Oden, J.T. and Pires, E.B., "Numerical Analysis of Certain Contact Problems in Elasticity with Non-Classical Friction Laws", Comp. and Struct., Vol. 16, No. 1-4, 481-485, 1983.

101. Oden, J.T. and Reddy, J.N., "An Introduction to the Mathematical Theory of Finite Elements", Wiley-Interscience, New York, 1976.

102. Oden, J.T. and Reddy, J.N., "Variational Methods in Theoretical Mechanics", 2nd Edition, Berlin/New York, 1983.

103. Ohtake, K., Oden, J.T. and Kikuchi, N., "Analysis of Certain Unilateral Problems in von Karman Plate Theory by a Penalty Method - Part 1. A Variational Principle with Penalty", Comp. Meth. Appl. Mech. Engrg., 24, 187-213, 1980.

104. Ohte, S., "Analysis of Elastic Contact Stress by Using Finite Element Method", (in Japanese), Trans. of JSME, 38, 2210-2216, 1972.

105. Okamoto, N. and Nakazawa, M., "Finite Element Incremental Contact Analysis with Various Frictional Conditions", I.J. Num. Meth. Engrg., Vol. 14, 337-357, 1979.

106. Olson, M.D., "The Mixed Finite Element Method in Elasticity and Elastic Contact Problems", Hybrid and Mixed Finite Element Methods, ed. by Atluri, S.N., Gallagher, R.H. and Zienkiewicz, O.C., John Wiley and Sons, 1983.

107. Padovan, J., Tovichakchaikul, S, and Zeid, I., "Finite Element Analysis of Steadily Moving Contact Fields", Comp. and Struct., Vol. 18, No. 2, 191-200, 1984.

108. Panagiotopoulos, P.D., "A Nonlinear Approach to the Unilateral Contact -, and Friction-Boundary Value Problem in the Theory of Elasticity", Ing.-Arch., 44, 421-432, 1975.

109. Panagiotopoloulos, P.D., "Inequality Problems in Mechanics and Applications - Convex and Nonconvex Energy Functions", Birkhauser, Boston, 1985.

110. Pian, T.H.H., "Finite Element Methods by Variational Methods with Relaxed Continuity Requirement", Int. Conf. on Variational Methods in Engineering, ed. by Brebbia, C.A., Southampton Univ.

Press, 1973.

111. Pian, T H.H. and Kubomura, K., "Formulation of Contact Problems by Assumed Stress Hybrid Elements", Nonlinear Finite Element Analysis in Structural Mechanics, Proc. Europe-U.S. Workshop (ed. by Wunderlich, Stein, Bathe), Ruhr University, Bocham, Germany, July 28-31, 1980.

112. Pian, T.H.H. and Tong, P., "Variational Formulations of Finite Displacement Analysis", in High Speed Computing of Elastic Structures (ed. Fraeije de Veubeke), IUTAM Symposium, Univ. of Liege, Liege, August, 1971.

113. Poritsky, H., "Stresses and Deflections of Cylindrical Bodies in Contact with Application to Contact of Gears and of Locomotive Wheels", J. Appl. Mech., Vol. 17, 191-201, 1950.

114. Rabier, P., Martins, J.A.C. and Oden, J.T., "Existence and Local Uniqueness of Solutions to Contact Problems in Elasticity with Nonlinear Friction Laws", Int. J. Engrg. Sci., Vol. 24, No. 11, 1755-1768, 1986.

115. Rice, J.M., McMeeking, R.M. and Parks, D.M., "Recent Finite Element Studies in Plasticity and Fracture Mechanics", Comp. Meth. Appl. Mech. Engrg., 17/18, 411-442, 1979.

116. Rostovtsev, N.A., "An Integral Equation Encountered in the Problem of a Rigid Foundation Bearing on Nonhomogeneous Soil", J. Appl. Math. Mech., Vol. 25, 238-246, 1961.

117. Rudin,, W., "Real and Complex Analysis", McGraw-Hill, New York, 1966.

118. Sanker, T.S. and Fabrikant, V., "Asymmetric Contact Problem Including Wear for Nonhomogeneous Half Space", J. Appl. Mech., Vol. 49, 43-46, 1982.

119. Shibagaki, W., "Functional Analysis and Foundation of Numerical Analysis", (in Japanese), Morikita-shuppan, Tokyo, 1985.

120. Showalter, R.E., "Hilbert Space Methods in Partial Differential Equations", Pitman Press, London, 1977.

121. Sneddon, I.N., "Fourier Transforms", McGraw-Hill, New York, 1951.

122. Sneddon, I.N., "Applications of Integral Transforms in the Theory of Elasticity", Springer-Verlag, Berlin, 1975.

123. Sobolev, S.L., "Applications of Functional Analysis in Mathematical Physics", American Mathematical Society, Providence, R.I., 1963.

124. Spence, D.A., "An Eigenvalue Problem for Elastic Contact with Finite Friction", Proc. Comb. Phil. Soc., 73, 249-268, 1973.

125. Steuermann, E., "To Hertz' Theory of Local Deformations in Compressed Elastic Bodies", C.R. Acad. Sci. URSS, 25, 359-361, 1939.

126. Stoker, J.J., "Nonlinear Elasticity", Gordon and Breach, New York, 1968.

127. Strang, G. and Fix, G.J., "An Analysis of the Finite Element Method", Prentice-Hall, Englewood Cliffs, 1973.

128. Tanabe, H., "Functional Analysis", (in Japanese), Vols. 1,2, Jikkyo-shuppan, Tokyo, 1978.

129. Timoshenko, S.P. and Goddier, J.N., "Theory of Elasticity", 3rd Edition, McGraw-Hill, New York, 1970.

130. Tonti, E., "Variational Formulation for Every Nonlinear Problem", Int. J. Engrg. Sci., Vol. 22, No. 11/12, 1343-1371, 1984.

131. Treves, F., "Basic Linear Partial Differential Equations", Academic Press, 1975.

132. Tricomi, F.G., "Integral Equations", Interscience, 1957.

133. Truesdell, C. and Noll, W., "The Nonlinear Field Theories of Mechanics", Handbuch der Physik, III/3, Springer-Verlag, Berlin, 1965.

134. Tsuta, T. and Yamaji, S., "Finite Element Analysis of Contact Problem", Theory and Practice in Finite Element Structural Analysis, Univ. of Tokyo Press, 177-194, 1973.

135. Tsueng, J. and Olson, M.D., "The Mixed Finite Element Method Applied to Two-Dimensional Elastic Contact Problems", I.J. Num. Meth. Engrg., Vol. 17, 991-1014, 1981.

136. Washizu, K., "Variational Methods in Elasticity and Plasticity", 3rd Edition, Pergamon Press, 1982.

137. Wilson, E.A. and Parsons, B., "Finite Element Analysis of Elastic Contact Problems Using Differential Displacements", Int. J. Num. Meth. Engrg., 2, 387-395, 1970.

138. Yong, R.N., "Analytical Predictive Performance for Physical Performance of Mobility", J. Terramechanics, Vol. 10, 47-60, 1973.

139. Yong, R.N., "Some Further Problems in the Design of Wheels and Tracks", J. Terramechanics, Vol. 13, NO. 2, 63-73, 1976.

140. Yong, R.N., Boonsinsuk, P. and Fattah, E.A., "Tyre Load Capacity and Energy Loss with Respect to Varying Soil Support Stiffness", J. Terramechanics, Vol. 17, No. 2, 131-147, 1980.

141. Yong, R.N., Boonsinsuk, P., Ishikawa, F., and Caporuscio, F., "Characterization of Full-Size Tires on a Rigid Unyielding Surface", Report submitted to Defense Research Establishment Suffield, Geotechnical Research Centre, McGill University, November 1987.

142. Yong, R.N., Boonsinsuk, P., Ishikawa, F., and Caporuscio, F., "Interactions Between Tires and Soils Under Static Loading Conditions", Report submitted to Defense Research Establishment Suffield, Geotechnical Research Centre, McGill University, March 1988.

143. Yong, R.N. and Fattah, E.A., "Influence of Contact Characteristics on Energy Transfer and Wheel Performance on Soft Soil", Proc. 5th Int. Conf. ISTVS, Detroit, Vol. 2, 241-310, 1975.

144. Yong, R.N. and Fattah, E.A., "Prediction of Wheel-Soil Interaction and Performance Using the Finite Element Method", J. Terramechanics, Vol. 13, No. 4, 227-240, 1976.

145. Yong, R.N. and Fukue, M., "Performance of Snow in Confined Compression", J. Terramechanics, 14 (2), 59-82, 1977.

146. Yong, R.N. and Ishikawa, F., "An Engineering Approach to Analysis of Interaction Between Linear and Nonlinear Solids", presented to Proc. of Int. Conf. on Computational Mechanics (ed. by Yagawa, G. and Atluri, S.N.), May 1986, Tokyo.

147. Yong, R.N., Ishikawa, F. and Fukue, M., "Iterative Method for Solution of Interaction Problems Between a Rigid Tire and a Supporting Snowpack", J. of Snow Engineering (Japan), No. 4, Sept. 1987.

148. Yong, R.N. and Japp, R.D., "Stress-Strain Behaviour of Clays in Dynamic Compression", Vibration Effects of Earthquakes on Soils and Foundations, ASTM STP 450, American Society for Testing and Materials, 1968.

149. Yong, R.N. and Metaxas, I., "Influence of Age-Hardening and Strain-Rate on Confined Compression and Shear Behaviour of Snow", J. Terramechanics, Vol. 22, No. 1, 37-49, 1985.

150. Yong, R.N. and Webb, G.L., "Energy Dissipation and Drawbar Pull Prediction in Soil-Wheel Interaction", Proc. 3rd Int. Conf. ISTVS, Essen, Vol. 1, 93-142, 1969.

151. Yong, R.N. and Windisch, E., "Determination of Wheel Contact Stresses from Measured Instantaneous Soil Deformations", J. Terramechanics, Vol. 7, 57-67, 1970.

152. Yosida, K., "Functional Analysis", 6th Edition, Springer-Verlag, Berlin/New York, 1980.

153. Zienkiewicz, O.C., "The Finite Element Method", 3rd Edition, McGraw Hill Book Co., 1977.

APPENDIX A

APPENDIX A

COMPLEX VARIABLE METHOD FOR TWO-DIMENSIONAL CONTACT PROBLEMS

1. Preliminaries: Airy Stress Function

In two-dimensional linear elasticity, the field equation can be defined in an open domain R with a sufficiently smooth boundary as follows:

(1) Translational Equilibrium Equation

$$\text{div } \underset{\sim}{T} = -\rho \underline{F} \tag{A.1}$$

where div $\underset{\sim}{T}$ is the divergence of the Cauchy stress tensor $\underset{\sim}{T}$; $\underline{F}$ the body force per unit mass; ρ denotes the mass density per unit volume. ($(\underset{\sim}{\cdot})$ and $(\underline{\cdot})$ denote quantities of a second order tensor and a vector respectively);

(2) Beltrami-Mitchell Compatibility Equation (in two-dimensional plane strain condition)

$$\text{div grad } \Theta = -\frac{2\rho(\lambda+G)}{\lambda+2G} \text{ div } \underline{F} \tag{A.2}$$

where div grad = Laplace operator, $\Theta = \underset{\sim}{T}:\underset{\sim}{T} = T_{11} + T_{22} = T_{xx} + T_{yy}$, $\lambda = E\nu/(1+\nu)(1-2\nu)$, $G = E/2(1+\nu)$, (E = modulus of elastsicity, ν = Poisson's ratio);

(3) Constitutive Relationship

$$\underset{\sim}{T} = \underset{\approx}{C} : \underset{\sim}{e}$$

$$= (\lambda\, e_{kk}\, \delta_{ij} + 2G e_{ij})\, \underline{e}_i \otimes \underline{e}_j \quad \text{(sum on k and i,j=1,2)} \qquad (A.3)$$

where $\underset{\approx}{C}$ is an elastic (fourth order) tensor, and $\underset{\sim}{e}$ is the engineering strain tensor, i.e., $\underset{\sim}{e} = 1/2(\text{grad } \underline{u} + (\text{grad } \underline{u})^T)$; $\underline{u}$ is a displacement vector; $(\cdot)^T$ denotes the transpose of $(\cdot)$; δ_{ij} is the Kronecker delta; $\otimes$ is the tensor product.

If the body forces are neglected in Eqs. A.1, A.2, then they can be simplified as

$$\text{div } \underset{\sim}{T} = 0 \qquad (A.1')$$

$$\text{div grad } \theta = 0 \qquad (A.2')$$

Let us introduce a function U(X), which belongs to the space of $C^n(R)$, $n > 4$, (i.e., collection of n-times continuously differentiable functions in R), such that stresses are represented by the function as follows:

$$T_{xx} = D_y^2 U(X);\ T_{yy} = D_x^2 U(X);\ T_{xy} = -D_x D_y U(X) \qquad (A.4a)$$

where T_{xx}, T_{yy} and T_{xy} are the components of the (Cauchy) stress tensor; $U(X) = U(x,y)$; D_x and D_y denote the partial derivatives with respect to x and y, respectively, i.e., $D_x = \partial/\partial x$, $D_y = \partial/\partial y$ and $D_x^2 = \partial^2/\partial x^2$, $D_y^n = \partial^n/\partial y^n$, etc.

The representation of the stresses in Eq. A.4a automatically satisfy the (translational) equilibrium equation in Eq. A.1'. But since they must also satisfy the compatibility equation in Eq. A.2', substitution of Eq. A.4a into Eq. A.2' leasds to the biharmonic

equation,

$$D^4 U(X) = D^2(D^2 U(X)) = D_x^4 U(X) + 2D_x^2 D_y^2 U(X) + D_y^4 U(X) = 0 \qquad (A.4b)$$

where $D^2(\cdot) = \text{div grad } (\cdot) = (D_x^2 + D_y^2)(\cdot)$.

The biharmonic function (i.e. Airy stress function) is often expressed by U in place of U(X), hereafter.

2. Complex Representation of Airy Stress Function

Although there are several ways to define complex representation of stresses, we basically follow the way given by Muskhelishvili:

Let $D^2U = P$, then $D^2(D^2U) = D^2P = 0$. So P is a harmonic function in the domain R. Let Q be a harmonic conjugate of P, then

$$f(z) = P(x,y) + i\,Q(x,y) \quad (z = x+iy;\ i = \sqrt{-1}) \qquad (A.5)$$

will represent a holomorphic function in R.

Now let $\phi(z)$ be another holomorphic function such that $f(z) = 4\phi'(z) = 4\,\frac{d\phi(z)}{dz}$, then

$$\phi(z) = \frac{1}{4}\int^z f(z)\,dz = p + iq \qquad (A.6)$$

$$\phi'(z) = p_{,x} + iq_{,x} = \frac{1}{4}(P + iQ) \qquad (A.7)$$

where $(\cdot)_{,1} = D_x(\cdot)$, and $(\cdot)_{,2} = D_y(\cdot)$ hereafter.

Since $\phi(z)$ is holomorphic in R, p and q satisfy Cauchy-Riemann equations so that Eqs. A.6 and A.7 imply

$$p_{,1} = q_{,2} = \frac{1}{4}P; \quad p_{,2} = -q_{,1} = -\frac{1}{4}Q \qquad (A.8a,b)$$

Hence $$P = 4\,p_{,1} = 4\,q_{,2} \qquad (A.9)$$

Since the function P (=Re f(z)) is represented as $P = D^2U$ using Eqs. A8a,b it is seen that U-xp - yq is also a harmonic function in R.

i.e. $$D^2(U-xp-yq) = D^2U - 2p_{,1} - 2q_{,2}$$
$$= P - 2\left(\frac{1}{4}P + \frac{1}{4}P\right) \qquad (A.10)$$
$$= 0$$

Putting $p_1 = U - xp - yq$, then $U = xp + yq + p_1$ (A.11)

But in order to express stress function U, we do not need both functions p and q in Eq. A.11. We illustrate as follows:

$D^2(U-2xp) = 0$ and let $p_2 = U-2xp$. Then we obtain

$$U = 2xp + p_2 \qquad (A.12)$$

Similarly U - 2yq is also a harmonic function such that

$$D^2(U-2yq) = 0. \text{ Putting } p_3 = U-2yq,\ U = 2yc_1 + p_3 \qquad (A.13)$$

Now let us define another holomorphic function $\chi(z)$ given by $\chi(z) = p_1 + i\,\gamma$ where p_1 is a harmonic function defined in Eq. A.11 and γ is an arbitrary conjugate harmonic function of p_1. Then the stress function U defined in Eq. A.11 can be written as

$$U = \mathrm{Re}[\bar{z}\phi(z) + \chi(z)] \qquad (A.14)$$

which satisfies the biharmonic equations. This was originally defined by Goursat in 1898.

Or equivalently

$$2U = \bar{z}\phi(z) + z\overline{\phi(z)} + \chi(z) + \overline{\chi(z)} \qquad (A.15)$$

i.e. Let A(z) be a complex function such as $\phi(z)$, $\chi(z)$, $f(z)$.

Then $A(z) = u(x,y) + i\,v(x,y)$ where $u(x,y) = \mathrm{Re}\,A(z)$ and $v(x,y) = \mathrm{Im}A(z)$

and, $\overline{A(z)} = u(x,y) - iv(x,y)$.

We note here that since the Airy stress function U is expressed by the functions of $\phi(z)$ and $\chi(z)$, U is of class C^{∞} (infinitely differentiable) in R.

3. Complex Representations of Stresses and Displacements

Substituting Eq. A.15 into Eq.4a,

$$T_{xx} + i\,T_{xy} = U_{,22} - i\,U_{,12} = (-i)\,[U_{,1} + i\,U_{,2}]_{,2} \qquad (A.16)$$

$$T_{yy} - i\,T_{xy} = U_{,11} + i\,U_{,12} = [U_{,1} + i\,U_{,2}]_{,1} \qquad (A.17)$$

where

$$U_{,1} + i\,U_{,2} = \phi(z) + z\overline{\phi'(z)} + \overline{\chi'(z)} \qquad (A.18)$$

(i.e. $(\cdot)_{,\alpha} = (\cdot)_{,z}\, z_{,\alpha} + (\cdot)_{,\bar{z}}\, \bar{z}_{,\alpha} \quad \alpha = 1,2$)

where $(\cdot)_{,z} = \partial/\partial z(\cdot)$.

We now introduce a new complex function $\psi(z)$ defined by $\psi(z) = \chi'(z)$. Expressing stresses in terms of holomorphic functions, Eqs. A.16 and A.17 give

$$T_{xx} + i\,T_{xy} = \phi'(z) + \bar{\phi}'(z) - z\phi''(z) - \overline{\psi'(z)} \qquad (A.16)'$$

$$T_{yy} - i\,T_{xy} = \phi'(z) + \bar{\phi}'(z) + z\phi''(z) + \psi'(z) \qquad (A.17)'$$

Now in order to define displacements in terms of the holomorphic functions we will consider the constitutive equation given in Eq. A.3.

The constitutive law is

$$T_{ij} = C_{ijkl}\, e_{kl} \quad (i,j,k,l = 1,2) \qquad (a)$$

where $C_{ijkl} = \lambda\delta_{ij}\,\delta_{kl} + 2G\,\delta_{ik}\delta_{jl}$

Considering $e_{ij} = 1/2(u_{i,j} + u_{j,i})$ and $\theta_1 = \text{div}\,\underline{u} = e_{11} + e_{22}$, we have,

$$\lambda\theta_1 + 2G\,u_{1,1} = T_{11} = U_{,22} \tag{b.1}$$

$$\lambda\theta_1 + 2G\,u_{2,2} = T_{22} = U_{,11} \tag{b.2}$$

$$G(u_{1,2} + u_{2,1}) = T_{12} = -U_{,12} \tag{b.3}$$

where $(T_{11},T_{12},T_{22}) = (T_{xx},T_{xy},T_{yy})$, $(u_1,u_2) = (u,v)$, $(e_{11},e_{12},e_{22}) = (e_{xx},e_{xy},e_{yy})$.

Solving the first two equations in (b) for $u_{1,1}$ and $u_{2,2}$, one obtains

$$2G\,u_{1,1} = -U_{,11} + JD^2U \tag{b.1'}$$

$$2G\,u_{2,2} = -U_{,22} + JD^2U \tag{b.2'}$$

where $J = \frac{\lambda + 2G}{2(\lambda+G)}$ and D^2 is the Laplace operator.

Since $D^2U = P = 4p_{,1} = 4q_{,2}$, Eqs. b.1' and b.2' become

$$2G\,u_{1,1} = -U_{,11} + 4J\,p_{,1} \tag{c.1}$$

$$2G\,u_{2,2} = -U_{,22} + 4J\,q_{,2} \tag{c.2}$$

Integrating the above equations,

$$2G\,u_1 = -U_{,1} + 4J\,p + f(y) \tag{d.1}$$

$$2G\,u_2 = -U_{,2} + 4J\,q + q(x) \tag{d.2}$$

In order to determine $f(y)$ and $g(x)$ we substitute Eqs. d.1 and d.2 into Eq. b.3, and setting $p_{,2} = -q_{,1}$ in Eq. A.8b, we obtain

$$\frac{df(y)}{dy} + \frac{dg(x)}{dx} = 0 \tag{e}$$

In order that this equation be always true for all x and y we must have

$$\frac{df(y)}{dy} = -\frac{dg(x)}{dx} = \alpha \quad (\alpha: \text{constant})$$

Hence

$$f(y) = \alpha y + \beta \tag{f.1}$$

$$g(x) = \alpha x + \gamma \tag{f.2}$$

However, when considering strains, the right hand terms will vanish or cancel each other. So the functions f(y) and g(x) merely represent rigid body motion. So we can set f(y) = g(x) = 0 in Eqs. d.1 and d.2.

Thus considering Eqs. A.6, A.18, d.1 and d.2, we finally obtain

$$2G(u_x + i\,u_y) = K\,\phi(z) - z\,\overline{\phi'(z)} - \overline{\psi(z)} \tag{A.19}$$

where $u_x = u_1$, $u_y = u_2$ and $K = (3-\nu)/(1+\nu)$ for plane stress condition. For plane strain let $K = K'$, $\nu = \nu'$ and substituting $\nu' = \nu/(1-\nu)$ one obtains $K' = 3-4\nu$ for plane strain condition.

We note here that Eqs. A.16' and A.17' can also be written as follows:

$$T_{xx} + T_{yy} = 2[\phi'(z) + \overline{\phi'(z)}] = 4\mathrm{Re}\,[\phi'(z)] \tag{A.16"}$$

$$T_{yy} - T_{xx} + i2\,T_{xy} = 2\,[z\phi''(z) + \psi'(z)] \tag{A.17"}$$

Thus we define the complex representation of stresses and displacements in Eqs. A.16', A.17' (or Eqs. A.16", A.17") and Eq. A.19, respectively.

4. Boundary Conditions Where Traction Force and/or Displacements are Given A Priori

We first consider the case where traction, denoted by t_{vi}, in which $\underline{v}$ and $\underline{s}$ denote respectively the normal and tangent vectors to the boundary. By Cauchy's formula:

$$t_{vi} = T_{ji}\lambda_j$$

where $\lambda_1 = \cos(x,v) = \cos(y,s) = \frac{dy}{ds}$

$$\lambda_2 = \cos(y,v) = -\cos(x,s) = -\frac{dx}{ds}$$

$$T_{xx}\lambda_1 + T_{xy}\lambda_2 = U_{,22}\left(\frac{dy}{ds}\right) - U_{,11}\left(-\frac{dx}{ds}\right)$$

$$= \frac{d(U_{,2})}{ds} = t_{v_1}(s) \qquad (A.20)$$

$$T_{xy}\lambda_1 + T_{yy}\lambda_2 = -U_{,12}\left(\frac{dy}{ds}\right) + U_{,11}\left(-\frac{dx}{ds}\right)$$

$$= -\frac{d(U_{,1})}{ds} = t_{v_2}(s) \qquad (A.21)$$

Integrating Eqs. A.20 and A.21 along the arc C of the boundary.

$$U_{,1} = -\int_{s_o}^{s} t_{v_2}(s)\,ds = f_1(s) + C_1$$

$$U_{,2} = \int_{s_o}^{s} t_{v_1}(s)\,ds = f_2(s) + C_2$$

Applying Eq. A.18 to the above equations, $\psi(z) = \chi'(z)$.

On C_T (boundary for traction force)

$$\phi(z) + z\phi'(z) + \psi(z) = f_1 + if_2 + \text{const.} \qquad (A.22)$$

This is the boundary condition on C_T where the traction is given a priori.

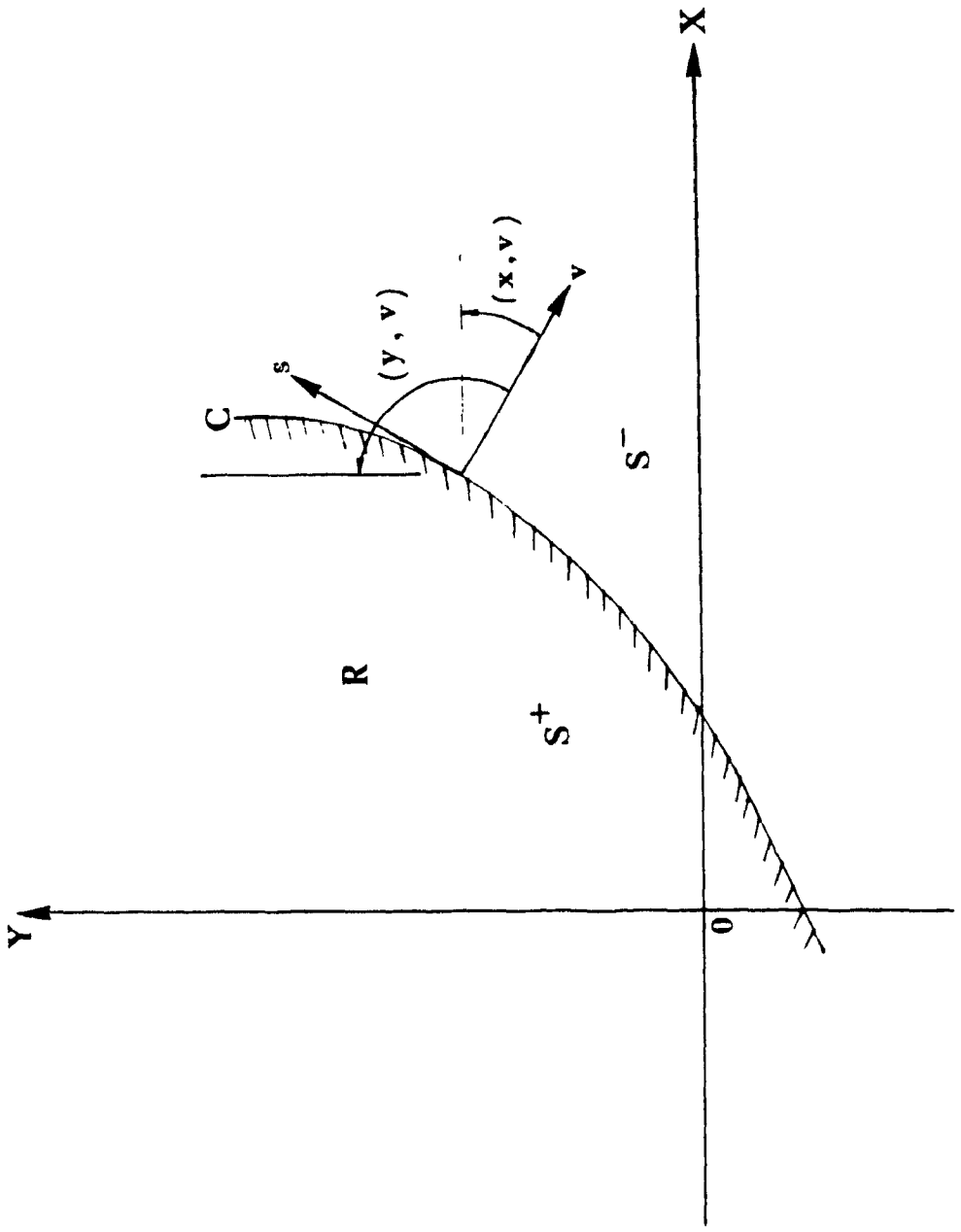


Fig. A.1 Notations Used for a Boundary on an Arc

We now consider a boundary where the displacements, $u = g_1(s)$ and $v = g_2(s)$, are given a priori. Substituting them into Eq. A.19 we obtain

$$\text{on } Cu \qquad K\phi(z) - z\bar{\phi}'(z) - \bar{\psi}(z) = 2G(g_1(s) + ig_2(s)) \tag{A.23}$$

It is noted that boundary conditions for stresses and displacements in a domain R can always be expressed in terms of the complex stress functions, $\phi(z)$ and $\psi(z)$, which are holomorphic in R.

A two-dimensional elasticity problem is essentially solved when the Airy stress function $U(x,y)$ is determined, say by solving the biharmonic equation given in Eq. A.4b. But since the Airy stress function U can be expressed in terms of $\phi(z)$ and $\chi(z)$ as shown in Eq. A.14 any original boundary problem of elasticity can be transformed into the determination of the holomorphic functions $\phi(z)$ and $\psi(z)$ $(= \chi'(z))$ under the boundary conditions given in Eqs. A.22 and A.23.

5. On the Expression of $U_{,1} \pm i\, U_{,2}$ (Eqs. A.16, A.17)

Rewriting Eqs. A.16 and A.17, as was done for equation A.18, one obtains

$$U_{,1} + i\, U_{,2} = \phi(z) + z\overline{\phi'}(z) + \bar{\psi}(z) \tag{A.24}$$

Let $C_T = [A,B]$ and let (X_1, X_2) be the resultant vector of forces applied from S^-, shown in Fig. A.1.

According to Eqs. A.20 and A.21,

$$t_{v_1} + i\, t_{v_2}\, ds = -id\,(U_{,1} + i\, U_{,2})$$

$$= -id\,(\phi(z) + z\bar{\phi}'(z) + \bar{\psi}(z))$$

Integrating over the arc [A,B], then

$$X_1 + iX_2 = \int_{[AB]} (t_{v_1} + it_{v_2})\, ds = - i\, [U_{,1} + i\, U_{,2}]_A^B$$

$$= - i\, [\phi(z) + z\bar{\phi}'(z) + \overline{\psi(z)}]_A^B \qquad (A.25)$$

where $[\ ]_A^B$ denotes the change in the expression as z moves from B to A. Thus, it is observed that the resultant force is obtained through the two points A and B, the initial and end point respectively, independent of the geometrical boundary of the arc AB.

Next we will consider the resultant moment about the origin of the coordinates.

It is, in general, expressed as,

$$\underline{M} = \int_{[A,B]} (\underline{r} \times \underline{t}_v)\, ds \quad \text{where } \underline{r} = x_i \underline{e}_i$$

$$\underline{t}_v = t_{v_i} \underline{e}_i$$

($\underline{e}_i$ = base vector)

$$= \int_{[A,B]} (xt_{v_2} - yt_{v_1})\, \underline{e}_3\, ds \quad (= M_3 \underline{e}_3)$$

$$\underline{M} = M_i \underline{e}_i = M_1 \underline{e}_1 + M_2 \underline{e}_2 + M_3 \underline{e}_3$$

$M_1 = M_2 = 0$ (w.r.t. x and y)

$M_3 \neq 0$

Let $M = M_3$.

$$M = \int_{[A,B]} (xt_{v_2} - yt_{v_1})\, ds$$

Then by Eqs. A.20 and A.21,

$$M = - \int_{[A,B]} \{x\, d(U_{,1}) + y\, d(U_{,2})\}$$

$$= - [x\, U_{,1} + y\, U_{,2}]_A^B + \int_{[A,B]} \{U_{,1}\, dx + U_{,2}\, dy\}$$

$$= - [x\, U_{,1} + y\, U_{,2}]_A^B + [U]_A^B \qquad (A.26)$$

But we have that

$$x\,U_{,1} + y\,U_{,2} = \mathrm{Re}\,\{z(U_{,1} - i\,U_{,2})\}$$

$$= \mathrm{Re}\,\{z(\overline{\phi(z)} + z\phi'(z) + \psi(z))\} \tag{A.27}$$

by considering the complex conjugate of Eq. A.18.

We also consider Eq. A.14, that is,

$$U = \mathrm{Re}\,\{\bar{z}\phi(z) + \chi(z)\}$$

One then can see that

$$M = \mathrm{Re}\,[\chi(z) - z\psi(z) - z\bar{z}\phi'(z)]_A^B \tag{A.28}$$

Therefore, we should notice that the force vector and moment component obtained in Eqs. A.25 and A.28 respectively are expressed through the equations $U_{,1} + i\,U_{,2}$ in Eq. A.18.

6. General Formulation and Propositions for the Half-Plane

We assume that the elastic body occupies the semi-infinite lower half-plane as shown in the Fig. A.2. Let R be a simply connected semi-circular region. Now it will be assumed that the stresses, and likewise the rotation, tend to zero as $|z| \to \infty$. The resultant vector of forces (X,Y), applied on the boundary, is considered to be finite.

However, we first consider the multiply-connected infinite region, as shown in Fig. A.3, which consists of non-intersecting simple contours, C_1, C_2, ---- , C_n. Let C_d be a circle about the origin with radius d sufficiently large enough so that all the contours lie inside C_d. Ther $|z| > |z_k|$ (k=1,---,n) for all z outside

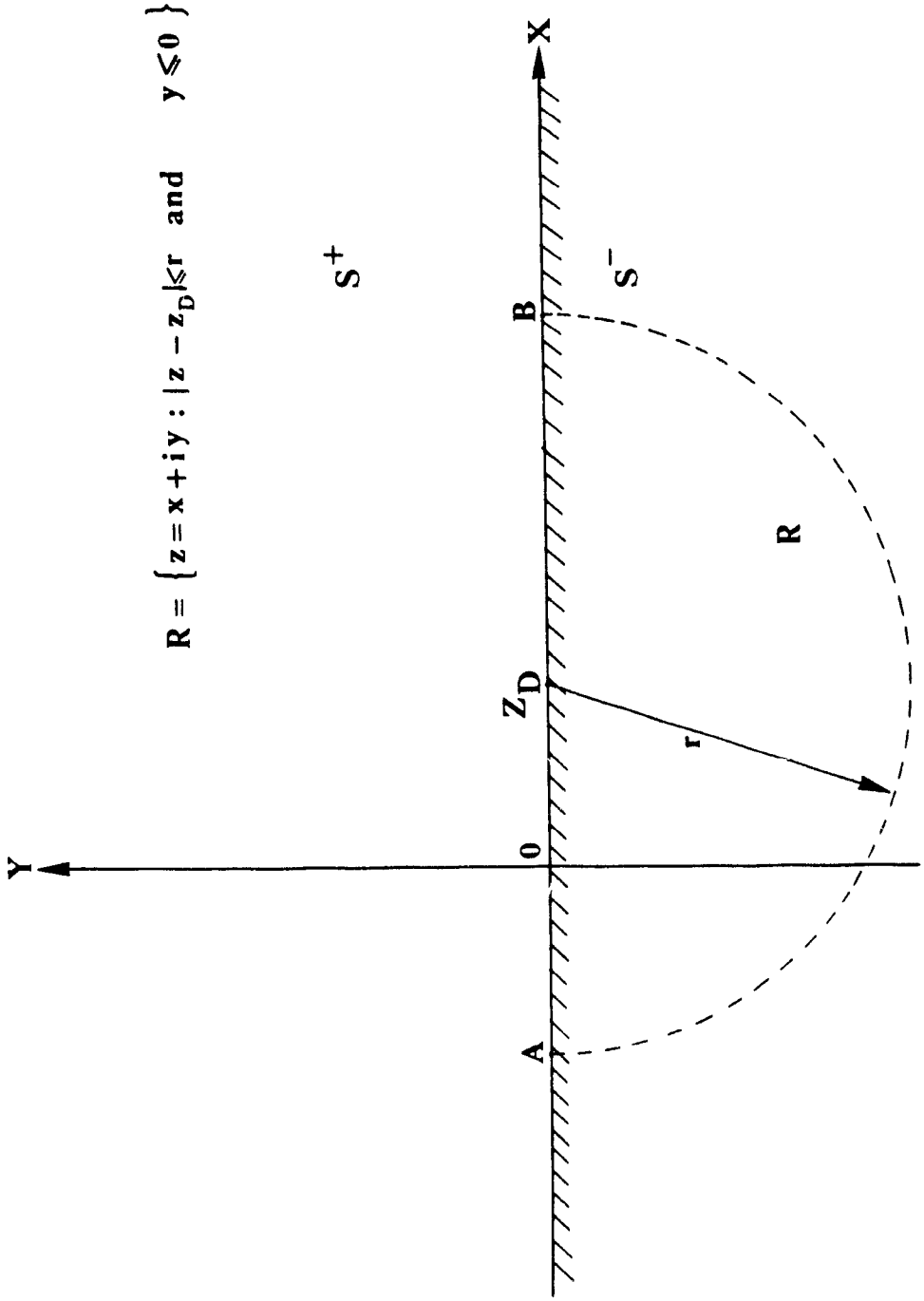


Fig. A.2 An Elastic Lower Half-Plane

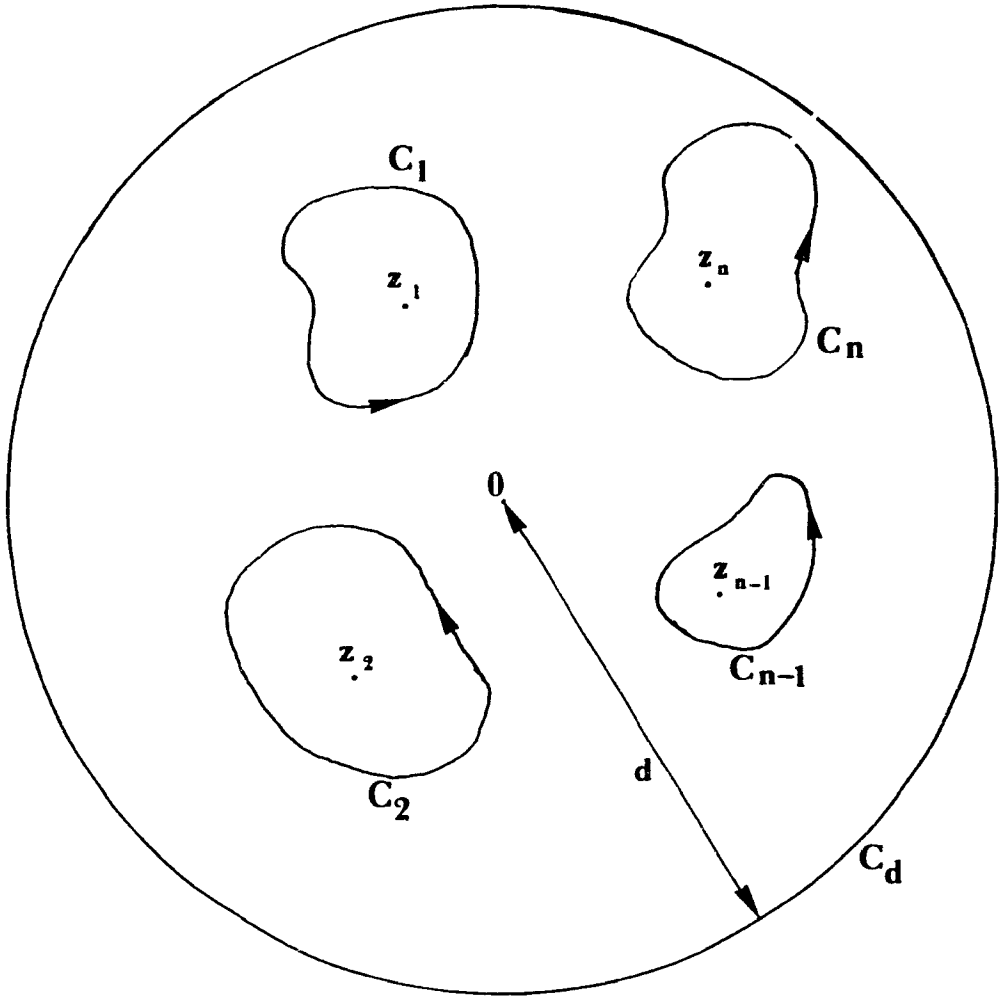


Fig. A.3 Multiple-Connected Infinite Region

C_d. It is then possible to write the complex functions $\phi(z)$, $\psi(z)$ in the following forms when $|z|$ is sufficiently large (e.g. Muskhelishvili [86], p. 126);

$$\phi(z) = -\frac{X + iY}{2\pi(k+1)} \log z + \Gamma z + \phi_o(z) \qquad (A.29)$$

$$\psi(z) = \frac{k(X - iY)}{2\pi(k+1)} \log z + \Gamma' z + \psi_o(z) \quad (k=3-4\nu) \qquad (A.30)$$

where $\phi_o(z)$ and $\psi_o(z)$ are holomorphic functions outside C_d, including infinity ($|z| = \infty$), i.e. $\phi_o = \sum_{n=0}^{\infty} a_n z^{-n}$, $\psi_o = \sum_{n=0}^{\infty} b_n z^{-n}$; $\Gamma = B+iC$ and $\Gamma' = B' + iC'$.

IF $T_{xx}(\infty)$, $T_{xy}(\infty)$, $T_{yy}(\infty)$ and $\omega(\infty)$ are the stresses and a rotation respectively, at infinity, then the following equations hold,

$$T_{xx}(\infty) = 2B - B'; \quad T_{xy}(\infty) = 2B + B'; \quad T_{yy}(\infty) = C';$$

$$\omega(\infty) = (k+1)\, C/2G.$$

The stress components are not altered no matter how we choose a_o and b_o in the series for $\phi_o(z)$, $\psi_o(z)$ and C. Assuming $a_o = b_o = 0$, then $\phi_o(z) = \psi_o(z) = 0$ and $C = 0$.

Now in the present infinite half-plane problem, while the region does not appear to be multiply connected, whenever $|z|$ is large enough, $\phi(z)$ and $\psi(z)$ are assumed to be expressed in the same way as

$$\phi'(z) = \frac{A}{z} + o(\frac{1}{z}), \quad \psi'(z) = \frac{B}{z} + o(\frac{1}{z}) \qquad (A.31a,b)$$

where $o(1/z) \to 0$ as $|z| \to \infty$. A and B are complex constants, $\phi'(z)$ and $\psi'(z)$ are considered to be holomorphic everywhere in the finite region.

Integrating eq. A.31 once,

$$\phi(z) = A \log z + o(1) + \text{const.}$$
$$\psi(z) = B \log z + o(1) + \text{const.} \qquad \text{(A.32a,b)}$$

Since log z is a multi-valued function, we need a branch such as $\log |z| + i\theta$ where $\theta \in [-\pi, \pi)$.

The constants A, B, which are related to the resultant vector X, Y, will be determined in the following way.

Let X' and Y' be the resultant vectors of the external forces, applied on the segment AB (see Fig. A.2). Furthermore, we assume that $X', Y' \to (X,Y)$ as $A \to -\infty$ and $B \to +\infty$. Now by Eq. A.25 we have

$$X_1' + iX_2' = i[\phi(z) + z\bar{\phi}'(\bar{z}) + \bar{\psi}(\bar{z})]_A^B \qquad \text{(A.33)}$$

In order to evaluate the right hand side of Eq. A.33, one may replace the evaluation of the resultant vector of the force applied on AB with that of the resultant vector of the forces applied on the semi-circle AB as shown in Fig. A.2. Now if the points A and B are sufficiently far away on the different sides of the origin o (in the sense that $|z_D| \ll |z_D - z_o| = r$ so that $|z_D| \ll |z_A|, |z_B|$), then the substitution of Eqs. A.31 and A.32 into Eq. A.33 gives:

$$[\phi(z) + z\bar{\phi}'(\bar{z}) + \psi(\bar{z})]_A^B = A \log \left(\frac{r''}{r'}\right) + A\pi i + \bar{B} \log \left(\frac{r''}{r'}\right) - \bar{B}\pi i + \varepsilon \qquad \text{(A.34)}$$

where $r' = |z_A|$ and $r'' = |z_B|$; ε is an arbitrary small real value such that it will vanish as r' and r" tend to infinite.

Now since the resultant force vector, $X_1' + iX_2'$, must be bounded

(in the sense that $|X'|, |Y'| < \sqrt{\bar{X}^2 + \bar{Y}^2} < \infty$) so long as r' and r" are bounded, the following condition must be imposed on A and B.

That is,

$$A + \bar{B} = 0 \tag{A.35}$$

Under this condition given by Eq. A.35 extending the radius r" (Fig. A.2) to infinity, then $X' + iY' \to X + iY$ which is bounded. Therefore, by Eq. A.33 one obtains

$$X + iY = i\,[\phi(z) + z\bar{\phi}'(\bar{z}) + \bar{\psi}(\bar{z})]_{-\infty}^{+\infty} = -\pi(A-\bar{B})$$

Or by Eq. A.35,

$$X + iY = -2\pi A$$

Thus $A = -\dfrac{X+iY}{2\pi}$; $B = \dfrac{X-iY}{2\pi}$ (A.36)

Hence, in the region where $|z|$ is large enough, Eqs. A.31, A.32 and A.36 give

$$\left.\begin{aligned} \phi'(z) &= -\frac{X+iY}{2\pi z} + o(\tfrac{1}{z}), \quad \psi'(z) = \frac{X-iY}{2\pi z} + o(\tfrac{1}{z}) \\ \phi''(z) &= \frac{X+iY}{2\pi z^2} + o(\tfrac{1}{z^2}) \end{aligned}\right\} \tag{A.37}$$

$$\left.\begin{aligned} \phi(z) &= -\frac{X+iY}{2\pi}\log z + o(1) + \text{const.} \\ \psi(z) &= \frac{X-iY}{2\pi}\log z + o(1) + \text{const.} \end{aligned}\right\} \tag{A.38}$$

where $o(1/z) < \varepsilon/|z|$ and $o(1) < \varepsilon$ (ε depends only on z and $\varepsilon \to 0$ as $|z| \to \infty$).

From the equations in (A.37) we notice that the stress components are dominated by $o(\frac{1}{z})$ for $|z|$ large. For the displacements u, v we have, by Eqs. A.19, A.37 and A.38, the following result

$$2G(u + iv) = -\frac{K(X + iY)}{2\pi} \log z - \frac{X + iY}{2\pi} \log \bar{z} + \frac{X - iY}{2\pi} \frac{z}{\bar{z}} + o(1) + \text{const.} \tag{A.39}$$

Thus the displacements are not bounded as $|z| \to \infty$. This is an inevitable feature in the two-dimensional elasticity problem involving an elastic half-plane.

7. Transformation of the General Formulae for the Half-Plane

It will be assumed that the elastic body occupies the lower half-plane as shown in Fig. A.2. Setting $\phi'(z) = \Phi(z)$ and $\psi'(z) = \Psi(z)$, the holomorphic function defined in Eqs. A.16', A.17' and Eq. A.19 can be rewritten as

$$T_{xx} + i\, T_{xy} = \Phi(z) + \bar{\Phi}(\bar{z}) - z\overline{\Phi'(z)} - \overline{\Psi(z)} \tag{A.40}$$

$$T_{yy} - i\, T_{xy} = \Phi(z) + \bar{\Phi}(\bar{z}) + z\bar{\Phi}'(\bar{z}) - \overline{\Psi(z)} \tag{A.41}$$

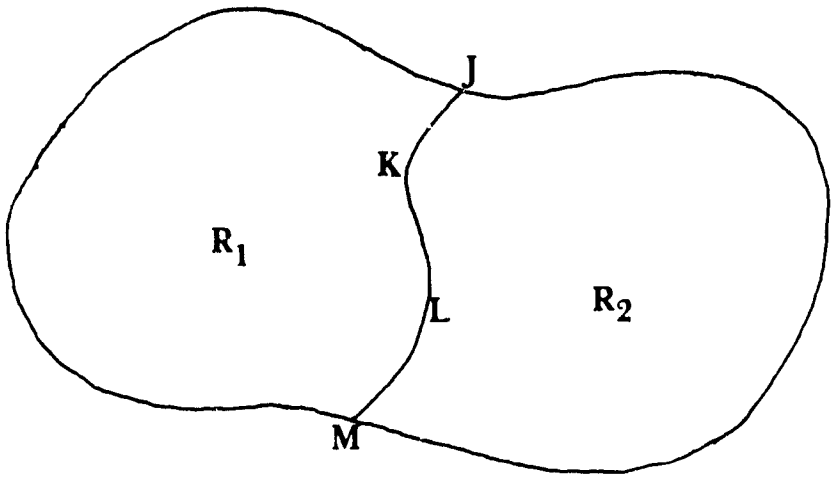
$$2G(u_{,1} + v_{,1}) = K\,\Phi(z) - \Phi(\bar{z}) - z\bar{\Phi}'(\bar{z}) - \overline{\psi(z)} \tag{A.42}$$

We must keep in mind that the holomorphic functions $\phi(z)$ and $\psi(z)$ have been defined only in the lower half plane S^- for the moment. We need and can extend those holomorphic functions defined in S^- into S^+ after the following preparation.

We first examine the property of an arbitrary holomorphic function, say $F_1(z)$, defined only in R_1 and on the boundary JKLM as shown in Fig. A.4.

Suppose there exists a holomorphic function $F_2(z)$ in R_2 and on JKLM such that $F_1(z) = F_2(z)$ on $\overline{JKLM}$. Then the function

$$F(z) = \begin{cases} F_1(z) & z \text{ in } R_1 \\ F_2(z) & z \text{ in } R_2 \end{cases} \tag{A.43}$$



$$R = R_1 \cup \{\widehat{JKLM}\} \cup R_2$$

Fig. A.4 Two Connected Regions for Defining Analytic Continuation

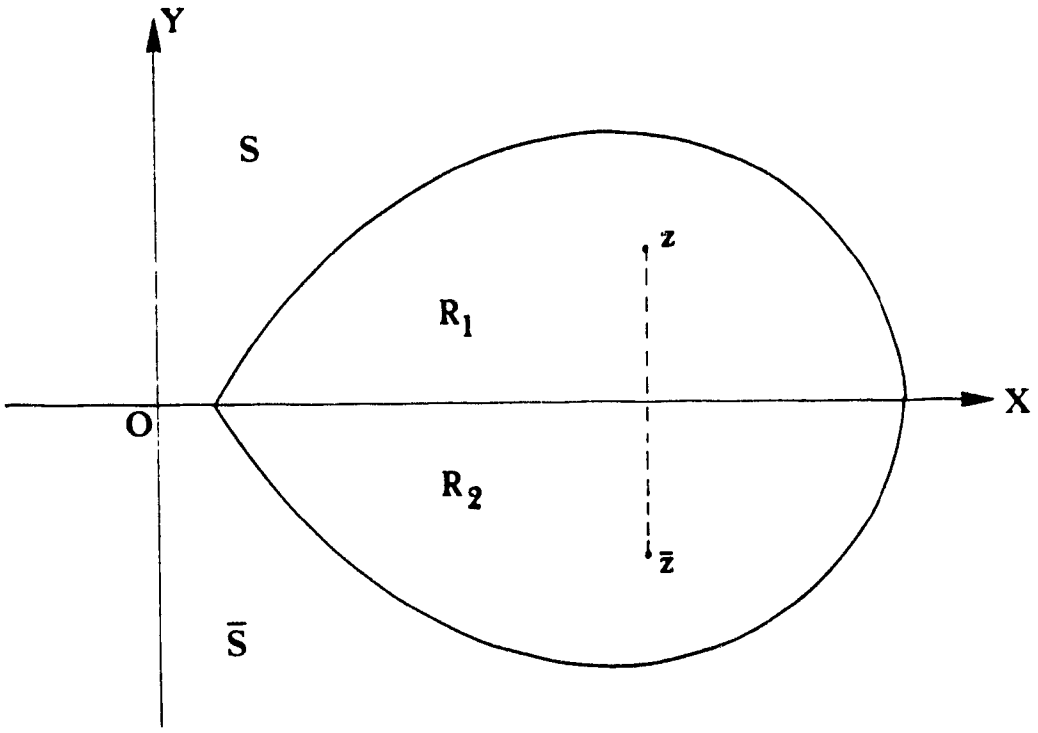


Fig. A.5 Two Connected Regions Symmetric With Respect to x-Axis for Defining Schwartz Principle

is a holomorphic function in R which is a union of the two domains, R_1 and R_2. $F_2(z)$ is called an analytical continuation of $F_1(z)$. This general idea of the analytic continuation of holomorphic functions can be applied to the present half-plane problem. That is, if the function $F_1(z)$ is holomorphic in R_1, except for some points which are singular points such as poles and branches, then the function $\overline{F_1}(z)$ (conjugate complex of $F_1(z)$) in R has the same property as the function $F_1(z)$ in S. (Fig. A.5). This is due to Schwartz reflection principle, which states that the analytic continuation of $F_1(z)$ into region R_2 considered as a mirror image, is given by

$$F_2(z) = \overline{F_1(\bar{z})} = \bar{F}_1(z) \qquad z \text{ in } R_2 \tag{A.44}$$

where $\bar{F}_1(z)$ is a conjugate complex of $F_1(z)$ and defined as

$$\bar{F}_1(z) = \overline{F_1(\bar{z})} = U(x,-y) - iV(x,-y)$$

if $$F_1(z) = U(x,y) + iV(x,y) \qquad z \text{ in } R_1$$

We can show that $F_2(z) = \bar{F}_1(z)$ is holomorphic in R_1 provided that $F_1(z)$ is holomorphic in R_1.

$$\bar{F}_1(z) = U(x,-y) - iV(x,-y) \quad (z \text{ in } R_2 \,,\ y < 0)$$

$$\frac{\partial}{\partial z}\bar{F}_1(z) = \frac{1}{2}\left[\frac{\partial}{\partial x} + i\,\frac{\partial}{\partial y}\right](U(x,-y) - iV(x,-y)$$

$$= \frac{1}{2}\left\{\frac{\partial U}{\partial x} - \frac{\partial V}{\partial y} - i\left(\frac{\partial u}{\partial y} + \frac{\partial v}{\partial x}\right)\right\} = 0$$

These partial derivatives are evaluated at $(x,-y)$, $y < 0$. Thus the complex derivative $\frac{d}{dz}\overline{F_1(\bar{z})} = \overline{F_1'(\bar{z})}$ exists for z in R_2. Therefore $F_2(z) = \overline{F_1}(z)$ is holomorphic in R_2.

Let $\mathbb{R}$ be a set of points in the real axis. If $F_1^+(t) = \lim_{z\to t^+} F_1(z)$ (z in R_1 and t in $\mathbb{R}$) exists, then $\overline{F}_1^-(t) = \lim_{z\to t^-} \overline{F}_1(z)$ exists, and the following equality holds:

$$\overline{F}_1^-(t) = \overline{F_1^+(t)} \tag{A.45}$$

We note that if $F_1(z)$ were defined in R_2 first, then we have that $F_2(z) = \overline{F}_1(z) = F_1(\bar{z})$ (z in R_1). This implies that

$$\overline{F}_1^+(t) = \overline{F_1^-(t)} \tag{A.46}$$

Now we are ready to transform and re-express Eqs. A.40, A.41 and A.42 in terms of the one complex stress function $\Phi(z)$ after redefining $\Phi(z)$ in the upper half-plane S^+.

Let us define a new function $\Phi(z)$ in S^+ as follows:

$$\begin{aligned}\Phi(z) &= -\overline{\Phi(\bar{z})} - z\overline{\Phi'(\bar{z})} - \overline{\Psi(\bar{z})} \\ &= -\bar{\Phi}(z) - z\dot{\Phi}'(z) - \dot{\Psi}(z) \qquad (z \text{ in } S^+)\end{aligned} \tag{A.47}$$

Since $\Phi(z)$ and $\Psi(z)$ are holomorphic in S^-, each term of the right hand side in Eq. A.47 is holomorphic in S^+, thus $\Phi(z)$ in Eq. A.47 is holomorphic in S^+.

Let us now assume that z is in S^- implying that $\dot{z}$ is in S^+. Replacing the variable z by $\bar{z}$ in Eq. A.47, we have

$$\begin{aligned}\Phi(z) &= -\bar{\Phi}(\bar{z}) - \bar{z}\overline{\Phi'}(\bar{z}) - \overline{\Psi}(\bar{z}) \\ &= -\dot{\bar{\Phi}}(\dot{z}) - \bar{z}\dot{\Phi}'(\dot{z}) - \dot{\Psi}(\dot{z}) \qquad (z \text{ in } S^-)\end{aligned} \tag{A.48}$$

Then taking conjugate complex values on both sides of Eq. A.48

$$\bar{\Phi}(\bar{z}) = -\Phi(z) - z\Phi'(z) - \Psi(z) \quad (z \text{ in } S^-)$$

$$= \bar{\Phi}(z)$$

Thus $$\Psi(z) = -\Phi(z) - \bar{\Phi}(z) - z\Phi'(z) \quad (z \text{ in } S^-) \tag{A.49}$$

It is noted that, without extending $\Phi(z)$ into S^+, Eq. A.49 does not make sense since it involves $\bar{\Phi}(z) = \bar{\Phi}(\bar{z})$.

Substituting Eq. A.49 into Eqs. A.16', A.17', A.40, A.41 and A.42 gives

$$T_{xx} + T_{yy} = 2[\Phi(z) + \bar{\Phi}(z)] \tag{A.50}$$

$$T_{yy} - T_{xx} + 2i\, T_{xy} = 2[(\bar{z}-z)\Phi'(z) - \Phi(z) - \bar{\Phi}(z)] \tag{A.51}$$

$$T_{yy} - i\, T_{xy} = \Phi(z) - \Phi(\bar{z}) + (z-\bar{z})\, \overline{\Phi'}(z) \tag{A.52}$$

$$2G(u_{,1} + i\, v_{,1}) = K\Phi(z) + \Phi(\bar{z}) - (z-\bar{z})\, \overline{\Phi'}(\bar{z}) \tag{A.53}$$

Thus the stresses and the displacements have finally been expressed in terms of one complex function $\Phi(z)$ which is holomorphic in both S^+ and S^-. These equations are necessary to formulate boundary value problems in two-dimensional elasticity.

We further define sectionally continuous functions and sectionally holomorphic functions as follows.

Let L be the union of a finite number of simple, non-intersecting arcs and contours in the complex plane, $\mathbb{C}$. Let S' be a connected region in the plane except for points in L ($\rightarrow S' = \mathbb{C} - L$) as shown in Fig. A.6. Let $\Phi(z)$ be a complex function which is holomorphic in S'. We assume that each arc L_n (n=1,2,...,6) has a given direction, then about a point t_o of L_n' (not including end points: $L_n - \{a_n\} - \{b_n\}$) it is possible to define left (in S^+) and right (in S^-) neighbourhoods of

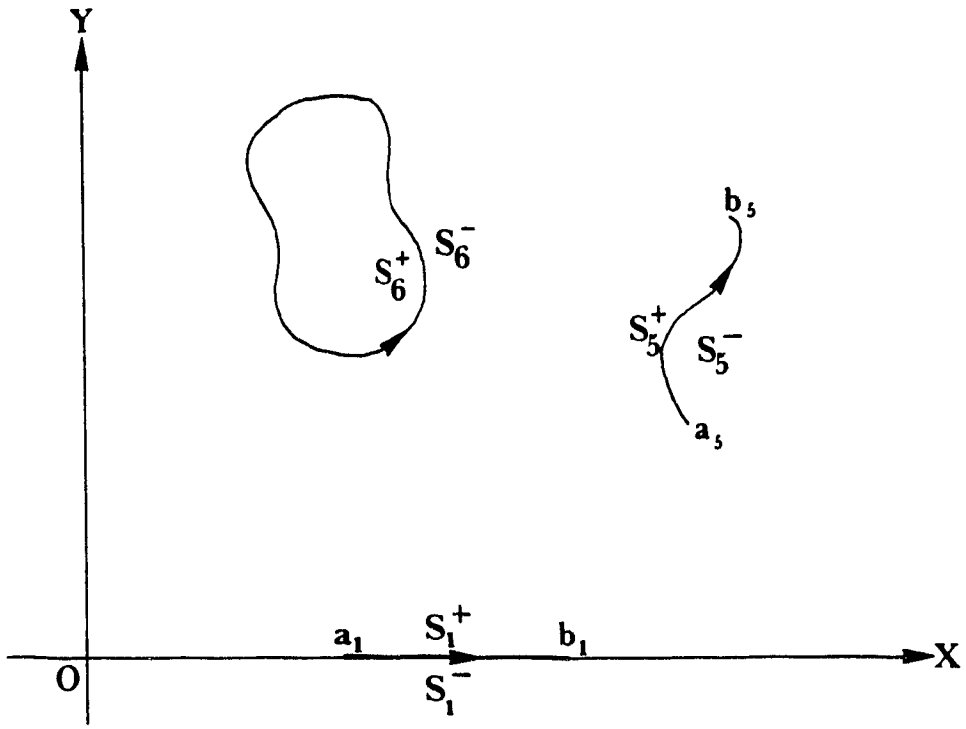


Fig. A.6 Union of Simple, Non-Intersecting Arcs and Contours in Complex Plane

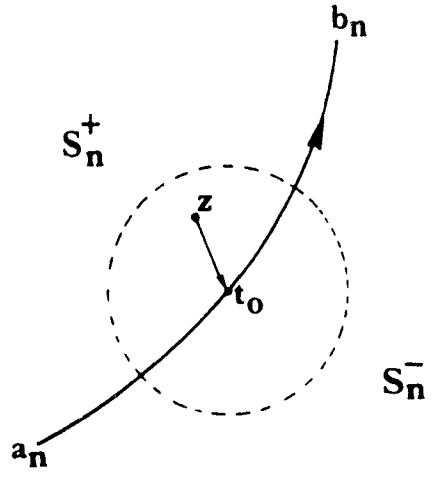


Fig. A.7 Limit Point on an Arc

t_o. Now if $\Phi(z)$ has a unique limit as $z \to t_o$ along any path in the left neighbourhood of t_o we denote this limit $\Phi^+(t_o)$ as shown in Fig. A.7 (i.e. $\Phi^+(t_o) = \lim_{z \to t_o} \Phi(z)$, $z \in S_n^+$).

Similarly if the unique limit exists on approach to t_o from the right neighbourhood it is denoted by $\Phi^-(t_o)$. (i.e. $\Phi^-(t_o) = \lim_{z \to t_o} \Phi(z)$, $z \in S_n^-$). However, limits of such holomorphic functions may not exist, in general, and yet the existence of the limits is not necessary if the theory of hyperfunctions is considered (see Ref. [53,60,61,85] or Appendix B.I: Method 7). A function $\Phi(z)$ in the neighbourhood of L_n' and for which $\Phi^+(t_o)$, $\Phi^-(t_o)$ exist at all interior points t_o of L_n' is said to be sectionally continuous in the neighbourhood of L'. To be more precise, $\Phi(z)$ is sectionally continuous in the neighbourhood of L if and only if, for all t_o in L_n', for any given $\varepsilon > 0$ there exists a $\delta > 0$, depending on ε and z in S^+ (or S^-), such that $0 < |z - t_o| < \delta(\varepsilon, z)$ implies $|\Phi(z) - C_n| < \varepsilon$ provided that C_n $(n = 1,2)$ are limits of $\Phi(z)$ at t_o $(C_1 = \Phi^+(t_o), C_2 = \Phi^-(t_o))$.

Moreover a complex function $\Phi(z)$ is said to be sectionally holomorphic if

(1) it is holomorphic for all z in $C - L$,

(2) it is sectionally continuous in the neighbourhood of L,

(3) it is such that at an end point a_n (or b_n) of each L_n, $\lim_{z \to a_n} (z-a_n)\Phi(z) = 0$ (or $|\Phi(z)| = o(|z-a_n|^{-\lambda})$, $0 \leq \lambda < 1$).

We note that every arc L_n defined above is called "the line of discontinuity" or "the boundary of $\Phi(z)$". If a sectionally holomorphic function has a singularity in the form of a branch point at an end a_n (or b_n) of an arc L_n, such a singularity is referred to

as a weak singularity since the condition (3) is satisfied.

We also should impose the following condition on $\Phi(z)$, that is

$$\lim_{y\to 0} \; y\,\Phi'(t+iy) = 0 \text{ for all } t \text{ in } L_n' = L_n - \{a_n\}-\{b_n\} \qquad (A.54)$$

8. A Definition of Riemann-Hilbert (Boundary) Problem

We first define Hölder condition and Cauchy integral on an arc.

(1) Hölder condition (H-condition)

A function $f(t)$ defined on an arc L is said to satisfy a Holder condition on L if for every two points t_1 and t_2 on L,

$$|f(t_1) - f(t_2)| < A\ |t_1-t_2|^{\mu} \qquad 0 < \mu < 1;\ A > 0) \qquad (A.55)$$

(2) Cauchy integral on an arc L

Let $f(t)$ be a complex function which satisfies the H-condition defined above on an arc L. Then Cauchy integral

$$\Phi(z) = \frac{1}{2\pi i} \int_L \frac{f(t)\,dt}{dt} \qquad (A.56)$$

is a sectionally holomorphic function in the whole complex plane cut along the arc L' (i.e. C-L). Furthermore, the limiting values $\phi^+(t)$, $\phi^-(t)$ exist on L, except for the end points, and they satisfy the following relations

$$\Phi^+(t_o) - \Phi^-(t_o) = f(t_o) \qquad (A.57)$$

$$\Phi^+(t_o) + \Phi^-(t_o) = \frac{1}{\pi i} \int_L \frac{f(t)\,dt}{(t-t_o)} \quad t_o \text{ in } L'(=L-\{a\}-\{b\}) \qquad (A.58)$$

Equation A.58 is interpreted as a principle value and it exists if $f(t)$ satisfies the H-condition. These results were first derived by J. Plemelj in 1908 (see ref. [86], Chapter II). They are called Plemelj formulae.

A Riemann-Hilbert Problem

The whole and only issue of this appendix is briefly stated as follows. A given (free) boundary-value problem in two-dimensional linear elasticity is first transformed to a single boundary equation, considering boundary conditions, which will be expressed as,

$$\Phi^{+}(t) - k\,\Phi^{-}(t) = f(t) \qquad t \text{ in } C_L \qquad (A.59)$$

where $f(t)$ satisfies the H-(continuity) condition, and k will be defined depending on the problems.

Then a sectionally holomorphic function $\Phi(z)$, which will also be re-stated in a more rigorous way, satisfying the boundary equation A.59 will be sought, so that stresses and rotations can be found from Eqs. A.50, A.51, A.52, and A.53. A problem, seeking a sectionally holomorphic function which satisfies a boundary equation like that in Eq. A.59, is called the Riemann-Hilbert problem. An interesting fact is that the Riemann-Hilbert problem can be studied more rigorously in a general manner if the theory of hyperfunctions (or Sato distributions), which was established by M. Sato in 1958 (see refs. [53,60,61,85]), is considered in the analysis. An elaboratre definition of the Riemann-Hilbert problem, which is connected to contact problems, will be given in the following section.

9. A Transformation of Contact Problem to a Riemann-Hilbert Problem

In this final section of Appendix A, we will solve a contact problem, where one solid slides quasi-statically over the boundary of the half-plane under the condition of limiting friction along the

surface of the half-plane (see Muskhelishvili [86]). At the end of this section 9.4, the three types of explicit formulae in obtaining contact pressure distribution and contact length are shown, which are classified depending on the profiles of contacting solids.

9.1 Development of the Riemann-Hilbert Problem for a Sliding Contact Problem

We first rewrite Eqs. A.51 and A.52 as,

$$T_{yy} - i\,T_{xy} = \Phi(z) - \Phi(\bar{z}) + (z-\bar{z})\,\bar{\Phi}'(z) \tag{A.60}$$

$$2G(u_{,1} + i\,v_{,1}) = K\Phi(z) + \Phi(z) - (z-z)\,\Phi'(z) \tag{A.61}$$

where the shear modulus, $G = E/2(1+\nu)$ (i.e. E = modulus of elasticity; ν = Poisson's ratio) and $K = 3-4\nu$ (plane strain condition).

Let us consider first that two elastic solids S_1 (e.g. half-plane) and S_2 are in contact under the following conditions:

(1) stresses and rotations in the solids S_1 and S_2 vanish at infinity.

(2) an external force exerted by the solid S_1 (or S_2) to another solid S_2 (of S_1) are known a priori,

(3) the slope of the contact portion, an arc $\overset{\frown}{ab}$, is sufficiently small.

Let $\Phi_1(z)$ and $\Phi_2(z)$ be sectionally holomorphic functions defined in the solids S_1 and S_2 respectively. The functions are actually holomorphic in the entire complex plane, except at the segment L = $\overline{ab}$ (i.e. a line of discontinuity) of the real axis. Then Eqs. A.50, A.51, A.52 and A.53 can be expressed in terms of the holomorphic

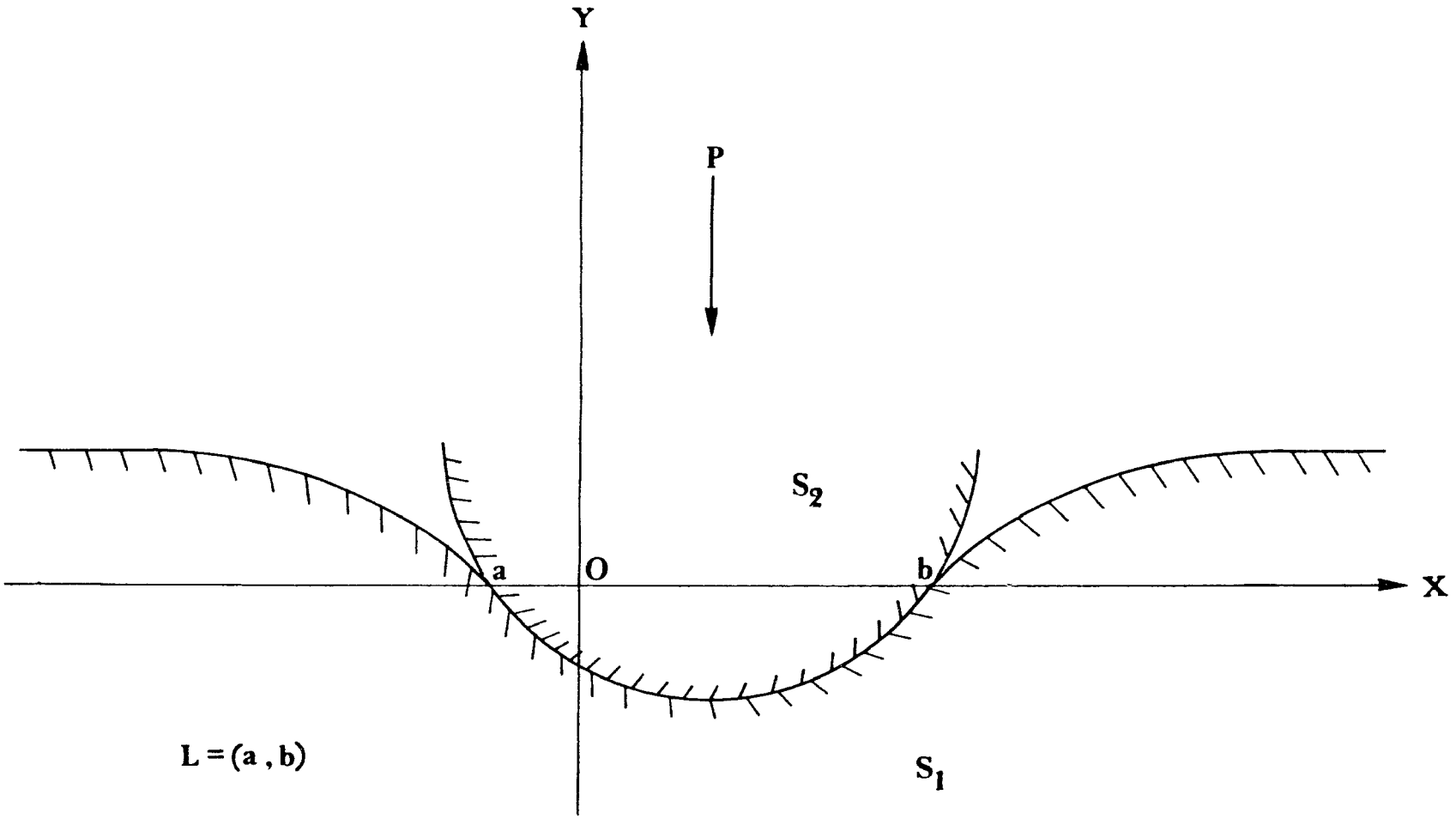


Fig. A.8 An Elastic Solid Contacting with an Elastic Half-Plane Under a Vertical Loading

functions $\Phi_1(z)$ and $\Phi_2(z)$ for each elastic solid.

Making use of Eq. A.60, the contact stresses for the solids S_1 and S_2 are respectively expressed as,

$$T_{yy}^{(1)} - i\, T_{xy}^{(1)} = \Phi_1^+(t) - \Phi_1^-(t) \quad \text{on L} \tag{A.62a}$$

$$T_{yy}^{(2)} - i\, T_{xy}^{(2)} = \Phi_2^+(t) - \Phi_2^-(t) \quad \text{on L} \tag{A.62b}$$

where the numbers (1), (2) in the superscript stand for the solids S_1 and S_2, respectively.

Since the contacting solids S_1 and S_2 are at an equilibrium state, the magnitude of the normal and the shear stresses at the contact surface must be equal and opposite for each elastic solid. Thereby the set of equations A.62a,b leads to the following equation

$$\Phi_1^+(t) + \Phi_2(t)^+ = \Phi_1^-(t) + \Phi_2^-(t) \quad \text{on L} \tag{A.63}$$

Applying the theorem by Painleve, then the sum of the two functions $\Phi_1(z) + \Phi_2(z)$, is holomorphic in the entire complex plane. By using the condition that both functions $\Phi_1(z)$ and $\Phi_2(z)$ vanish at infinity, we have the following result which holds in the entire complex plane.

$$\Phi_1(z) + \Phi_2(z) = 0 \tag{A.64a}$$

or

$$\Phi_1(z) = -\Phi_2(z) \tag{A.64b}$$

Hence the above result implies that the contact problem is reduced to finding the one holomorphic function either $\Phi_1(z)$ or $\Phi_2(z)$.

Let T(t) and P(t) be the shear and the normal stresses (i.e., $T(t) = T_{xy}(t)$ and $P(t) = T_{yy}(t)$) respectively, on the contact surface

L such that

$$T(t) = k\, P(t) \qquad \text{on } L \tag{A.65}$$

where k is a constant coefficient of friction. Next we consider the elastic solid S_2 only since for the two elastic solids there is a relation given by $\Phi_1(z) = -\Phi_2(z)$ obtained in Eq. A.64. Hereafter $\Phi_2(z)$ and the elastic solid S_2 are denoted, for the sake of simplicity, as $\Phi(z)$ and S respectively.

Consideration of Eq. A.65 with Eq. A.60 leads to the following relationship:

$$P(t)\,(1+ik) = \Phi(z) - \Phi(\bar{z}) + (z-\bar{z})\,\overline{\Phi'}(\bar{z}) \tag{A.66}$$

and hence at the boundary,

$$P(t)\,(1+k^2) = (1-ik)(\Phi^+(t) - \Phi^-(t)) \tag{A.67}$$

since $T_{xy} = k\, T_{yy} = k\,(-P(t))$ for the resultant vector $(X,Y) = (T,-P)$. Taking the complex conjugate and the limit of Eq. A.66,

$$P(t)\,(1+k^2) = (1+ik)(\bar{\Phi}^-(t) - \bar{\Phi}^+(t)) \tag{A.68}$$

where $\bar{\Phi}^-(t) = \dot{\Phi}^+(\bar{t})$ and $\dot{\Phi}^+(t) = \bar{\Phi}^-(\bar{t})$.

Subtracting Eq. A.68 from Eq. A.67, one can obtain the following equation, i.e.

$$(1-ik)\,\Phi^+(t) + (1+ik)\,\bar{\Phi}^+(t) = (1-ik)\,\Phi^-(t) + (1+ik)\,\bar{\Phi}^-(t) \tag{A.69}$$

Then again using the Painleve theorem, one can obtain the complex function, $(1-ik)\ \Phi(z) + (1+ik)\ \Phi(z)$, being holomorphic in the entire complex plane, vanishing at infinity, hence

$$(i-ik)\ \Phi(z) + (1+ik)\ \bar{\Phi}(z) = 0 \tag{A.70}$$

Next consider Eq. A.61 for the two elastic solids S_1 and S_2. First for the solid S_1 one obtains

$$2G_1(u^{(1)}_{,t} + iv^{(1)}_{,t}) = K_1\Phi_1(z) + \Phi_1(z) + \Phi_1(\bar{z}) - (z-\bar{z})\,\overline{\Phi_1'(z)} \quad (A.71)$$

where ,t denotes the derivative with respect to t.

Taking the complex conjugate of Eq. A.71

$$2G_1(u^{(1)}_{,t} - iv^{(1)}_{,t}) = K_1\,\overline{\Phi_1(z)} + \overline{\Phi_1(\bar{z})} - (\bar{z}-z)\,\bar{\Phi}_1'(\bar{z}) \quad (A.72)$$

Subtracting Eq. A.72 from Eq. A.71, and taking the limit, i.e. z in S_1 approaches t in L,

$$4\,iv^{(1)}_{,t} = \frac{K_1}{G_1}\,\Phi_1^+(t) + \frac{1}{G_1}\,\Phi_1^-(t) - \frac{K_1}{G_1}\,\overline{\Phi_1^+(t)} - \frac{1}{G_1}\,\overline{\Phi_1^-(t)} \quad (A.73)$$

The same operations are carried out for the solid S_2, thus obtaining,

$$4\,iv^{(2)}_{,t} = \frac{K_2}{G_2}\,\Phi_2^-(t) + \frac{1}{G_2}\,\Phi_2^+(t) - \frac{K_2}{G_2}\,\overline{\Phi_2^-(t)} - \frac{1}{G_2}\,\overline{\Phi_2^+(t)} \quad (A.74)$$

Let $f_1(t)$ and $f_2(t)$ be real-valued differentiable functions on the segment L, describing the profiles of the solids S_1 and S_2 respectively, prior to loading. After the vertical load is applied, the following relation holds on the contact surface

$$f_1(t) + v^{(1)-}_{(t)} = f_2(t) + v^{(2)+}_{(t)} \quad (A.75)$$

or

$$v^{(1)-}_{(t)} - v^{(2)+}_{(t)} = f_2(t) - f_1(t) = f(t) \quad (A.76)$$

Differentiating both sides of Eq. A.76,

$$(v^{(1)'}_{(t)})^- - (v^{(2)'}_{(t)})^+ = f'(t) \quad (A.77a)$$

or

$$v^{(1)}_{,t} - v^{(2)}_{,t} = f'(t) \quad (A.77b)$$

provided that the limits and the differentiations of the vertical displacements "$v^{(i)}$" (i=1,2) are interchangeable, i.e.

$$v^{(1)}_{,t} = (v^{(1)'}_{(t)})^{-} = \frac{d}{dt}\,(v^{(1)-}_{(t)}) = (\frac{dv^{(1)}(t)}{dt})^{-} \qquad (A.78a)$$

or

$$v^{(2)}_{,t} = (v^{(2)'}_{(t)})^{+} = \frac{d}{dt}\,(v^{(2)+}_{(t)}) = (\frac{dv^{(2)}(t)}{dt})^{+} \qquad (A.78b)$$

Subtracting Eq. A.74 from Eq. A.73 under the consideration of Eqs. A.77 and A.64; i.e. $\Phi_1(z) = -\Phi_2(z)$, one can obtain the following equation:

$$4i\,[v^{(1)}_{,t} - v^{(2)}_{,t}] = 4i\,f'(t)$$
$$= \frac{K_1}{G_1}\,\Phi_2^{+}(t) + \frac{\Phi_2^{-}(t)}{G_1} - \frac{K_1}{G_1}\,\overline{\Phi}_2^{-}(t) - \frac{\overline{\Phi}_2^{+}(t)}{G_1} + \frac{K_2}{G_2}\,\Phi_2^{-}(t) + \frac{\Phi_2^{+}(t)}{G_2} - \frac{K_2}{G_2}\,\overline{\Phi}_2^{+}(t)$$
$$- \frac{\overline{\Phi}_2^{-}(t)}{G_2} \qquad (A.79)$$

where the shear modulus $G_i = E_i/2(i+\nu_i)$ and $K_i = 3 - 4\nu_i$ (i=1,2).

Applying the result obtained in Eq. A.70 to Eq. A.79,

$$4i\,f'(t) = \{\frac{K_1}{G_1} + \frac{1-ik}{G_1(1+ik)} + \frac{1}{G_2} + \frac{K_2}{G_2}\,(\frac{1-ik}{1+ik})\}\,\Phi^{+}(t)$$

$$+ \{\frac{1}{G_1} + \frac{K_1}{G_1}\,(\frac{1-ik}{1+ik}) + \frac{K_2}{G_2} + \frac{1-ik}{G_2\,(1+ik)}\}\,\Phi^{-}(t) \qquad \text{on L} \qquad (A.80)$$

Hence

$$\Phi^{+}(t) + \frac{c+ikd}{c-ikd}\,\Phi^{-}(t) = 4i\,f'(t)\,\frac{G_1G_2(1+ik)}{c-ikd} \qquad \text{on L} \qquad (A.81)$$

where

$$c = G_1(K_2+1) + G_2(K_1+1) \qquad (A.82a)$$

$$d = G_1(K_2-1) - G_2(K_1-1) \qquad (A.82b)$$

Furthermore Eq. A.81 can be written in a more compact form,

$$\Phi^{+}(t) = q\,\Phi^{-}(t) + f_o \qquad \text{on L} \qquad \text{(A.83a)}$$

where

$$q = -\frac{G_1(K_2+1) + G_2(K_1+1) + ik\,\{G_1(K_2-1) - G_2(K_1-1)\}}{G_1(K_2+1) + G_2(K_1+1) - ik\,\{G_1(K_2-1) - G_2(K_1-1)\}} \qquad \text{(A.84a)}$$

$$f_o = 4i\,f'(t)\,\frac{G_1G_2(1+ik)}{G_1(K_2+1) + G_2(K_1+1) - ik\,\{G_1(K_2-1) - G_2(K_1-1)\}} \qquad \text{(A.84b)}$$

The Reimann-Hilbert problem in Eq. A.83a was obtained by considering the slop of displacements at the contact surface L. Next considering that the surface outside of the contact is free from any stresses or loads, then another Riemann-Hilbert problem can be obtained for Eq. A.60 as,

$$\Phi^{+}(t) - \Phi^{-}(t) = 0 \qquad \text{not on L} \qquad \text{(A.83b)}$$

Solving a contact problem between two solids is equivalent to solving the system of the two linear equations given in Eqs. A.83a,b for a sectionally holomorphic function $\Phi(z)$. Such a sectionally holomorphic function is clearly holomorphic in the complex plane cut along L (Eq. A.83a).

Next the real value "α" is introduced into Eq. A.83 to simplify the problem as follows.

In doing so, we first put;

$$\tan \pi\alpha = k\,\frac{G_1(K_2-1) - G_2(K_1-1)}{G_1(K_2+1) + G_2(K_1+1)} \qquad \text{(A.85)}$$

then

$$c \pm ikd = (c^2 + k^2d^2)^{1/2} e^{\pm i\pi\alpha} = c \frac{e^{\pm i\pi\alpha}}{\cos \pi\alpha} \tag{A.86}$$

We will then see that consideration of Eqs. A.85 and A.86 will greatly simplify the expression of "g" and "f_o" given in Eqs. A.84a and A.84b, respectively.

First, substituting Eq. A.86 into Eq. A.84a, the coefficient "g" can be shown as,

$$g = - e^{i2\pi\alpha} \tag{A.87}$$

In the same way f_o in Eq. A.84b can be re-expressed as,

$$f_o = 4i\, f'(t) \frac{G_1G_2(1+ik)\, e^{i\pi\alpha} \cos \pi\alpha}{G_1(K_2+1) + G_2(K_1+1)} \tag{A.88}$$

The simplification of the terms such as "g" and "f_o", just obtained in Eqs. A.87 and A.88, will also naturally simplify the analysis of the Riemann-Hilbert problem given in Eq. A.83.

9.2 The General Solution to the Riemann-Hilbert Problem Governing the Contact Problem

The general solution of Eq. A.83 is obtained as follows without difficulty (see Muskhelishvili [86], Imai [53]):

$$\Phi(z) = \frac{X(z)}{2\pi i} \int_L \frac{f_o}{X^+(t)} \frac{dt}{t-z} + X(z)\, P_{n-1}(z) \tag{A.89}$$

where $X(z)\, P_{n-1}(z)$ is the general solution of the homogeneous cae of Eq. A.83 (i.e., $f_o = 0$) and it must be such that $X(z)P_{n-1}(z)$ vanishes at infinity since $\Phi(z)$ is imposed to vanish at infinity; $P_{n-1}(z)$ is

the polynomial of degree n-1. The function X(z) is also a sectionally holomorphic function, and it is the homogeneous solution to Eq. A.83. The function X(z) and the polynomial $P_{n-1}(z)$ are explicitly defined as follows:

Put X(z) as,

$$X(z) = (z-a)^{-\gamma} (b-z)^{\gamma-1} \qquad \text{on } \mathbb{C}\setminus L \tag{A.90}$$

where the points a and b are the end points of L = (a,b), and $\gamma = \beta_1 + i\beta_2$ (β_1, β_2: real values).

In order to find γ, we invesitgate X(z) as the point z (not on L) traces a path beginning at the point t on L, then leading the upper side of L (i.e. $\mathbb{C}^+ \cup (-\infty, a)$) around the end "a" to approach the point t from the lower side (i.e. $\mathbb{C}^-$) of L. Then one can obtain the following relationship between $X^+(t)$ and $X^-(t)$ as

$$X^+(t) = X^-(t) \exp(i2\pi\gamma) \tag{A.91}$$

This automatically satisfies the homogeneous equation ($f_o = 0$ in Eq. A.83)

$$X^+(t) = g\, X^-(t) \tag{A.92}$$

f g is given by

$$e^{i2\pi\gamma} = g \tag{A.93a}$$

i.e.

$$\gamma = \frac{1}{2\pi i} \log g \tag{A.93b}$$

Substituting g in Eq. A.87 into Eq. A.93a,b, then γ is obtained as follows,

$$\gamma = \frac{1}{2\pi i} \log (-e^{i2\pi\alpha})$$

hence obtaining,

$$\gamma = \frac{1}{2} + \alpha \tag{A.94}$$

where α is obtained from Eq. A.85.

Thus $X(z)$ can be written as

$$X(z) = \frac{1}{(z-a)^{1/2+\alpha}\,(b-z)^{1/2-\alpha}} \tag{A.95}$$

with the properties that $\lim_{|z|\to\infty} z\,X(z) = 1$ and $X(z)$ has weak singularities at $z = a$ and b.

Next the polynomial $P_{n-1}(z)$ in Eq. A.89 can be determined under the following condition:

$$|\Phi(z)| \to 0 \quad \text{as } |z| \to 0 \tag{A.96}$$

According to Eq. A.37, for large $|z|$, $\Phi(z)$ $(= \phi'(z))$ tends to have the following form,

$$\Phi(z) = -\frac{X+iY}{2\pi}\,\frac{1}{z} + o(1/z) \tag{A.97}$$

where (X,Y) given in Eq. A.37, is a pair of resultant force vectors.

Put $(X,Y) = (T,-P)$ being a pair of the tangent and the normal forces. Then Eq. A.97 is written as

$$\Phi(z) = -\frac{T-iP}{2\pi}\,\frac{1}{z} + o(1/z)$$

$$\equiv \frac{i\,P(1+ik)}{2\pi}\,\frac{1}{z} + o(1/z) \tag{A.98}$$

where k is a coefficient of friction.

Now considering Eq. A.89, where $X(z)$ is given in Eq. A.95, for large $|z|$ it is shown to be such that

$$\Phi(z) = \frac{P_{n-1}(z)}{(z-a)^{\gamma}\,(b-z)^{1-\gamma}} + o(1/z) \tag{A.99a}$$

The condition given in Eq. A.96 requires $P_{n-1}(z)$ to be a constant, say D, thus Eq. A.99a is,

$$\Phi(z) = \frac{D}{z(1-a/z)^{\gamma}\,(h/z-1)^{1-\gamma}} + o(1/z) \tag{A.99b}$$

Now making use of Eq. A.97,

$$\lim_{z\to\infty} z\,\Phi(z) = \frac{i\,P(1+ik)}{2\pi} \tag{A.100}$$

and using Eq. A.99b,

$$\lim_{z\to\infty} z\,\Phi(z) = \frac{D}{-i\,e^{i\pi\alpha}} = \frac{i\,D}{e^{i\pi\alpha}} \tag{A.101}$$

Thus D is given as,

$$D = \frac{P(1+ik)}{2\pi}\,e^{i\pi\alpha} \quad (= P_{n-1}(z)) \tag{A.102}$$

Hence the final form of the sectionally holomorphic function (i.e., the defining function in the thoery of hyperfunctions) $\Phi(z)$, satisfying the Riemann-Hilbert "contact" problem given in Eq. A.83, is obtained by substituting Eqs. A.88, A.90, and A.102 into Eq. A.89 as follows:

$$\Phi(z) = \frac{2\,M(1+ik)\,\exp(i\pi\alpha)\,\cos\pi\alpha}{\pi(z-a)^{\gamma}\,(b-z)^{1-\gamma}} \int_L \frac{(t-a)^{\gamma}(b-t)^{1-\gamma}\,f'(t)}{t-z}\,dt$$

$$+ \frac{P(i+ik)\,\exp(i\pi\alpha)}{2\pi\,(z-a)^{\gamma}\,(b-z)^{1-\gamma}} \qquad z \text{ in } \mathbb{C}\setminus L \tag{A.103}$$

where γ and α are given in Eqs. A.94 and A.85 respectively, as,

$$\gamma = 1/2 + \alpha\ , \tag{A.104a}$$

$$\alpha = \frac{1}{\pi}\,\tan^{-1}\left\{k\frac{G_1(K_2-1) - G_2(K_1-1)}{G_1(K_2+1) + G_2(K_1+1)}\right\}\ , \tag{A.104b}$$

$$M = \frac{G_1G_2}{G_1(K_2+1) + G_2(K_1+1)}\ , \tag{A.104c}$$

P the vertical load, and f'(t) is given in Eq. A.77b.

9.3 Contact Pressure and Contact Area

Considering that $\Phi(z)$ is obtained in the form, $\Phi(z) = X(z)F(z)$ where $F(z)$ is holomorphic everywhere except on L , and substituting it into Eq. A.95, one obtains the following equation:

$$F^{+}(t_o) - F^{-}(t_o) = f_* \qquad t_o \text{ on } L \qquad (A.105)$$

where $f_* = f_o/X^{+}(t_o)$

Next considering Eq. A.89 with $F(z)$ being holomorphic in $C\setminus L$, one obtains

$$F^{+}(t_o) + F^{-}(t_o) = \frac{1}{\pi i} \int_L \frac{f_* dt}{t-t_o} + 2P_{n-1}(t_o) \qquad t_o \text{ on } L \qquad (A.106)$$

Elimination of $F^{-}(t_o)$ in Eqs. A.105 and A.106 leads to

$$\Phi^{+}(t_o) = \frac{f_*}{2} X^{+}(t_o) + \frac{X^{+}(t_o)}{2\pi i} \int_L \frac{f_*}{t-t_o} dt + P_{n-1}(t_o)\, X^{+}(t_o) \qquad (A.107)$$

Contact stresses are given by using Eq. A.60 as follows,

$$P(t_o) + i\, T(t_o) = \Phi^{+}(t_o) - \Phi^{-}(t_o) \qquad \text{on } L \qquad (A.108)$$

Eliminating $\Phi^{-}(t_o)$ in Eq. A.108 by making use of Eq. A.83 and substituting $\Phi^{+}(t_o)$ in Eq. A.107 into it,

$$P(t_o) + i\, T(t_o) = \left(\frac{q-1}{q}\right) \Phi^{+}(t_o) + \frac{f_o}{q}$$

$$= \frac{q+1}{2} \frac{f_o}{q} + \frac{q-1}{q} \frac{X^{+}(t_o)}{2\pi i} \int_L \frac{f_*\, dt}{t-t_o} + \frac{q-1}{q} P_{n-1}\, X^{+}(t_o) \qquad (A.109a)$$

Considering $T = kP$ (Eq. A.65), f_o (Eq. A.88), P_{n-1} (Eq. A.102) and f_* (Eq. A.105), then the above equation leads to,

$$P(t_o) + i\,T(t_o) = P(t_o)(1+ik)$$

$$= -4M(1+ik)\sin\pi\alpha\cos\pi\alpha\, f'(t_o) + \frac{4(1+ik)M\cos^2\pi\alpha}{\pi} X^+(t_o) \int_L \frac{f'(t)\,dt}{X^+(t)\,(t-t_o)} + \frac{P(1+ik)\cos\pi\alpha\, X^+(t_o)}{\pi} \quad \text{on } L \qquad (A.109b)$$

Hence the pressure is obtained as,

$$P(t_o) = -4M f'(t_o)\sin\pi\alpha\cos\pi\alpha + 4M\cos^2\pi\alpha \frac{X^+(t_o)}{\pi} \int_L \frac{f'(t)\,dt}{X^+(t)(t-t_o)} + P\cos\pi\alpha \frac{X^+(t_o)}{\pi} \quad \text{on } L \qquad (A.110)$$

where $M = G_1G_2/(G_1(K_2+1) + G_2(K_1+1))$.

Once material properties (i.e. Poisson's ratio, modulus of elasticity) and profiles of two contacting solids, and (unknown) contact lengths are given, one can compute contact pressures by means of the formula obtained in Eq. A.110. In order to obtain pressure distribution, however, we need to evaluate the integration in Eq. A.110.

We put the integration in Eq. A.110 as,

$$I(z) = \int_L \frac{f'(t)\,dt}{X^+(t)\,(t-z)} \qquad z \text{ on } L = (a,b) \qquad (A.111)$$

where $$\frac{1}{X^+(t)} = (t-a)^{\gamma}\,(b-t)^{1-\gamma} \qquad (A.112)$$

Assuming only a vertical load is applied, then "a" and "b" can be put as $a = -a$ and $b = a$. Equation A.112 is then written as

$$\frac{1}{X^+(t)} \equiv \frac{1}{X(t)} = (a+t)^{\gamma}\,(a-t)^{1-\gamma} \qquad (A.113)$$

where $\gamma = 1/2 + \alpha$ and $1-\gamma = 1/2 - \alpha$.

Since the residue theorem is applied for the integration, the integrand can be expanded into a series. First 1/X(t) can be represented in a series, under the consideration that the profiles of contacting solids are approximated by polynomials of the degree up to six.

Introducing the new variable x = a/t, Eq. A.113 is expressed as

$$\frac{1}{X(t)} = \left[\sum_{n=0}^{\infty} \frac{\gamma^n \{\log(1+x)\}^n}{n!}\right] \left[\sum_{n=0}^{\infty} \frac{(1-\gamma)^n \{\log(1-x)\}^n}{n!}\right]$$

After tedius algebraic work, one obtains:

$$\begin{aligned}\frac{1}{X(t)} &= t \sum_{n=0}^{\infty} C_n \left(\frac{a}{t}\right)^n \\ &= t \left\{1 + C_1 \frac{a}{t} + C_2 \left(\frac{a}{t}\right)^2 + C_3 \left(\frac{a}{t}\right)^3 + C^4 \left(\frac{a}{t}\right)^4 + C_5 \left(\frac{a}{t}\right)^5 \right. \\ &\quad \left. + C_6 \left(\frac{a}{t}\right)^6 + \cdots\cdots \right\} \end{aligned} \tag{A.114}$$

where
$$\left.\begin{aligned} C_o &= 1 \\ C_1 &= 2\gamma - 1 \\ C_2 &= 2\gamma(\gamma-1) \\ C_3 &= 2\gamma(\gamma-1)(2\gamma-1)/3 \\ C_4 &= 2\gamma(\gamma-1)(\gamma^2-\gamma+1)/3 \\ C_5 &= \gamma^2(\gamma-1)^2(2\gamma-1)/12 \\ C_6 &= \gamma^2(\gamma-1)^2(\gamma+1)(\gamma-2)/36 \end{aligned}\right\} \tag{A.115}$$

Two types of integrations, which depend on the profiles of contacting solids, are carried out in the following. The profiles are given by polynomials with arbitrary coefficients.

(i) Integration (I_1) for Profile of S_2: $f = g_1 = d_1 t^2/R$ (A.116a)

Differentiating $f = g_1$, then $g_1'(t)$ is given by

$$q_1' = D_1\, t/R \tag{A.116b}$$

where $D_1 = 2d_1$ and R are arbitrary coefficients for now.

The integration is then represented as

$$I_1(t_o) = \frac{D_1}{R} \int_{-a}^{a} \frac{(a+t)^{\gamma}(a-t)^{1-\gamma}\, t}{(t-t_o)}\, dt \tag{A.117}$$

Applying the residue theorem to Eq. A.117 by considering Eq. A.114,

$$I_1(t_o) = \frac{2\pi i\, D_1}{R(1-q)} \{(a+t_o)^{\gamma}(a-t_o)^{1-\gamma} t_o + i \cos \pi\alpha \sum_{n=0}^{\infty} C_n\, t_o^{2-n}\, a^n\} \tag{A.118}$$

Since

$$\frac{1}{1-q} = \frac{1}{2}\,(1-i\,\frac{\sin 2\pi\alpha}{(1+\cos 2\pi\alpha)}) = \frac{1}{2}\,(1-i \tan \pi\alpha), \tag{A.119}$$

taking only the real part of $I_1(t_o)$ (i.e. $\mathrm{Re}\,[I_1(t_o)]$), Eq. A.117 is given by

$$\mathrm{Re}[I_1(t_o)] = D_1 \frac{\pi}{R} \{(a+t_o)^{\gamma}(a-t_o)^{1-\gamma}\, t_o \tan \pi\alpha - \cos \pi\alpha \sum_{n=0}^{2} C_n\, t_o^{2-n}\, a^n\} \tag{A.120}$$

(ii) Integration (I_2) for Profile of S_2: $f = g_2 = d_2 t^4/R^3$ (A.121a)

Then g_2' is

$$q_2' = D_2 \frac{t^3}{R^3} \tag{A.121b}$$

where $D_2 = 4d_2$.

Again, by virtue of the residue theorem and Eq. A.119,

$$I_2(t_o) = \frac{D_2}{R^3} \int_{-a}^{a} \frac{(a+t)^{\gamma}(a-t)^{1-\gamma}\, t^3}{(t-t_o)}\, dt$$

$$= D_2 \frac{2\pi i}{R^3(1-q)} \{(a+t_o)^{\gamma}(a-t_o)^{1-\gamma}\, t_o^3 + i \cos \pi\alpha \sum_{n=0}^{4} C_n\, t_o^{4-n}\, a^n\}$$

$$\mathrm{Re}[I_2(t_o)] = D_2 \frac{\pi}{R^3} \{(a+t_o)^{\gamma}(a-t_o)^{1-\gamma} t_o^3 \tan \pi\alpha - \cos \pi\alpha \sum_{n=0}^{4} C_n t_o^{4-n}\, a^n\} \tag{A.122}$$

Assuming that profiles of contacting solids are described by the pair of functions given in (i) and (ii), then the pressure, obtained in Eq. A.110, can be written by means of the explicit forms of two integrations obtained in Eqs. A.120 and A.122 as follows. Replacing the variable t_o by t, the pressure is

$$P(t) = -4M(f_1'+f_2') \sin \pi\alpha \cos \pi\alpha + 4M \cos^2 \pi\alpha \frac{X(t)}{\pi} [\mathrm{Re}\{I_1(t) + I_2(t)\}] + P \cos \pi\alpha \frac{X(t)}{\pi} \quad (A.123)$$

where α, M, f_1', f_2', Re $I_1(t)$ and Re $I_2(t)$ are given in Eqs. A.104b,c, A.116, A.121, A.120 and A.122, respectively.

The formula for the pressure distribution in Eq. A.123 is further simplified, after lengthy algebraic work, by imposing the condition that the pressure at the edge $t = \pm a$ is zero (i.e. $P(\pm a) = 0$).

Hence the final formula for the pressure distribution is given by

$$P(t) = \frac{4M \cos^3 \pi\alpha}{R} (a+t)^{1-\gamma}(a-t)^{\gamma}\{D_1+D_2 \frac{a^2}{R^2} (1+C_2 + \frac{t^2}{a^2}\} \quad (A.124)$$

where C_2, D_1 and D_2 are given in Eqs. A.115, A.116 and A.121, respectively.

The formula of contact length is also obtained simultaneously when the condition $P(t) = 0$ at $t = \pm a$ is imposed in Eq. A.123. First the real part of the integration is given by,

$$\mathrm{Re}[I_1+I_2](t = \pm a) = -\pi \cos \pi\alpha \{D_1 \frac{a^2}{R} \sum_{n=0}^{2} h_1(n) C_n + D_2 \frac{a^4}{R^3} \sum_{n=0}^{4} h_2(n) C_n\} \quad (A.125)$$

where

$$h_1(n) = \begin{cases} +1 & \text{at } t = a \\ (-1)^{2-n} & \text{at } t = -a \end{cases} \quad (n = 0,1,2),$$

and $$h_2(n) = \begin{cases} +1 & \text{at } t = a \\ (-1)^{4-n} & \text{at } t = -a \end{cases} \qquad (n=0,1,2,3,4)$$

Substituting Eq. A.125 into Eq. A.123, and setting $P(\pm a) = 0$, one obtains the following force equilibrium equation.

$$V_4 a^4 \sum_{n=0}^{4} h_2(n)\, C_n + V_2 a^2 \sum_{n=0}^{2} h_1(n)\, C_n - P = 0 \qquad (A.126)$$

or

$$V_4(1+C_2+C_4)\, a^4 + V_2(1+C_2)a^2 = P \qquad (A.127)$$

where

$$V_2 = 4D_1 M \pi \cos^2 \pi\alpha/R, \qquad (A.128a)$$

and

$$V_4 = 4D_2 M \pi \cos^2 \pi\alpha/R^3 \qquad (A.128b)$$

Hence the half of contact length is given by,

$$a = \left(\frac{A}{2}\right)^{1/2} \left[-1 + \left\{1+4P \frac{V_4(1+C_2+C_4)}{\{V_2(1+C_2)\}^2}\right\}^{1/2}\right]^{1/2} \qquad (A.129)$$

where

$$A = \frac{V_2(1+C_2)}{V_4(1+C_2+C_4)} \qquad (A.130)$$

9.4 Contact Pressure and Contact Length for a Contacing Body with Three Different Profiles

The three types of formulae of contact pressures and contact lengths, which depend on profiles of contacting solids, are shown in the following:

(1) Case 1: $f = t^2/2R \; (= g_1)$ (A.131a)

$$f' = \frac{t}{R} \qquad (D_1 = 1) \qquad (A.131b)$$

Contact Pressure:

$$P(t) = \frac{4M\cos^3 \pi\alpha}{R} (a+t)^{1-\gamma}(a-t)^{\gamma} \qquad (A.132)$$

Contact Length:

$$a = \left[\frac{P}{V_2(1+C_2)}\right]^{1/2} \qquad (A.133)$$

(ii) Case 2: $f = t^2/2R + 25t^4/128R^3 \ (= g_1 + g_2)$ (A.134a)

$$f' = \frac{t}{R} + \frac{25}{32}\frac{t^3}{R^3} \quad (D_1 = 1 \text{ and } D_2 = \frac{25}{32}) \qquad (A.134b)$$

Contact Pressure:

$$P(t) = \frac{4M\cos^3 \pi\alpha}{R} \left\{1+ \frac{25}{32}\frac{a^2}{R^2}(1+C_2+\frac{t^2}{a^2})\right\} (a+t)^{1-\gamma}(a-t)^{\gamma} \qquad (A.135)$$

Contact Length:

$$a = (\frac{A}{2})^{1/2}\left[-1 + \left\{1+4P\frac{V_4(1+C_2+C_4)}{\{V_2(1+C_2)\}^2}\right\}^{1/2}\right]^{1/2} \qquad (A.136)$$

(iii) Case 3: $f = t^4/3R^3 \ (= g_2)$ (A.137a)

$$f' = \frac{4}{3}\frac{t^3}{R^3} \qquad (D_2 = \frac{4}{3}) \qquad (A.137b)$$

Contact Pressure:

$$P(t) = \frac{16M\cos^3 \pi\alpha}{3R} (\frac{a}{R})^2 (1+C_2+\frac{t^2}{a^2})(a+t)^{1-\gamma}(a-t)^{\gamma} \qquad (A.138)$$

Contact Length:

$$a = \left[\frac{P}{V_4'(1+C_2+C_4)}\right]^{1/4} \qquad (A.139)$$

where $V_4' = \frac{16M\pi}{3R^3}\cos^2 \pi\alpha$ (A.140)

APPENDIX B

APPENDIX B

I. A BRIEF REVIEW OF TWO- AND THREE-DIMENSIONAL CONTACT PROBLEMS

Analytical Methods for Three-Dimensional Contact Problems

Method 1 (Three-Dimensional Hertz Theory)

This theory was developed based on two fundamental results: (i) a relationship between normal pressure p(r,s) applied on an elastic half-space, and its vertical displacements at the surface. The displacement w at any point in the half-space due to the pressure p is given by Love [58] as:

$$w(x,y,z) = \frac{1}{4\pi G}\,(2(1-\nu)q - z\,D_z q) \tag{B.1}$$

where G, ν are the shear modulus and the Poisson's ratio, D_z is a partial derivative operator with respect to the z-coordinate, g(x,y,z) is a scalar function called a Newtonian potential (i.e. a Boussinesq-Cerruti potential).

Such a Newtonian potential is expressed by a single layer potential,

$$q(x,y,z) = \iint_S \frac{p(r,s)}{R}\,dr\,ds \tag{B.2}$$

where p(r,s) ($\equiv p(r,s,0)$) is a surface density function at (r,s,0) and R is the distance between two points, (r,s,0) and (x,y,z), i.e.

$R = ((r-x)^2 + (s-y)^2 + z^2)^{1/2}$; 1/R called the Newtonian kernel. The integration in Eq. B.2 will uniformly converge, thus the potential g being continuous in $\mathbb{R}^3$, if the function p is bounded in a domain S. (e.g. Kellog [63]);

(ii) a geometric condition due to the undeformed profiles of two solids (e.g. f_1 and f_2) and an approach of contact, H, due to the vertical deformations of solids (only) so that within the area of contact

$$\bar{w}_1 + \bar{w}_2 = H - d(z_2, z_1) \tag{B.3}$$

where $\bar{w}_1$ and $\bar{w}_2$ are displacements for the two solids pressed against each other, H the approach, $d(z_2, z_1)$ the distance function, i.e. $d(z_2, z_1) = (f_2 + f_1)(x)$.

Assuming then that the two contacting solids are represented by two elastic half-spaces, Eqs. B.1, B.2 and B.3 lead to an integral equations:

$$w_1(x,y,0) + w_2(x,y,0) = \tilde{M} \iint_S \frac{p(r,s)}{\tilde{R}} \, dr \, ds \tag{B.4}$$
$$= H - d(z_2, z_1)$$

where $\tilde{R}^2 = (x-r)^2 + (y-s)^2$, $\tilde{M} = \frac{1}{2\pi} \left(\frac{1-\nu_1}{G_1} + \frac{1-\nu_2}{G_2}\right)$,

and ν_1, ν_2 , G_1, G_2 are the Poisson's ratios, shear moduli for the solids S_1 and S_2 respectively.

A few comments are made on the above formulation. The normal displacement in the form of Eq. B.1 is derived, and is expressed by means of only one potential (given in Eq. B.2) as being a harmonic function, provided that shear stresses on the surface (z = 0) are imposed as zero. Hence this approach naturally is limited to frictionless contact problems. Although Hertz solved the integral equation in Eq. B.4 by means of a potential of an ellipsoid under the assumption that profiles of contacting solids are given in quadratic

form, the equation can be solved numerically for profiles approximated by a higher order polynomial (Ahmadi, Keer and Mura [4]). However, since the potential given in Eq. B.2 exists only if the density function p is bounded (e.g. $p \in L^1(S)$, continuous, piecewise continuous) in the surface S, the method is not applicable to those problems given in Fig. 2.1(c), (d) and the contacts shown in Fig. 2.1(a), (b) which are complete. It is also possible to recast the problem, which in the end leads to a Fredholm integral equation of the second kind instead of Eq. B.4, by considering a contact problem as a second boundary-value problem (or a Neumann problem), e.g. Kellog [63].

Method 2 (Hankel Transform)

A contact problem, which will be solved by this method, is an axisymmetric frictionless contact problem occurring between an axisymmetric rigid punch and an elastic half-space. The method is assumed to have the following information: (i) a profile of rigid punch with a magnitude of penetration and/or displacement field in the contact area, (ii) normal stress outside the contact area and tangential stress on the whole surface are zero. Hence, solving the contact problem is equivalent to solving a mixed boundary-value problem in elasticity. In the following, the method in which the integral transform, known as a Hankel (or Fourier-Bessel) transform takes an important role. This will be shown step by step with an example at the end (refer to Sneddon [122]).

First, the displacement solution to the equilibrium equation, where no body forces are present, can be shown as follows (see e.g. Gurtin [46], Fung [34], Lur'e [77]):

$$\underline{u} = \underline{B} - \frac{1}{4(1-\nu)} \text{ grad } (\underline{r}\cdot\underline{B} + A) \tag{B.5}$$

where $(\underline{\cdot})$ denotes a vector, $\underline{r}$ the position vector, $\underline{B}$ and A are the Papkovich-Neuber potentials, ν is the Poisson's ratio and grad is the gradient operator, i.e., grad $= \underline{e}_i \frac{\partial}{\partial x_i} \equiv \underline{e}_i D_{x_i}$ ($\underline{e}_i$ are base vectors, x_i are commonly used and referred to as $x_1 = x$, $x_2 = y$, $x_3 = z$).

For the equilibrium, the two potentials must satisfy the Laplacian operator such that

$$\text{div grad } \underline{B} = \underline{0} \quad \text{and div grad } A = 0 \tag{B.6}$$

Hence, the potentials are harmonic functions.

Introducing new harmonic functions, g, $\underline{C}$ and $\underline{E}$, then the potentials can be expressed as

$$\underline{B} = -4(1-\nu)\,\underline{C} + \text{curl } \underline{E} \tag{B.7}$$

and

$$A = -4(1-\nu)g - \underline{r} \cdot \text{curl } \underline{E} \tag{B.8}$$

where curl $\underline{E} = \underline{e}_1(D_yE_z - D_zE_y) + \underline{e}_2(D_zE_x - D_xE_z) + \underline{e}_3(D_xE_y - D_yE_x)$, D_x, D_y and D_z are partial derivative operators with respect to the coordinates x, y and z respectively.

Substituting Eqs. B.7 and B.8 into Eq. B.5, one obtains

$$\underline{u} = \text{grad } g + \text{curl } \underline{E} + \text{grad } (\underline{r}\cdot\underline{C}) - 4(1-\nu)\underline{C} \tag{B.9}$$

Considering the components of z-axis only for the harmonic vectors, $\underline{C}$ and $\underline{E}$, Eq. B.9 is reduced to

$$\underline{u} = \text{grad } q + \text{curl } (\underline{e}_3 E_z) + \text{grad } (zC_z) - 4(1-\nu)\underline{e}_3 C_z \quad (B.10)$$

Since there are no rotations for an axisymmetric problem, $E_z = 0$, and putting $C_z = h$, the displacement vector $\underline{u} = (u_r, u_\theta, u_z)$ in cylindrical coordinates can be written as

$$u_r = D_r(q + zh) \quad (B.11a)$$

$$u_\theta = 0 \quad (B.11b)$$

$$u_z = D_z(q + zh) - 4(1-\nu)h \quad (B.11c)$$

where D_r, D_z are the partial derivative operators as usual.

Introducing a function F in terms of the functions g and h as

$$F = -\int^z (q + zh)dz, \quad (B.12)$$

we obtain

$$\text{div grad } F = -2h \quad (B.13)$$

Then, the displacements can be expressed by only one function F as follows:

$$u_r = -D_{rz}F \quad (B.14a)$$

$$u_\theta = 0 \quad (B.14b)$$

$$u_z = -D_{zz}F + 2(1-\nu) \text{ div grad } F \quad (B.14c)$$

The stresses can be similarly shown by means of the function F only (see Sneddon [101]). Therefore, an axisymmetric problem is reduced to a problem of finding the function F. Now applying the Laplacian operator in Eq. B.13 and considering h as being harmonic, the

following partial differential equation can be obtained.

$$L^*(F) = 0 \tag{B.15}$$

where L^* is the biharmonic operator in cylindrical coordinates given by $L^* = (D_{rr} + r^{-1} D_r + D_{zz})^2$ (symmetric with respect to the z-axis).

Equation B.15 can be solved by the Hankel transform since the (infinite) half-space is considered as a domain. Seeking a solution in the form of a series to Eq. B.15 such that

$$F = \sum_{n=0}^{\infty} F_n(r,z) \cos r\theta \tag{B.16}$$

Then the following equation must hold:

$$L_n(F_n) = 0 \tag{B.17}$$

where $L_n = (D_{rr} + r^{-1}D_r - n^2r^{-2} + D_{zz})^2$

Applying the Hankel transform (denoted by HK hereafter) to Eq B.17,

$$HK[L_n(F_n)] = \int_0^{\infty} L_n(F_n)\, J_n(tr)\, dr$$

$$= (\frac{d^2}{dt^2} - t^2)^2 G_n(t,z) = 0 \tag{B.18}$$

where $J_n(tr)$ is the Bessel function of order n.

Equation B.18 is an ordinary differential equation, seeking an unknown function G_n, which is the Hankel transform of order n of the function F_n, and is given as

$$G_n(t,z) = HK[F_n] = \int_0^{\infty} F_n(r,z)\, J_n(tr)\, r\, dr \tag{B.19}$$

The Hankel transform in Eq. B.19 exists (i.e. the integration converges) if $F_n(r,z)$ is continuous almost everywhere on $E = \mathbb{R}_{r+} \cup \{0\}$ (or $0 \leq r < \infty$) and $rF_n \in L^1(E)$ (or $\int_0^\infty |r\, F_n(r,z)|dr < \infty$ for all $z > 0$). $L^1(E)$ is the Lebesque space.

This is called the Fourier-Bessel theorem, and if $F_n(r,z)$ satisfies this condition, then the following reciprocal relation holds:

$$F_n = HK^{-1}[HK[F_n]] = HK^{-1}[G_n]$$

$$= \int_0^\infty G_n(t,z) J_n(tr)\, t\, dt \qquad (B.20)$$

where HK^{-1} is the inversion of the Hankel transform.

The solution of the ordinary differential equation in Eq. B.18 is given by

$$G_n(t,z) = (A_n + B_n z)e^{tz} + (C_n + D_n z)e^{-tz} \qquad (B.21)$$

where the coefficients A_n, B_n, C_n and D_n will be determined from boundary conditions.

Then F_n is Eq. B.18 can be obtained by substituting G_n in Eq. B.21, provided that the coefficients are determined. After obtaining F_n in this way, the displacements in Eqs. B.14(a),(b),(c) can be derived from the substitution of F ($=F_o$; $n = 0$ for axisymmetric problems).

Example Problem

An axisymmetric frictionless contact problem, based on a mixed boundary-value problem, between a rigid punch and an elastic half-

space is considered. The boundary conditions (at z = 0) on vertical displacement v, normal stress T_{zz} and tangential stress T_{rz} are given as

$$v(r) \equiv u_z(r,0) = w(r) \qquad 0 < r < a \tag{B.22a}$$

$$P(r) \equiv T_{zz}(r,0) = 0 \qquad a < r < \infty \tag{B.22b}$$

$$T(r) \equiv T_{rz}(r,0) = 0 \qquad 0 < r < \infty \tag{B.22c}$$

First, considering Eqs. B.14c, B.20 and B.21, where n = 0 for an axisymmetric problem, one obtains the expression of the vertical displacement by,

$$u_z(r,z) = \int_0^\infty \left((1-2\nu)\frac{d^2H}{dz^2} - 2(1-\nu)t^2H\right) J_o(tr)\, t\, dt \tag{B.23}$$

and similarly those for stresses given by,

$$T_{zz}(r,z) = 2G \int_0^\infty (1-\nu)\frac{d^3H}{dz^3} - (2-\nu)t^2\frac{dH}{dz}) J_o(tr)\, t\, dt \tag{B.24}$$

$$T_{rz}(r,z) = 2G \int_0^\infty (\nu\frac{d^2H}{dz^2} + (1-\nu)\, t^2\frac{dH}{dz}) J_1(tr)\, t^2\, dt \tag{B.25}$$

where $H = G_o(t,z) = (A + B)\, e^{tz} + (C + Dz)\, e^{-tz}$ (B.26)

Once the coefficients in Eq. B.26 are determined, the problem is solved. Since the displacement vanishes at infinity, F (= F_0 for an axisymmetric problem) must vanish at infinity. This condition requires A = B = 0. Next, considering the boundary condition in Eq. B.22c and Eq. B.25,

$$T(r) = 2G \int_0^\infty (tC - 2\nu D) J_1(tr)\ t^3\ dt = 0, \qquad (B.27)$$

one thus obtains a relationship $C = 2\nu D/t$.

Accordingly, $H\ (= G_o)$ in Eq. B.26 is expressed as

$$H = \frac{D}{t}\ (2\nu + tz) e^{-tz} \qquad (B.28)$$

Substituting H in Eq. B.28 into Eqs. B.23 and B.24, and considering the boundary conditions, then

$$v(r) = w(r) = -\ 2(1-\nu) \int_0^\infty D J_o(tr)\ t^2\ dt \quad (0 \leqslant r \leqslant a) \qquad (B.29)$$

$$P(r) = 2G \int_0^\infty D J_o(tr)\ t^3\ dt = 0 \qquad (a < r < \infty) \qquad (B.30)$$

Now, in Eqs. B.29 and B.30, putting

$$t^2 D = a^2 f(x),\ ta = s,\ r = as,\ w(r) = -2(1-\nu)\ a\ q(s)$$

one comes up with the following pair of integral equations with an unknown function $f(x)$:

$$\int_0^\infty f(x)\ J_o(xs)\ dx = q(s) \qquad (0 \leqslant s \leqslant 1) \qquad (B.31a)$$

$$\int_0^\infty f(x)\ J_o(xs)\ x\ dx = 0 \qquad (1 < s < \infty) \qquad (B.31b)$$

In order to find the unknown function $f(x)$, which is equivalent to finding D, we consider a rigid punch with a flat surface displacing the elastic half-space by the magnitude d, i.e. $w(r) = d$ (a constant). We can solve the pair of integral equations without much difficulty as,

$$f(x) = \frac{2d}{m\pi a} \frac{\sin x}{x} \qquad (m = -2(1-\nu)) \qquad (B.32)$$

thus D is obtained as

$$D = - \frac{d}{(1-\nu)\pi} \frac{\sin at}{t^2} \tag{B.33}$$

Substituting D in Eq. B.33 into Eq. B.30, the pressure P(r), exerted by w(r) = d, is given by

$$P(r) = - \frac{2Gd}{(1-\nu)\pi} \int_0^\infty \sin at \, J_0(tr) \, dt$$

$$= - \frac{2Gd}{(1-\nu)\pi} (a^2-r^2)^{-1/2} \tag{B.34}$$

A more detailed study of this method was given by Gladwell [38,39,41] for the various contact profiles and the state of contact surface (i.e. frictionless, adhesive and in limiting friction).

Analytical Methods for Two-Dimensional Contact Problems

Method 3 (Two-Dimensional Hertz Theory)

The two-dimensional Hertz theory (abbreviated hereinafter as 2-D) has essentially no differences in assumptions and/or conditions from those stated in the three-dimensional (abbreviated hereinafter as 3-D) (e.g. Poritsky [113]). There is one difficulty in the establishment of the 2-D Hertz theory, which results from an undesirable behaviour of displacement in plane elasticity. That is, the vertical displacement is unbounded at infinity, due to a vertical point load applied at a surface of an elastic half-plane. This will then lead to the following indeterminant expression of the vertical displacement V(x) at the surface, produced by pressure applied over a portion, i.e. an interval L = (-a,a), which is equivalent to a superposition of displacements due to point loads over the portion

with magnitudes in accordance with the pressure at every position,

$$v(x) = -\frac{2(1-\nu^2)}{\pi E} \int_L p(t) \log |x-t| \, dt + C \qquad x \in L \qquad (B.35)$$

where C is an unknown constant, and ν, E are the Poisson's ratio and modulus of elasticity, respectively.

Since the constant C remains undetermined, while the integration may be seen to be a surface potential, the procedure used in the 3-D Hertz theory cannot be used directly. Instead, essentially the following approach is seen to be taken by Portisky [113] and Gladwell [41]:

1. Consider a contact problem between a rigid punch with a parabolic profile (simulating a circular punch) and an elastic half-plane. Determine a (surface) displacement field of the half-plane due to this contact by applying an assumed (contact) pressure.
2. The assumed pressure distribution p(t) may be obtained in much the same way as Hertz did for the 3-D contact. That is, to first assume a potential of an ellipse, $x^2/a^2 + y^2/b^2 = 1$. Then we have a total vertical force F,

$$F = \pi ab\, q \qquad (q = \text{homogeneous density}) \qquad (B.36)$$

and the differential force at x is given by

$$\begin{aligned} \Delta F &= 2\, q\, \Delta x b\, (1 - \frac{x^2}{a^2})^{1/2} \\ &= 2\, q\, \Delta x \frac{b}{a} (a^2 - x^2)^{1/2} \end{aligned} \qquad (B.37)$$

Eliminating q in Eq. B.37 using Eq. B.36, then the pressure distribution p(x) can be obtained as

$$p(x) = \lim_{\Delta x \to 0} \frac{\Delta F}{\Delta x} = \frac{2F}{\pi a^2} (a^2 - x^2)^{1/2}, \quad x \in L. \tag{B.38}$$

3. Substituting the pressure distribution obtained in Eq. B.38 into B.35 will give a displacement, a part from the constant term, which corresponds to the punch with a radius R, thus

$$v(x) = - \frac{F(1-\nu)}{\pi a^2 G} x^2 = - \frac{x^2}{2R} \qquad x \in L \tag{B.39}$$

which links the force F to the contact area (actually length) 2a, the constants of the material and the radius R, i.e.

$$\frac{F(1-\nu)}{\pi a^2 G} = \frac{1}{2R} \tag{B.40}$$

4. Finally a 2-D contact problem between two elastic solids with circular profiles of radii R_1, R_2, will be solved by considering all the results obtained above, and the assumptions and conditions used in the 3-D Hertz theory.

Referring to Eq. B.3 in the 3-D Hertz theory, vertical displacements v_1, v_2 of the two solids must again hold the following condition,

$$v_1 + v_2(x) = H - d(z_2, z_1) \qquad x \in L \tag{B.41}$$

where H is the approach of the solid surfaces, i.e.

$$d(z_2, z_1) = f_2(x) + f_1(x) = \frac{x^2}{2R_2} + \frac{x^2}{2R_1} \qquad x \in L \tag{B.42}$$

The contact pressure is then simulated by the one obtained in Eq. B.38, i.e.

$$p(x) = \frac{2F}{\pi a^2}(a^2 - x^2)^{1/2} \qquad x \in L \tag{B.43}$$

where the total force F can be obtained by considering Eqs. B.39, B.40 and B.41 as

$$F = \frac{1}{2}\left(\frac{1}{R_1} + \frac{1}{R_2}\right) \frac{\pi a^2 G_1 G_2}{G_1(1-\nu_2) + G_2(1-\nu_1)} \tag{B.44}$$

(G_i, ν_i (i= 1,2) are shear moduli and Poisson's ratios of solids S_1, S_2 respectively).

Method 4 (Singular Integral Equations)

Method 4, which we also call the singular integral equation (abbreviated as SIE) approach, is applied to a contact problem, occurring on a half-plane, where either a slope of contact surface or a profile of a rigid punch is known a priori. The two SIEs will be considered in the following. The first one is applicable to frictionless problems and the other is applicable to frictional problems.

The first one can easily be obtained by differentiating Eq. B.35 with respect to x as,

$$v'(x) = \frac{2(1-\nu^2)}{\pi E} \int_L \frac{p(t)}{t-x}\, dt \tag{B.45}$$

where $v'(x) = dV(x)/dx$ and ν, E are the Poisson's ratio and the modulus of elasticity of the half-plane, respectively.

The SIE, obtained in Eq. B.45 with the singular kernal $1/(t-x)$, is the Fredholm integral equation of the first kind with an unknown pressure p(t). The integration is carried out in the sense of a Cauchy principal value.

The second SIE can be derived in the same manner from the equation of vertical (boundary) displacement which is obtained by considering not only pressure p(t), that led to Eq. B.35, but also shear stress q(t). After differentiating such an equation, one comes up with

$$\int_L \frac{p(t)}{t-x}\,dt = -\frac{\pi(1-2\nu)}{2(1-\nu)}\,q(x) + \frac{\pi E}{2(1-\nu^2)}\,v' \qquad (B.46)$$

If the shear stress q(t) applied over a contact surface L is set as $q(x) = k\,p(x)$, where k is a constant coefficient of friction, so that the contact simulates a quasi-statically sliding motion, one obtains the second SIE as,

$$p(x) - \frac{2(1-\nu)}{\pi k(1-2\nu)} \int_L \frac{p(t)}{x-t}\,dt = \frac{E\,v'(x)}{k(1-2\nu)(1+\nu)} \qquad x \in L \qquad (B.47)$$

which is a Fredholm integral equation of the second kind.

The first SIE in Eq. B.45 can be considered as an integral equation, involving the finite Hilbert transform H_L defined as

$$H_L(p) = \frac{1}{\pi} \int_L \frac{p(t)}{t-x}\,dt \qquad x \in L \qquad (B.48)$$

where the surface L is a bounded interval.

Unlike the usual Hilbert transform, i.e. $L = \mathbb{R} = (-\infty, \infty)$ in Eq. B.46, which is a bounded (hence continuous) linear operator mapping $L^p(\mathbb{R})$ into $L^p(\mathbb{R})$ ($L^p(\mathbb{R})$ = Lebesque space; $1 < p < \infty$) and is a unitary operator, i.e. a (bounded) isometric bijective operator, if p=2, the finite Hilbert transform cannot be simply inverted for solving Eq. B.45 since v'(x) is not known at $x \in \mathbb{R}\setminus L$ even if p(x) = 0

at $x \in \mathbb{R}\backslash L$.

The frictionless contact problem, described by Eq. B.45, can be solved on the basis of the theory of hyperfunctions (see e.g. Imai [53], Kaneko [60]). These singular integral equations were classically studied and applied in various elasticity problems by Muskhelishvili [87], Tricomi [132] and Vekua (see Muskhelishvili [87]).

Furthermore, it is noted that such singular integral equations will also be easily transformed to Riemann-Hilbert problems, considered in the following Method 7, where the concept of the theory of hyperfunctions will naturally appear.

Method 6 (Fourier Transform)

This method (see Gladwell [41]) is straightforward, once the (displacement) potentials, namely Papkovich-Neuber potentials, for the displacement solution of the 2-D problem, where no body forces are present, are explicitly given by means of a Fourier transform. It is capable of solving contact problems where the slopes are given a priori, just like Methods 2, 4 and 5. A summary of this method will be stated in the following:

1. The two displacement potentials, B and A, are put, by means of the conjugate (or inverse) Fourier transform F* as

$$B(x,y) = F^* \left(|t|t^{-2} M(t) \exp(-|t|y) : t \to x\right) \tag{B.49a}$$

and

$$A(x,y) = F^* \left(t^{-2} N(t) \exp(-|t|y) : t \to x\right) \tag{B.49b}$$

where the conjugate Fourier transform F* is defined as $F^*(f(t)) = (F^*f)_{(x)} = (2\pi)^{1/2} \int_R f(t) \exp(-itx)\, dt$ for an arbitrary function $f(t)$, $y > 0$.

We will assume for now that the functions mapped by Fourier transform F have nice properties on operations such as the inversion formula, i.e. $F^*Ff = f$ and $FF^*g = g$ and differentiabilities. For example, if the Fourier transform denoted by F is defined on a linear space S (defined later), then $F: S_x \to S_t$ is bijective. The space S is a dense subset of the space $L^p(\mathbb{R}^n)$, $1 < p < \infty$. The determination of M(t) and N(t) in Eqs. B.49 is essentially the problem of this method, which can be found in the following way.

2. Substitute the potentials B, A in Eqs. 3.49 into the following expressions of displacements (u, v) and stresses (T_{xx}, T_{xy}, T_{yy}) which are given in matrix form as:

$$\begin{pmatrix} u \\ v \end{pmatrix} = \frac{1}{2G} \begin{bmatrix} -y D_x & -D_x \\ (K - y K_y) & -D_y \end{bmatrix} \begin{pmatrix} B \\ A \end{pmatrix} \qquad \text{(B.50a)}$$

and the stresses are

$$\begin{pmatrix} T_{xx} \\ T_{xy} \\ T_{yy} \end{pmatrix} = \begin{bmatrix} 2\nu D_y - y D_{xx} & -D_{xx} \\ (1-2\nu) D_x - y D_{xy} & D_{xy} \\ 2(1-\nu) D_y - y D_{yy} & D_{yy} \end{bmatrix} \begin{pmatrix} B \\ A \end{pmatrix} \qquad \text{(B.50b)}$$

where G is the shear modulus, $K = 3 - 4\nu$, ν the Poisson's ratio,

and D_x, D_{xy} etc. are, as usual, referred to as the partial derivative operators, e.g. D_x and D_{xy} denote the partial derivative operators with respect to x and to both x and y respectively.

Now Eqs. B.50 for the displacements and the stresses are functions of the unknown functions M(t) and N(t) in Eq. B.49, which can be compactly expressed as

$$\underline{u} = F^*(\underline{f}(M(t), N(t)) \tag{B.51a}$$

and

$$\underline{T} = F^*(\underline{g}(M(t), N(t)) \tag{B.51b}$$

where $(\underline{\cdot})$ denotes a vector so that $\underline{u} = (u,v)$ and $\underline{T} = (T_{xx}, T_{xy}, T_{yy})$ and the conjugate Fourier transform F* operates on the vector functions $\underline{f}$ and $\underline{g}$ containing the unknowns M(t) and N(t).

3. Operating the Fourier transform F in Eqs. B.53, considering that the Fourier inversion formula holds, one obtains:

$$F(\underline{u}) = \underline{f}\ (M(t), N(t)) \tag{B.52a}$$

and

$$F(\underline{T}) = \underline{g}\ (M(t), n(t)) \tag{B.52b}$$

Next, the unknowns M(t), N(t) can be linked with stress boundary conditions given by

$$T_{xy}(x,0) = 0, \quad T_{yy}(x,0) = -P(x), \quad x \in (-\infty, \infty) \tag{B.53a,b}$$

which imply that contact problems considered by this method should be frictionless. Considering the boundary condition of

the shear stress (the first equation in Eq. B.53) and $F(T_{xy})$ in Eq. 52b, the following equation can be found

$$(1-2\nu)\ M(t) + N(t) = 0 \tag{B.54}$$

Then the boundary condition of the (unknown) pressure (the second equation in Eqs. B.53). $F(T_{yy})$ in Eq. B.52b and Eq. B.54 will give

$$T_{yy}(x,o) = -F^*\ (M(t)) = -\ p(x) \tag{B.55}$$

thus obtaining

$$M(t) = F(p\ (x)\ ) = P\ (t) \tag{B.56}$$

Hence, once the mixed boundary conditions for a contact problem, where a displacement (or its slope) of an elastic half-plane is prescribed, are given, the problem is reduced to a pair of integral equations, which can be solved by a further reduction to a singular integral equation, expressed by means of a finite Hilbert transform, which already appeared previously in Methods 4 (and 5). The steps to obtaining such an integral equation will be briefly described by considering the following contact problem.

4. A frictionless contact problem over a contact surface $L = (-a,a)$ is specified by the boundary conditions

$$v(x,0) = f(x) + d \qquad x \in L \tag{B.57a}$$

$$T_{xy}(x,0) = 0 \qquad x \in \mathbb{R} \equiv (-\infty,\infty) \tag{B.57b}$$

$$T_{yy}(x,0) = 0 \qquad x \in \mathbb{R}\backslash L \tag{B.57c}$$

Considering these boundary condtions for the vertical

displacements and the normal stesses given in Eqs. B.51, it is easily reduced to the following pair of integral equations:

$$\frac{(1-\nu)}{G} F^*(-i \text{ sign } (t)\ P(t)) = \frac{df(x)}{dx}\ , \quad x \in L \qquad \text{(B.58a)}$$

$$F\ (P(t)) = 0 \qquad x \in \mathbb{R}\backslash L \qquad \text{(B.58b)}$$

From a relationship established between the Fourier and Hilbert transform, Eq. B.58a can be reduced to a singular integral equation, after considering Eq. B.58b;

$$\frac{1-\nu}{G\pi} \int_L \frac{p(t)}{t-x}\, dt = \frac{df(x)}{dx}\ , \qquad x \in L \qquad \text{(B.59)}$$

since

$$F^*(-1 \text{ sign } (t)\ P(t)) = H(p(t)) \quad (\text{in } L^2(\mathbb{R})) \qquad \text{(B.60)}$$

where $H(\cdot)$ is the Hilbert transform defined by

$$H(\cdot) = \frac{1}{\pi} \int_{\mathbb{R}} \frac{(\cdot)}{t-x}\, dt\ , \qquad x \in \mathbb{R} \qquad \text{(B.61)}$$

It is noted that Eq. B.60 is obtained by means of a character of Fourier transform which is a unitary operator on $L^2(\mathbb{R})$, i.e. Eq. B.60 holds only if $p(t) \in L^2(\mathbb{R})$, although the Hilbert transform in Eq. B.61 is an automorphism of $L^p(\mathbb{R})$, $1 < p < \infty$, and also a unitary map on $L^2(\mathbb{R})$.

Since the Fourier transform is exclusively used as the main tool in this method, a few theorems related to the inversion formula and differentiabilities of (conjugate) Fourier transforms are stated below without proof (see e.g. Treves [131], Mizohata [84] and Kuroda [69], Hormander [51], Tanabe [121]).

Theorem 1. If $f(x) \in L^1(\mathbb{R}^n) \cap L^p(\mathbb{R}^n)$, $1 \leq p < \infty$, then

$$f(x) = \lim_{\varepsilon \to 0} (2\pi)^{-n/2} \int_{\mathbb{R}} (Ff)(t) \exp(-\varepsilon|t|^2 + itx)\, dt \qquad \text{(in } L^p\text{)} \tag{B.62}$$

which holds in the sense of L^p-Gaussian sum.

The theorem is practically important. If $f(x) \in L^1(\mathbb{R}^n)$, then $(Ff)(t)$ is bounded and uniformly continuous, but not generally in $L^1(\mathbb{R}^n)$. Hence, the inversion will not be assured, and assuming $(Ff)(t)$ in $L^1(\mathbb{R}^n)$ is not practically useful.

While the Fourier inversion formula is well defined in the function spaces such as $L^2(\mathbb{R}^n)$, S (i.e. space of rapidly decreasing test functions) and its dual S' (i.e. space of tempered distributions) the usefullness of the theorem can be inferred from the following example (appearing in contact problems). That is, if $f(x)$ is given by

$$f(x) = \begin{cases} x^{-1/2} & x \in (0,1] \\ 0 & x > 1 \end{cases} \tag{B.63}$$

then $f(x) \in L^1(\mathbb{R})$, but $f(x) \in L^2(\mathbb{R})$.

Theorem 2. Let $f(x) \in L^1(\mathbb{R}^n)$ in all the following cases. if a function $f \in C_0^m(\mathbb{R}^n)$, i.e. the closure of the set $\{x: D^m f(x) \neq 0\}$ is bounded, or $f(x)$ is such that $|x|^n |D^a f(x)| \to 0$ (uniformly) as $|x| \to \infty$ and $D^a f(x) \in L^1(\mathbb{R}^n)$, $|a| < m-1$, then

1. $F(D^a f(x)) = (it)^a F(f(x))$ $\qquad |a| \leq m,\ i = (-1)^{1/2}$ $\qquad$ (B.64a)

2. $|t^a (Ff)(t)| \leq \|D^a f(x)\|_{L^1}$ $\qquad |a| \leq m$ $\qquad$ (B.64b)

where $D^a f(x) = (D_{x_1})^{a_1} + \ldots + (D_{x_n})^{a_n} = (\frac{\partial}{\partial x_1})^{a_1} + \ldots + (\frac{\partial}{\partial x_n})^{a_n}$,
$a = (a_1, \ldots, a_n) \in N^n$ $|a| = a_1 + a_2 + \ldots + a_n$, $(it)^a = (it_1)^{a_1} \ldots (it_n)^{a_n}$

If $(1+|x|)^m f(x) \in L^1(\mathbb{R}^n)$ (in $\mathbb{R}$, $x^m f(x) \in L^1(\mathbb{R})$), $m \geq 0$.

3. $$D^a (Ff)_{(t)} = F((-ix)^a f(x)), \quad |a| \leq m \tag{B.65a}$$

4. $$|D^a (Ff)_{(t)}| \leq \| x^a f(x) \|_{L^1} \quad |a| \leq m \tag{B.65b}$$

If $f(x) \in C_o^{2n}(\mathbb{R}^n)$, the Fourier inversion formula holds, i.e.

$$F^*F = I \quad \text{in } L^1(\mathbb{R}^n_x) \tag{B.66a}$$

$$FF^* = I \quad \text{in } L^1(\mathbb{R}^n_t) \tag{B.66b}$$

$$\|Ff\|_{L^2} = \|F^*f\|_{L^2} = \|f\|_{L^2} \qquad \text{(Parseval-Plancherel)} \tag{B.66c}$$

where I is an identity operator.

If $f(x) \in C_o^{2n}(\mathbb{R}^n)$, then the Fourier inversion formula holds, i.e. $F^* F = I$ in $L^1(\mathbb{R}^n_x)$ and $FF^* = I$ in $L^1(\mathbb{R}^n_t)$.

The above theorems are important when handling the Fourier transform on $L^1(\mathbb{R}^n)$ space, since the Fourier image (transform) of a function in $L^1(\mathbb{R}^n_x)$ is not necessarily in $L^1(\mathbb{R}^n_t)$, without further restrictions on functions in $L^1(\mathbb{R}^n_x)$. The Fourier images on L^2-functions, however, are always in L^2-spaces, i.e. Fourier transform on $L^2(\mathbb{R}^n_x)$ is a unitary operator, mapping $L^2(\mathbb{R}^n)$ into itself, and the inverstion formula holds in the L^2-sense. Although many types of functions, coming up in physical problems, are in L^1, L^2 or $L^1 \cap L^2$, there are still various functions not in these spaces. For example, if a function $f(x) = 1$ (or any other constants) for all x in $\mathbb{R}$, then

the function does not belong to neither of the above spaces. This requires us to consider a larger space, which is a dual space (S') of the space of rapidly decreasing test functions (S), i.e. S' is a collection of continuous linear functionals on S, and an element of S' is called a tempered (or temperate) distribution. The following inclusions of the spaces $L^p(\mathbb{R}^n)$, S and S' (in $\mathbb{R}^n$) are known,

$$D \overset{d}{\subset} S \overset{d}{\subset} L^p \subset S' \subset D' \qquad (1 \leqslant p \leqslant \infty) \qquad (B.67)$$

where D is a space of test functions (i.e. If $f \in D$, $f \in C_o^\infty(\mathbb{R}^n)$ and D' is its dual space; and element in D' is called a Schwartz distribution (or a generalized function); for arbitrary sets A and B, $A \overset{d}{\subset} B$ means A is a dense subset of B so that the closure of A is identical to B ($\bar{A} = B$).

However, for frictionless contact problems, only L^p spaces (p = 1 or 2) would be necessary since contact stresses are known to vanish outside the (finite) contact surface (i.e. contact stresses belong to $C_o^m(\mathbb{R}^n)$) even if an infinite elastic domain is considered to be one of the contacting solids.

Method 7 (Complex Variable Method)

This method is derived on the basis of the theory of complex functions by Muskhelishvili [86,87], which is applicable to various complicated 2-D elasticity problems, including contact problems (frictionless, frictional and adhesive contacts). We will sometimes call this method the complex variable method (abbreviated as CVM).

Every contact problem will be reduced to a pair of governing equations which are referred to as the Riemann-Hilbert problem with a solution, being holomorphic except (a bounded interval of) the real axis, from which contact stresses can be determined. Such a holomorphic function is said to be a sectionally holomorphic function, and is also sometimes called a complex potential. Besides in the following, the contact problem described as a Riemann-Hilbert problem is shown to be intimately linked to the singular integral equations obtained in the previous methods (4, 5 and 6).

Since the details of this method are well described in Appendix A (see section 9, in particular) and in Chapter 4, only some of the results will be given in the following where $\mathbb{C}$ and $\mathbb{R}$ denote the complex plane and the real axis, respectively.

Let $\Phi(z)$ be a holomorphic in $\mathbb{C}\backslash\mathbb{R}$. Then the stresses and the rotations in a half-plane are expressed as (Eqs. A.60 and A.61):

$$T_{yy} - i\,T_{xy} = \Phi(z) - \Phi(z) + (z-z)\,\bar{\Phi}'(z) \tag{B.68}$$

$$2G(u_{,x} + iv_{,x}) = K\,\Phi(z) + \Phi(z) - (z-\bar{z})\,\bar{\Phi}'(z) \tag{B.69}$$

where G is the shear modulus; $K = 3-4\nu$ (for plane strain condition), ν = Poisson's ratio; both notations "$'$" and "$,$" denote the ordinary derivative with respect to x. Let S_1 and S_2 be elastic solids. The stresses at the boundary (i.e. the contact surface) on the real axis denoted by R can be expressed for S_1 and S_2 respectively as shown in Eqs. A.62a and A.62b. Therefore, the stresses in the solids, as well as on the contact surface, can be determined once the

function is found. If the undeformed profiles of the two solids are respectively given by the Holder continuous functions $f_1(t)$ and $f_2(t)$, then the following equation is derived, as a result of kinematics of contact surface (i.e. Eq. A.88), neglecting the horizontal displacements:

$$v_1 - v_2 = f_2(t) - f_1(t) \equiv f(t) \qquad t \text{ on } L \tag{B.70}$$

where v_i are the vertical displacements for the solids S_i $(i=1,2)$ and $L \subset \mathbb{R}$ denotes a set of points of the contact surface.

Differentiating Eq. B.70 with respect to t gives

$$v_{1,t} - v_{2,t} = f'(t) \tag{B.71}$$

Substituting the boundary values of Eq. B.69 (i.e. Eqs. A.85 and A.86) into Eq. 2.49, one obtains a Riemann-Hilbert problem as shown in Eq. A.95:

$$\begin{aligned} \Phi^+(t) &= q\,\Phi^-(t) + f_o && t \in L \\ \Phi^+(t) &- \Phi^-(t) = 0 && t \notin L \end{aligned} \tag{B.72}$$

where q and f_o are given in Eq. A.95; $\Phi^+(t)$, $\Phi^-(t)$ are limiting values.

Equation B.72 can be further reformulated by assuming that the form of the solution to the equation is given as

$$\Phi(z) = X(z)\,F(z) \tag{B.73}$$

where the functions $X(z)$ and $F(z)$ are both holomorphic in $\mathbb{C} \setminus L$ such that $X(z)$ is a solution of the homogeneous equation of Eq. B.74 (i.e. $f_o = 0$).

Substitution of $\Phi(z)$ in Eq. B.73 into Eq. B.72 leads to the following (i.e. Eq. A.113)

$$F^+(t) - F^-(t) = \frac{f_o}{X(t)^+} \qquad t \text{ on } L \qquad (B.74)$$

where $X^+(t) = q\, X^-(t)$.

The general solution to Eq. B.72 is then given (Eq. A.118) as,

$$\Phi(z) = \frac{X(z)}{2\pi i} \int_L \frac{f_o}{X(t)^+} \frac{dt}{(t-z)} + X(z)\, P_{n-1}(z) \qquad z \text{ on } C\, L \qquad (B.75)$$

where $P_{n-1}(z)$ is the polynomial function of the order (n-1). The function $X(z)\, P_{n-1}(z)$ is a homogeneous solution such that $X(z)P_{n-1}(z) \to 0$ as $|z| \to \infty$, since $\Phi(z)$ is imposed to vanish at infinity.

Then the contact pressure can be obtained (as shown in Eqs. A.62a,b) from Eq. B.68 as.

$$P(t) - i\, T(t) = \Phi^+(t) - \Phi^-(t) \qquad t \text{ on } L \qquad (B.76a)$$

$$\equiv \Phi^+(t+i0) - \Phi^-(t-i0) \qquad t \text{ on } L \qquad (B.76b)$$

where $P(t) = T_{yy}(t,0)$ and $T(t) = T_{xy}(t,0)$.

It is worth noting, regarding the character of $\Phi(z)$, that the difference in the two limiting values on the right hand side of Eq. 76b defines hyperfunction, e.g. Morimoto [85] implying that the stresses on the left hand side can be interpreted as hyperfunctions. A hyperfunction can be (loosely but sufficiently in applications) defined and interpreted as follows. Let a domain D, containing a part (or all) of the real axis Γ, be in the complex plane such that, $D_+ = \{z = x+iy \text{ in } D:\ y > 0\}$ and $D_- = \{z = x+iy \text{ in } D:\ y < 0\}$. Let $F_+(z)$ and $F_-(z)$ be holomorphic in D_+ and D_-, respectively. Then a hyperfunction $f(x)$ is defined as

$$f(x) = \lim_{\varepsilon \to 0} \{F_+(x+i\varepsilon) - F_-(x-i\varepsilon)\} \qquad x \text{ on } D \cap \mathbb{R} \qquad (B.77a)$$

$$= F_+(x+i0) - F_-(x-i0) \qquad x \text{ on } D \cap \mathbb{R} \qquad (B.77b)$$

$f(x)$ is an ordinal function if the limit in Eq. B.77a exists, e.g., $F_+(z) = z$, $F_-(z) = 0$ then $f(x) = x$. But the Dirac delta function (distribution) for example, will not be defined in that sense, i.e. let $F(z) = F_+(z) = F_-(z) = \frac{-1}{2\pi i}\left(\frac{1}{z}\right)$, then the Dirac delta function $\delta(x)$ is defined as

$$\delta(x) = -\frac{1}{2\pi i}\left[\frac{1}{x + i0} - \frac{1}{x - i0}\right] \qquad (B.78)$$

which has only a symbolic meaning, with a compact support at one point $x = 0$.

The pair of holomorphic functions, $F_+(z)$ and $F_-(z)$, in Eqs. B.77 are called defining functions (e.g. Morimoto [85], Kaneko [60] and Imai [53]). While in contact problems, a hyperfunction in Eqs. B.77 defines contact stresses (in a form of complex functions) as shown in Eqs. B.76 with a defining function given by B.75, densities of sheet vortex and line source in fluid mechanics (e.g. Batchelor [12]) on $\mathbb{R} \cap D$ can also be defined in the same way if the velocity vectors in D_+ and D_- are irrotational solenoidal fields, i.e. for a velocity vector $\underline{v}$ in D_+ (or D_-), it must be such that div $\underline{v} = 0$ and curl $\underline{v} = \underline{0}$ in D_+ (or D_-). A common thing to both contact and fluid mechanics is that physical values such as contact stresses, sheet vortex and line source are defined at the discontinuous surface (line).

II. A LINK BETWEEN THE COMPLEX VARIABLE METHOD (METHOD 7) AND THE SINGULAR INTEGRAL EQUATION APPROACH (METHODS 4, 5 AND 6)

We will consider the following boundary-value problem where surface tractions over a surface L are assumed to be described by

$$P(t) = -p(t), \quad T(t) = -c\,p(t), \ (c = \text{a constant}) \text{ on } L \tag{B.79}$$

where $P(t)$ and $T(t)$ denote respectively, the pressure and the tangential stress distributed over the surface L.

We will evaluate the slope of the surface L due to the tractions in Eq. B.79. Using Eq. B.76a,b (i.e. Eq. A.62a,b), then the above stresses are given by means of a sectionally holomorphic function as,

$$\begin{aligned} \Phi^{+}(t) &= \Phi^{-}(t) = P(t) + i\,T(t) \\ &= -\,p(t)\,(1+ic) \qquad\qquad t \text{ on } L \end{aligned} \tag{B.80}$$

The above equation corresponds to one of the Riemann-Hilbert problems of this kind. Hence, recalling the Plemelj formuale (e.g. Eq. A.57 and A.58), a particular solution to Eq. B.80 can be shown as

$$\Phi_o(z) = \frac{1}{2\pi i} \int_L \frac{-p(t)\,(1+ic)}{t-z}\,dt \tag{B.81}$$

which satisfies the second equation (Eq. A.58) of the Plemelj formulae as,

$$\Phi_o^{+}(t) + \Phi_o^{-}(t) = \frac{1}{\pi i} \int_L \frac{-p(s)\,(1+ic)}{s-t}\,ds \tag{B.82}$$

or

$$\begin{aligned} i(\Phi_o^{+}(t) + \Phi_o^{-}(t)) &= \frac{1}{\pi} \int_L \frac{-p(s)\,(1+ic)}{s-t}\,ds \\ &= H_L\,(-p(1+ic)) \end{aligned} \tag{B.83}$$

where H_L denotes the finite Hilbert transform (Eq. B.48). The general solution can be expressed as

$$\Phi(z) = \Phi_o(z) + \Phi_*(z) \qquad t \text{ on } L \qquad (B.84)$$

where $\Phi_*(z)$ is the difference between the general and the particular solutions, which means that $\Phi_*(z)$ is a homogeneous solution to Eq. B.80.

Since $\Phi_*(z)$ is such that

$$\Phi_*^+(t) - \Phi_*^-(t) = 0 \qquad t \text{ on } L \qquad (B.85)$$

and $\Phi(z)$ must vanish at infinity, $\Phi_*(z)$ vanishes in the entire complex plane including infinity. Thus the general solution $\Phi(z)$ is given by $\Phi_o(z)$ in Eq. B.81, i.e. $\Phi(z) = \Phi_o(z)$.

Once the pressure $p(t)$ in Eq. B.79 is given, we can evaluate Eq. B.81, from which the slope of the surface L will be determined by means of Eq. B.69 (Eq. A.61).

In two-dimensional elasticity, surface tractions and the corresponding slope of the surface are linked by the following integral equation (see e.g. Spence [124], Johnson [55]):

$$T(t) + A\, H_L(P(s)) = B\, v' \qquad t \text{ on } L \qquad (B.86)$$

where H_L is the finite Hilbert transform (Eq. B.48) and A and B are material constants given by

$$A = \frac{2(1-\nu)}{1-2\nu} \quad \text{and} \quad B = \frac{E}{(1-2\nu)(1+\nu)}$$

If one considers a contact problem with limiting friction (i.e. $T(t) = -k\,P(t)$, k = constant of friction), then Eq. B.86 is reduced to the singular integral equation (Eq. B.47). Such a singular integral equation, governing contact problems, can be transformed to a corresponding Riemann-Hilbert problem by considering Eqs. B.80, B.83 and B.86, and setting the constant c in Eq. B.79 to be the constant of friction.

First, substituting Eqs. B.80 and B.83 into Eq. B.86, and arranging it, one obtains

$$\left(1 + \frac{Ai}{k}\right)\,\Phi^{+}(t) - \left(1 - \frac{Ai}{k}\right)\,\Phi^{-}(t) = -\frac{1+ik}{k}\,B\,v' \qquad (B.87)$$

Dividing both sides of the above equation by $(1 + Ai/k)$ and rearranging, one obtains the Riemann-Hilbert problem for contact problems as,

$$\Phi^{+}(t) = g\,\Phi^{-} + f_o \qquad t \text{ on } L \qquad (B.88a)$$

where $$g = \frac{1-Ai/k}{1+Ai/k} = -\frac{2(1-\nu) + ik\,(1-2\nu)}{2(1-\nu) - ik\,(1-2\nu)}$$

and

$$f_o = \frac{i(1+ik)\,E\,v'}{(1+\nu)\,(2(1-\nu) - ik\,(1-2\nu))}$$

The associated equation for Eq. B.88a is given by

$$\Phi^{+}(t) - \Phi^{-}(t) = 0 \qquad t \text{ on } R\backslash L \qquad (B.88b)$$

It is noted that Eq. B.88a has the same form as Eq. B.72 (Eq. A.95). If a solid S_1 is assumed to be rigid in Eq. A.95, then Eq.

A.95 becomes identical to Eq. B.88a. Therefore, the Riemann-Hilbert problem, described by Eqs. B.88a,b, which governs a frictional contact problem (e.g., between a rigid punch and an elastic-half-plane), is seen to be equivalent to the singular integral equation in Eq. B.47. An equivalent relationship for a frictionless contact problem can also be obtained.

III. TWO COMPUTATIONAL METHODS FORMULATING CONTACT PROBLEMS

Method 1 : Finite Element Method

There are many works on contact analysis based on the displacement finite element methods, starting in the beginning of the 1970's, e.g. Wilson and Parles [137], Ohte [104], Chan and Tuba [16], Gaertner [35], Tsuta and Yamaji [134], and Okamoto and Nakazawa [105], while there are a few works based on the hybrid finite element method, e.g. Pian and Kubomura [111], and the mixed finite element method, Oden [94], and Tseng and Olsen [135]. The hybrid finite element methods is obtained by regarding continuity requirements across interelement boundaries as constraints and using the method of Lagrange multipliers to enforce the constraints in an average variational sense. Although both these methods, based on the Lagrange multipliers, would be very useful for some special problems, unlike the displacement method, it will be extremely tedious for the formulation and hard to satisfy the stability of solutions.

Only the contact analysis based on the displacement finite element method is reviewed here, by considering two elastic solids in contact as shown in Fig. B.1.

We follow the formulation by Okamoto and Nakazawa [105] who considered the contacting solids being subjected to incremental loading. Then for each solid S_i (i = 1 or 2 hereafter), assuming the contact stresses being external tractions, the following standard equilibrium equation due to the incremental virtual work can be shown:

$$\int_{V_i} \Delta \underset{\sim}{T} : \delta \Delta \underset{\sim}{e} dV = \int_{V_i} \rho \Delta \bar{\underline{f}} \cdot \delta \Delta \underline{u} dV + \int_{S_t} \Delta \bar{\underline{t}} \cdot \delta \Delta \underline{u} dS + \int_{S_c} \Delta \underline{R} \cdot \delta \Delta \underline{u} dS \qquad (B.89)$$

where Δ stands for an increment, $\underset{\sim}{T}$ the Cauchy stress, $\underset{\sim}{e}$ the engineering strain, V_i the volume of the solid S_i, ρ the mass density, $\bar{\underline{f}}$ the given force per unit mass, $\underline{u}$ the displacement vector, $\bar{\underline{t}}$ the given traction force, S_t the surface where the traction force is applied, $\underline{R}$ the contact force and S is the contact surface ($\bar{(\cdot)}$ describes a prescribed quantity).

We then can obtain the stiffness equations for the solids S_1 and S_2 by considering a reasonable displacement field. The stiffness equation for the solid S_1 is

$$\underline{\underline{K}}^{(1)} \underline{q}^{(1)} = \Delta \bar{\underline{Q}}^{(1)} + \Delta \underline{Q}_r \qquad (B.90a)$$

and for the solid S_2

$$\underline{\underline{K}}^{(2)} \underline{q}^{(2)} = \Delta \bar{\underline{Q}}^{(2)} - \Delta \underline{Q}_r \qquad (B.90b)$$

where $\underline{\underline{K}}^{(i)}$ is the (standard) stiffness matrices, $\underline{q}^{(i)}$ the nodal displacement vectors, $\Delta \underline{Q}^{(i)}$ the equivalent nodal forces obtained from

the first and the second term in Eq. B.89.

The second terms of the right hand side in Eqs. B.90a,b are given by

$$\Delta Q_r = \int_{S_c} \Delta \underline{R} \cdot \delta \Delta \underline{u} \, dS \tag{B.91}$$

Equation B.91 cannot be integrated since the contact force vector $\underline{R}$ is unknown, hence ΔQ_r is treated as an unknown variable vector.

Considering the contact conditions such as open, stick, sliding and mixed conditions for displacements and stresses on the contact surface (see Okamoto and Nakazawa [105]), the following equation is finally obtained from Eqs. B.90a,b,

$$\begin{bmatrix} \underline{\underline{K}}^{(1)} & \underline{\underline{0}} & \underline{\underline{K}}^{(1c)} \\ \underline{\underline{0}} & \underline{\underline{K}}^{(2)} & \underline{\underline{K}}^{(2c)} \\ \underline{\underline{K}}^{(c1)} & \underline{\underline{K}}^{(c2)} & \underline{\underline{K}}^{(cc)} \end{bmatrix} \begin{Bmatrix} \Delta \underline{q}^{(1)} \\ \Delta \underline{q}^{(2)} \\ \Delta \underline{R}^{*} \end{Bmatrix} = \begin{Bmatrix} \Delta \underline{\bar{Q}}^{(1)} \\ \Delta \underline{\bar{Q}}^{(2)} \\ \underline{\delta}^{(c)} \end{Bmatrix} \tag{B.92}$$

where the matrices such as $K^{(1c)}$, $K^{(c1)}$ etc., and the vectors ΔR^* and $\delta^{(c)}$ came out from the contact conditions, e.g., for open condition (i.e. the points of surfaces of the two solids are not in contact), there are no contact forces implying that $\Delta R^*_{1i} = \Delta R^*_{2i} = 0$, i=x,y,z the local coordinates. If the surfaces on contact slide (locally) over, then the contact forces are $\Delta R^*_{1i} = -\Delta R^*_{2i} = +k \Delta R^*_z$ (i=x,y) where k is the constant of friction, and so on.

Since the stiffness matrices in the contact problems are not symmetric, the frontal solution technique based on the Crout's elimination is developed for solving the incremental equation in an iterative manner by trial and error.

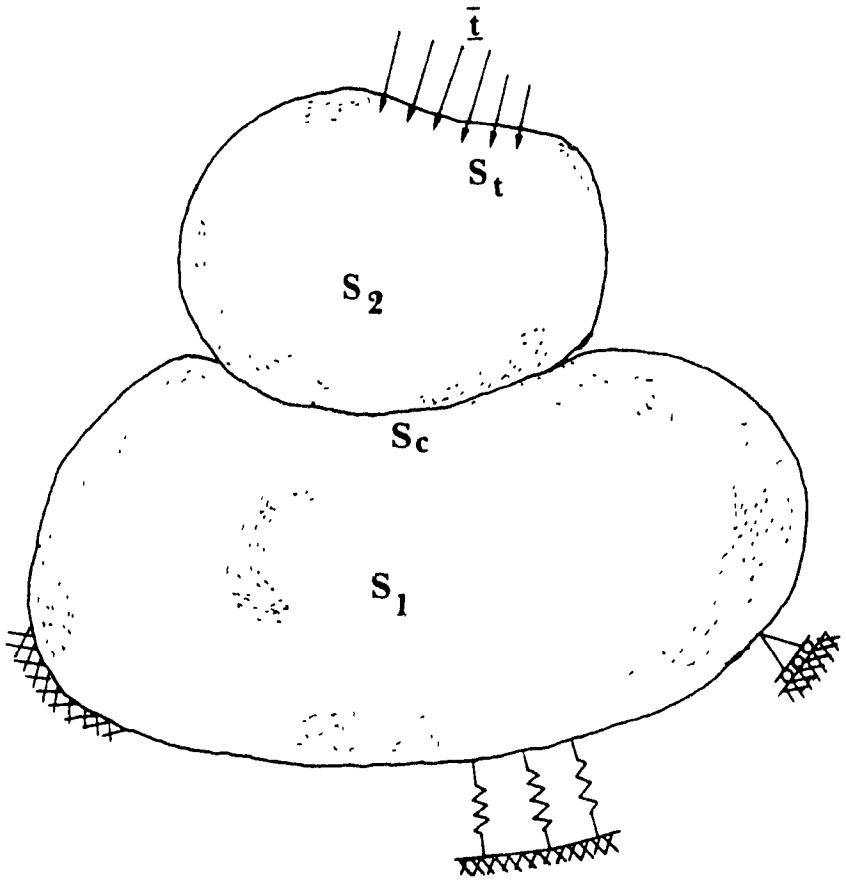


Fig. B.1 A Contact Problem Between Two Linearly Elastic Solids With Various Supports

Method 2:Variational Inequalities

Contact problems will be most naturally formulated, on the basis of the energy principles, as variational inequalities (e.g. Duvaut and Lios [24], Oden [94], Oden and Kikuchi [96] and Kikuchi [65,66]) in which the existence and uniqueness of solutions can be studied. One important physical law in elasticity theory was questioned by this approach (see e.g. Duvaut and Lions [24]). That is, when Coulomb's law is extended so as to apply the static frictional phenomena in elasticity, it leads to classes of boundary-value problems for which no existence theory is yet available, and even if a solution exists, its uniqueness is not guaranteed. In order to overcome such difficulties, more delicate analyses on friction have been carried out, e.g. Kikuch [64], Oden and Pires [99,100].

In order to describe a variational inequality for a contact problem, we will consider the well-known Signorini problem with no friction, avoiding complications appearing from pointwise friction problems, in which a linearly elastic solid comes into contact with a rigid foundation as shown in Fig. B.2. Discussing the variational inequality, we will use the terminologies in the abstract mathematics since it is rather difficult to make the statement clear without their use.

The elastic solid $\bar{D}$ (i.e. the closure of D) in $\mathbb{R}^3$ is the union of an open interior D, and the boundary ∂D. The boundary δD is assumed to consist of three disjoint parts ∂D_u, ∂D_t and ∂D_c, where ∂D_u and ∂D_t are the portions of the boundary on which the

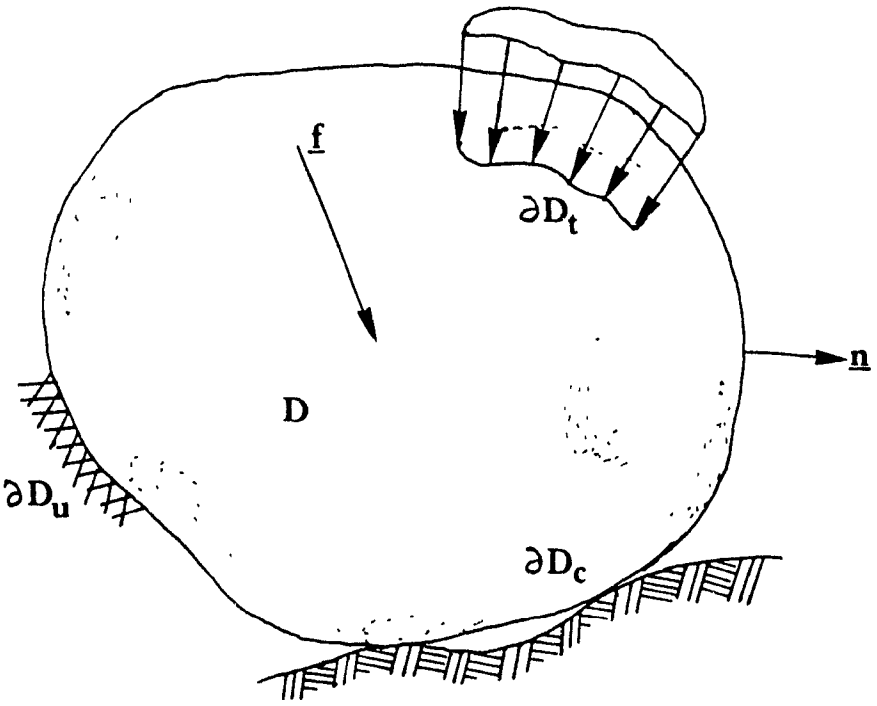


Fig. B.2 A Linearly Elastic Solid in Contact With a Rigid Frictionless Foundation

displacements and tractions are, a priori, prescribed respectively, and δD_c is the candidate contact surface which will be given, a posteriori, along with the tractions (i.e. contact pressures) on ∂D_c, after the application of loads. The external body forces on the solid consist of prescribed surfaces tractions t per unit surface area and of body force field intensity f per unit volume.

Assuming the particles within the open bounded domain D are in static equilibrium, then the translational equilibrium equation in terms of the Cauchy stress tensor $\underset{\sim}{T}$ holds:

$$\text{div}\,\underset{\sim}{T} + \underline{f} = \underline{0} \qquad \text{in } D \tag{B.93a}$$

or in componentwise

$$T_{ij,j} + f_i = 0 \quad (i,j=1,2,3) \text{ in } D \tag{B.93b}$$

where "," denotes the usual partial differentiation under the Cartesian coordinates and $(\underset{\sim}{\cdot})$ and $(\underline{\cdot})$ denote the quantities of the second order tensor and the vector respectively.

The boundary conditions on ∂D_u and ∂D_t are described as follows:

For the displacement boundary ∂D_u being perfectly fixed, the displacement field $\underline{u}$ is prescribed as

$$\underline{u} = \underline{0} \qquad \text{on } \partial D_u \tag{B.94}$$

and for the stress boundary ∂D_t, the prescribed traction $\bar{\underline{t}}$ is expressed as

$$\underline{n} \cdot \underset{\sim}{T} = \bar{\underline{t}} \qquad \text{on } \partial D_t \tag{B.95}$$

where the vector n denotes the unit outward normal to the whole boundary ∂D of D.

We note that since the solid is assumed to be linearly elastic, the Hooke's law holds so that the Cauchy stress is given as

$$\underset{\sim}{T} = \underset{\approx}{E} : \underset{\sim}{e} \tag{B.96a}$$

or in componentwise

$$T_{ij} = E_{ijkl}\, e_{kl} \tag{B.96b}$$

where E_{ijkl} are usual elastic constants of material and $\underset{\sim}{e}$ is the engineering strain tensor, i.e., $e_{ij} = 1/2\,(u_{i,j} + u_{j,i})$. Assuming that $u_{i,j} \equiv u_{j,i}$, then Eq. B.96b is

$$T_{ij} = E_{ijkl}\, u_{k,l} \tag{B.96c}$$

where the elasticity coefficients E_{ijkl} satisfy the following conditions:

1. $E_{ijkl} \in L^{\infty}(D)$, $\max_{1\leq i,j,k,l\leq 3} \| E_{ijkl}(x) \|_{L^{\infty}} \leq M \in \mathbb{R}^{+}$ (B.97)
2. $E_{ijkl} = E_{klij} = E_{jikl}$ a.e. in D (B.98)
3. there exists $C > 0$ such that
$$E_{ijkl}(x)\, A_{ij} A_{kl} > C\, A_{ij} A_{ij} \tag{B.99}$$
for all measurable symmetric second order tensors $\underset{\sim}{A}$.

The condition (1) in Eq. B.97 is to establish the boundness of the elasticity coefficients in the domain D, while condition (2), $E_{ijkl} = E_{klij}$, guarantees the existence of the strain energy function W(e) so that

$$\underset{\sim}{T} = \frac{\partial W}{\partial \underset{\sim}{e}} \tag{B.100}$$

Condition (3) is to suffice strict convexity of the strain energy function i.e.

$$W(h\,\underset{\sim}{e}^1 + (1-h)\,\underset{\sim}{e}^2) < hW(\underset{\sim}{e}^1) + (1-h)\,W(\underset{\sim}{e}^2) \tag{B.101}$$

for all strains $\underset{\sim}{e}^1$, $\underset{\sim}{e}^2 \in \mathbb{R}^6$ and $h \in [0,1]$ and also guarantees the coercivity of total potential energy, i.e. Let $F(\underline{u})$ be a total potential energy functional on the closed convex subset K (i.e. the kinematically admissible space) of the reflexive Banach space V. $K \subset V$. It is known that if $F(u)$ is coercive on K, i.e.

$$F(\underline{u}) \to \infty \qquad \text{as} \quad \|\underline{u}\|_K \to \infty \tag{B.102}$$

then $F(\underline{u})$ attains its minimum on K, i.e. there is at least one element (displacement field) $\underline{u} \in K$. which is unique if $F(\underline{u})$ is strictly convex. such that

$$F(\underline{u}) < F(\underline{v}) \quad \text{for all} \quad \underline{v} \in K \tag{B.103}$$

The coercivity of $F(\underline{u})$ is equivalent to the convexity and the differentiability (Gâteaux) of $F(\underline{u})$.

So far the boundaries ∂D_u and ∂D_t. of which the quantities are prescribed, have been considered. In the case of the boundary ∂D_c. although the surface of ∂D_c and any quantities are not known a priori. we can describe the conditions as constraints on ∂D_c prior to the application of loading as follows. First considering the (small) normal displacements of the boundary ∂D, which is restricted to the presence of the rigid foundation, one can impose a constraint due to

the fact that the normal displacement cannot exceed a (normalized) distance s away from the initial configuration of the solid, i.e.

$$\gamma_n(\underline{u}) - s \leqslant 0 \qquad \text{on } \partial D_c \tag{B.104}$$

where $\gamma_n(\underline{u})$ is the normal trace of the displacement $\underline{u}$, i.e. $\gamma_n(\underline{u}) = \underline{u}\cdot\underline{n}$ on ∂D_c for $\underline{u}$ being sufficiently smooth; s is given, after linearlization, as $s = (h(x) - g(x))n_3$; $h(x)$ and $g(x)$ are the functions describing the boundaries of the elastic solid and the rigid foundation respectively; n_3 is the component of the outward normal $\underline{n}$.

If $\underline{u}\cdot\underline{n} = s$, the contact is established, whilst $\underline{u}\cdot\underline{n} < s$ indicates the existence of the gap between the elastic solid and the rigid foundation. Hence Eq. B.104 represents a nonpenetration condition.

The next condition is due to the normal stress T_n, i.e., $T_n = T_{ij}n_in_j = E_{ijkl}u_{k,l}n_in_j$, depending on the contact

$$T_n = 0 \text{ if } \underline{u}\cdot\underline{n} < s \tag{B.105a}$$

and

$$T_n \leqslant 0 \text{ if } \underline{u}\cdot\underline{n} = s \tag{B.105b}$$

Equations B.105a,b imply that

$$T_n \leqslant 0 \qquad \text{on } \partial D_c \tag{B.106a}$$

$$T_n(u\cdot n - s) = 0 \qquad \text{on } \partial D_c \tag{B.106b}$$

Hence, summarizing the Signorini problem, a frictionless contact problem between an elastic solid and a rigid foundation, the displacement field must satisfy the following system of equations and inequalities:

1. Translational Equilibrium Equations

$$\text{div } \underset{\sim}{T}(\underline{u}) + \underline{f} = \underline{0} \qquad \text{in } D \tag{B.107}$$

2. Boundary Conditions

$$\underline{u} = \underline{0} \qquad \text{on } \partial D_u \tag{B.108}$$

$$\underline{n}\, T(\underline{u}) = \underline{t} \quad \text{on } \partial D_t \tag{B.109}$$

3. Contact Constraints

$$\left.\begin{aligned} &\underline{u}\cdot\underline{n} \leqslant s && (B.110)\\ &T_n(\underline{u}) \leqslant 0 && (B.111)\\ &T_n(\underline{u})\ (\underline{u}\cdot\underline{n} - s) = 0 && (B.112) \end{aligned}\right\} \text{ on } \partial D_c$$

Then the displacement field can be sought such that the displacements satisfy the equality and inequality equations, in Eqs. B.107 through B.112, in the variational sense. Such a variational problem is called the variational inequality problem. In order to establish such an inequality problem, one must define some function spaces for each physical quantity such as the displacements $\underline{u}$ in D and on ∂D, the body force $\underline{f}$ in D, the stresses $\underset{\sim}{T}$ in D and on ∂D as tractions, as follows.

Inside the open domain D, these quantities are defined on the standard Sobolev spaces $H^s(D)$ (see Adams [1], Sobolev [123], Oden [90,101], Mizohata [84], Hormander [51], Treves [131], Lions and Magenes [74])

$$\underline{u} \in (H^1(D))^3,\ \underline{f} \in (L^2(D))^3 \tag{B.113}$$

and

$$\underset{\sim}{T}(\underline{u}) \in (L^2(D))^6,\ \text{div } \underset{\sim}{T}(\underline{u}) \in (L^2(D))^3 \tag{B.114}$$

$$\text{Let } \tilde{L}(D) = \{\underset{\sim}{T}(\underline{u}) : \underset{\sim}{T}(\underline{u}) \in (L^2(D))^6 \text{ and div } \underset{\sim}{T}(\underline{u}) \in (L^2(D))^3\} \quad (B.115)$$

On the boundary ∂D, $\underline{u}$ and $\underset{\sim}{T}$ are defined by means of linear continuous mappings γ and $\bar{\gamma}$ so that

$$\gamma \text{ mapps } \underline{u} \in (H^1(D))^3 \text{ into } H^{1/2}(\partial D) \quad (B.116)$$

and

$$\bar{\gamma} \text{ mapps } \underset{\sim}{T}(\underline{u}) \in \tilde{L}(D) \text{ into } H^{-1/2}(\partial D_t) \quad (B.117)$$

i.e. for all $\underline{u} \in (H^1(D))^3$, $\gamma(\underline{u}) \in (H^{1/2}(\partial D))^3$

for all $\underset{\sim}{T}(\underline{u}) \in \tilde{L}(D)$, $\bar{\gamma}(\underset{\sim}{T}(\underline{u})) = \underline{n} \cdot \underset{\sim}{T}(\underline{u}) \in (H^{-1/2}(\partial D_t))^3$

The space of kinematically admissible displacements is defined as

$$V = \{\underline{v} \in (H^1(D))^3 : \underline{v} = \underline{0} \text{ a.e. on } \partial D_u\} \quad (B.118)$$

due to the perfect constraints assumed on ∂D_u.

The subset K of V so-called admissible space considering the constraints on ∂D_c is also defined as

$$K = \{\underline{v} \in V : \underline{n} \cdot \underline{v} \leq s \text{ in } H^{1/2}(D_c)\} \quad (B.119)$$

where $\underline{n} \cdot \underline{v}$ is interpreted in the sense of trace of functions in V onto ∂D_c, i.e. $\gamma_n(\underline{v}) = \gamma(\underline{v}) \cdot \underline{n} \equiv \underline{n} \cdot \underline{v} \in H^{1/2}(\partial D_c)$ which is the normal trace as shown in Eq. B.104. K is the closed, convex subset of V.

All the function spaces necessary for the variational principles were defined. Furthermore, the boundary of the domain D is assumed to be Lipschitzian, e.g. Adams [1], Fichera [31]. Applying the virtual work method, to the mixed boundary-value problem (Eqs. B.107, B.108,

B.109), i.e. multiplying the translational equilibrium equation in Eq. B.107 by an arbitrary displacement $\underline{v} \in V$ and using the Green-Gauss formula, one obtains

$$a(\underline{u},\underline{v}) = \langle \underline{f}, \underline{v} \rangle_D + \langle \bar{\gamma}(\underset{\sim}{T}(\underline{u})), \underline{v} \rangle_{\partial D} \tag{B.120}$$

where $a(u.v) = \int_D E_{ijkl}\, u_{k,l}\, v_{i,j}\, dV$ is the virtual work produced by the action of stresses $T_{ij}(\underline{u}) = E_{ijkl}\, u_{k,l}$ on strains caused by the virtual work $\underline{v}$; the right hand terms are virtual work done by the external forces such as body force $\underline{f}$ and the tractions $\bar{\gamma}(\underset{\sim}{T}(\underline{u})) = \underline{n}\cdot\underset{\sim}{T}(\underline{u})$ such that $\langle \underline{f}, \underline{v} \rangle_D = \int_D \underline{f}\cdot\underline{v}\, dV$ and $\langle \bar{\gamma}(\underset{\sim}{T}(\underline{u})), \underline{v} \rangle_{\partial D} \equiv \langle \underline{n}\cdot\underset{\sim}{T}(\underline{u}), \underline{v} \rangle_{\partial D} = \int_{\partial D} \underline{n}\cdot\underset{\sim}{T}(\underline{u}) \cdot \underline{v}\, ds$.

Now if $\underline{u}, \underline{v} \in V$, then $a(\cdot\,,\cdot)$ is a symmetric bilinear form mapping $V \times V \to \mathbb{R}$; $\langle \cdot\,,\cdot \rangle_D$ and $\langle \cdot\,,\cdot \rangle_{\partial D}$ are duality pairings such that

$$\langle \cdot\,,\cdot \rangle_D : (L^2(D))^3 \times (H^1(D))^3 \to \mathbb{R} \tag{B.121}$$

and

$$\langle \cdot,\cdot \rangle_{\partial D} : (H^{-1/2}(\partial D))^3 \times (H^1(D))^3 \to \mathbb{R} \tag{B.122}$$

Next we decompose the duality pairing $\langle \cdot,\cdot \rangle_{\partial D}$ into two parts; one is for the prescribed tractions on ∂D_t and another one is for the contact force on ∂D_c, i.e.

$$\langle \bar{\gamma}(\underset{\sim}{T}(\underline{u})), \underline{v} \rangle_{\partial D} = \langle \underline{t}, \underline{v} \rangle_{\partial D_t} + \langle T_n(\underline{u}), \underline{v} \rangle_{\partial D_c} \tag{B.123}$$

so that Eq. B.120 is

$$a(\underline{u},\underline{v}) = \langle \underline{f}, \underline{v} \rangle_D + \langle \underline{t}, \underline{v} \rangle_{\partial D_t} + \langle T_n(\underline{u}), \underline{v} \rangle_{\partial D_c} \tag{B.124}$$

for all $\underline{v} \in V$

Now we consider the subset K of V, which is equivalent to the constraints in Eqs. B.110, B.111, B.112; and suppose that the elastic solid is initially in contact so that Eqs. B.111 and B.112 are modified as

$$\left.\begin{aligned} T_n(\underline{u}) - \bar{T}_n \leqslant 0 \qquad & (B.125) \\ \text{and} \qquad (T_n(\underline{u}) - \bar{T}_n)\ (\underline{u}\cdot\underline{n} - s) = 0 \qquad & (B.126) \end{aligned}\right\} \text{ on } \partial D_c$$

where $T_n(\underline{u})$ and $\bar{T}_n$ are respectively, the normal stress due to the incremental load and the initial normal stress on ∂D_c.

Considering the inequalities in Eqs. B.125, B.126 on the subset K of V, the following inequality follows:

$$T_n(\underline{u})\ (\underline{w} - \underline{u})\cdot\underline{n} \geqslant -\bar{T}_n(\underline{w} - \underline{u})\cdot\underline{n} \qquad (B.127a)$$

or

$$T_n(\underline{u})\,(w_n - u_n) \geqslant -\bar{T}_n(w_n - u_n) \qquad (B.127b)$$

where $w_n = w\cdot n$ and $u_n = u\cdot n$.

The vector $\underline{u}$ is the true displacement sought, while $\underline{w}$ is the kinematically admissible displacement field with the constraint. Hence the difference of $\underline{w}$ and $\underline{u}$, $\underline{w} - \underline{u}$, is considered to be the kinematically admissible variation vanishing at the prescribed boundary ∂D_u. The inequality in Eqs. B.127a,b with Eq. B.124 finally yields the variational inequality of the Signorini contact problem:

$$a(\underline{u},\ \underline{w}-\underline{u}) \geqslant \langle \underline{f},\ \underline{w}-\underline{u}\rangle_D + \langle \underline{t},\ \underline{w}-\underline{u}\rangle_{\partial D_t} - \langle \bar{T}_n\underline{n},\ \underline{w}-\underline{u}\rangle \qquad (B.128)$$

$$\text{for all } \underline{w} \in K$$

Replacing the right hand side by $f(\underline{w}-\underline{u})$, Eq. B.128 is then compactly described as

$$a(\underline{u}, \underline{w}-\underline{u}) > f(\underline{w}-\underline{u}) \qquad \text{for all } \underline{w} \in K \tag{B.129}$$

For the above variational inequality problem, there exists a unique solution since $a(\cdot, \cdot)$ is coercive and $f \in V'$ (i.e. the dual space of V). If the solution is regular (i.e. sufficiently smooth), then it is also the solution to the classical Signorini problem.

In the case of two solids being linearly elastic, a variational inequality exactly the same type as that in Eq. B.129 is derived with the constraint set K. The constraint set K on the contact boundary in Eq. B.119 is replaced by,

$$K = \{(\underline{v}^1, \underline{v}^2) \in (H^1(D_1))^3 \times (H^1(D_2))^3 : \underline{v}^i \big|_{\partial D_u} = 0,$$
$$i = 1,2,\ v_n^1 + s \geq v_n^2 \text{ in } H^{1/2}(\partial D_c)\} \tag{B.130}$$

where $\underline{v}^i$ are the kinematically admissible displacements for the elastic solids D_i, $i=1,2$; s is the normalized gap between the two solids.

The variational inequality formulated for the two elastic solids in contact, which is under the consideration of the constraint set K in Eq. B.130, is defined as

$$a(\underline{u}, \underline{v}-\underline{u}) \geq f(\underline{v} - \underline{u}) \quad \text{for all } \underline{v} \in K \tag{B.131}$$

where

$$a(\underline{u}, \underline{v}) = \sum_{i=1}^{2} a_i(\underline{u}^i, \underline{v}^i) \tag{B.132}$$

$$f(\underline{v}) = \sum_{i=1}^{2} f_i(\underline{v}^1) \tag{B.133}$$

It is however, reported by Oden [94], and Oden and Kikuchi [96] that the direct approximation of Eq. B.131 on the constraint set $K \subset V$ is generally difficult. For this reason the numerical techniques called the penalty methods combined with the finite element methods (i.e. the penalty finite element methods) have been applied to the variational inequality problems, e.g. Oden, Kikuch and Song [97], Oden [94], and Oden and Kikuchi [96].

APPENDIX C

Experimental Results on Tire-Rigid Base Interactions

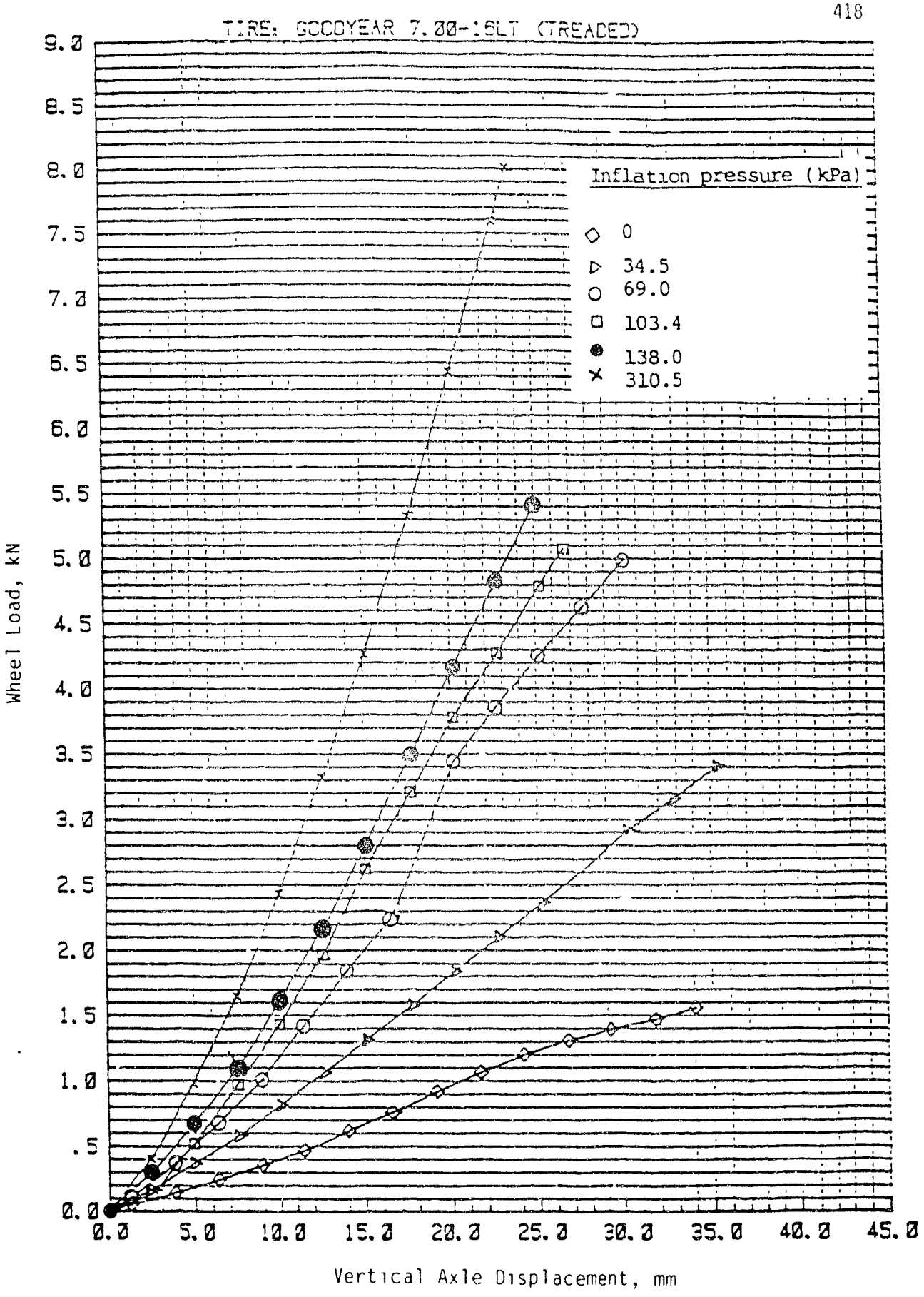


Fig. C.1a Load-Displacement Relationship for GOODYEAR 7.00-16LT (treaded)

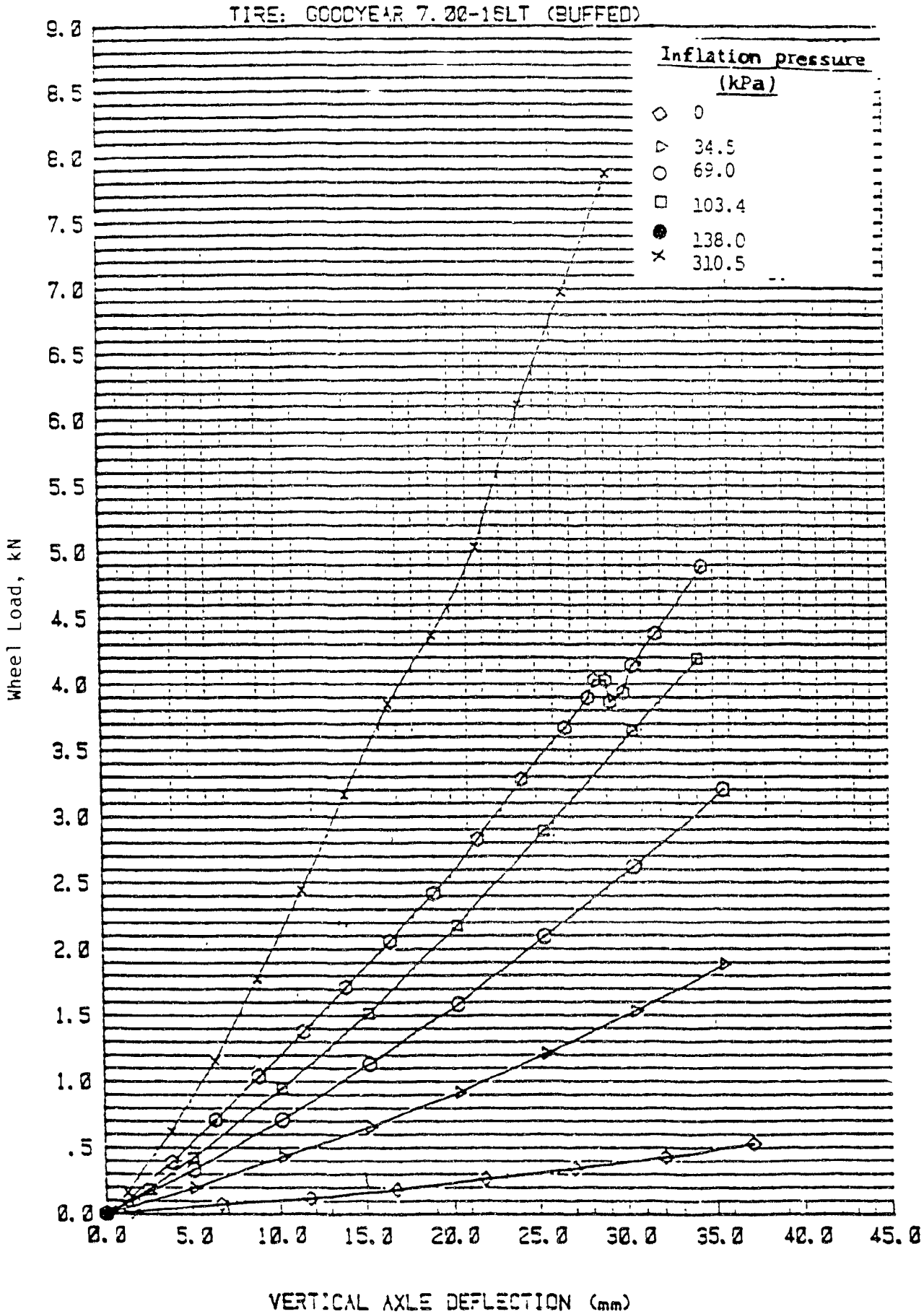


Fig. C.1b Load-Displacement Relationship for GOODYEAR 7.00-16LT (buffed)

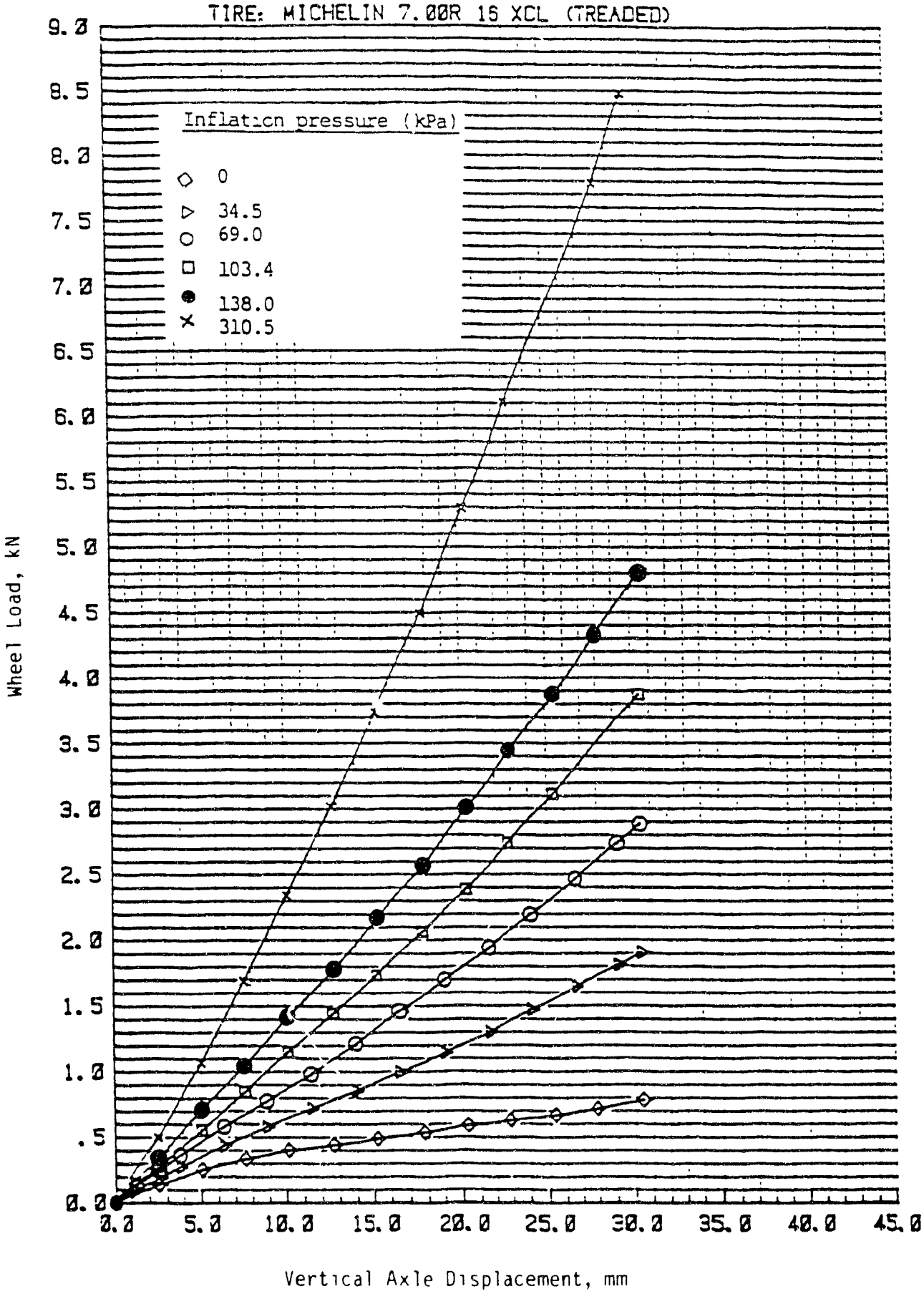


Fig. C.1c Load-Displacement Relationship for MICHELIN 7.00R-16XCL (treaded)

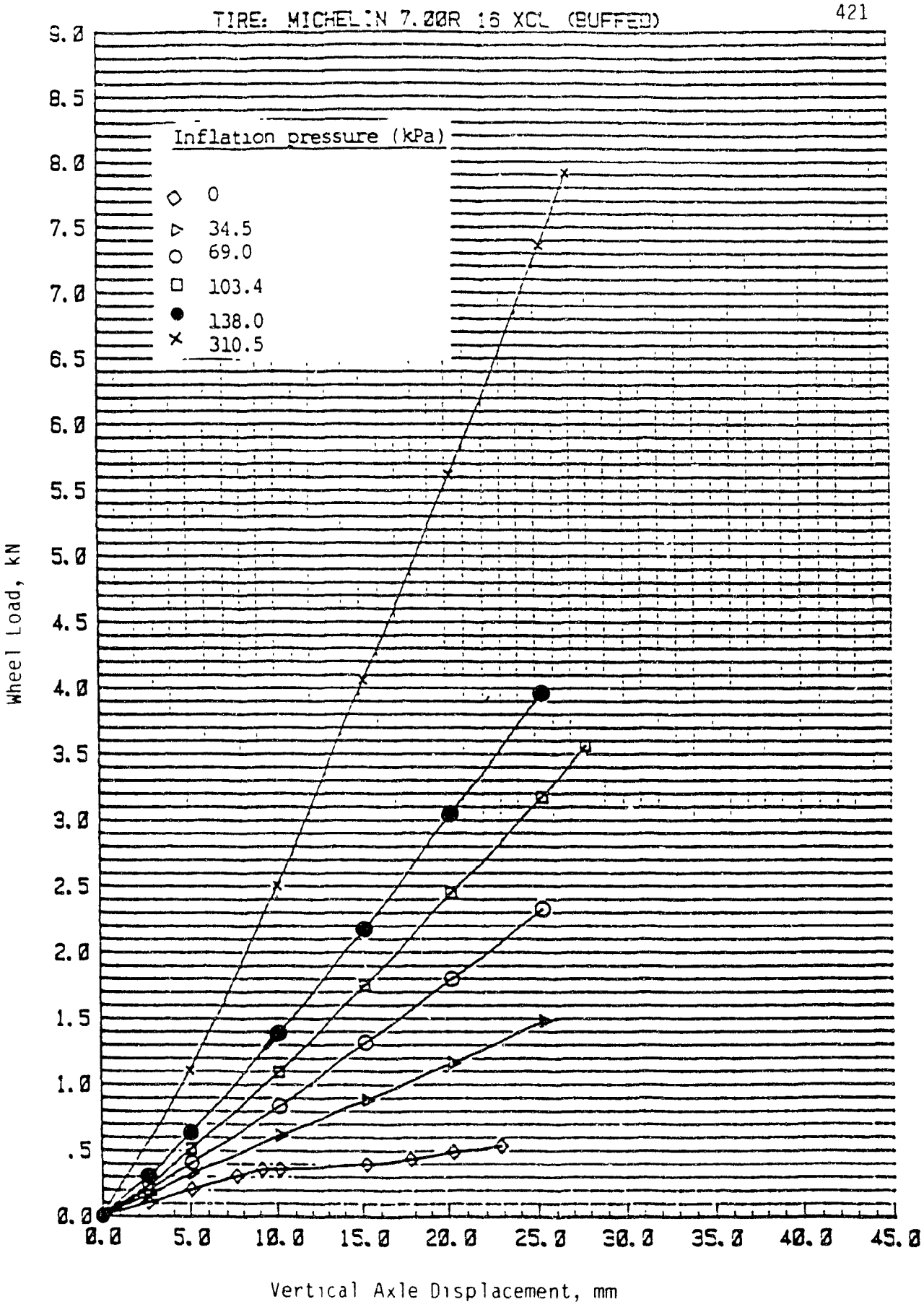


Fig. C.1d Load-Displacement Relationship for MICHELIN 7.00R-16XL (buffed)

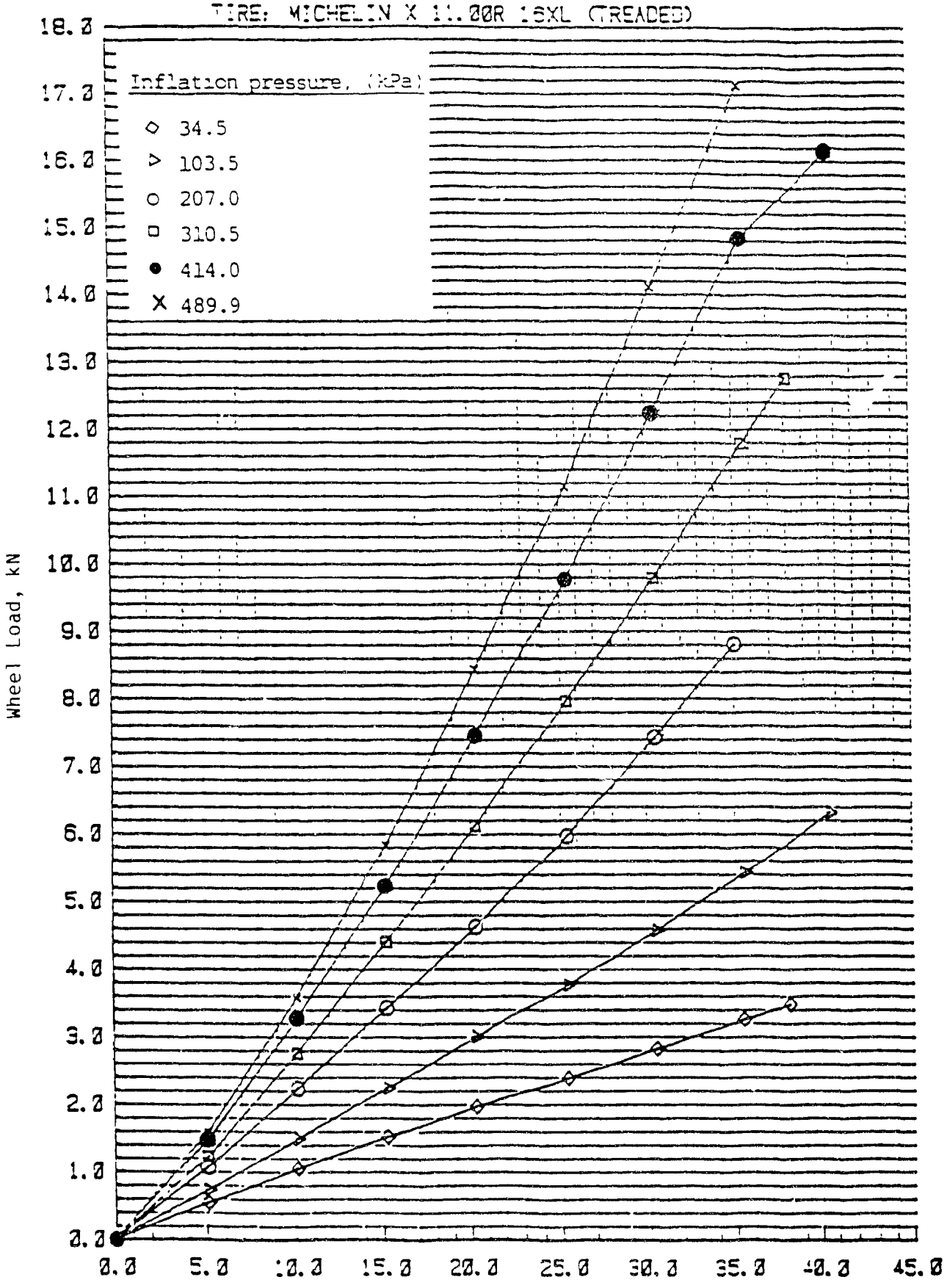


Fig. C.1e Load-Displacement Relationship for MICHELIN 11.00R-16XL (treaded)

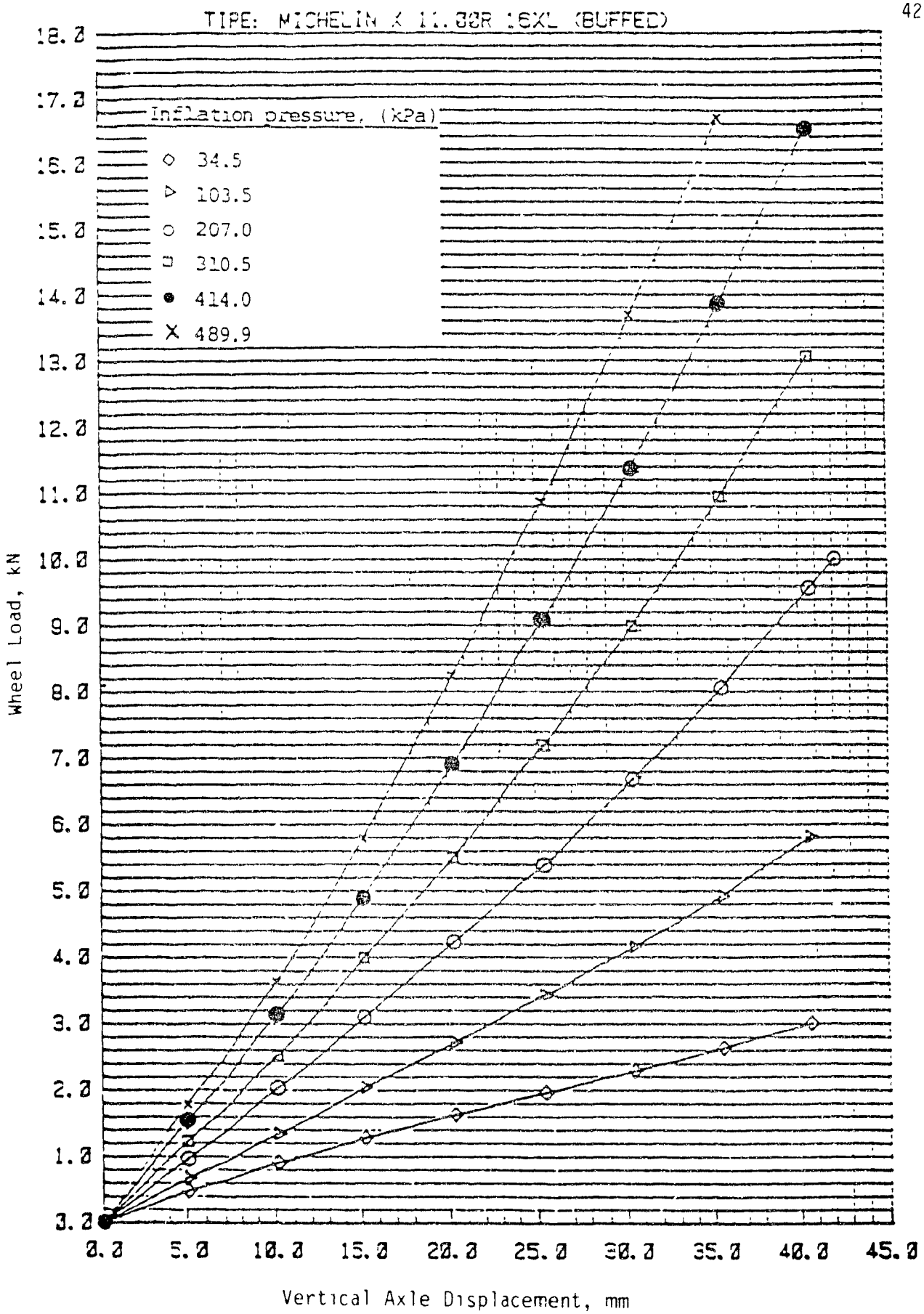


Fig. C.1f Load-Displacement Relationship for MICHELIN 11.00R-16XL (buffed)

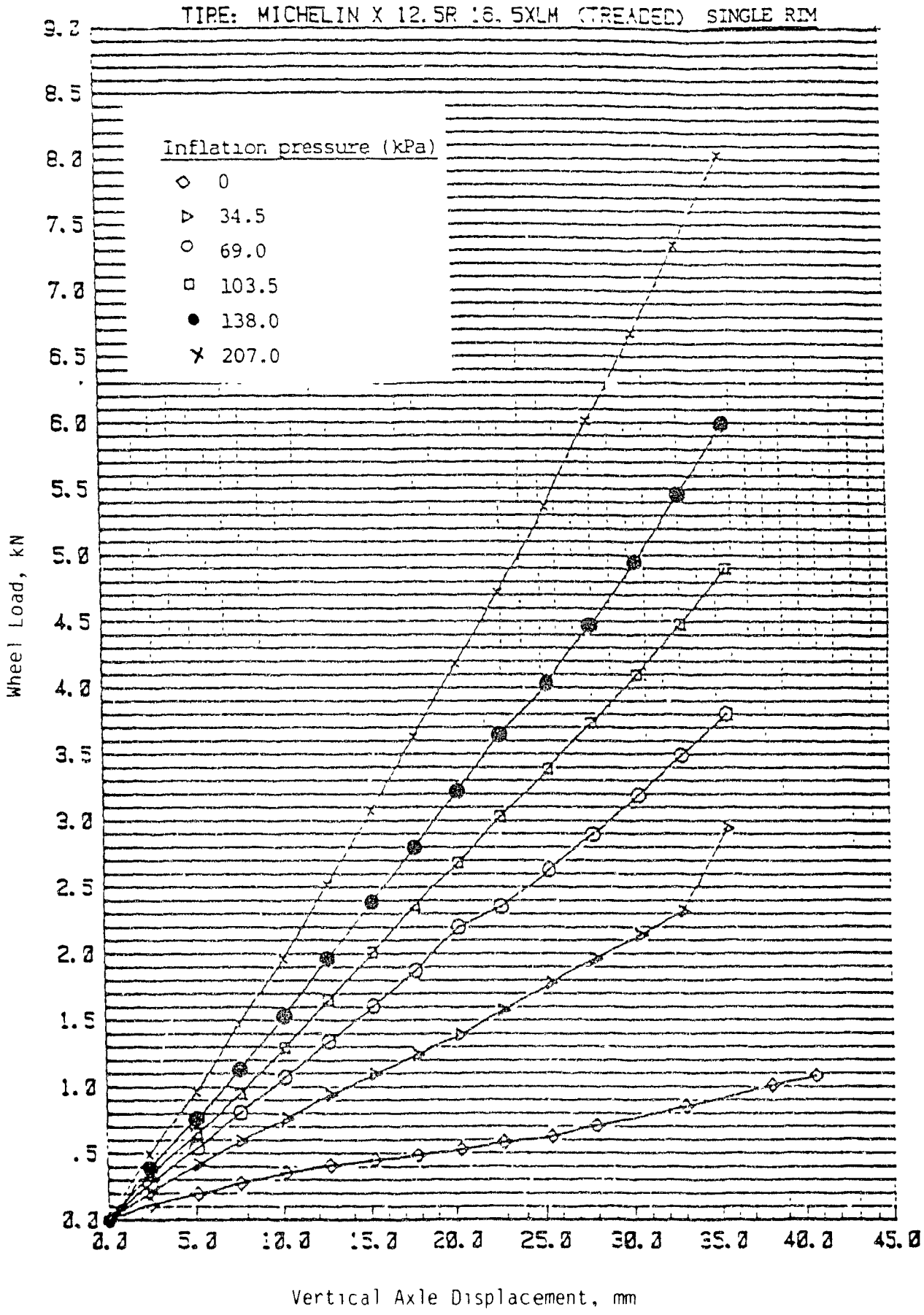


Fig. C.1g Load-Displacement Relationship for MICHELIN 12.5R-16.5XLM (treaded) (single rim)

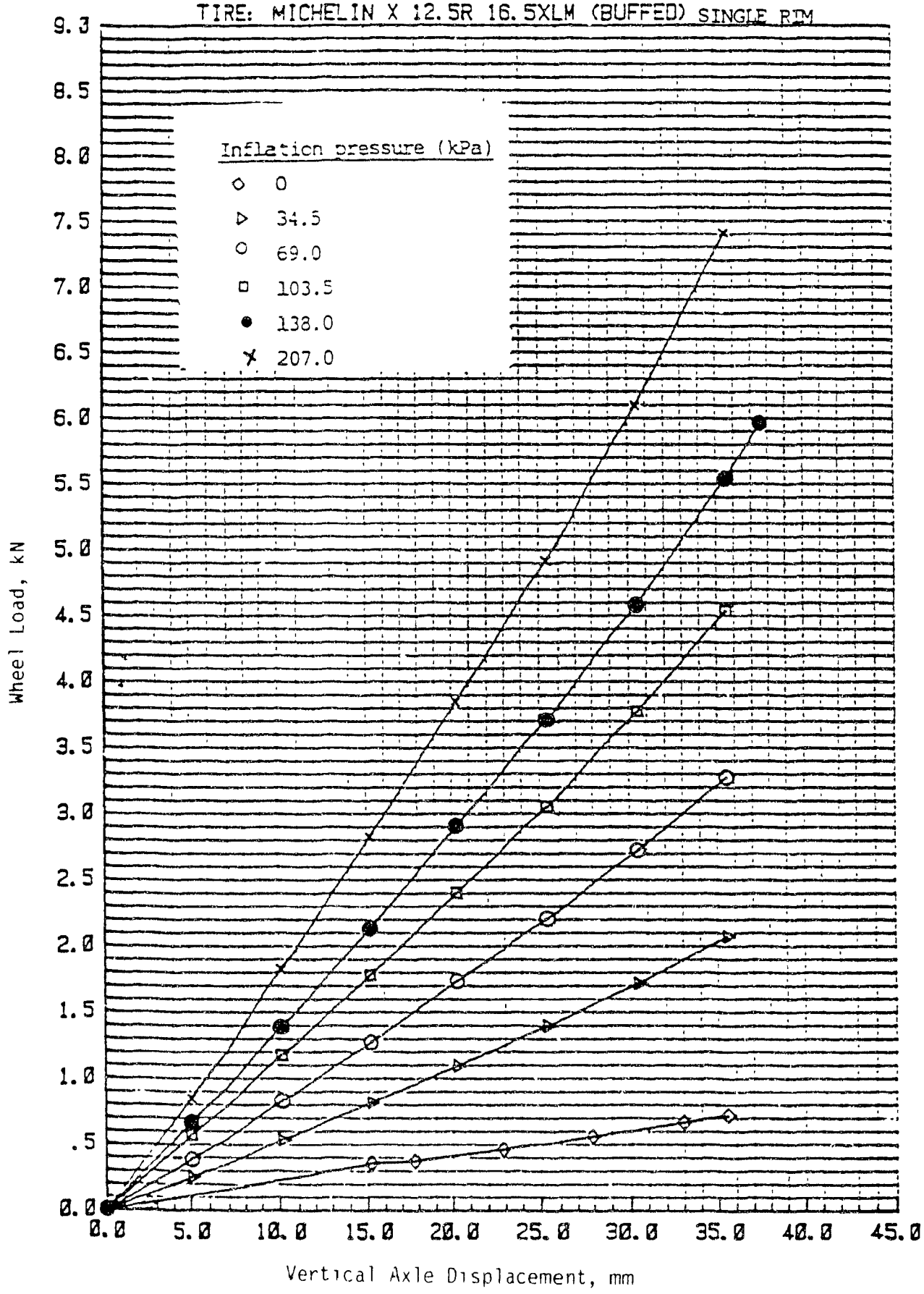


Fig. C.1h Load-Displacement Relationship for MICHELIN 12.5R-16.5XLM (buffed (single rim)

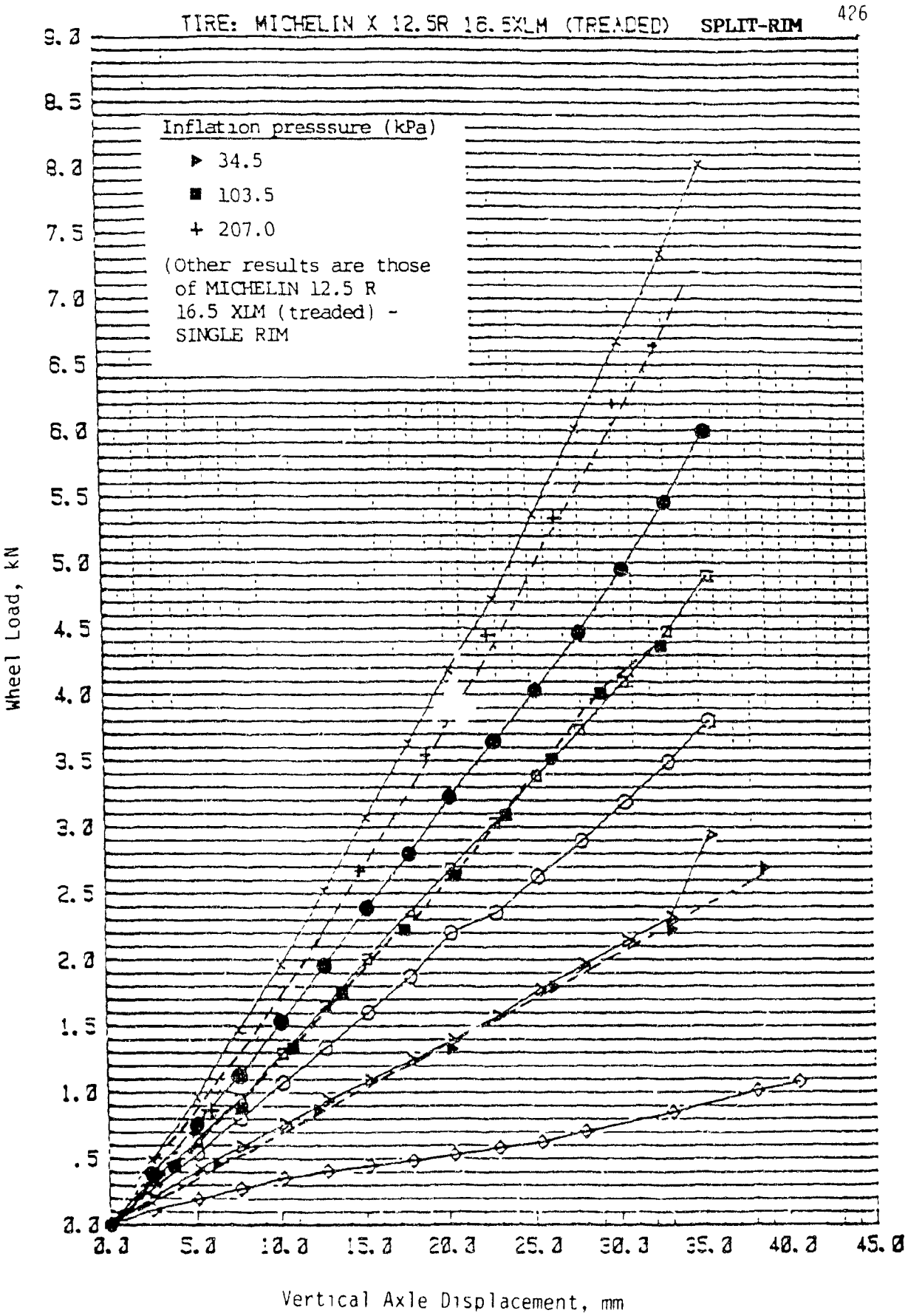


Fig. C.11 Load-Displacement Relationship for MICHELIN 12.5R-16.5XLM (treaded (split rim)

TABLE C.1a Comparison of Axle Displacement

(Load = 3.0 kN, Inflation Pressure = 103.5 kPa)

TIRE	Fig. No.	Tire Deflection mm	Tire Deflection %
GOODYEAR 7.00-16LT			
treaded	C.1a	16.8	11.2
buffed	C.1b	26.0	17.3
MICHELIN 7.00R 16XCL			
treaded	C.1c	24.3	16.0
buffed	C.1d	24.0	15.8
MICHELIN 11.00R 16XL			
treaded	C.1e	20.2	8.9
buffed	C.1f	22.2	9.8
MICHELIN 12.5R 16.5XLM (single rim)			
treaded	C.1g	22.8	9.8
buffed	C.1h	25.0	10.8
MICHELIN 12.5R 16.5XLM (split rim)			
treaded	C.1i	22.5	9.7

Table C.1b Measure of Carcass Stiffness for Each Tire Based on Carcass Stiffness of Treaded GOODYEAR 7.00-16LT (310.5 kPa) as One Unit

	Presence of Tread	Inflation Pressure		Ratio of Carcass Stiffness (C.S.) $(\frac{\text{High C.S.}}{\text{Low C.S.}})$
		High	Low	
GOODYEAR 7.00-16LT	Treaded	1	0.3	3.33
	Buffed	0.8	0.17	4.71
MICHELIN 7.00R-16XCL	Treaded	0.87	0.2	4.35
	Buffed	0.9	0.18	5
MICHELIN 11.00R-16XL	Treaded	0.77	0.31	2.48
	Buffed	0.74	0.25	2.96
MICHELIN 12.5R-16.5XLM	Treaded	0.71	0.24	2.96
	Buffed	0.65	0.19	3.42

NOTE 1: Carcass stiffness (C.S.) is defined by the slope of Load-Displacement relationship (Figs. C.1a-h)

NOTE 2: A measure of carcass stiffness for each tire is obtained by dividing each carcass stiffness by the carcass stiffness of the treaded tire GOODYEAR 7.00-16LT (Inf. Press. = 310.5 kPa) i.e., C.S. of treaded GOODYEAR 7.00-16LT is about 0.31 kN/mm as shown in Fig. C.1a.

NOTE 3: High Inf. Press. for GOODYEAR 7.00-16LT and MICHELIN 7.00R-16XCL is 310.5 kPa, while High Inf. Press. for MICHELIN 11.00R-16XL and MICHELIN 12.5R-16.5SLM is 207 kPa. Low Inf. Press. for all four tires is 34.5 kPa.

TABLE C.2a Data on Contact Area - GOODYEAR 7.00-16LT (treaded)
(Rigid Surface)

$$\frac{A_R \text{ (rib or lug area)}}{A_T \text{ (total or gross contact area)}} = 0.686$$

INFLATION PRESSURE kPa	WHEEL LOAD (W) kN	MEASURED TOTAL CONTACT AREA (A_T) mm^2	REPRESENTATIVE RECTANGULAR CONTACT AREA		AVERAGE CONTACT PRESSURE ($\frac{W}{A_T}$) kPa
			WIDTH mm	LENGTH mm	
34.5	0.667	8140	77	105	82.0
	1.334	16270	116	140	82.0
	2.001	24410	142	172	82.0
	2.669	32540	153	212	82.0
	3.336	34180	152	225	97.6
103.5	0.89	7120	71	100	125.0
	1.779	14232	109	130	125.0
	2.669	21352	133	160	125.0
	3.558	28464	59	178	125.0
	4.448	30690	141	218	145.0
310.5	1.334	6402	57	112	208.0
	2.669	12811	93	138	208.0
	4.003	19214	117	162	208.0
	5.338	25622	141	182	208.0
	6.672	28450	148	192	234.5

TABLE C.2b Data on Contact Area - GOODYEAR 7.00-16LT (buffed)
(Rigid Surface)

$$\frac{A_R \text{ (rib or lug area)}}{A_T \text{ (total or gross contact area)}} = 1.0$$

INFLATION PRESSURE kPa	WHEEL LOAD (W) kN	MEASURED TOTAL CONTACT AREA (A_T) mm^2	REPRESENTATIVE RECTANGULAR CONTACT AREA		AVERAGE CONTACT PRESSURE ($\frac{W}{A_T}$) kPa
			WIDTH mm	LENGTH mm	
34.5	0.356	7300	59	124	48.7
	0.712	14630	75	194	48.7
	1.067	21950	95	232	48.7
	1.423	29270	113	258	48.7
	1.779	34000	116	292	52.3
103.5	0.890	8032	68	118	110.8
	1.779	16055	80	200	110.8
	2.669	24088	104	232	110.8
	3.558	32110	124	260	110.8
	4.448	39200	133	294	113.0
310.5	1.334	5410	54	100	246.5
	2.669	10820	83	130	246.5
	4.003	16240	80	202	246.5
	5.338	21650	95	228	246.5
	6.672	25200	101	250	265.0

TABLE C.2c Data on Contact Area - MICHELIN 7.00R-16XCL (treaded)
(Rigid Surface)

$$\frac{A_R \text{ (rib or lug area)}}{A_T \text{ (total or gross contact area)}} = 0.600$$

INFLATION PRESSURE kPa	WHEEL LOAD (W) kN	MEASURED TOTAL CONTACT AREA (A_T) mm^2	REPRESENTATIVE RECTANGULAR CONTACT AREA		AVERAGE CONTACT PRESSURE ($\frac{W}{A_T}$) kPa
			WIDTH mm	LENGTH mm	
34.5	0.356	4985	56	87	72.7
	0.711	9776	78	125	72.7
	1.067	14670	87	169	72.7
	1.423	19566	95	206	72.7
	1.779	24460	98	248	72.7
103.5	0.711	5809	53	110	122.4
	1.423	11626	76	153	122.4
	2.135	17443	94	186	122.4
	2.846	23252	107	216	122.4
	3.558	27000	110	244	132.0
310.5	1.601	6868	57	120	233.0
	2.846	12209	81	150	233.0
	4.270	18318	98	186	233.0
	5.693	24423	127	192	233.0
	7.117	28600	123	232	249.0

TABLE C.2d Data on Contact Area - MICHELIN 7.00R-16XCL (buffed)
(Rigid Surface)

$$\frac{A_R \text{ (rib or lug area)}}{A_T \text{ (total or gross contact area)}} = 1.0$$

INFLATION PRESSURE kPa	WHEEL LOAD (W) kN	MEASURED TOTAL CONTACT AREA (A_T) mm^2	REPRESENTATIVE RECTANGULAR CONTACT AREA		AVERAGE CONTACT PRESSURE ($\frac{W}{A_T}$) kPa
			WIDTH mm	LENGTH mm	
34.5	0.356	6454	56	116	55.0
	0.711	12930	81	159	55.0
	1.067	19420	103	188	55.0
	1.423	25870	118	220	55.0
	1.779	32340	120	265	55.0
	2.135	38820	146	265	55.0
103.5	0.711	6760	70	96	105.2
	1.423	13520	104	130	105.2
	2.135	20280	105	192	105.2
	2.846	27050	124	217	105.2
	3.558	25060	96	260	142.0
310.5	1.601	6644	111	60	241.0
	3.202	13288	102	130	241.0
	4.804	19937	105	190	241.0
	6.405	26580	126	210	241.0
	8.006	29081	130	223	275.3

TABLE C.2e Data on Contact Area - MICHELIN 11.00R-16XL (treaded)
(Rigid Surface)

$$\frac{A_R \text{ (rib or lug area)}}{A_T \text{ (total or gross contact area)}} = 0.580$$

INFLATION PRESSURE kPa	WHEEL LOAD (W) kN	MEASURED TOTAL CONTACT AREA (A_T) mm^2	REPRESENTATIVE RECTANGULAR CONTACT AREA		AVERAGE CONTACT PRESSURE ($\frac{W}{A_T}$) kPa
			WIDTH mm	LENGTH mm	
34.5	0.622	7480	72	104	83.0
	1.245	14940	93	160	83.0
	1.868	22420	110	204	83.0
	2.491	29890	123	243	83.0
	3.113	37370	129	290	83.0
207	1.601	8530	61	140	187.0
	3.202	17070	87	197	187.0
	4.804	25610	122	210	187.0
	6.405	34140	138	247	187.0
	8.006	39000	148	258	205.0
414	2,668	10220	74	138	261.0
	5.337	20440	110	185	261.0
	8.006	30660	143	214	261.0
	10.675	40890	171	239	261.0
	13.344	51110	195	261	261.0

TABLE C.2f Data on Contact Area - MICHELIN 11.00R-16XL (buffed)
(Rigid Surface)

$$\frac{A_R \text{ (rib or lug area)}}{A_T \text{ (total or gross contact area)}} = 1.0$$

INFLATION PRESSURE kPa	WHEEL LOAD (W) kN	MEASURED TOTAL CONTACT AREA (A_T) mm^2	REPRESENTATIVE RECTANGULAR CONTACT AREA		AVERAGE CONTACT PRESSURE ($\frac{W}{A_T}$) kPa
			WIDTH mm	LENGTH mm	
34.5	0.622	8210	78	105	76.0
	1.245	16434	93	176	76.0
	1.868	24658	103	240	76.0
	2.491	32881	119	276	76.0
	3.113	41091	127	323	76.0
207	1.601	7204	72	100	222.0
	3.202	14409	85	170	222.0
	4.804	21618	104	207	222.0
	6.405	28823	122	235	222.0
	8.006	36027	138	260	222.0
414	2.668	7737	69	112	345.0
	5.337	15477	95	162	345.0
	8.006	23217	114	204	345.0
	10.675	30958	137	225	345.0
	13.344	38819	152	255	345.0

TABLE C.2g Data on Contact Area - MICHELIN 12.5R-16.5XLM (treaded)
(Rigid Surface)

$$\frac{A_R \text{ (rib or lug area)}}{A_T \text{ (total or gross contact area)}} = 0.47$$

INFLATION PRESSURE kPa	WHEEL LOAD (W) kN	MEASURED TOTAL CONTACT AREA (A_T) mm^2	REPRESENTATIVE RECTANGULAR CONTACT AREA		AVERAGE CONTACT PRESSURE ($\frac{W}{A_T}$) kPa
			WIDTH mm	LENGTH mm	
34.5	0.533	10950	84	130	49.0
	1.067	21890	100	218	49.0
	1.601	32820	126	260	49.0
	2.135	43770	156	280	49.0
	2.668	50930	168	302	52.0
103.5	0.889	9700	67	144	92.0
	1.779	19400	112	173	92.0
	2.669	29100	133	219	92.0
	3.558	38800	163	237	92.0
	4.448	44230	163	272	101.0
207	1.334	8890	62	144	150.0
	2.668	17800	106	168	150.0
	4.003	26670	124	215	150.0
	5.337	35600	143	248	150.0
	6.672	42100	166	254	158.0

TABLE C.2h Data on Contact Area - MICHELIN 12.5R-16.5XLM (buffed)
(Rigid Surface)

$$\frac{A_R \text{ (rib or lug area)}}{A_T \text{ (total or gross contact area)}} = 1.0$$

INFLATION PRESSURE kPa	WHEEL LOAD (W) kN	MEASURED TOTAL CONTACT AREA (A_T) mm^2	REPRESENTATIVE RECTANGULAR CONTACT AREA		AVERAGE CONTACT PRESSURE ($\frac{W}{A_T}$) kPa
			WIDTH mm	LENGTH mm	
34.5	0.355	10205	78	130	35.0
	0.711	20410	111	184	35.0
	1.067	30620	135	226	35.0
	1.423	40790	160	254	35.0
	1.779	49000	173	284	36.3
103.5	0.889	10240	82	124	87.0
	1.779	20470	111	184	87.0
	2.668	30710	133	230	87.0
	3.558	40940	155	264	87.0
	4.448	46478	172	268	95.7
207	1.334	8440	84.4	100	158.0
	2.668	16910	103	164	158.0
	4.003	25330	123	208	158.0
	5.337	33820	150	226	158.0
	6.672	38900	165	236	171.5

TABLE C.3 Ratio of Lug (or Rib) to Gross (or Total) Contact Area

Tire	A_R/A_T
GOODYEAR 7.00-16LT	0.69
MICHELIN 7.00R-16XCL	0.6
MICHELIN 11.00R-16XL	0.58
MICHELIN 12.5R-16.5XLM	0.47

Note 1: A_R = Rib (or Lug) Area

Note 2: A_T = Total (or Gross) Contact Area

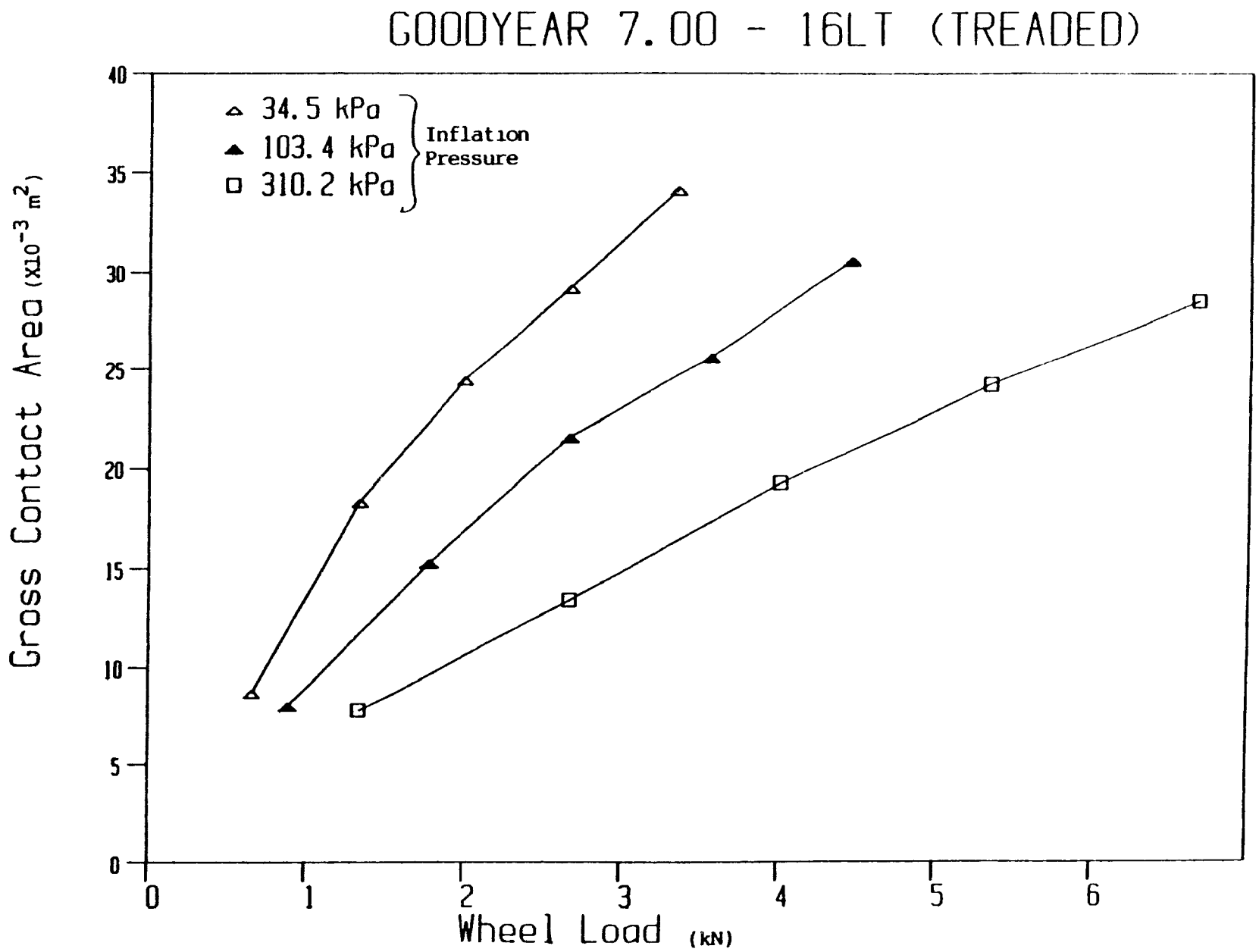


Fig. C.2a Gross Contact Area - Load Relationship for GOODYEAR 7.00-16LT (treaded)

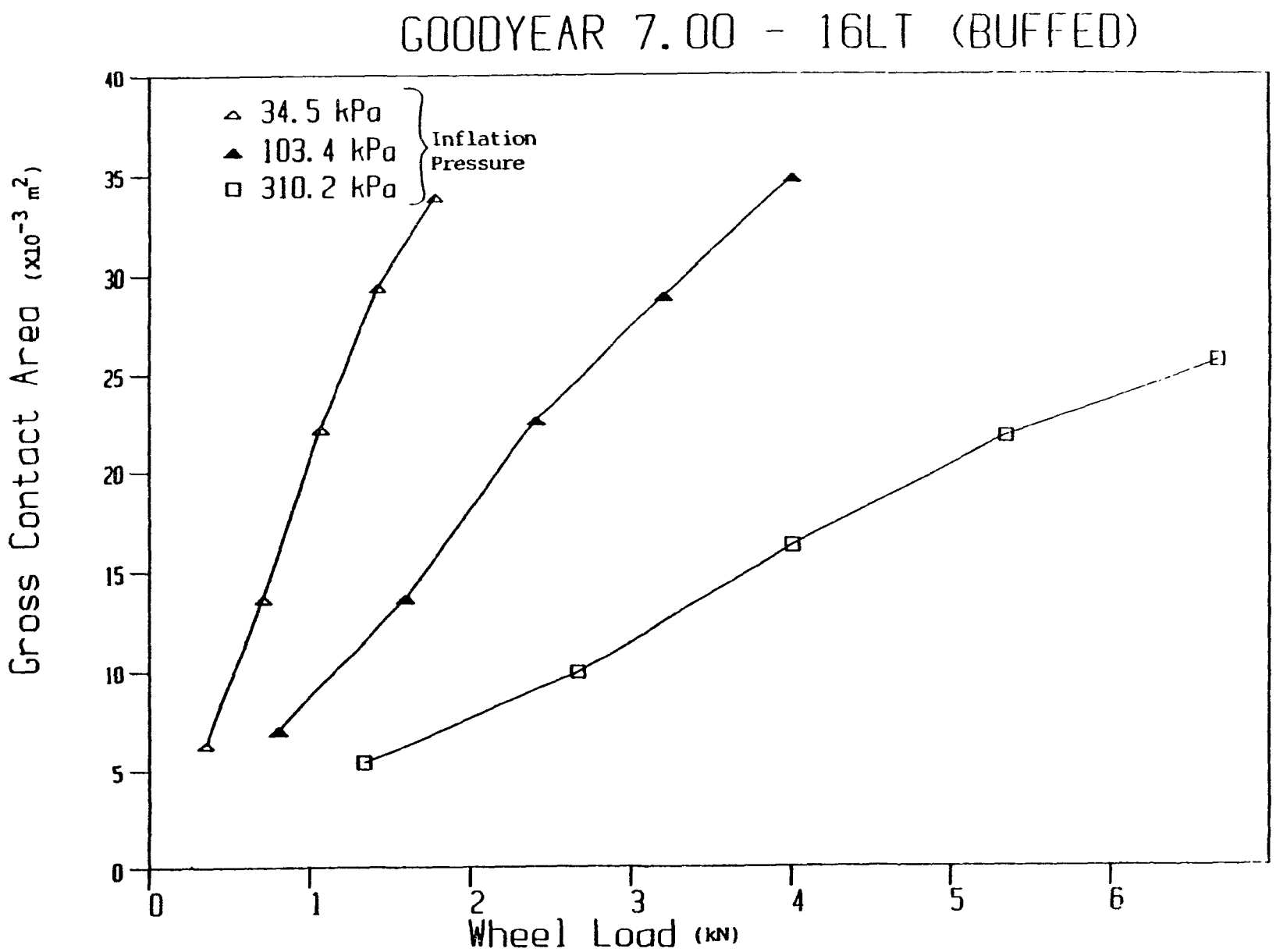


Fig. C.2b Gross Contact Area - Load Relationship for GOODYEAR 7.00-16LT (buffed)

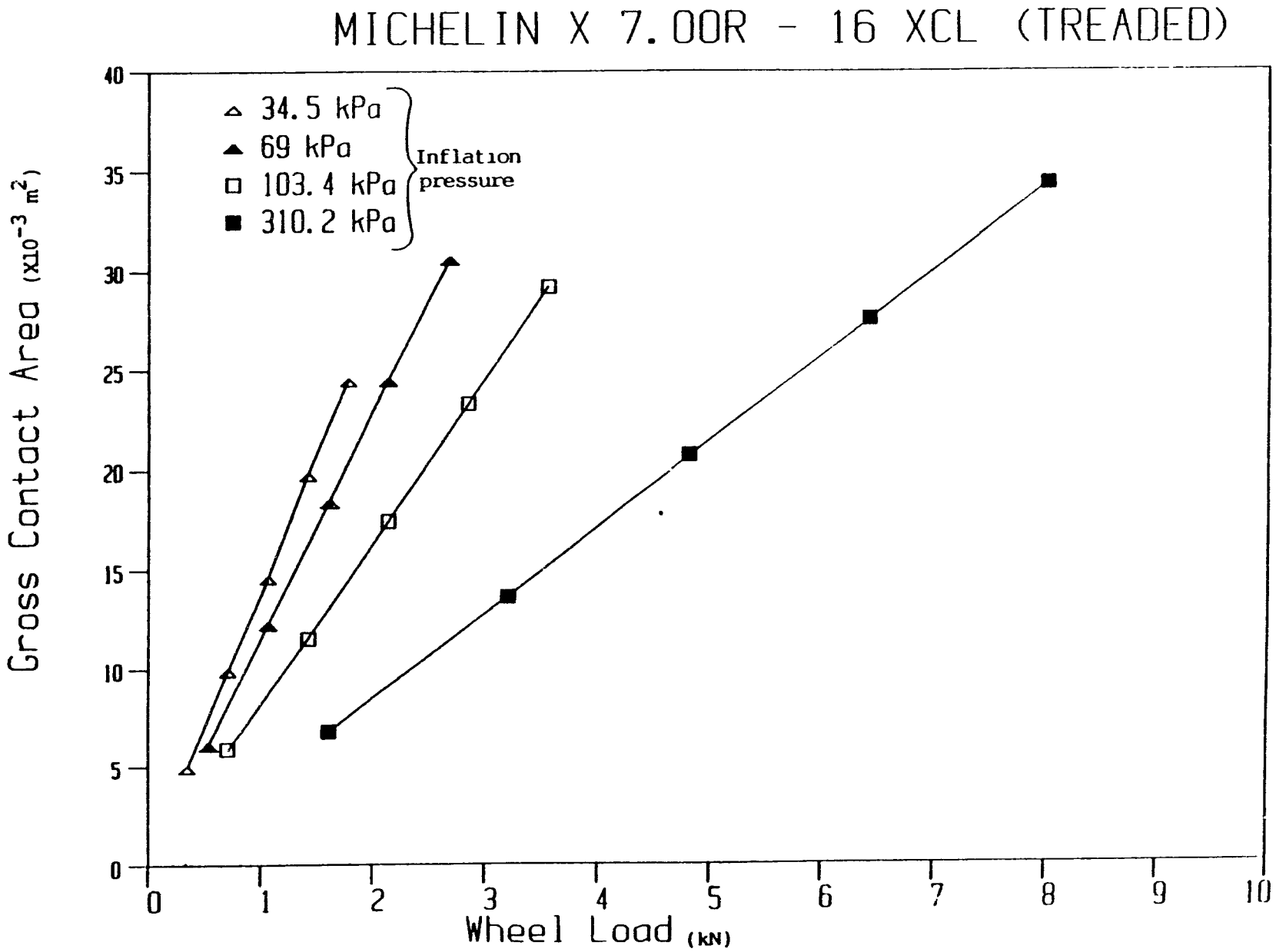


Fig. C.2c Gross Contact Area - Load Relationship for MICHELIN 7.00R-16XCL (treaded)

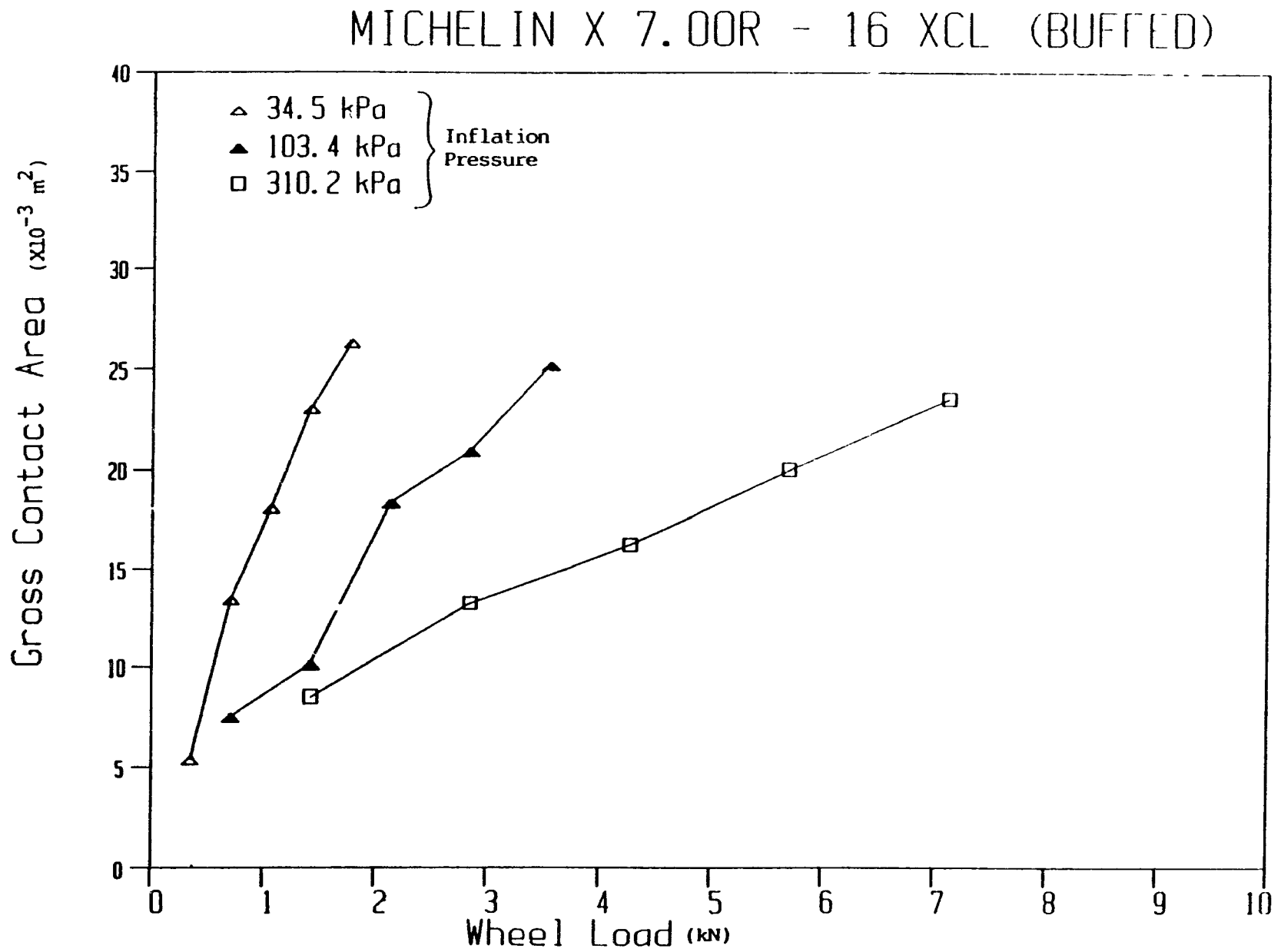


Fig. C.2d Gross Contact Area - Load Relationship for MICHELIN 7.00R-16XCL (buffed)

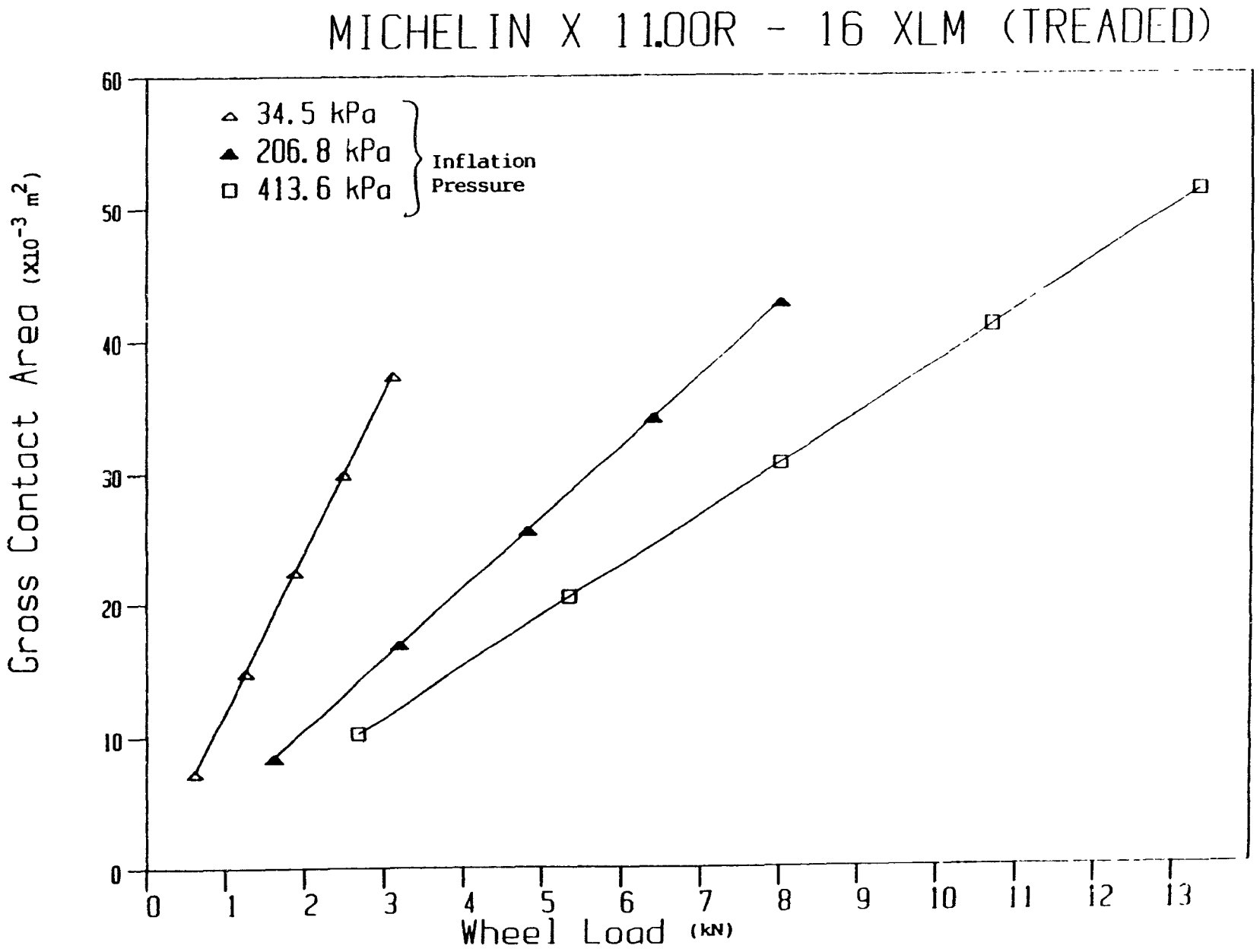


Fig. C.2e Gross Contact Area - Load Relationship for MICHELIN 11.00R-16XL (treaded)

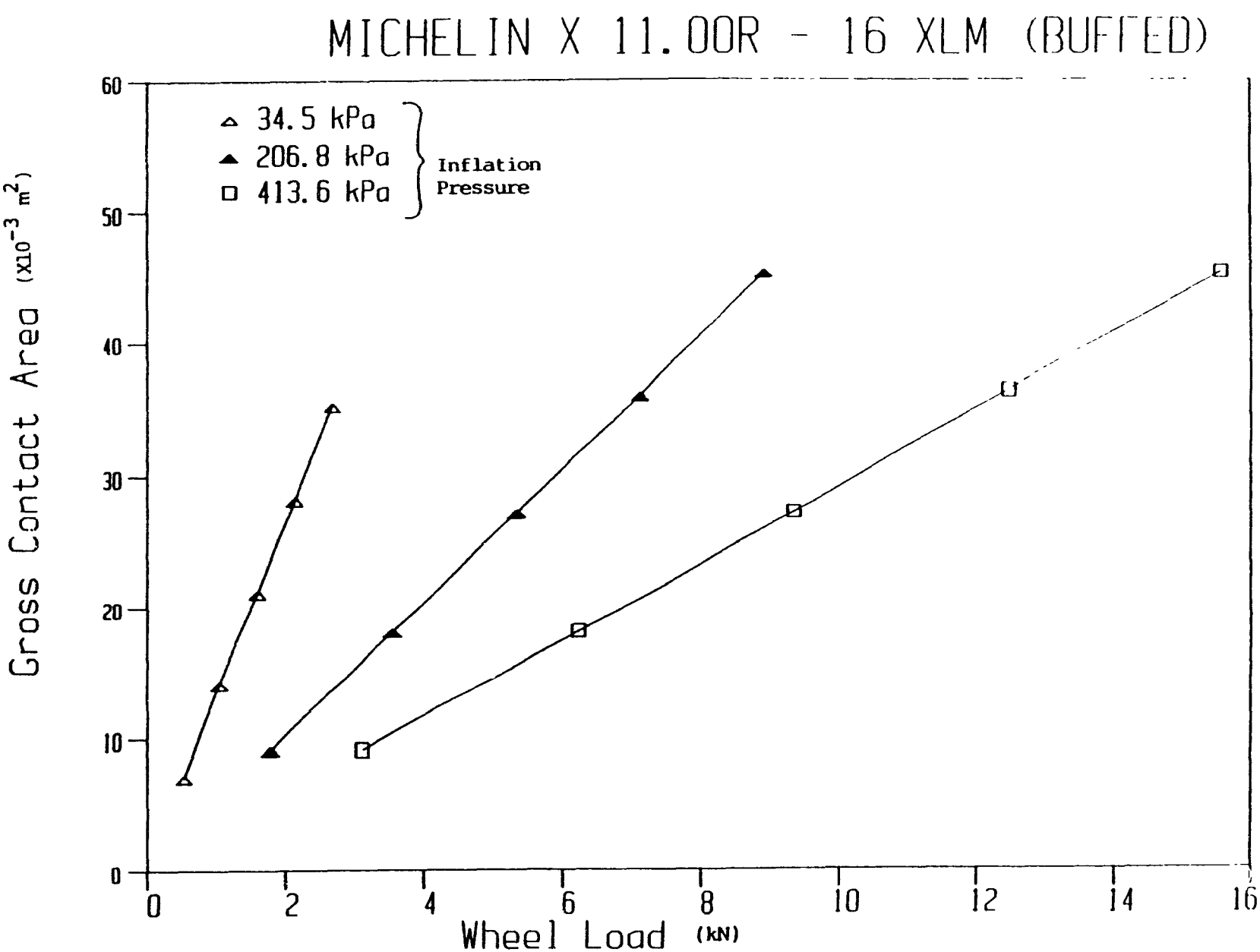


Fig. C.2f Gross Contact Area - Load Relationship for MICHELIN 11.00R-16XCL (buffed)

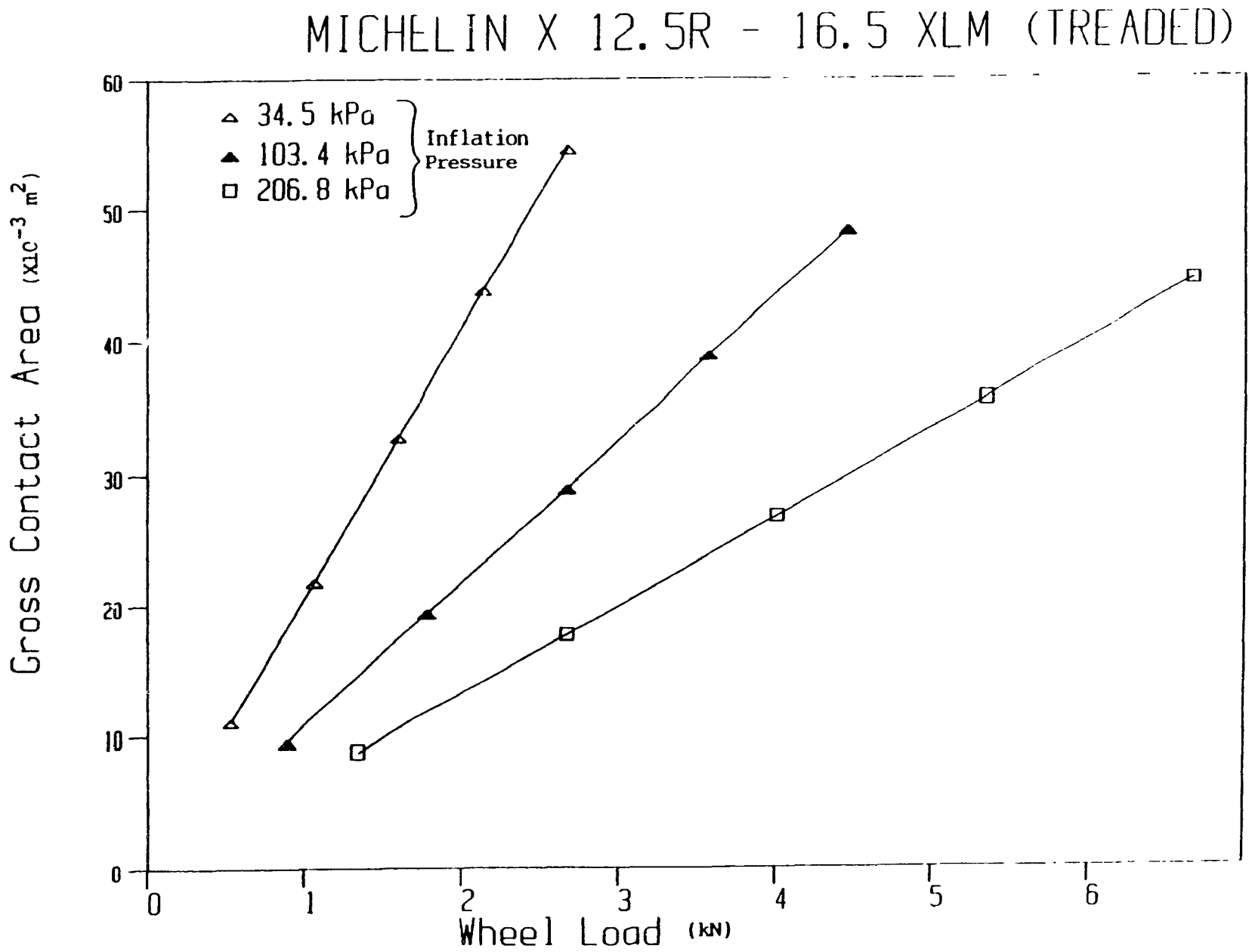


Fig. C.2g Gross Contact Area - Load Relationship for MICHELIN 12.5R-16.5XLM (treaded)

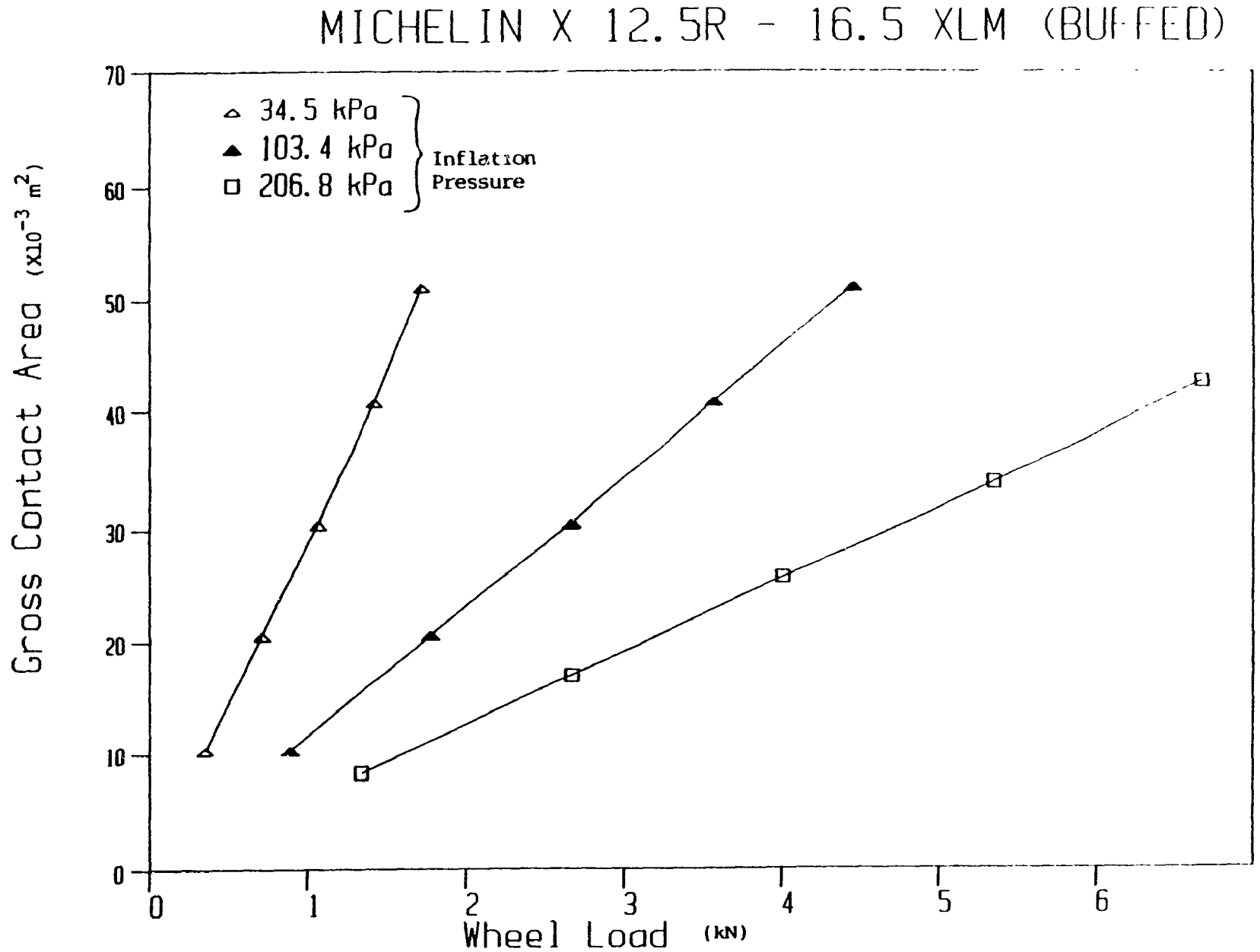


Fig. C.2h Gross Contact Area - Load Relationship for MICHELIN 12.5R-16.5XLM (buffed)

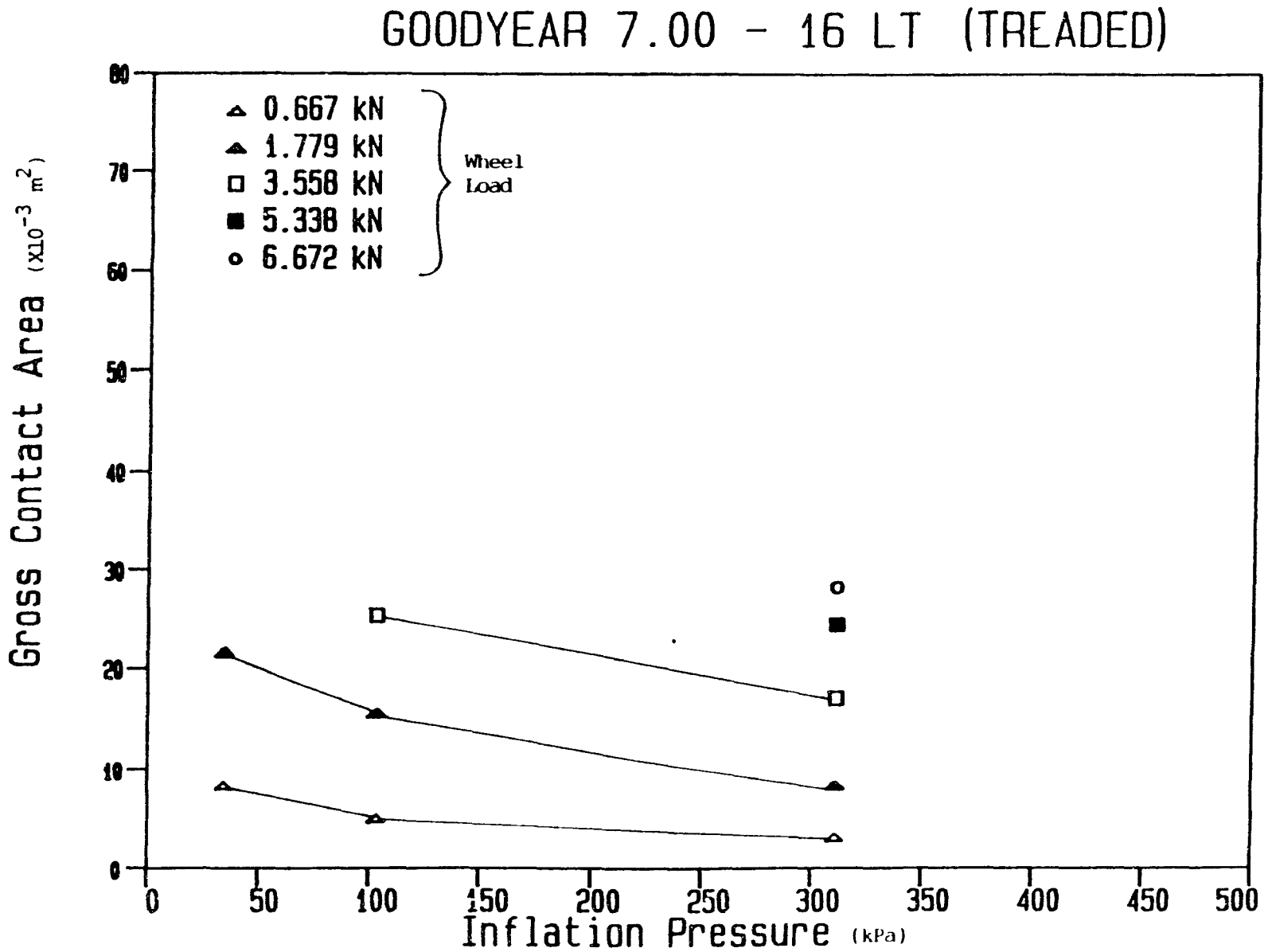


Fig. C.3a Gross Contact Area - Inflation Pressure Relationship for GOODYEAR 7.00-16LT (treaded)

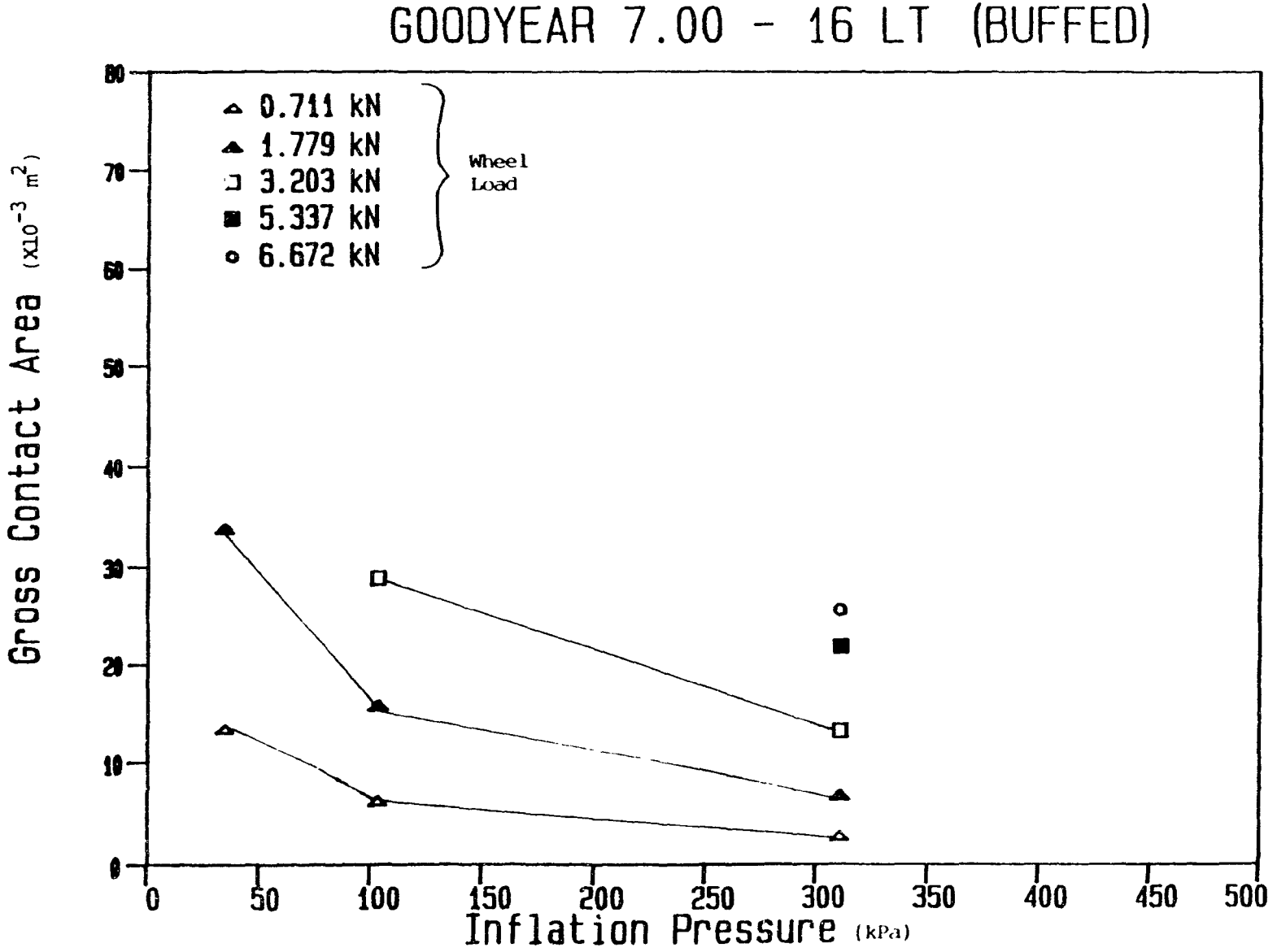


Fig. C.3b Gross Contact Area - Inflation Pressure Relationship for GOODYEAR 7.00-16LT (buffed)

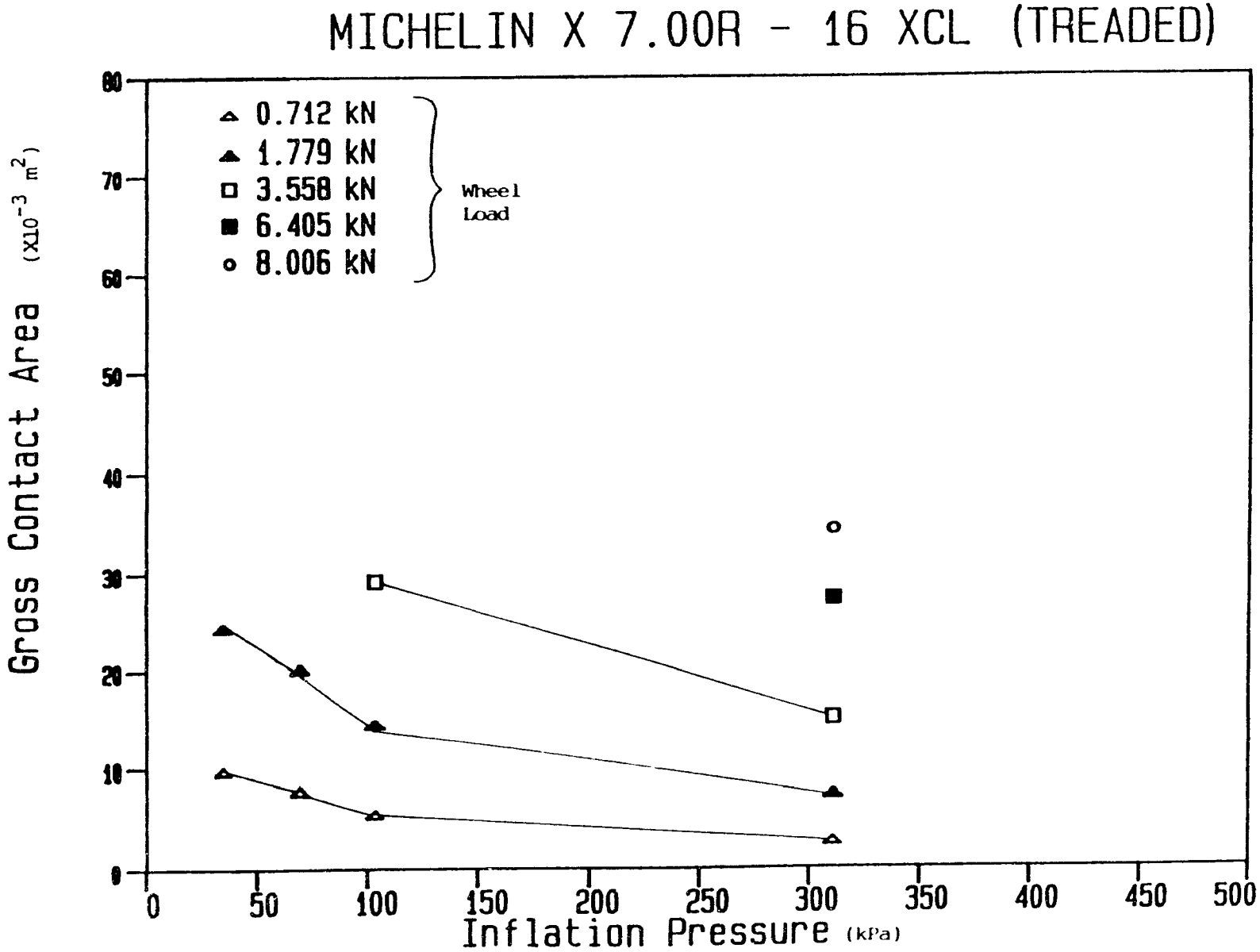


Fig. C.3c Gross Contact Area - Inflation Pressure Relationship for MICHELIN 7.00R-16XCL (treaded)

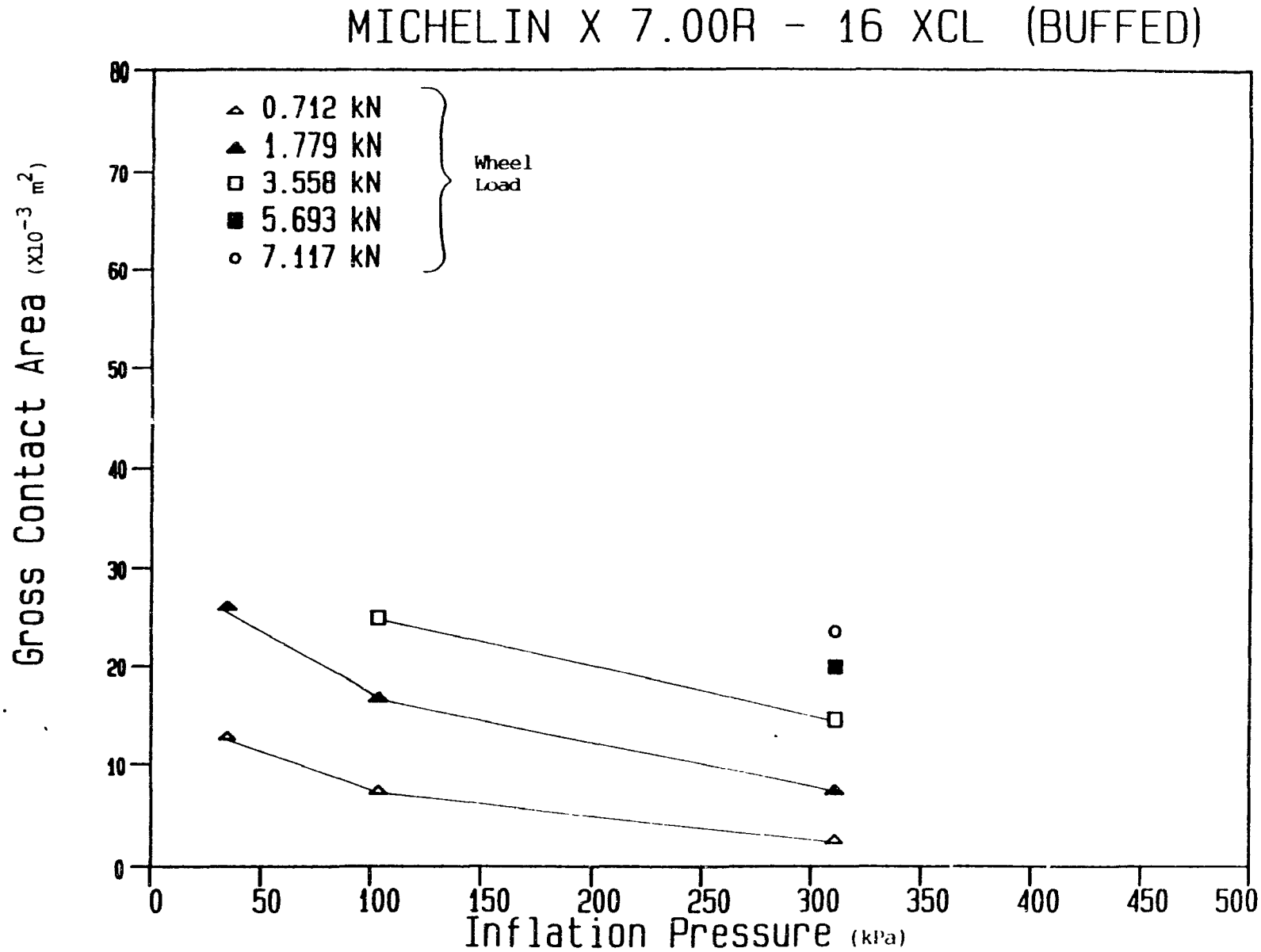


Fig. C.3d Gross Contact Area - Inflation Pressure Relationship for MICHELIN 7.00R-16XCL (buffed)

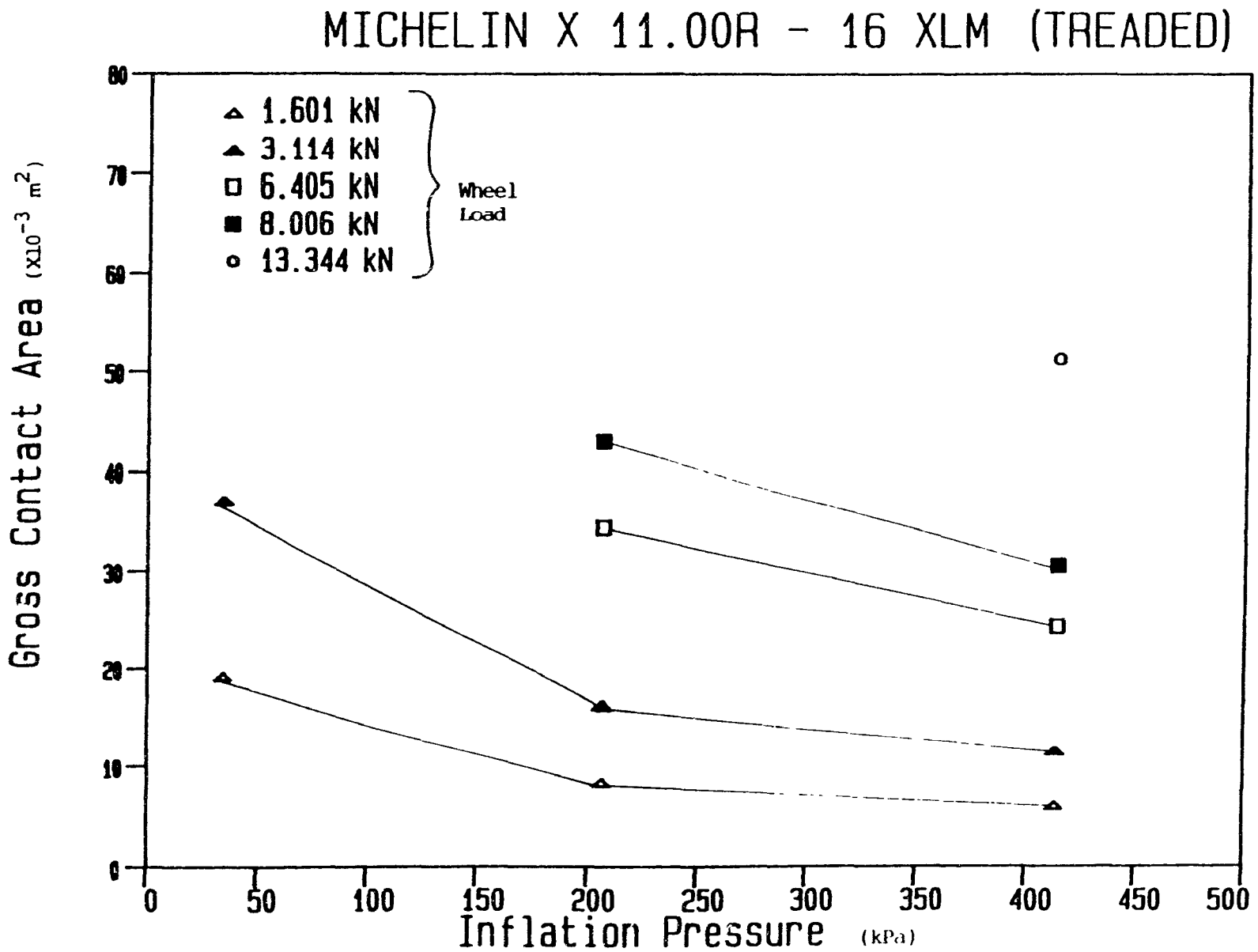


Fig. C.3e Gross Contact Area - Inflation Pressure Relationship for MICHELIN 11.00R-16XL (treaded)

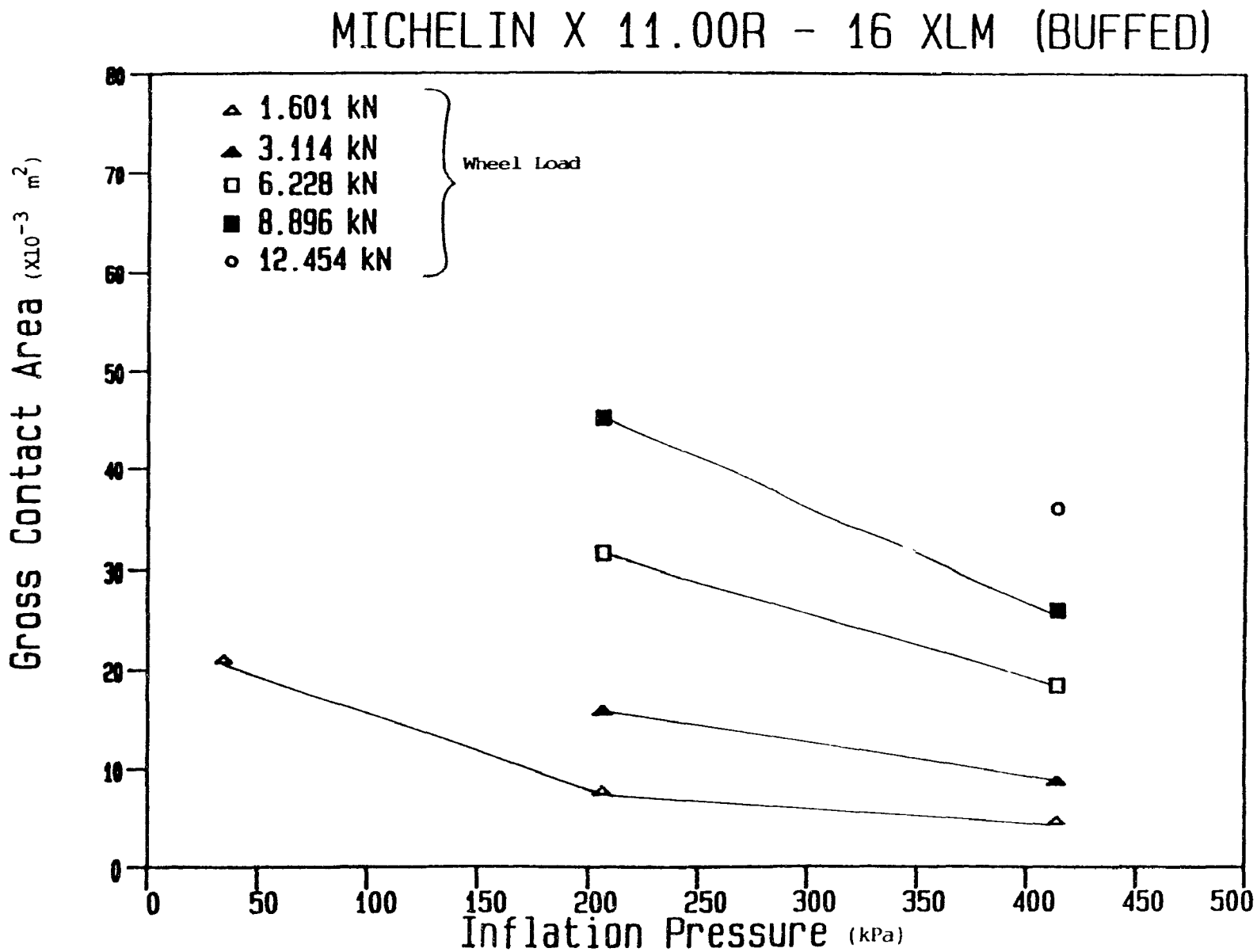


Fig. C.3f Gross Contact Area - Inflation Pressure Relationship for MICHELIN 11.00R-16XL (buffed)

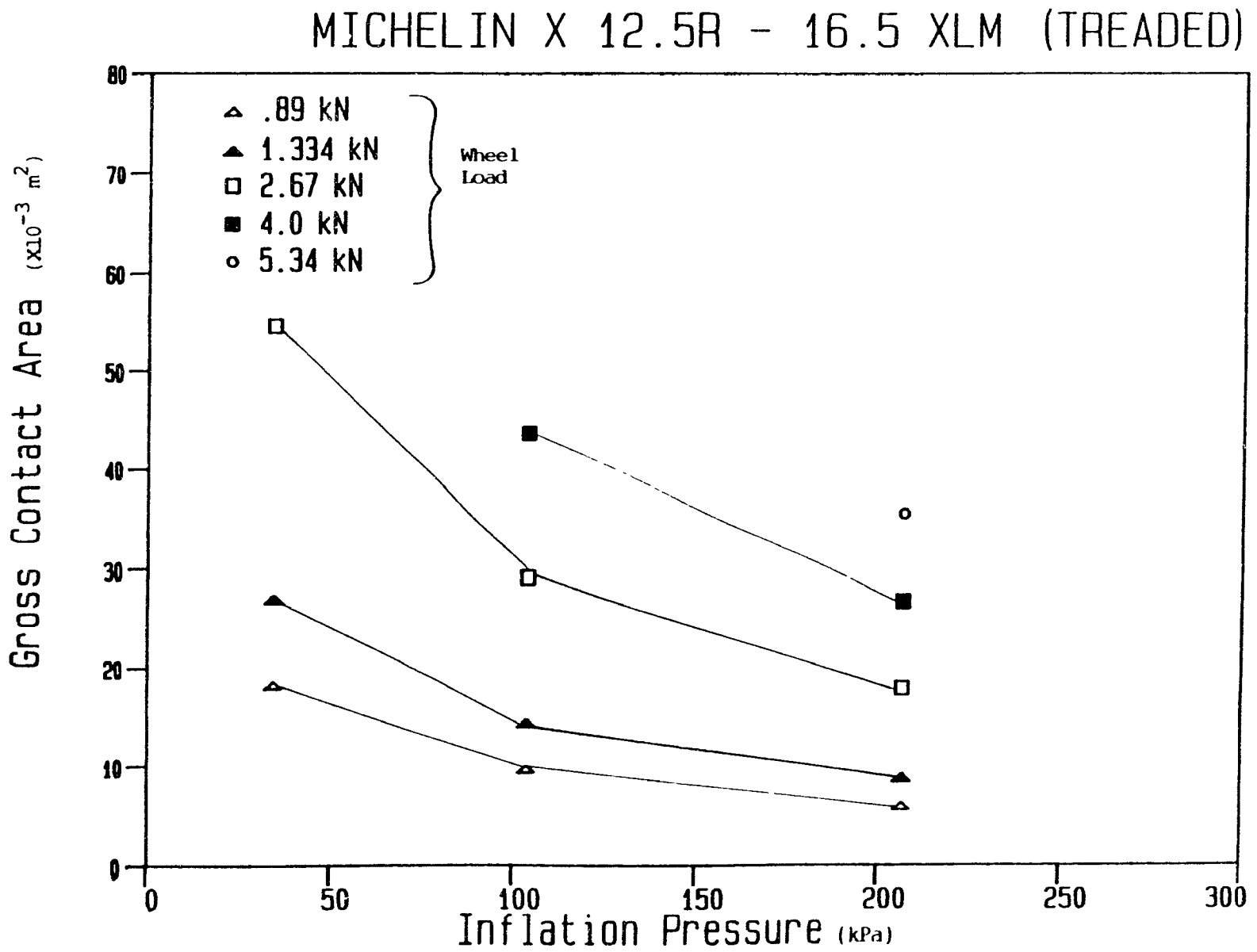


Fig. C.3g Gross Contact Area - Inflation Pressure Relationship for MICHELIN 12.5R-16.5XLM (treaded)

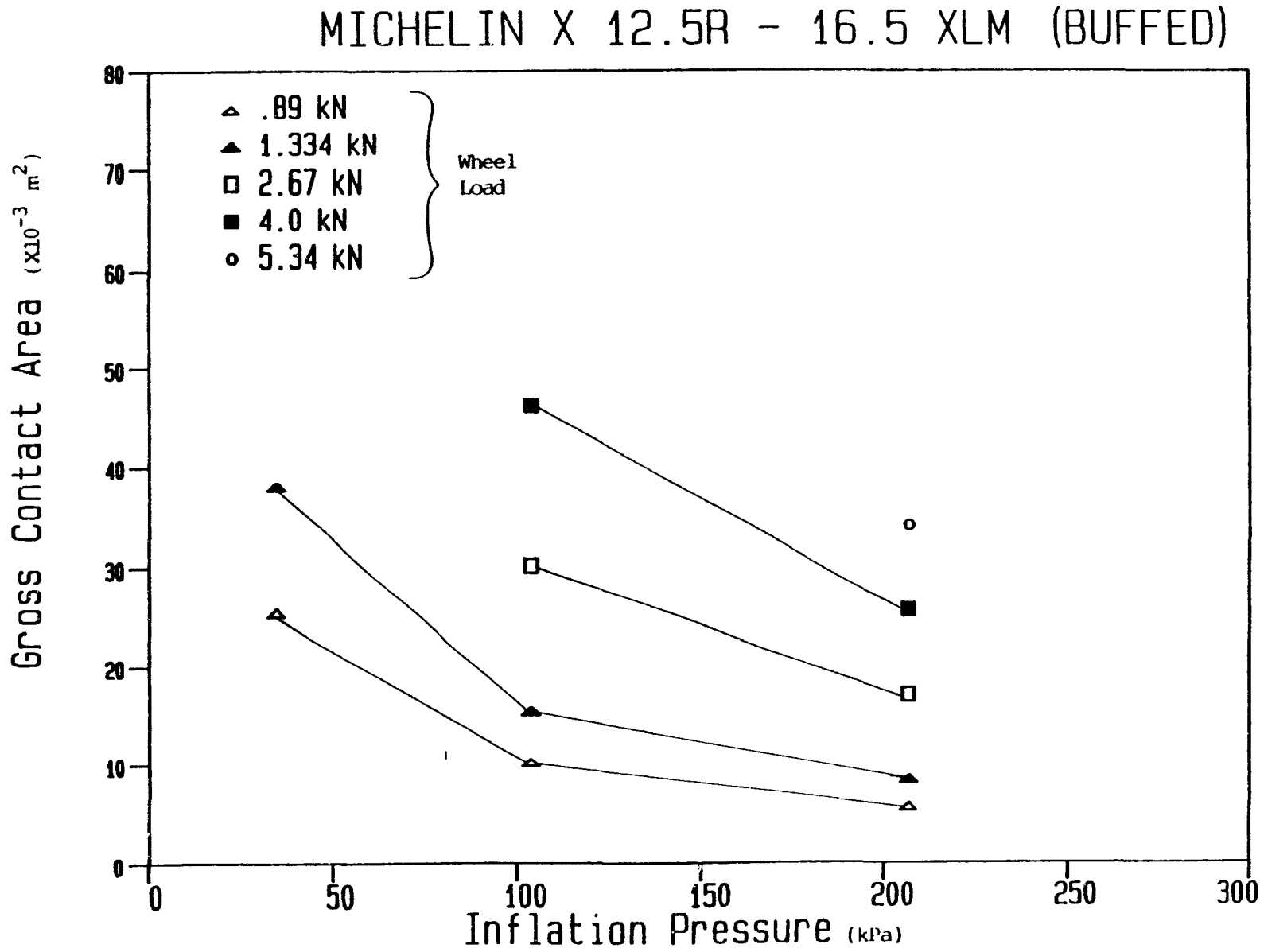


Fig. C.3h Gross Contact Area - Inflation Pressure Relationship for MICHELIN 12.5R-16.5XLM (buffed)

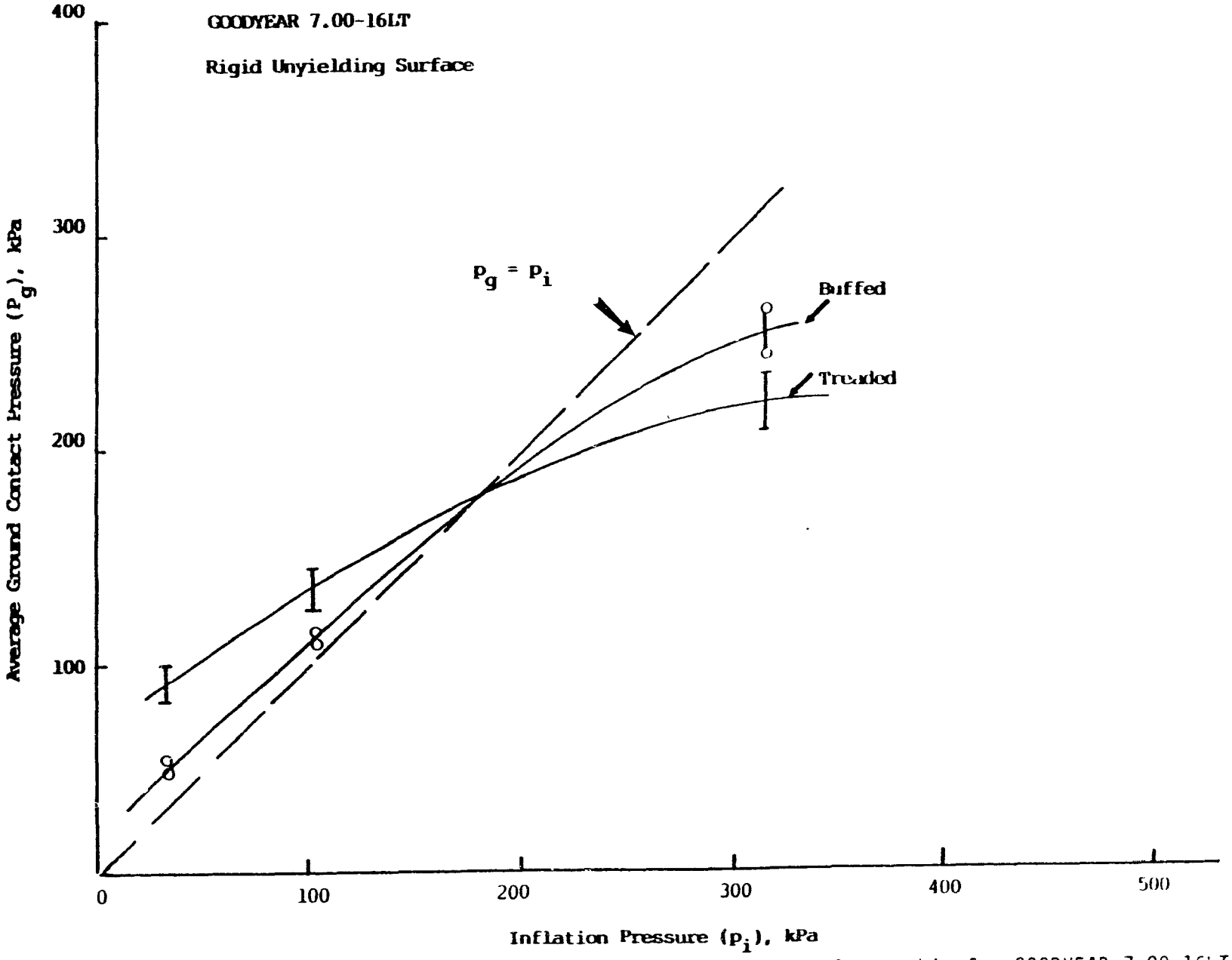


Fig. C.4a Average Ground Contact Pressure-Inflation Pressure Relationship for GOODYEAR 7.00-16LT

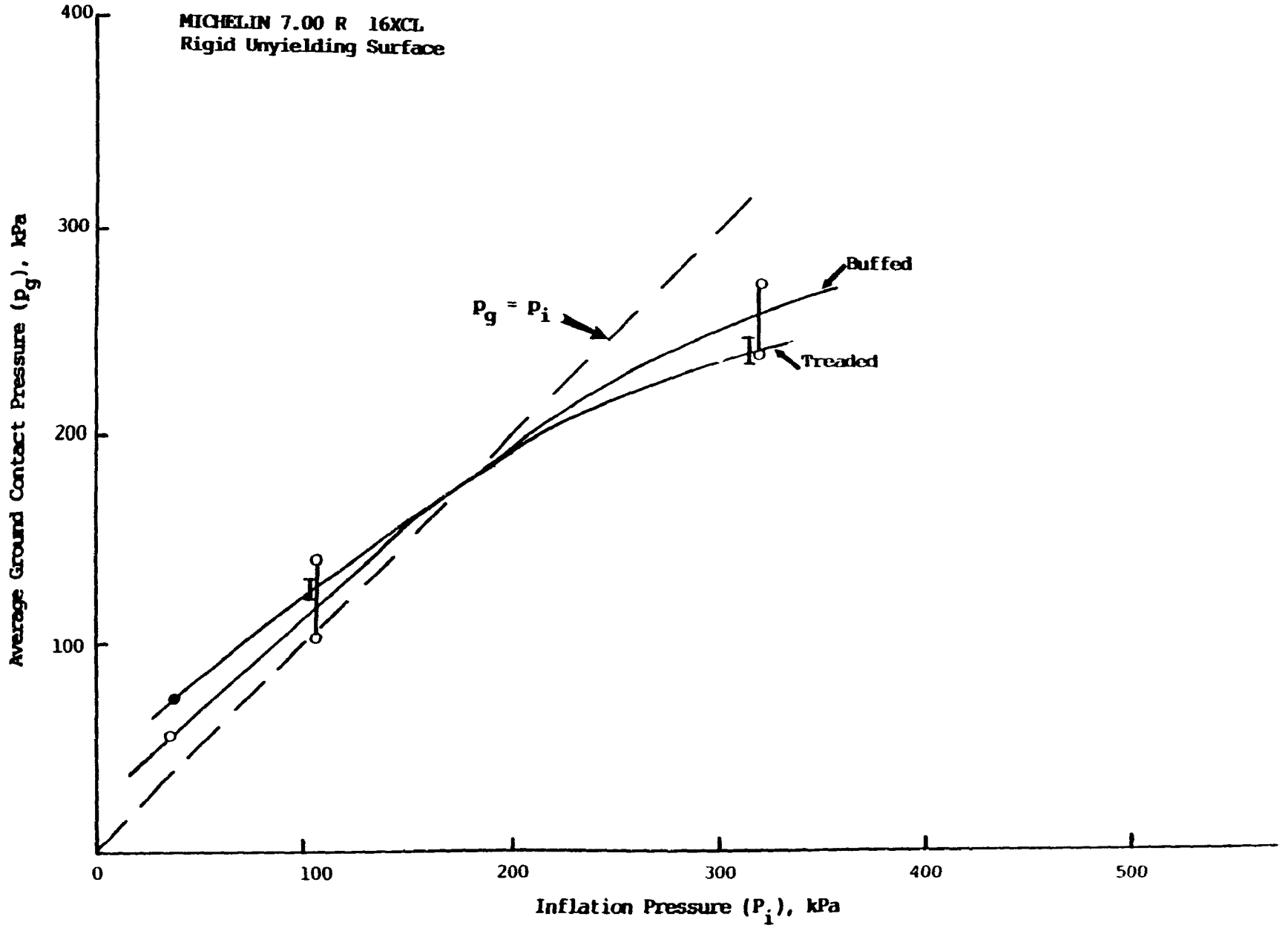


Fig. C.4b Average Ground Contact Pressure-Inflation Pressure Relationship for MICHELIN 7.00R-16XCL

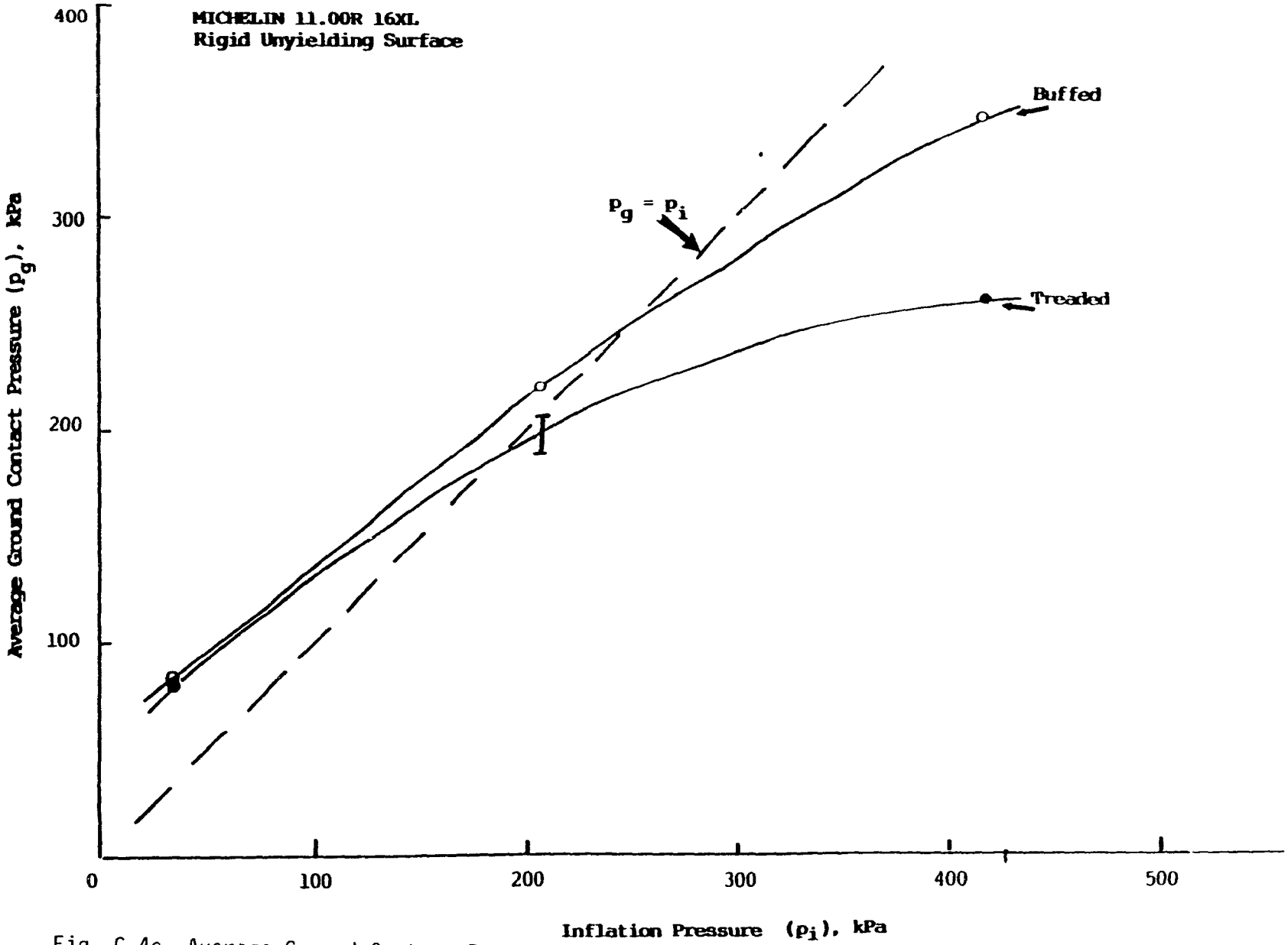


Fig. C.4c Average Ground Contact Pressure-Inflation Pressure Relationship for MICHELIN 11.00R-16XL

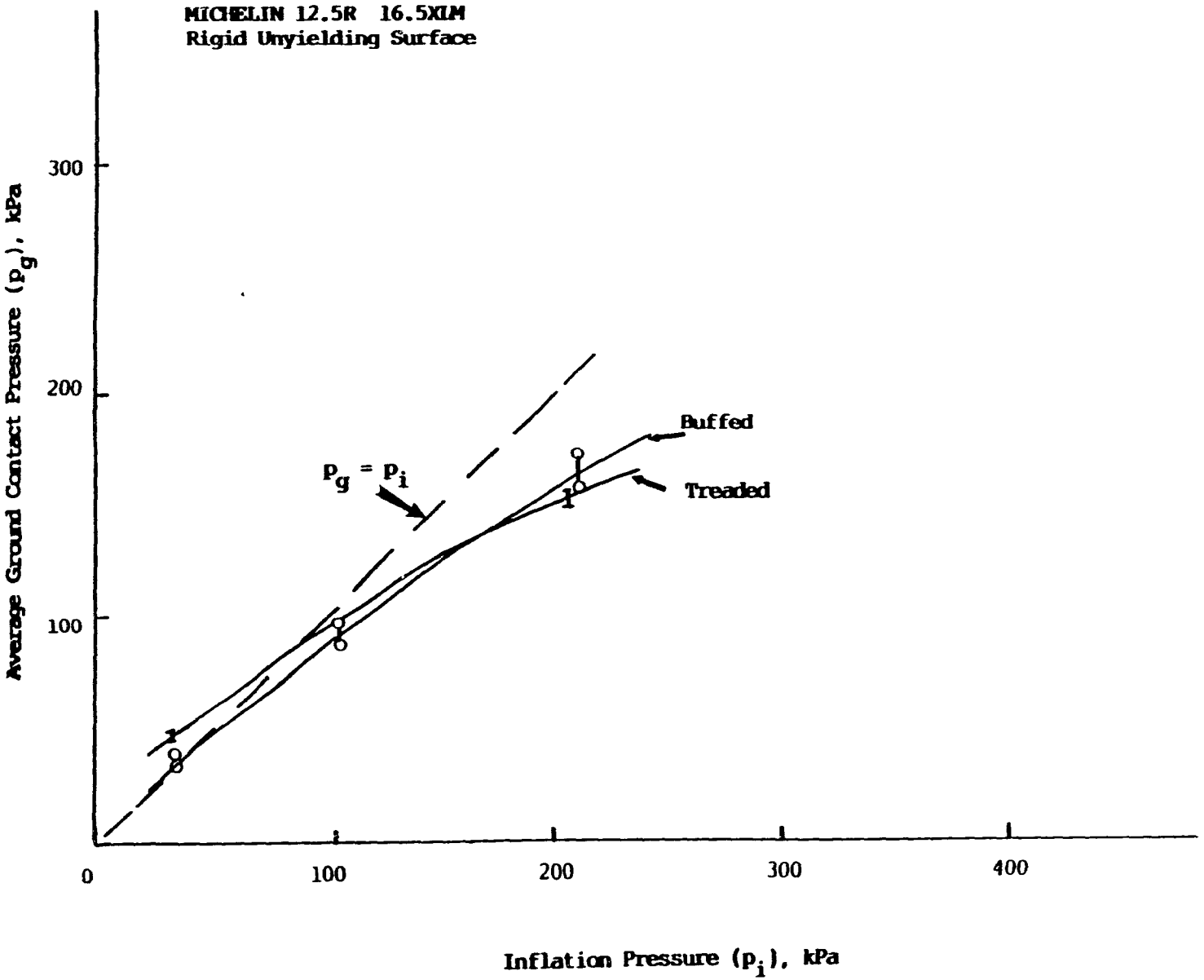


Fig. C.4a Average Ground Contact Pressure-Inflation Pressure Relationship for MICHELIN 12.5R-16.5XLM

TABLE C.4 Test Conditions Imposed in Pressure Distribution Determination

Tire	Inflation Pressure (kPa)	Wheel Load (kN)	Average Ground Contact Pressure (kPa) Based On		Fig. No.
			Gross Area	Lug Area	
GOODYEAR 7.00-16LT (treaded)	34.5	2.67	82.0	119.5	C.5a
GOODYEAR 7.00-16LT (treaded)	34.5	3.34	97.6	142.3	C.5b
GOODYEAR 7.00-16LT (treaded)	103.5	3.64	125.0	182.2	C.5c
GOODYEAR 7.00-16LT (treaded)	103.5	4.45	145.	211.4	C.5d
GOODYEAR 7.00-16LT (treaded)	310.5	5.46	208.0	303.2	C.5e
GOODYEAR 7.00-16LT (treaded)	310.5	6.68	234.5	341.8	C.5f
GOODYEAR 7.00-16LT (buffed)	34.5	0.356	48.7	48.7	C.6a
GOODYEAR 7.00-16LT (buffed)	34.5	0.712	48.7	48.7	C.6b
GOODYEAR 7.00-16LT (buffed)	34.5	1.067	48.7	48.7	C.6c/1-2
GOODYEAR 7.00-16LT (buffed)	34.5	1.423	48.7	48.7	C.6d/1-2
GOODYEAR 7.00-16LT (buffed)	34.5	1.779	52.3	52.3	C.6e/1-2
GOODYEAR 7.00-16LT (buffed)	103.5	0.890	110.8	110.8	C.6f
GOODYEAR 7.00-16LT (buffed)	103.5	2.668	110.8	110.8	C.6g/1-2
GOODYEAR 7.00-16LT (buffed)	103.5	3.564	110.8	110.8	C.6h/1-2
GOODYEAR 7.00-16LT (buffed)	103.5	4.454	113.0	110.8	C.6i/1-2
GOODYEAR 7.00-16LT (buffed)	310.5	1.334	246.5	246.5	C.6j

TABLE C.4 Continued

Tire	Inflation Pressure (kPa)	Wheel Load (kN)	Average Ground Contact Pressure (kPa) Based On		Fig. No.
			Gross Area	Lug Area	
GOODYEAR 7.00-16LT (buffed)	310.5	2.668	246.5	246.5	C.6k
GOODYEAR 7.00-16LT (buffed)	310.5	4.003	245.5	246.5	C.6l/1-2
GOODYEAR 7.00-16LT (buffed)	310.5	5.337	246.5	246.5	C.6m/1-2
GOODYEAR 7.00-16LT (buffed)	310.5	6.672	265.0	246.5	C.6n/1-3
MICHELIN 7.00R-16XCL (treaded)	34.5	0.356	72.7	121.2	C.7a
MICHELIN 7.00R-16XCL (treaded)	34.5	0.711	72.7	121.2	C.7b
MICHELIN 7.00R-16XCL (treaded)	34.5	1.067	72.7	121.2	C.7c
MICHELIN 7.00R-16XCL (treaded)	34.5	1.423	72.7	121.1	C.7d
MICHELIN 7.00R-16XCL (treaded)	34.5	1.779	72.7	121.1	C.7e
MICHELIN 7.00R-16XCL (treaded)	103.5	0.711	122.4	204.0	C.7f
MICHELIN 7.00R-16XCL (treaded)	103.5	1.423	122.4	204.0	C.7g
MICHELIN 7.00R-16XCL (treaded)	103.5	2.135	122.4	204.0	C.7h
MICHELIN 7.00R-16XCL (treaded)	103.5	2.845	122.4	204.0	C.7i
MICHELIN 7.00-16XCL (treaded)	103.5	3.558	132.0	220.0	C.7j

TABLE C.4 Continued

Tire	Inflation Pressure (kPa)	Wheel Load (kN)	Average Ground Contact Pressure (kPa) Based On		Fig. No.
			Gross Area	Lug Area	
MICHELIN 7.00R-16XCL (treaded)	310.5	1.601	233.0	388.3	C.7k
MICHELIN 7.00R-16XCL (treaded)	310.5	2.846	233.0	388.3	C.7l
MICHELIN 7.00R-16XCL (treaded)	310.5	4.270	233.0	388.3	C.7m
MICHELIN 7.00R-16XCL (treaded)	310.5	5.693	233.0	388.3	C.7n
MICHELIN 7.00R-16XCL (treaded)	310.5	7.117	249.0	415.0	C.7p
MICHELIN 7.00R-16XCL (buffed)	103.5	2.85	105.2	105.2	C.8a/1-2-3
MICHELIN 7.00R-16XCL (buffed)	310.5	8.02	275.3	275.3	C.8b/1-2-3-4
MICHELIN 11.00R-16XL (treaded)	34.5	2.50	83.0	143.1	C.9a
MICHELIN 11.00R-16XL (treaded)	34.5	3.12	83.0	143.1	C.9b
MICHELIN 11.00R-16XL (treaded)	207.0	6.42	187.0	322.4	C.9c
MICHELIN 11.00R-16XL (treaded)	207.0	8.02	205.0	353.4	C.9d
MICHELIN 11.00R-16XL (treaded)	414.0	10.69	261.0	450.0	C.9e
MICHELIN 11.00R-16XL (treaded)	414.0	13.34	261.0	450.0	C.9f

TABLE C.4 Continued

Tire	Inflation Pressure (kPa)	Wheel Load (kN)	Average Ground Contact Pressure (kPa) Based On		Fig. No.
			Gross Area	Lug Area	
MICHELIN 11.00R-16XL (buffed)	207.0	6.40	222.0	222.0	C.10a/1-2
MICHELIN 11.00R-16XL (buffed)	414.0	13.34	345.0	345.0	C.10b/1-2-3
MICHELIN 12.5R-16.5XLM (treaded)	34.5	2.67	52.	110.6	C.11a
MICHELIN 12.5R-16.5XLM (treaded)	103.5	4.45	101.	214.9	C.11b
MICHELIN 12.5R-16.5XLM (treaded)	207.0	6.68	158.	336.2	C.11c
MICHELIN 12.5R-16.5XLM (buffed)	103.5	0.89	87.0	87.0	C.12a
MICHELIN 12.5R-16.5XLM (buffed)	103.5	1.78	87.0	87.0	C.12b
MICHELIN 12.5R-16.5XLM (buffed)	103.5	3.56	87.0	87.0	C.12c/1-2
MICHELIN 12.5R-16.5XLM (buffed)	103.5	4.45	95.7	95.7	C.12d/1-3
MICHELIN 12.5R-16.5XLM (buffed)	207.0	1.34	158.0	158.0	C.12e
MICHELIN 12.5R-16.5XLM (buffed)	207.0	2.67	158.0	158.0	C.12f
MICHELIN 12.5R-16.5XLM (buffed)	207.0	4.01	158.0	158.0	C.12g/1-2
MICHELIN 12.5R-16.5XLM (buffed)	207.0	5.34	158.0	158.0	C.12h/1-2
MICHELIN 12.5R-16.5XLM (buffed)	207.0	6.67	171.5	171.5	C.12i/1-2

GOODYEAR 7.00-16LT treaded
Rigid surface
Inflation pressure = 34.5 kPa
Wheel load = 2.67 kN
Average ground contact pressure = 119.5 kPa (based on lug area)

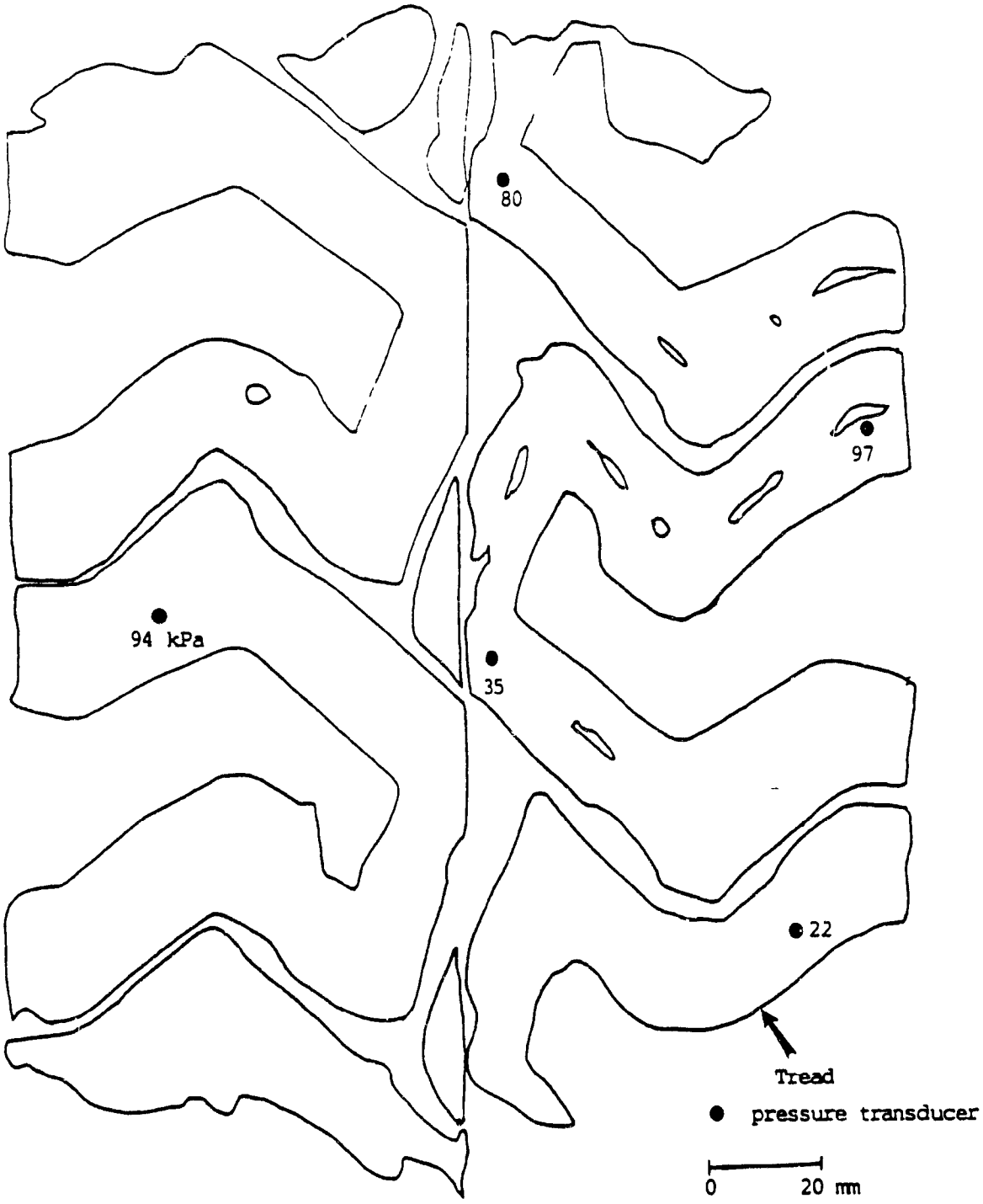


Fig. C.5a Pressure Transducer Readings Within the Footprint of GOODYEAR 7.00-16LT (treaded)

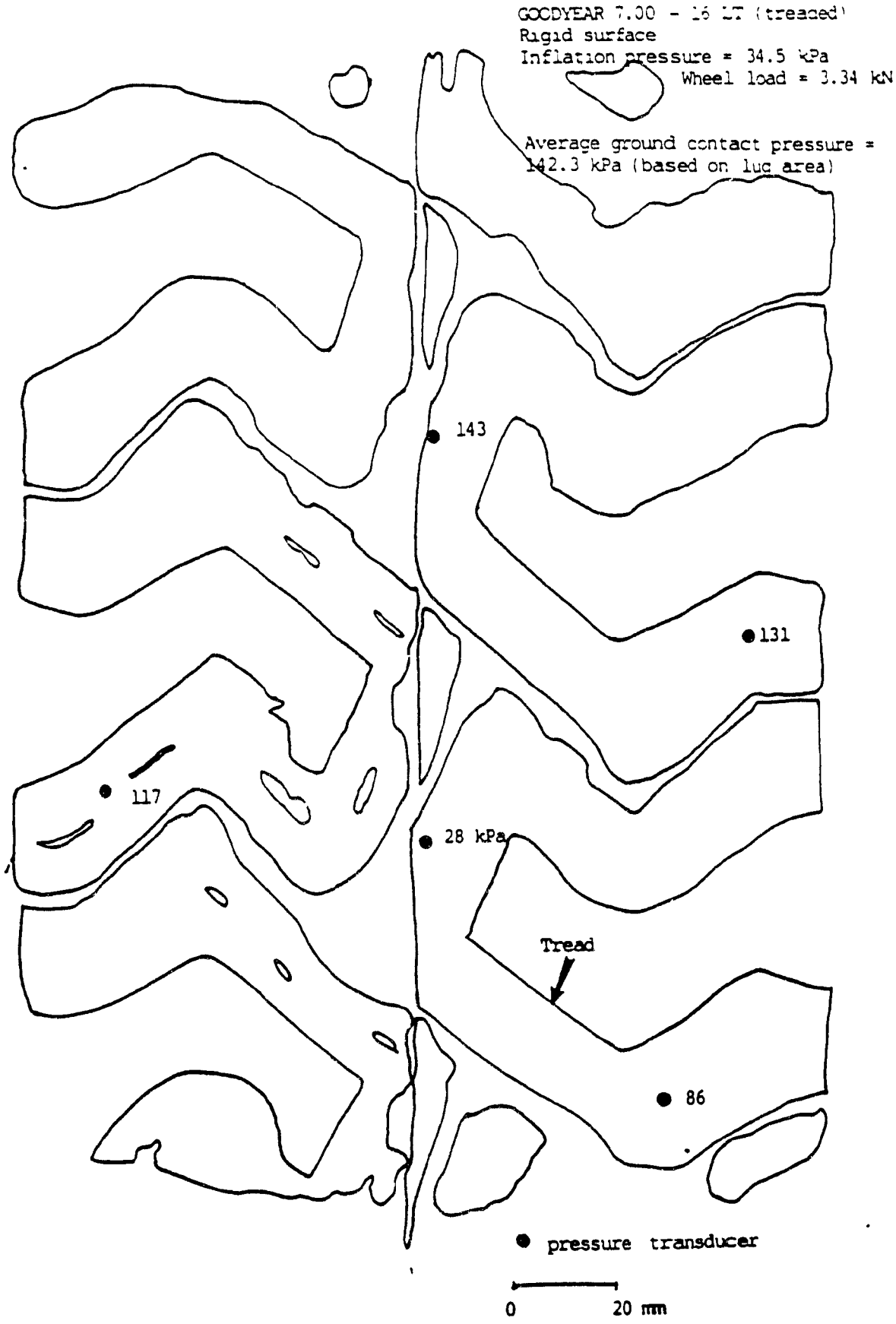


Fig. C.5b Pressure Transducer Readings Within the Footprint of GOODYEAR 7.00-16LT (treaded)

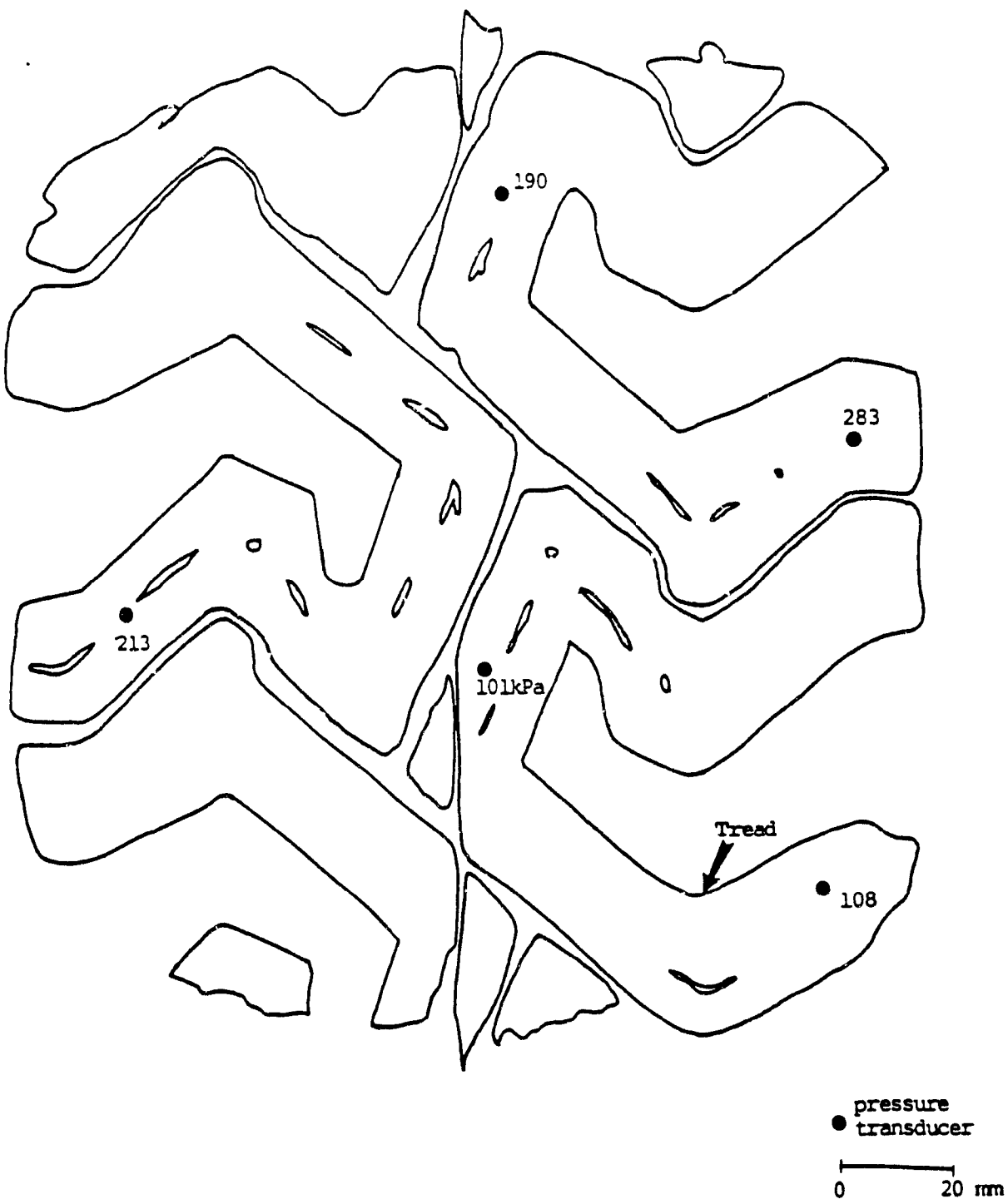


Fig. C.5c Pressure Transducer Readings Within the Footprint of GOODYEAR 7.00-16LT (treaded)

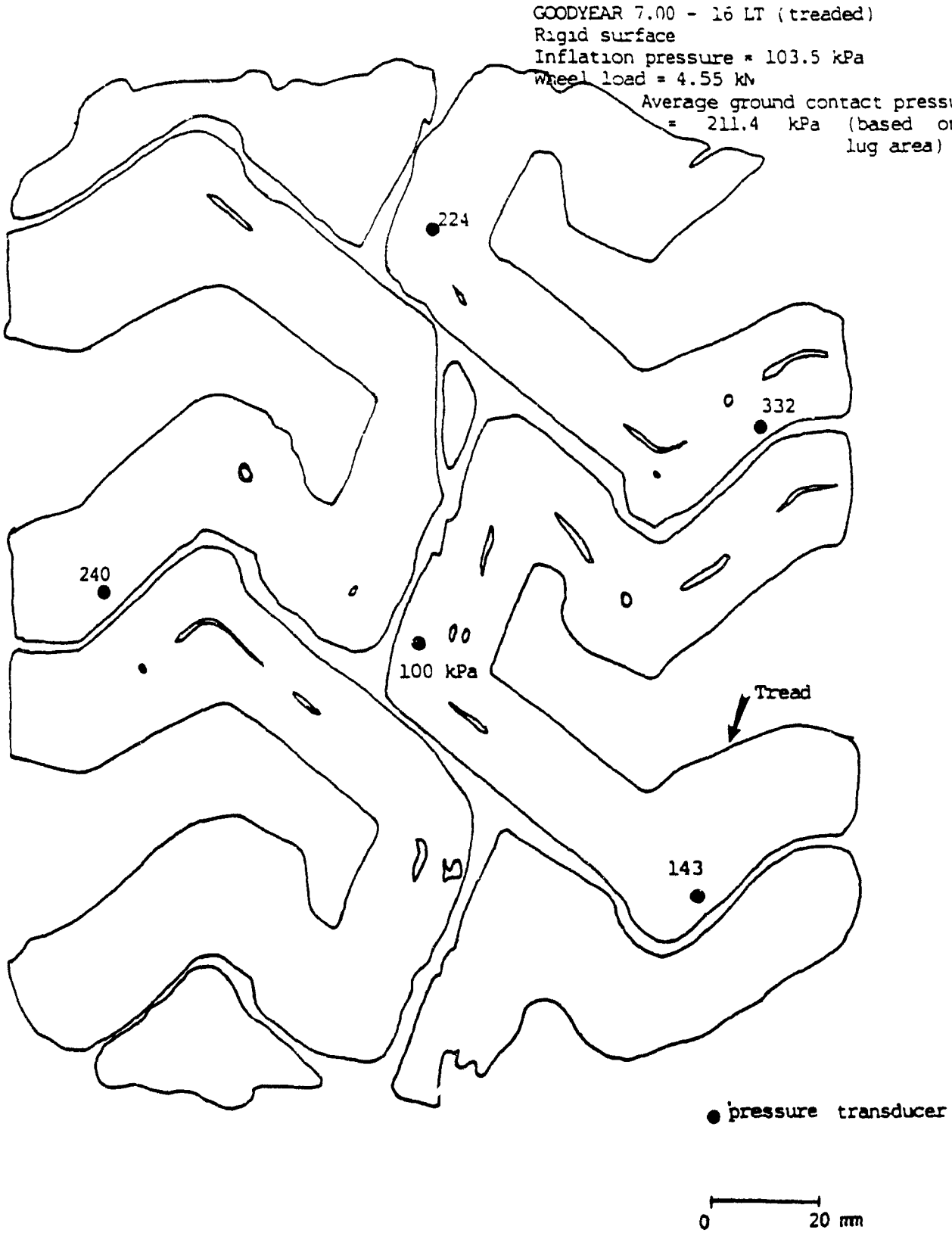


Fig. C.5d Pressure Transducer Readings Within the Footprint of GOODYEAR 7.00-16LT (treaded)

GOODYEAR 7.00 - 16 LT (treaded)
Rigid surface
Inflation pressure = 310.5 kPa
Wheel load = 5.46 kN

Average ground contact pressure = 303.2 kPa
(based on lug area)

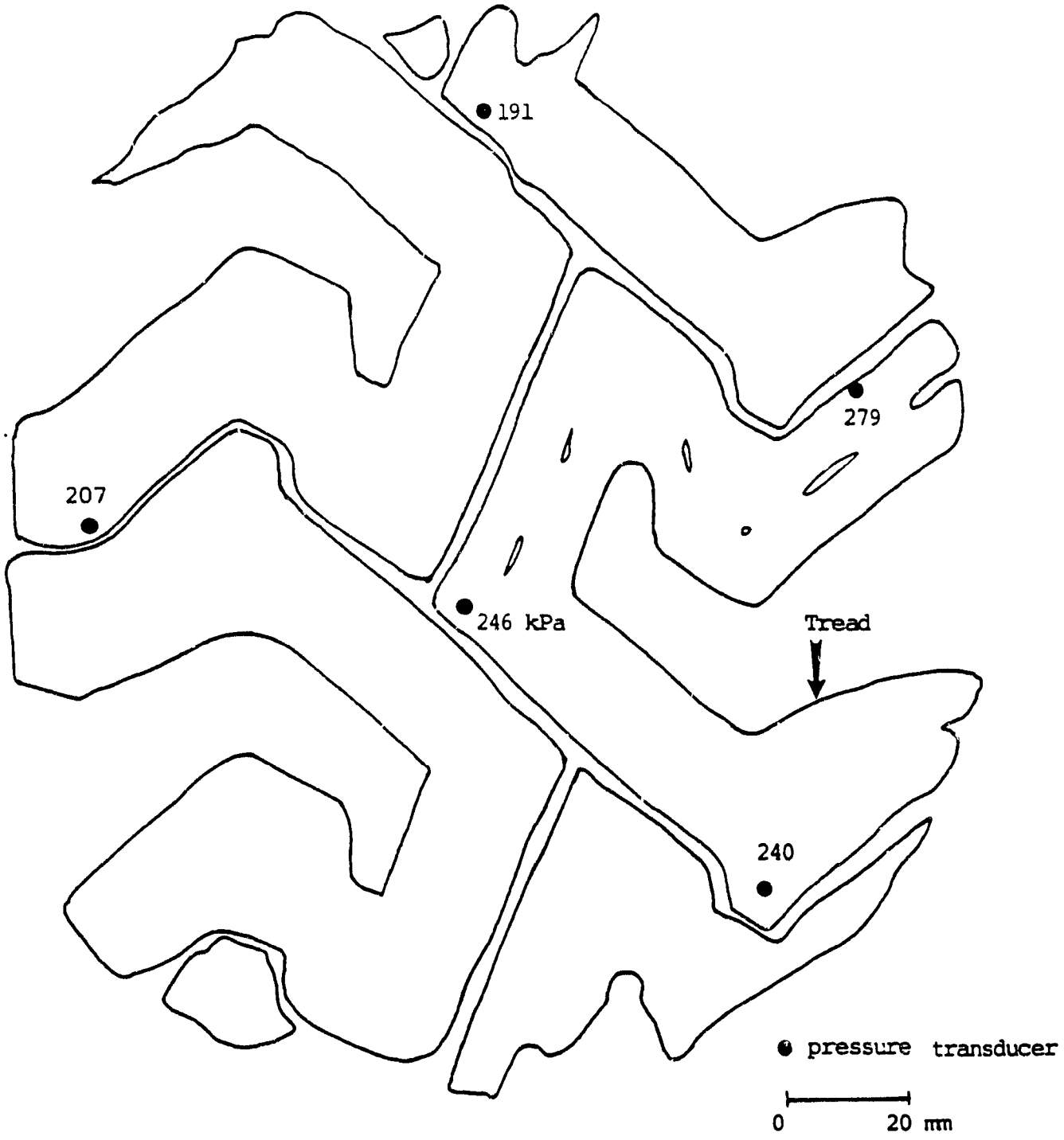


Fig. C.5e Pressure Transducer Readings Within the Footprint of GOODYEAR 7.00-16LT (treaded)

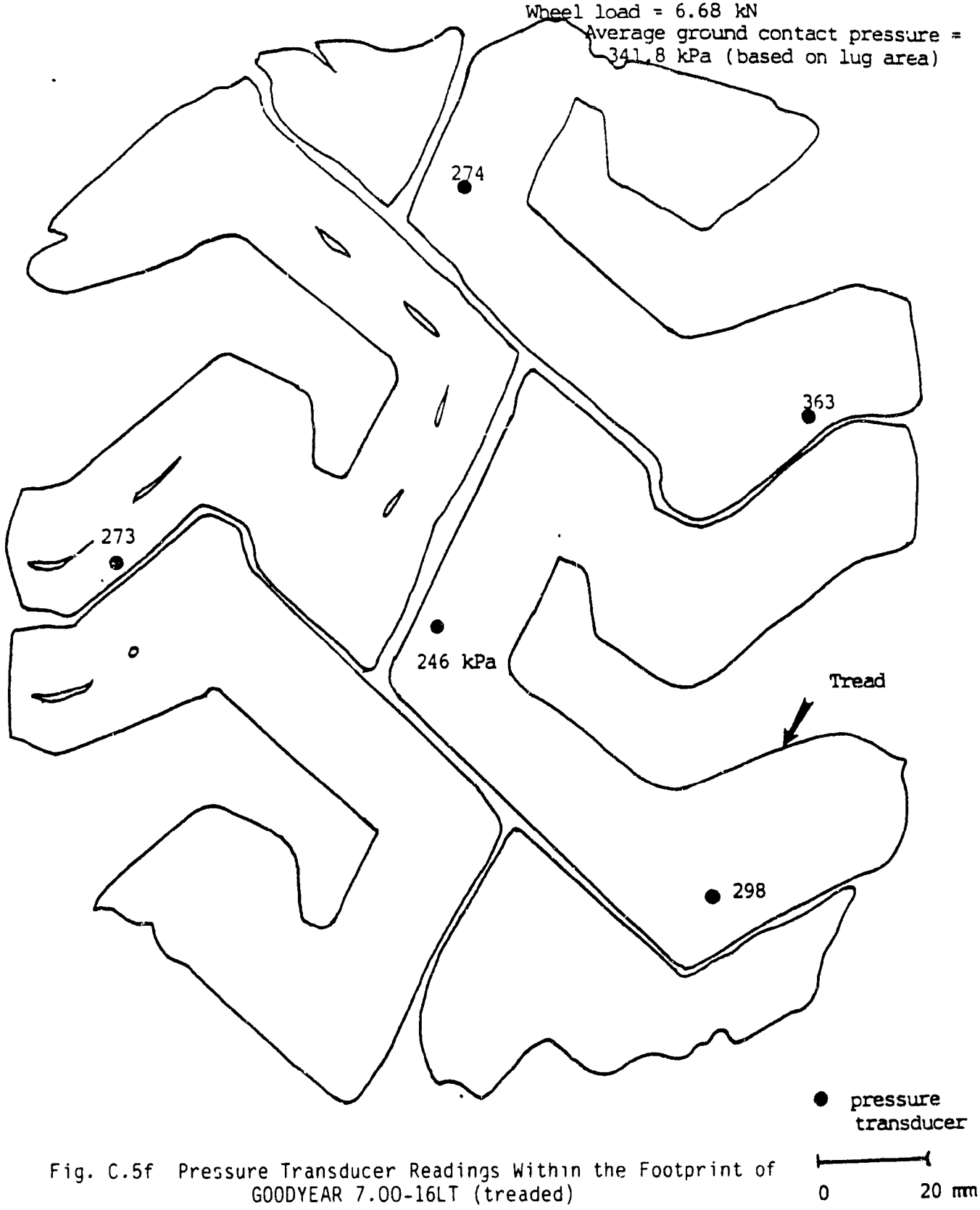


Fig. C.5f Pressure Transducer Readings Within the Footprint of GOODYEAR 7.00-16LT (treaded)

GOODYEAR 7.00-16 LT (buffed)

Rigid surface

Inflation pressure = 34.5 kPa

Wheel load = 0.356 kN

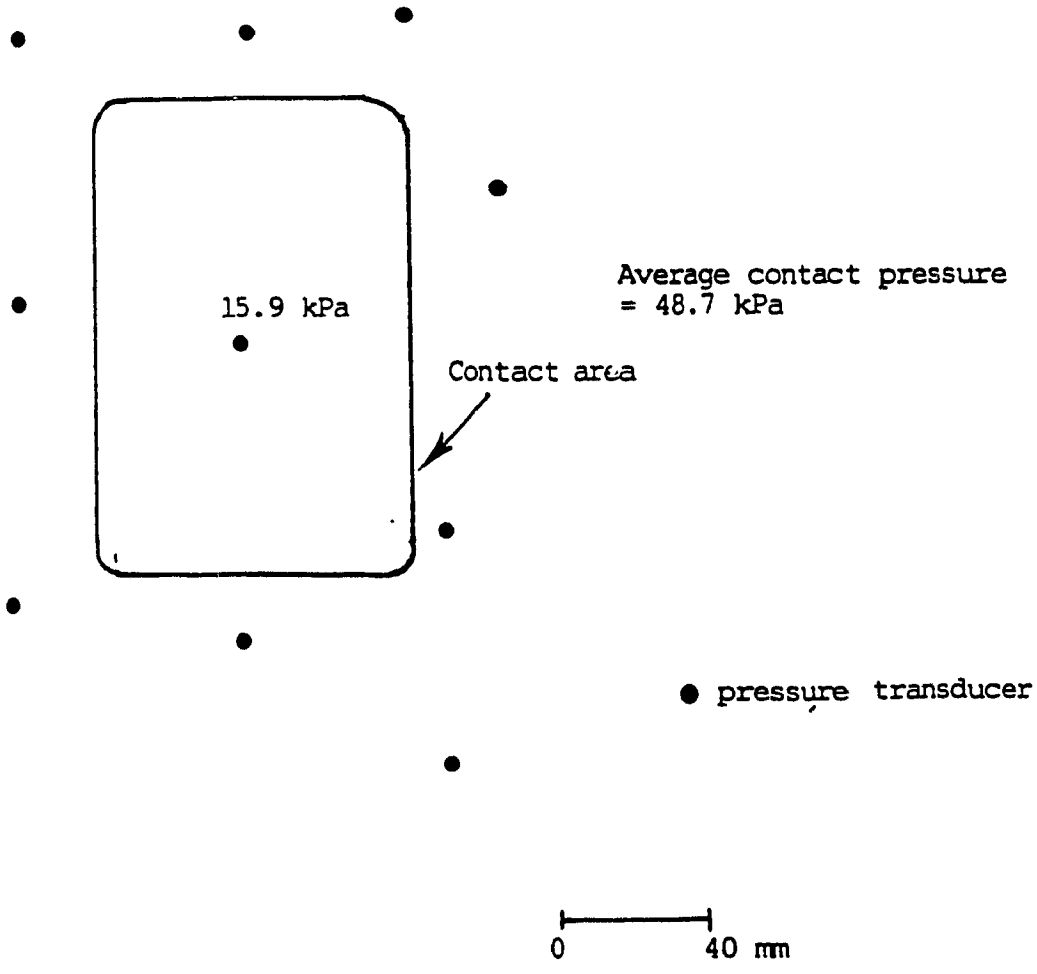


Fig. C.6a Pressure Transducer Readings Within the Footprint of GOODYEAR 7.00-16LT (buffed)

GOODYEAR 7.00 - 16 LT (buffed)
Rigid surface
Inflation pressure = 34.5 kPa
Wheel load = 0.712 kN

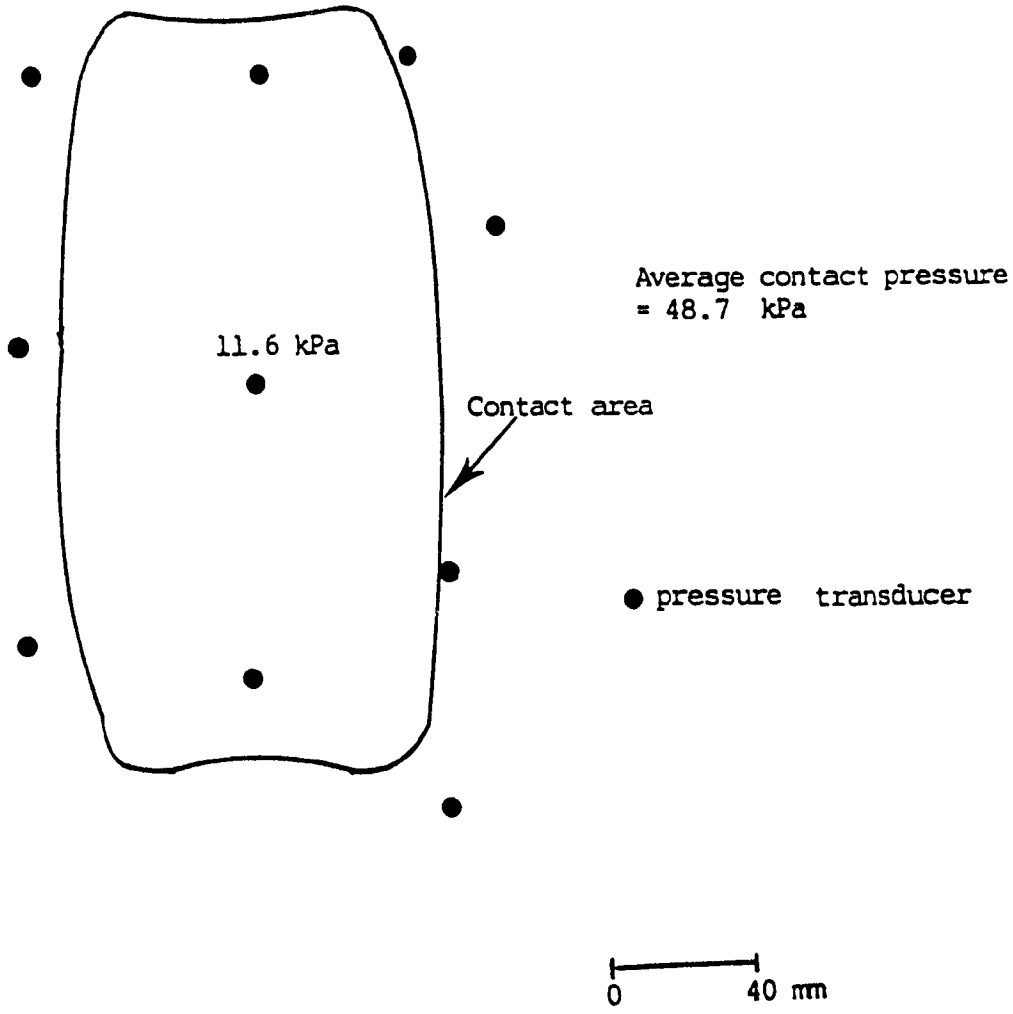


Fig. C.6b Pressure Transducer Readings Within the Footprint of GOODYEAR 7.00-16LT (buffed)

GOODYEAR 7.00 - 16 LT (buffed)
Rigid surface
Inflation pressure = 34.5 kPa
Wheel load = 1.067 kN

Average contact pressure
= 48.7 kPa

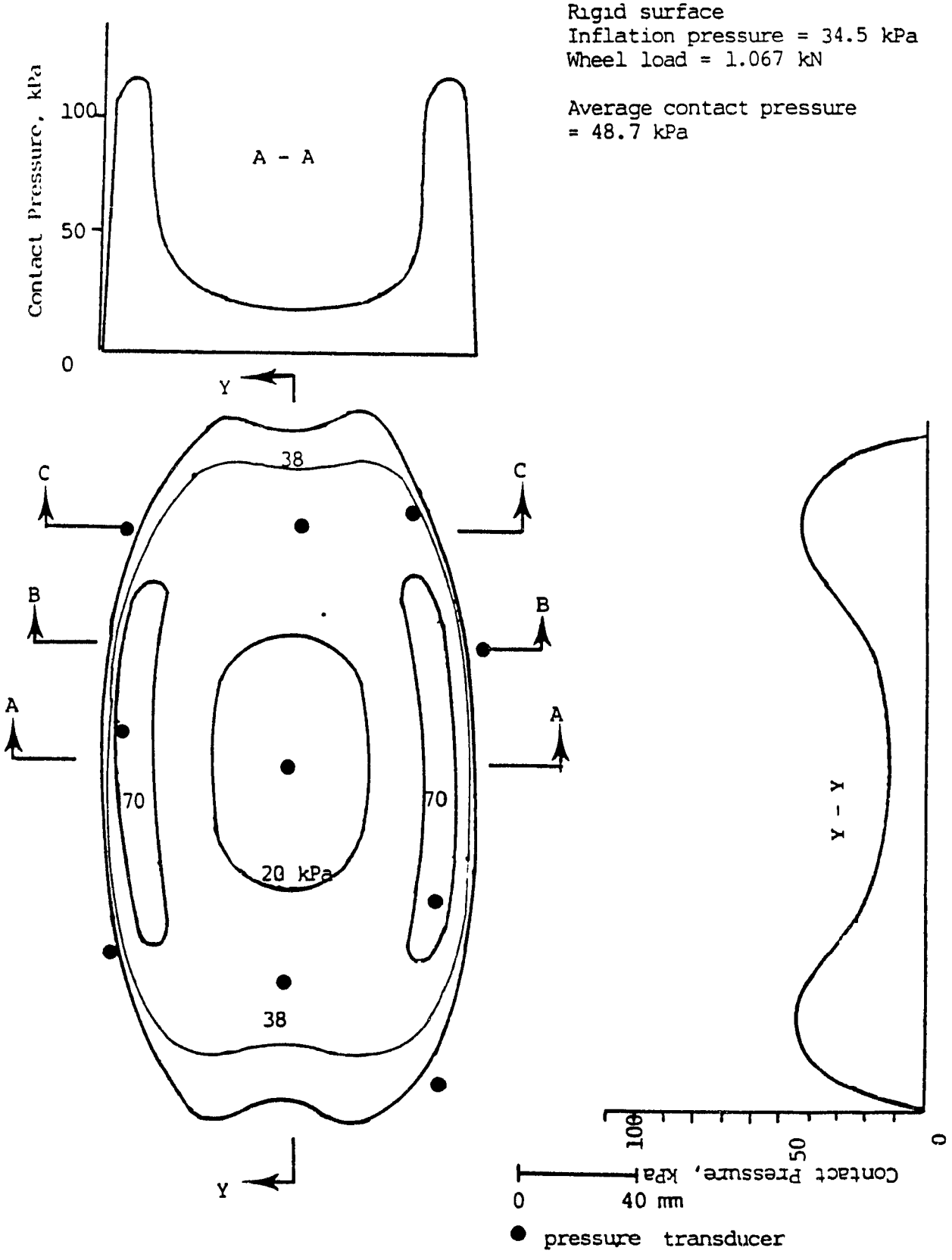


Fig. C.6c/1 Isobars of Pressure Distribution Within the Footprint of GOODYEAR 7.00-16LT (buffed)

GOODYEAR 7.00 - 16 LT (buffed)
Rigid surface
Inflation pressure = 34.5 kPa
Wheel load = 1.067 kN

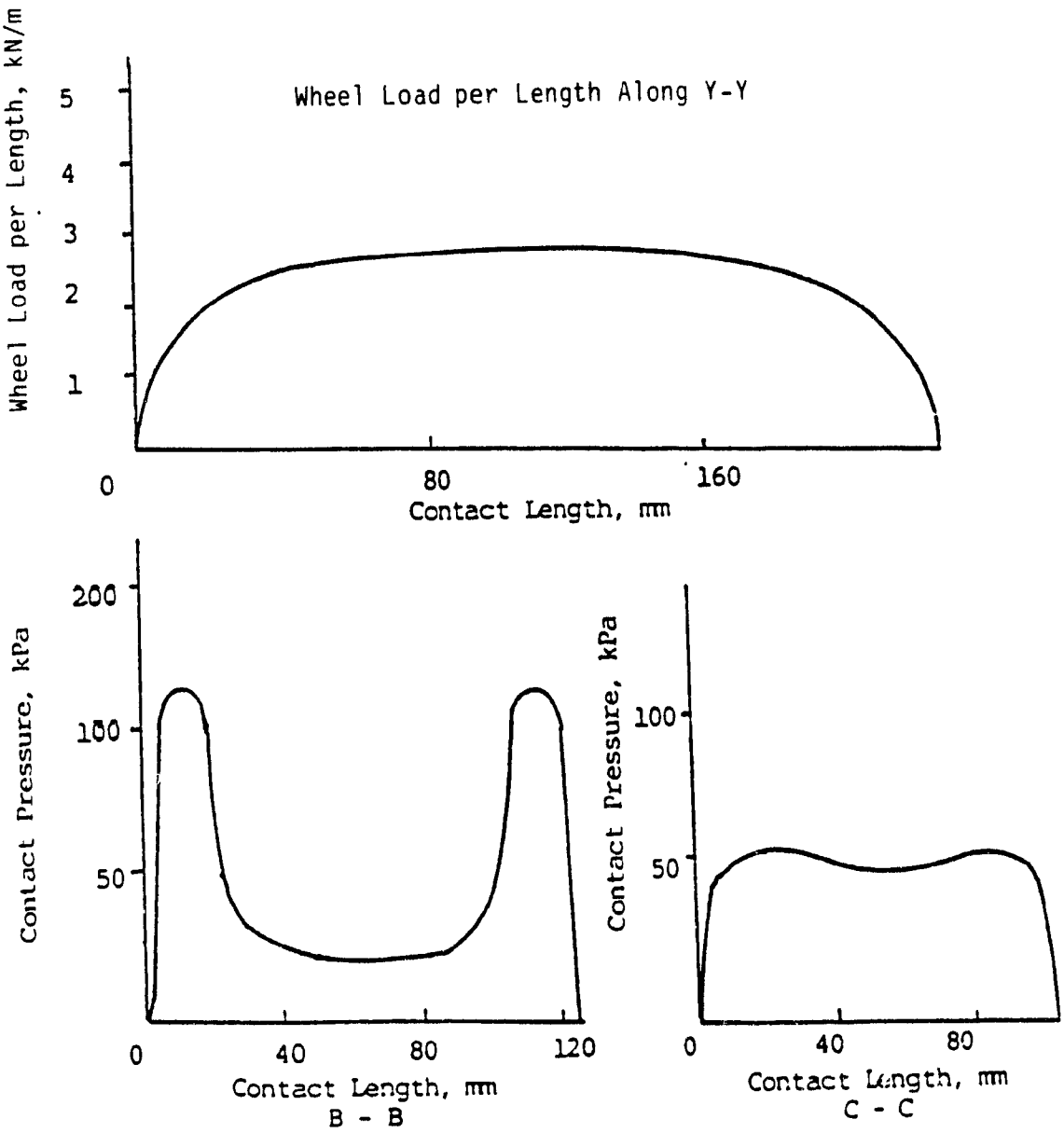


Fig. C.6c/2 Pressure Distribution Within the Footprint of GOODYEAR 7.00-16LT (buffed)

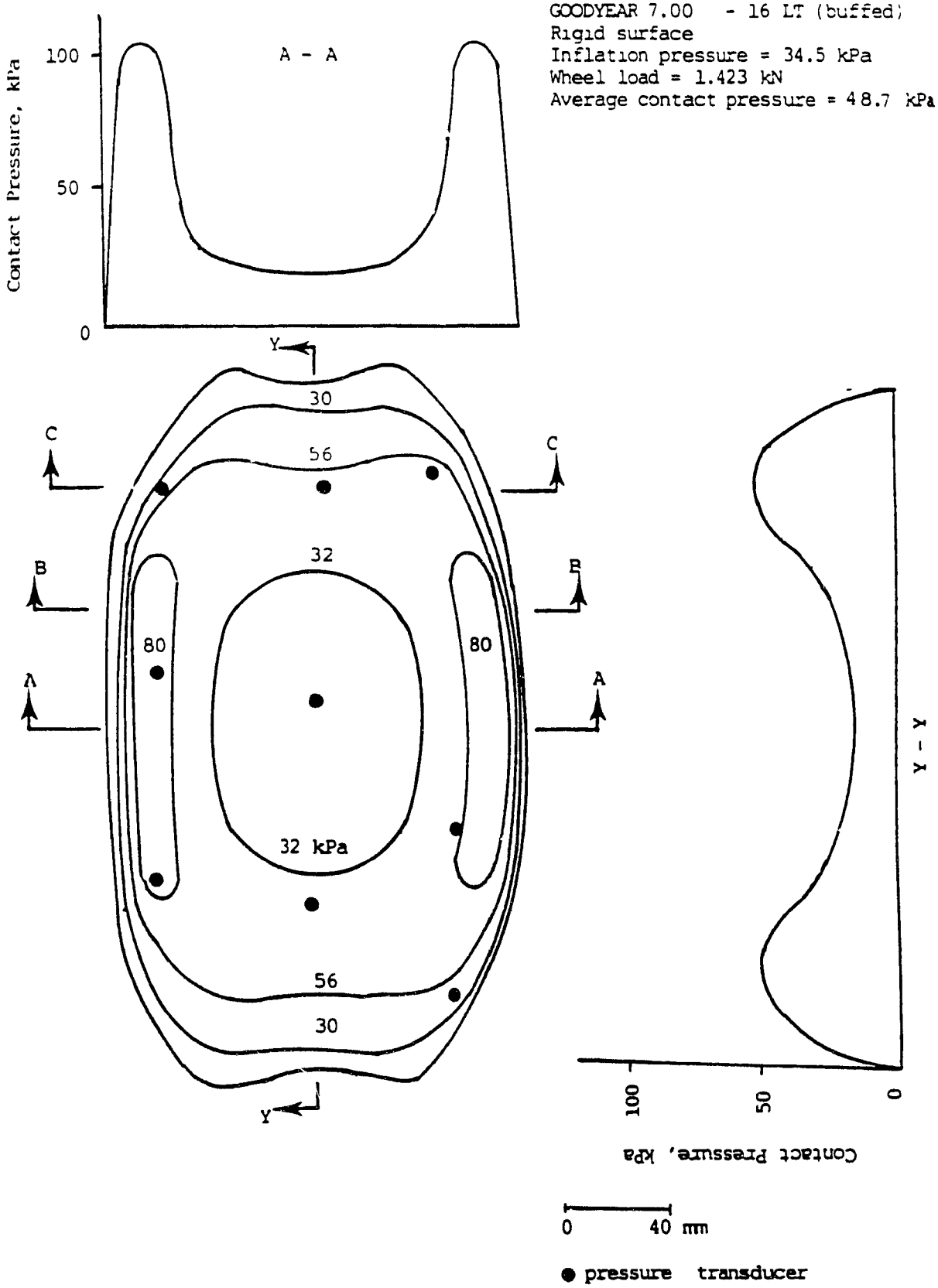


Fig. C.6d/1 Isobars of Pressure Distribution Within the Footprint of GOODYEAR 7.00-16LT (buffed)

GOODYEAR 7.00 - 16 LT (buffed)
Rigid surface
Inflation pressure = 34.5 kPa
Wheel load = 1.423 kN

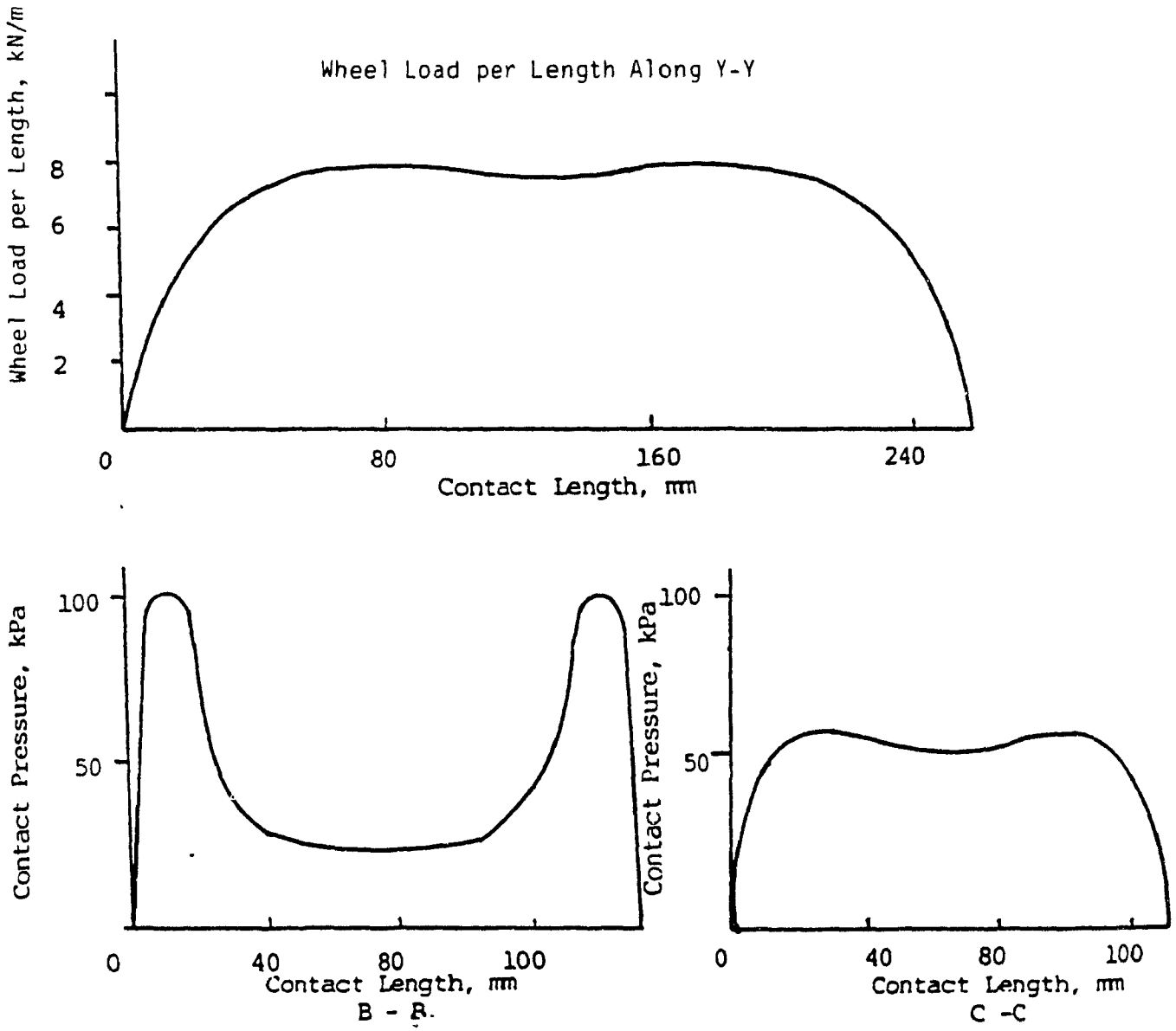


Fig. C.6d/2 Pressure Distribution Within the Footprint of GOODYEAR 7.00-16LT (buffed)

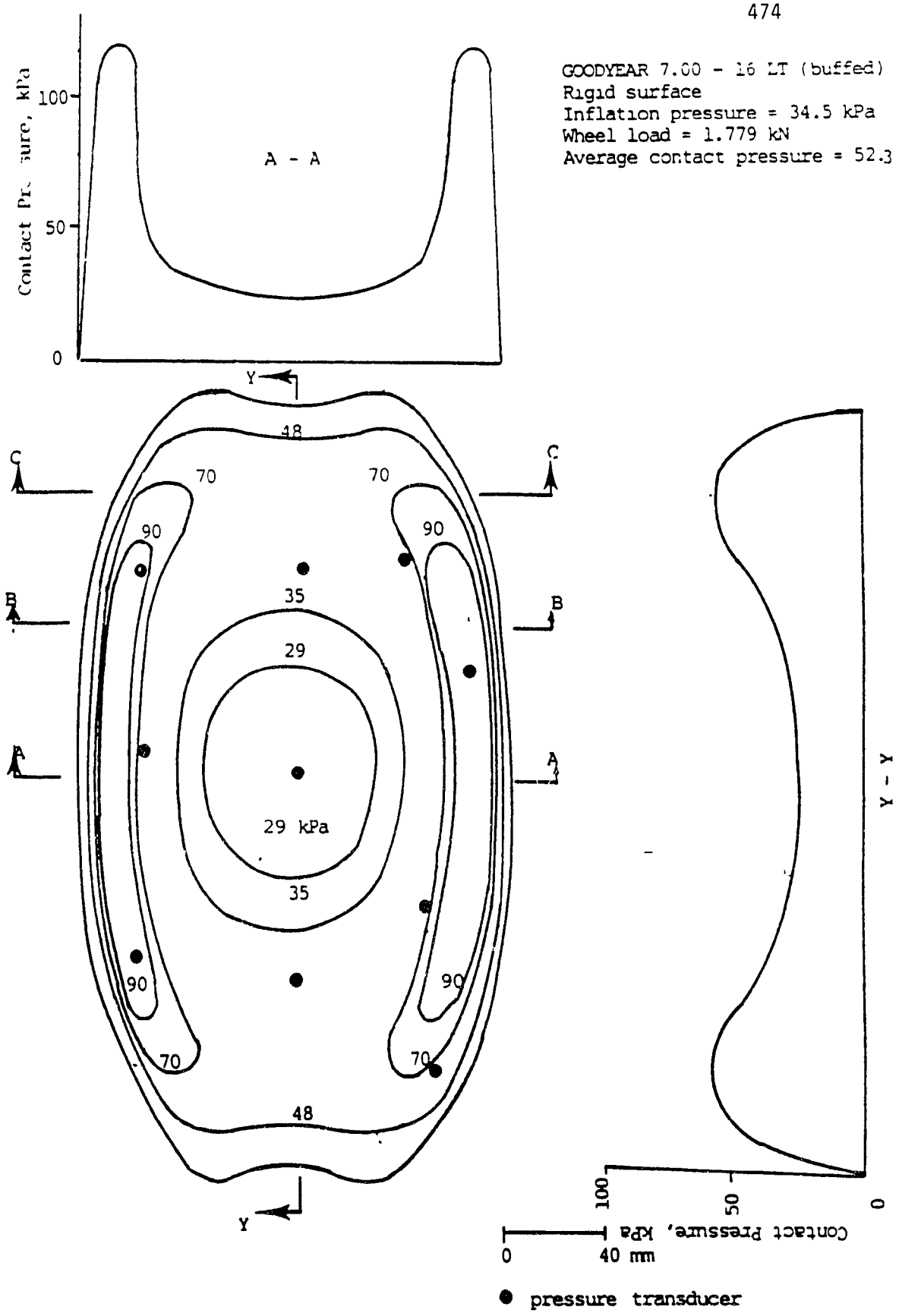
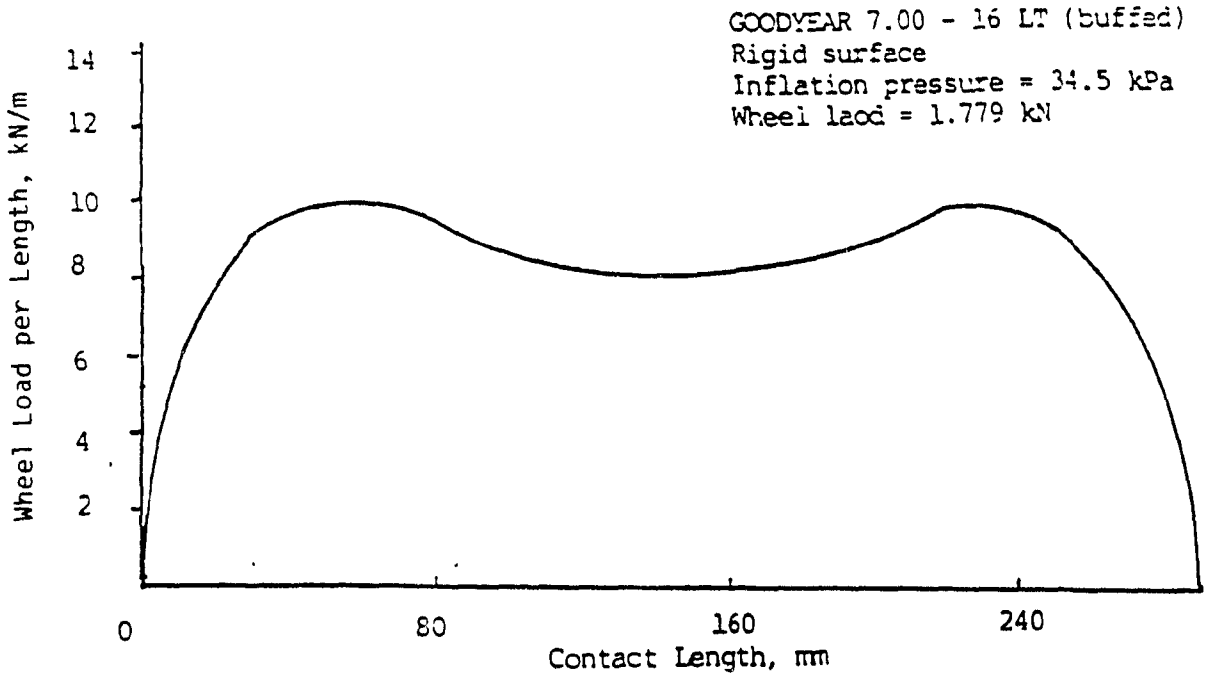


Fig. C.6e/1 Contact Pressure Distribution Within the Footprint of GOODYEAR 7.00-16LT (buffed)



Wheel Load per Length Along Y-Y

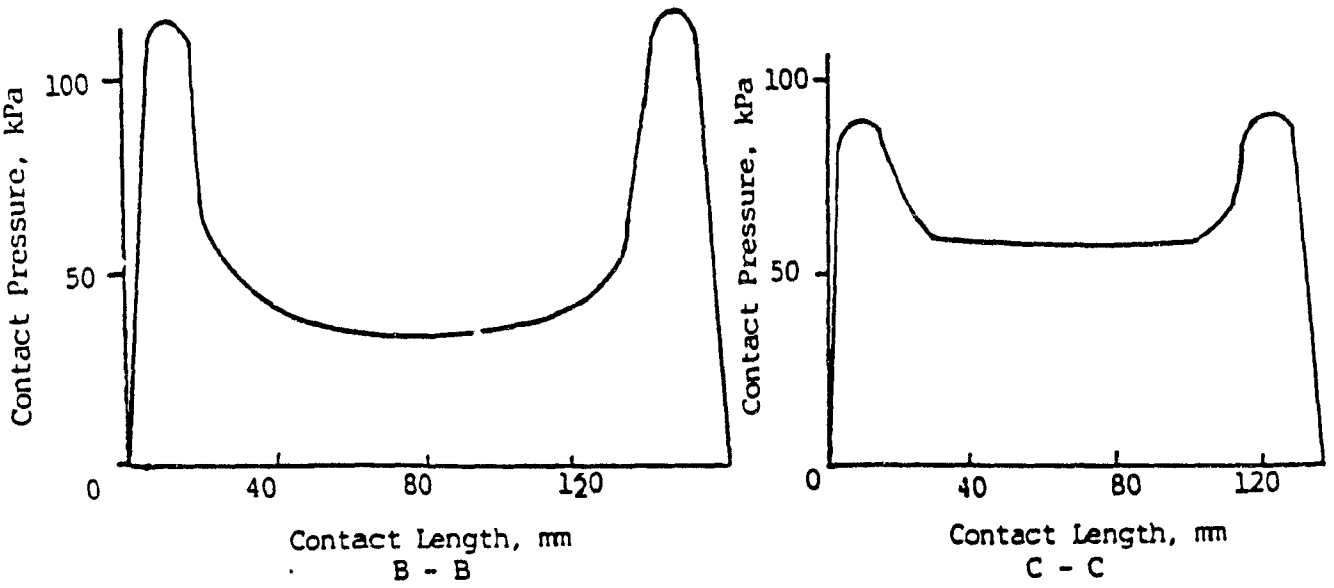


Fig. C.6e/2 Contact Pressure Distribution Within the Footprint of GOODYEAR 7.00-16LT (buffed)

GOODYEAR 7.00- 16 LT (buffed)
Rigid surface
Inflation pressure = 103.5 kPa
Wheel load = 0.890 kN

Average ground contact pressure = 110.8 kPa

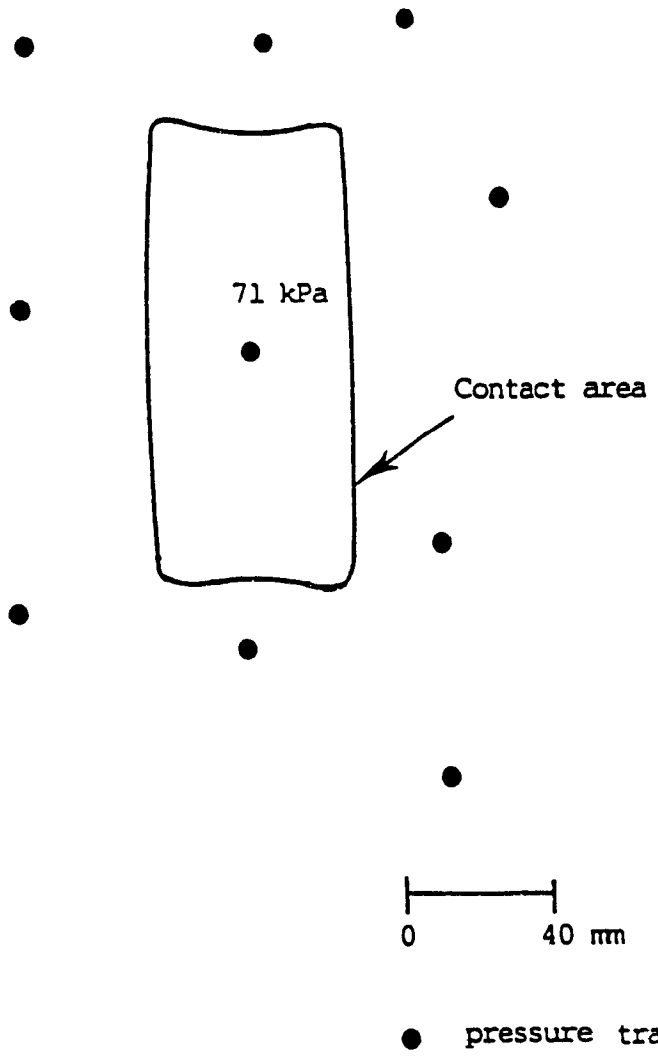


Fig. C.6f Pressure Transducer Readings Within the Footprint of GOODYEAR 7.00-16LT (buffed)

GOODYEAR 7.00 - 16 LT (buffed)
Rigid surface
Inflation pressure = 103.5 kPa
Wheel load = 2.668 kN
Average contact pressure = 110.8 kPa

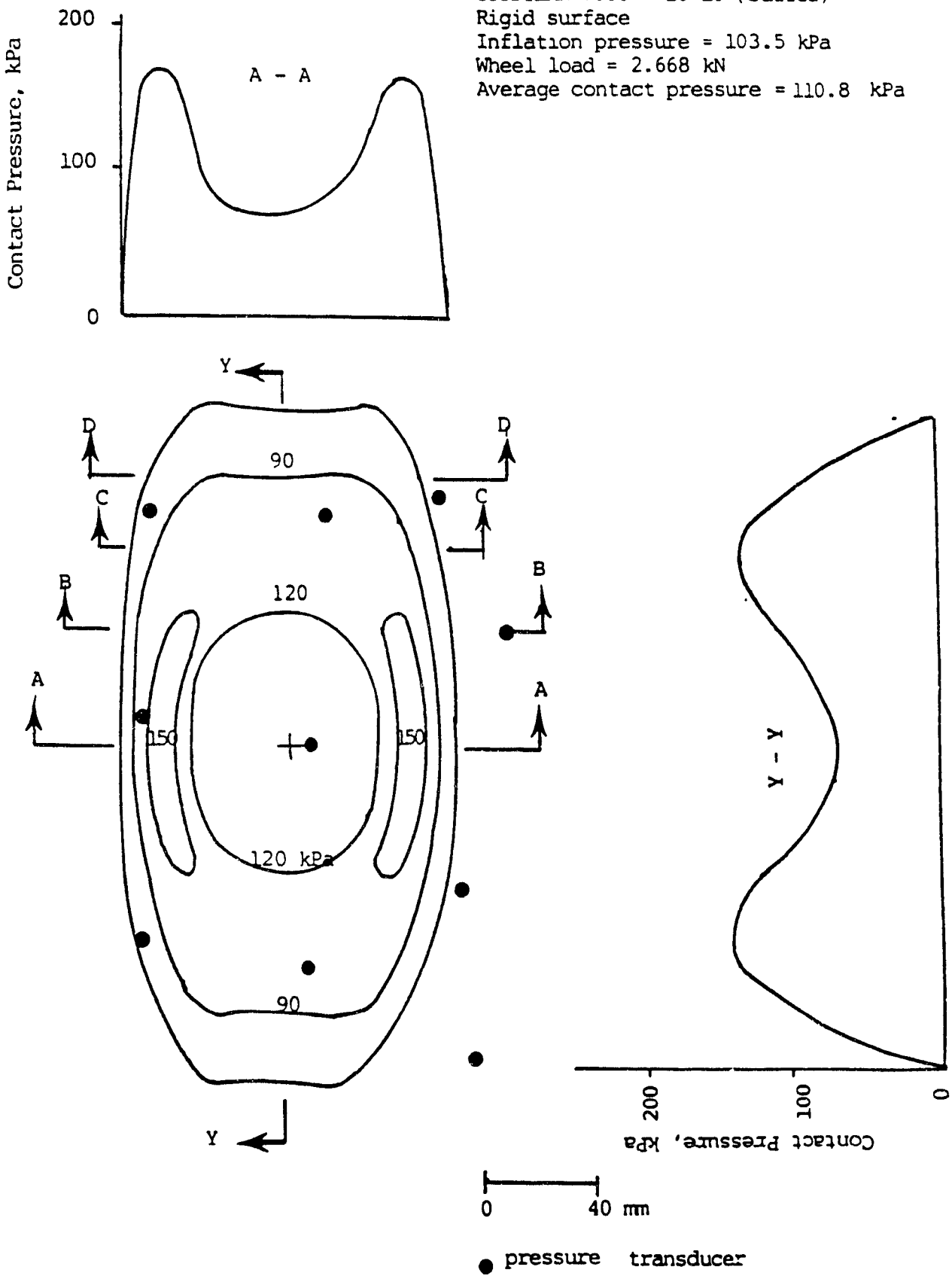


Fig. C.6g/1 Contact Pressure Distribution Within the Footprint of GOODYEAR 7.00-16LT (buffed)

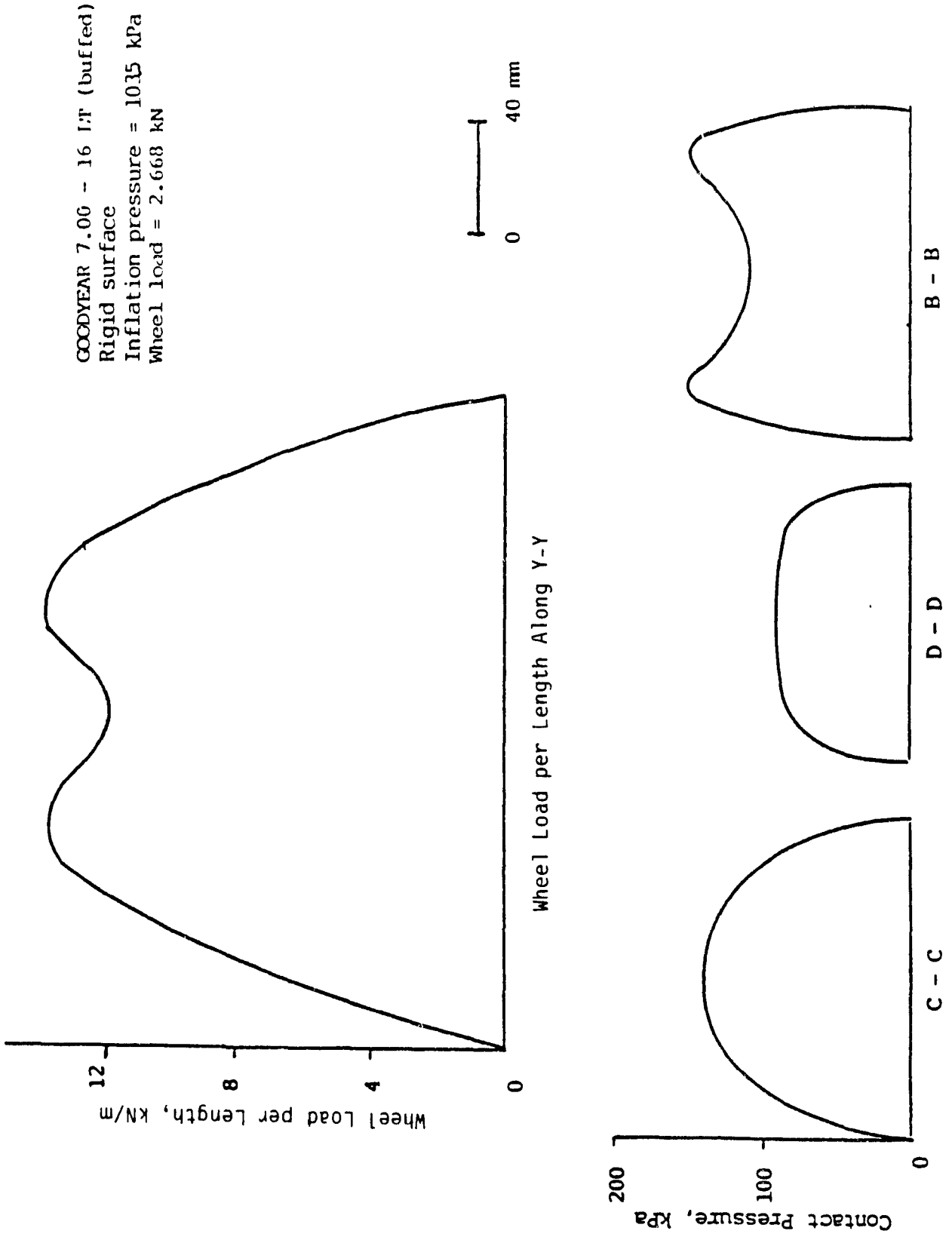


Fig. C.6g/2 Contact Pressure Distribution Within the Footprint of GOODYEAR 7.00-16LT (buffed)

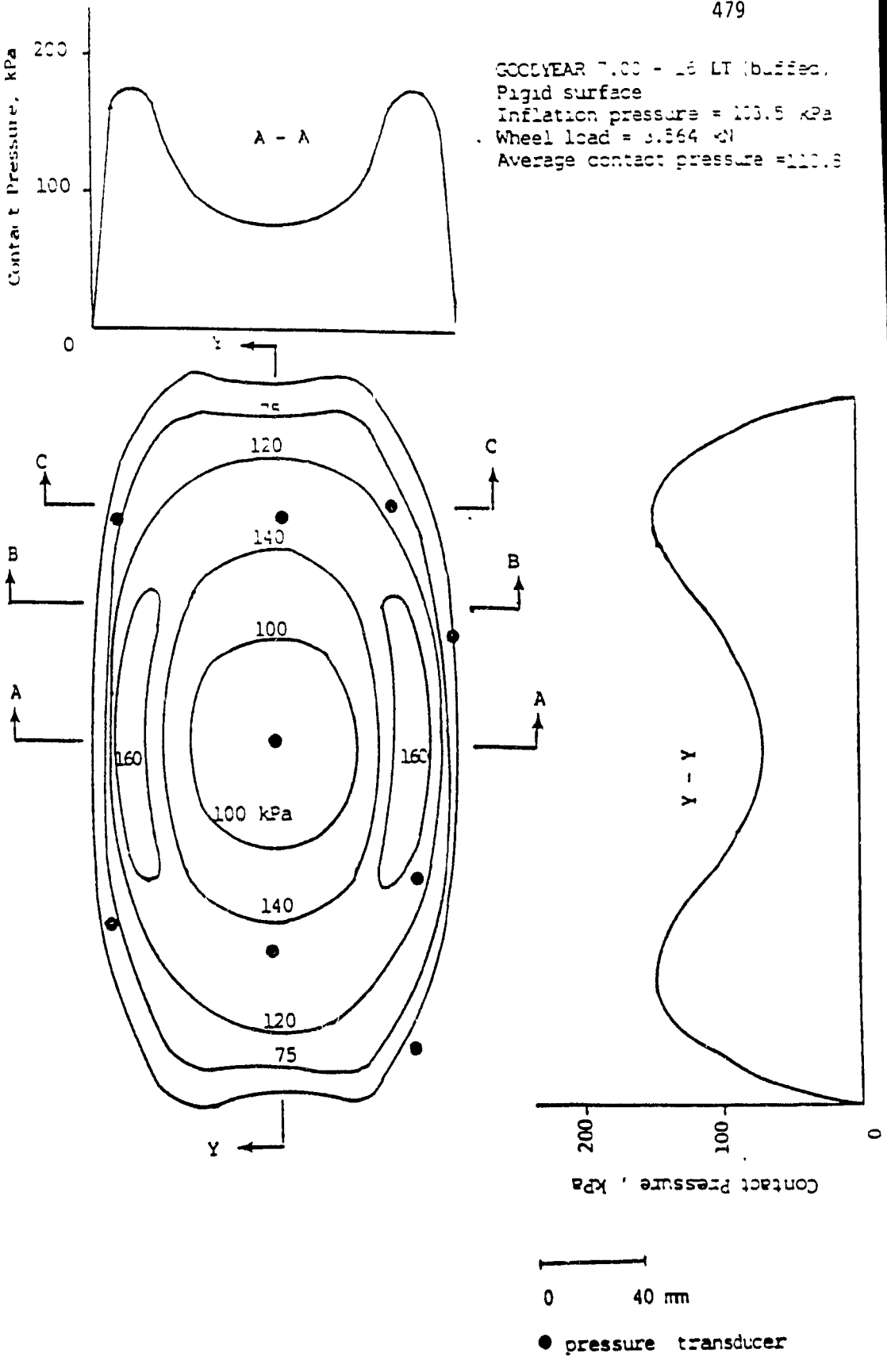


Fig. C.6h/1 Contact Pressure Distribution Within the Footprint of GOODYEAR 7.00-16LT (buffed)

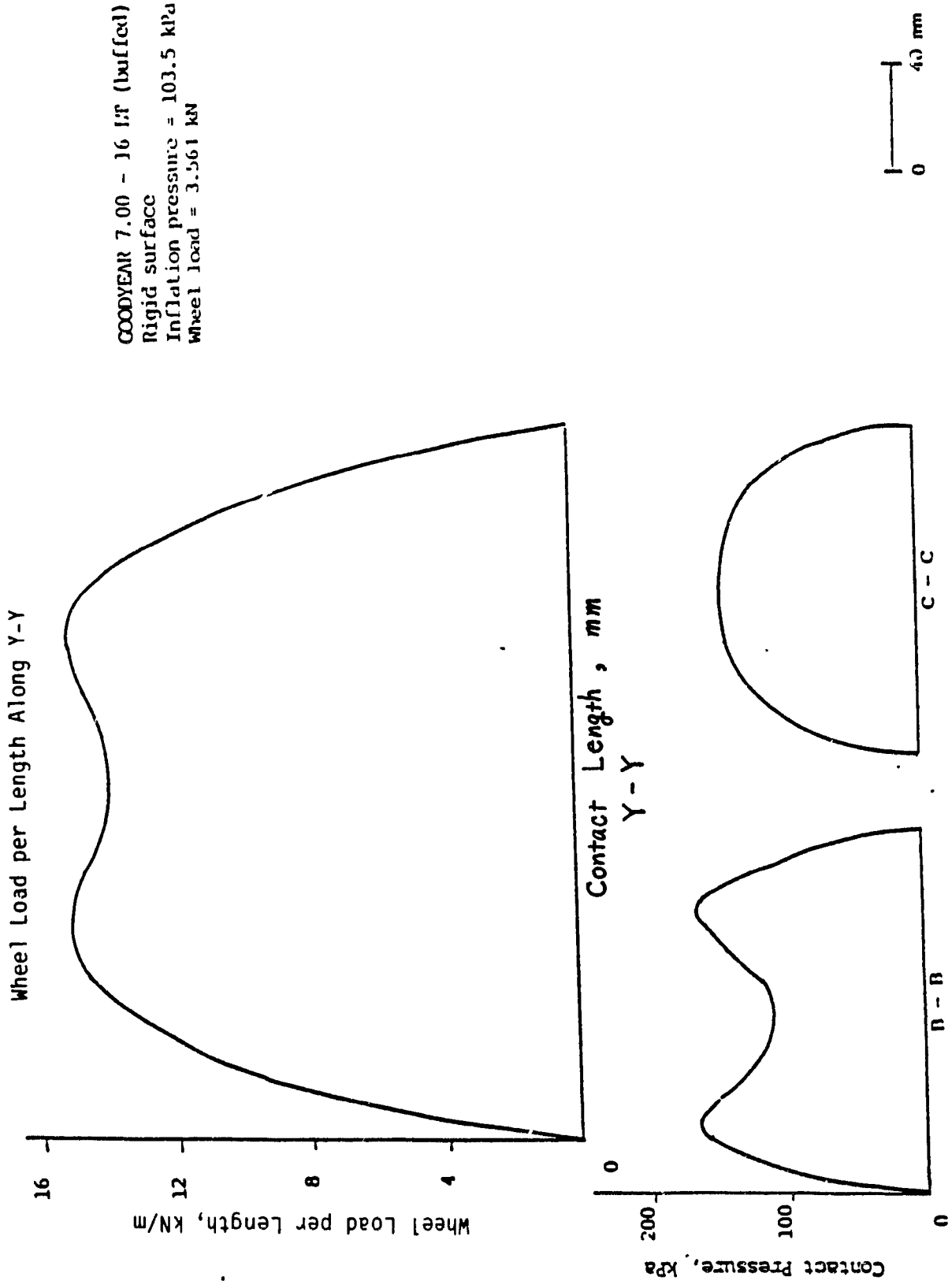


Fig. C.6h/2 Contact Pressure Distribution Within the Footprint of GOODYEAR 7.00-16LT (buffed)

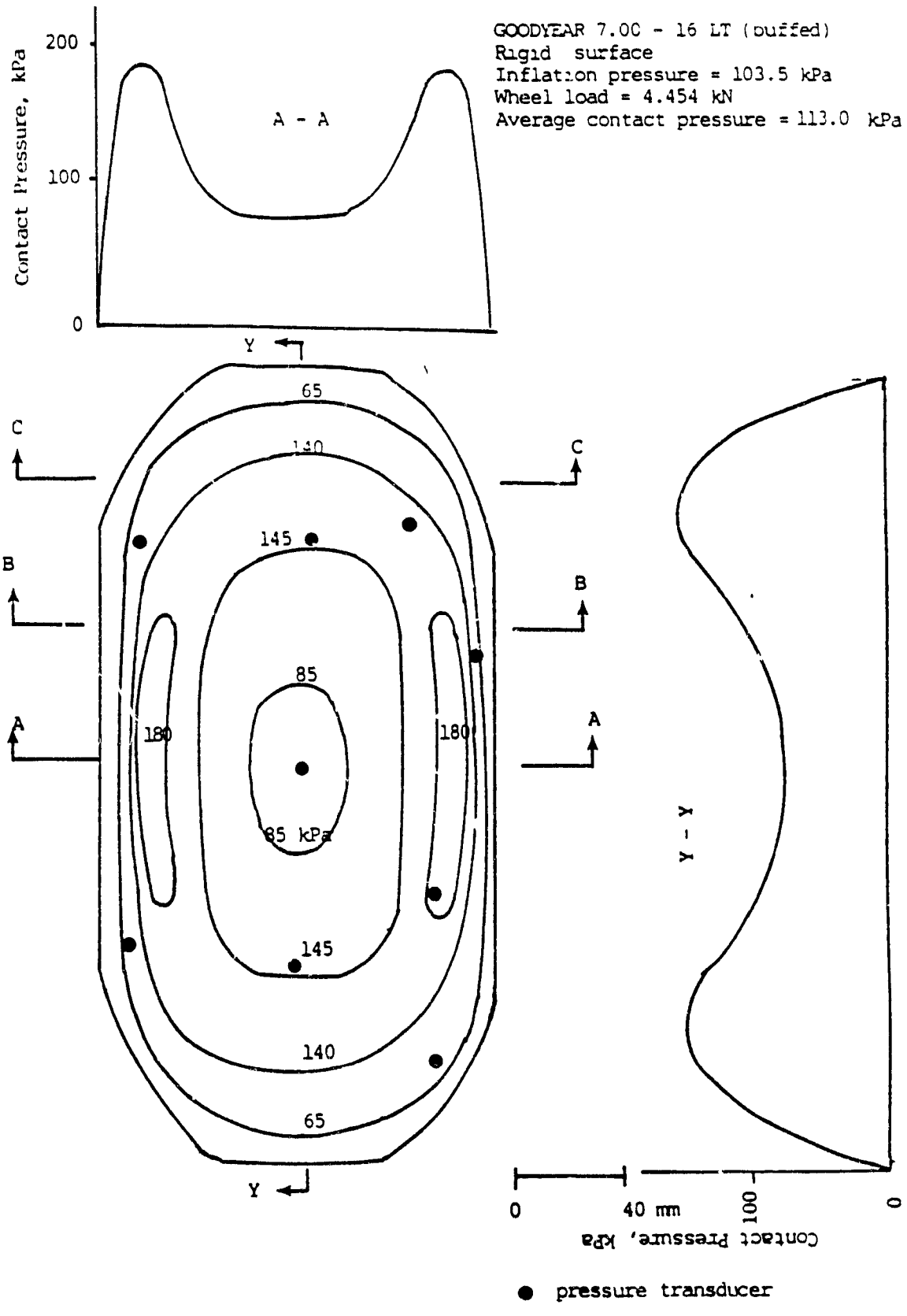


Fig. C.6i/1 Contact Pressure Distribution Within the Footprint of GOODYEAR 7.00-16LT (buffed)

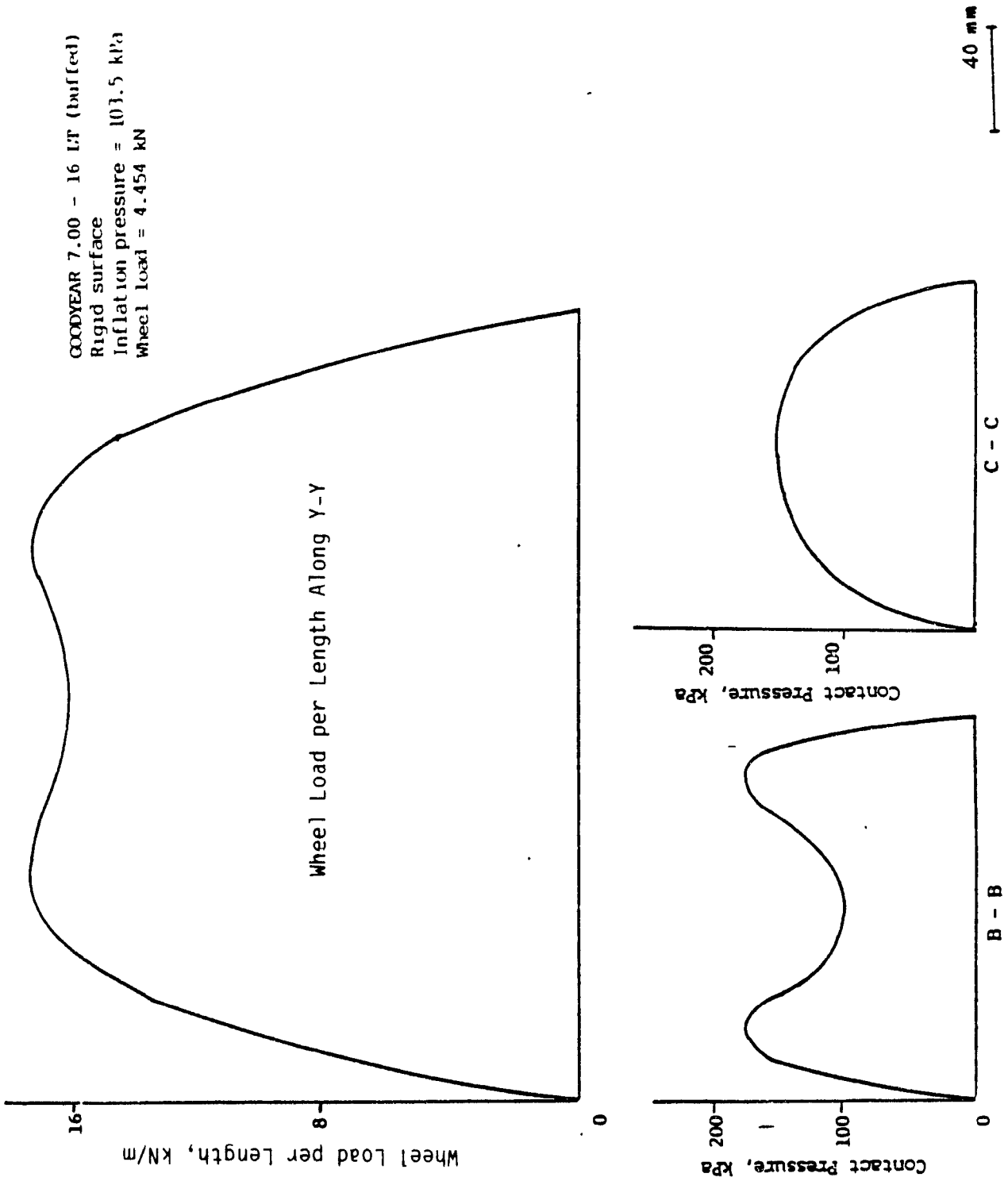


Fig. C.61/2 Contact Pressure Distribution Within the Footprint of GOODYEAR 7.00-16LT (buffed)

GOODYEAR 7.00 - 16 LT (buffed)
Rigid surface
Inflation pressure = 310.5 kPa
Wheel load = 1.334 kN

Average contact pressure = 246.5 kPa

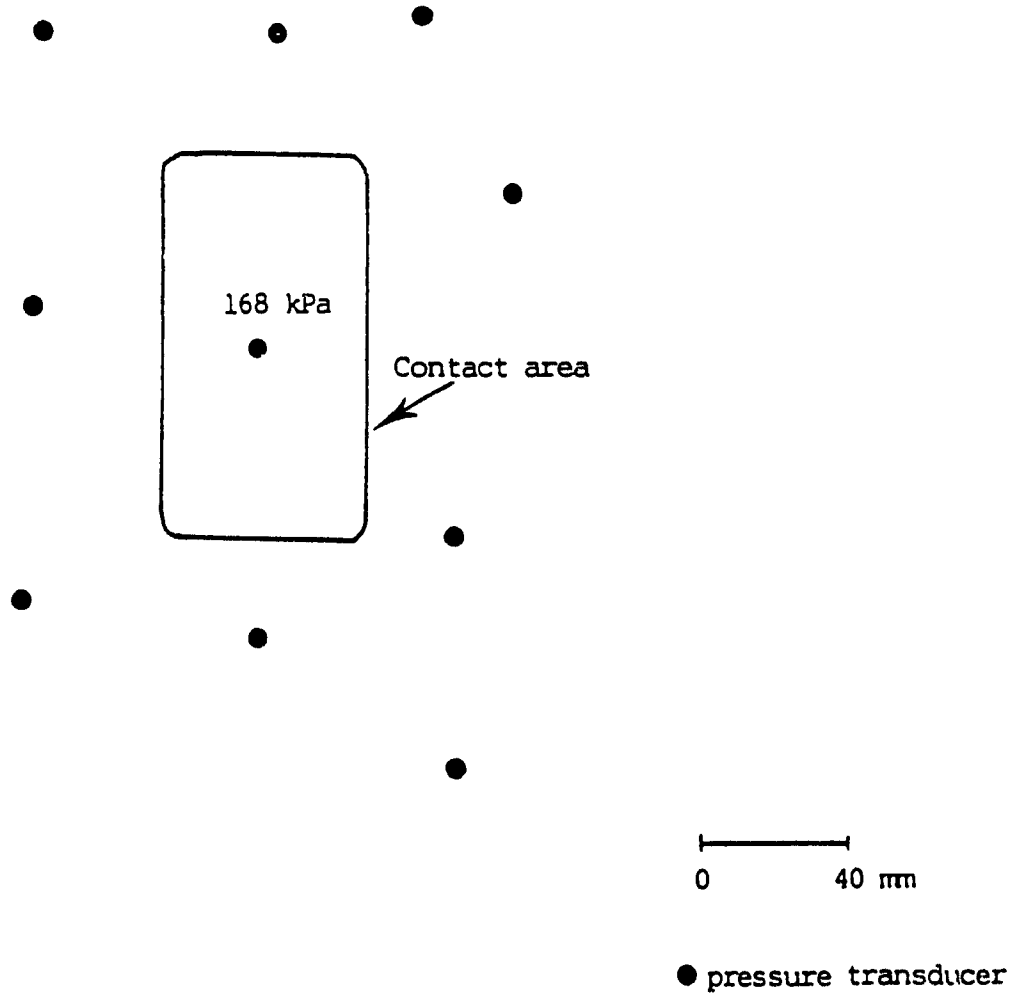


Fig. C.6j Pressure Transducer Readings Within the Footprint of GOODYEAR 7.00-16LT (buffed)

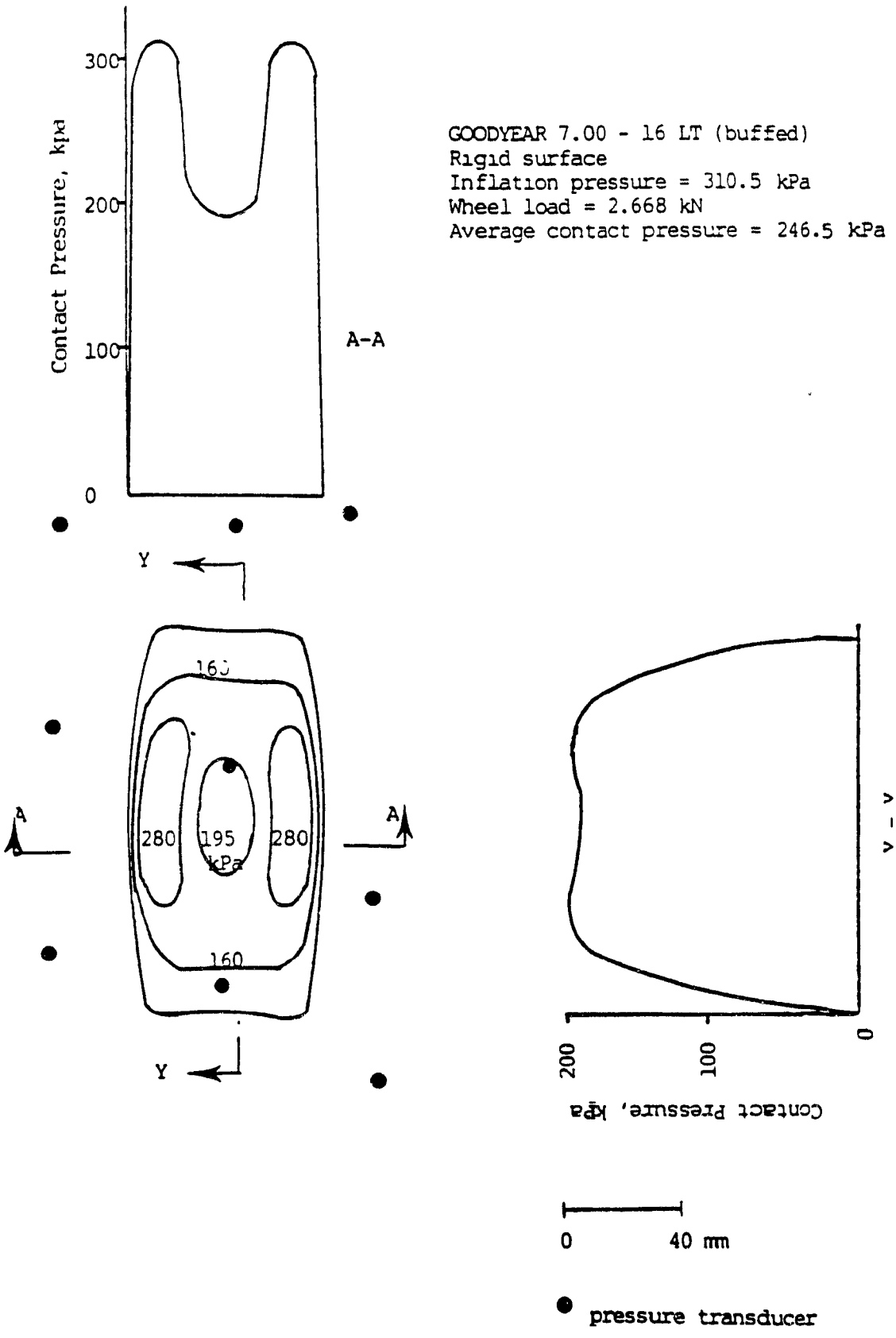


Fig. C.6k Contact Pressure Distribution Within the Footprint of GOODYEAR 7.00-16LT (buffed)

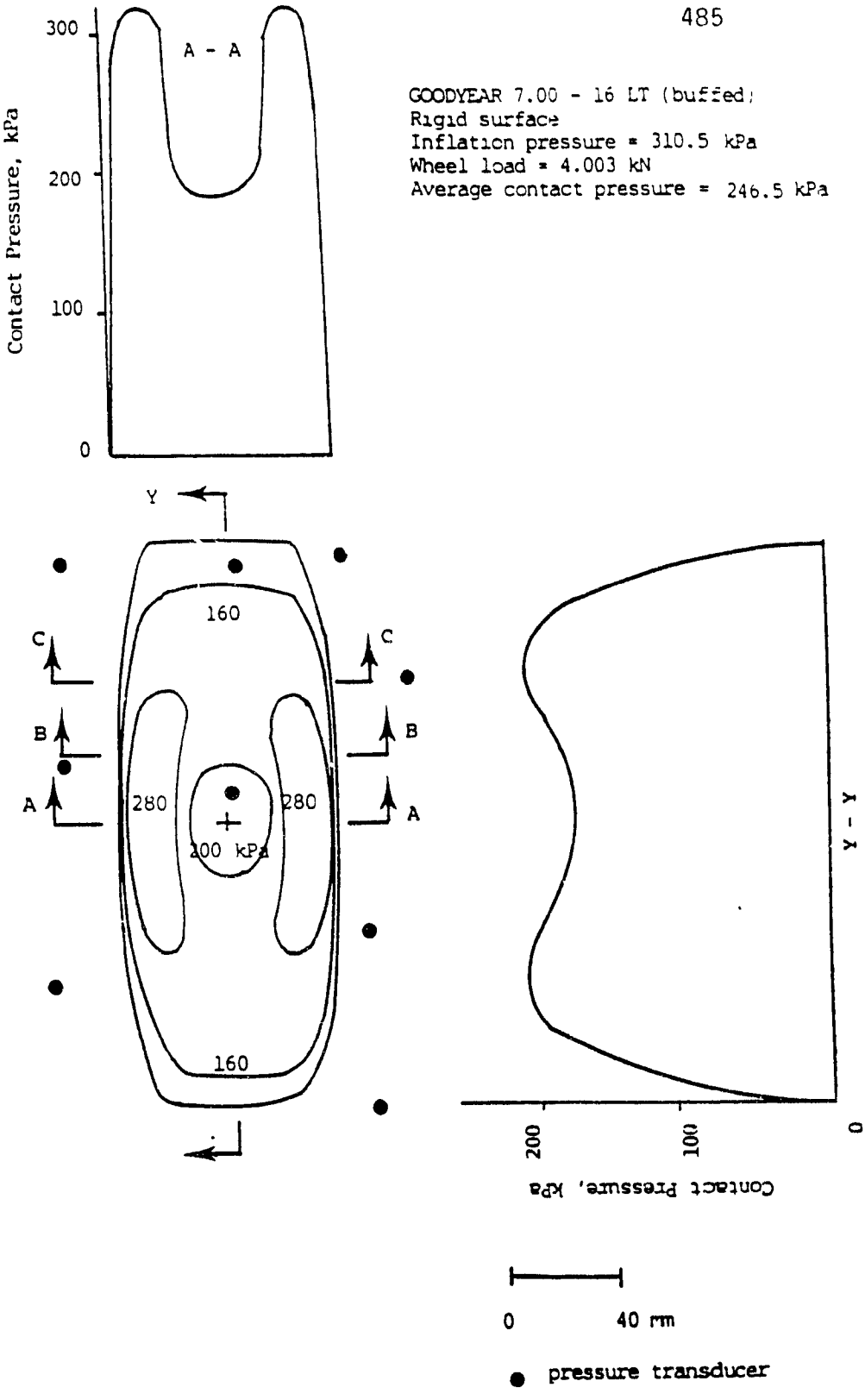


Fig. C.61/1 Contact Pressure Distribution Within the Footprint of GOODYEAR 7.00-16LT (buffed)

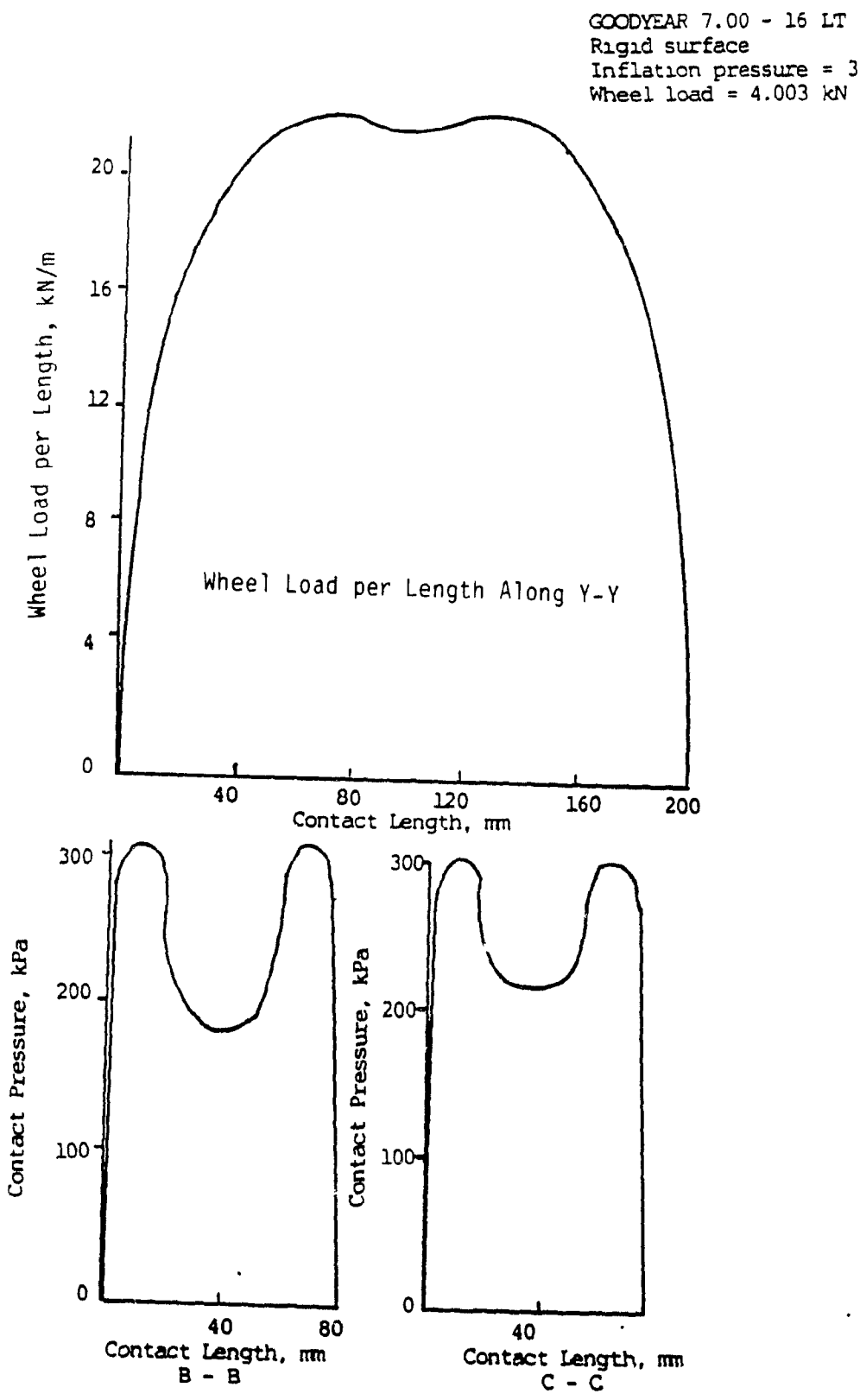


Fig. C.61/2 Contact Pressure Distribution Within the Footprint of GOODYEAR 7.00-16LT (buffed)

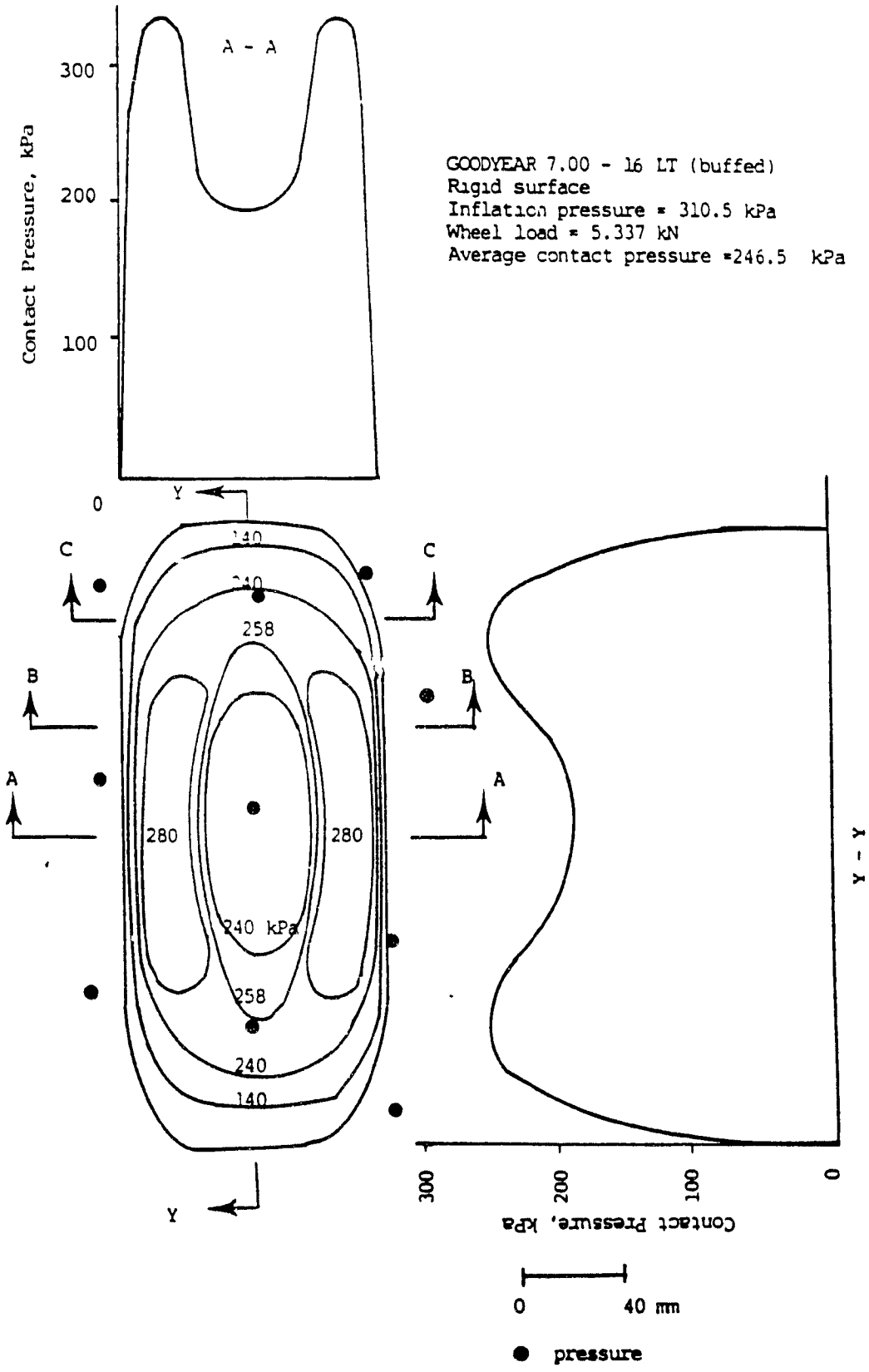


Fig. C.6m/1 Contact Pressure Distribution Within the Footprint of GOODYEAR 7.00-16LT (buffed)

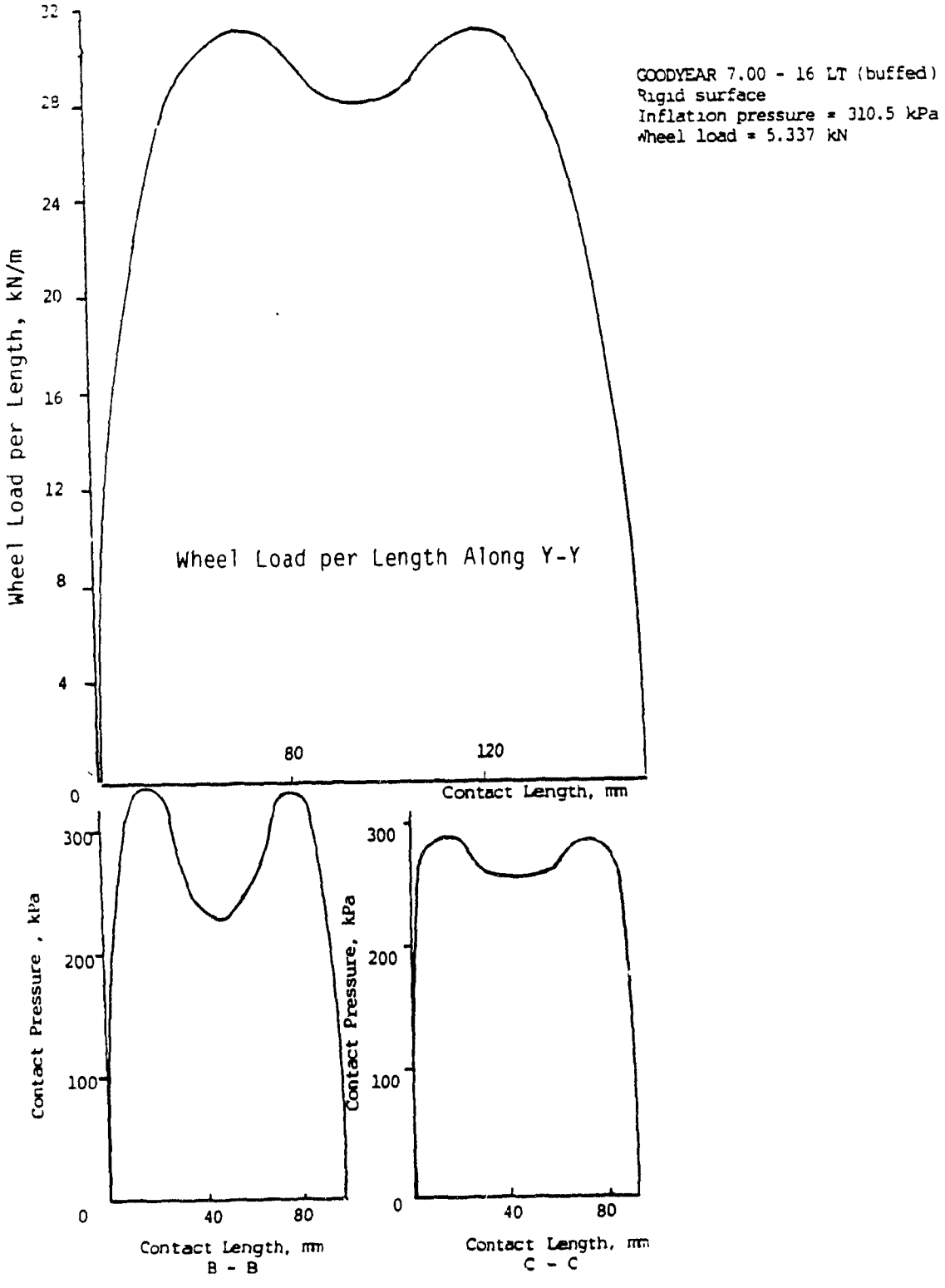


Fig. C.6m/2 Contact Pressure Distribution Within the Footprint of GOODYEAR 7.00-16LT (buffed)

GOODYEAR 7.00 - 16 LT (buffed)
Rigid surface
Inflation pressure = 310.5 kPa
Wheel load = 6.672 kN
Average contact pressure = 265.0 kPa

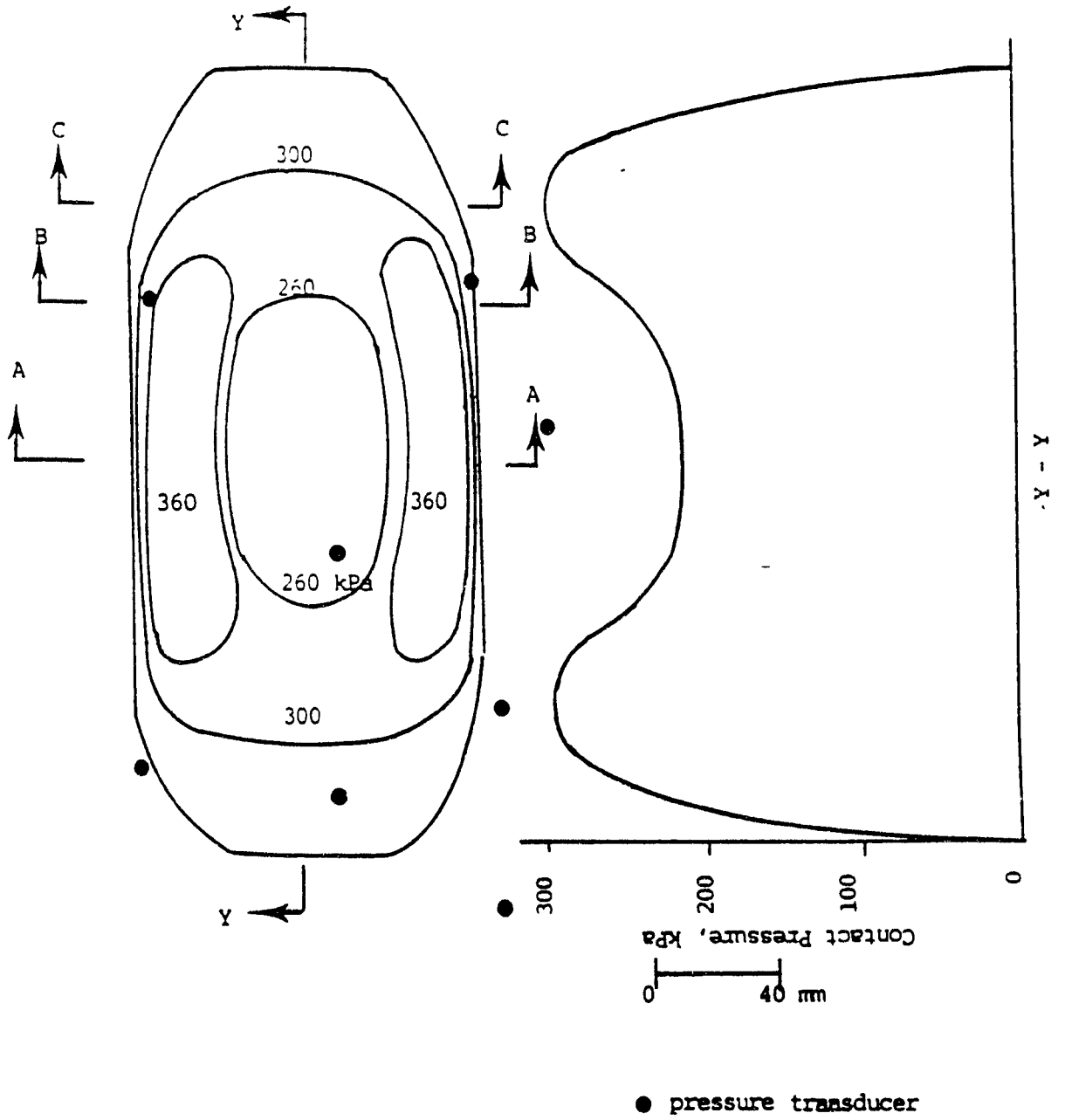


Fig. C.6n/1 Contact Pressure Distribution Within the Footprint of GOODYEAR 7.00-16LT (buffed)

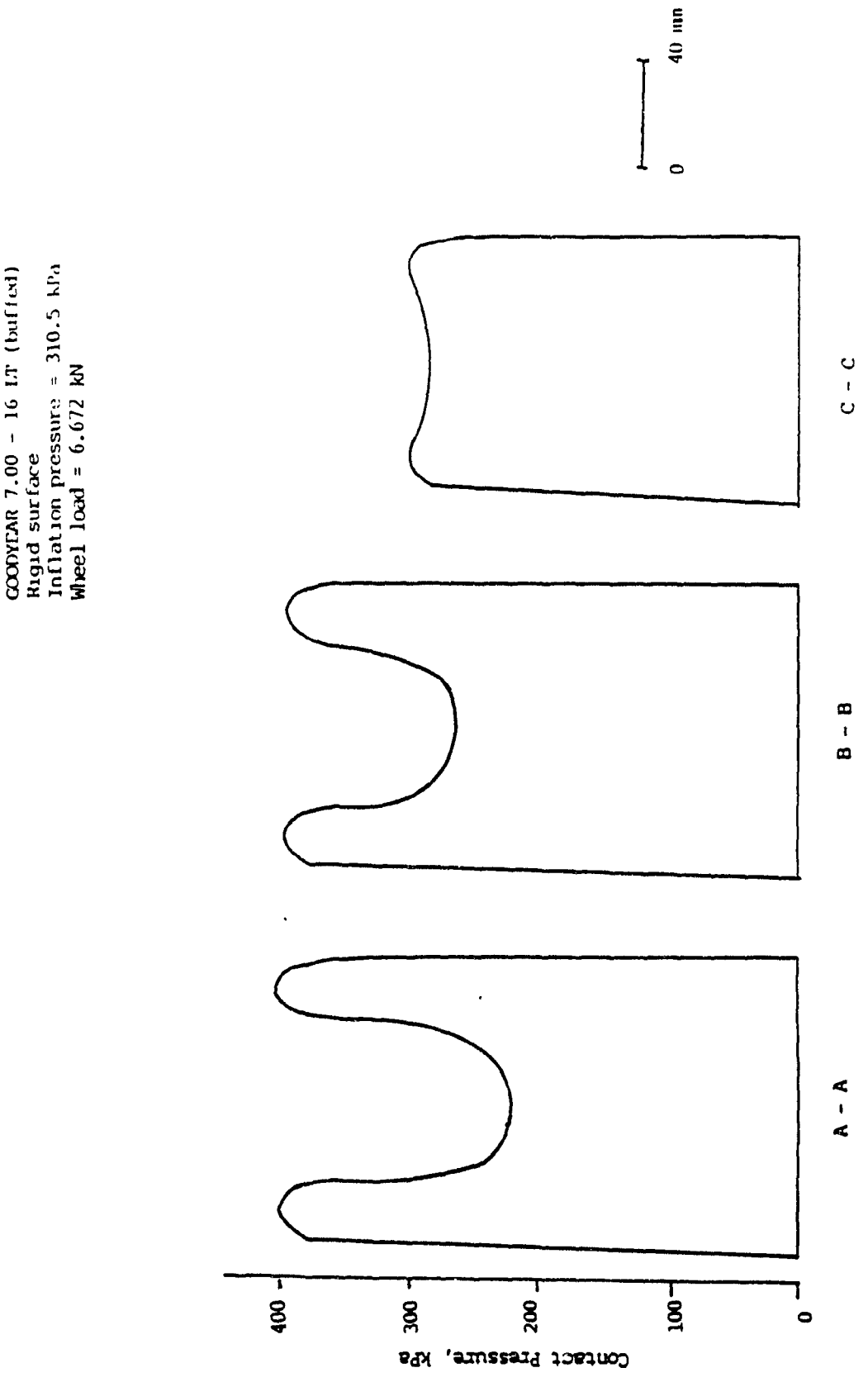


Fig. C.6n/2 Contact Pressure Distribution Within the Footprint of GOODYEAR 7.00-16LT (buffed)

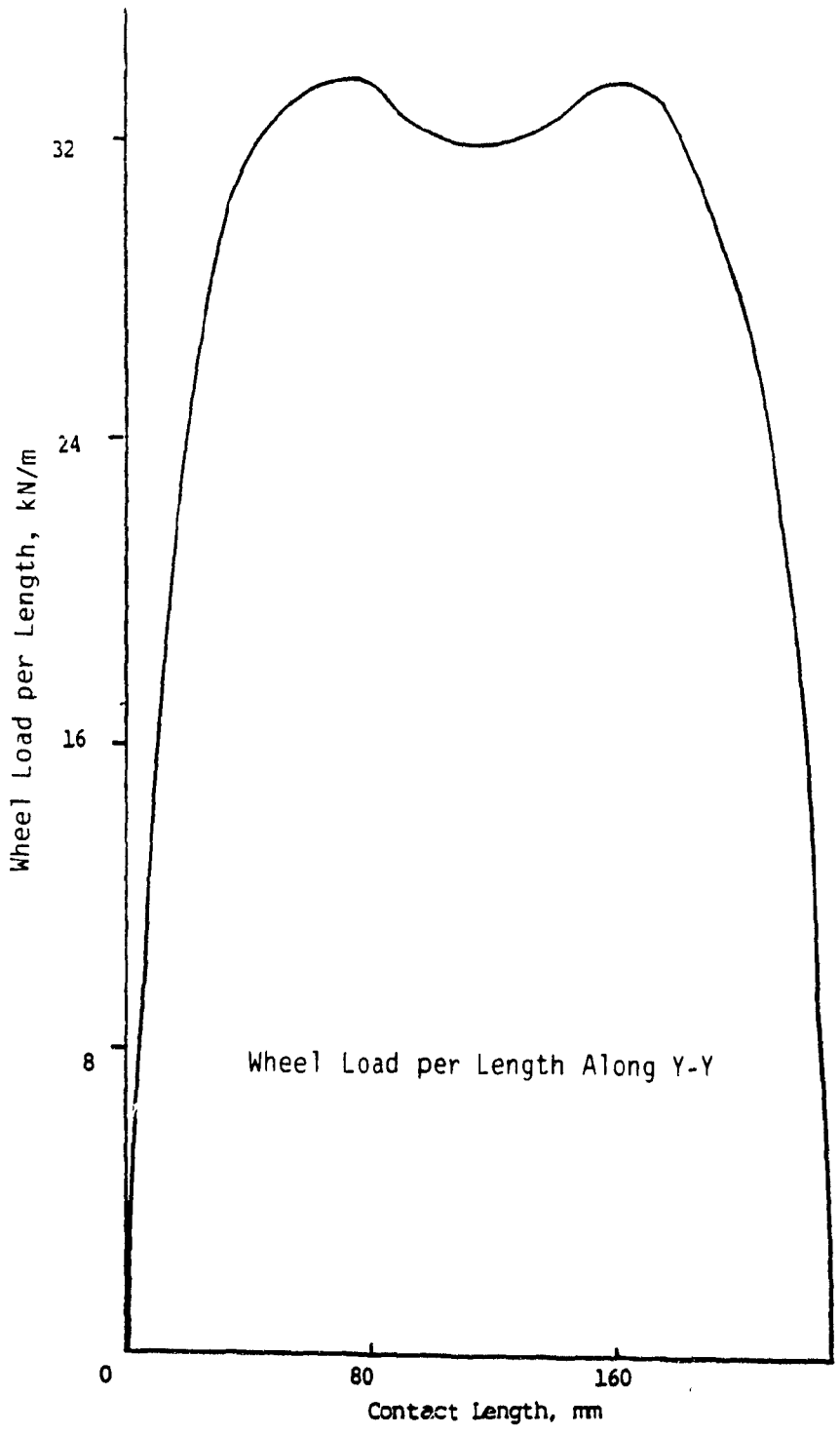


Fig. C.6n/3 Load per Length Along Y-Y of GOODYEAR 7.00-16LT (buffed)

MICHELIN 7.00 R 16XCL (treaded)
Rigid surface
Inflation pressure = 34.5 kPa
Wheel load = 0.356 kN

Average contact pressure = 121.2 kPa
(based on lug area)

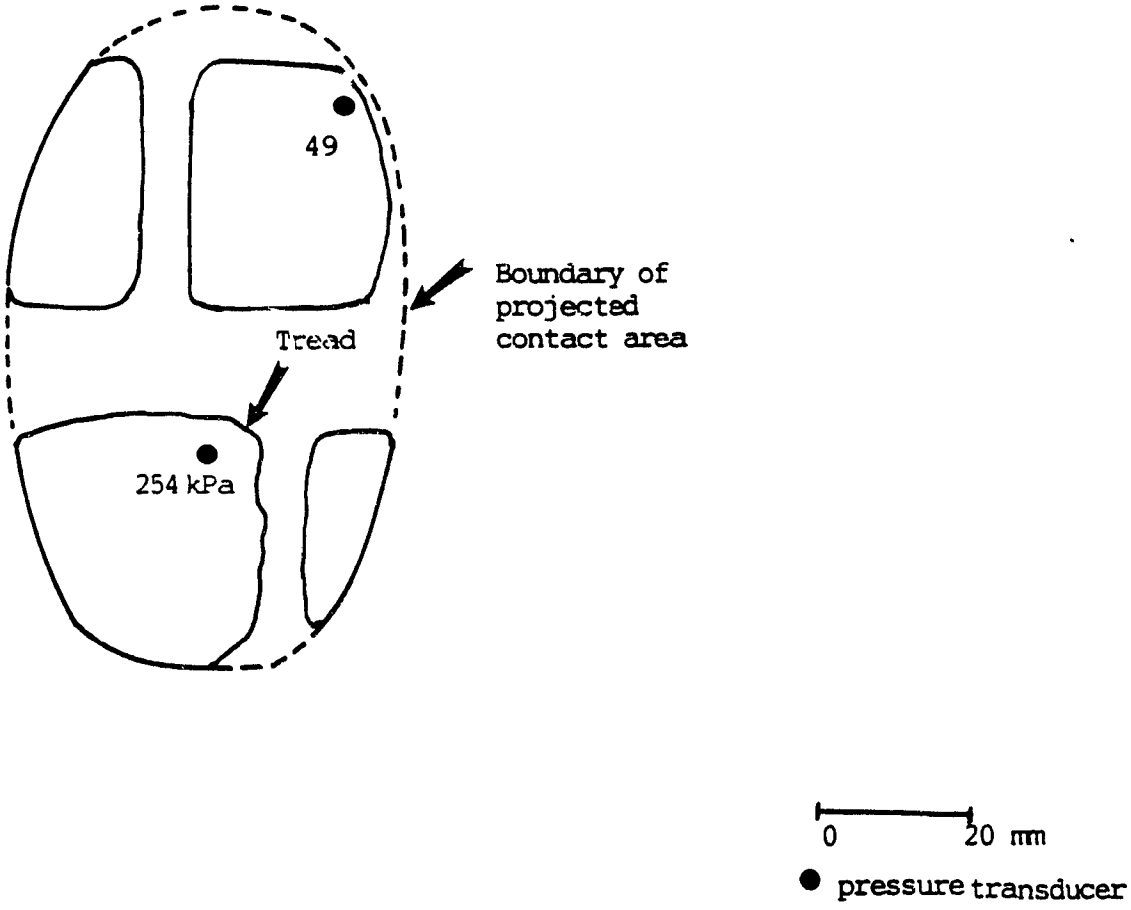


Fig. C.7a Pressure Transducer Readings Within the Footprint of MICHELIN 7.00R-16XCL (treaded)

MICHELIN 7.00R 16XCL (treaded)
Rigid surface
Inflation pressure = 34.5 kPa
Wheel load = 0.711 kN

Average contact pressure = 121.2 kPa
(based on lug area)

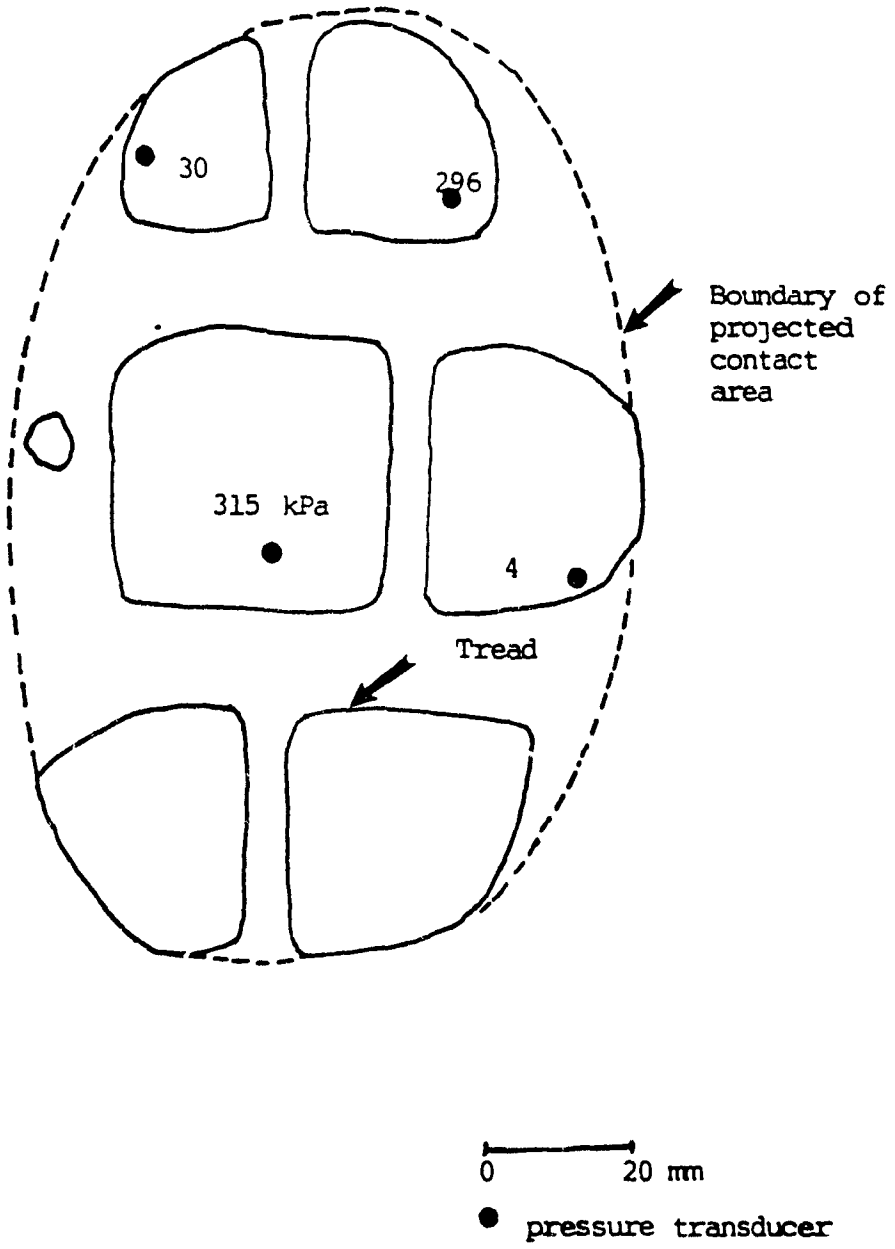


Fig. C.7b Pressure Transducer Readings Within the Footprint of MICHELIN 7.00R-16XCL (treaded)

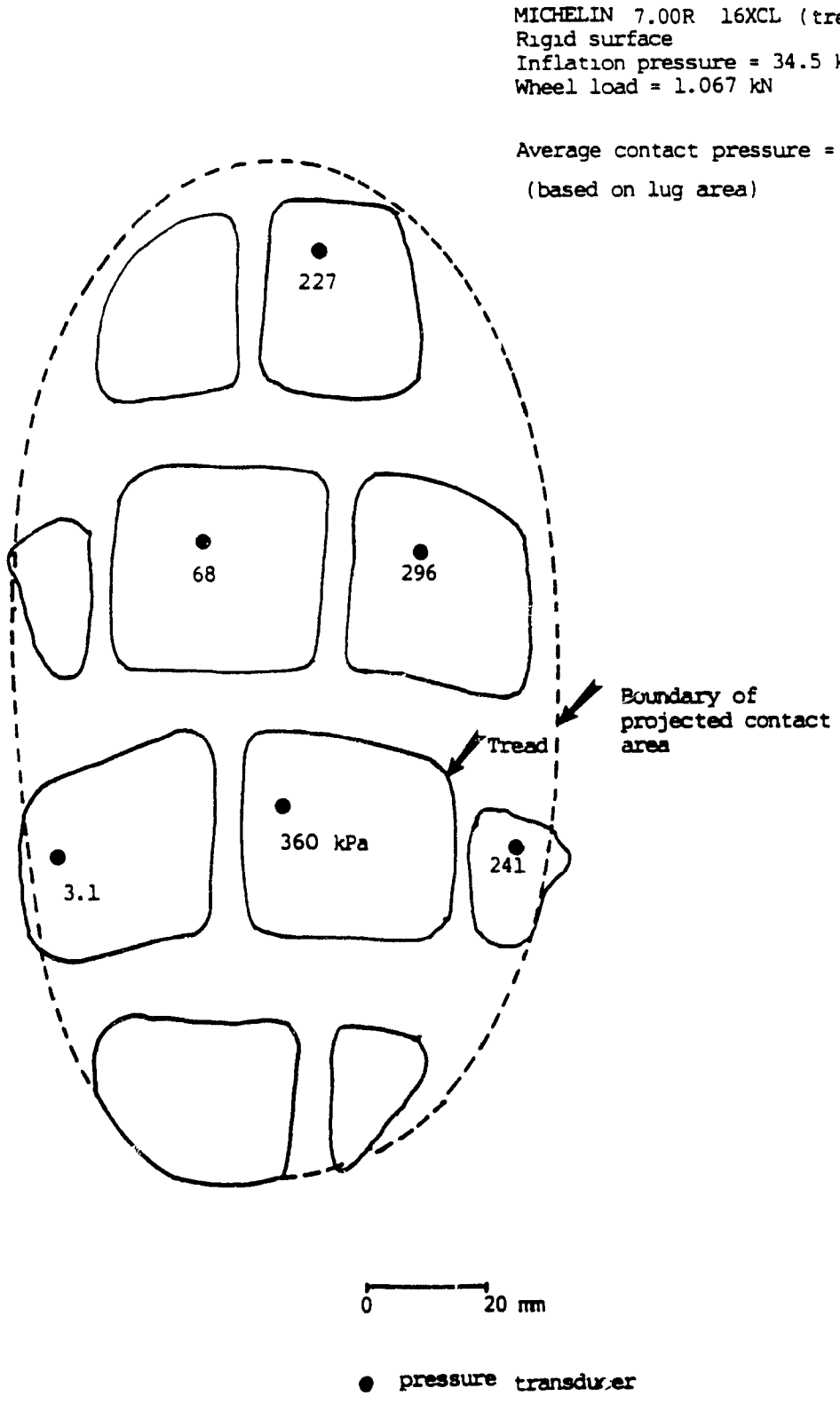


Fig. C.7c Pressure Transducer Readings Within the Footprint of MICHELIN 7.00R-16XCL (treaded)

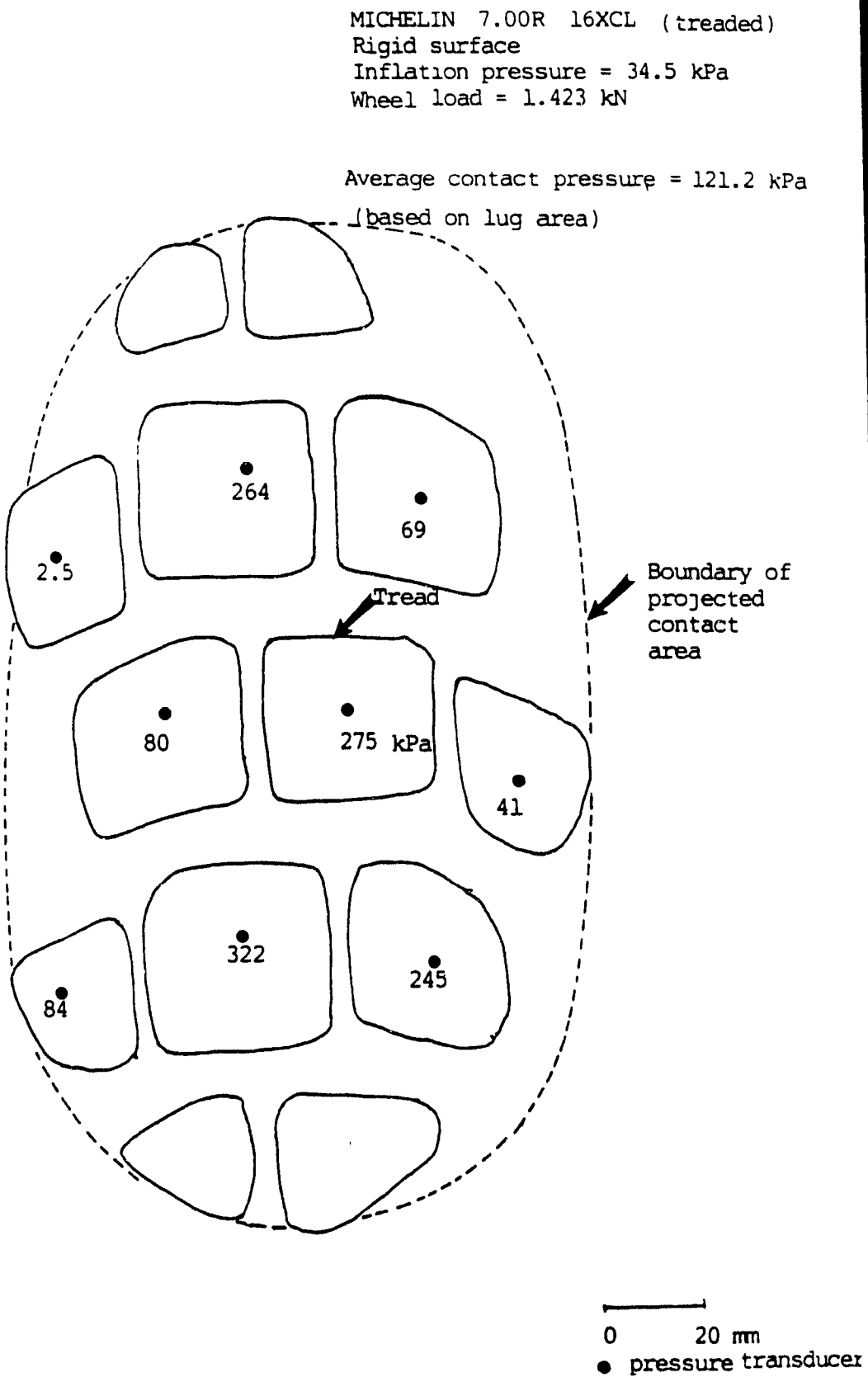


Fig. C.7d Pressure Transducer Readings Within the Footprint of MICHELIN 7.00R-16XCL (treaded)

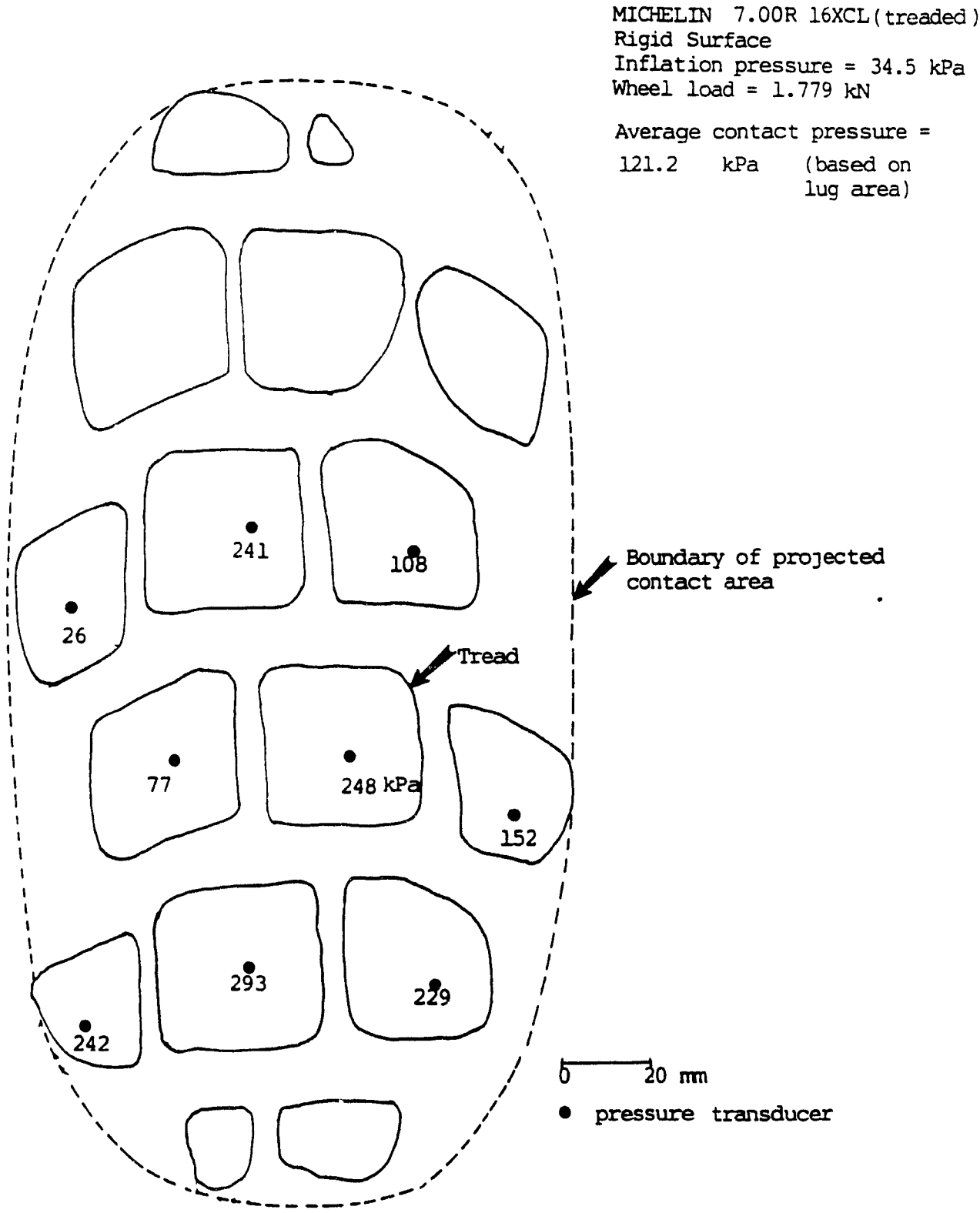


Fig. C.7e Pressure Transducer Readings Within the Footprint of MICHELIN 7.00R-16XCL (treaded)

MICHELIN 7.00R 16XCL (treaded)
Rigid surface
Inflation pressure = 103.5 kPa
Wheel load = 0.711 kN

Average contact pressure =
204.0 kPa

(based on lug area)

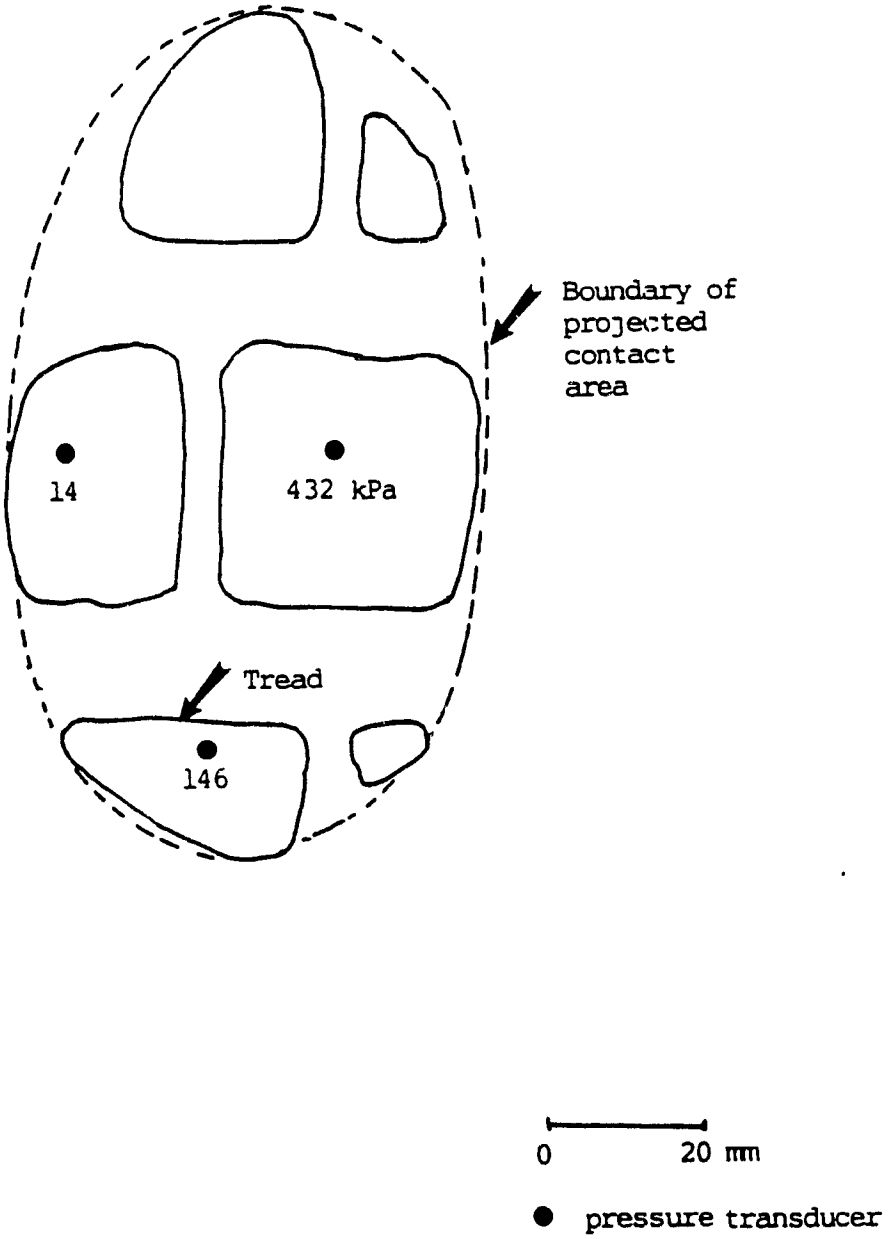


Fig. C.7f Pressure Transducer Readings Within the Footprint of MICHELIN 7.00R-16XCL (treaded)

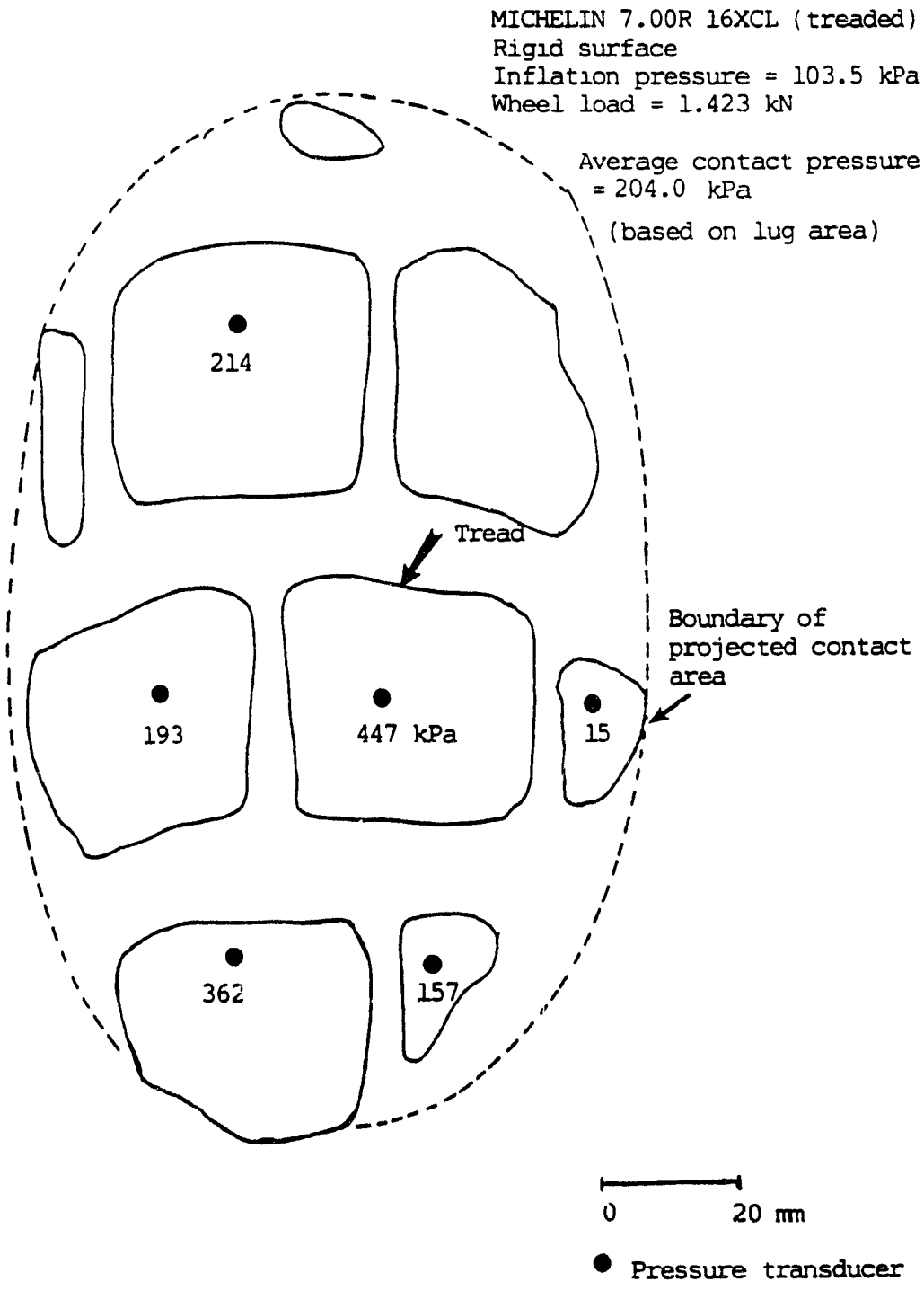


Fig. C.7g Pressure Transducer Readings Within the Footprint of MICHELIN 7.00R-16XCL (treaded)

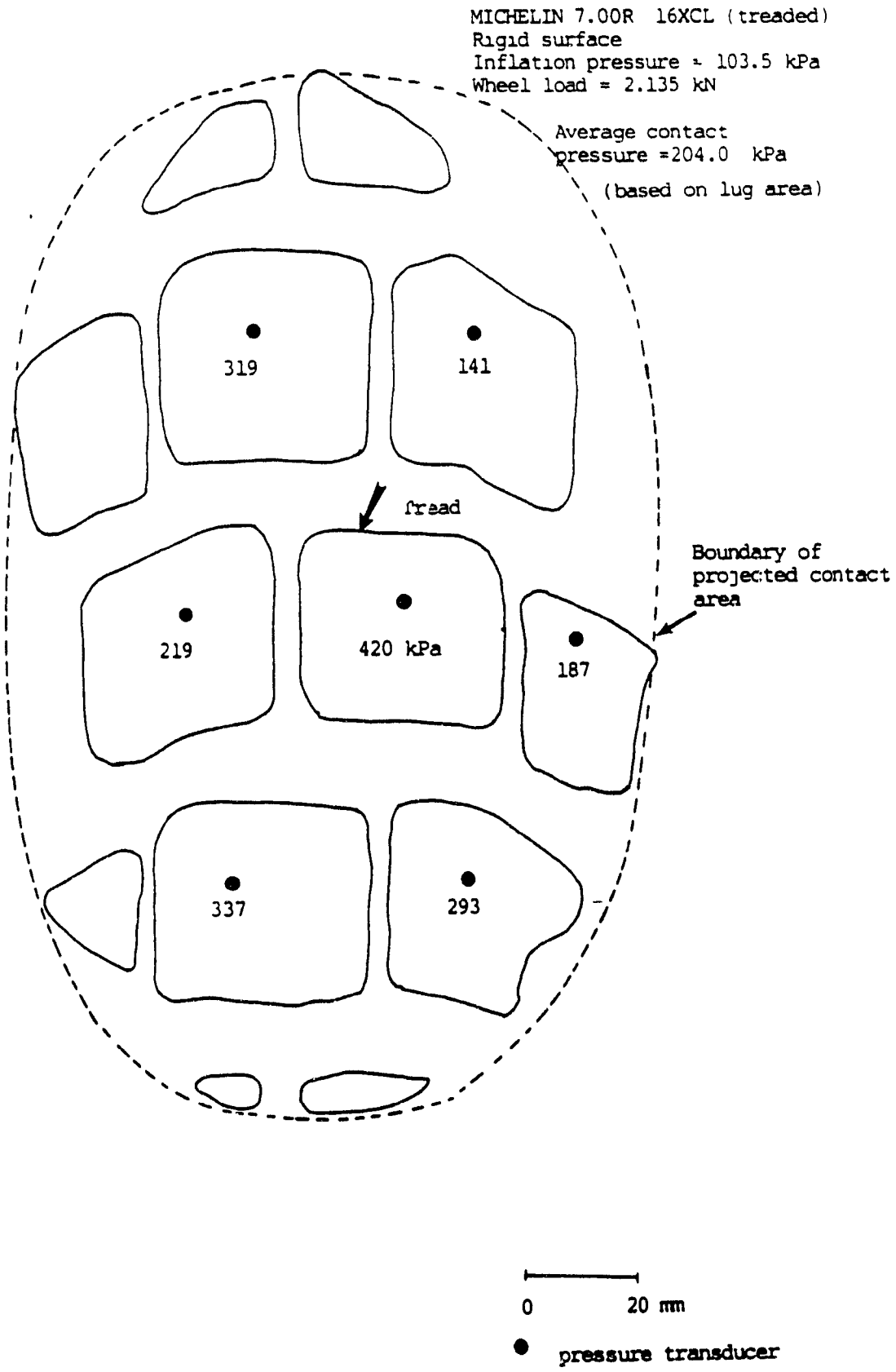


Fig. C.7h Pressure Transducer Readings Within the Footprint of MICHELIN 7.00R-16XCL (treaded)

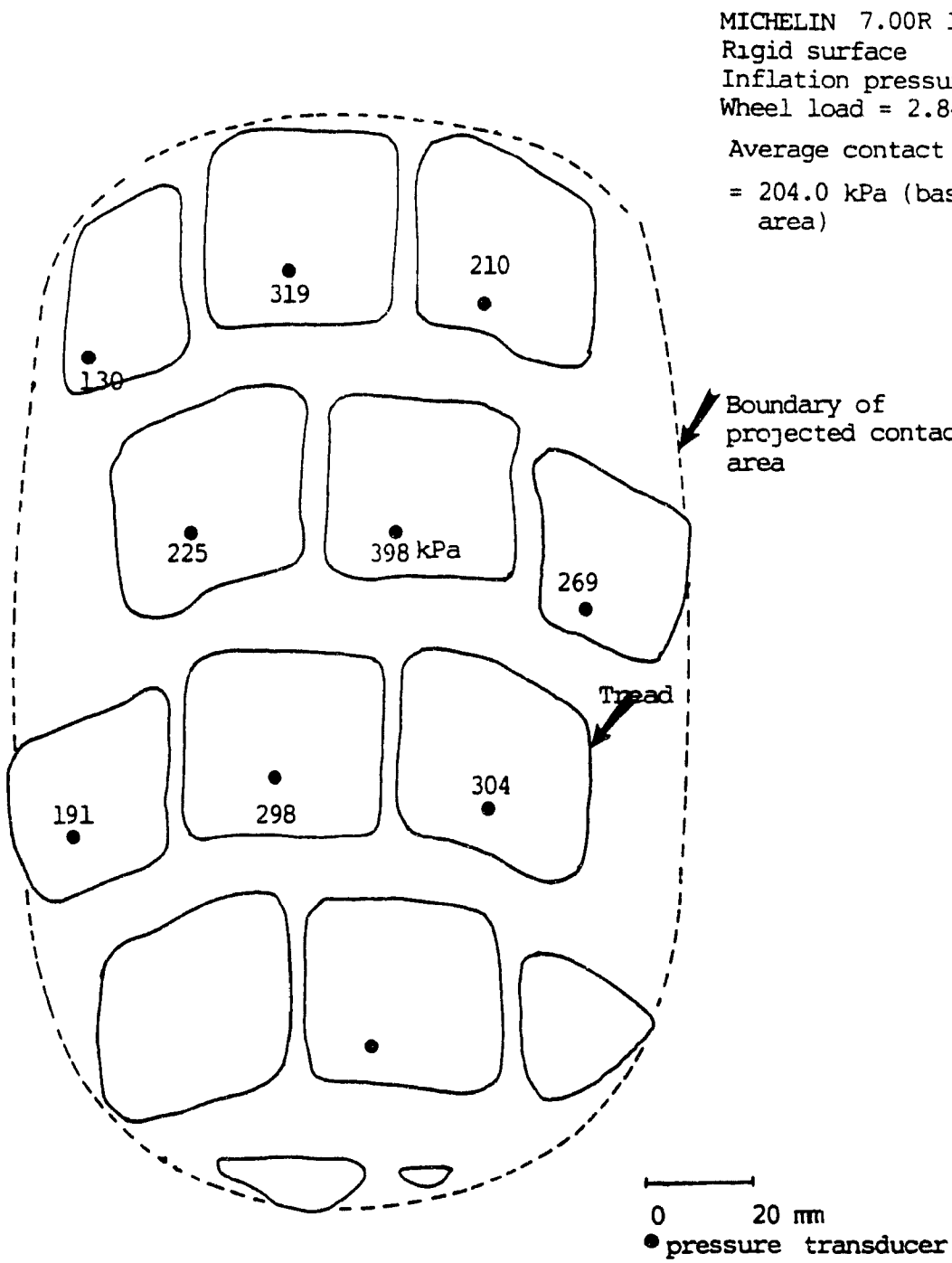


Fig. C.7i Pressure Transducer Readings Within the Footprint of MICHELIN 7.00R-16XCL (treaded)

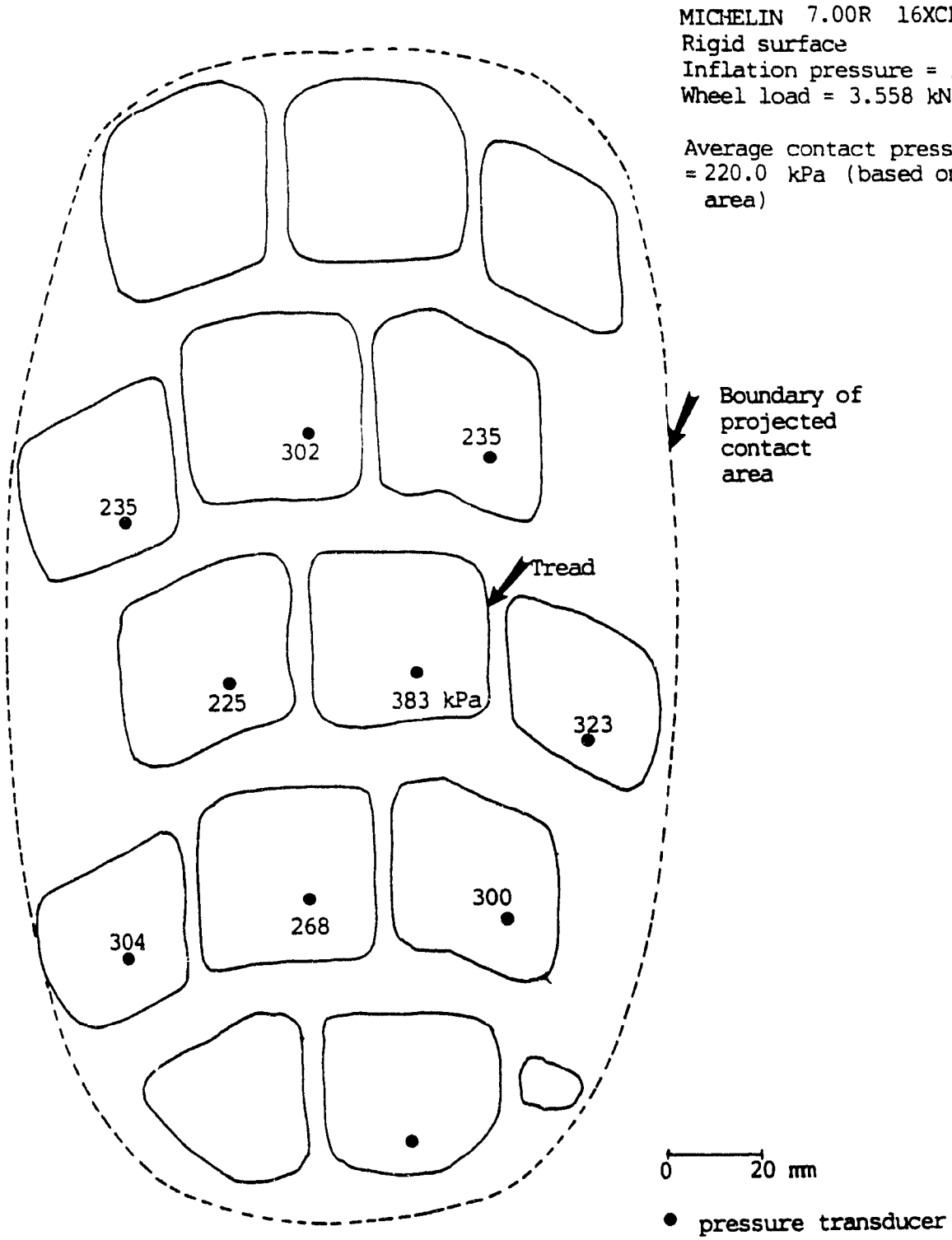


Fig. C.7j Pressure Transducer Readings Within the Footprint of MICHELIN 7.00R-16XCL (treaded)

MICHELIN 7.00R 16XCL (treaded)
Rigid surface
Inflation pressure = 310.5 kPa
Wheel load = 1.601 kN

Average contact pressure = 388.3 kPa
(based on lug area)

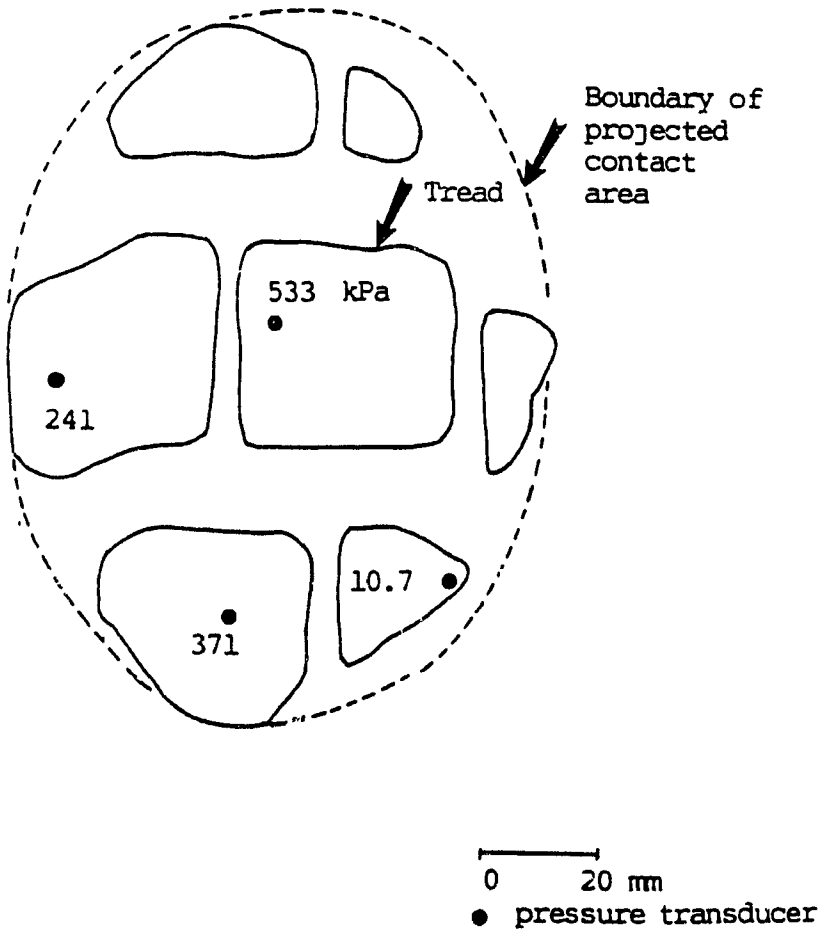


Fig. C.7k Pressure Transducer Readings Within the Footprint of MICHELIN 7.00R-16XCL (treaded)

MICHELIN 7.00R 16XCL (treaded)
Rigid surface
Inflation pressure = 310.5 kPa
Wheel load = 2.846 kN

Average contact pressure = 388.3 kPa
(based on lug area)

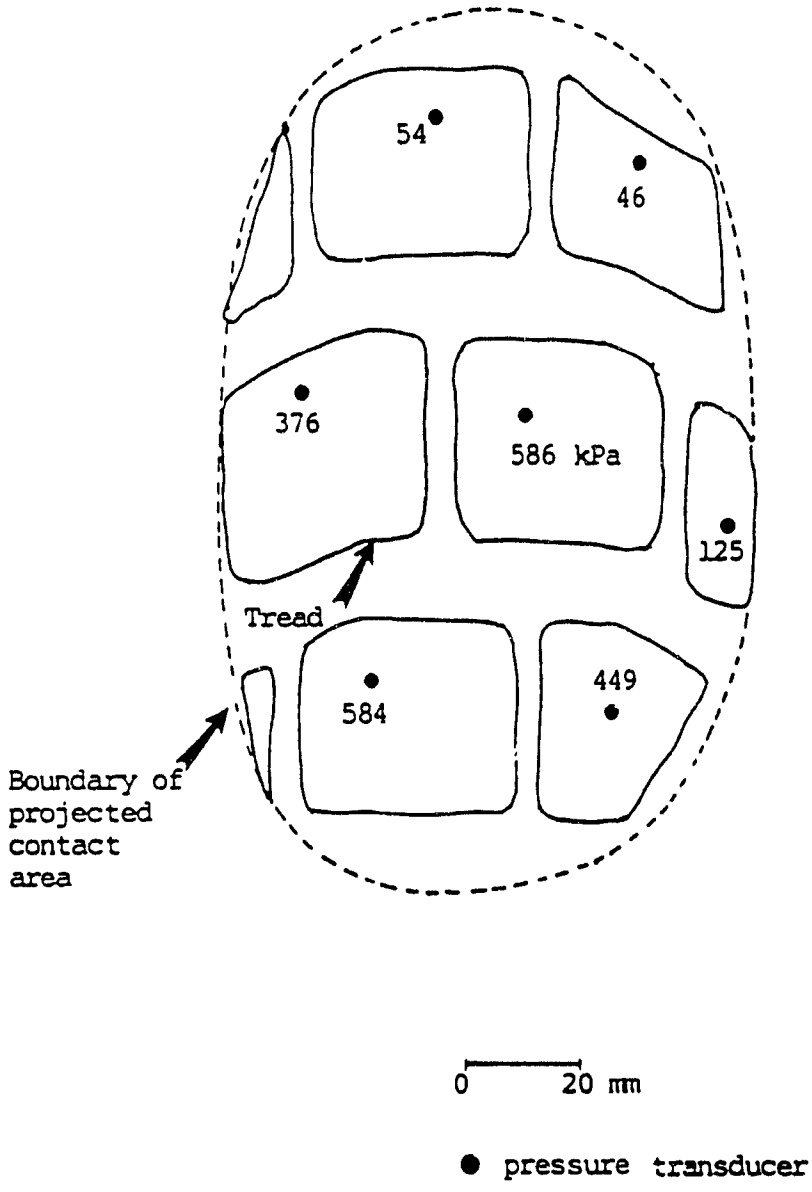


Fig. C.71 Pressure Transducer Readings Within the Footprint of MICHELIN 7.00R-16XCL (treaded)

MICHELIN 7.00R 16XCL (treaded)
Rigid surface
Inflation pressure = 310.5 kPa
Wheel load = 4.27 kN

Average contact pressure = 388.3 kPa (based on lug area

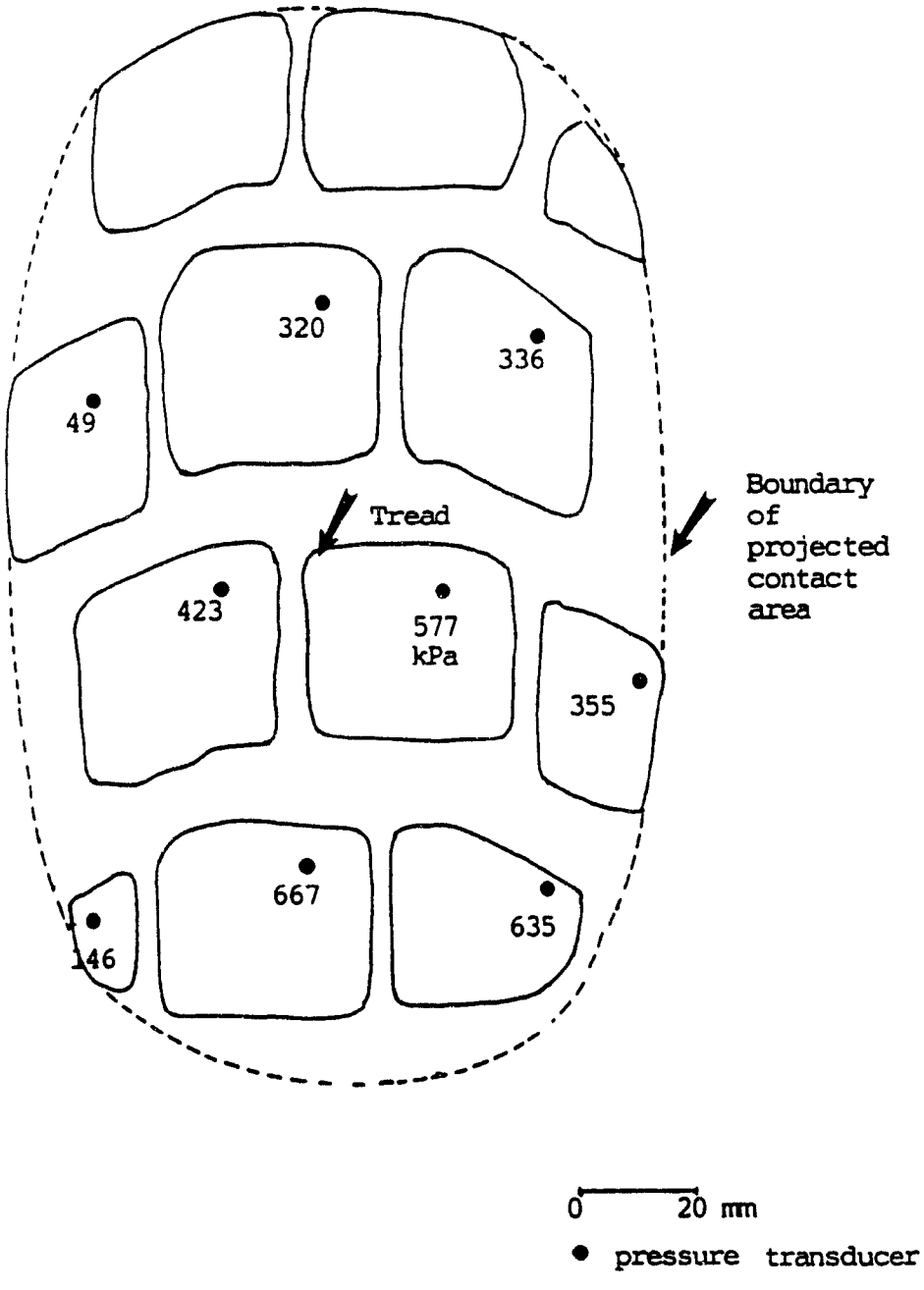


Fig. C.7m Pressure Transducer Readings Within the Footprint of MICHELIN 7.00R-16XCL (treaded)

MICHELIN 7.00R 16XCL (treaded)
Rigid surface
Inflation pressure = 310.5 kPa
Wheel load = 5.693 kN

Average contact pressure =
388.3 kPa (based on lug area)

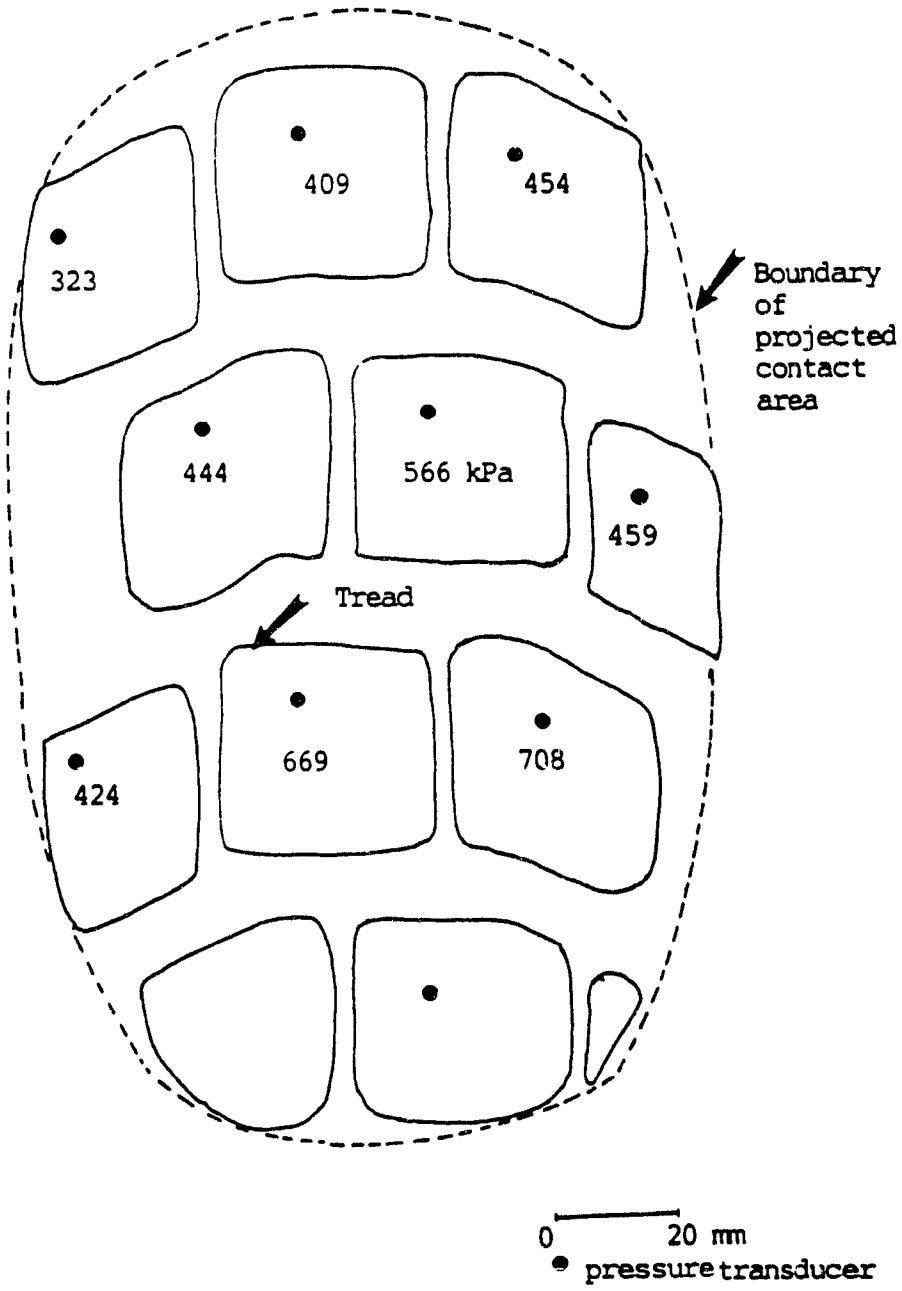


Fig. C.7n Pressure Transducer Readings Within the Footprint of MICHELIN 7.00R-16XCL (treaded)

MICHELIN 7.00R 16XCL (treaded)
Rigid surface
Inflation pressure = 310.5 kPa
Wheel load = 7.117 kN

Average contact pressure = 415 kPa
(based on lug area)

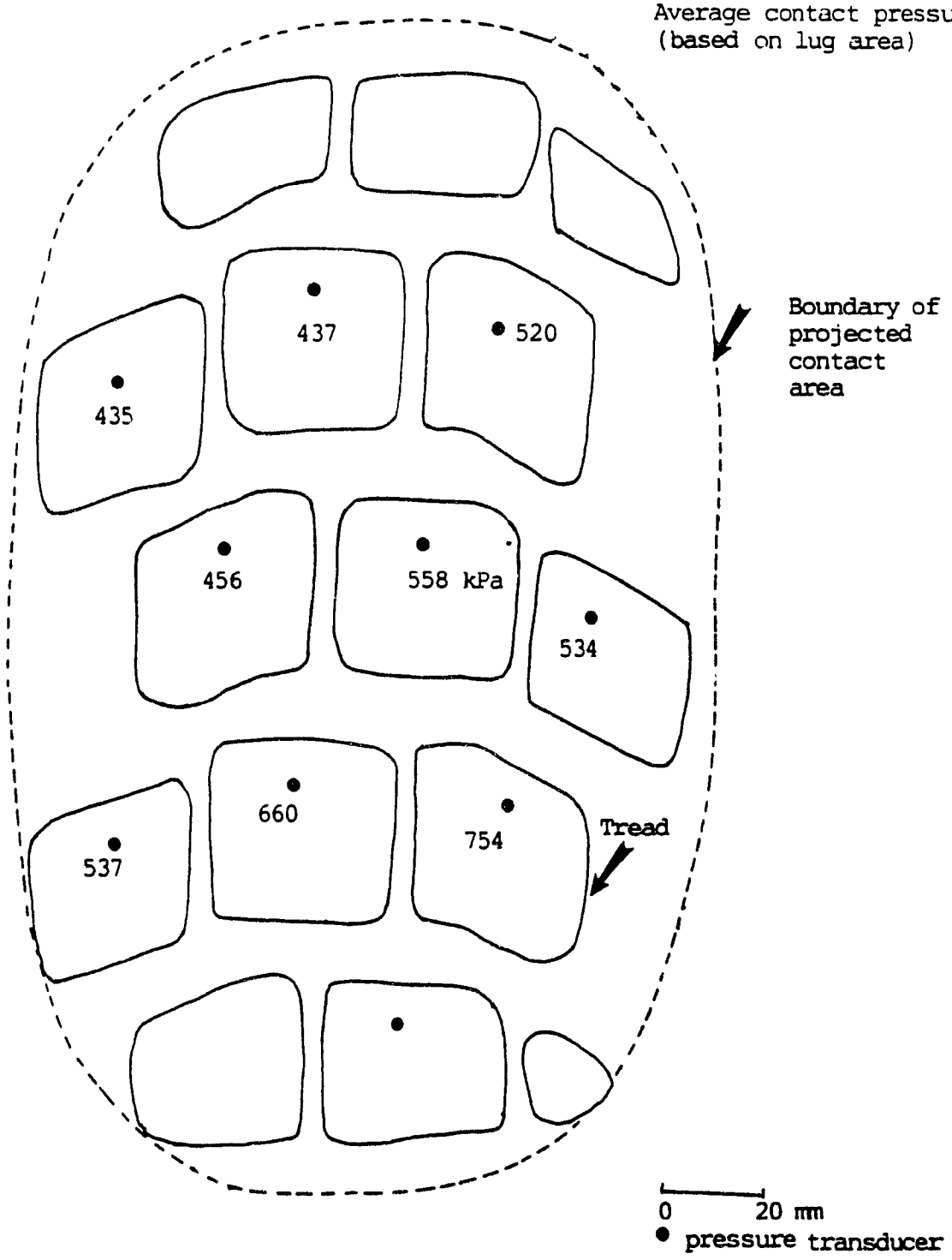


Fig. C.7p Pressure Transducer Readings Within the Footprint of MICHELIN 7.00R-16XCL (treaded)

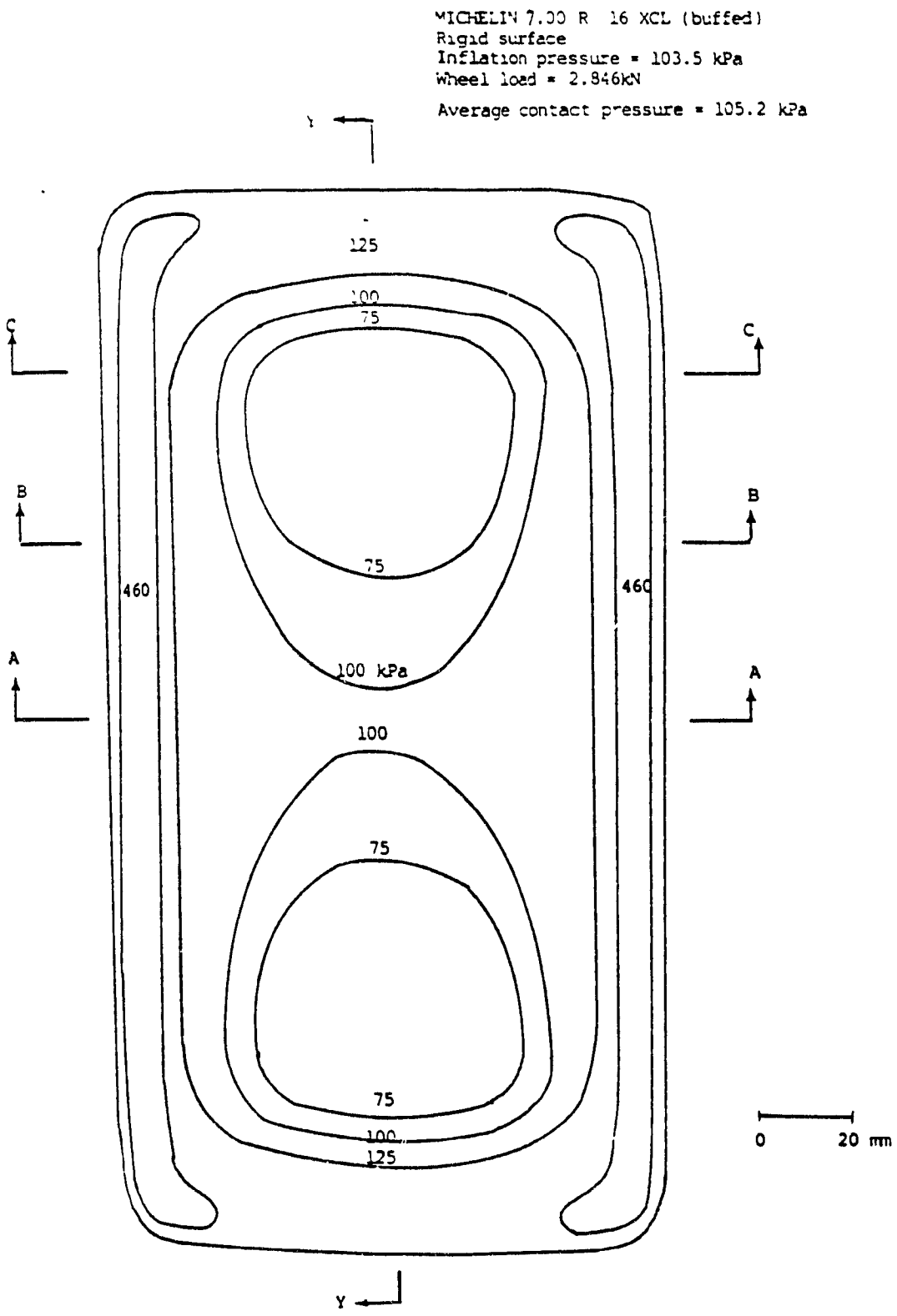


Fig. C.8a/1 Contact Pressure Distribution Within the Footprint of MICHELIN 7.00R-16XCL (buffed)

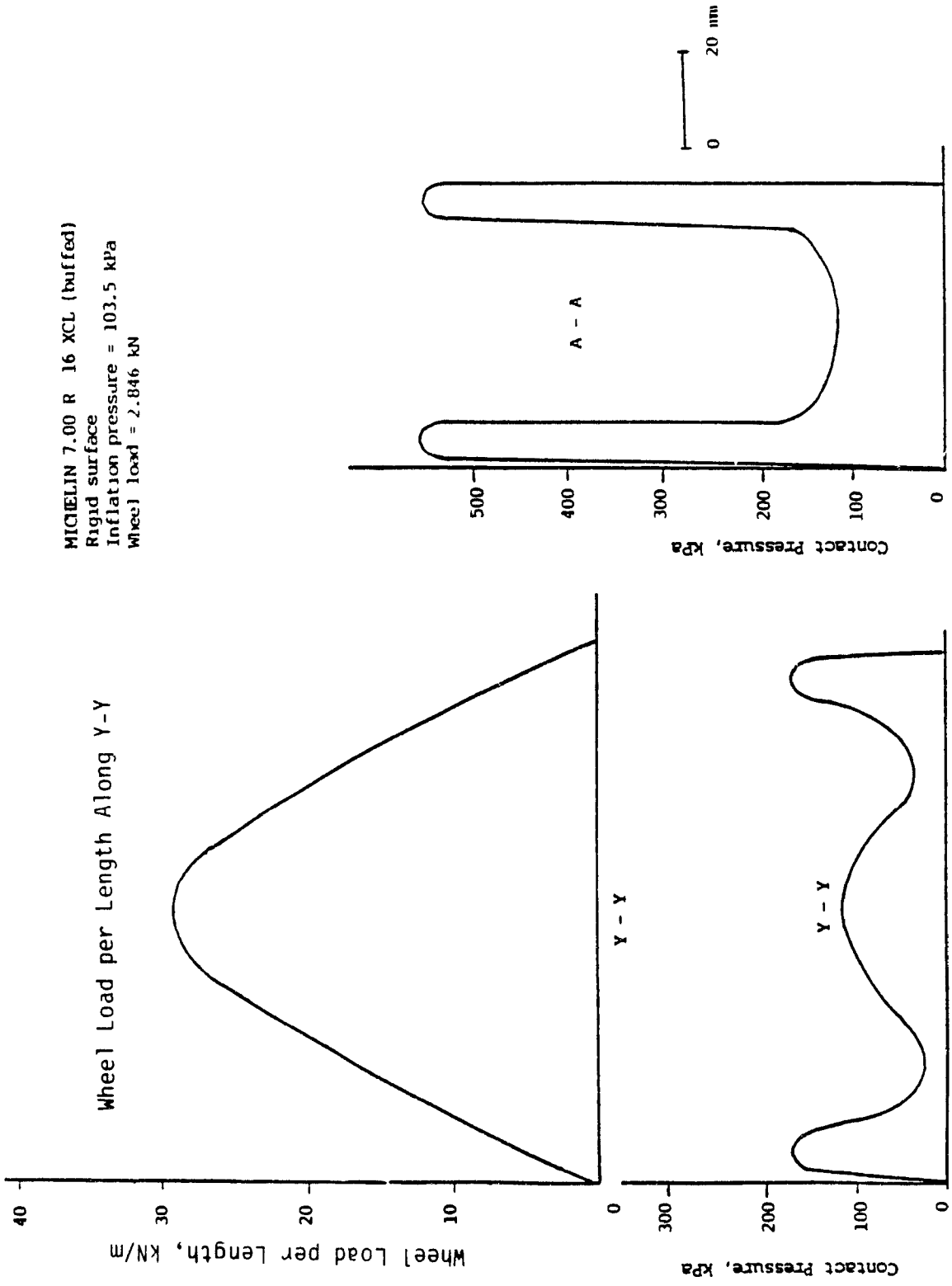


Fig. C.8a/2 Contact Pressure Distribution Within the Footprint of MICHELIN 7.00R-16XCL (buffed)

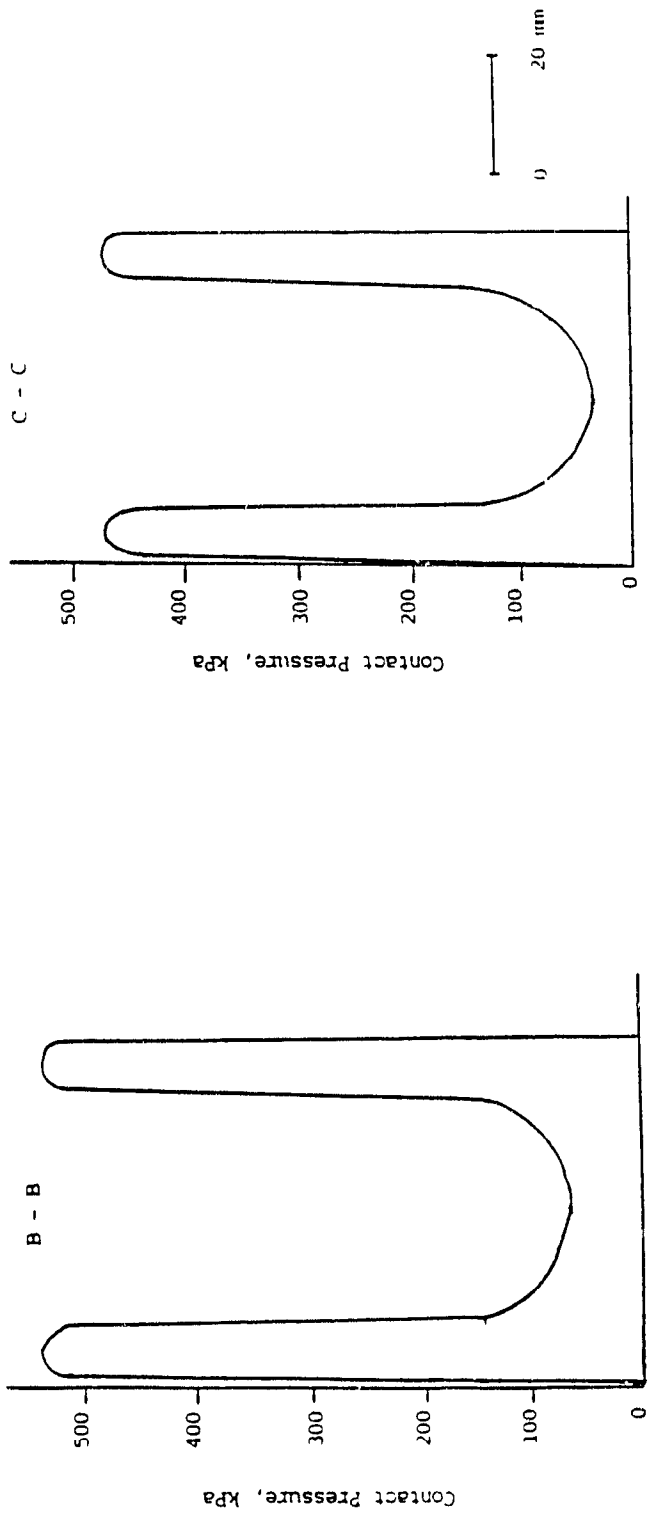


Fig. C.8a/3 Contact Pressure Distribution within the Footprint of MICHELIN 7.00R 16XCL (buffed)

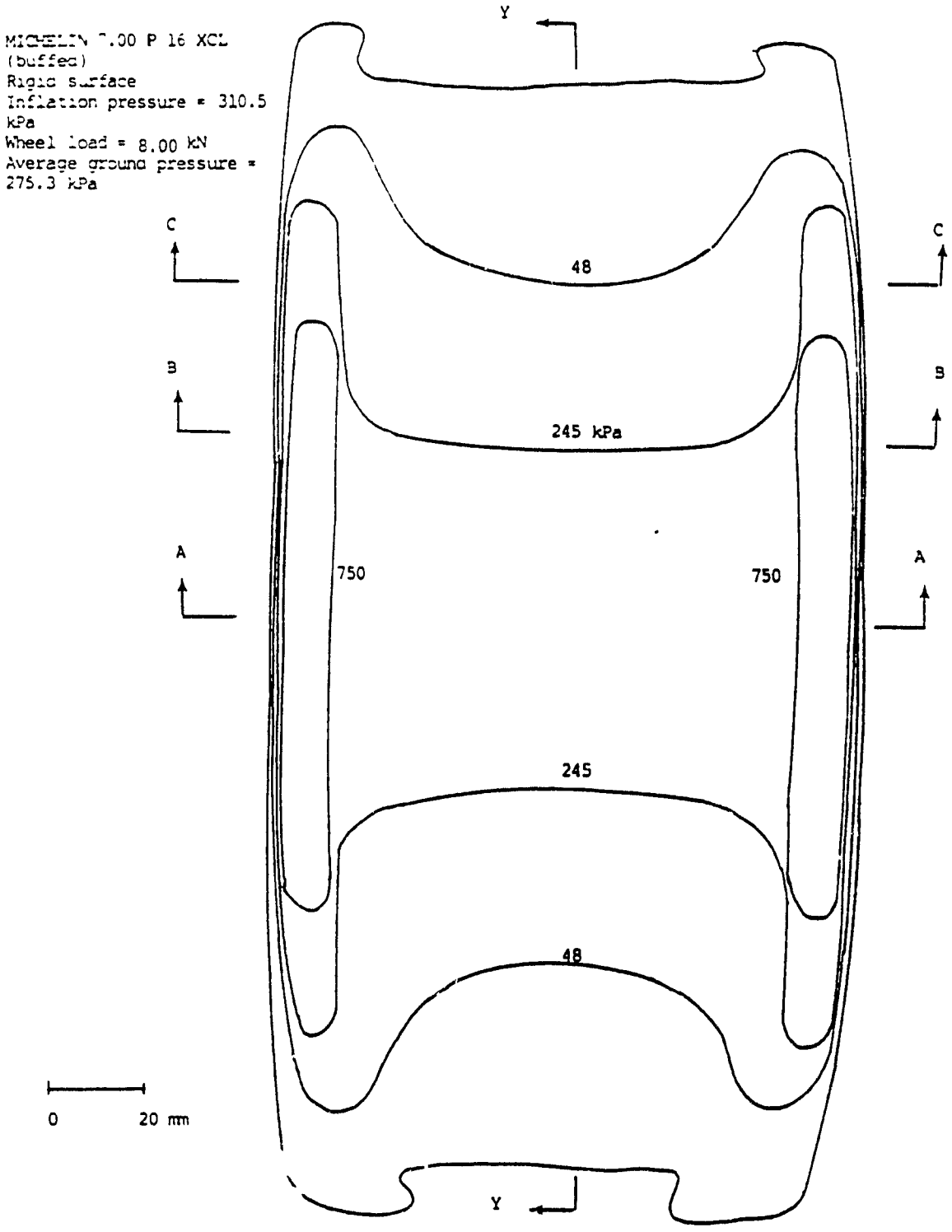


Fig. C.8b/1 Contact Pressure Distribution Within the Footprint of MICHELIN 7.00R-16XCL (buffed)

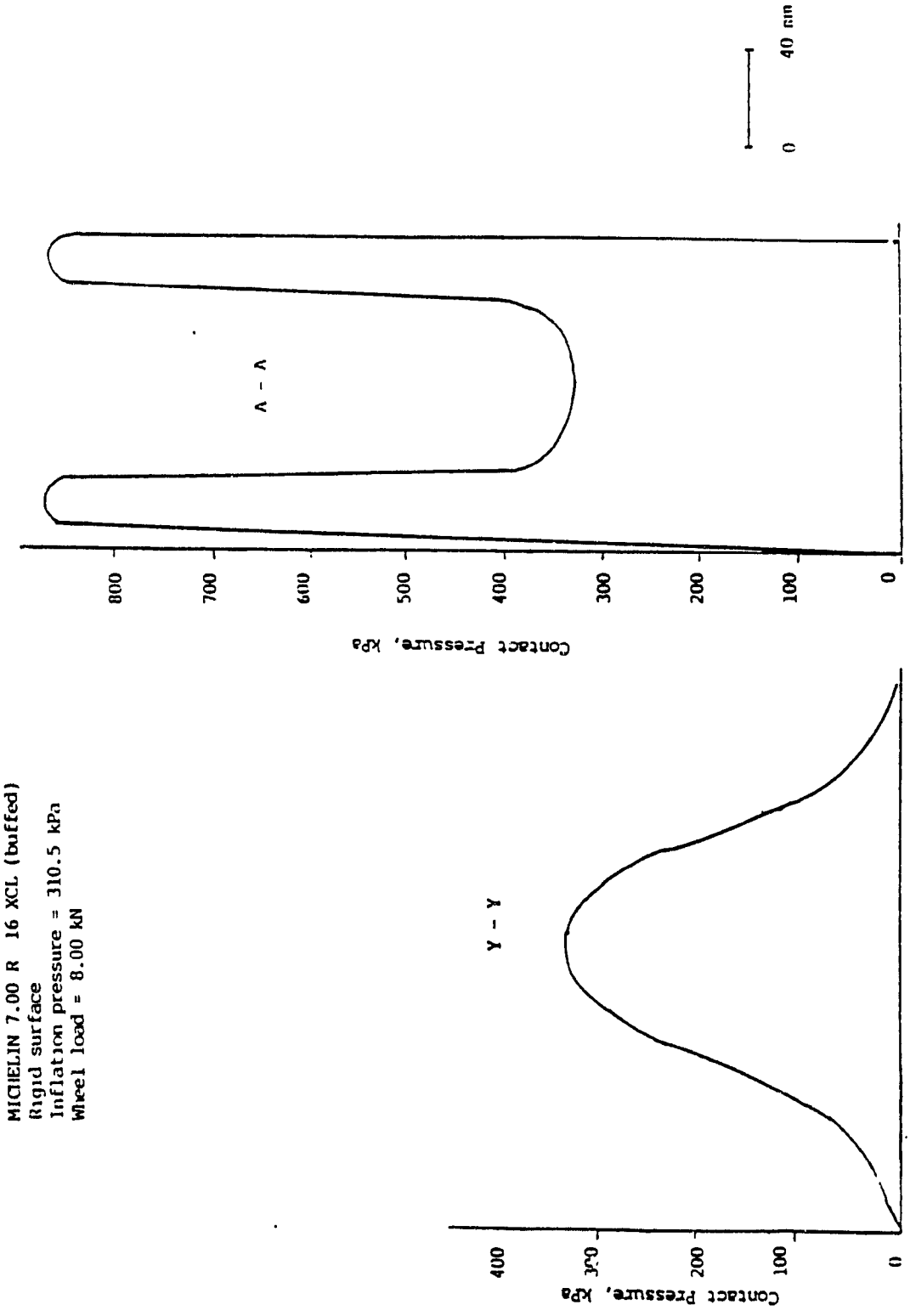


Fig. C.8b/2 Contact Pressure Distribution Within the Footprint of MICHELIN 7.00R-16XCL (buffed)

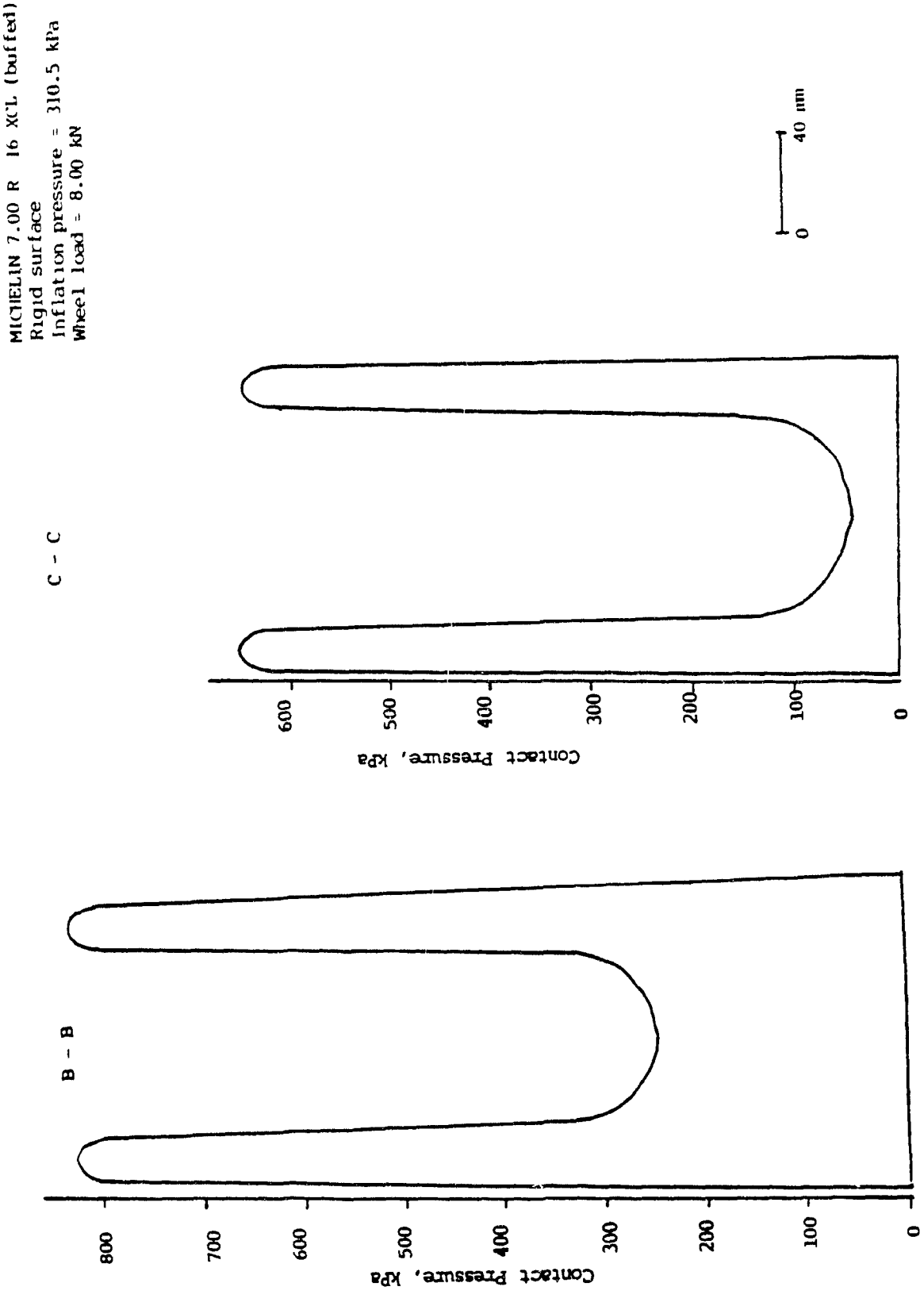


Fig. C.8b/3 Contact Pressure Distribution Within the Footprint of MICHELIN 7.00R-16XCL (buffed)

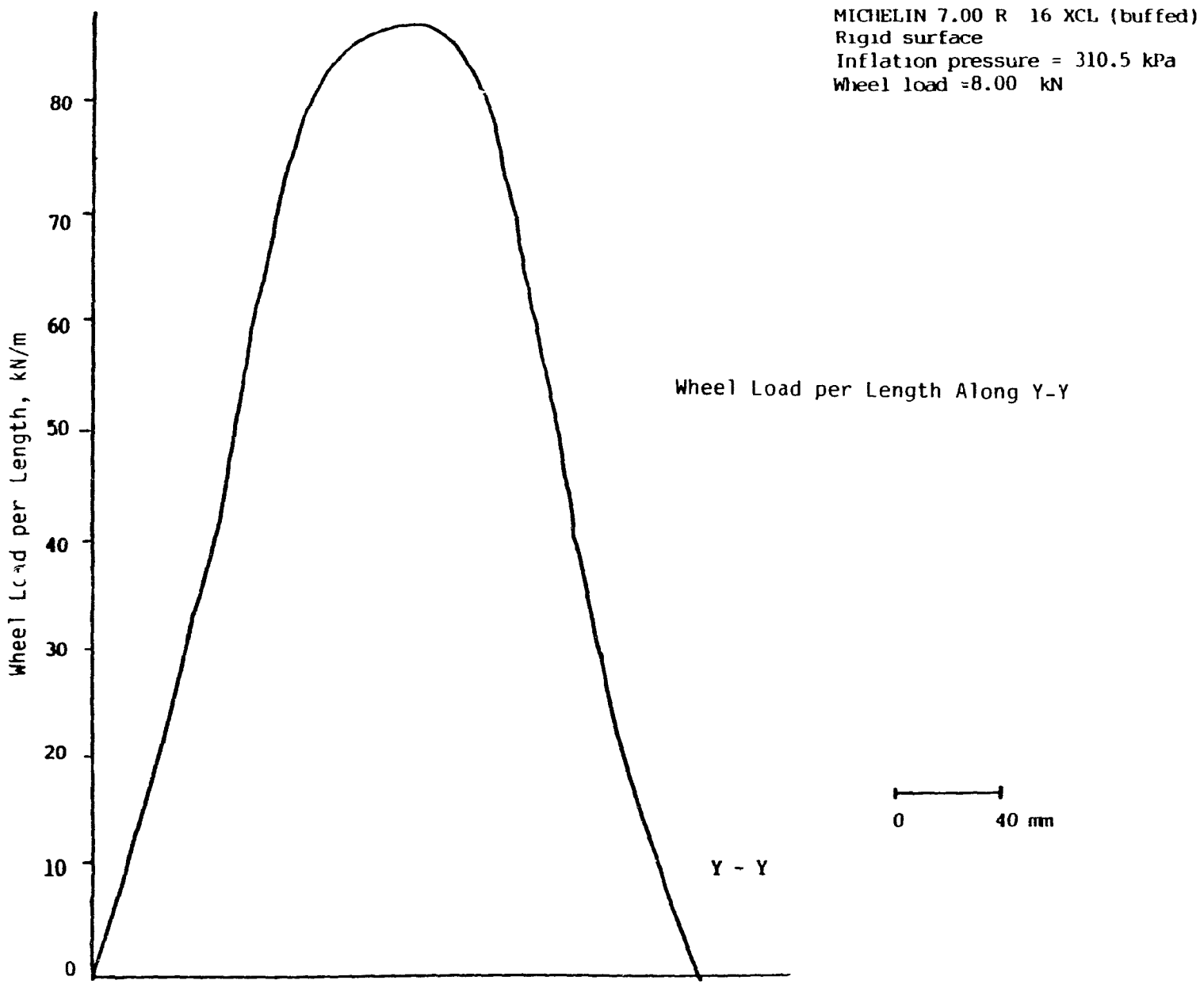


Fig. C.8b/4 Load per Length Along Y-Y of MICHELIN 7.00R-16XCL (buffed)

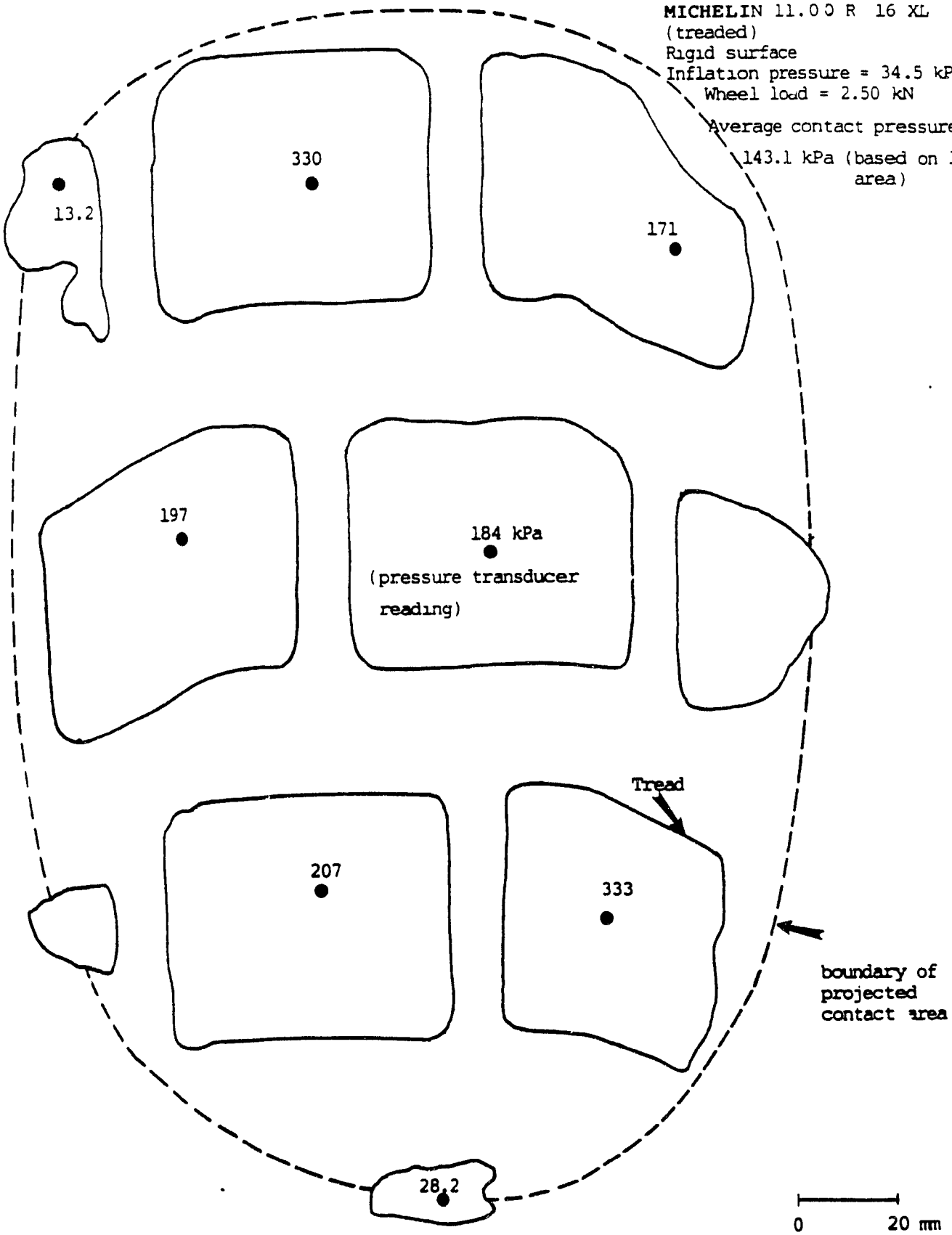


Fig. C.9a Pressure Transducer Readings Within the Footprint of MICHELIN 11.00-16XL (treaded)

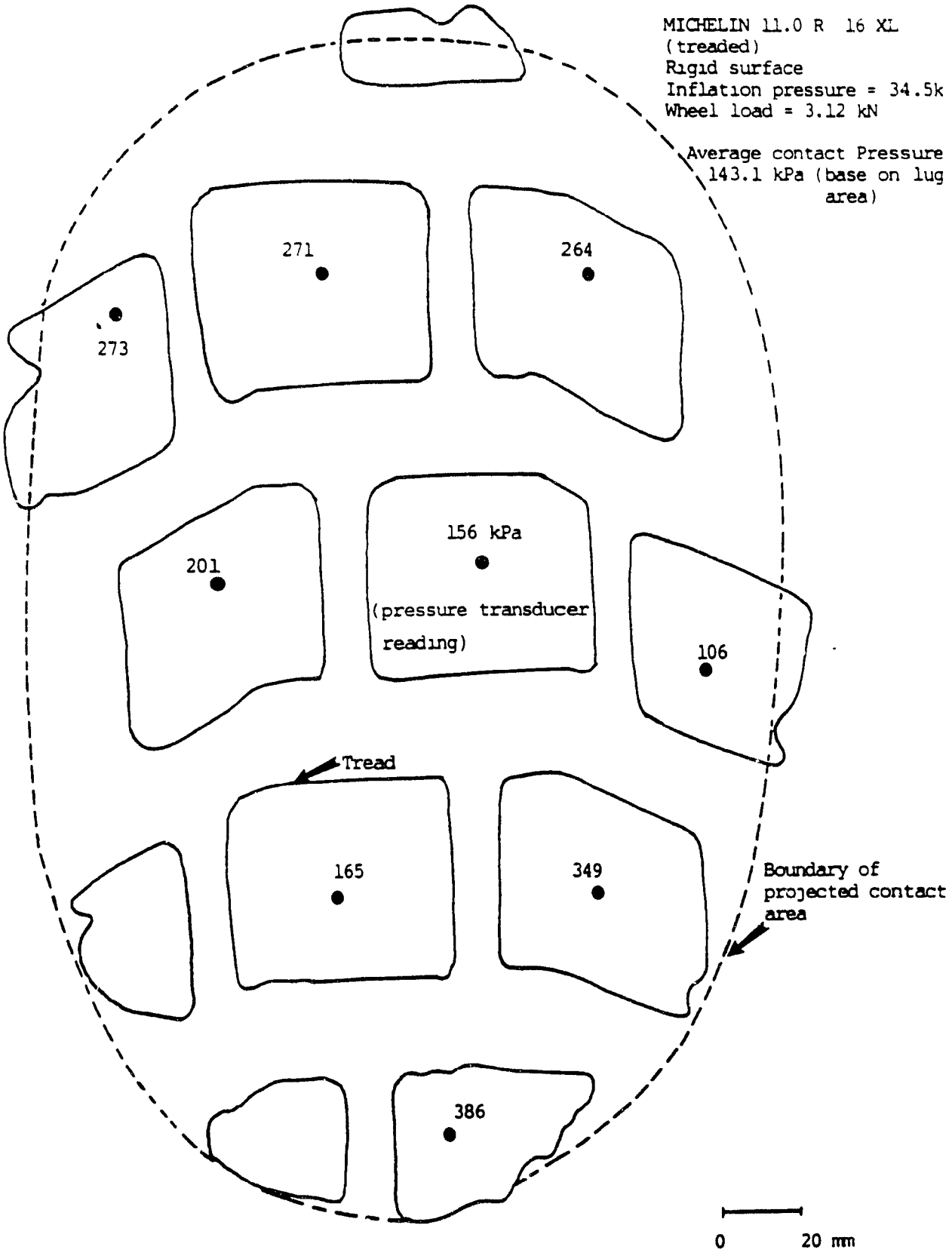


Fig. C.9b Pressure Transducer Readings Within the Footprint of MICHELIN 11.00-16XL (treaded)

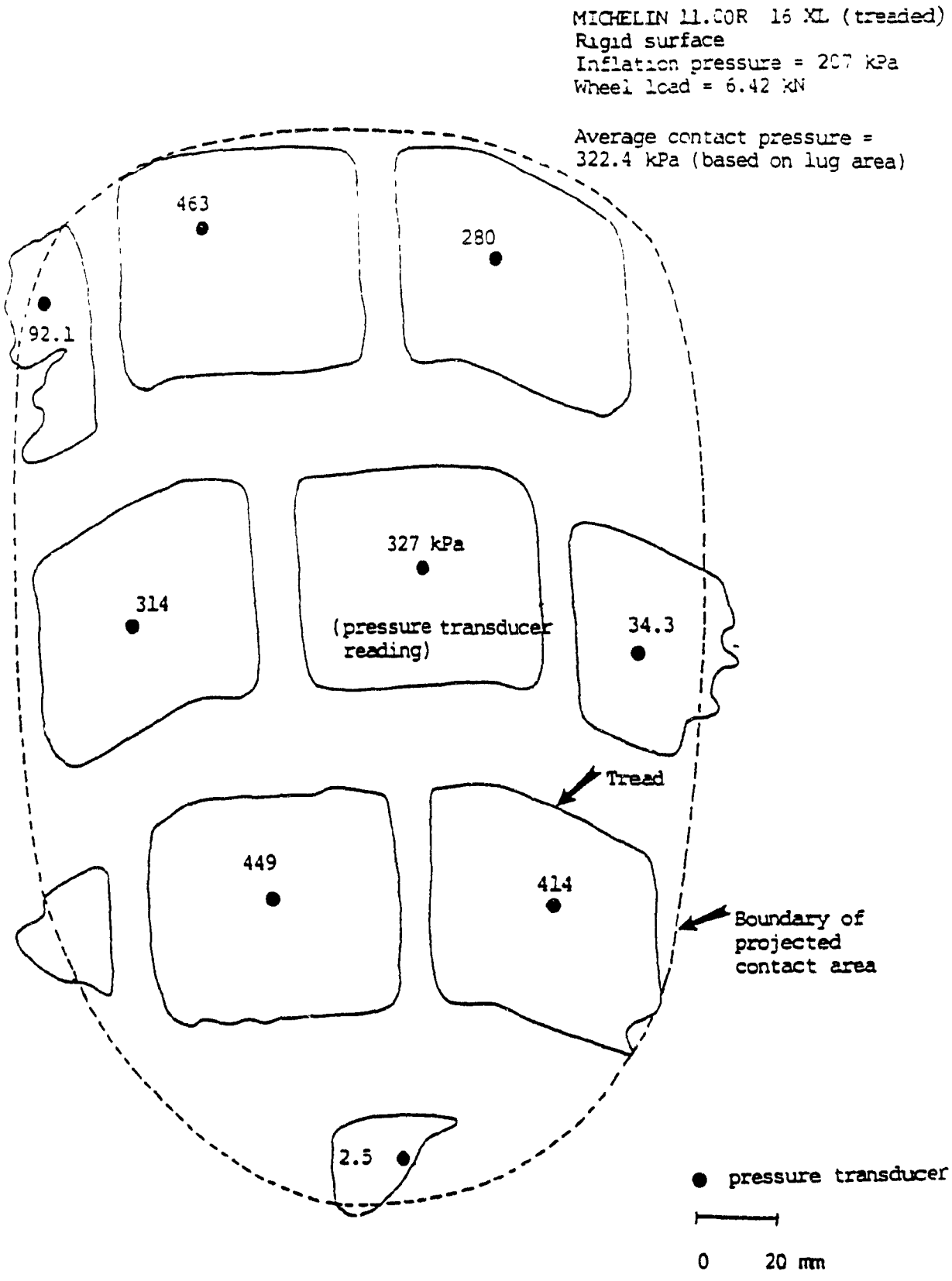


Fig. C.9c Pressure Transducer Readings Within the Footprint of MICHELIN 11.00-16XL (treaded)

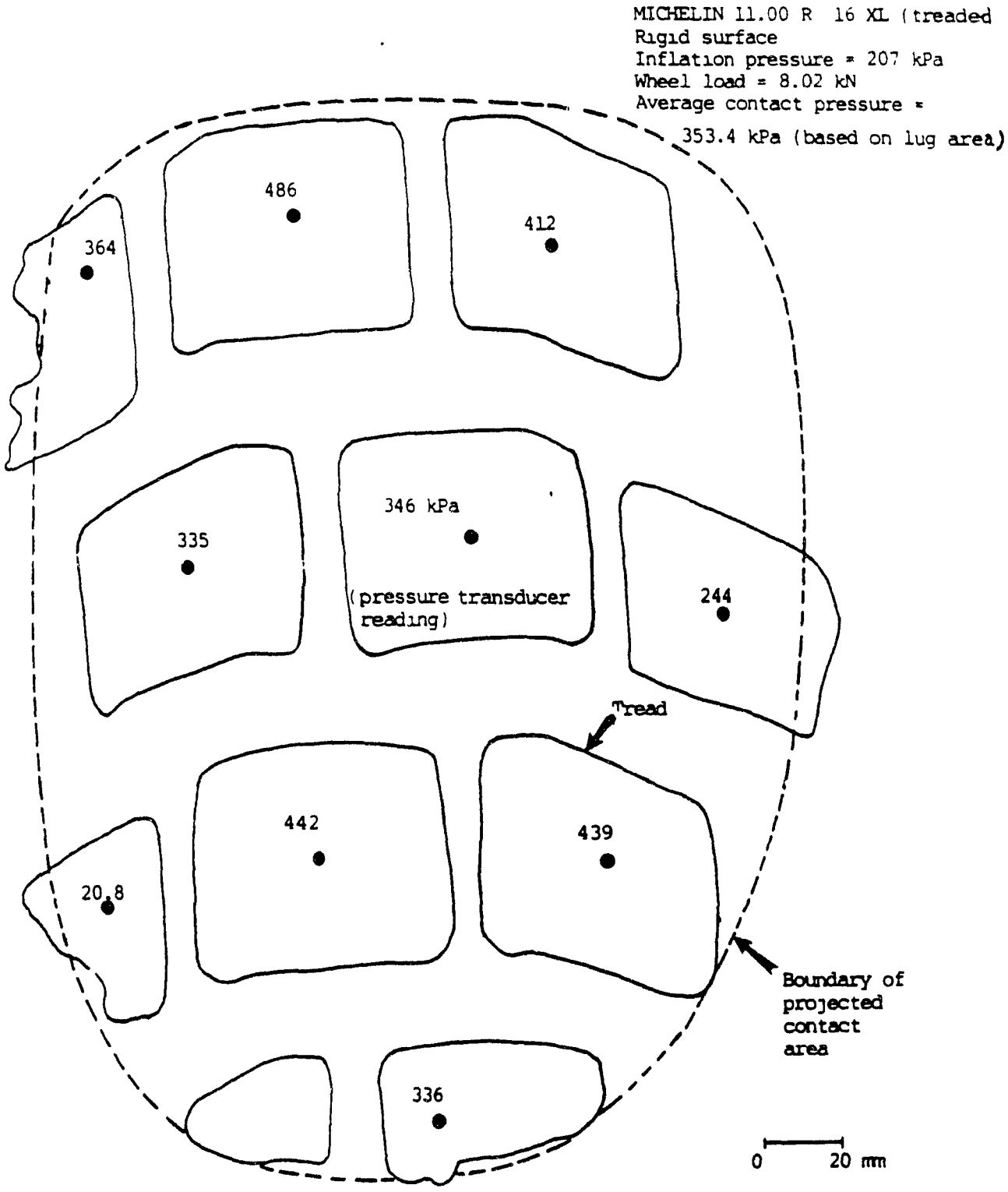


Fig. C.9d Pressure Transducer Readings Within the Footprint of MICHELIN 11.00-16XL (treaded)

MICHELIN 11.00 R 16 XL (treaded)
Rigid surface
Inflation pressure = 414 kPa
Wheel load = 10.69 kN
Average contact pressure =
450.0 kPa (based on lug area)

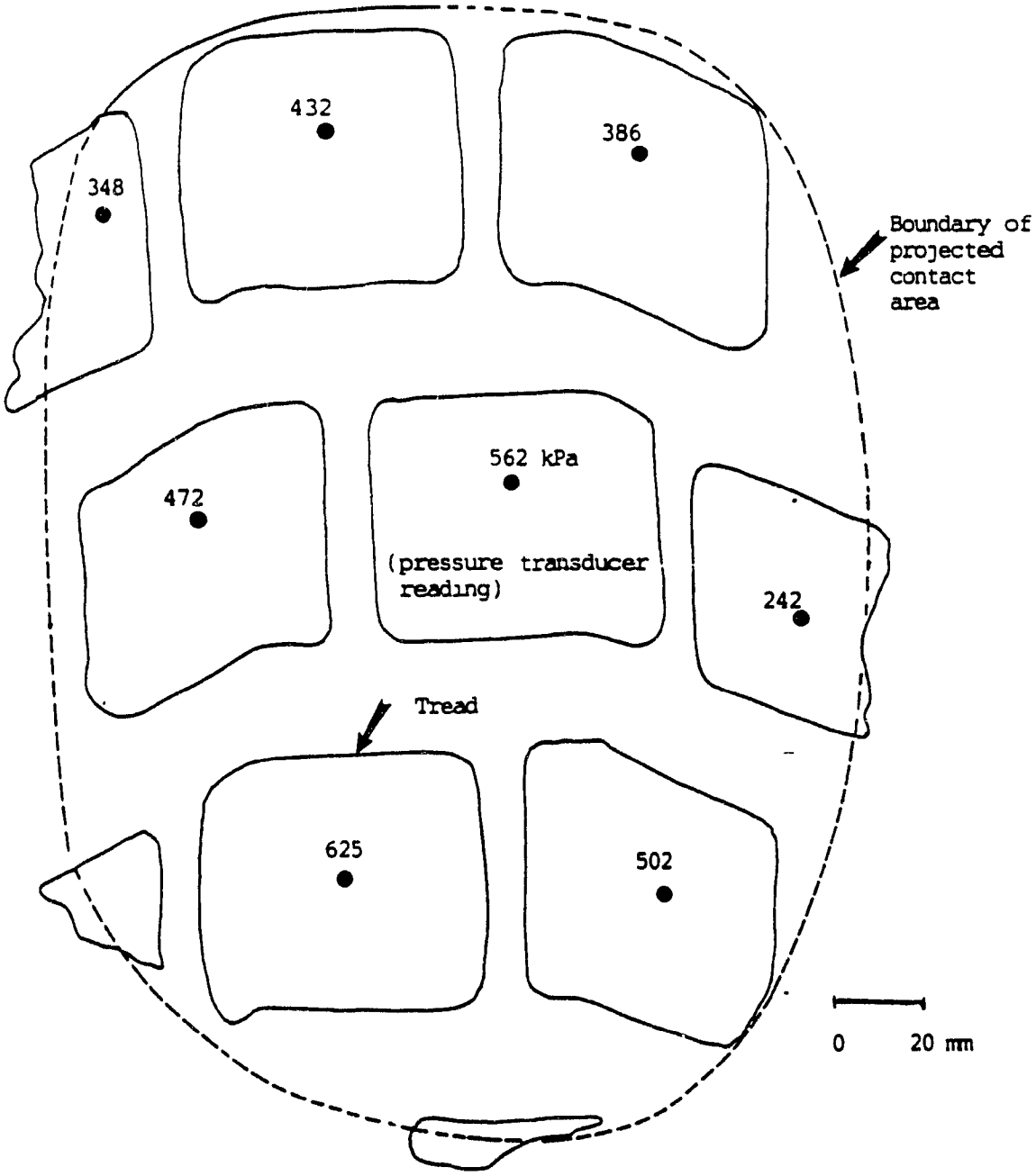


Fig. C.9e Pressure Transducer Readings Within the Footprint of MICHELIN 11.00-16XL (treaded)

MICHELIN 11.00 R 16 XL (treaded)
Rigid surface
Inflation pressure = 414 kPa
Wheel load = 13.34 kN
Average contact pressure = 450.0 kPa
(based on lug area)

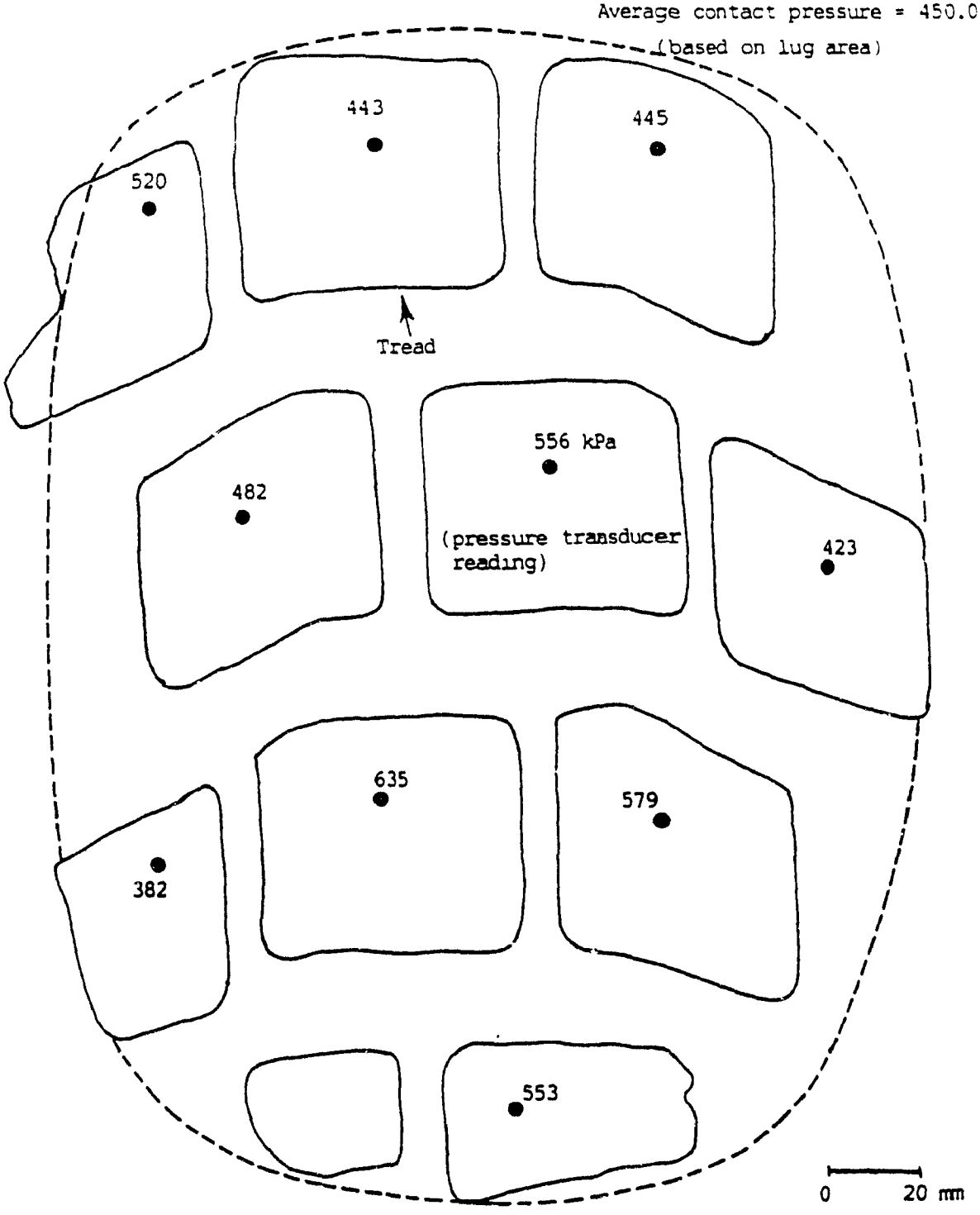


Fig. C.9f Pressure Transducer Readings Within the Footprint of MICHELIN 11.00-16XL (treaded)

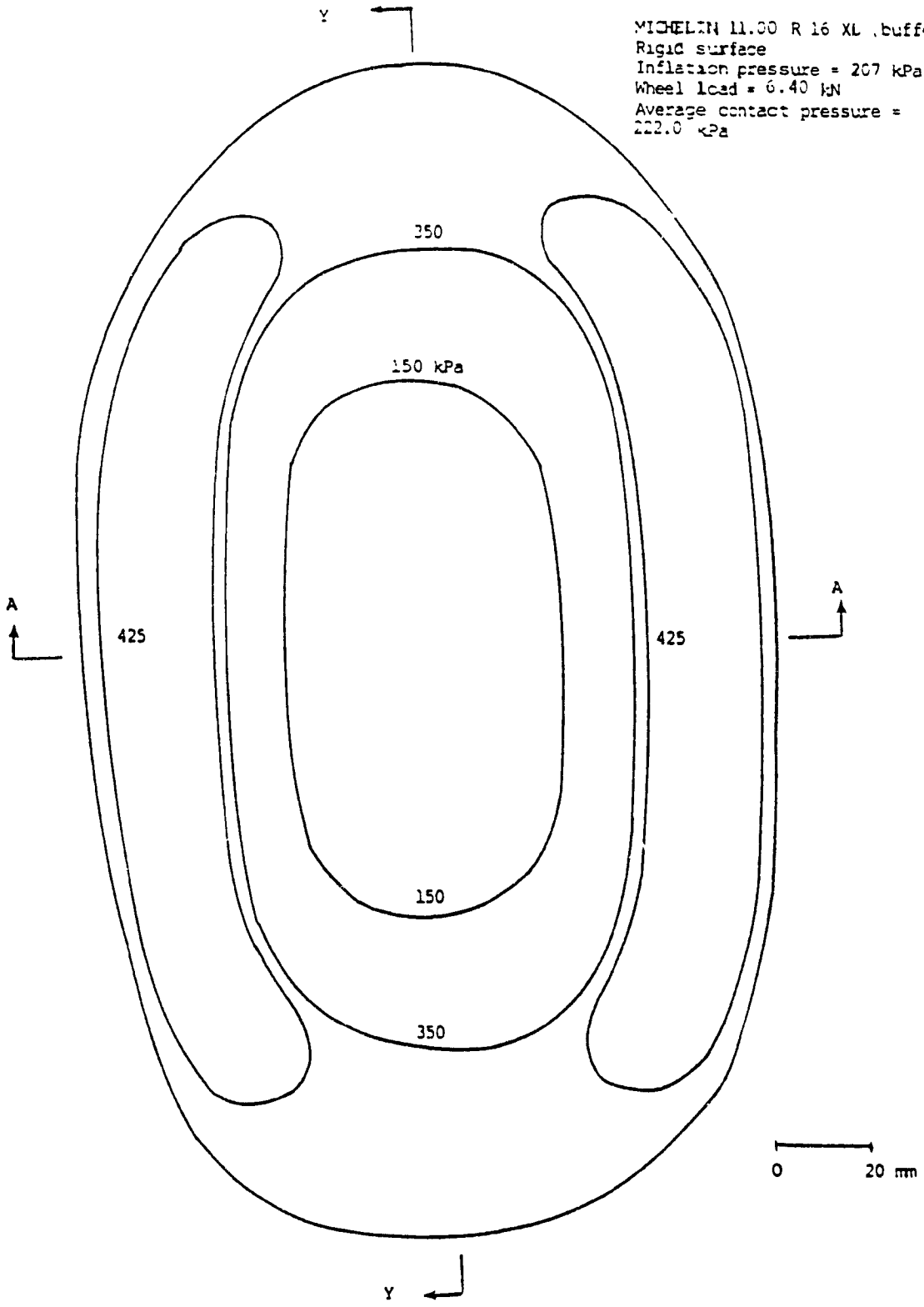


Fig. C.10a/1 Contact Pressure Distribution Within the Footprint of MICHELIN 11.00R-16XL (buffed)

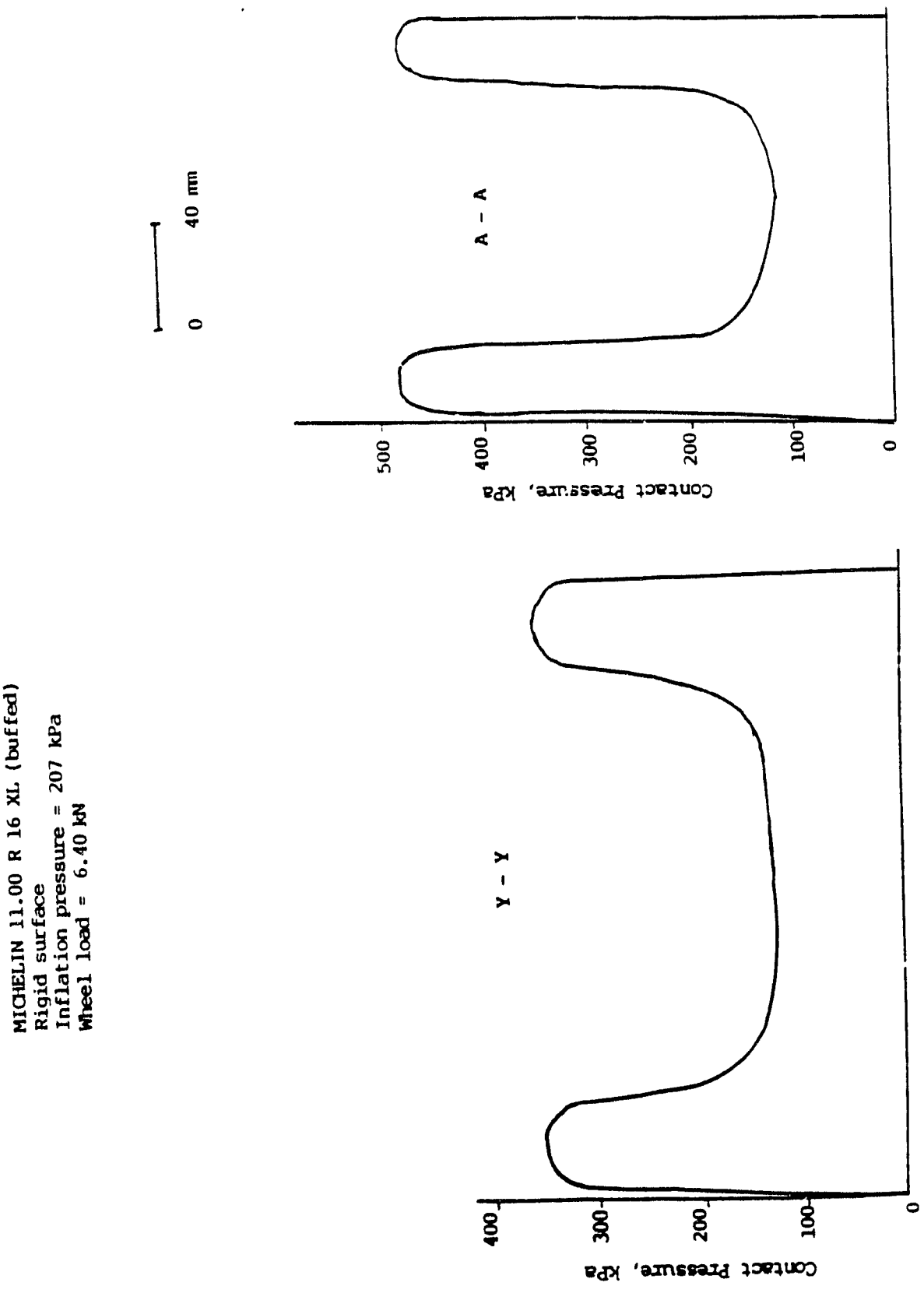


Fig. C.10a/2 Contact Pressure Distribution Within the Footprint of MICHELIN 11.00R-16XL (buffed)

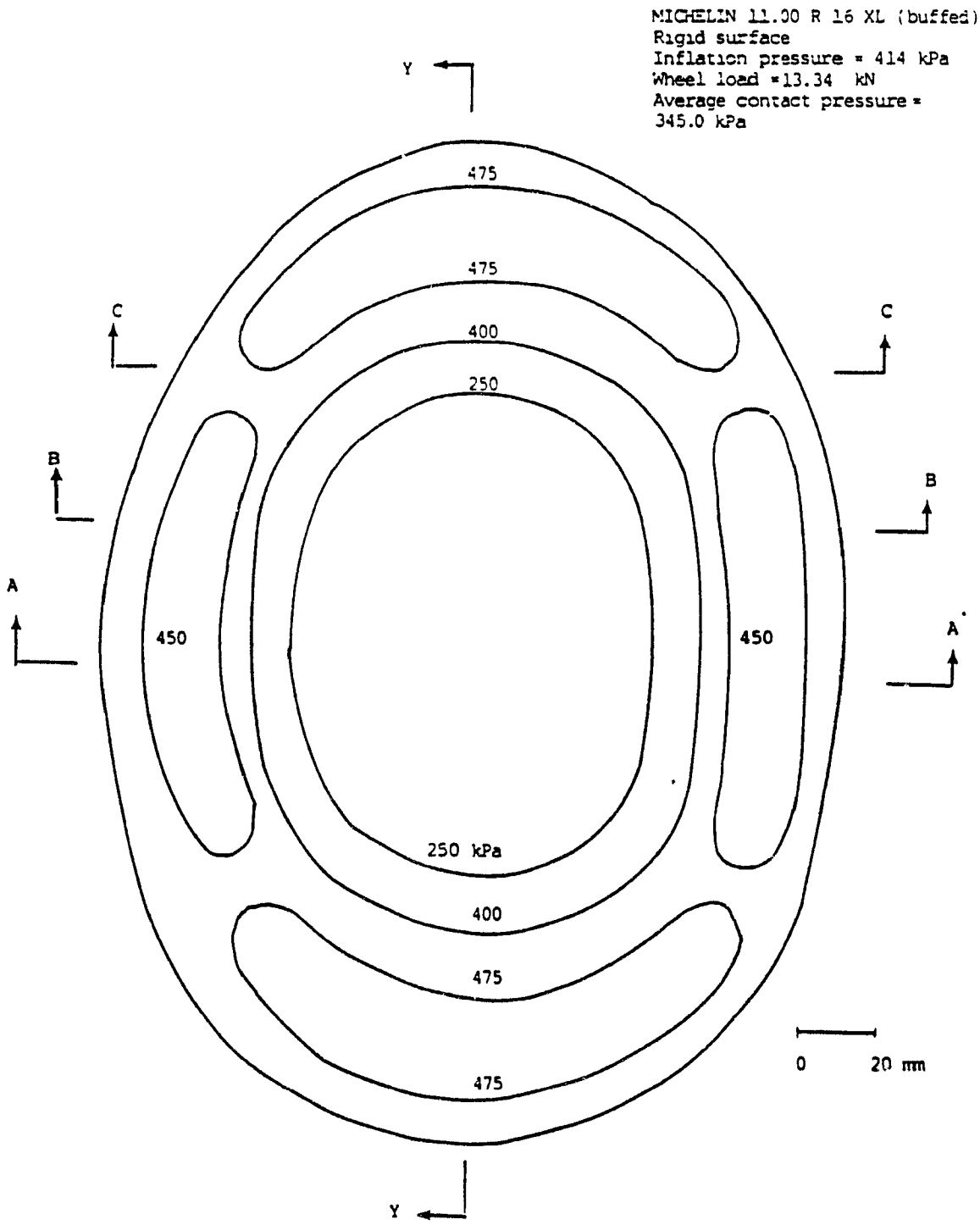


Fig. C.10b/1 Contact Pressure Distribution Within the Footprint of MICHELIN 11.00R-16XL (buffed)

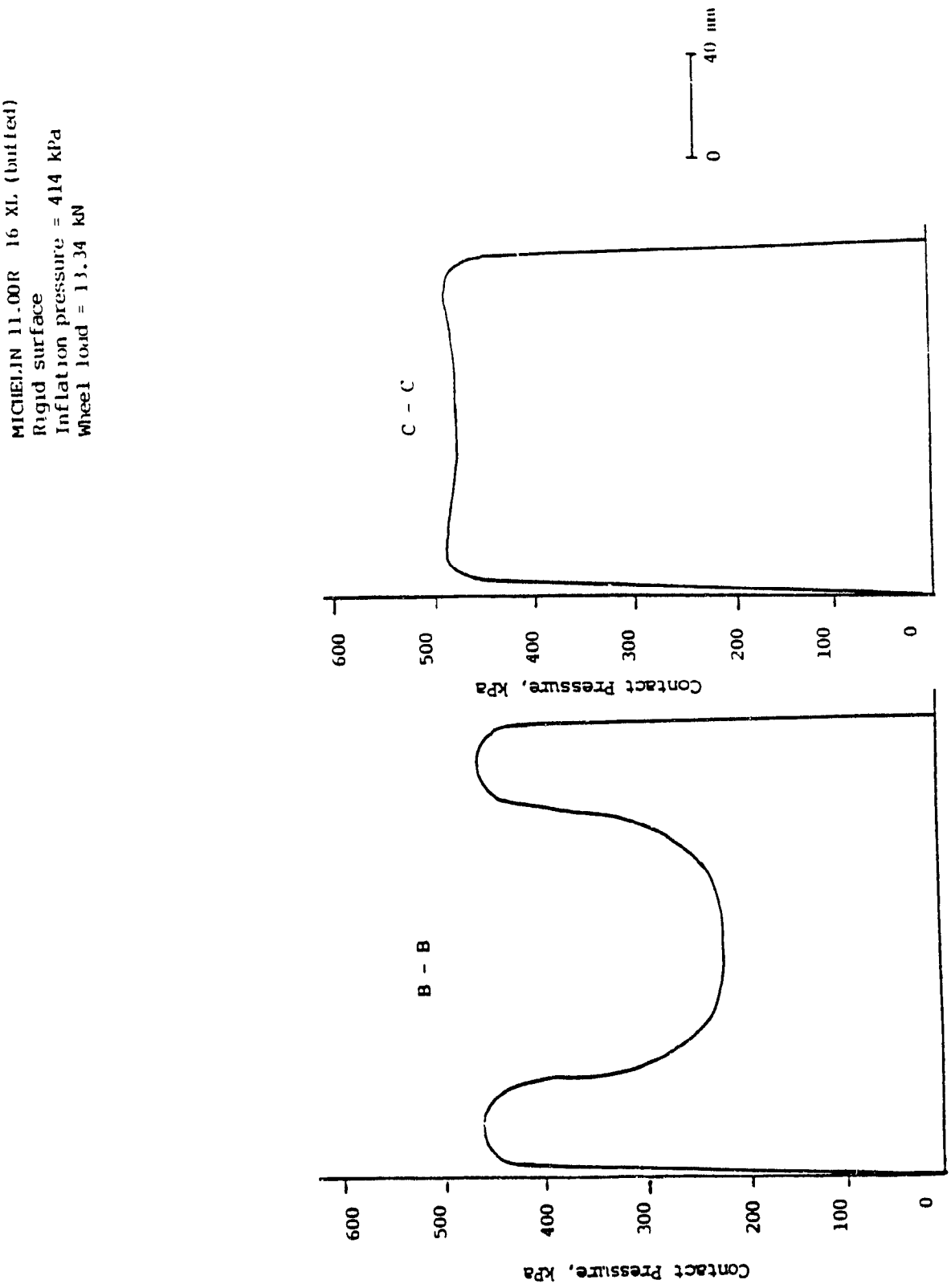


Fig. C.10b/2 Contact Pressure Distribution Within the Footprint of MICHELIN 11.00R-16XL (buffed)

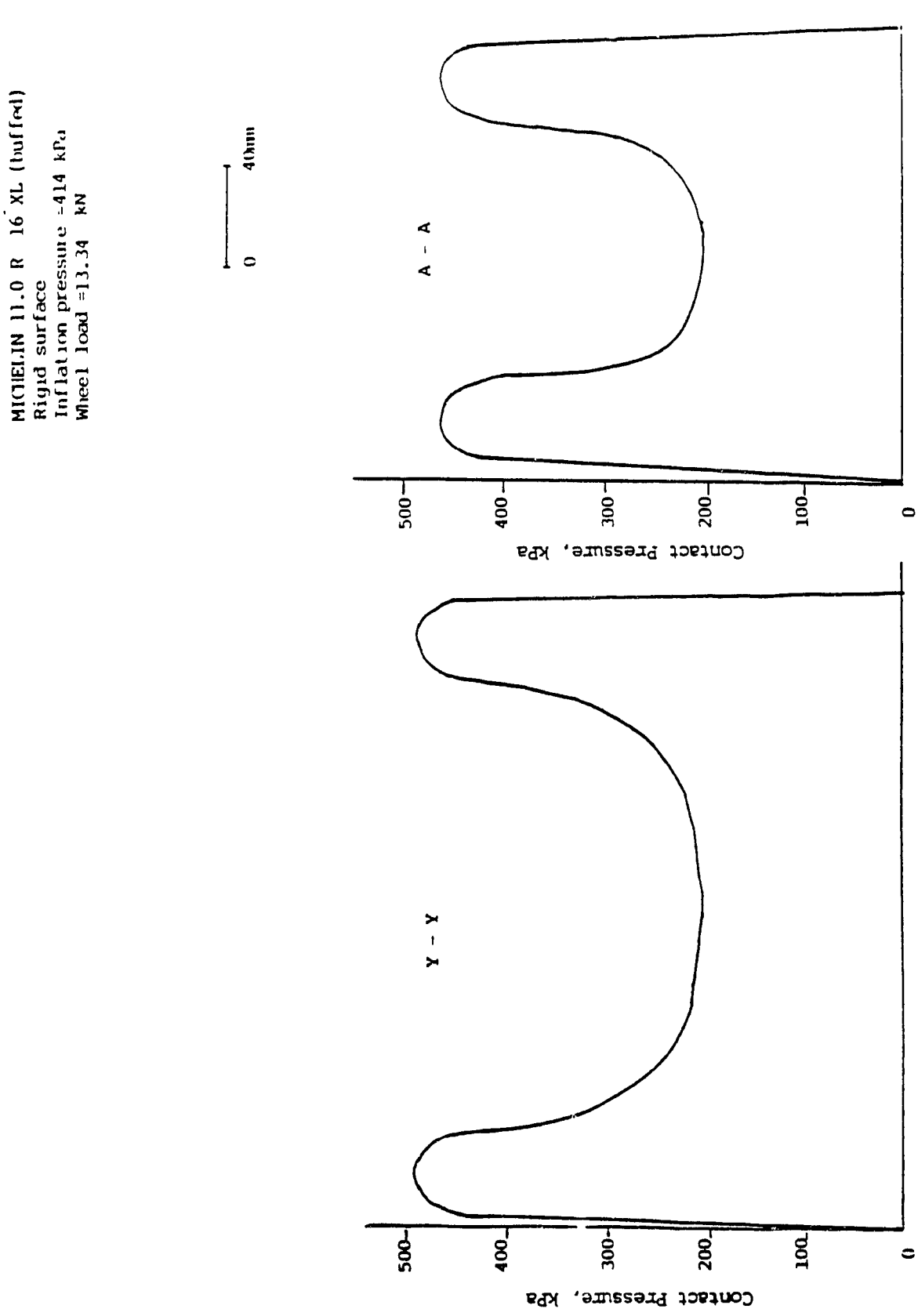


Fig. C.10b/3 Contact Pressure Distribution Within the Footprint of MICHELIN 11.00R-16XL (buffed)

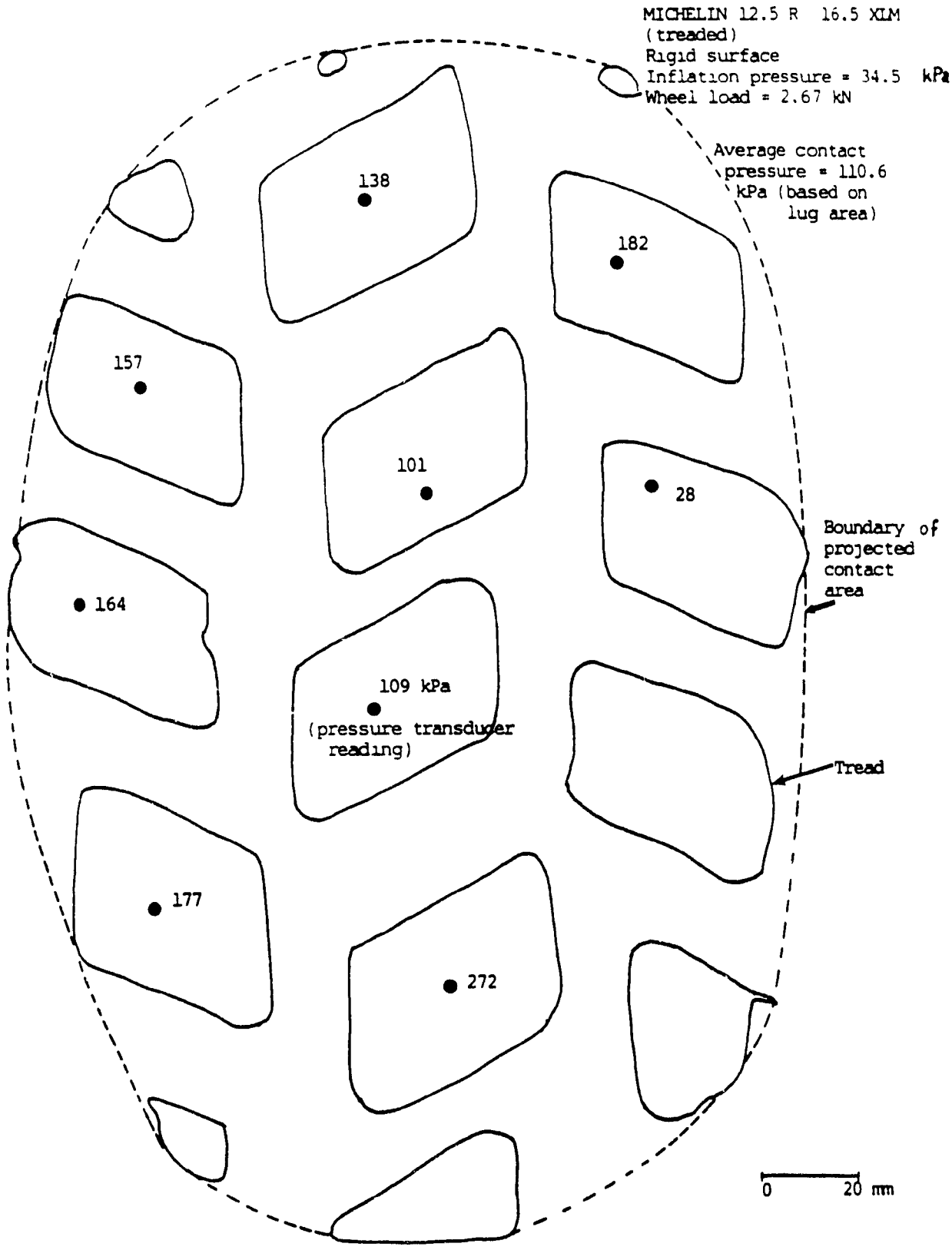


Fig. C.11a Pressure Transducer Readings Within the Footprint of MICHELIN 12.5R-16.5XLM (treaded)

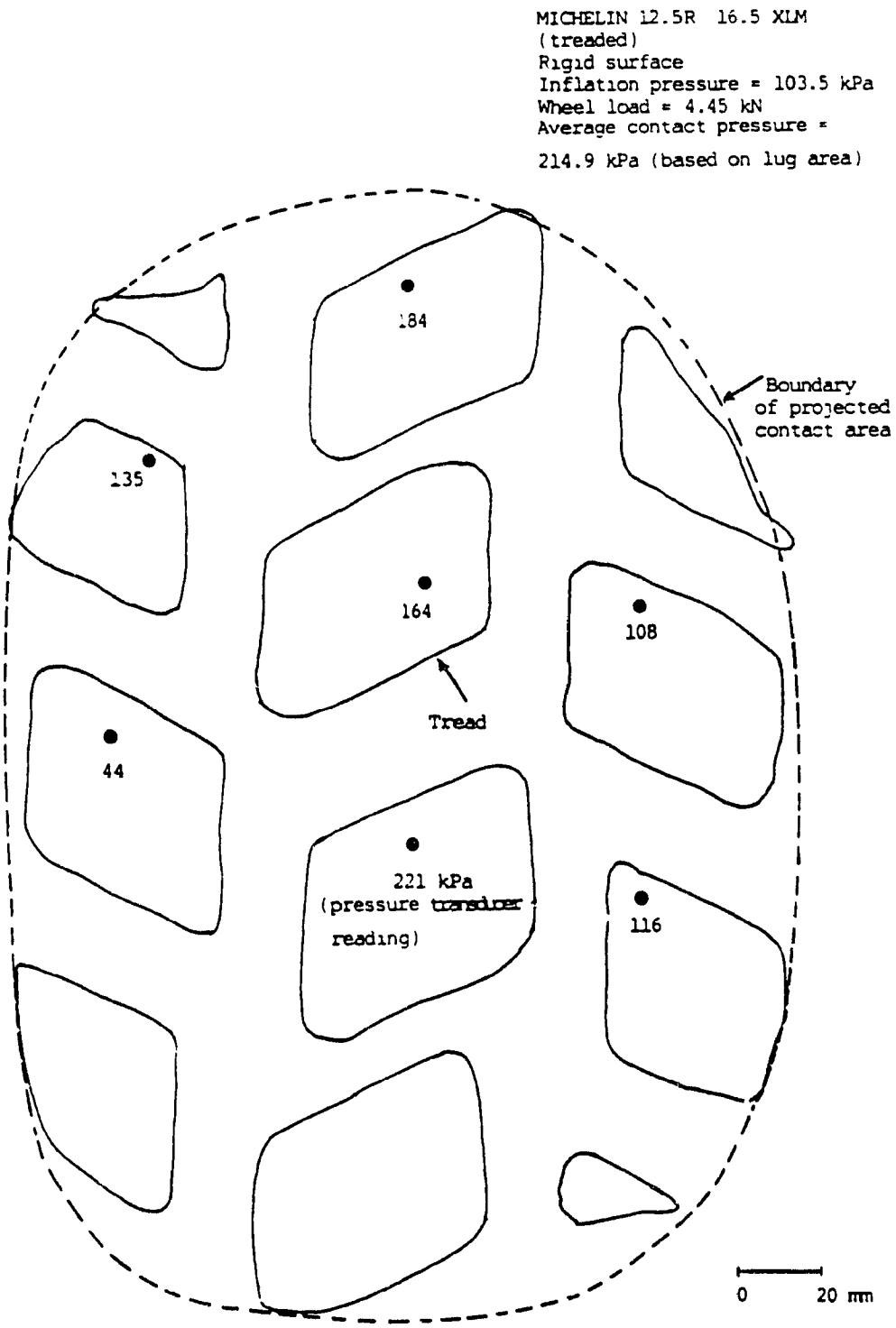


Fig. C.11b Pressure Transducer Readings Within the Footprint of of MICHELIN MICHELIN 12.5R-16.5XLM (treaded)

MICHELIN 12.5 R 16.5 XLM (treaded
Rigid surface
Inflation pressure = 207 kPa
Wheel load = 6.68 kN
Average contact pressure = 336.2 kPa (based on lug area)

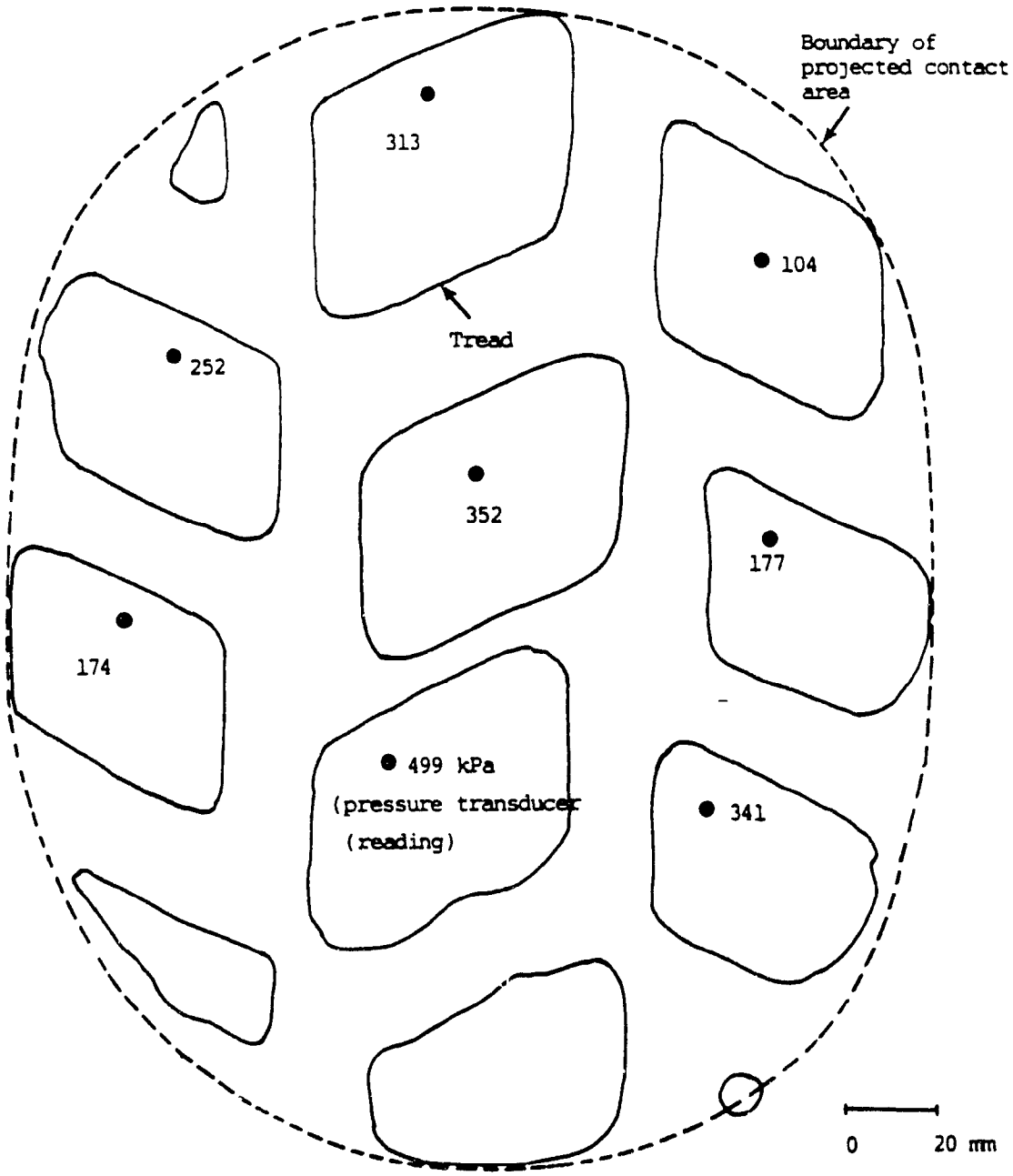


Fig. C.11c Pressure Transducer Readings Within the Footprint of MICHELIN 12.5R-16.5XLM (treaded)

MICHELIN 12.5 R 16.5 XLM (buffed)
Rigid surface
Inflation pressure = 103.5 kPa
Wheel load = 0.89 kN
Average contact pressure = 87.0 kPa

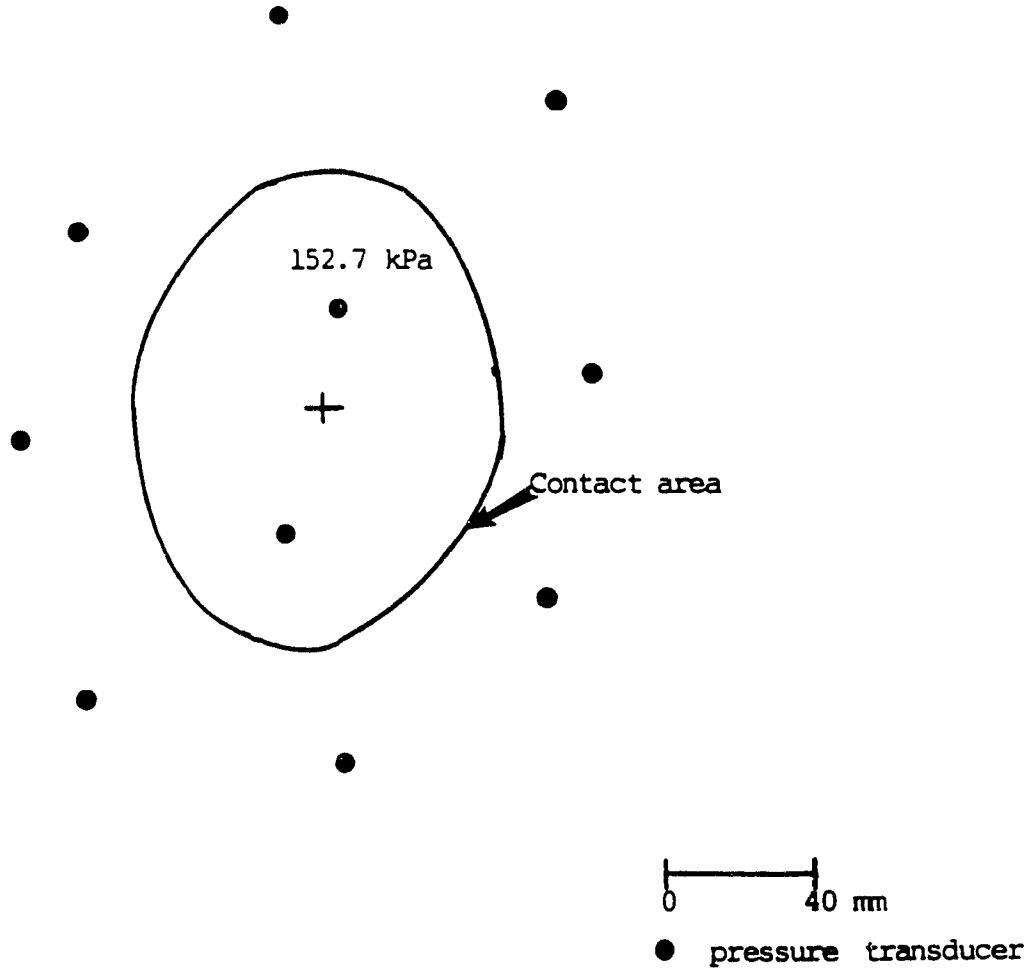


Fig. C.12a Pressure Transducer Readings Within the Footprint of MICHELIN 12.5R-16.5XLM (buffed)

MICHELIN 12.5 R 16.5 XLM (buffed)
Rigid surface
Inflation pressure = 103.5 kPa
Wheel load = 1.78 kN
Average contact pressure = 87.0 kPa

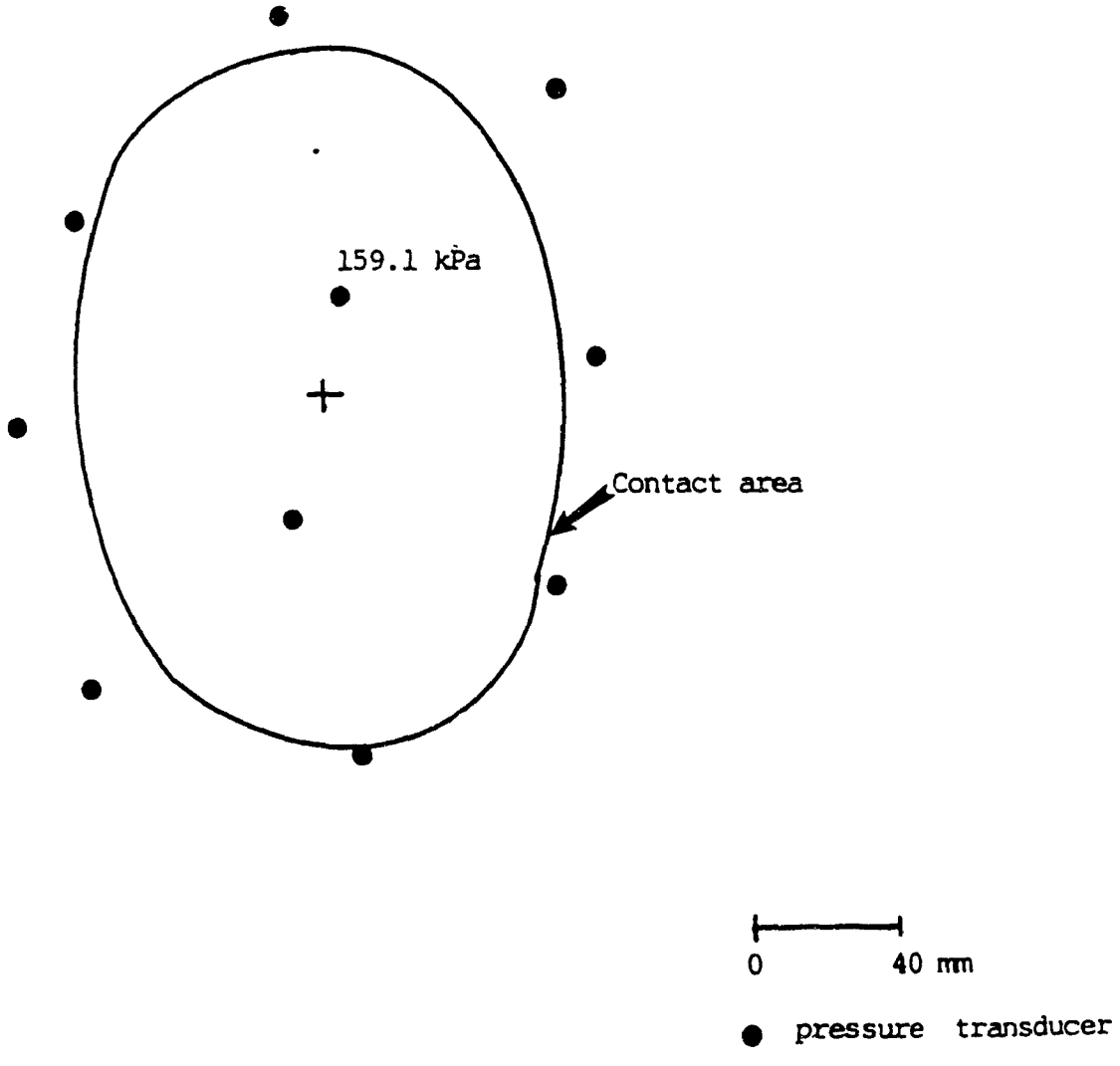


Fig. C.12b Pressure Transducer Readings Within the Footprint of MICHELIN 12.5R-16.5XLM (buffed)

MICHELIN 12.5 R 16.5 XLM (buffed)
Rigid surface
Inflation pressure = 103.5 kPa
Wheel load = 3.56 kN
Average contact pressure = 87.0 kPa

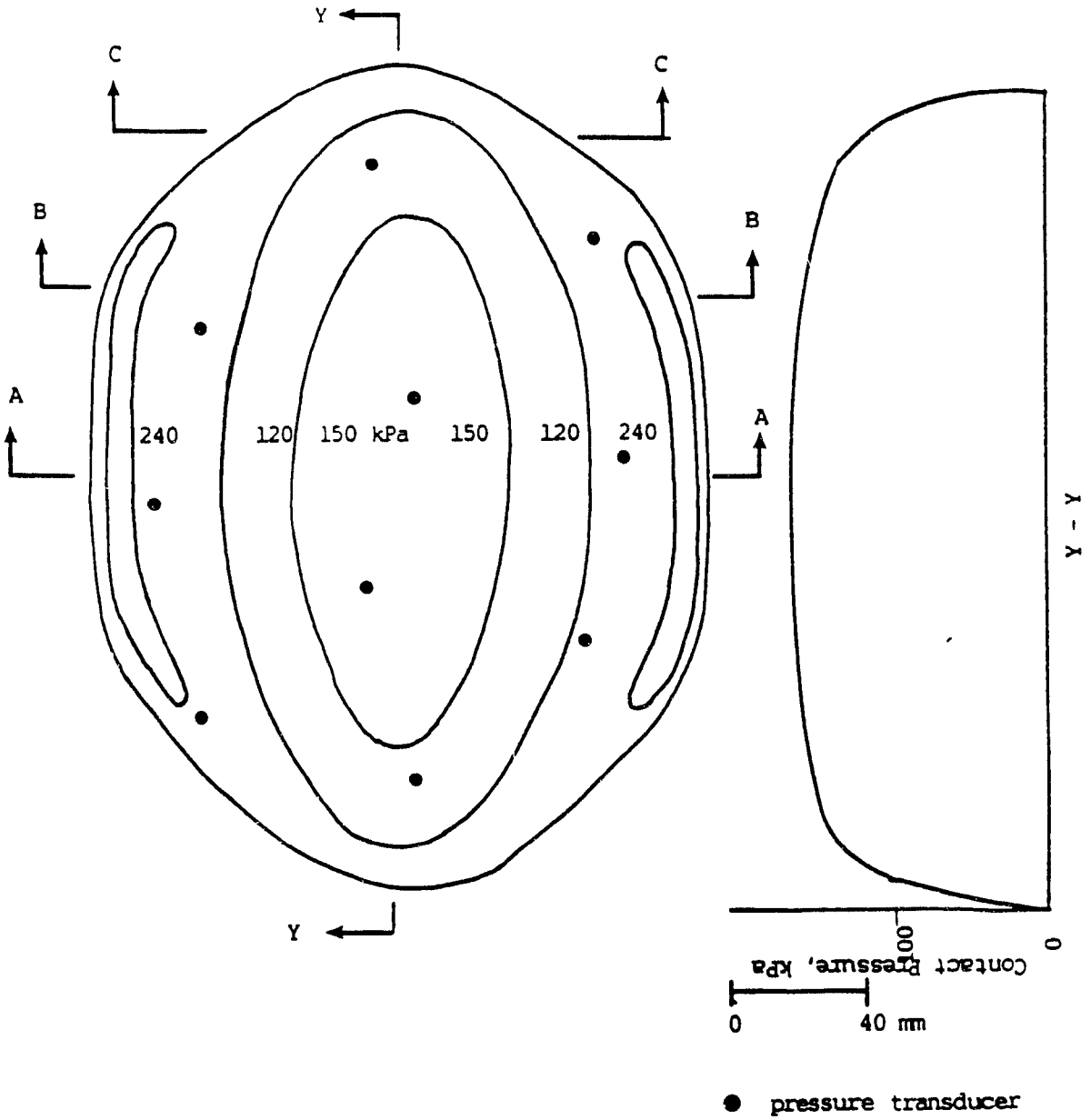


Fig. C.12c/1 Contact Pressure Distribution Within the Footprint of MICHELIN 12.5R-16.5XLM (buffed)

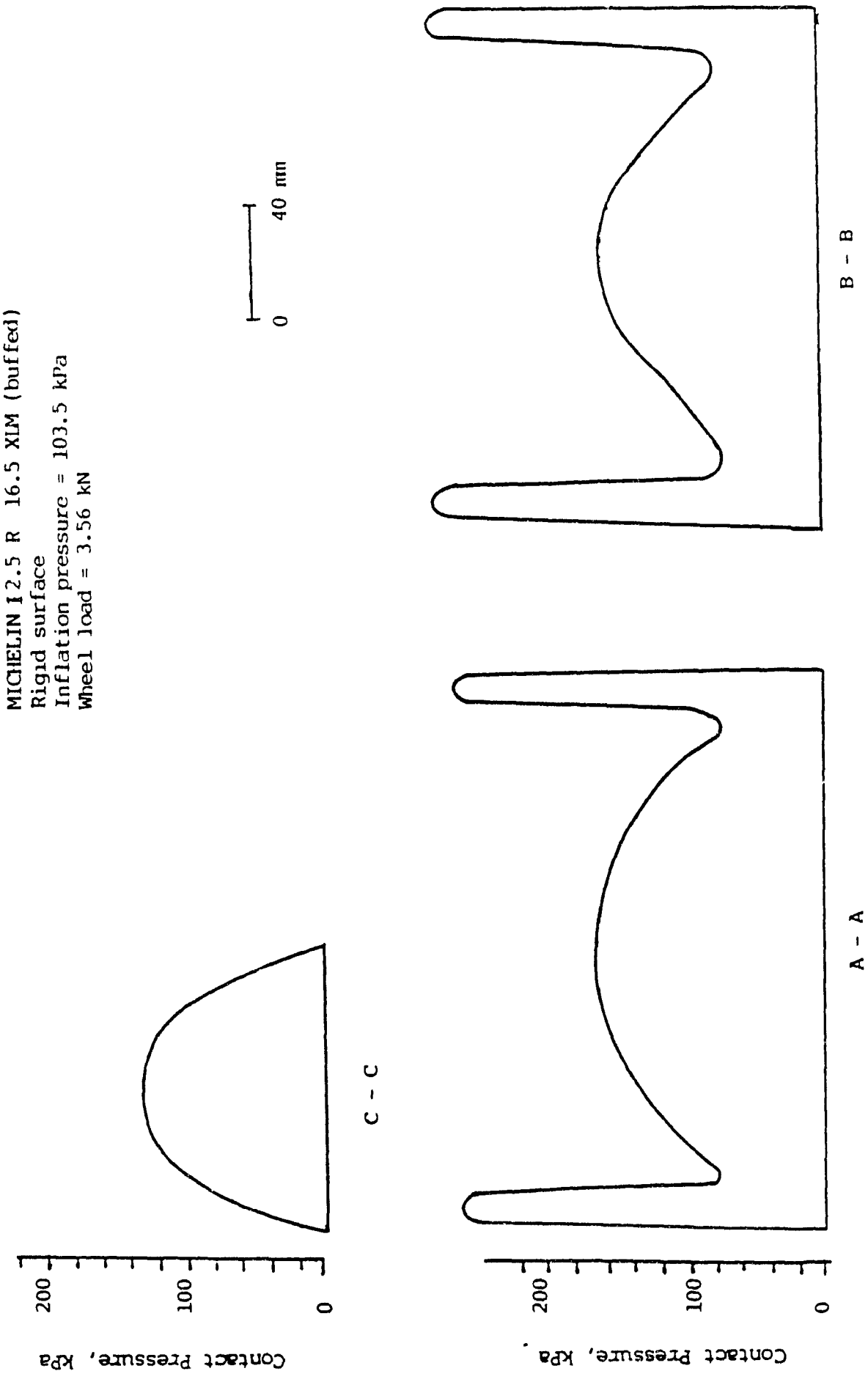


Fig. C.12c/2 Contact Pressure Distribution Within the Footprint of MICHELIN 12.5R-16.5XLM (buffed)

MICHELIN 12.5 R 16.5 XLM (buffed)
Rigid surface
Inflation pressure = 103.5 kPa
Wheel load = 4.45 kN
Average contact pressure = 95.7 kPa

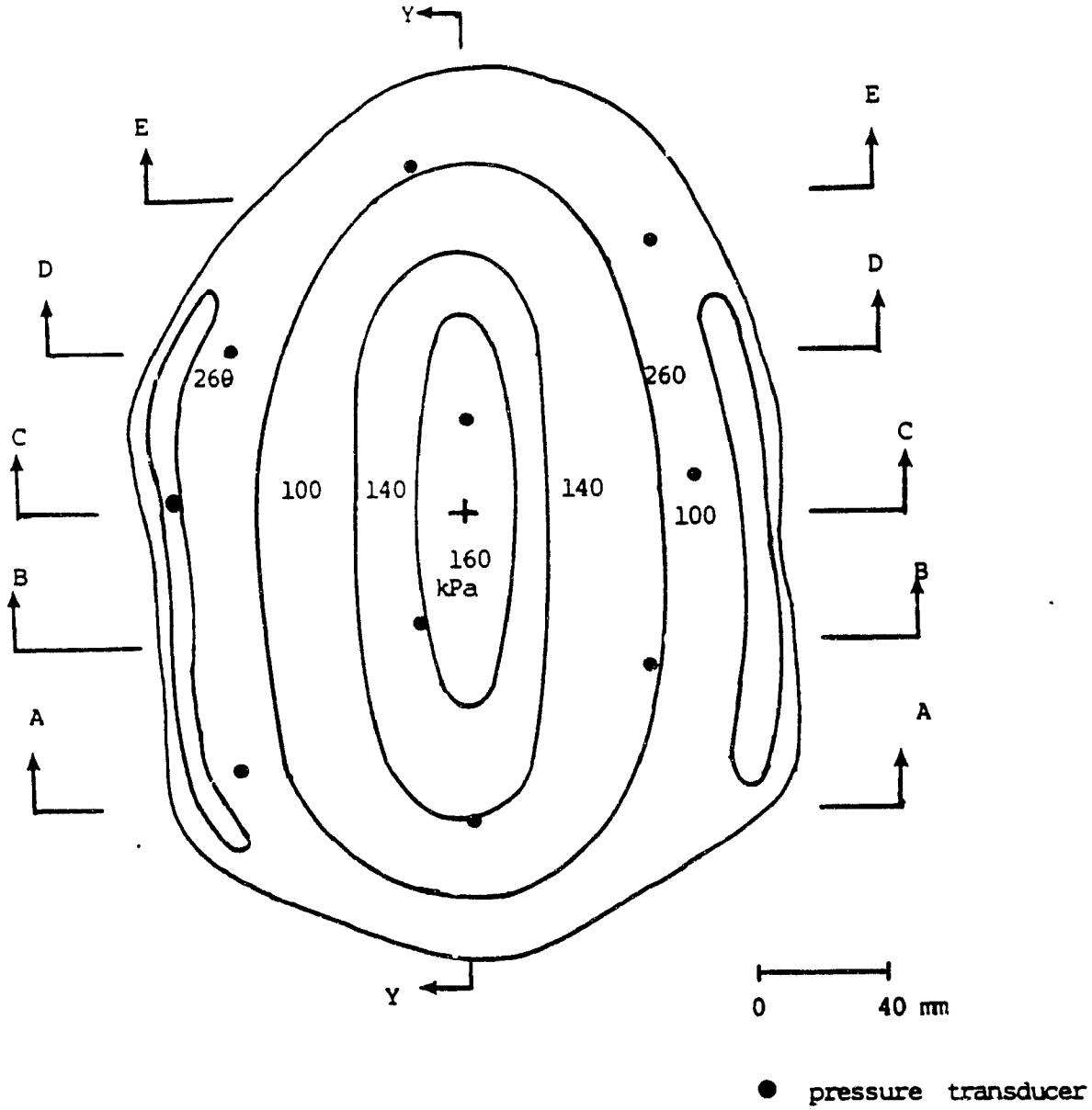


Fig. C.12d/1 Contact Pressure Distribution Within the Footprint of MICHELIN 12.5R-16.5XLM (buffed)

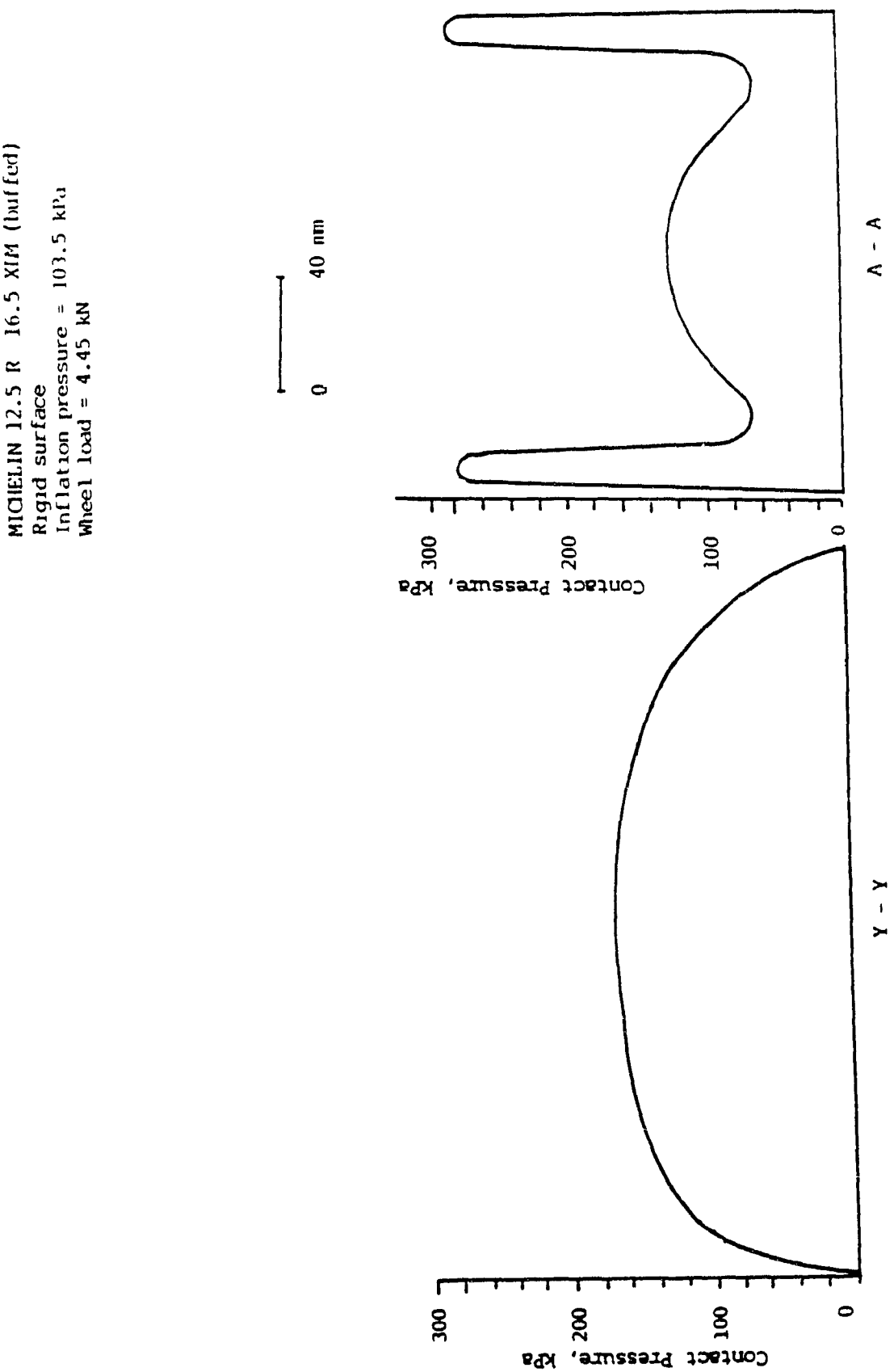


Fig. C.12d/2 Contact Pressure Distribution Within the Footprint of MICHELIN 12.5R-16.5XLM (buffed)

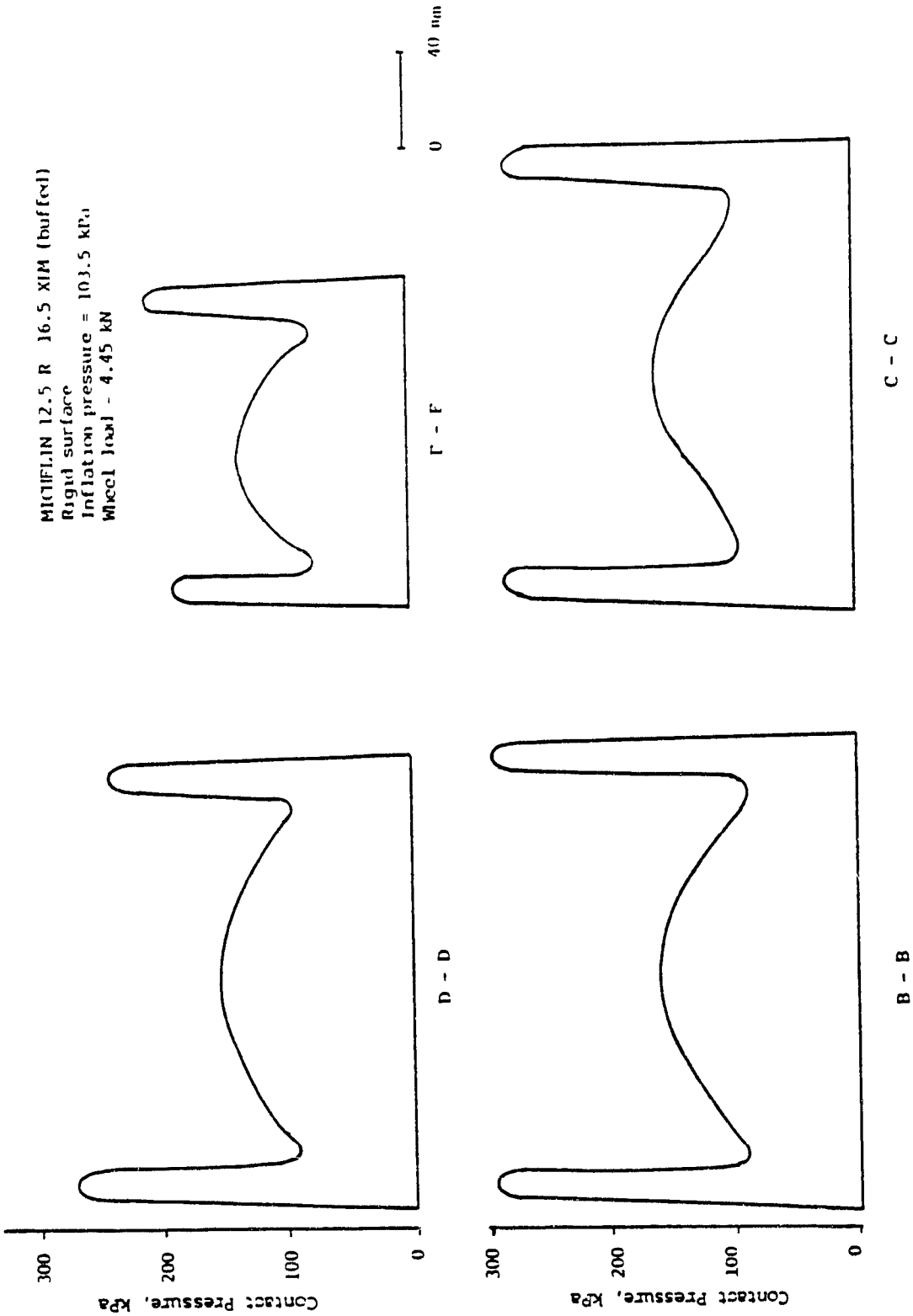


Fig. C.12d/3 Contact Pressure Distribution Within the Footprint of MICHELIN 12.5R-16.5XLM (buffed)

MICHELIN 12.5 R 16.5 XLM (buffed)
Rigid surface
Inflation pressure = 207 kPa
Wheel load = 1.34 kN
Average contact pressure = 158.0 kPa

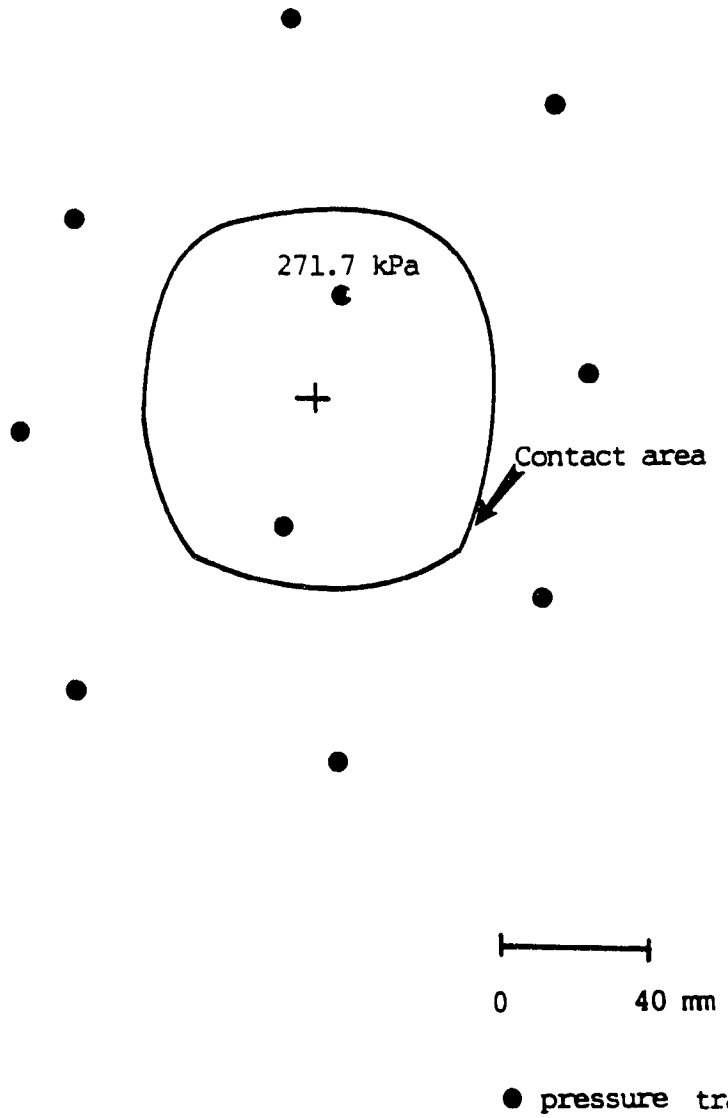


Fig. C.12e Pressure Transducer Readings Within the Footprint of MICHELIN 12.5R-16.5XLM (buffed)

MICHELIN 12.5 R 16.5 XLM (buffed)
Rigid surface
Inflation pressure = 207 kPa
Wheel load = 2.67 kN
Average contact pressure = 158.0 kPa

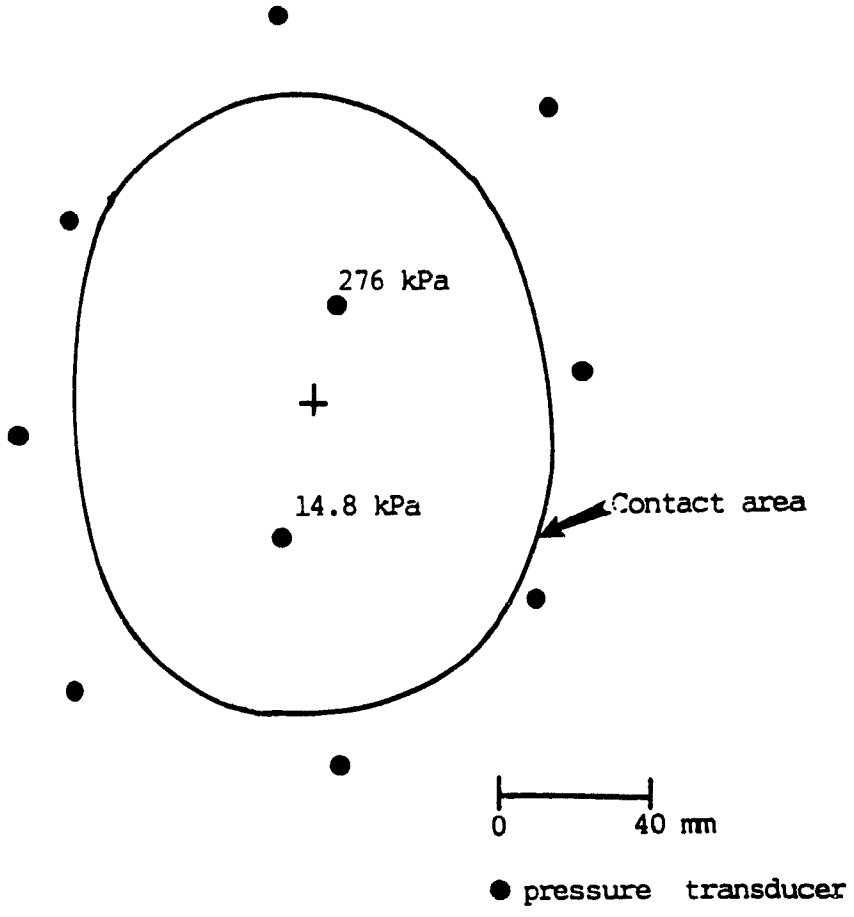


Fig. C.12f Pressure Transducer Readings Within the Footprint of MICHELIN 12.5R-16.5XLM (buffed)

MICHELIN 12.5 R 16.5 XLM (buffed)
Rigid surface
Inflation pressure = 207 kPa
Wheel load = 4.01 kN
Average contact pressure = 158.0 kPa

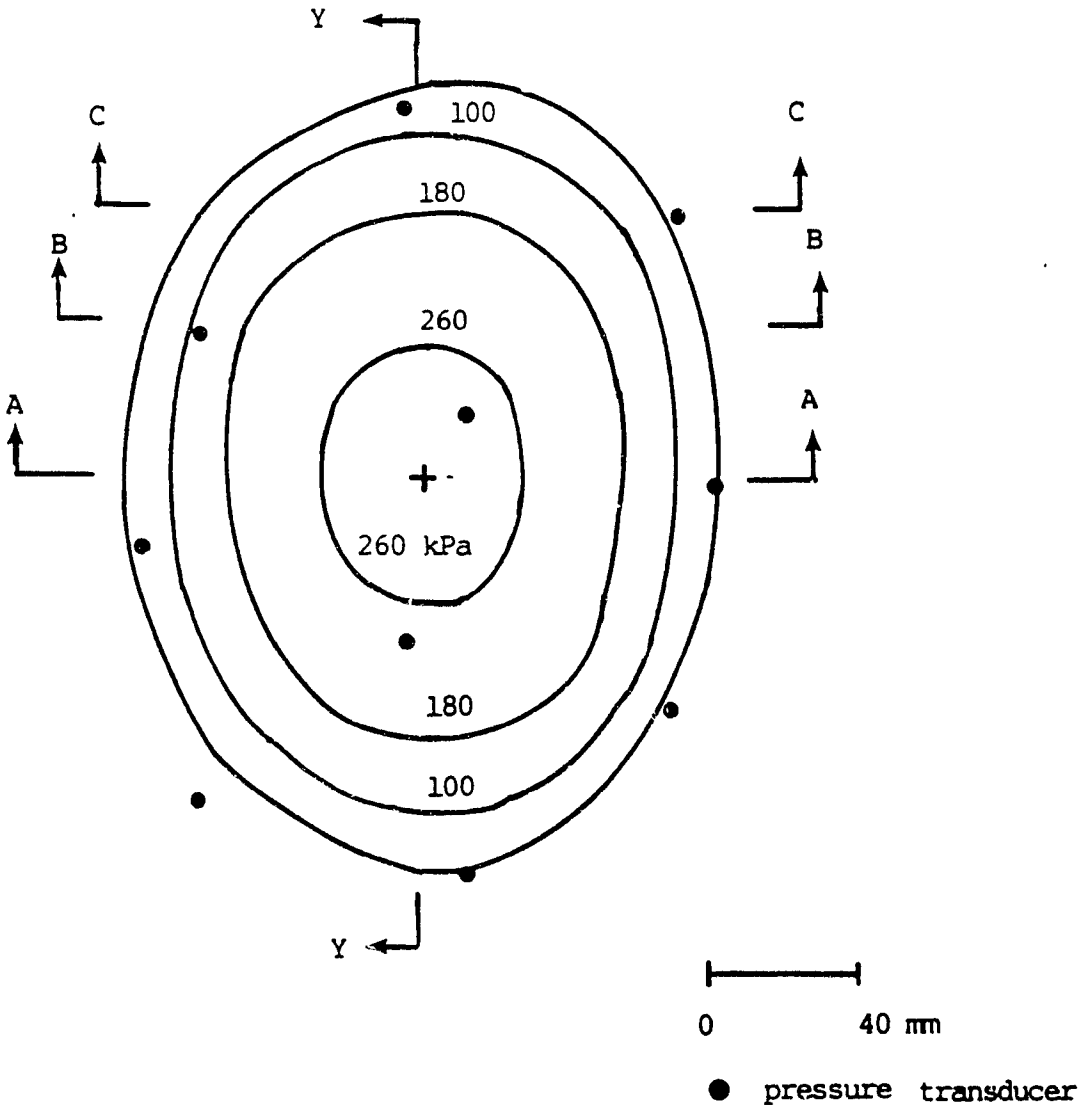


Fig. C.12g/1 Contact Pressure Distribution Within the Footprint of MICHELIN 12.5R-16.5XLM (buffed)

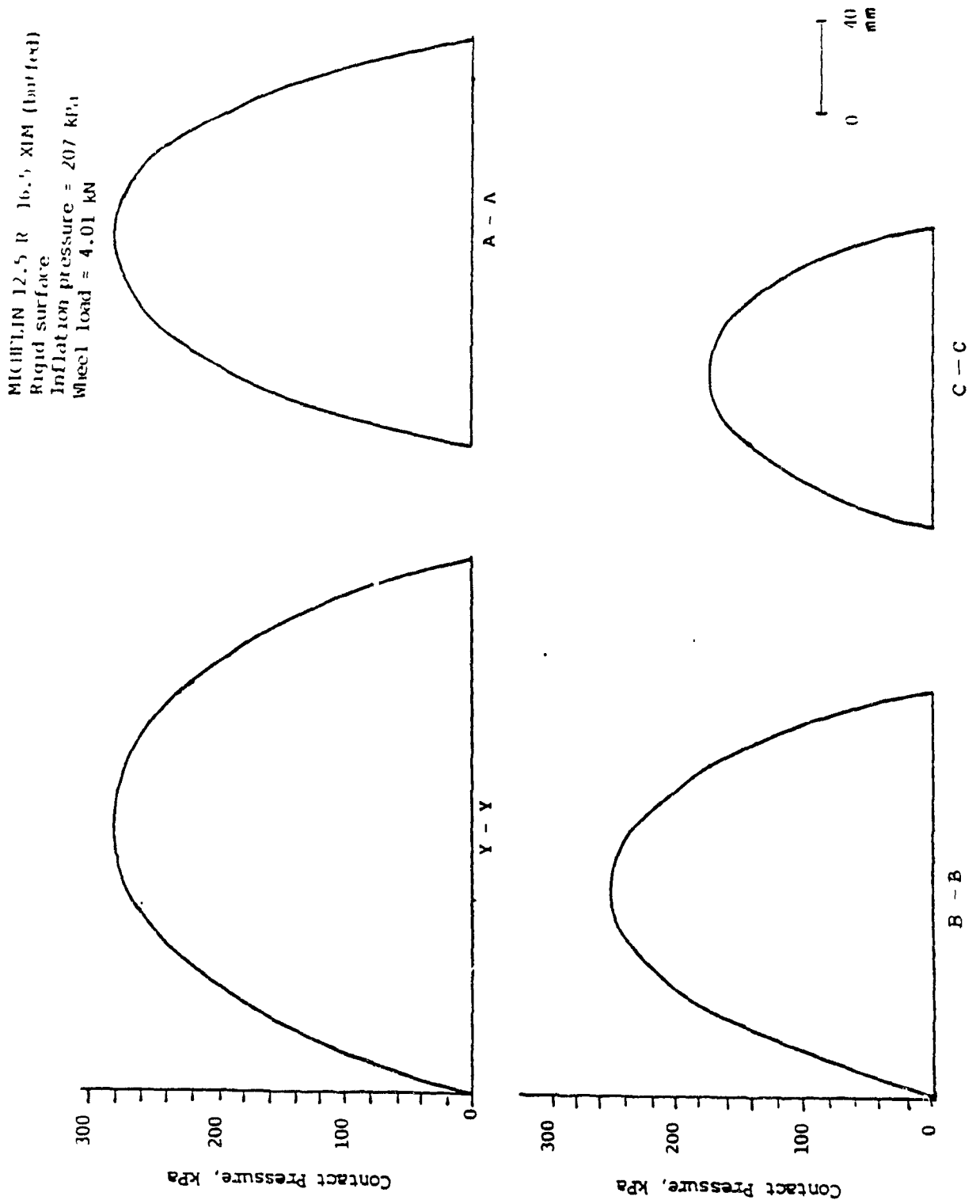


Fig. C.12g/2 Contact Pressure Distribution Within the Footprint of MICHELIN 12.5R-16.5XLM (buffed)

MICHELIN 12.5 R 16.5 XLM (buffed)
Rigid surface
Inflation pressure = 207 kPa
Wheel load = 5.34 kN
Average contact pressure = 158.0 kPa

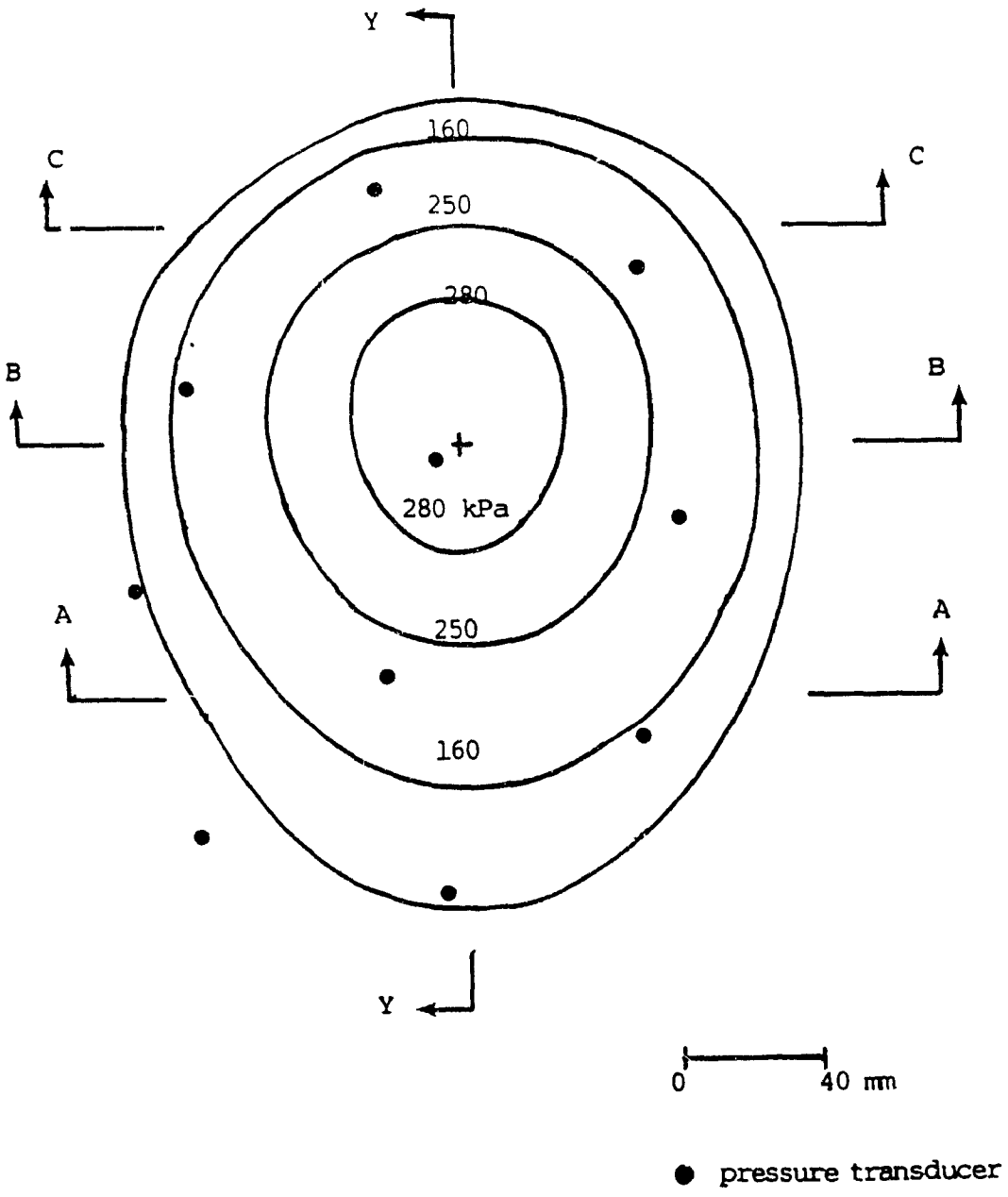


Fig. C.12h/1 Contact Pressure Distribution Within the Footprint of MICHELIN 12.5R-16.5XLM (buffed)

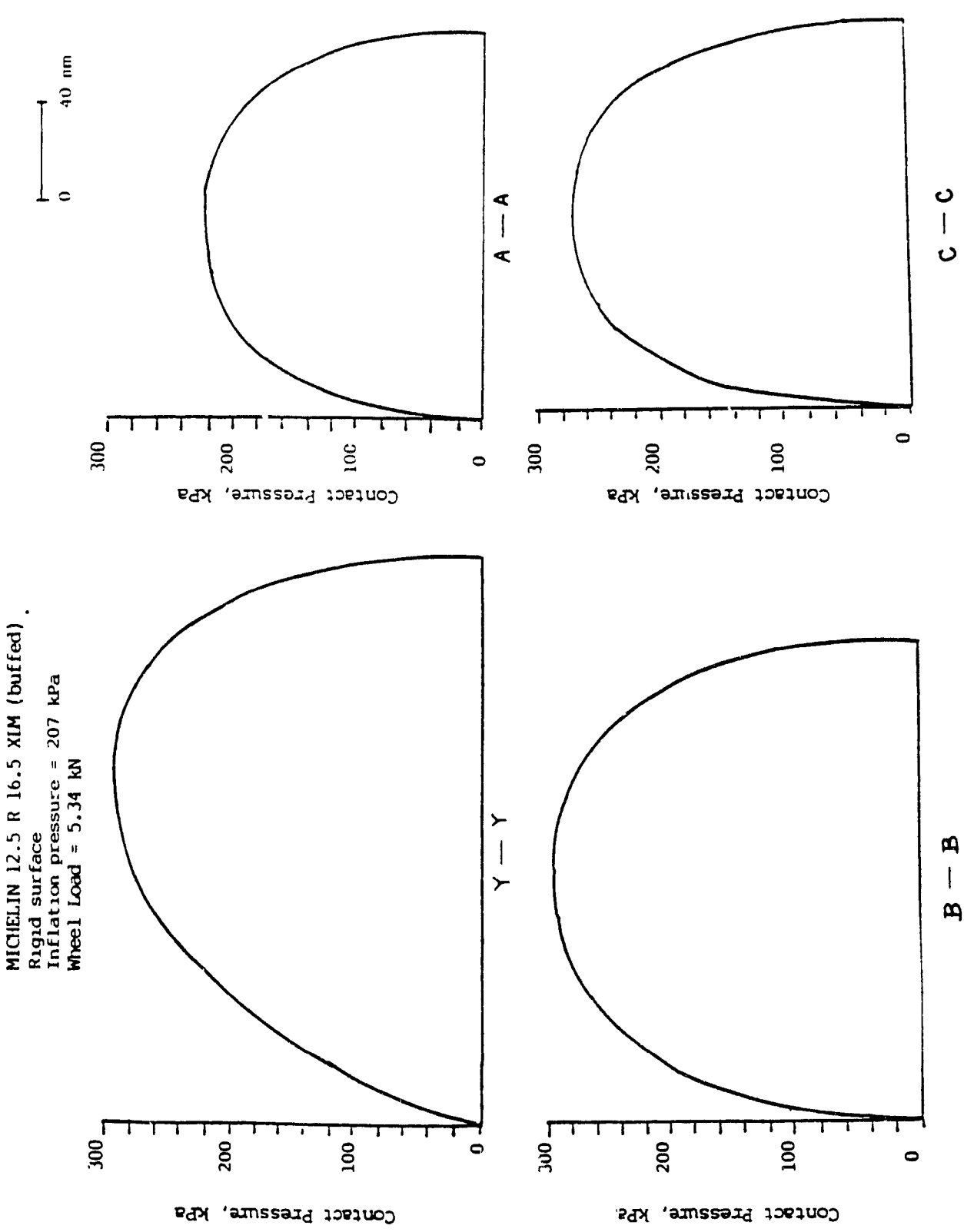


Fig. C.12h/2 Contact Pressure Distribution Within the Footprint of MICHELIN 12.5R-16.5XLM (buffed)

MICHELIN 12.5 R 16.5 XLM (buffed)
Rigid surface
Inflation pressure = 207 kPa
Wheel load = 6.67 kN

Average contact pressure = 171. kPa

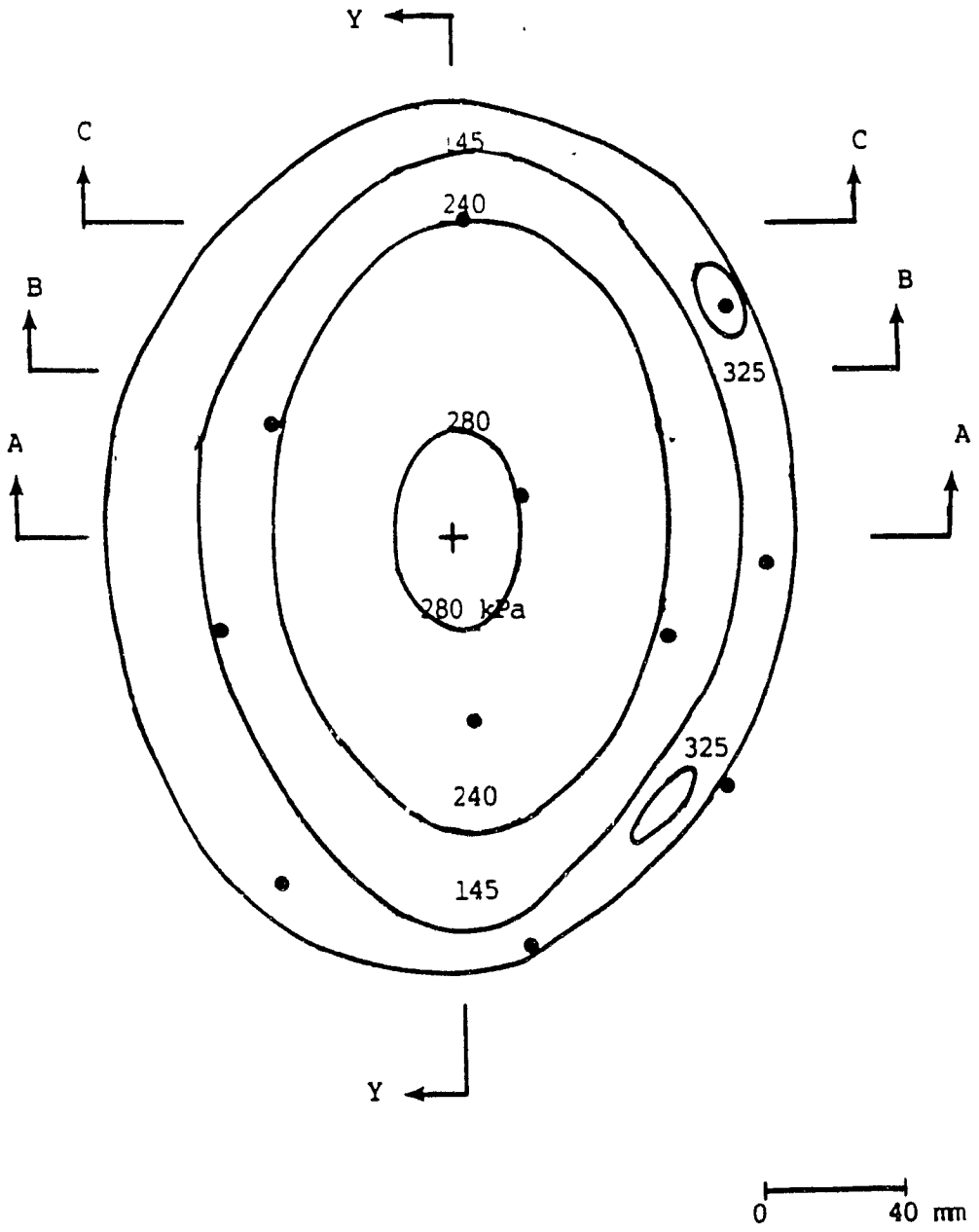


Fig. C.121/1 Contact Pressure Distribution Within the Footprint of MICHELIN 12.5R-16.5XLM (buffed)

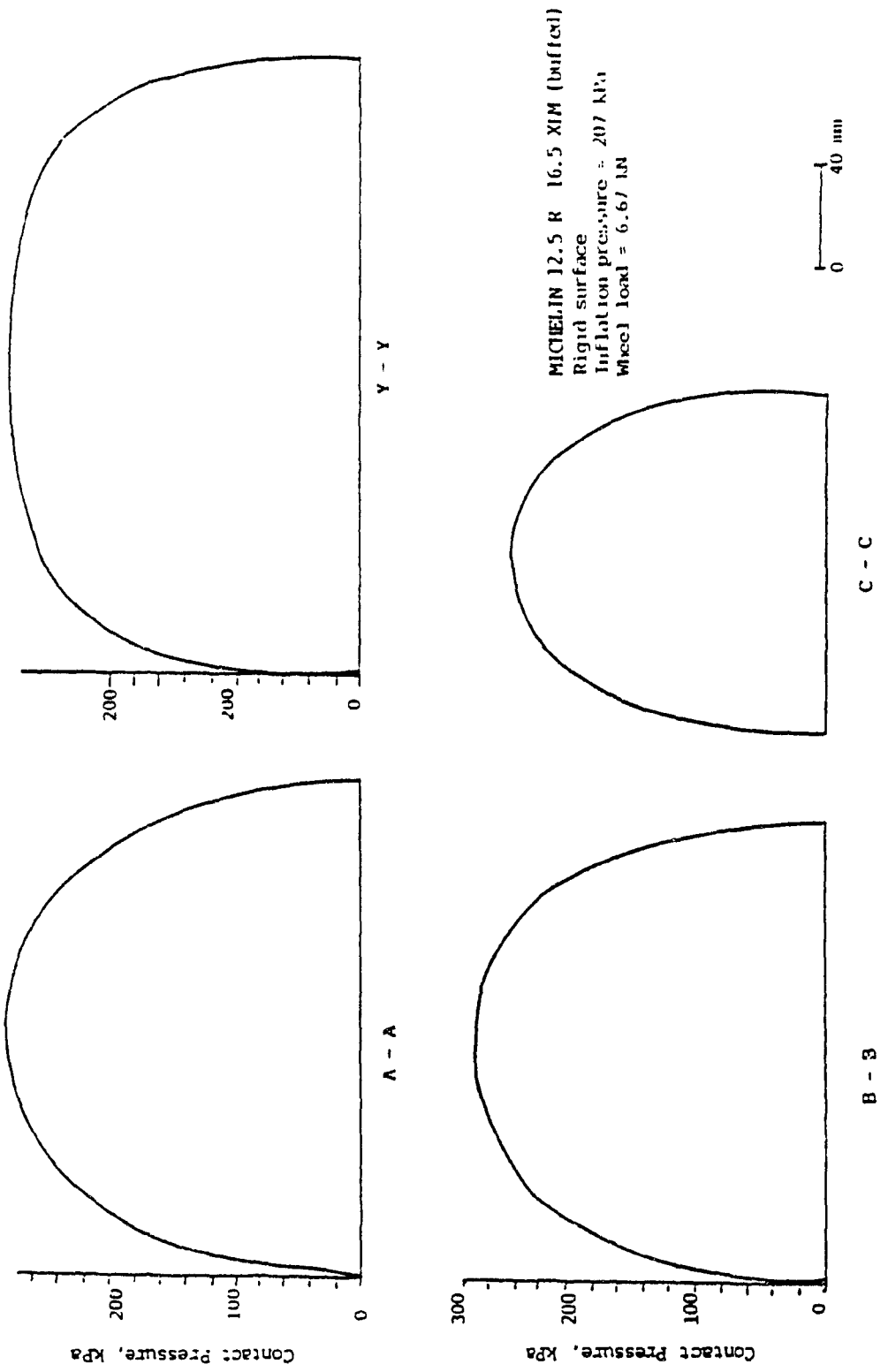


Fig. C.121/2 Contact Pressure Distribution within the Footprint of MICHELIN 12.5R-16.5XLM (buffed)

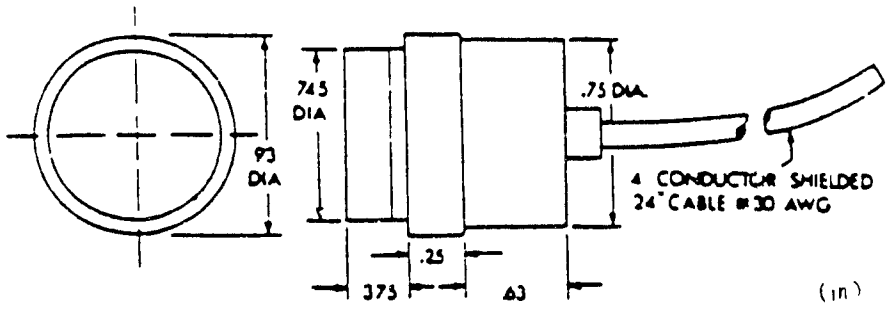


Fig. C.13 Description of Soil Stress Pressure Transducer

APPENDIX D

Experimental Results on Tire-Clay Interactions

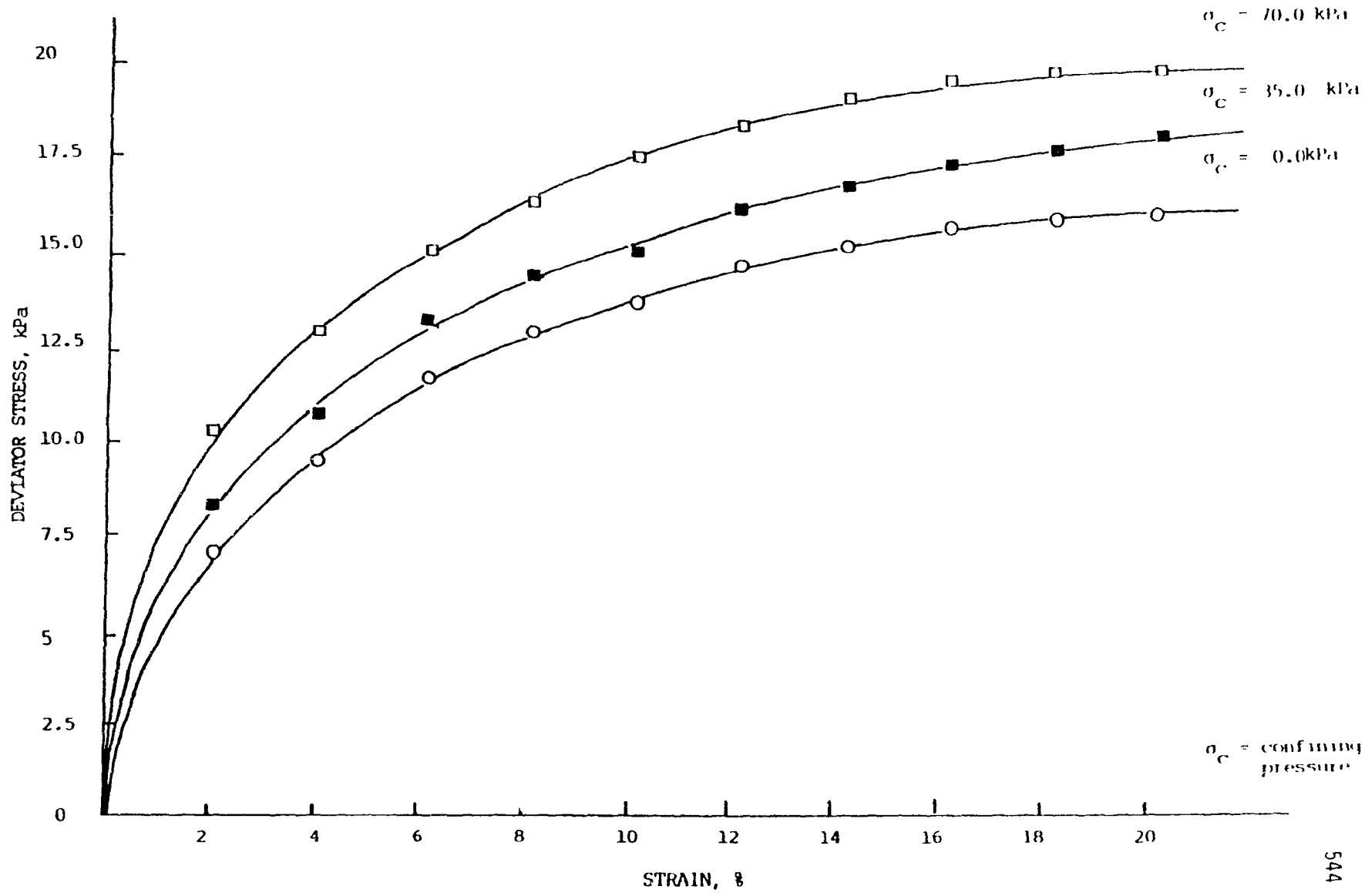


Fig. D.1 Stress-Strain Curves of Kaolinite Under Plane-Strain Triaxial Tests

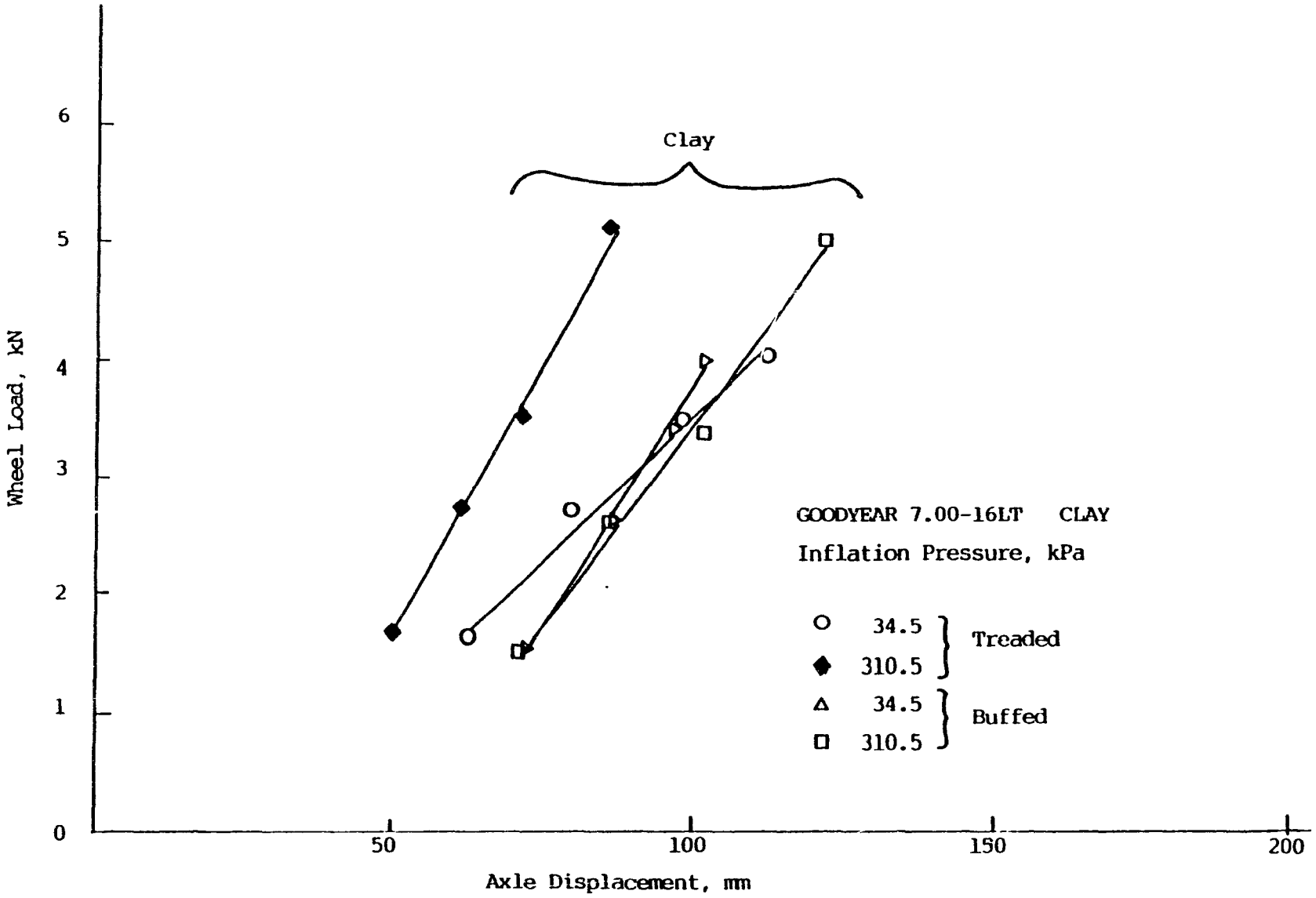


Fig. D.2a Load-Displacement Relationship of GOODYEAR 7.00-16LT on CLAY

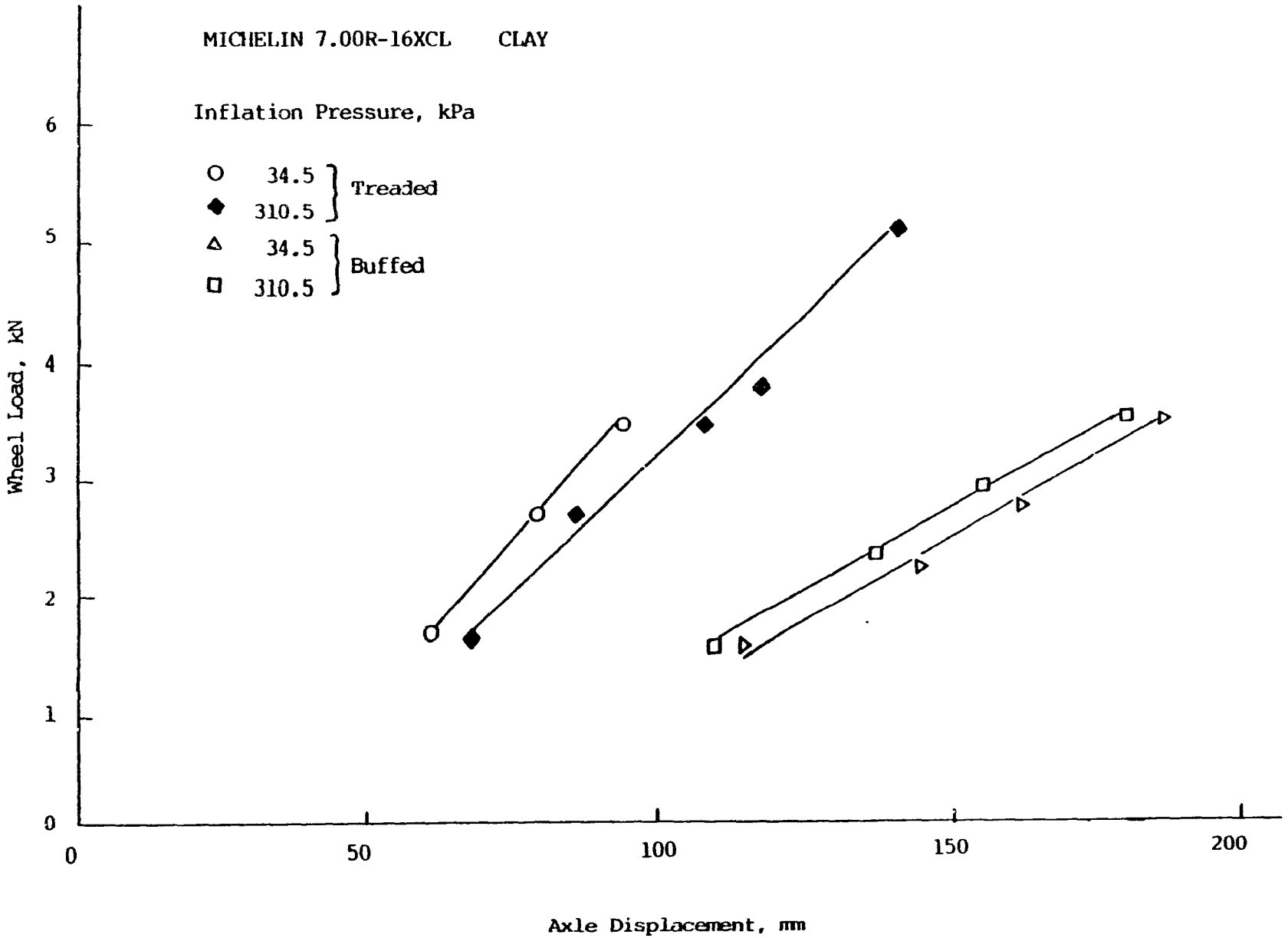


Fig. D.2b Load-Displacement Relationship of MICHELIN 7.00R-16XCL on CLAY

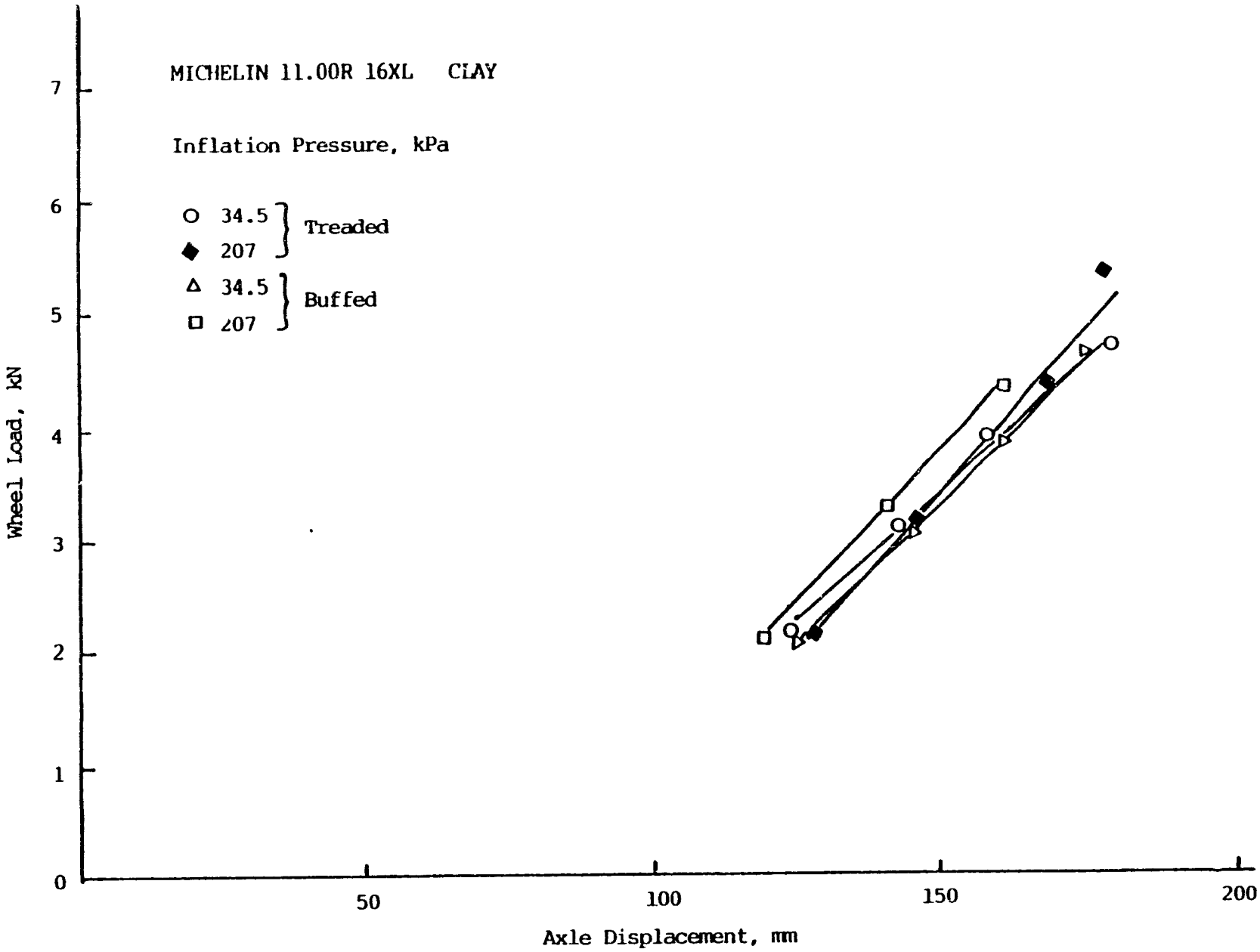


Fig. D.2c Load-Displacement Relationship of MICHELIN 1.00R-16XL on CLAY

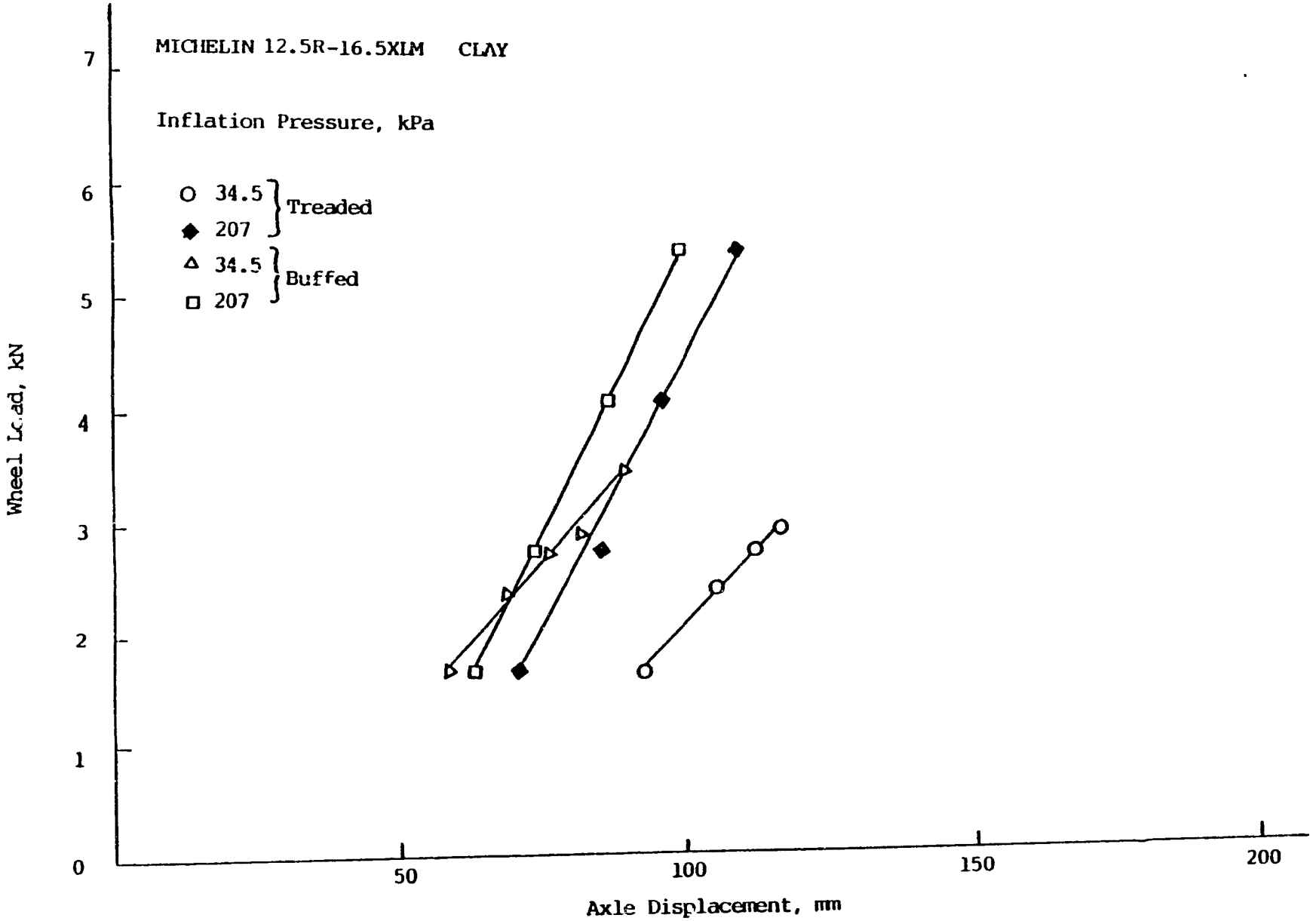


Fig. D.2d Load-Displacement Relationship of MICHELIN 12.5R-16.5XLM on CLAY

TABLE D.1a Data on Contact Area - GOODYEAR 7.00-16LT (treaded)

CLAY

INFLATION PRESSURE kPa	WHEEL LOAD (W) kN	MEASURED CONTACT AREA (A_T) mm^2	REPRESENTATIVE RECTANGULAR CONTACT AREA		AVERAGE CONTACT PRESSURE ($\frac{W}{A_T}$) kPa
			WIDTH mm	LENGTH mm	
34.5	1.670	60400	176	344	27.7
34.5	2.760	71520	182	394	38.6
34.5	3.562	80800	186	434	44.1
34.5	4.096	83920	182	462	48.8
310.5	1.670	58000	163	356	28.8
310.5	2.760	64800	165	394	42.6
310.5	3.562	74400	178	418	47.9
310.5	5.183	83040	183	454	62.4

TABLE D.1b Data on Contact Area - GOODYEAR 7.00-16LT (buffed)

CLAY

INFLATION PRESSURE kPa	WHEEL LOAD (W) kN	MEASURED CONTACT AREA (A_T) mm^2	REPRESENTATIVE RECTANGULAR CONTACT AREA		AVERAGE CONTACT PRESSURE ($\frac{W}{A_T}$) kPa
			WIDTH mm	LENGTH mm	
34.5	1.581	57600	156	368	27.5
34.5	2.671	72400	177	408	36.9
34.5	3.473	78840	188	420	44.0
34.5	4.007	85280	192	442	47.0
310.5	1.581	53800	139	386	29.4
310.5	2.671	71360	172	416	37.4
310.5	3.473	79120	181	436	43.9
310.5	5.094	95400	197	484	53.4

TABLE D.1c Data on Contact Area - MICHELIN 7 00R-16XCL (treaded)

CLAY

INFLATION PRESSURE kPa	WHEEL LOAD (W) kN	MEASURED CONTACT AREA (A_T) mm^2	REPRESENTATIVE RECTANGULAR CONTACT AREA		AVERAGE CONTACT PRESSURE ($\frac{W}{A_T}$) kPa
			WIDTH mm	LENGTH mm	
34.5	1.616	42080	118	358	38.4
34.5	2.693	57320	142	402	47.0
34.5	3.495	70280	161	438	49.8
310.5	1.616	57920	149	388	27.9
310.5	2.693	68760	165	416	39.2
310.5	3.495	80760	178	454	43.3
310.5	3.807	87840	185	476	43.3
310.5	5.143	96520	186	520	53.3

TABLE D.1d Data on Contact Area - MICHELIN 7.00R-16XCL (buffed)

CLAY

INFLATION PRESSSURE kPa	WHEEL LOAD (W) kN	MEASURED CONTACT AREA (A_T) mm^2	REPRESENTATIVE RECTANGULAR CONTACT AREA		AVERAGE CONTACT PRESSURE ($\frac{W}{A_T}$) kPa
			WIDTH mm	LENGTH mm	
34.5	1.598	78640	152	516	20.4
34.5	2.271	115080	212	544	19.7
34.5	2.760	128920	219	590	21.4
34.5	3.584	131640	217	608	27.3
310.5	1.598	93280	194	480	17.1
310.5	2.382	104240	201	518	22.8
310.5	2.983	114560	208	550	26.0
310.5	3.584	126320	212	596	28.4

TABLE D.1e Data on Contact Area - MICHELIN 11.00R-16XL (treaded)

CLAY

INFLATION PRESSURE kPa	WHEEL LOAD (W) kN	MEASURED CONTACT AREA (A_T) mm^2	REPRESENTATIVE RECTANGULAR CONTACT AREA		AVERAGE CONTACT PRESSURE ($\frac{W}{A_T}$) kPa
			WIDTH mm	LENGTH mm	
34.5	2.253	124240	207	600	18.2
34.5	3.250	145000	232	626	22.4
34.5	4.052	154200	239	646	26.3
34.5	4.853	180560	252	716	26.8
207	2.253	137720	233	590	16.4
207	3.250	145200	244	596	22.4

TABLE D.1f Data on Contact Area - MICHELIN 11.00R-16XL (buffed)

CLAY

INFLATION PRESSURE kPa	WHEEL LOAD (W) kN	MEASURED CONTACT AREA (A_T) mm^2	REPRESENTATIVE RECTANGULAR CONTACT AREA		AVERAGE CONTACT PRESSURE ($\frac{W}{A_T}$) kPa
			WIDTH mm	LENGTH mm	
34.5	2.213	128800	235	548	17.1
34.5	3.206	163840	262	626	19.5
34.5	4.007	168520	265	636	23.7
34.5	4.809	182120	270	674	26.4
207	2.213	145080	253	574	15.3
207	3.423	153480	254	604	22.3

TABLE D.1g Data on Contact Area - MICHELIN 12.5R-16.5XLM (treaded)

CLAY

INFLATION PRESSURE kPa	WHEEL LOAD (W) kN	MEASURED CONTACT AREA (A_T) mm^2	REPRESENTATIVE RECTANGULAR CONTACT AREA		AVERAGE CONTACT PRESSURE ($\frac{W}{A_T}$) kPa
			WIDTH mm	LENGTH mm	
34.5	1.701	98440	199	494	17.3
34.5	2.783	129640	245	530	21.5
34.5	2.961	142880	253	564	20.7
207	1.701	85960	208	414	19.8
207	2.783	98240	212	464	28.3
207	4.118	111200	227	490	37.1
207	5.454	125160	232	540	43.5

TABLE D.1h Data on Contact Area - MICHELIN 12.5R-16.5XLM (buffed)

CLAY

INFLATION PRESSURE kPa	WHEEL LOAD(W) kN	MEASURED CONTACT AREA (A_T) mm^2	REPRESENTATIVE RECTANGULAR CONTACT AREA		AVERAGE CONTACT PRESSURE ($\frac{W}{A_T}$) kPa
			WIDTH mm	LENGTH mm	
34.5	1.687	81480	203	402	20.7
34.5	2.404	100360	228	440	23.9
34.5	2.760	98000	215	456	28.2
34.5	2.939	111080	232	478	26.4
34.5	3.473	120440	241	500	28.8
207	1.687	86320	207	418	19.5
207	2.760	100280	218	460	27.5
207	4.096	110640	234	472	37.0
207	5.432	128640	239	538	42.2

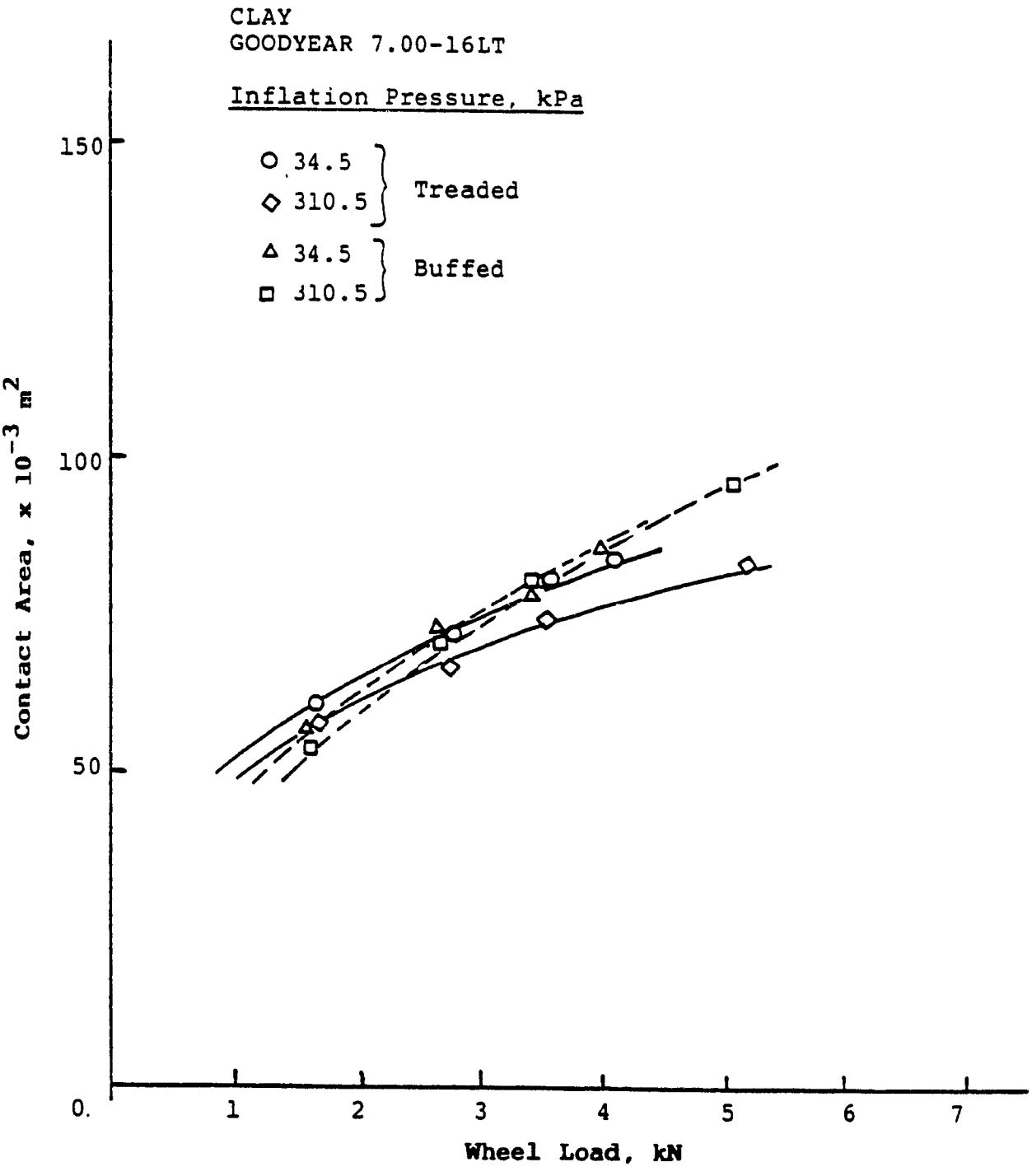


Fig. D.3a Contact Area-Axle Load Relationship of GOODYEAR 7.00-16LT on Clay

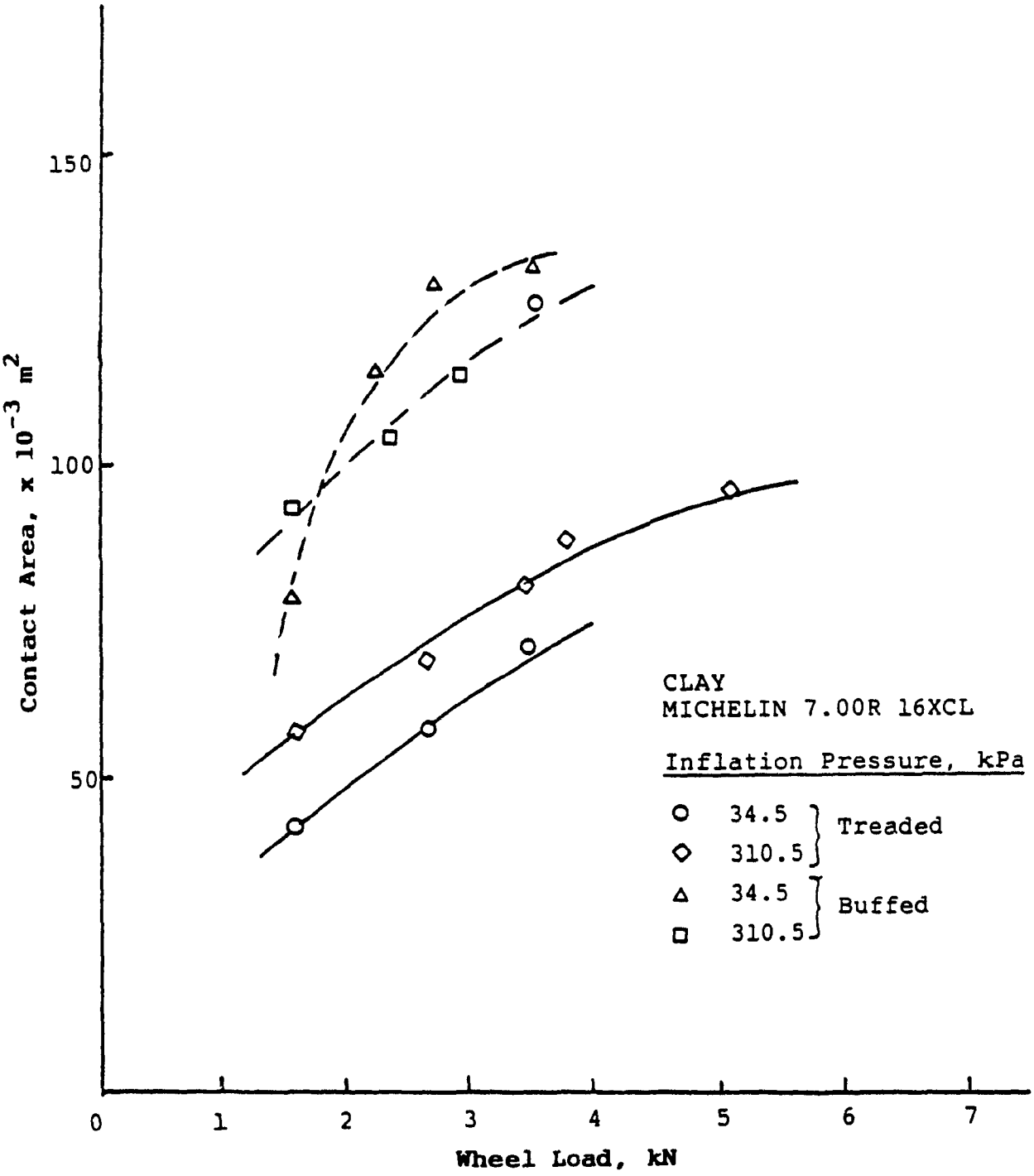


Fig. D.3b Contact Area-Axle Load Relationship of MICHELIN 7.00R-16XCL on Clay

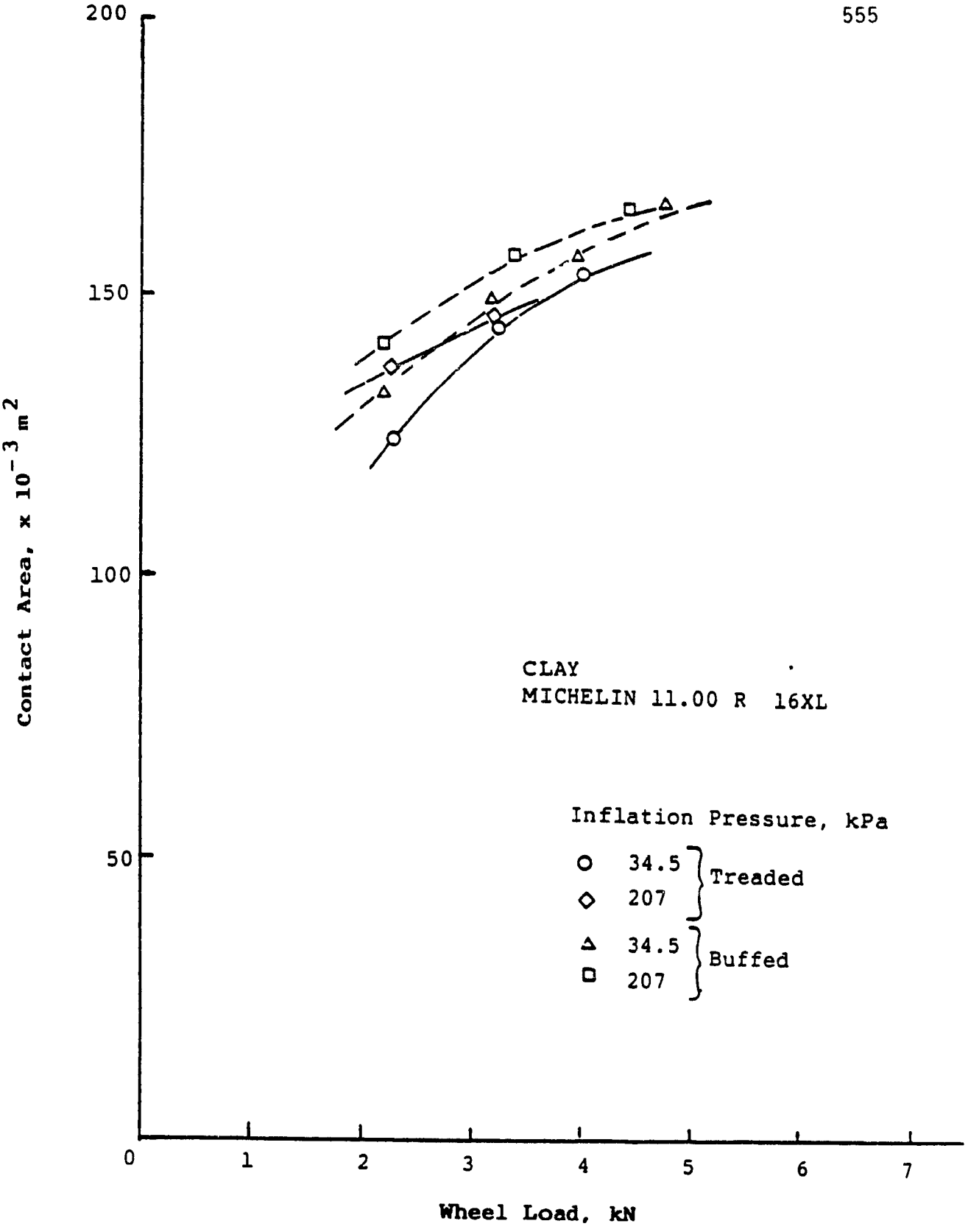


Fig. D.3c Contact Area-Axle Load Relationship of MICHELIN 11.00R-16XL on Clay

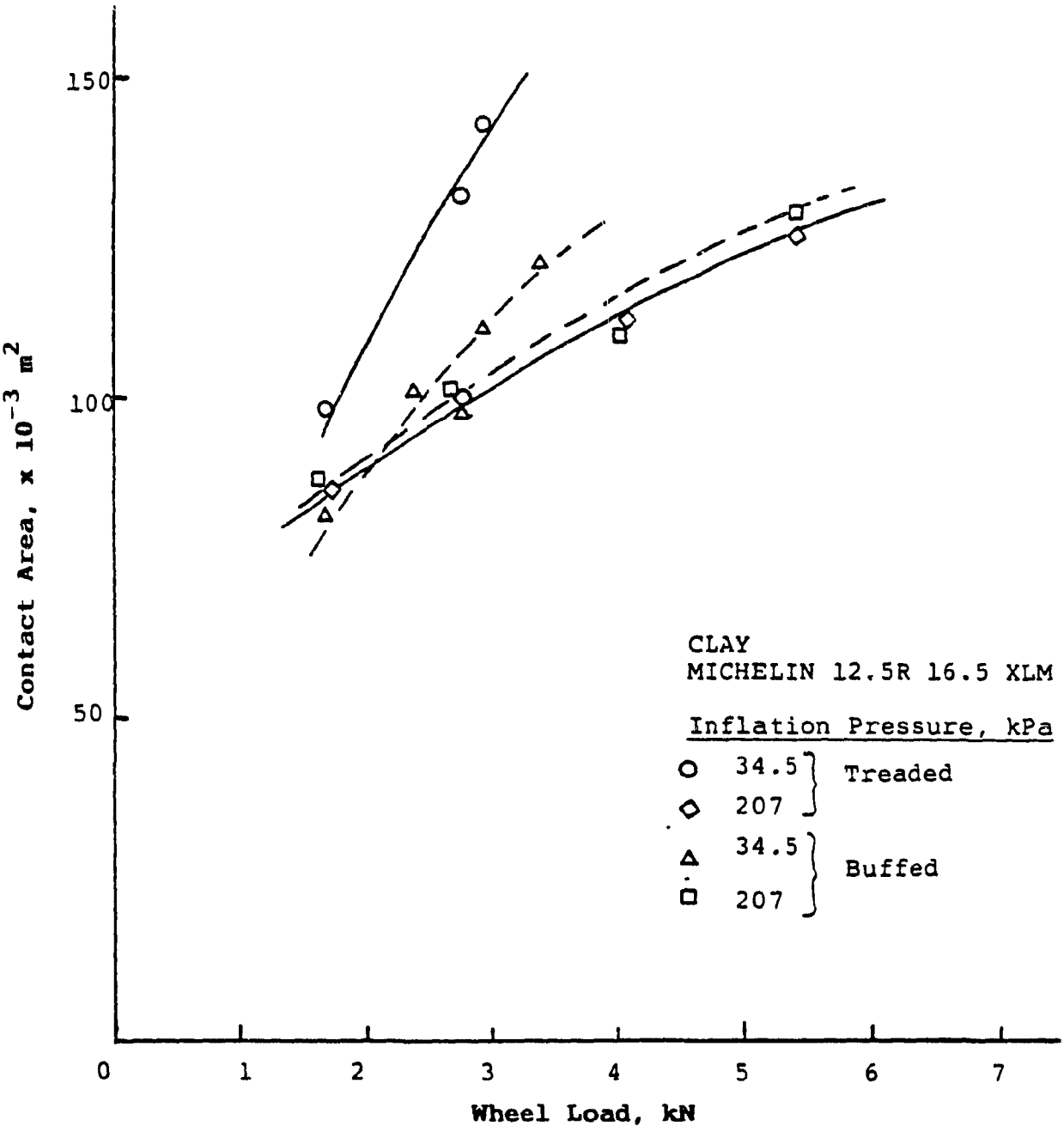


Fig. D.3d Contact Area-Axle Load Relationship of MICHLEIN 12.5R-16.5XLM on Clay

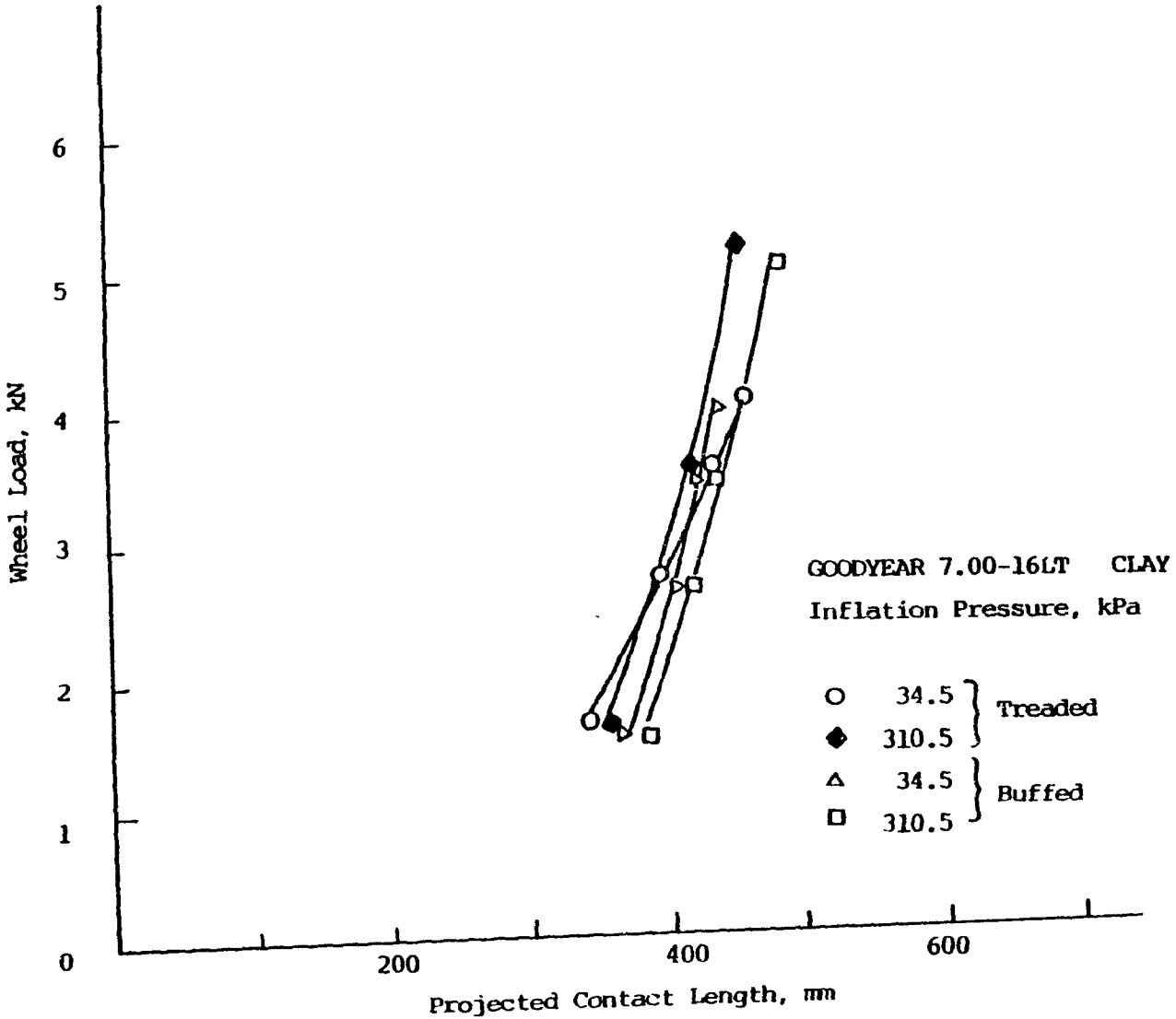


Fig. D.4a Load-Contact Length Relationship of GOODYEASR 7.00-16LT on CLAY

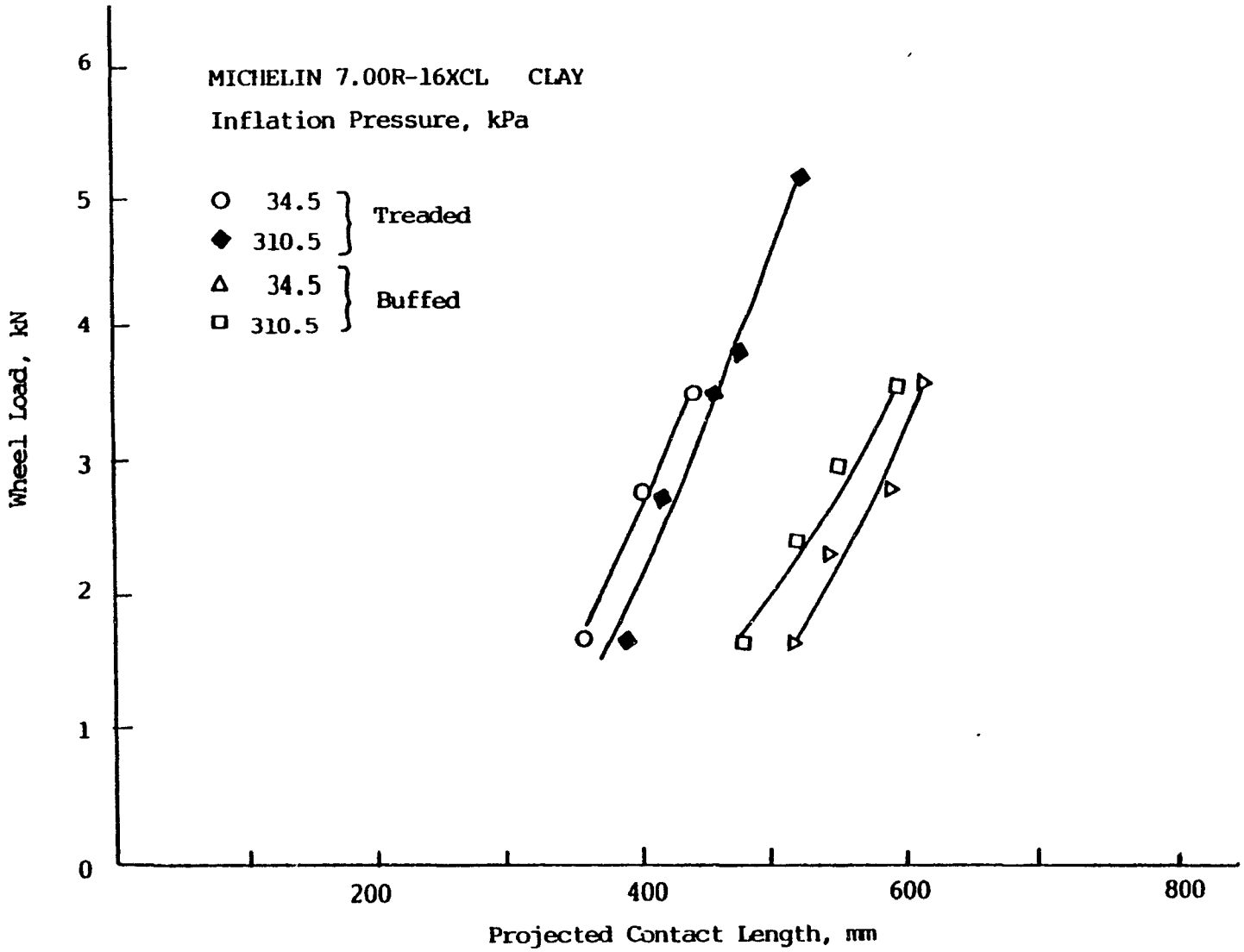


Fig. D.4b Load-Contact Length Relationship of MICHELIN 7.00R-16XCL on CLAY

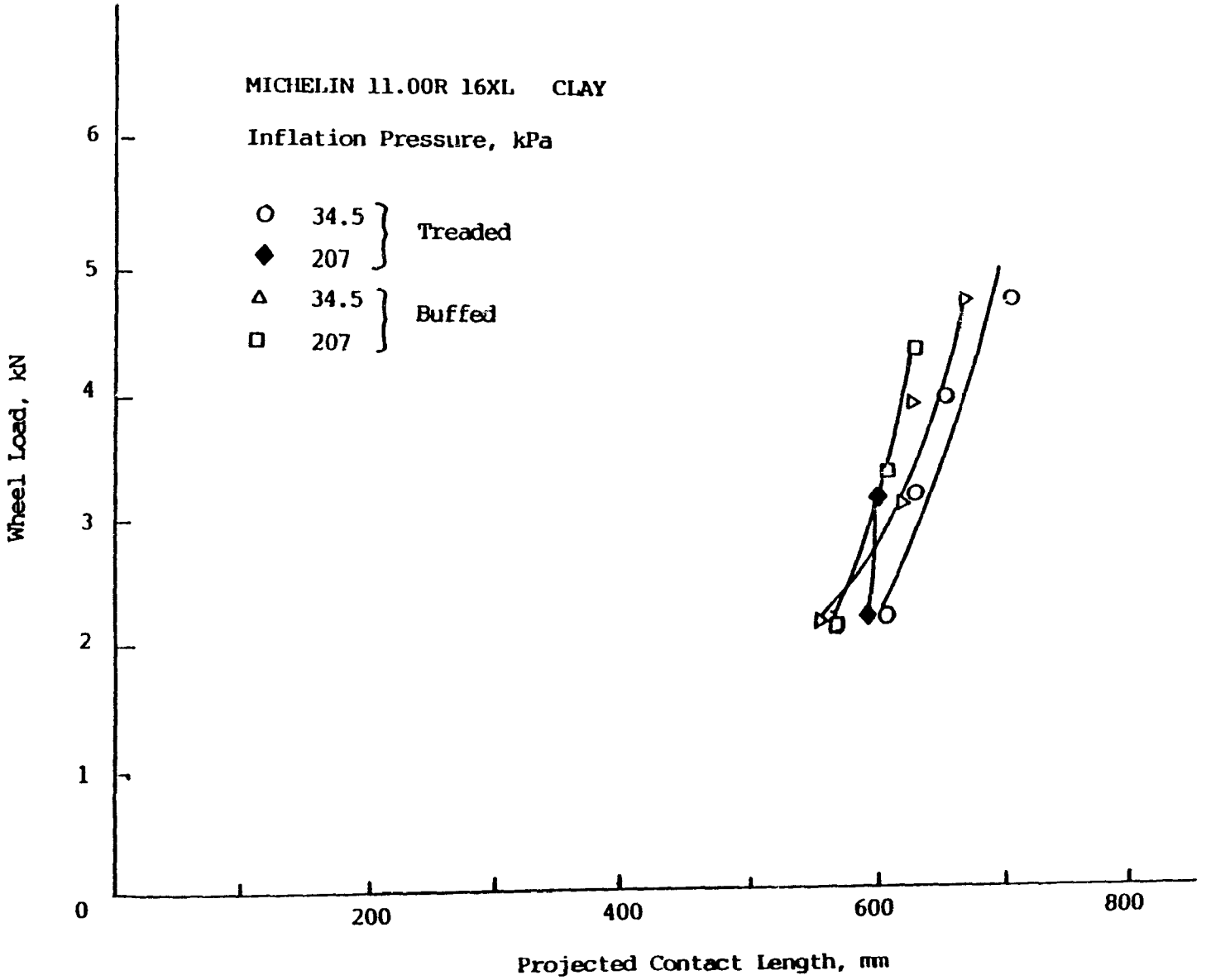


Fig. D.4c Load-Contact Length Relationship of MICHELIN 11.00R-16XL on CLAY

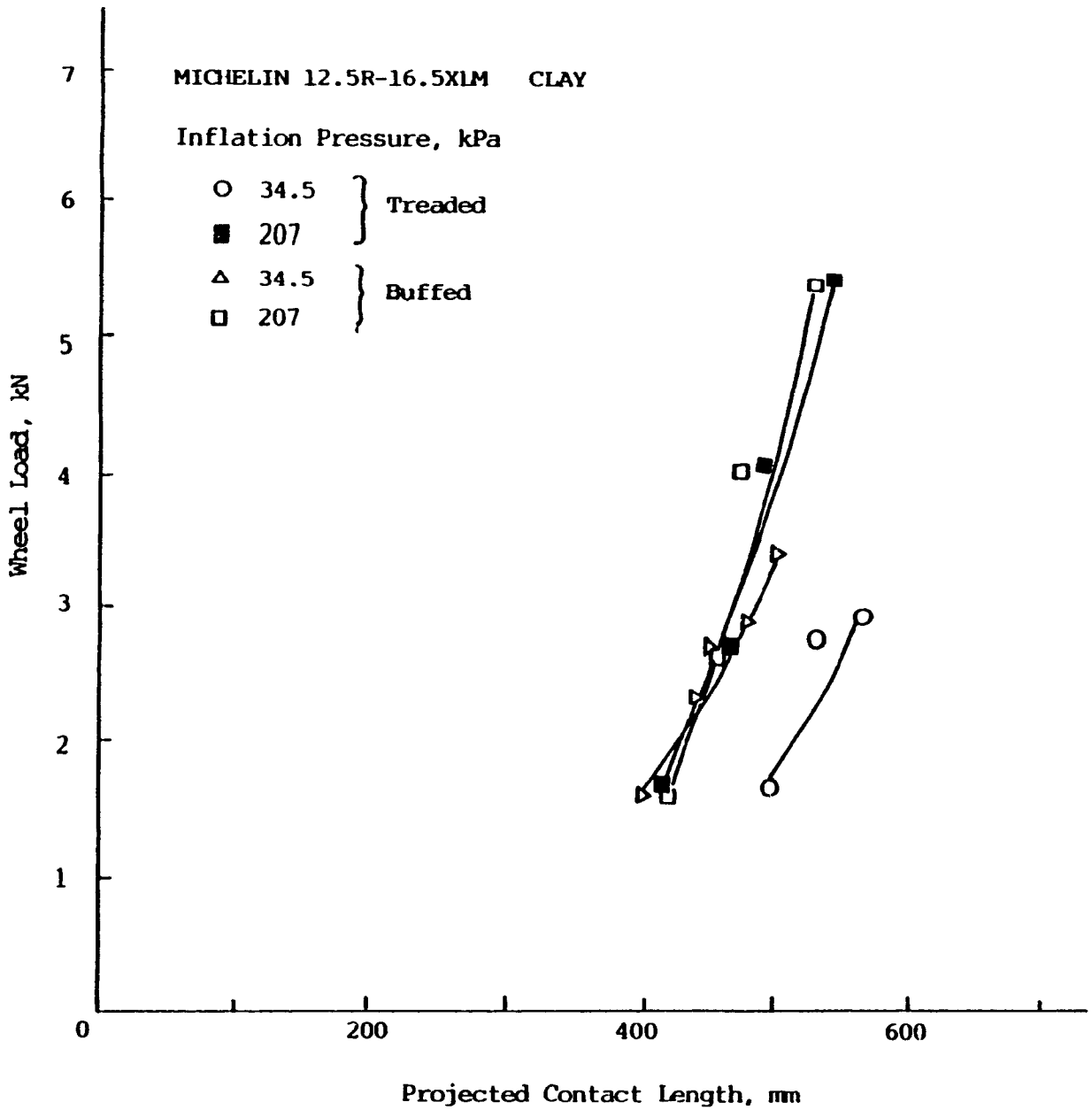


Fig. D.4d Load-Contact Length Relationship of MICHELIN 12.5R-16.5XLM on CLAY

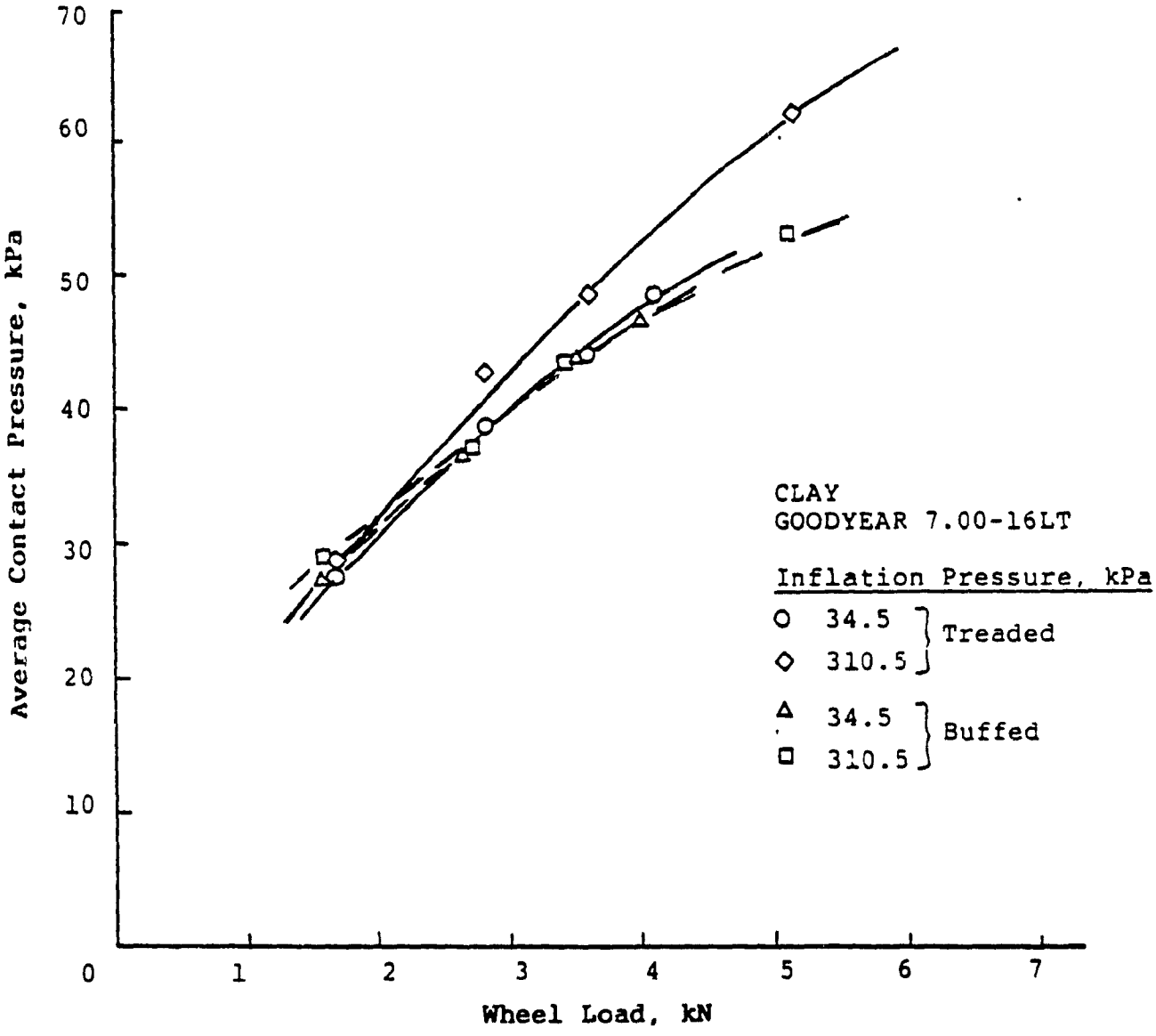


Fig. D.5a Average Contact Pressure-Axle Load Relationship of GOODYEAR 7.00-16LT on Clay

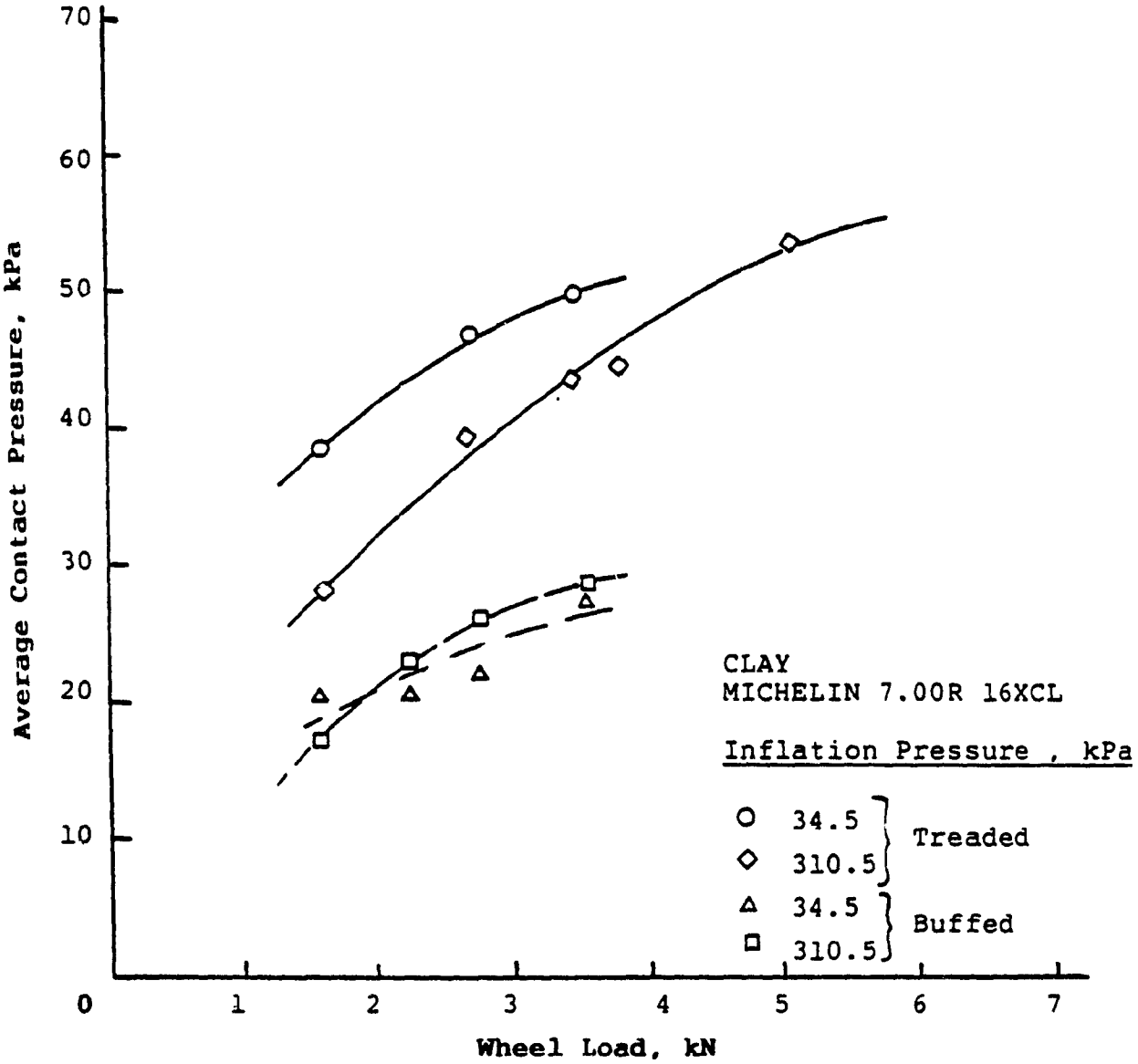


Fig. D.5b Average Contact Pressure-Axle Load Relationship of MICHELIN 7.00R-16XCL on Clay

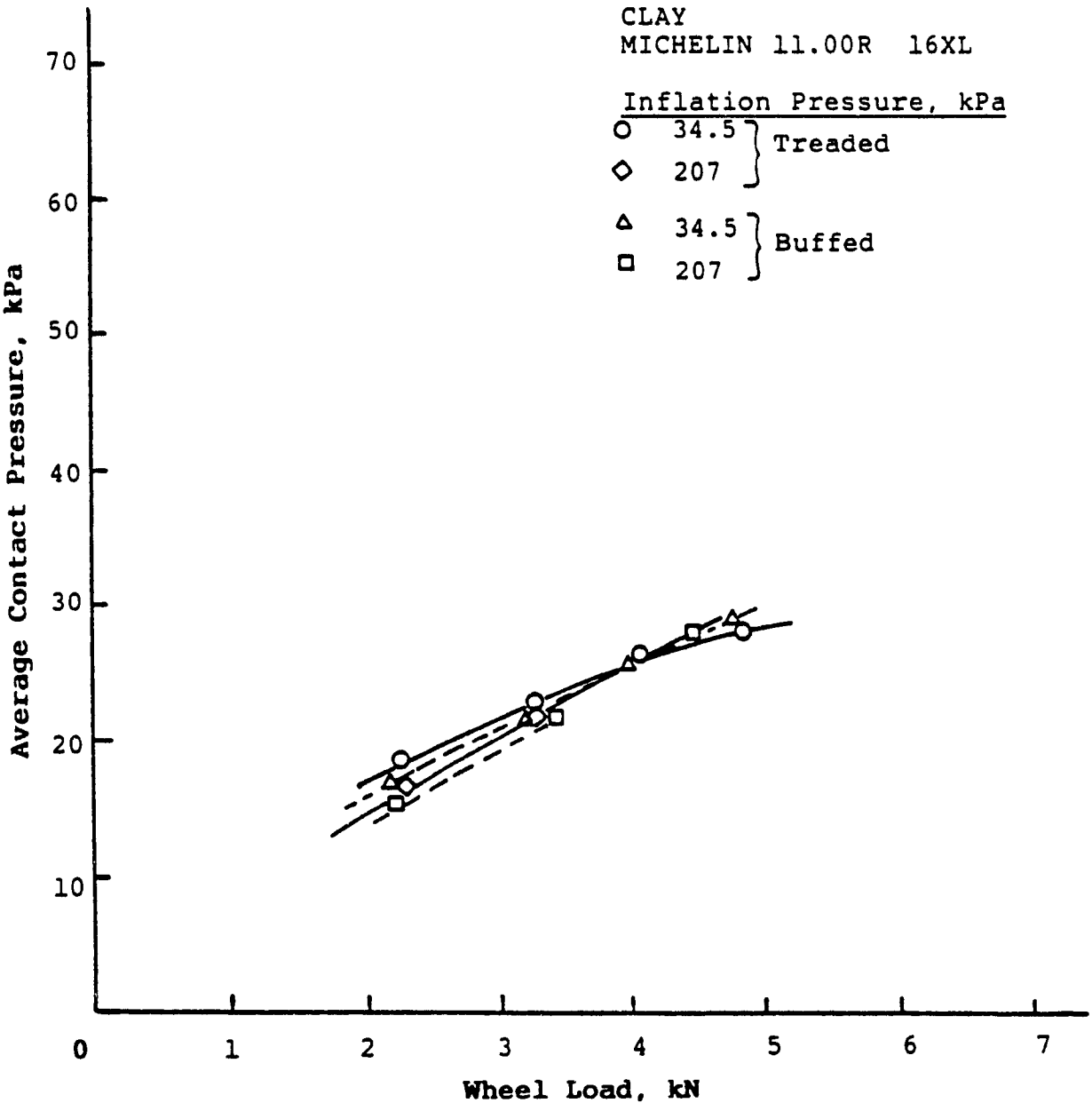


Fig. D.5c Average Contact Pressure-Axle Load Relationship of MICHELIN 11.00R-16XL on Clay

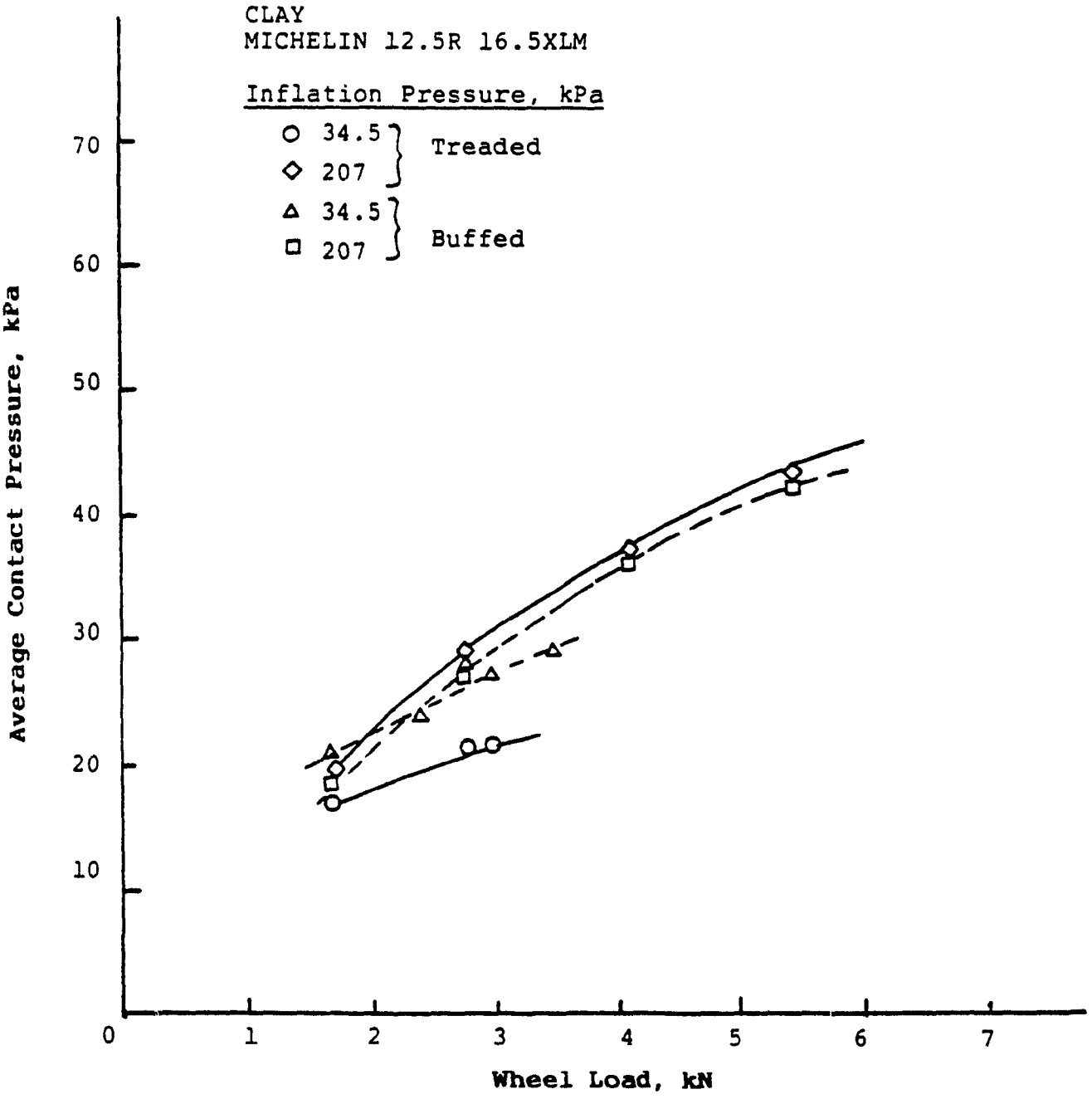


Fig. D.5d Average Contact Pressure-Axle Load Relationship of MICHELIN 12.5R-16.5XLM on Clay

TABLE D.2 Test Conditions Imposed in Determination of Tire-Clay Contact Pressure Distribution

TIRE	Inflation Pressure (kPa)	Wheel Load (kN)	Average Contact Pressure (kPa)	Figure No.
GOODYEAR 7.00-16LT (treaded)	34.5	4.096	48.8	D.6a-b
	310.5	3.562	47.9	D.7a-b
GOODYEAR 7.00-16LT (buffed)	34.5	4.007	47.0	D.8a-c
	310.5	3.473	43.9	D.9a-c
MICHELIN 7.00R-16XCL (treaded)	34.5	3.495	49.8	D.10a-c
	310.5	3.495	43.3	D.11a-c
MICHELIN 7.00R-16XCL (buffed)	34.5	3.584	27.3	D.12a-b
	310.5	3.584	28.4	D.13a-b
MICHELIN 11.00R-16XL (treaded)	34.5	3.250	22.4	D.14a-b
	207	3.250	22.4	D.15a-b
MICHELIN 11.00R-16XL (buffed)	34.5	3.206	19.5	D.16a-b
	207	3.423	22.3	D.17a-b
MICHELIN 12.5R-16.5XLM (treaded)	34.5	2.961	20.7	D.18a-b
	207	4.118	37.1	D.19a-c
MICHELIN 12.5R-16.5XLM (buffed)	34.5	3.473	28.8	D.20a-b
	207	4.096	37.0	D.21a-b

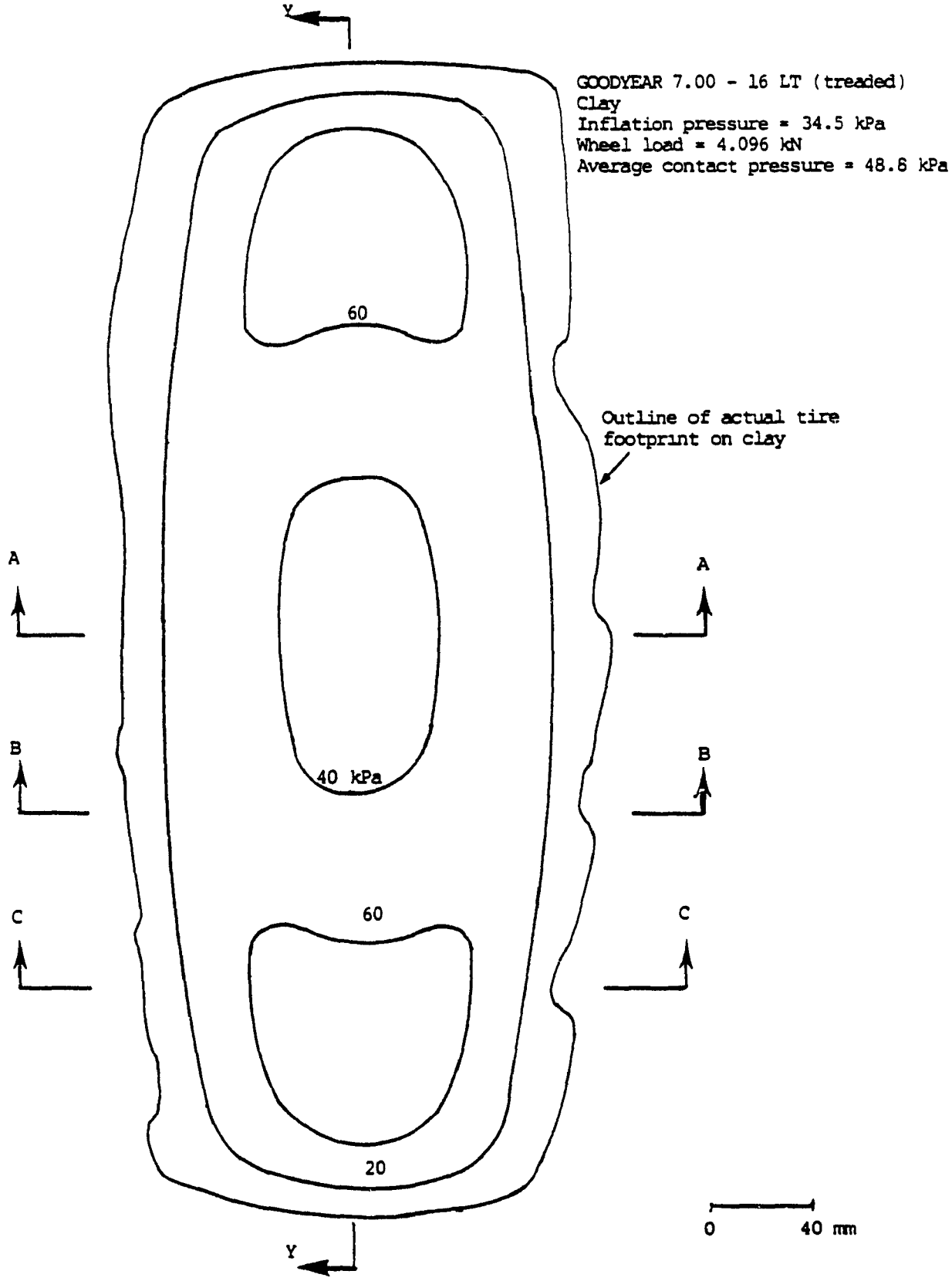


Fig. D.6a Isobars of Pressure Distribution Within the Footprint of GOODYEAR 7.00-16LT (treaded) on Clay

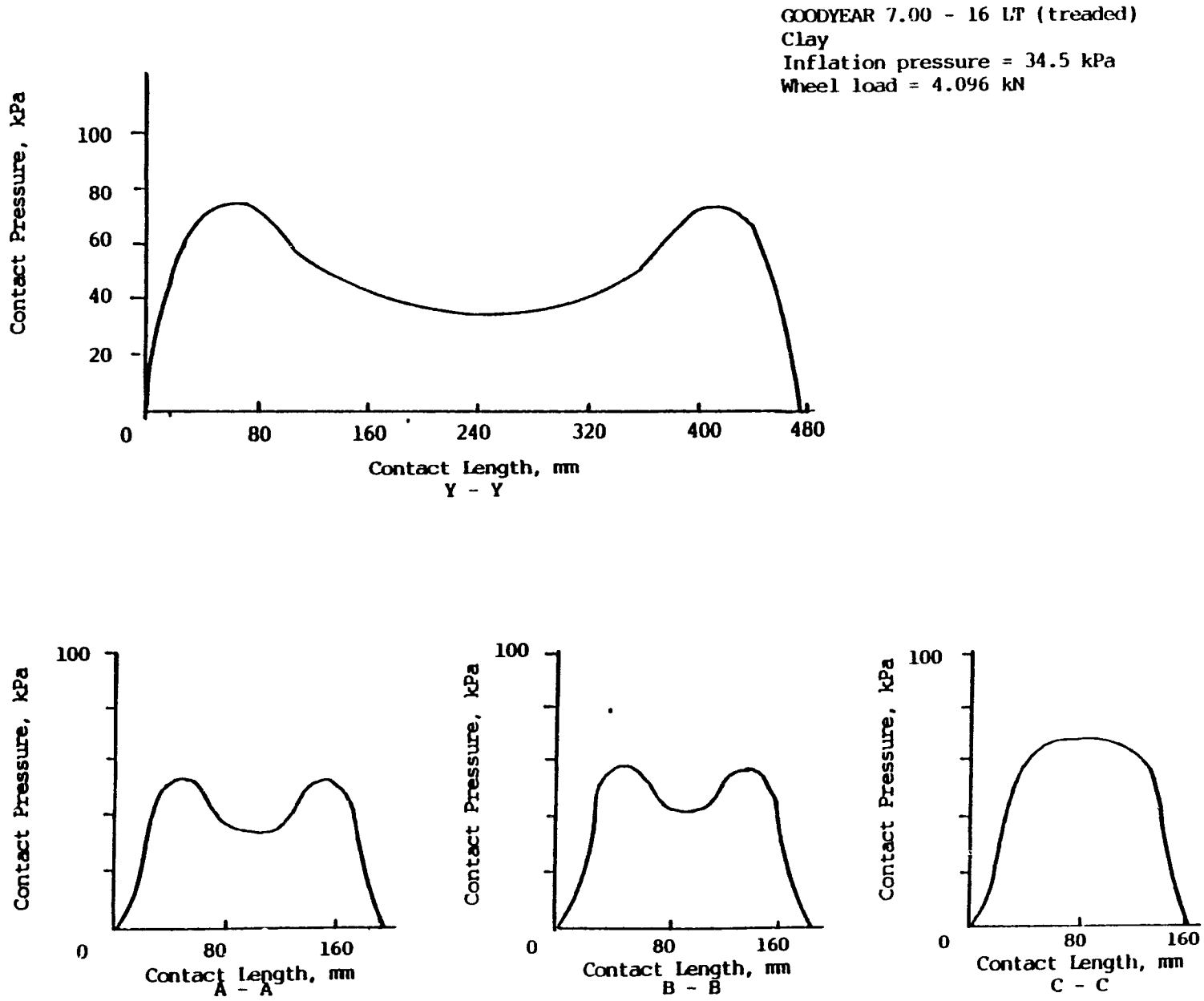


Fig. D.6b Profiles of Pressure Distribution Within the Footprint of GOODYEAR 7.00-16LT (treaded) on Clay

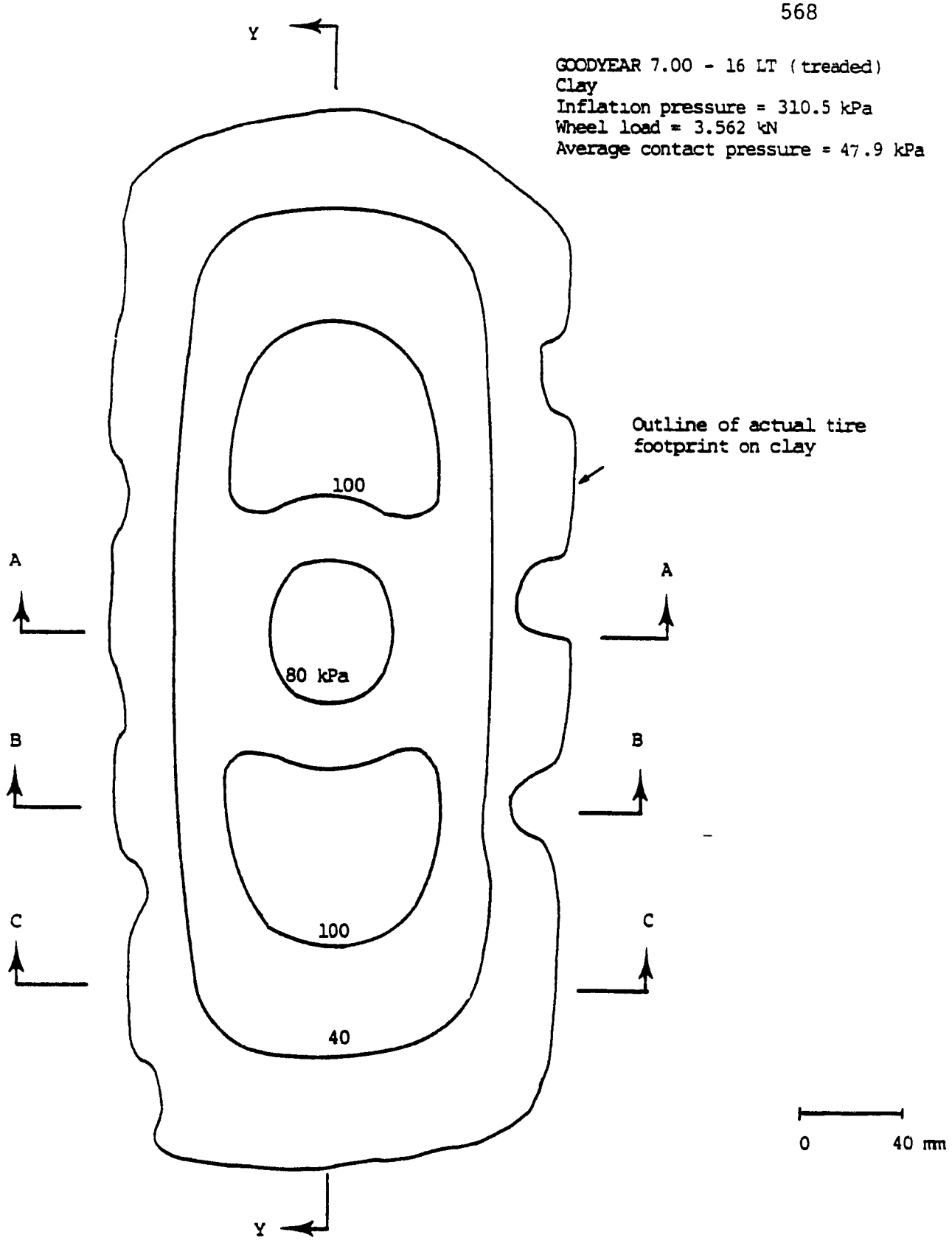
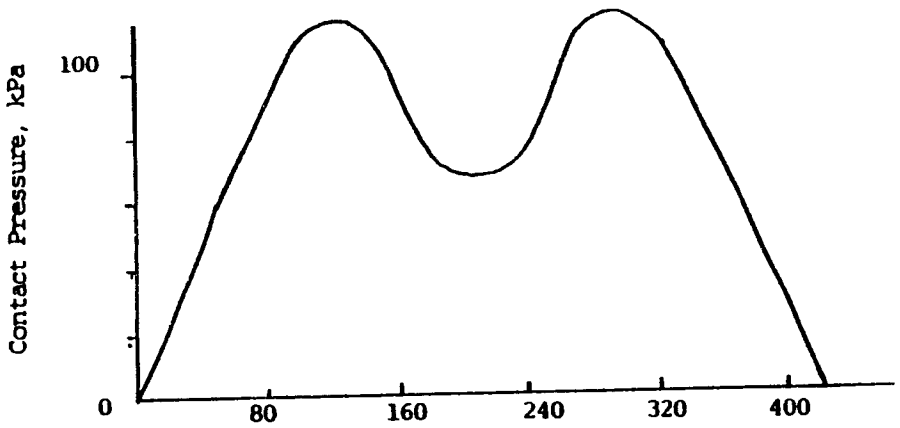


Fig. D.7a Isobars of Pressure Distribution Within the Footprint of GOODYEAR 7.00-16LT (treaded) in Clay



GOODYEAR 7.00 - 16 LT (treaded)
Clay
Inflation pressure = 310.5 kPa
Wheel load = 3.562 kN

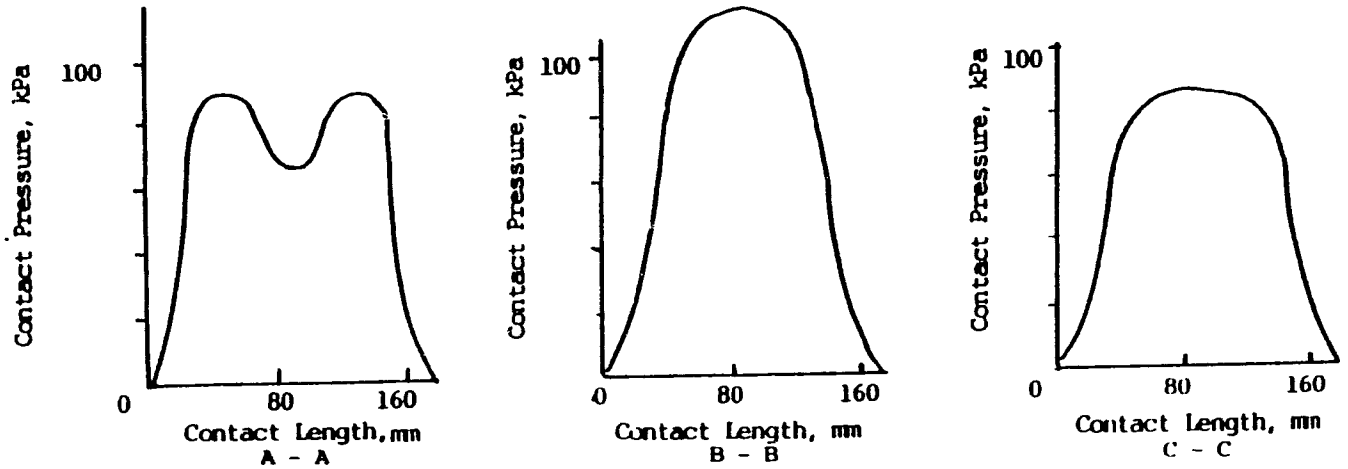


Fig. D.7b Profiles of Pressue Distribution Within the Footprint of GOODYEAR 7.00-16LT (treaded) in Clay

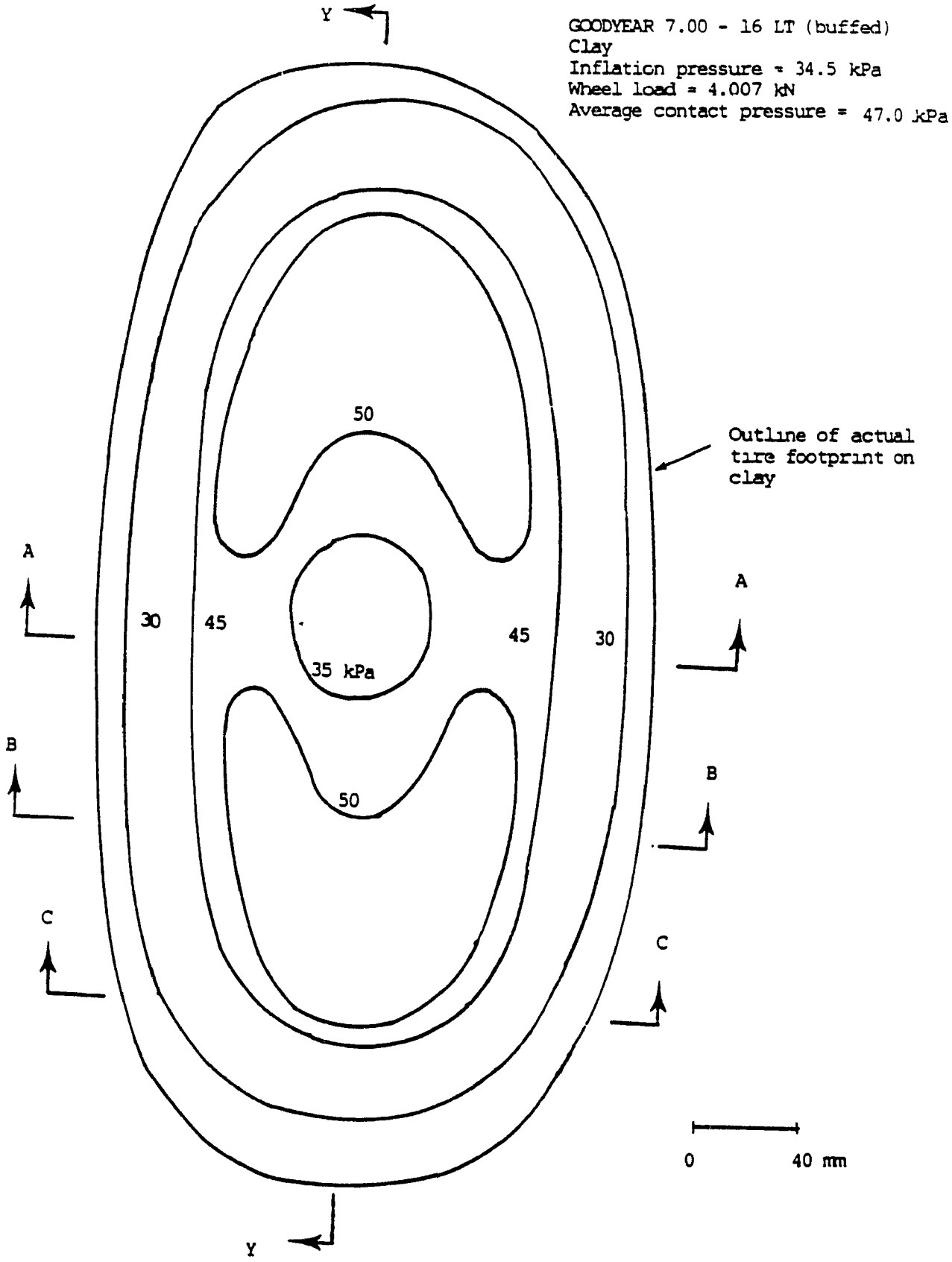
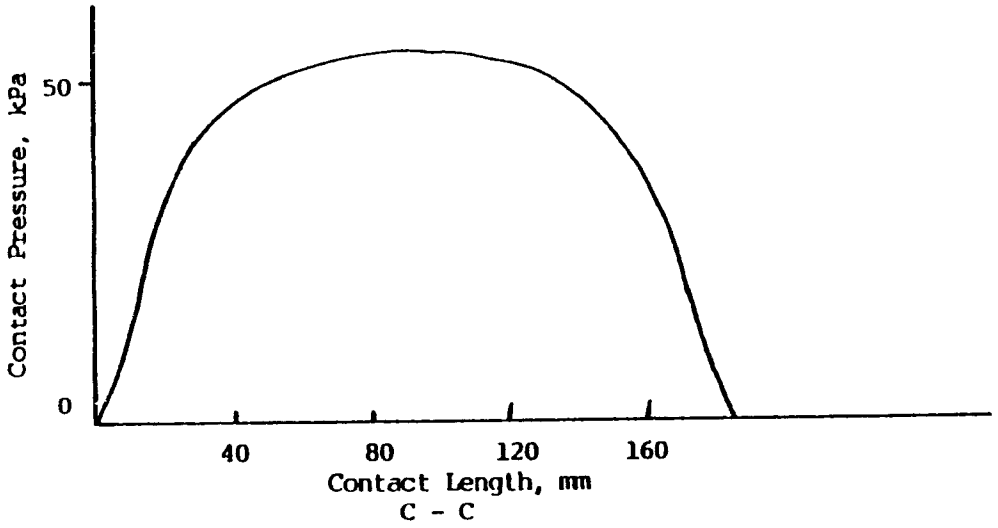
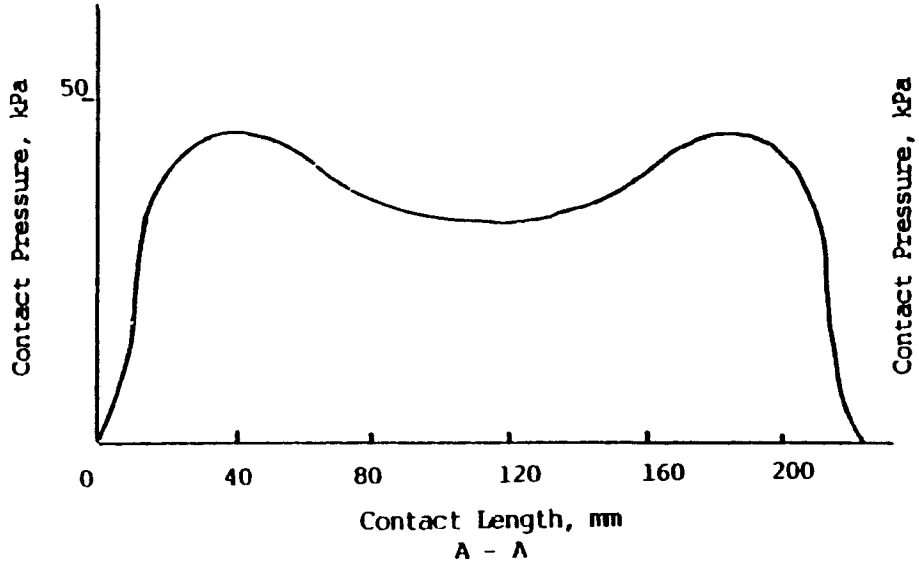


Fig. D.8a Isobars of Pressure Distribution Within the Footprint of GOODYEAR 7.00-16LT (buffed) in Clay





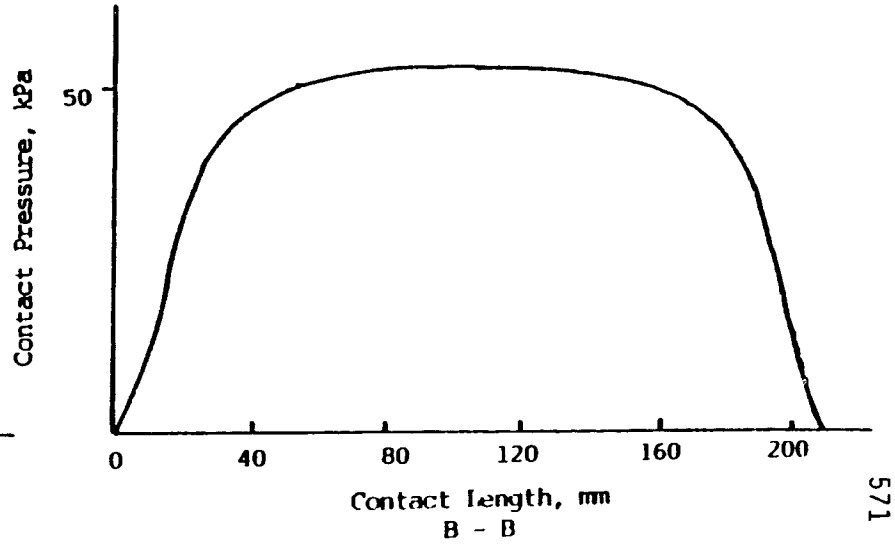


Fig. D.8b Profiles of Pressure Distribution Within the Footprint of GOODYEAR 7.00-16LT (buffed) in Clay

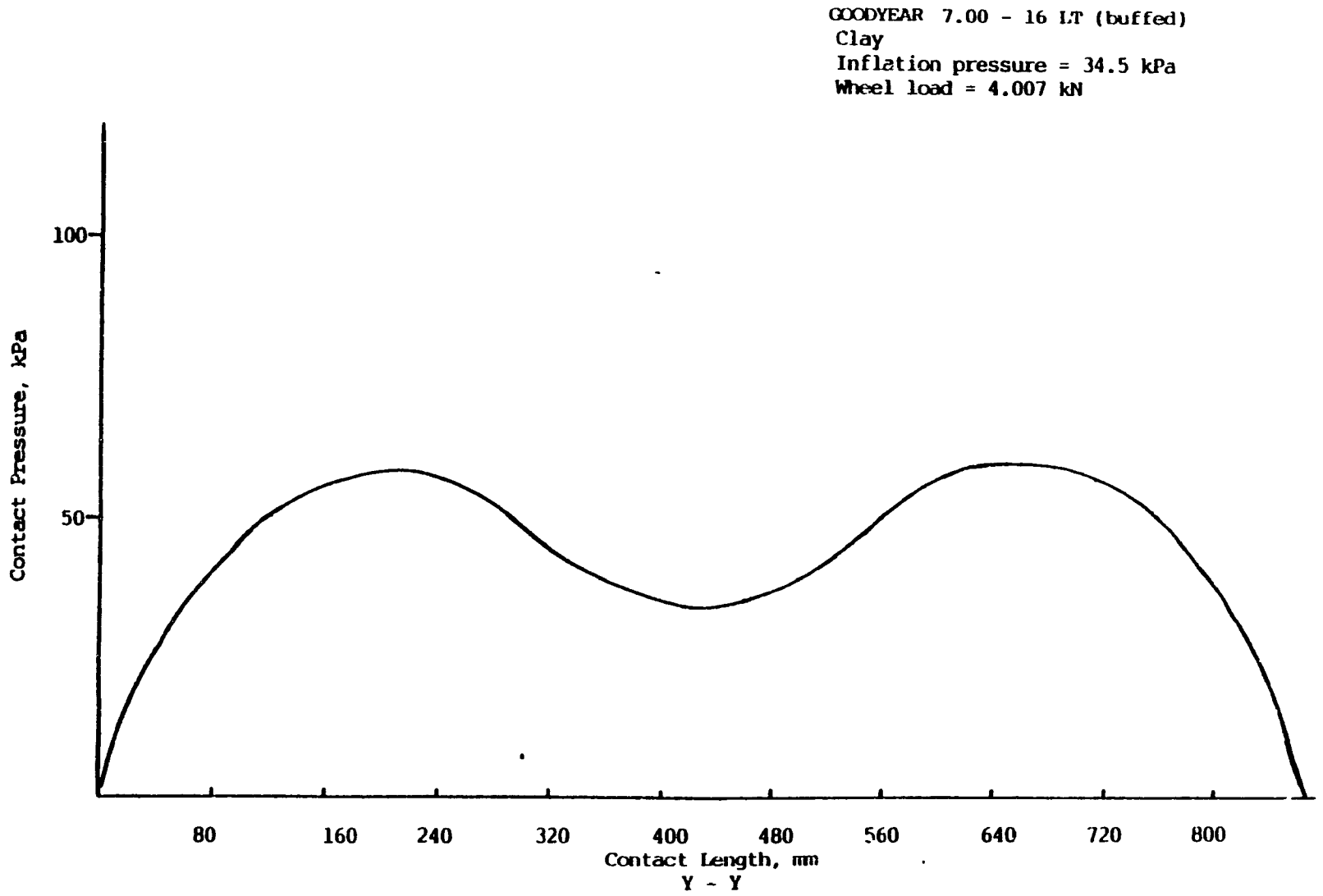


Fig. D.8c Profiles of Pressure Distribution Within the Footprint of GOODYEAR 7.00-16LT (buffed) in Clay

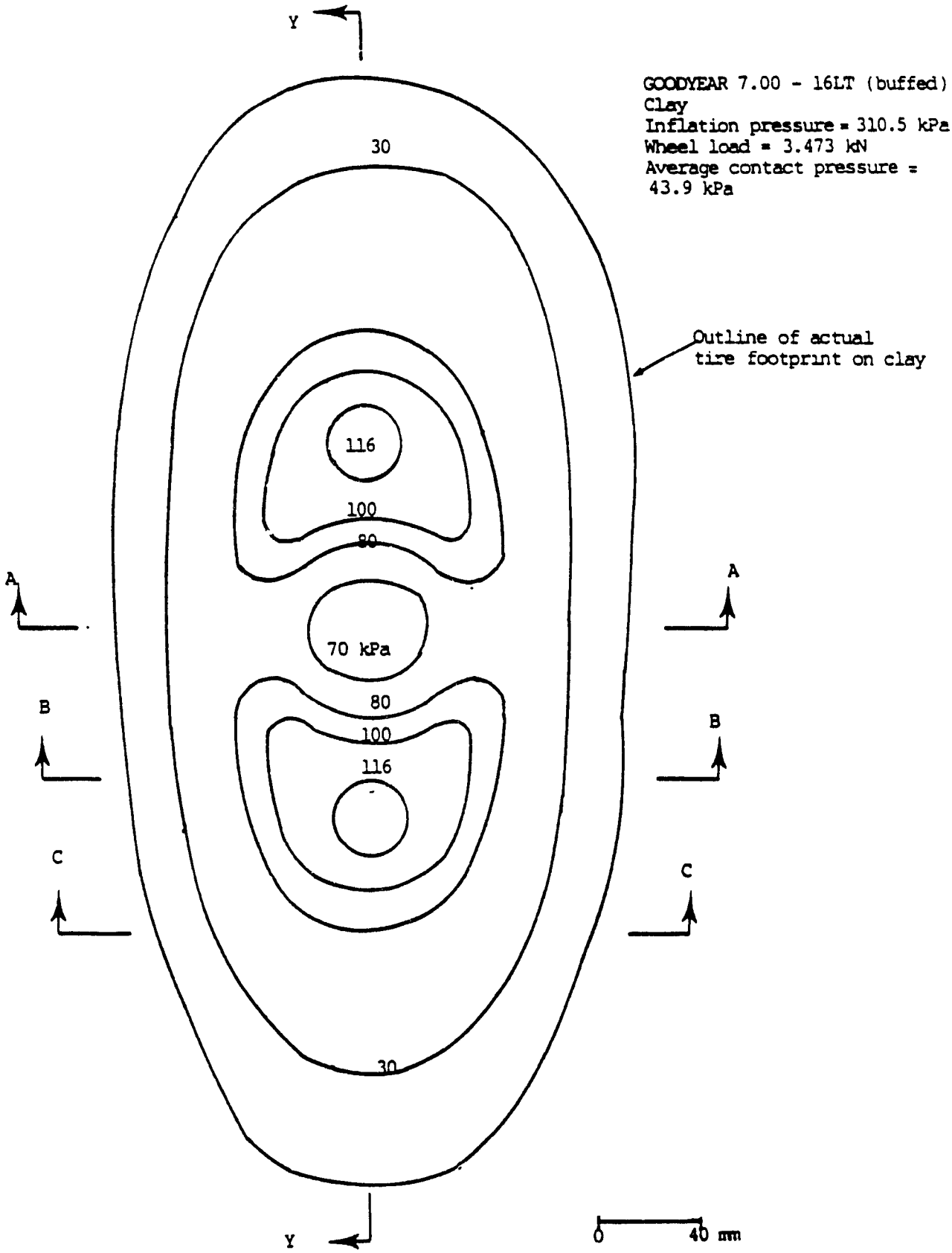
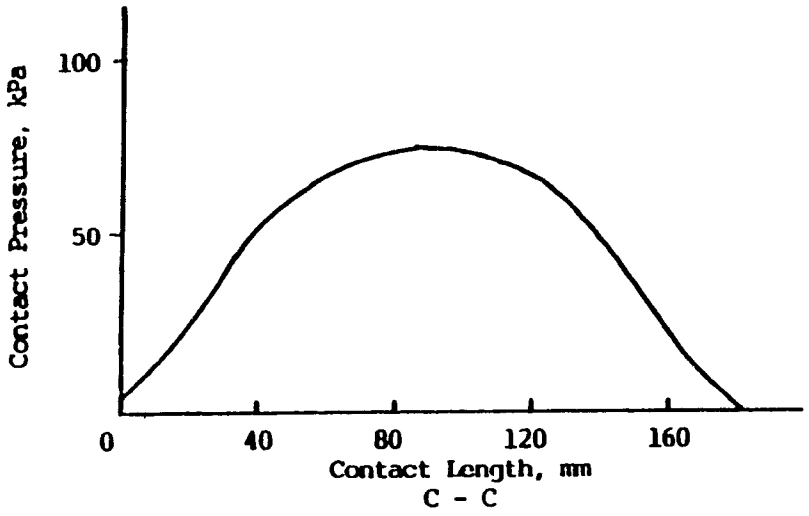
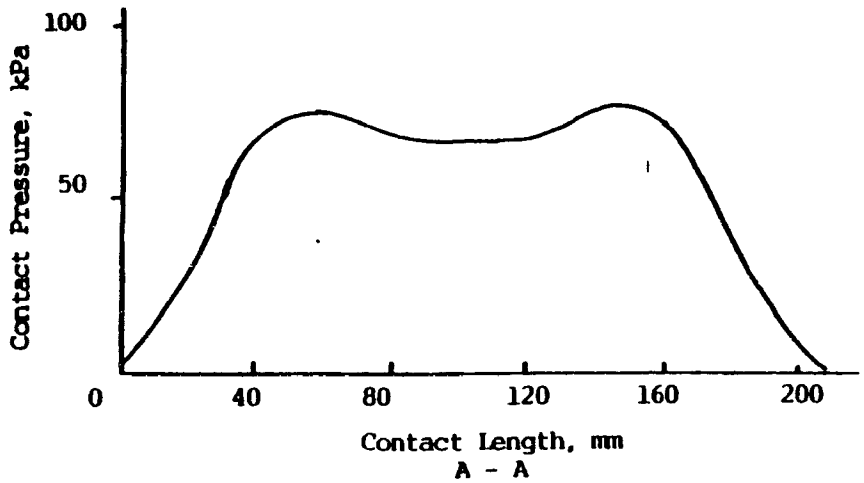


Fig. D.9a Isobars of Pressure Distribution Within the Footprint of GOODYEAR 7.00-16LT (buffed) in Clay

GOODYEAR 7.00 - 16 LT (buffed)
Clay
Inflation pressure = 310.5 kPa
Wheel load = 3.473 kN





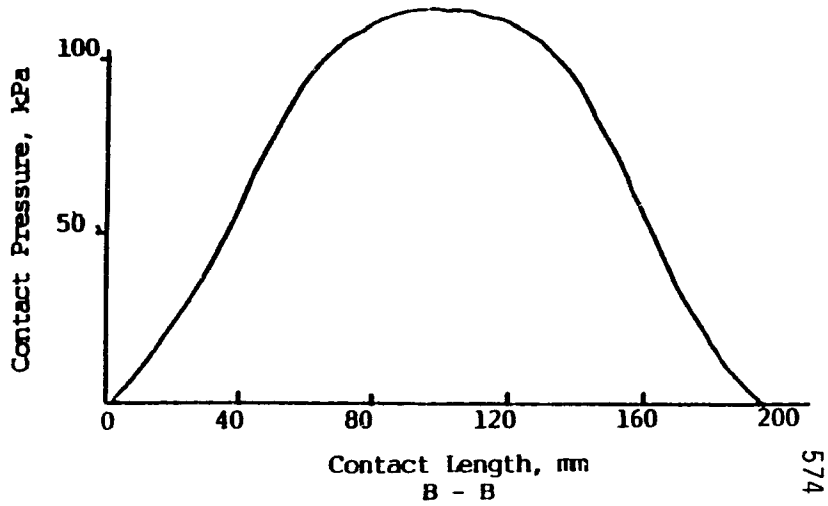


Fig. D.9b Profiles of Pressure Distribution Within the Footprint of GOODYEAR 7.00-16LT (buffed) in Clay

GOODYEAR 7.00 - 16 LT (buffed)
Clay
Inflation pressure = 310.5 kPa
Wheel load = 3.473 kN

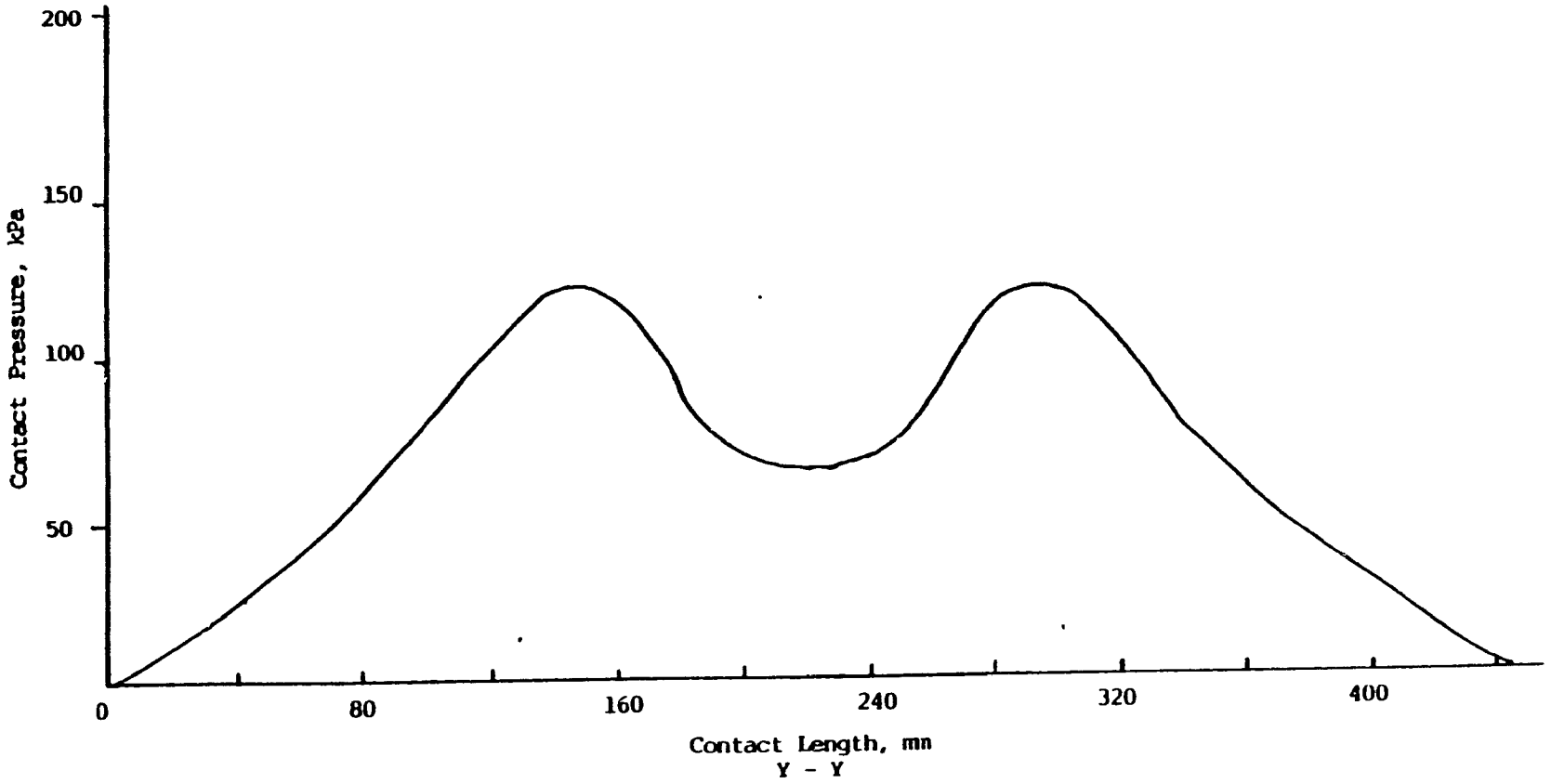


Fig. D.9c Profiles of Pressure Distribution Within the Footprint of GOODYEAR 7.00-16LT (buffed) in Clay

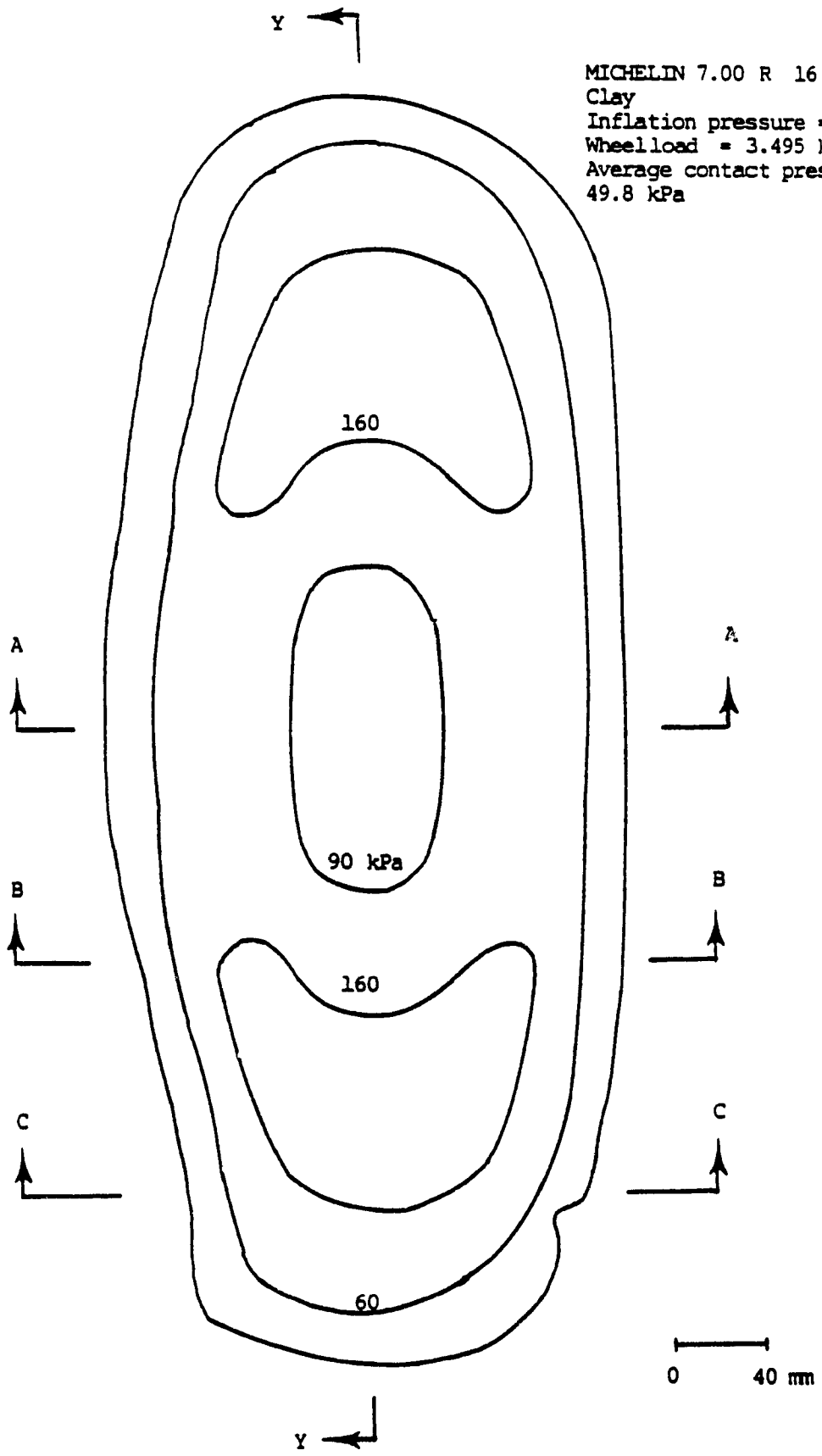


Fig. D.10a Isobars of Pressure Distribution Within the Footprint of MICHELIN 7.00R-16XCL (treaded) in Clay

MICHELIN 7.00 R 16 XCL (treaded)
Clay
Inflation pressure = 34.5 kPa
Wheel load = 3.495 kN

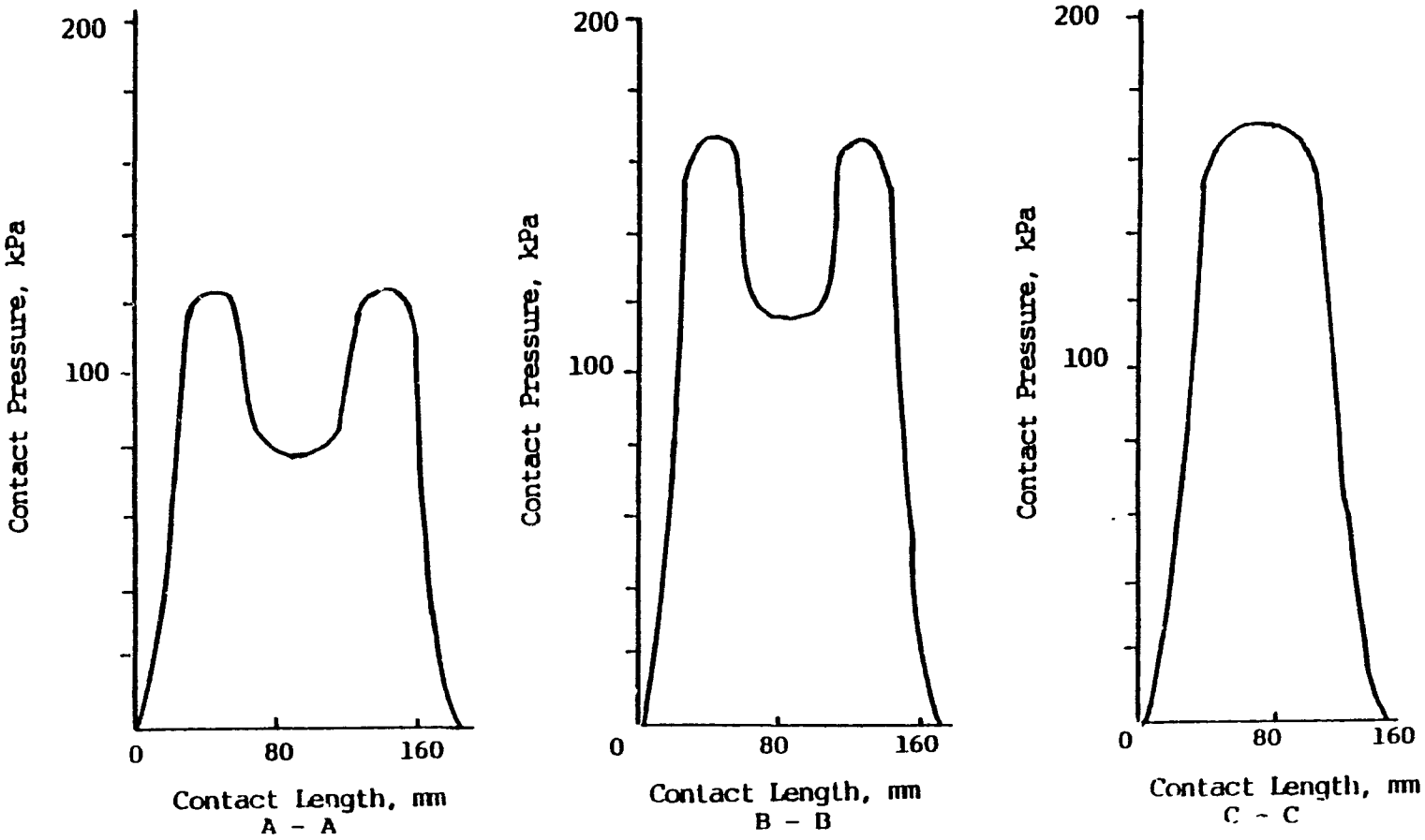


Fig. D.10b Profiles of Pressure Distribution Within the Footprint of MICHELIN 7.00R-16XCL (treaded) in Clay

MICHELIN 7.00 R 16 XCL (treaded)
Clay
Inflation pressure = 34.5 kPa
Wheel load = 3.495 kN

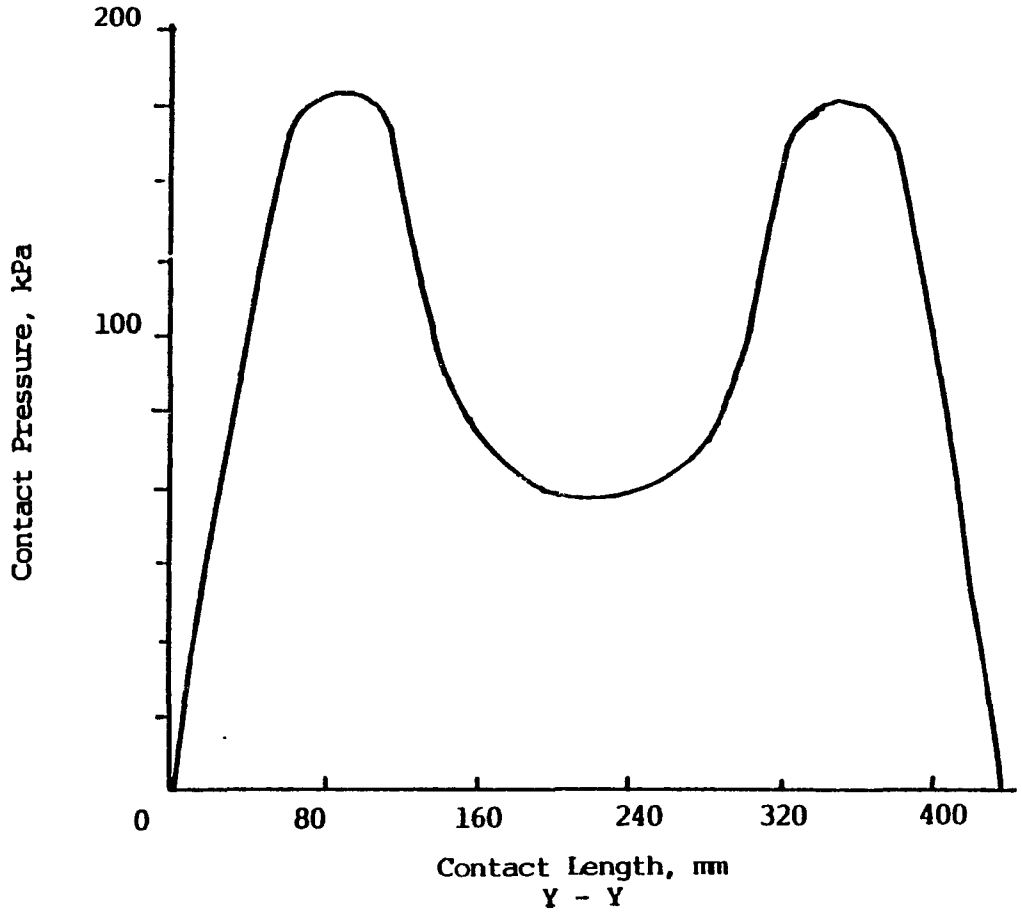


Fig. D.10c Profiles of Pressure Distribution Within the Footprint of MICHELIN 7.00R-16XCL (treaded) in Clay

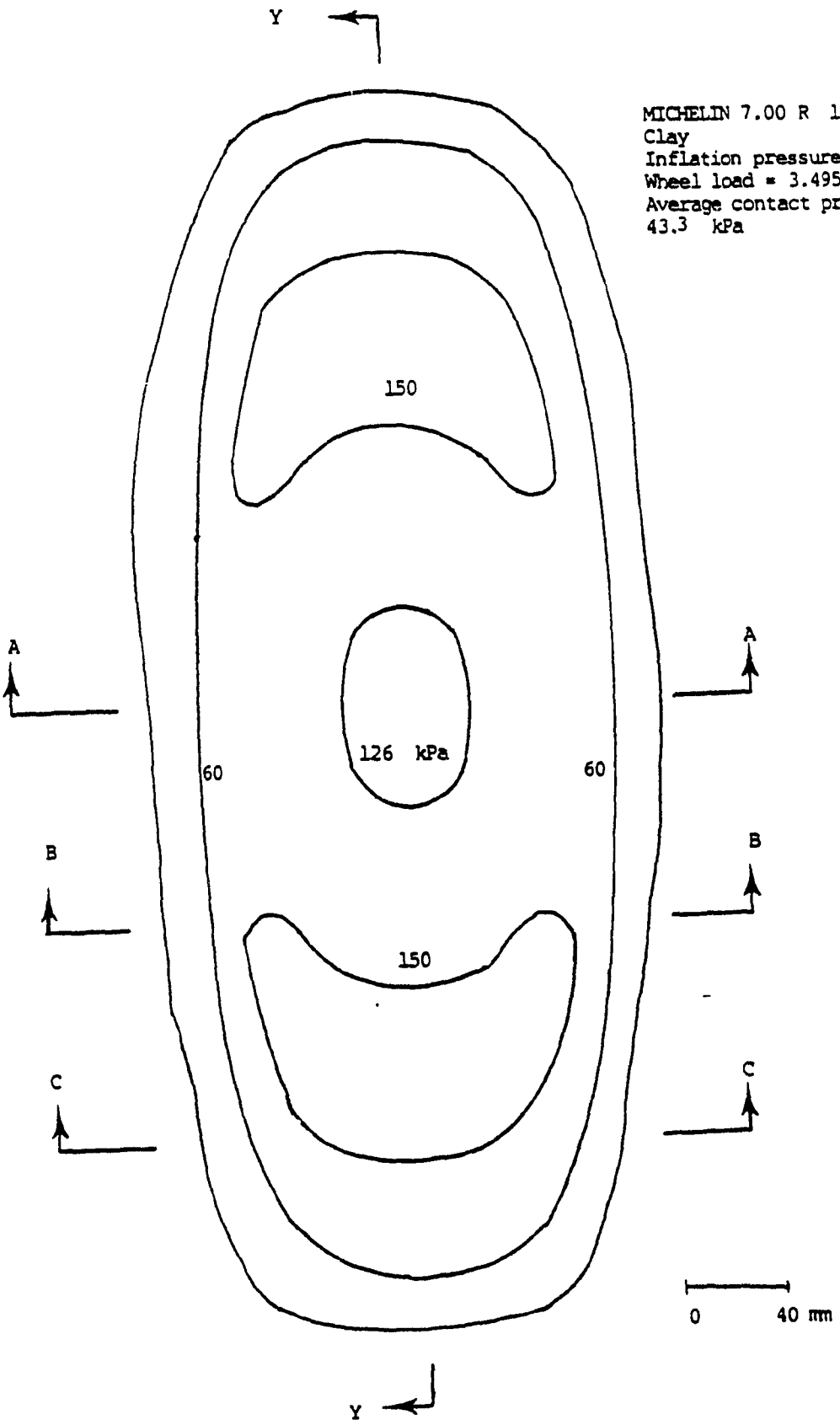


Fig. D.11a Isobars of Pressure Distribution Within the Footprint of MICHELIN 7.00R-16XCL (treaded) in Clay

MICHELIN 7.00 R 16XCL (treaded)
Clay
Inflation pressure = 310.5 kPa
Wheel load = 3.495 kN

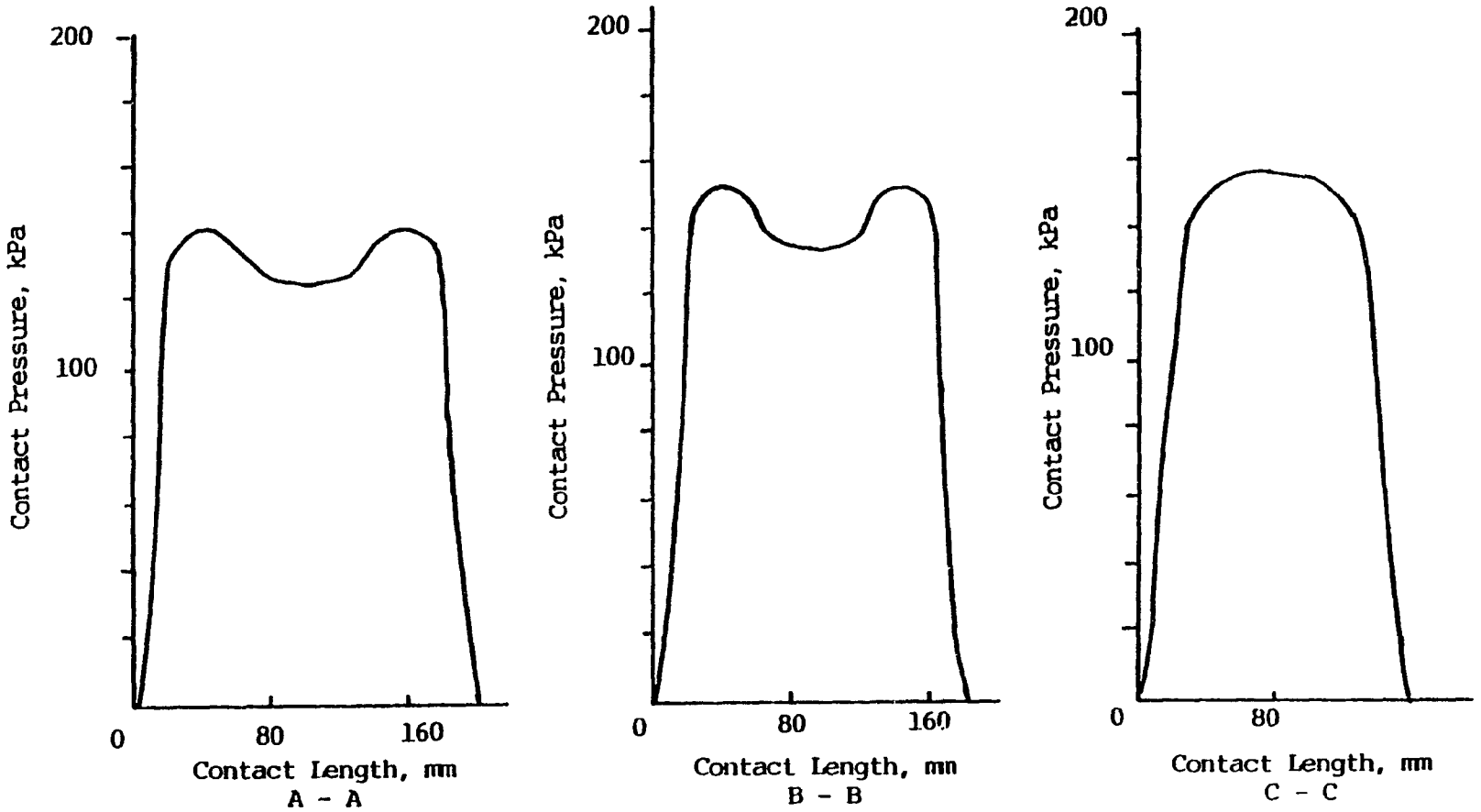


Fig. D.11b Profiles of Pressure Distribution Within the Footprint of MICHELIN 7.00R-16XCL (treaded) in Clay

MICHELIN 7.00 R 16XCL (treaded)
Clay
Inflation pressure = 310.5 kPa
Wheel load = 3.495 kN

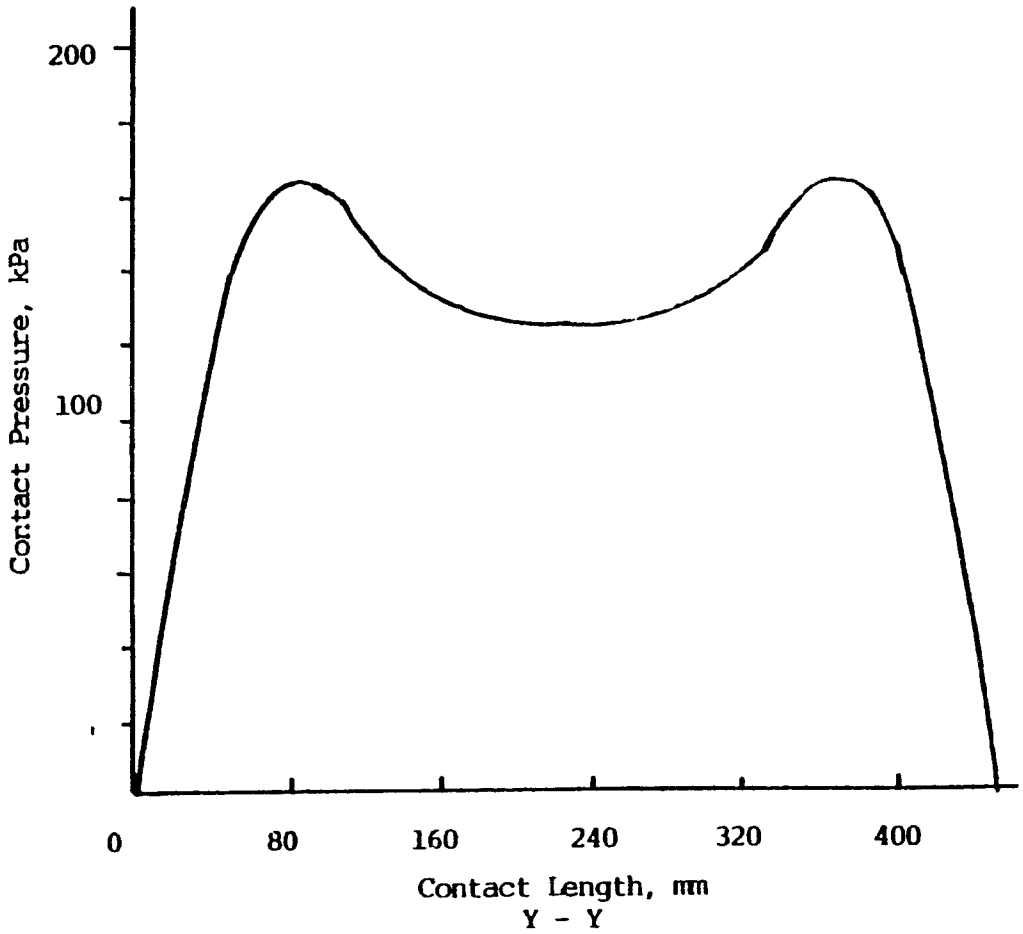


Fig. D.11c Profiles of Pressure Distribution Within the Footprint of MICHELIN 7.00R-16XCL (treaded) in Clay

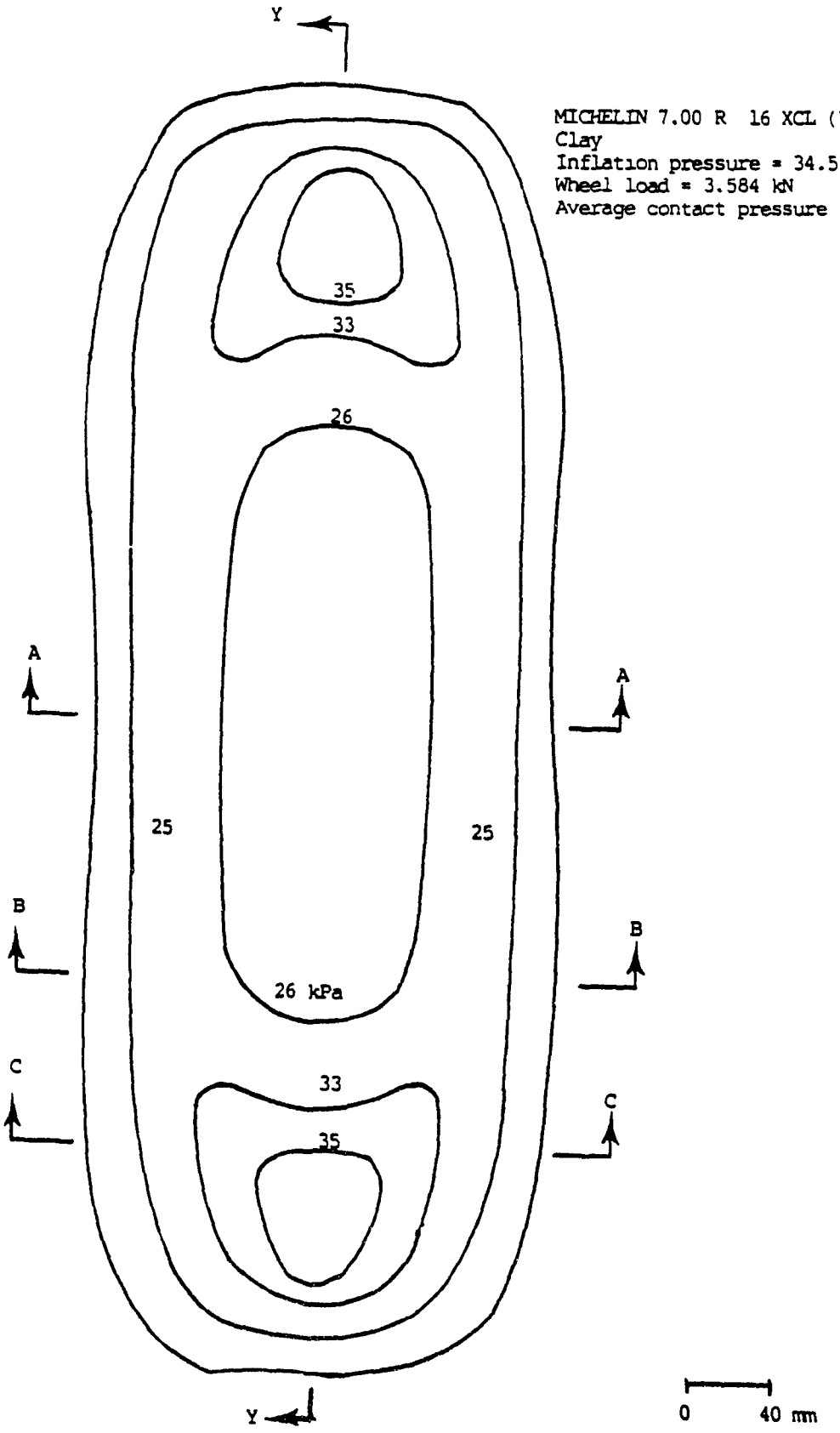


Fig. D.12a Isobars of Pressure Distribution Within the Footprint of MICHELIN 7.00R-16XCL (buffed) in Clay

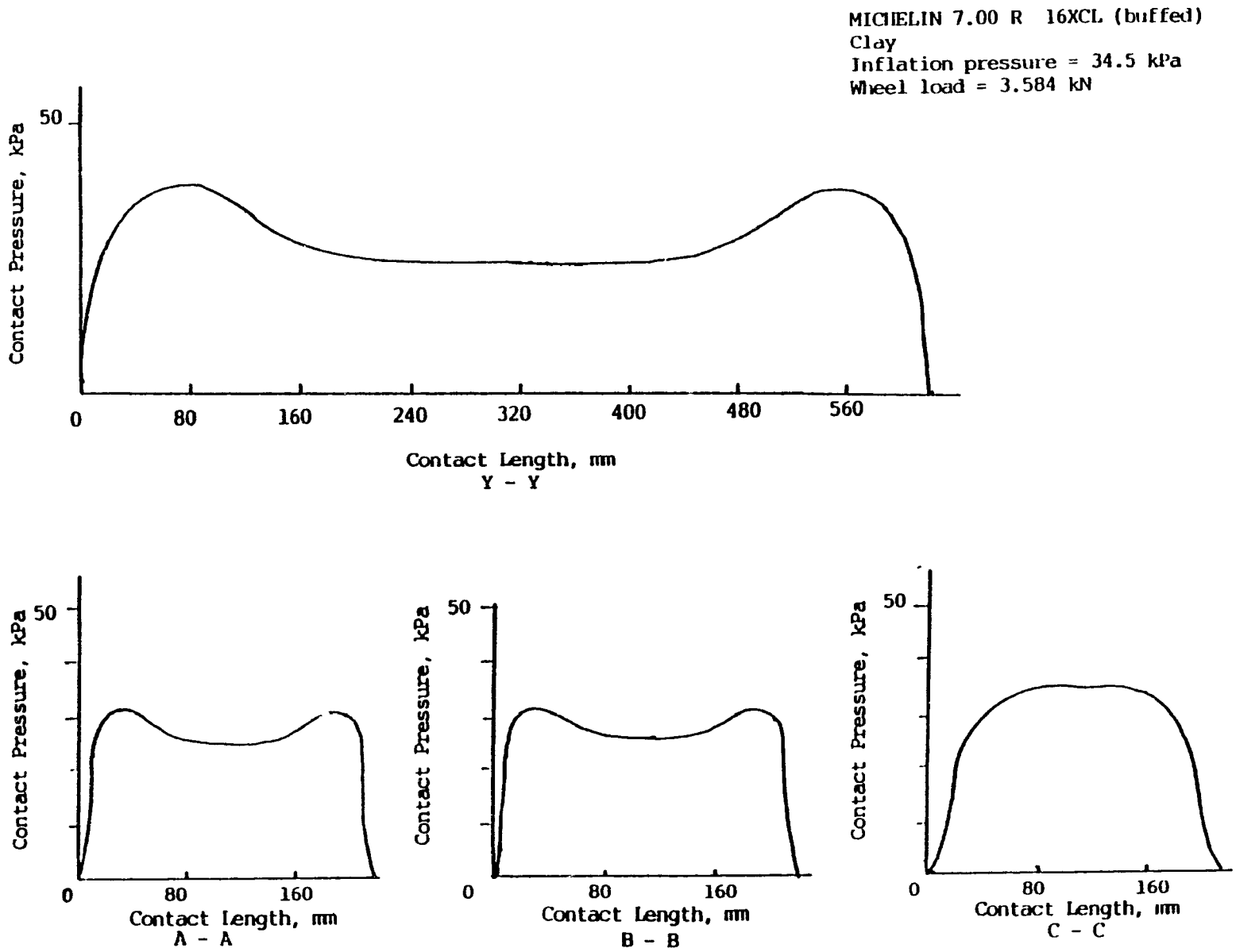


Fig. D.12b Profiles of Pressure Distribution Within the Footprint of MICHELIN 7.00R-16XCL (buffed) in Clay

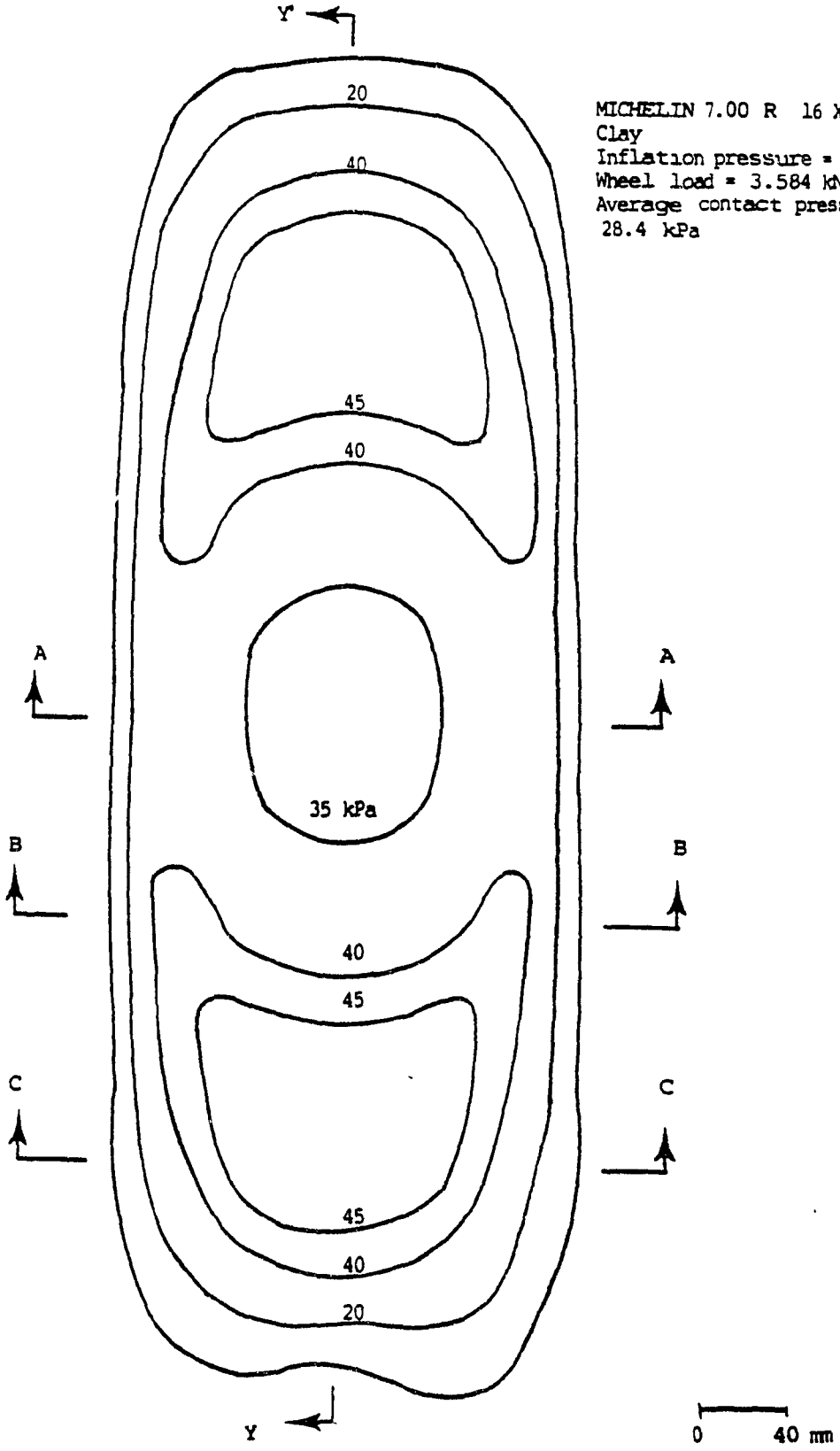


Fig. D.13a Isobars of Pressure Distribution Within the Footprint of MICHELIN 7.00R-16XCL (buffed) in Clay

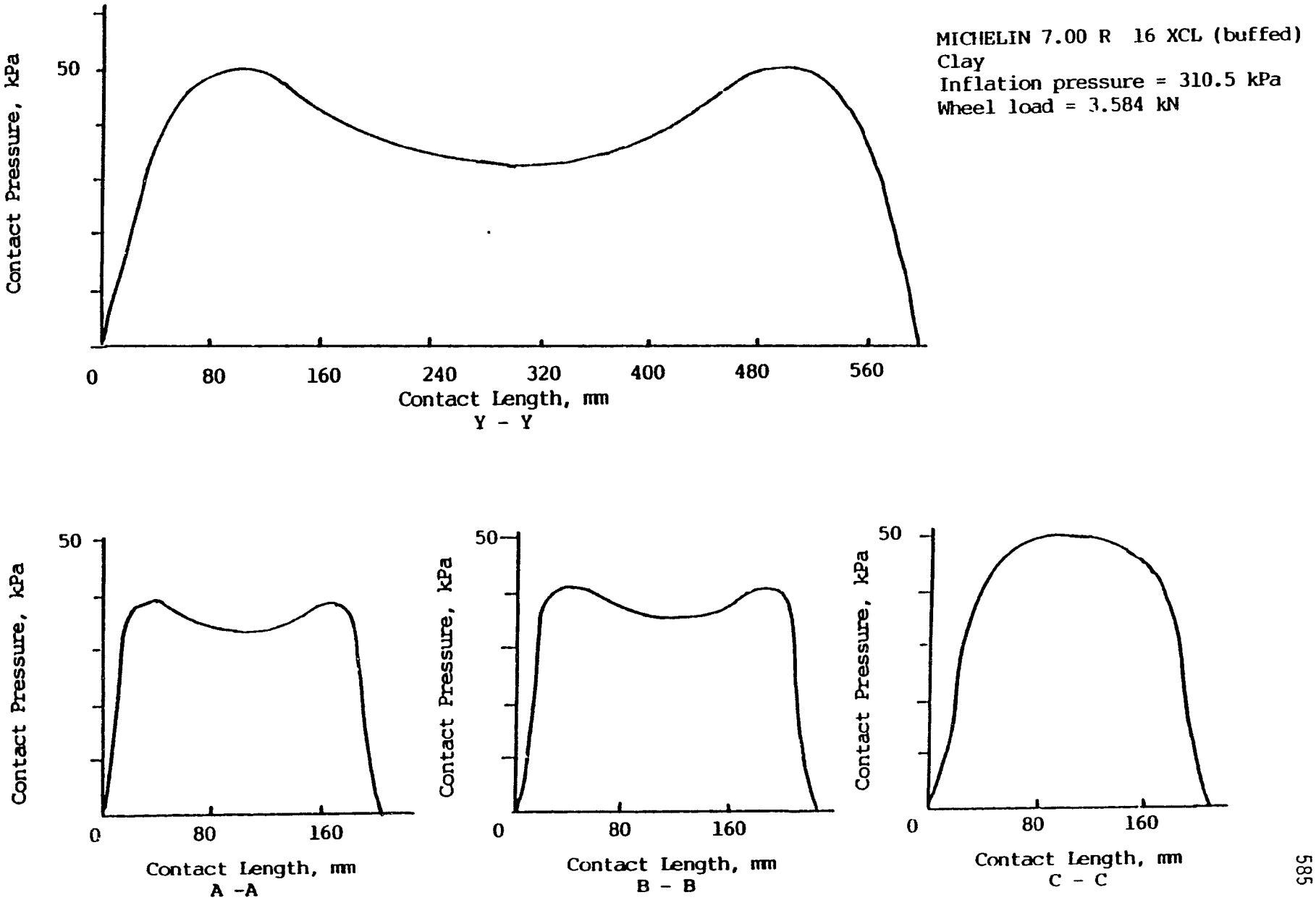


Fig. D.13b Profiles of Pressure Distribution Within the Footprint of MICHELIN 7.00R-16XCL (buffed) in Clay

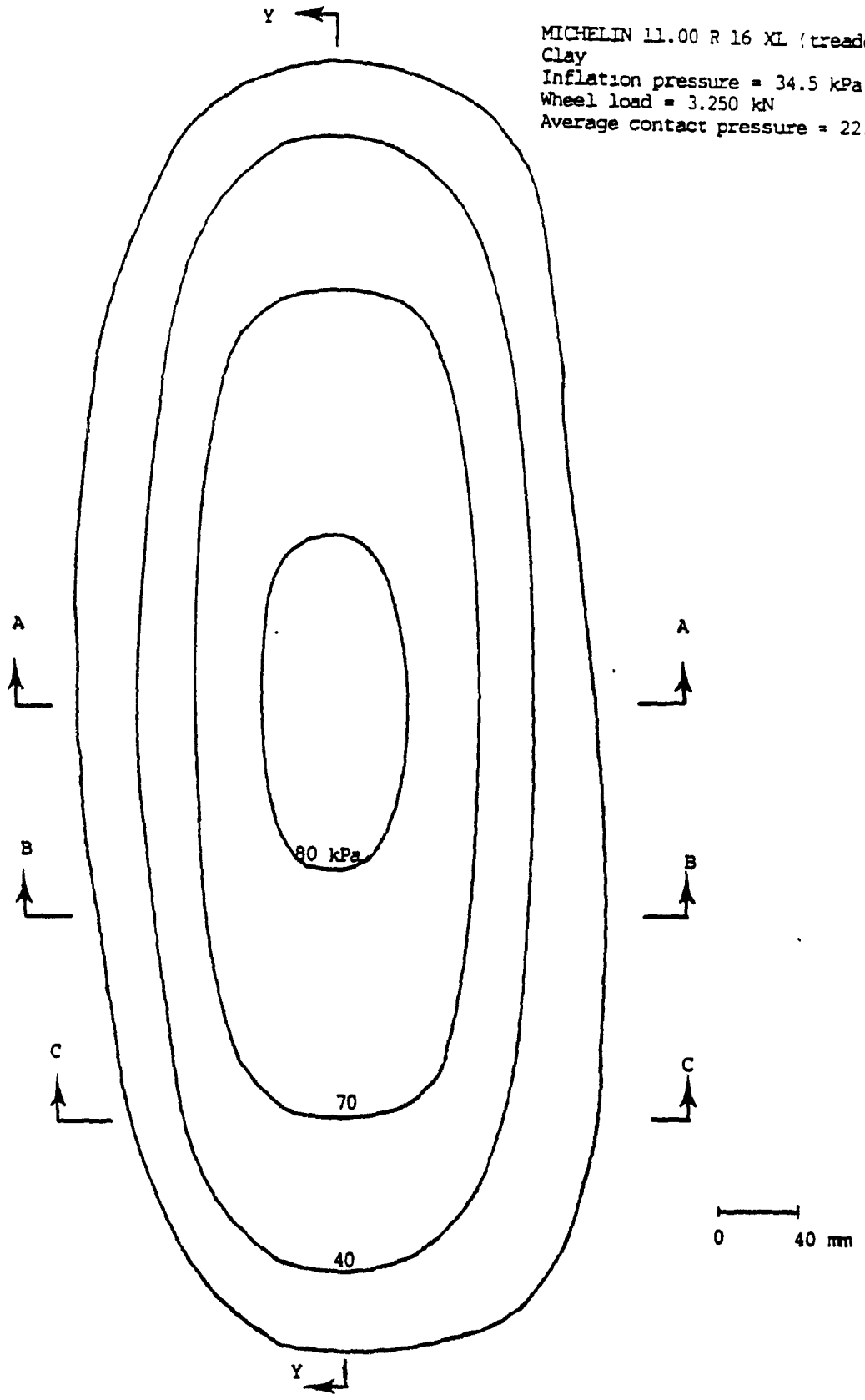


Fig. D.14a Isobars of Pressure Distribution Within the Footprint of MICHELIN 11.00R-16XL (treaded) in Clay

MICHELIN 11.00 R 16 XL (treaded)
Clay
Inflation pressure = 34.5 kPa
Wheel load = 3.250 kN

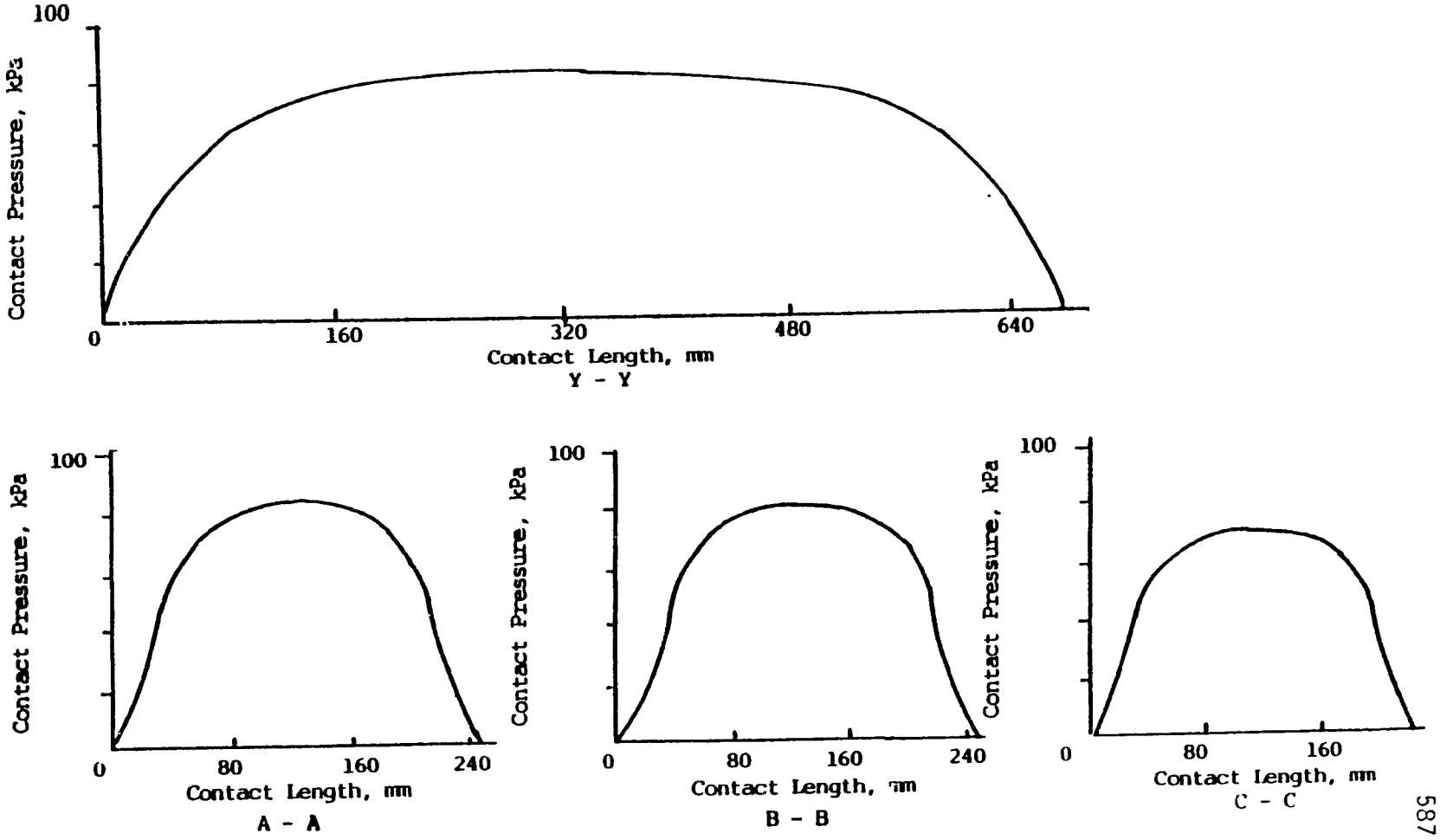


Fig. D.14b Profiles of Pressure Distribution Within the Footprint of MICHELIN 11.00R-16XL (treaded) in Clay

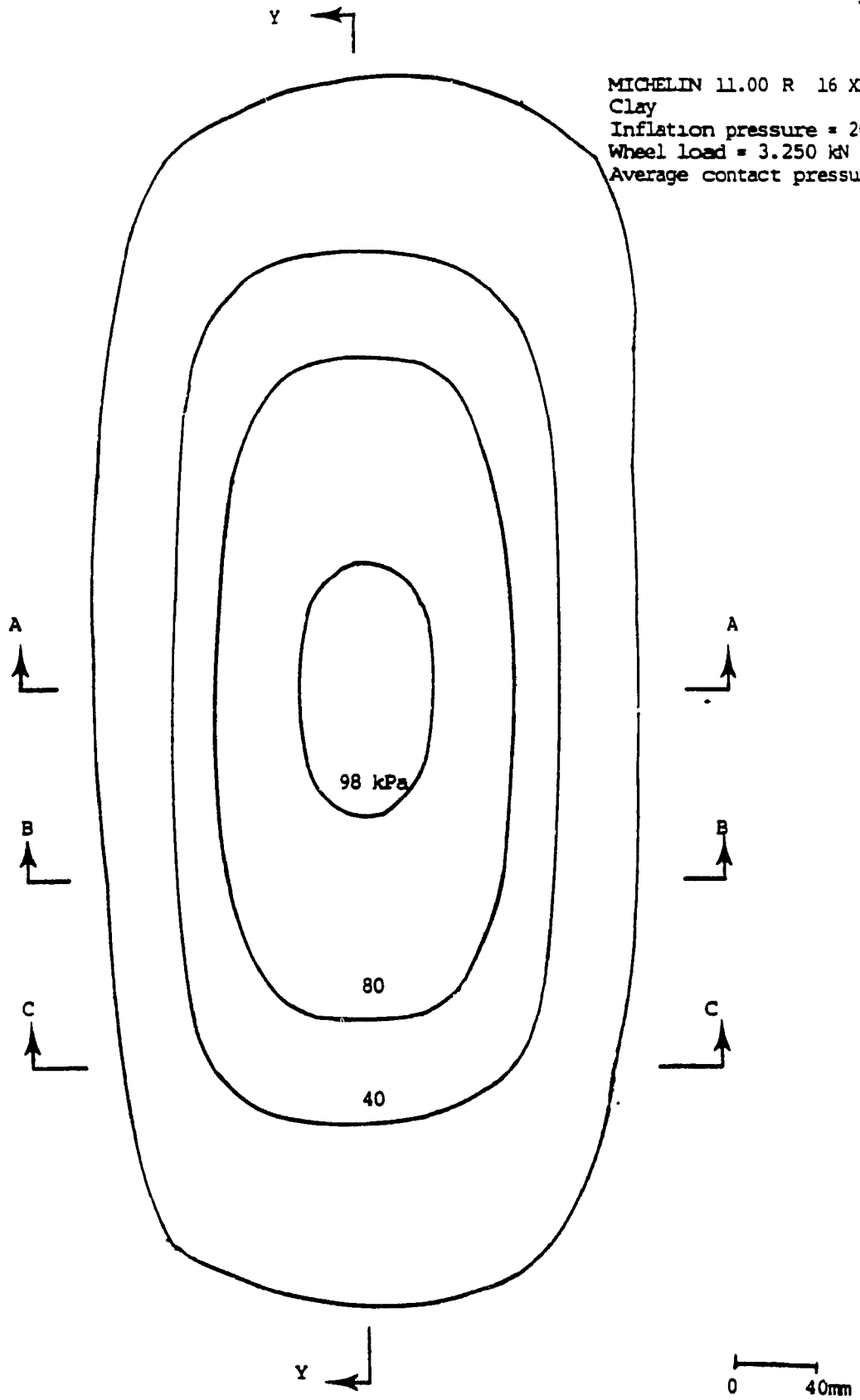


Fig. D.15a Isobars of Pressure Distribution Within the Footprint of MICHELIN 11.00R-16XL (treaded) in Clay

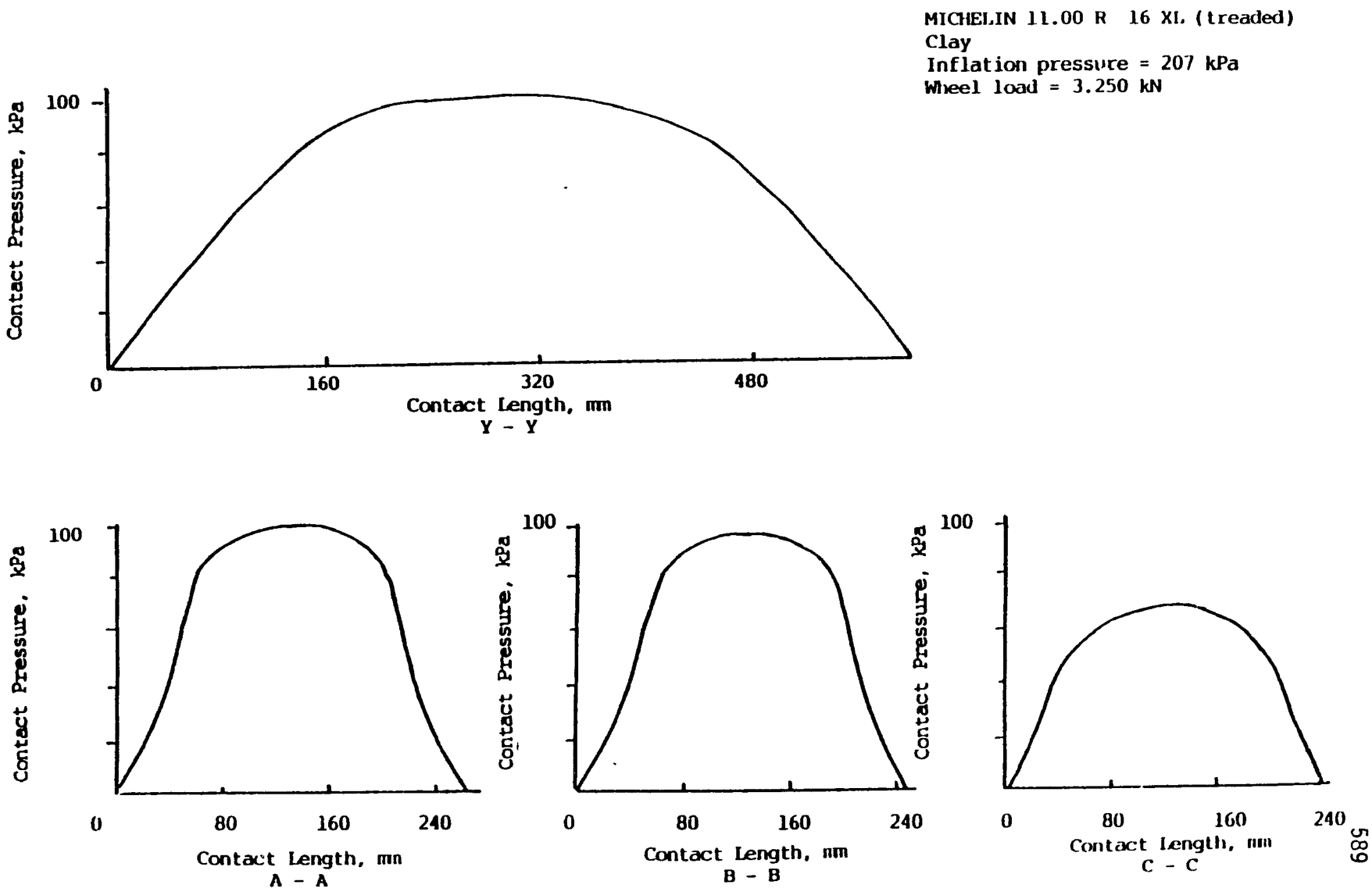


Fig. D.15b Profiles of Pressure Distribution Within the Footprint of MICHELIN 11.00R-16XL (treaded) in Clay

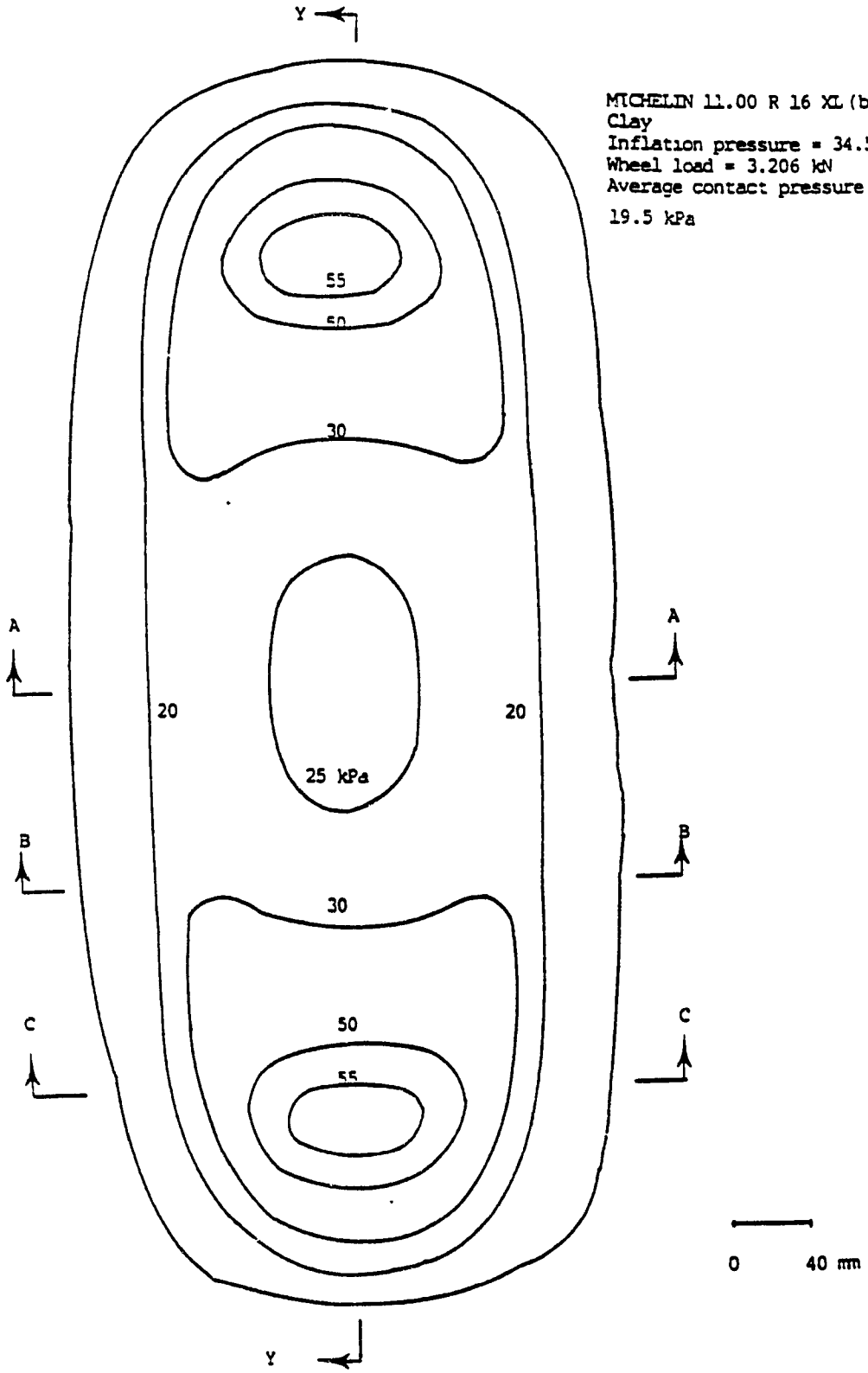


Fig. D.16a Isobars of Pressure Distribution Within the Footprint of MICHELIN 11.00R-16XL (buffed) in Clay

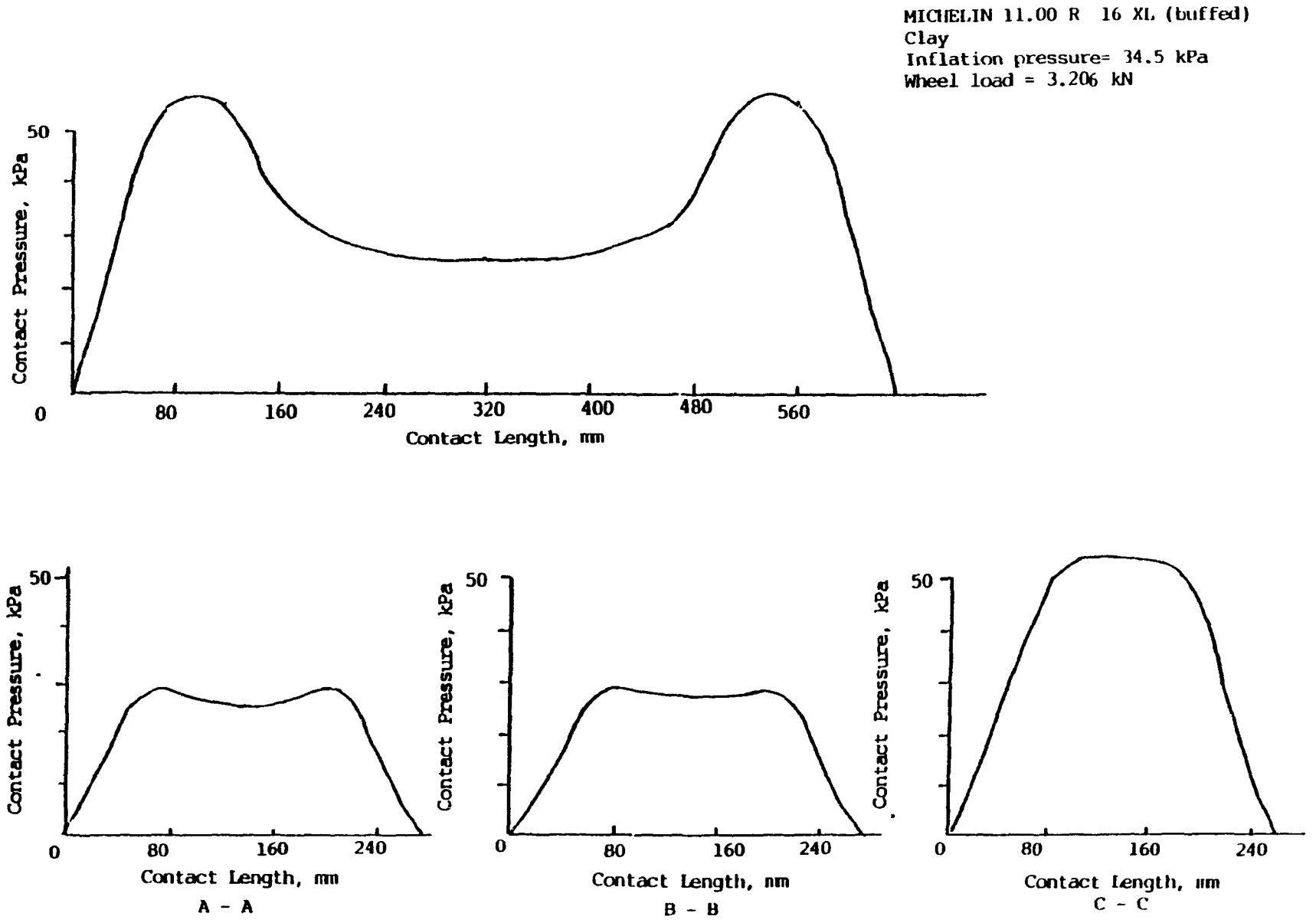


Fig. D.16b Profiles of Pressure Distribution Within the Footprint of MICHELIN 11.00R-16XL (buffed) in Clay

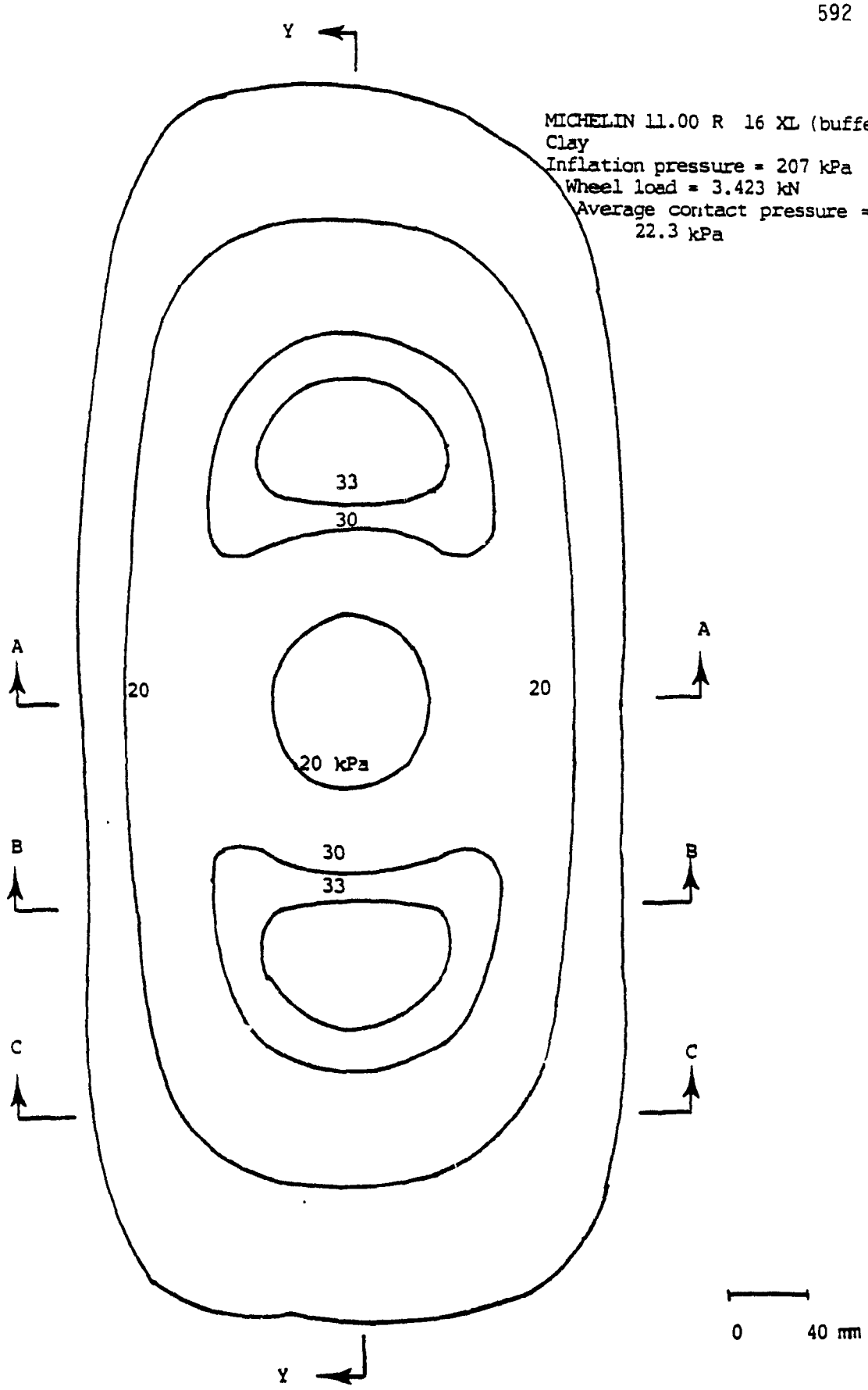


Fig. D.17a Isobars of Pressure Distribution Within the Footprint of MICHELIN 11.00R-16XL (buffed) in Clay

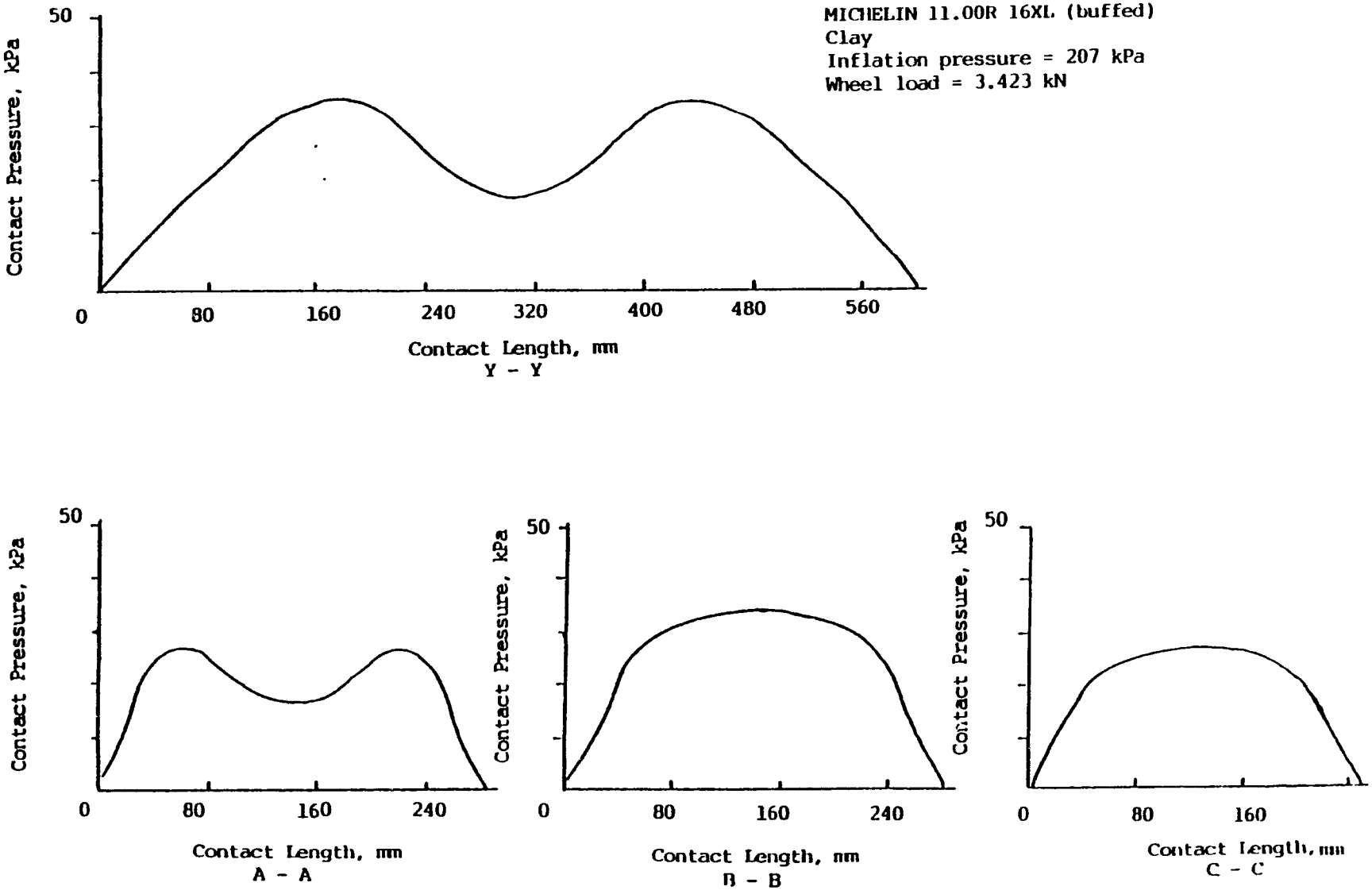


Fig. D.17b Profiles of Pressure Distribution Within the Footprint of MICHELIN 11.00R-16XL (buffed) in Clay

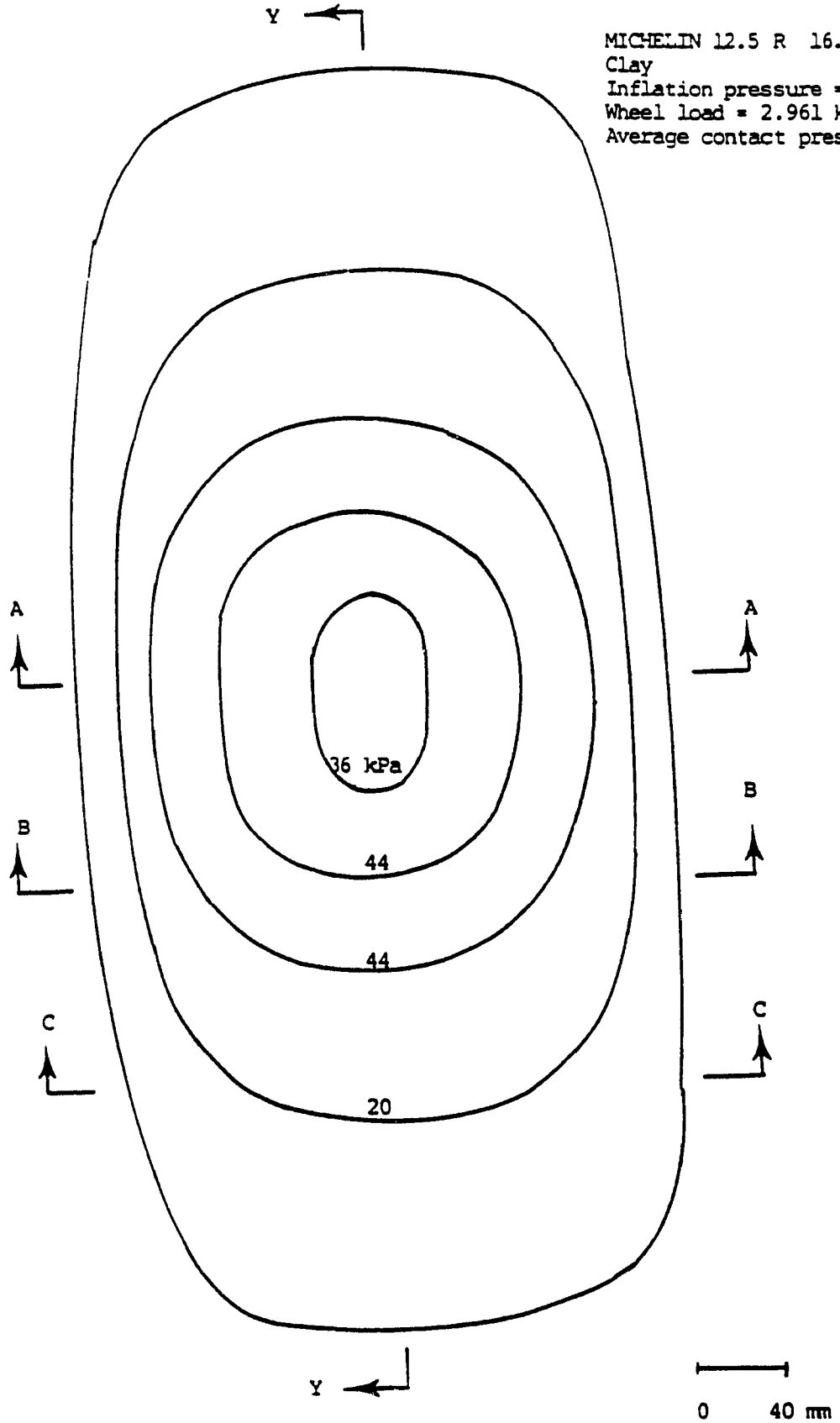


Fig. D.18a Isobars of Pressure Distribution Within the Footprint of MICHELIN 12.5R-16.5XLM (treaded) in Clay

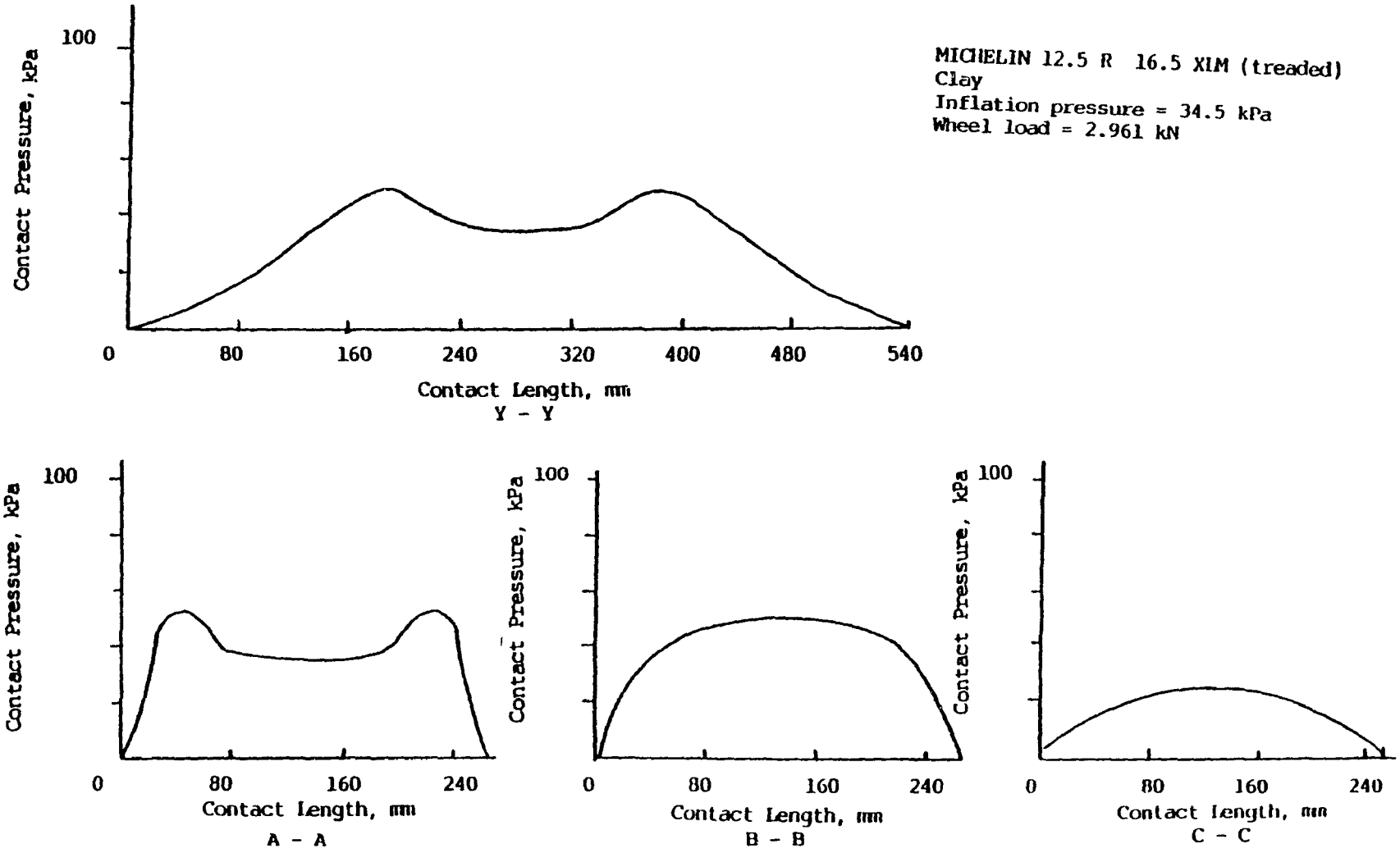


Fig. D.18b Profiles of Pressure Distribution Within the Footprint of MICHELIN 12.5R-16.5XLM (treaded) in Clay

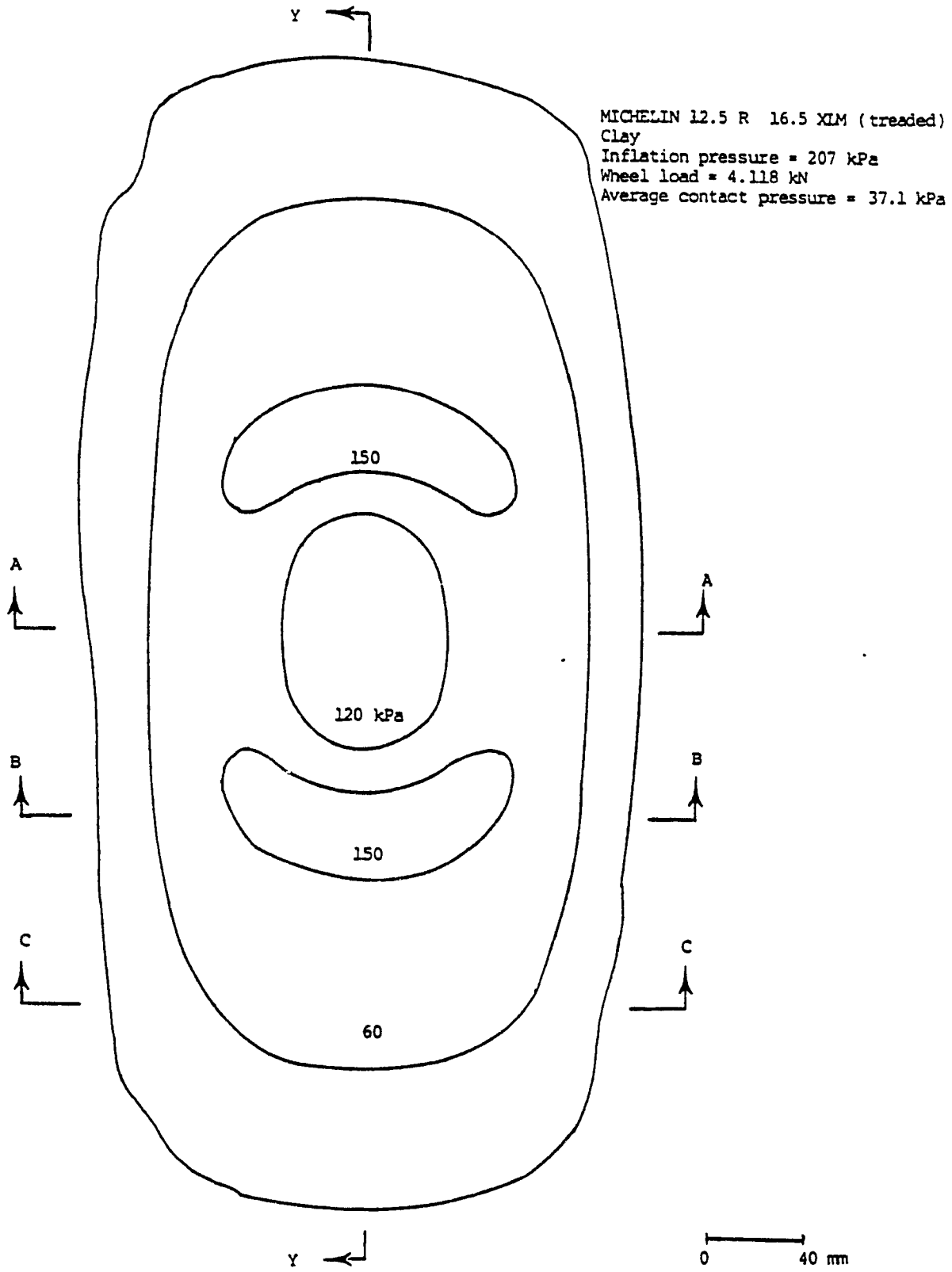


Fig. D.19a Isobars of Pressure Distribution Within the Footprint of MICHELIN 12.5R-16.5XLM (treaded) In Clay

MICHELIN 12.5 R 16.5 XIM (treaded)
Clay
Inflation pressure = 207 kPa
Wheel load = 4.118 kN

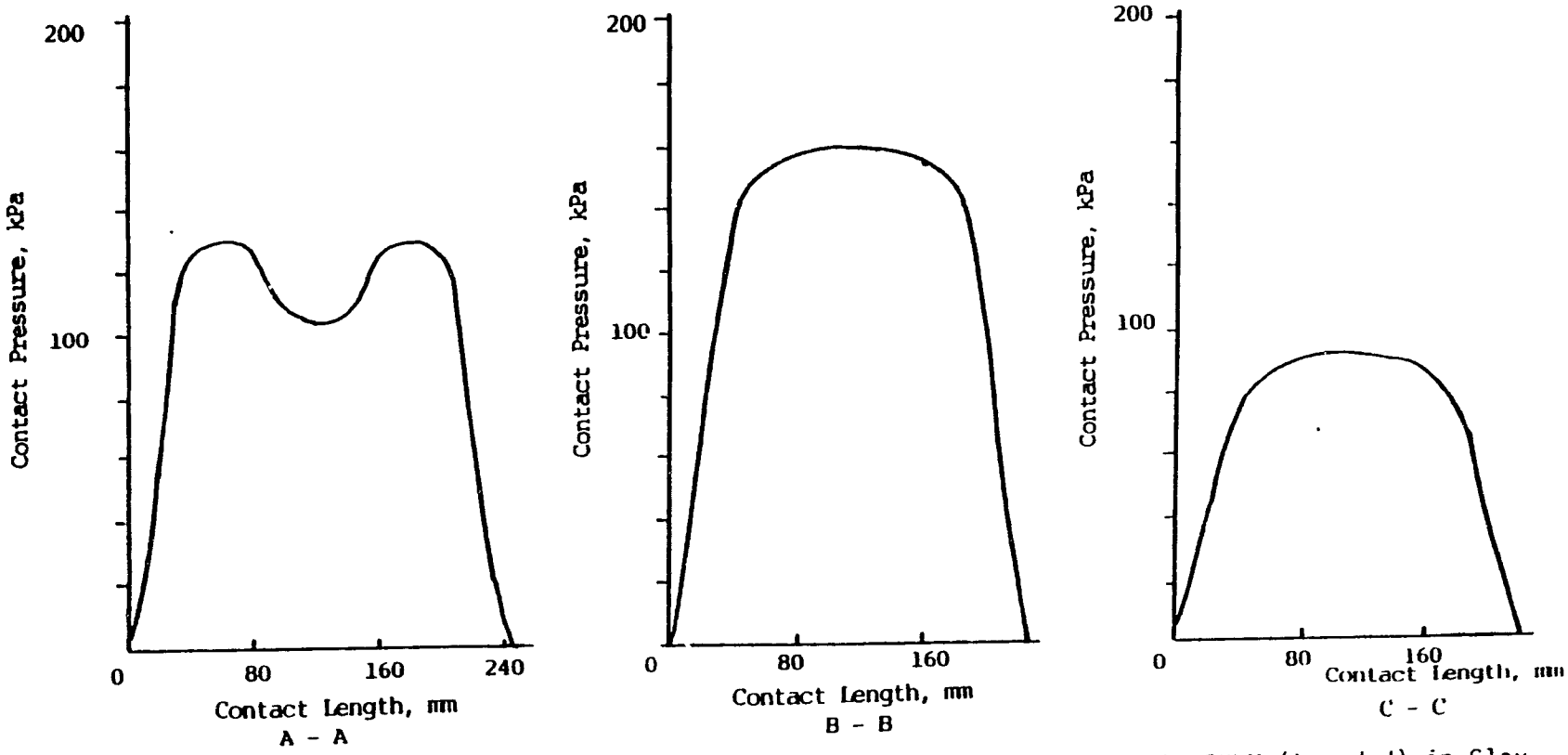


Fig. D.19b Profiles of Pressure Distribution Within the Footprint of MICHELIN 12.5R-16.5XLM (treaded) in Clay

MICHELIN 12.5 R 16.5 XLM (treaded)
Clay
Inflation pressure = 207 kPa
Wheel load = 4.118 kN

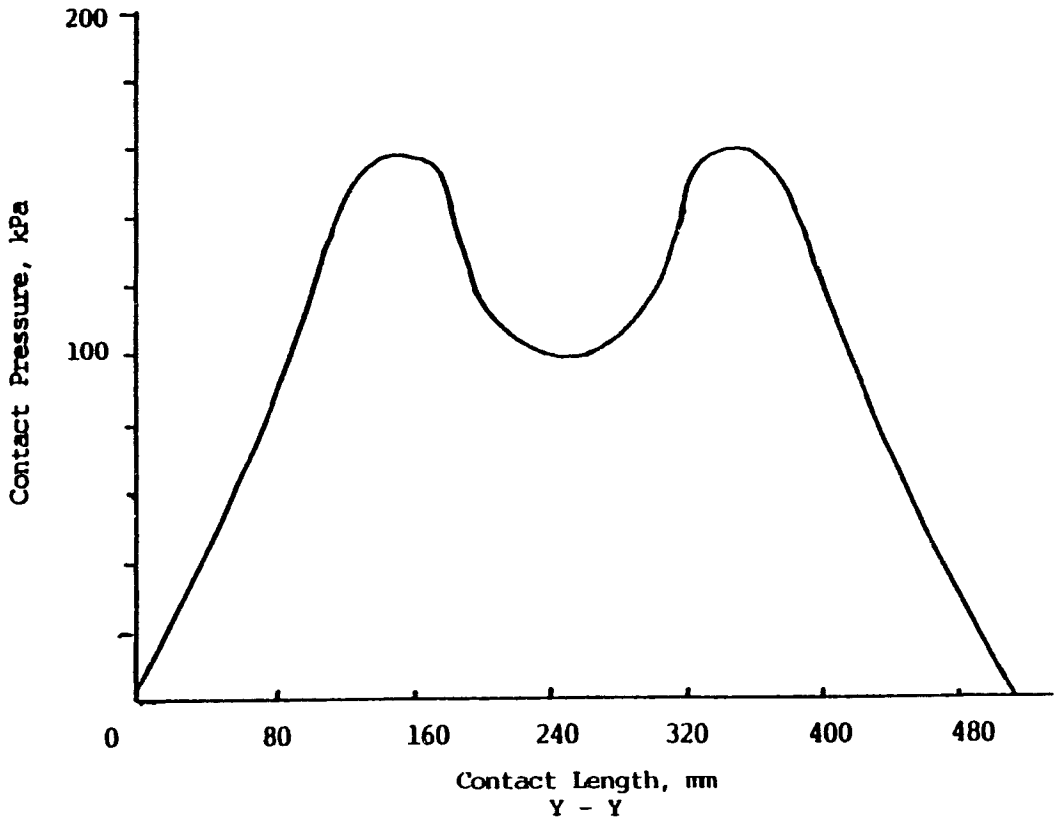


Fig. D.19c Profiles of Pressure Distribution Within the Footprint of MICHELIN 12.5R-16.5XLM (treaded) in Clay

MICHELIN 12.5 R 16.5 XLM (buffed)
Clay
Inflation pressure = 34.5 kPa
Wheel load = 3.473 kN
Average contact pressure
= 28.8 kPa

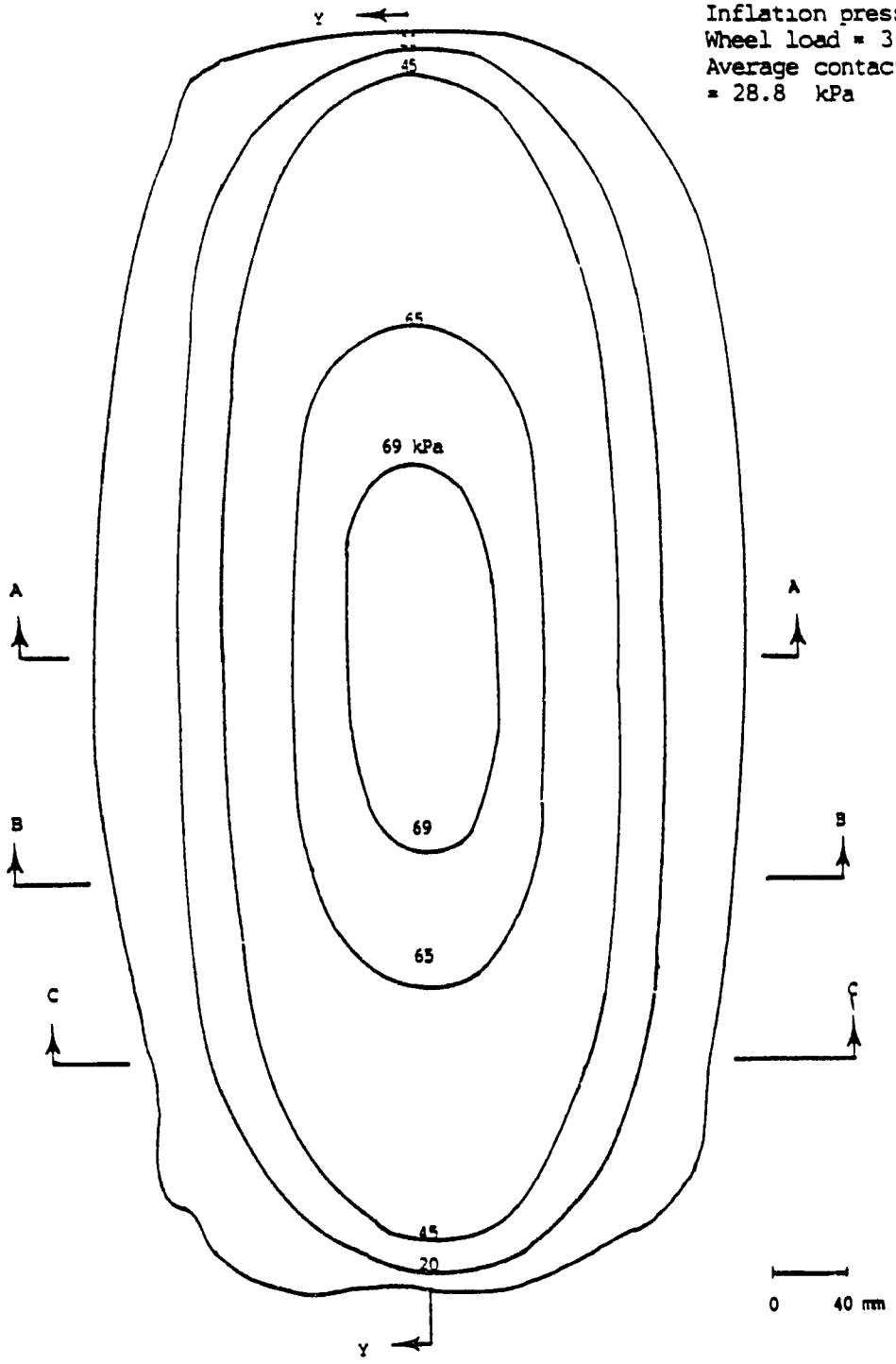


Fig. D.20a Isobars of Pressure Distribution Within the Footprint of MICHELIN 12.5R-16.5XLM (buffed) in Clay

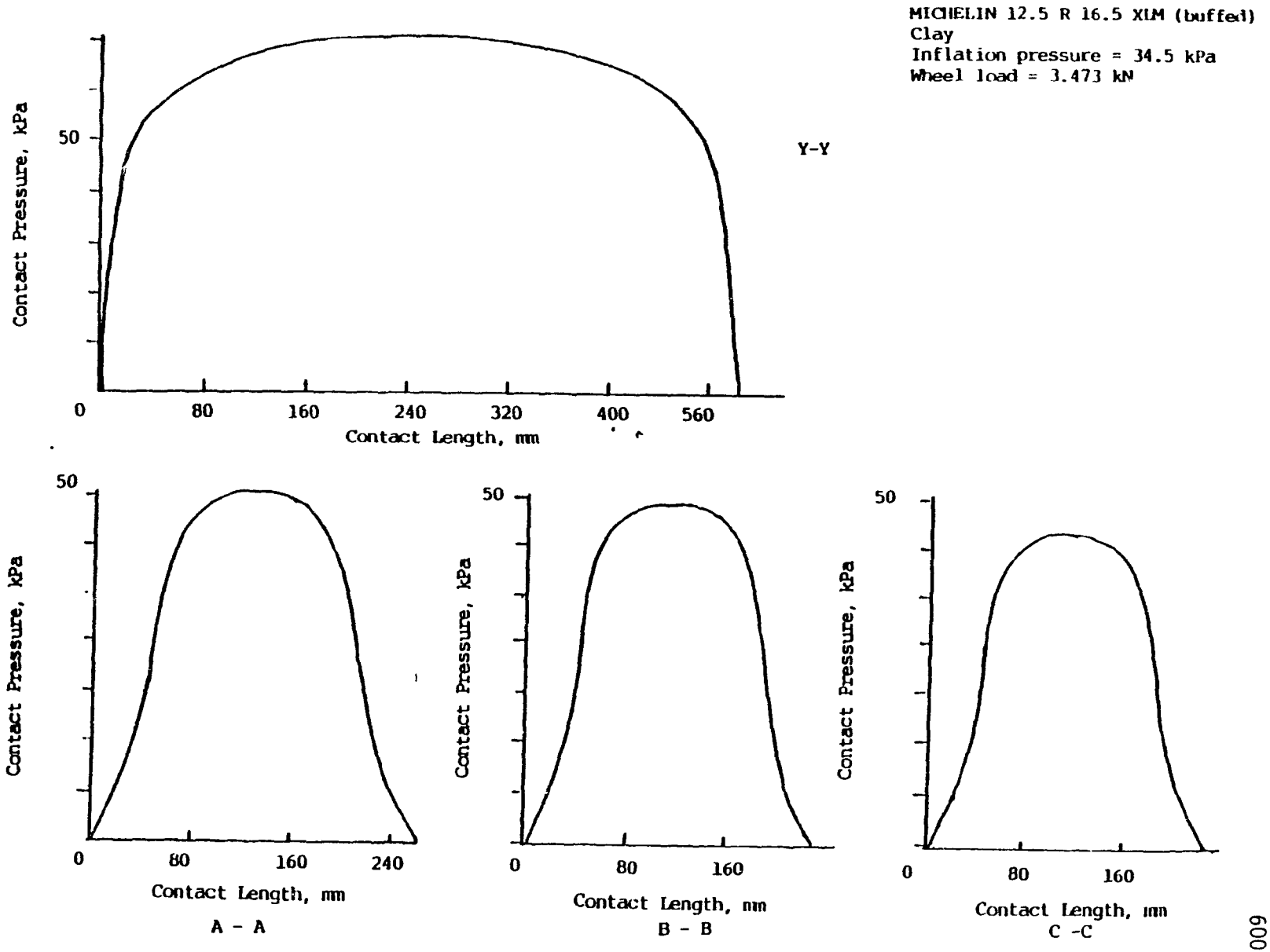


Fig. D.20b Profiles of Pressure Distribution Within the Footprint of MICHELIN 12.5R-16.5XLM (buffed) in Clay

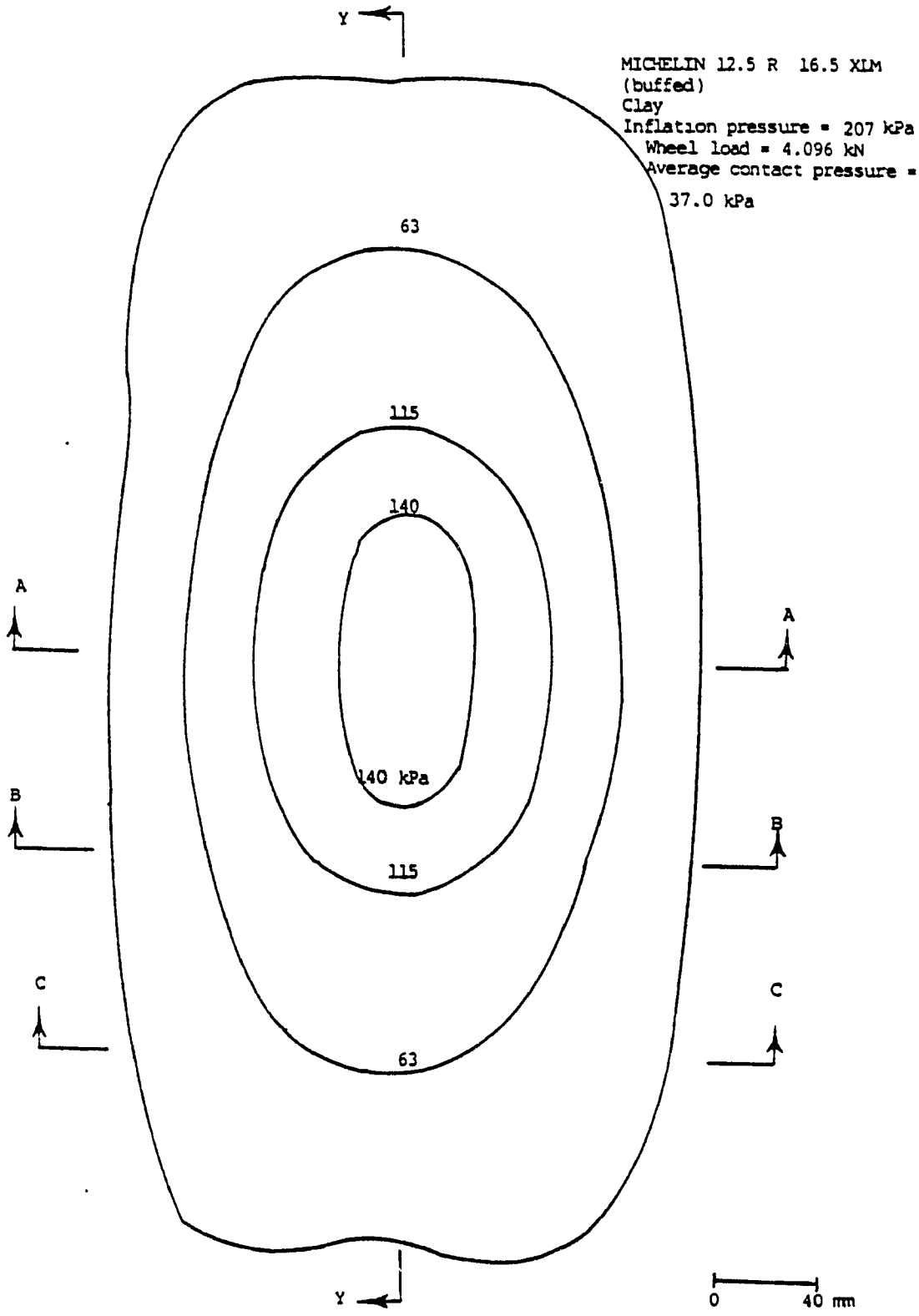


Fig. D.21a Isobars of Pressure Distribution Within the Footprint of MICHELIN 12.5R-16.5XLM (buffed) in Clay

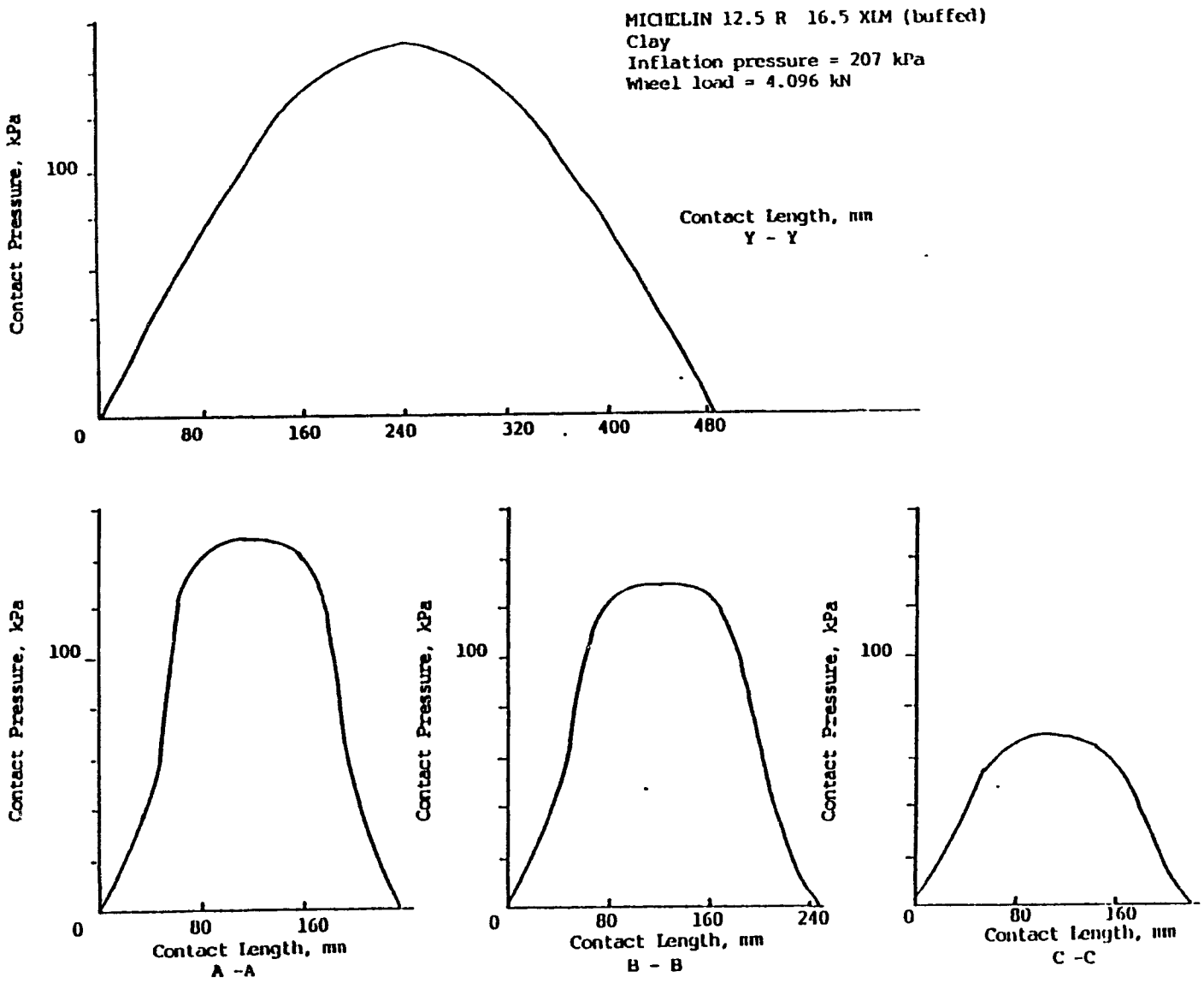


Fig. D.21b Profiles of Pressure Distribution Within the Footprint of MICHELIN 12.5R-16.5XLM (buffed) in Clay

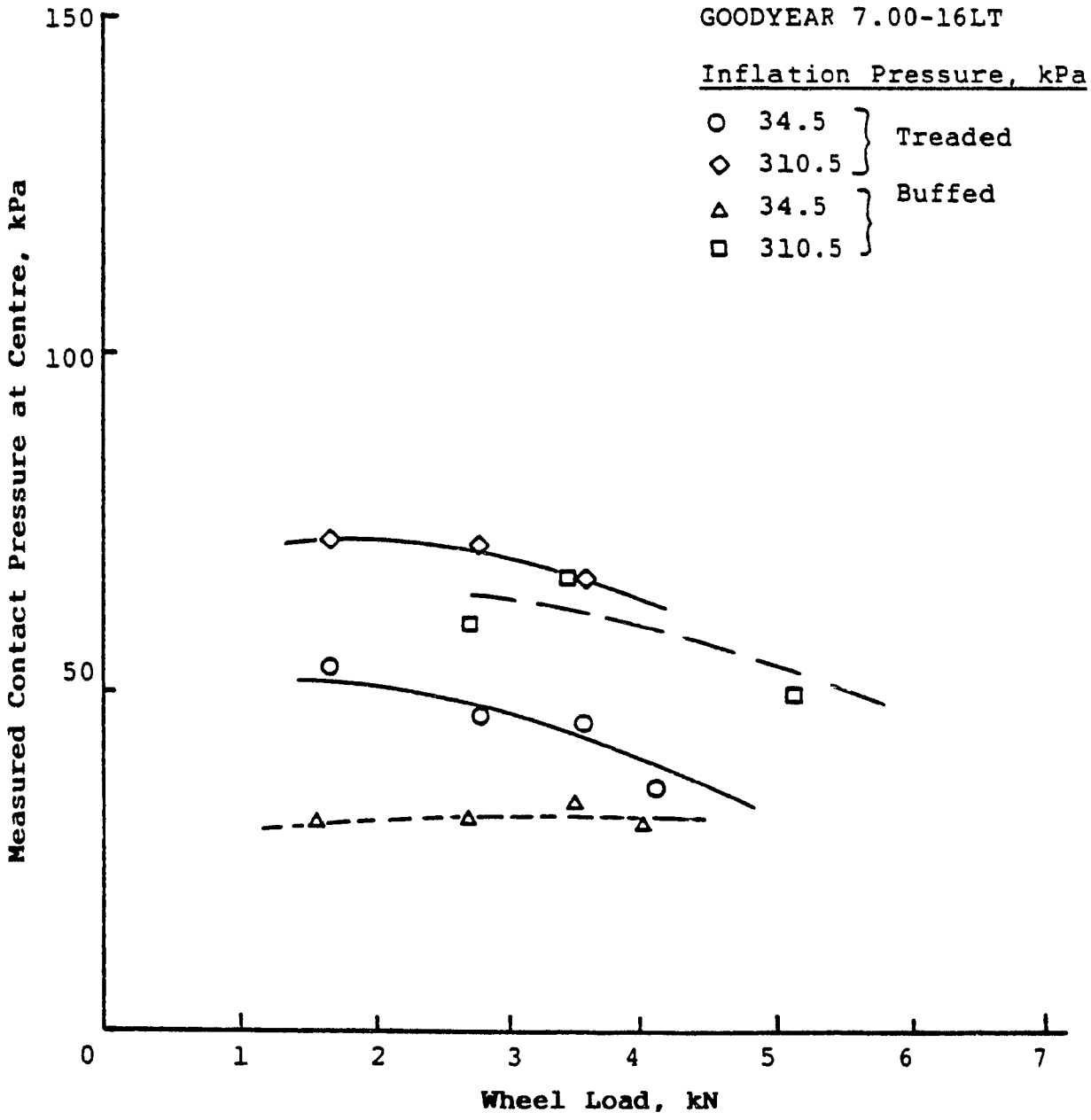


Fig. D.22a Variation of Contact Pressure (at Center) With Wheel Load for GOODYEAR 7.00-16LT on Clay

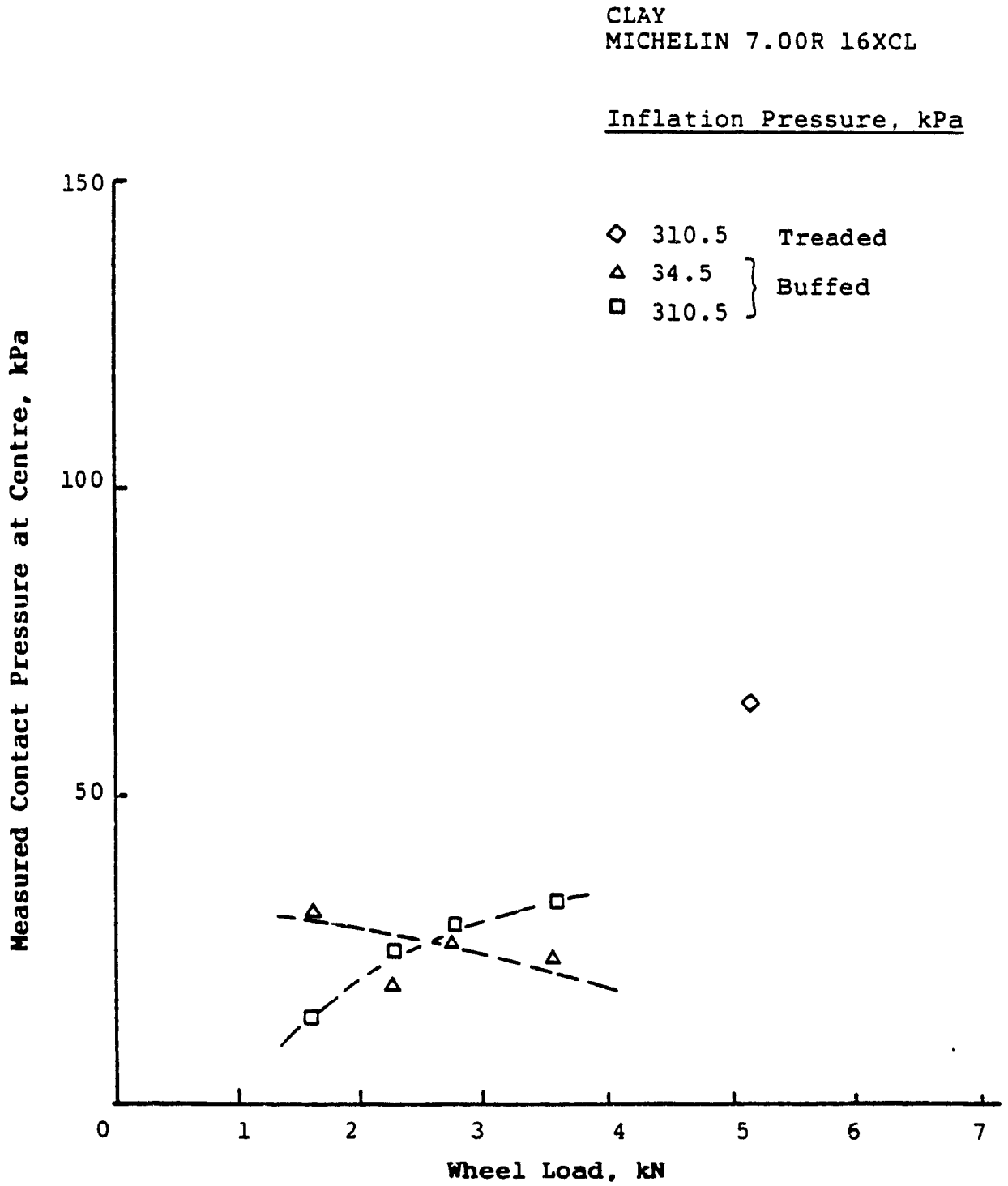


Fig. D.22b Variation of Contact Pressure (at Center) With Wheel Load for MICHELIN 7.00R-16XCL on Clay

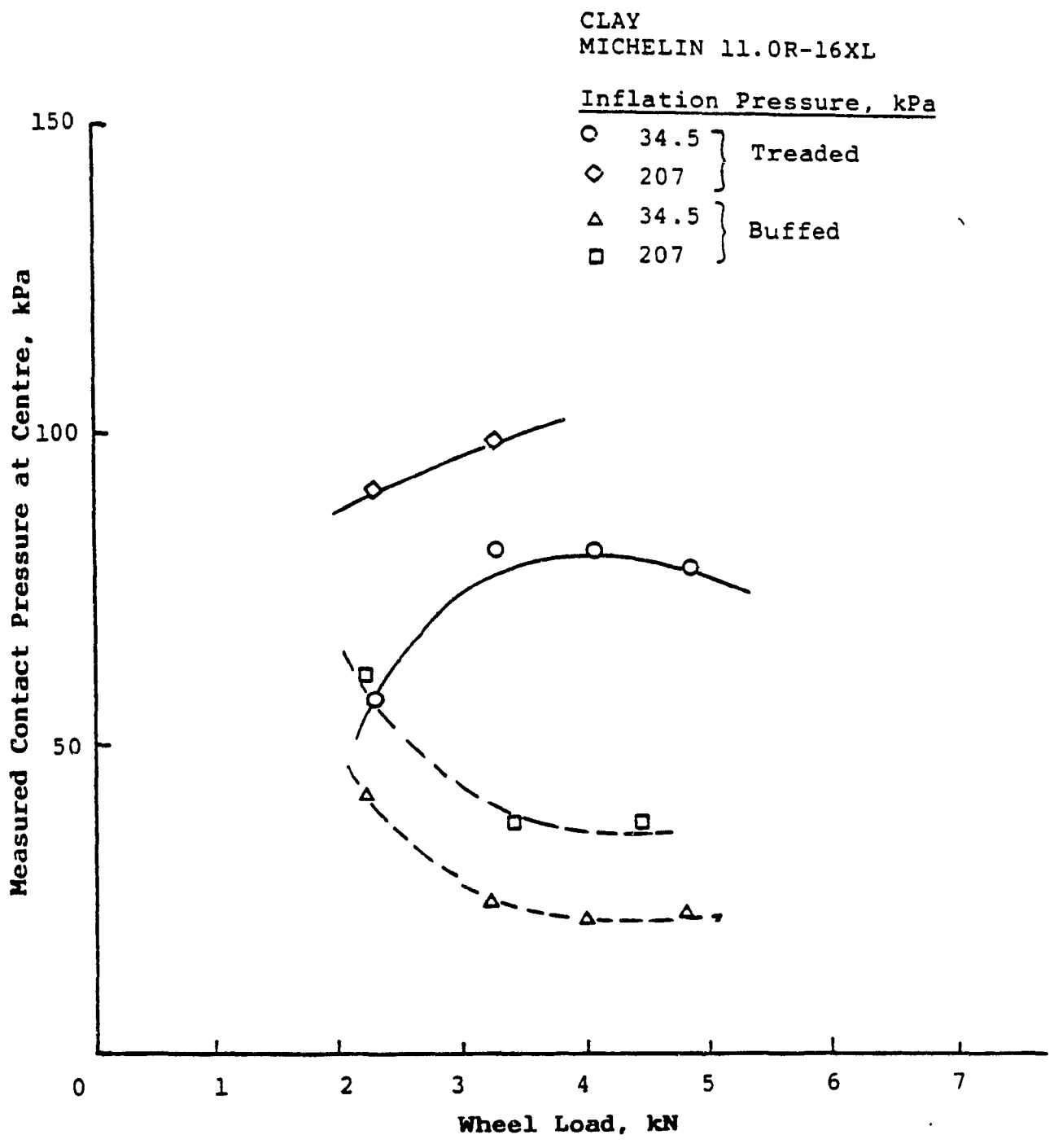


Fig. D.22c Variation of Contact Pressure (at Center) With Wheel Load for MICHELIN 11.00R-16XL on Clay

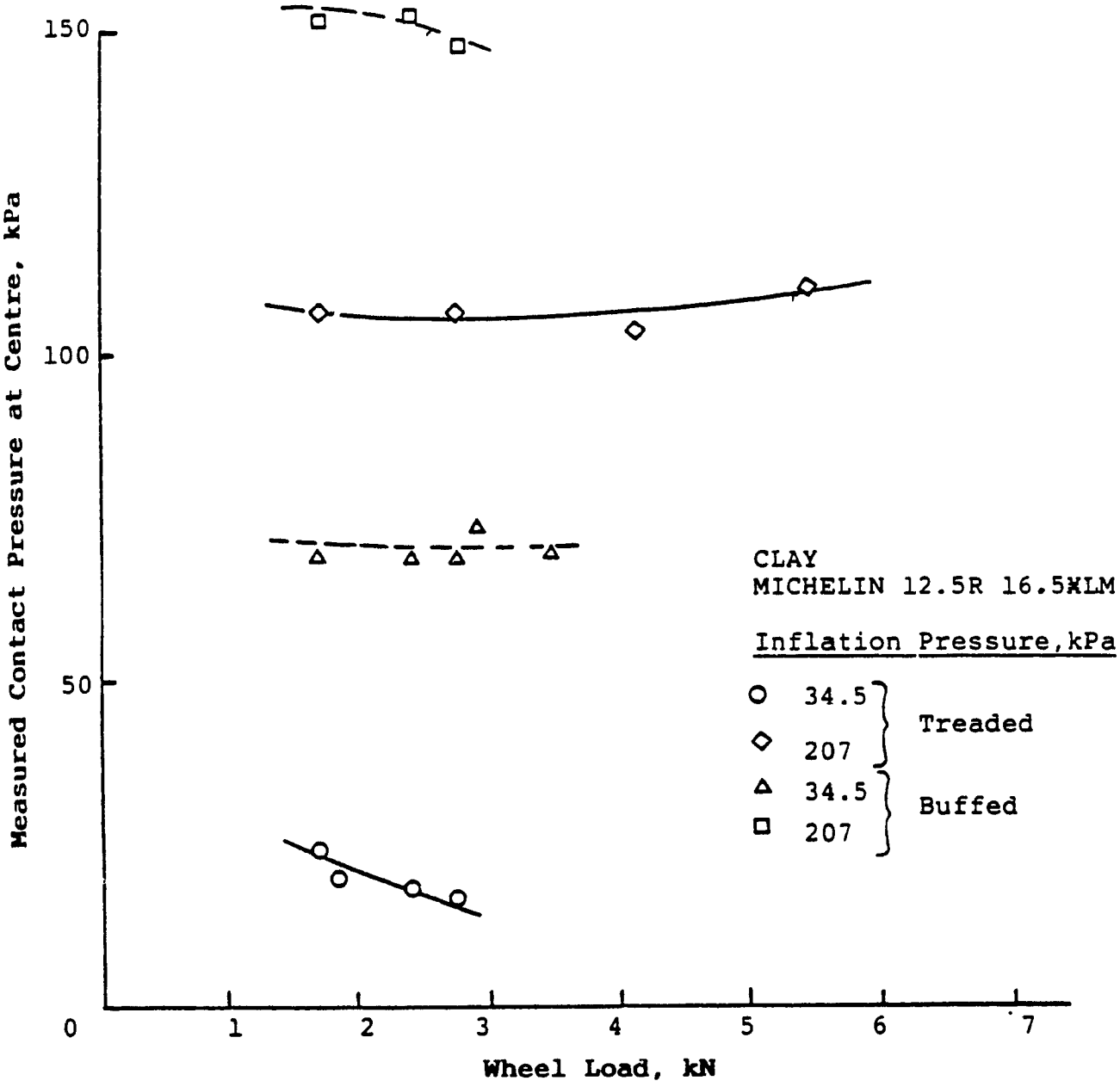


Fig. D.22d Variation of Contact Pressure (at Center) With Wheel Load For MICHELIN 12.5R-16.5XLM on Clay

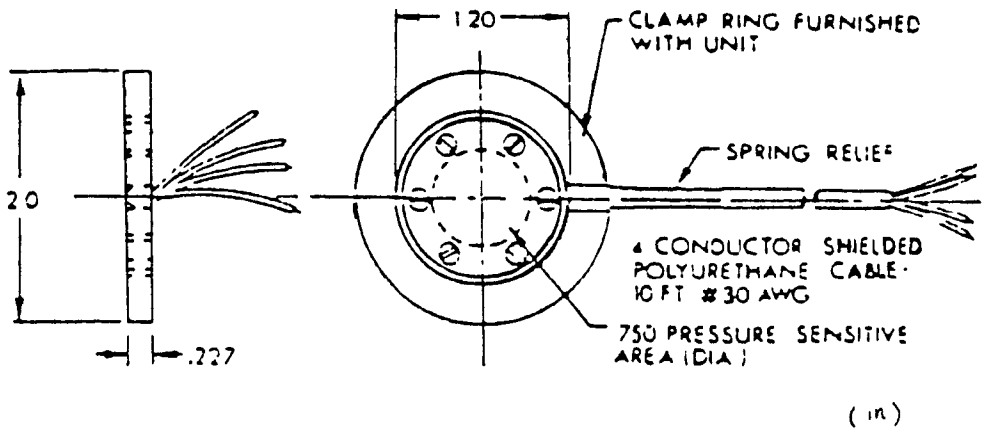


Fig. D.23 Descriptions of Soil Stress Gauge

APPENDIX E

Experimental Results on Tire-Sand Interactions

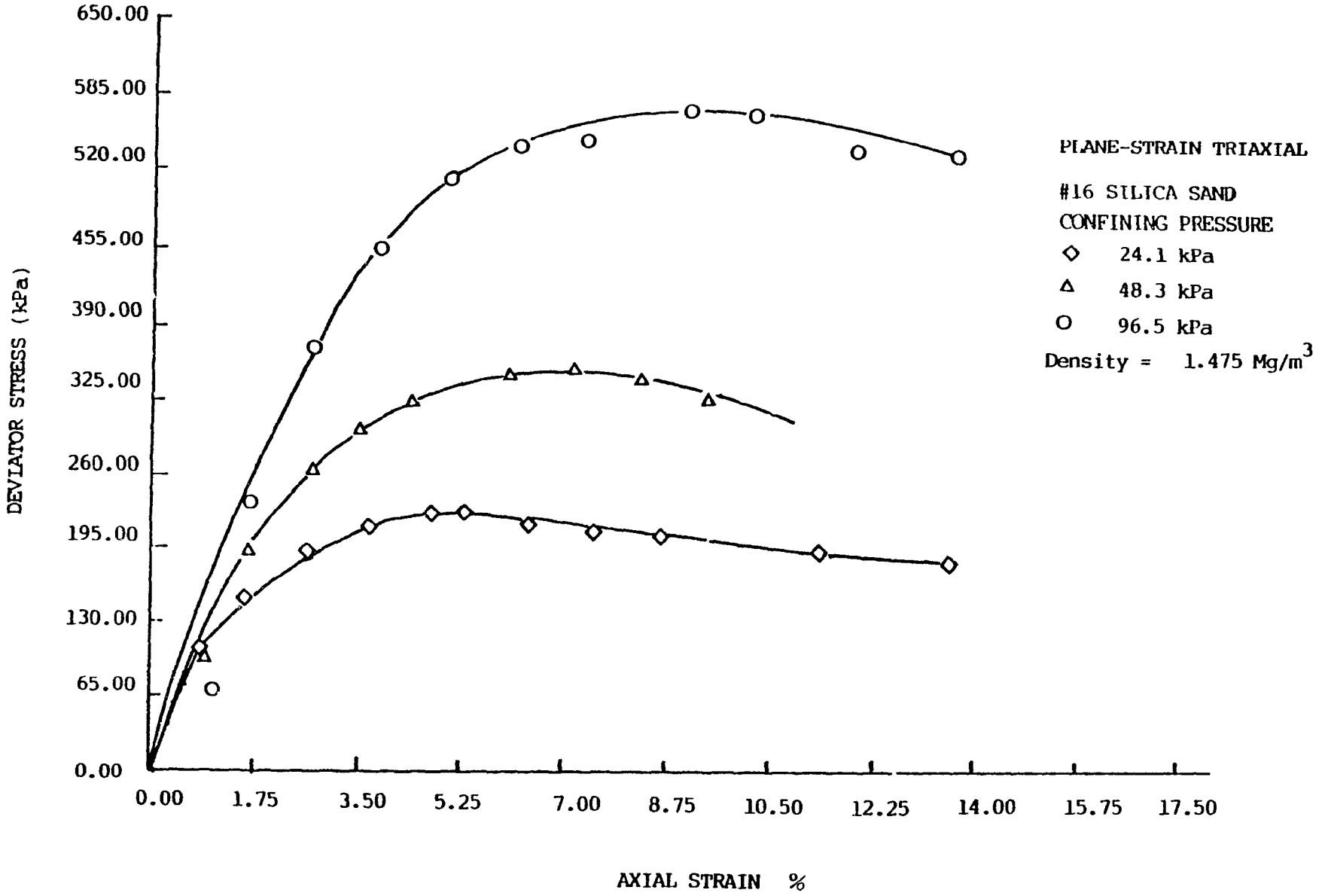


Fig. E.1 Stress-Strain Relationship of Silica Sand (Triaxial Test)

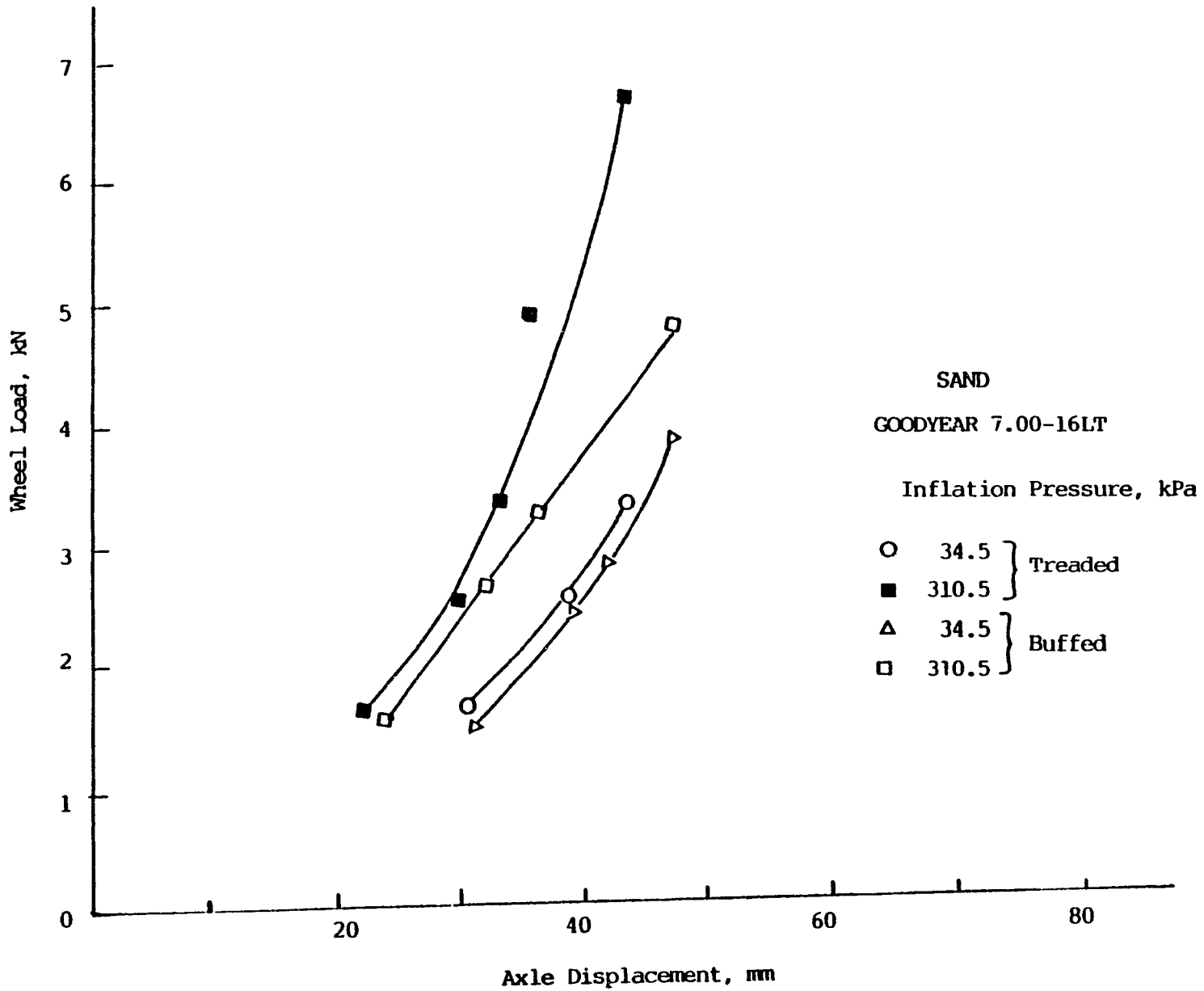


Fig. E.2a Load-Displacement Relationship of GOODYEAR 7.00-16LT on SAND

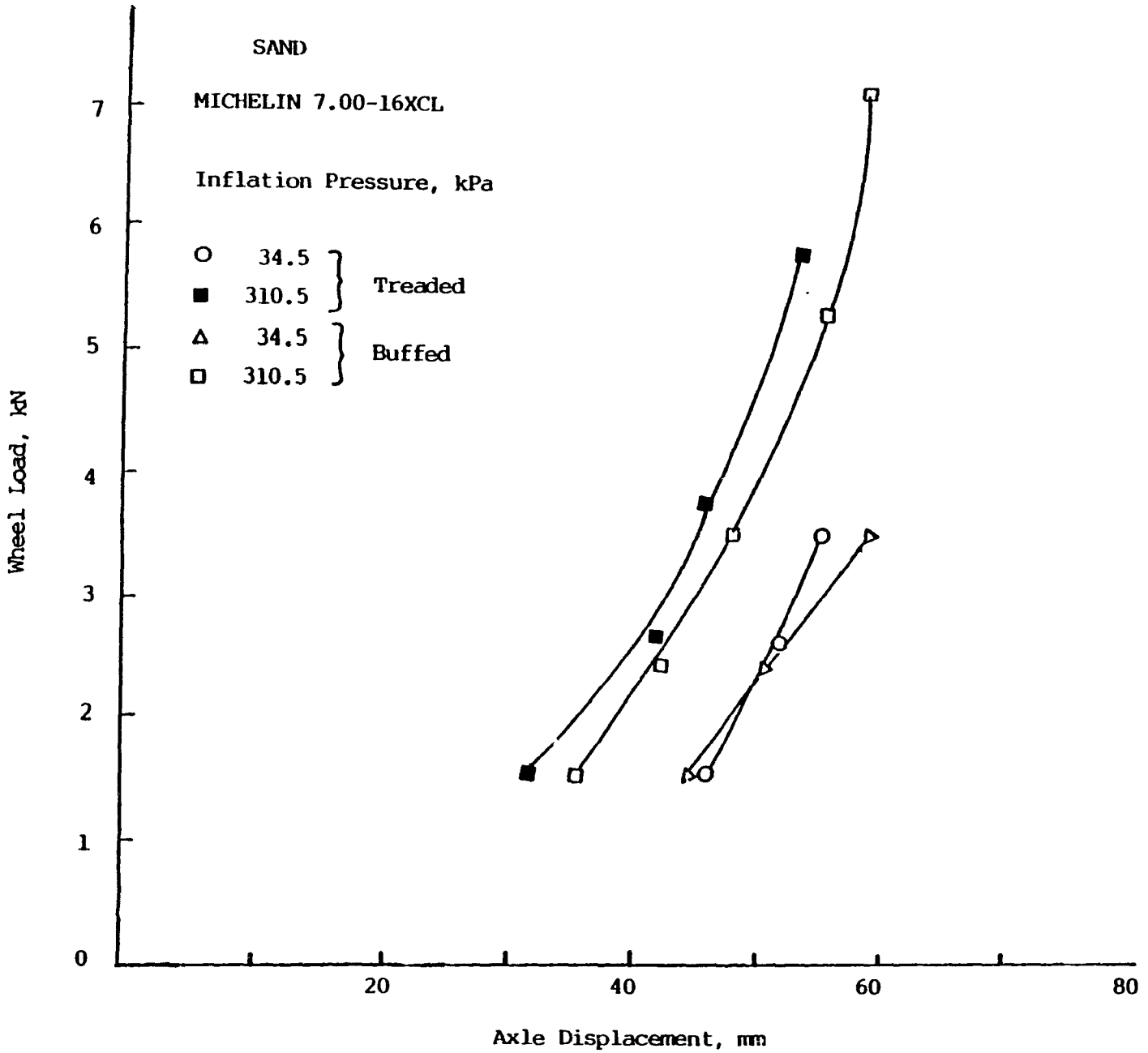


Fig. E.2b Load-Displacement Relationship of MICHELIN 7.00-16XCL on SAND

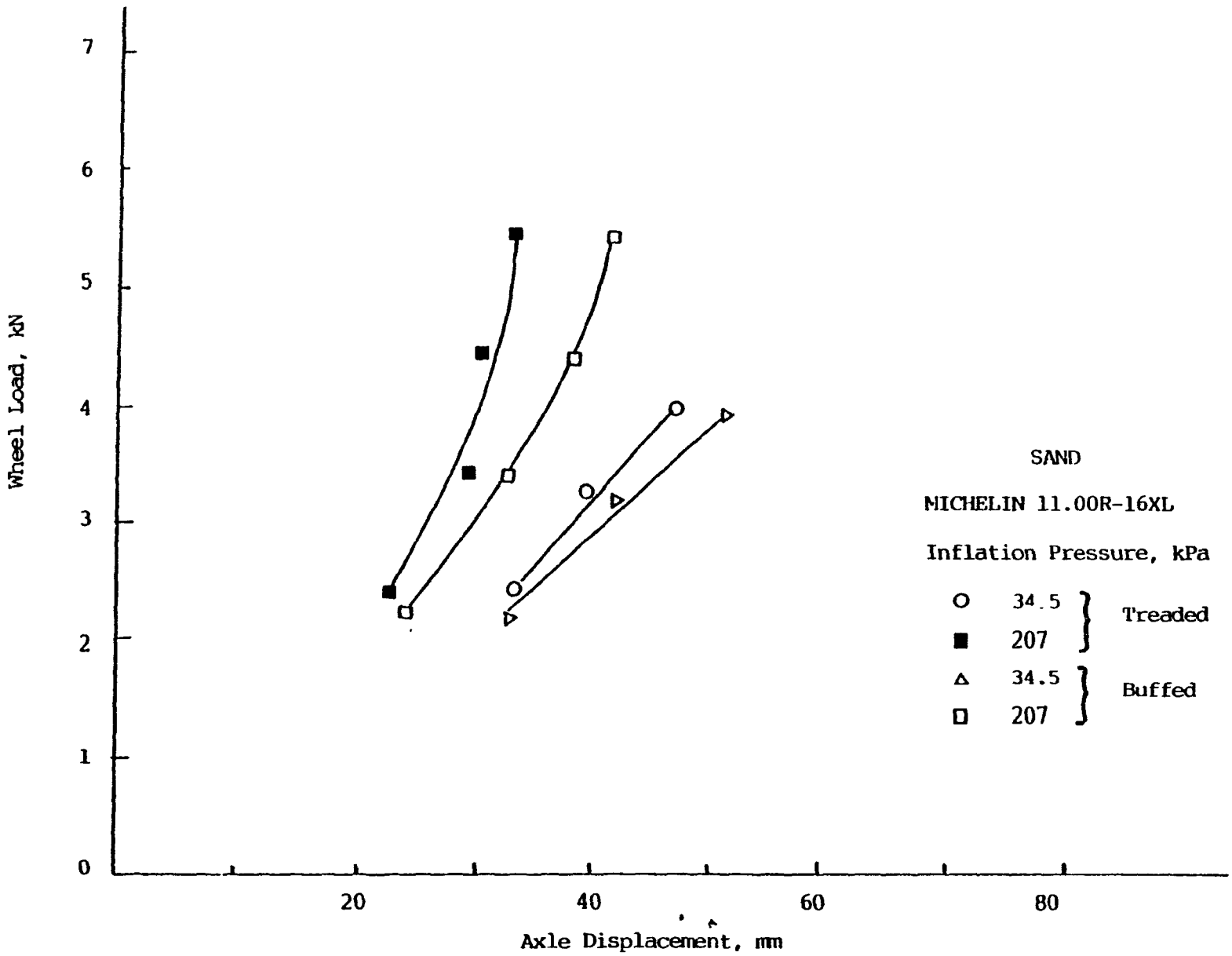


Fig. E.2c Load-Displacement Relationship of MICHELIN 11.00R-16XL on SAND

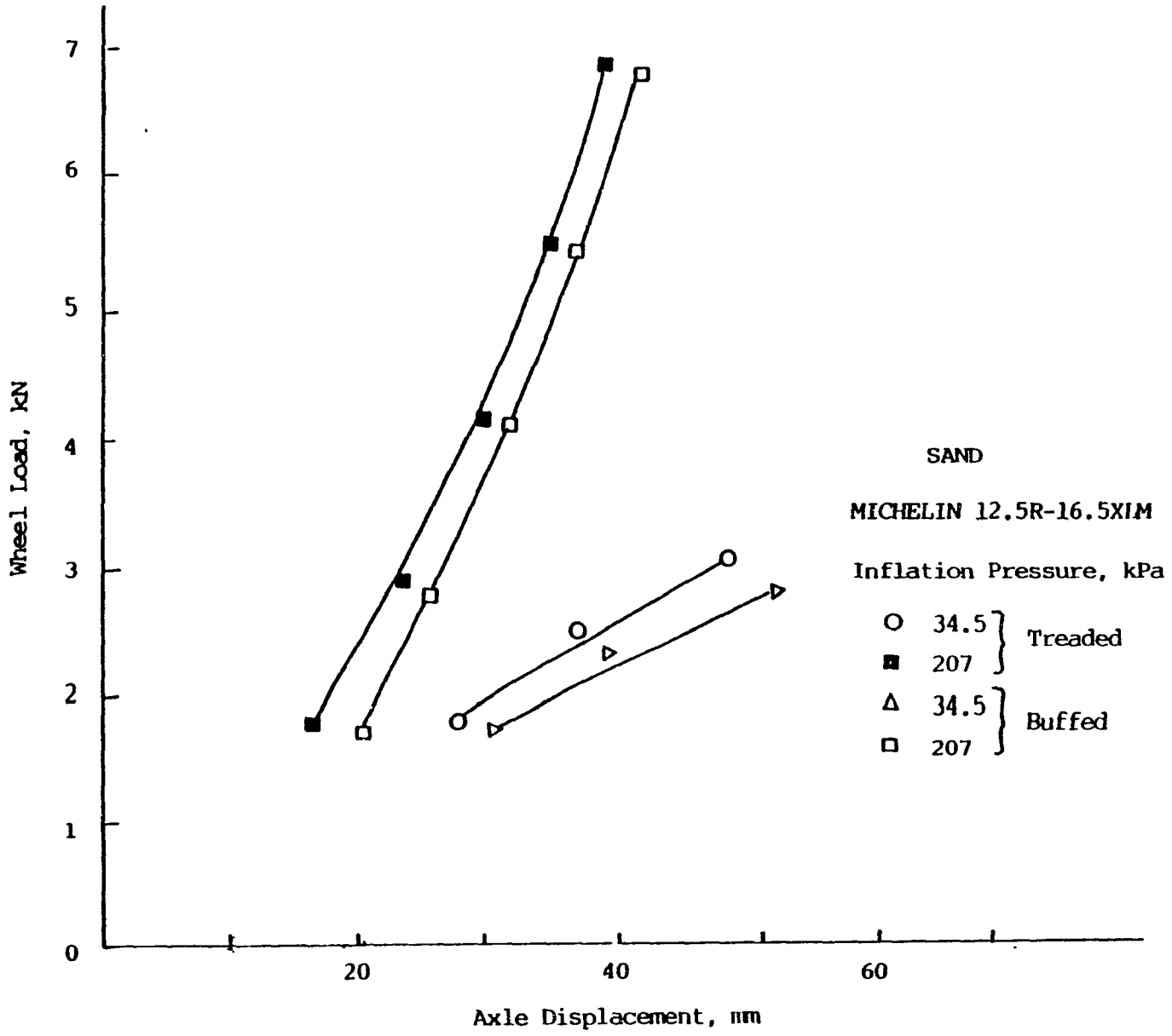


Fig. E.2d Load-Displacement Relationship of MICHELIN 12.5R-16.5XLM on SAND

TIRE	Inflation Pressure kPa	Wheel Load (W) kN	Measured Contact Area (A_T) mm^2	Representative Rectangular Contact Area		Average Contact Pressure (W/A_T) kPa	Fig. No.
				Width mm	Length mm		
GOODYEAR 7.00-16Lt (treaded)	34.5	3.548	59400	180	330	59.7	E.3a-b
	310.5	3.548	48280	170	284	73.5	E.4a-b
GOODYEAR 7.00-16LT (buffed)	34.5	2.467	64416	176	366	38.3	E.5a-b
	310.5	2.653	49000	140	350	54.2	E.6a-b
MICHELIN 7.00R-16XCL (treaded	34.5	2.507	82680	156	530	30.3	E.7a-b
	310.5	2.507	44928	144	312	55.8	E.8a-b
MICHELIN 7.00R-16XCL (buffed)	34.5	2.489	56472	156	362	44.4	E.9a-b
	310.5	2.676	42032	148	284	64.1	E.10a-b
MICHELIN 11.0-16XL (treaded)	34.5	4.043	92008	212	434	43.9	E.11a-b
	207.0	4.489	81700	215	380	54.9	E.12a-b
MICHELIN 11.00R-16XL (buffed)	34.5	4.003	111104	248	448	36.0	E.13a-b
	207.0	4.448	100536	236	426	44.2	E.14a-b
MICHELIN 12.5R-16.5XLM (treaded)	34.5	2.841	75264	196	384	37.7	E.15a-b
	207.0	2.841	74108	194	382	38.3	E.16a-c
MICHELIN 12.5R-16XLM (buffed)	34.5	2.765	86940	210	414	31.8	E.17a-b
	207.0	2.765	58464	168	348	47.3	E.18a-b

TABLE E.1 Data on Contact Area in Sand

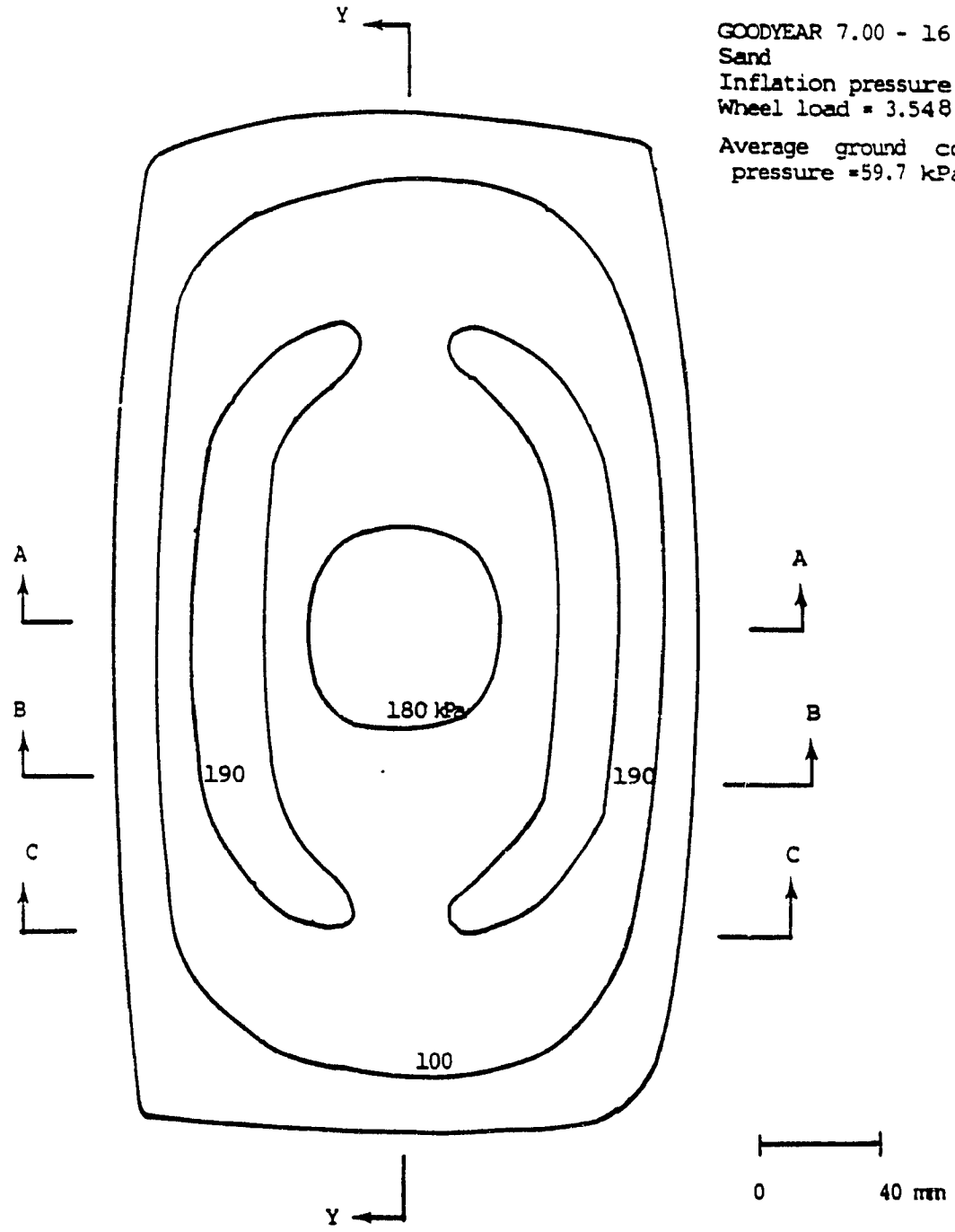
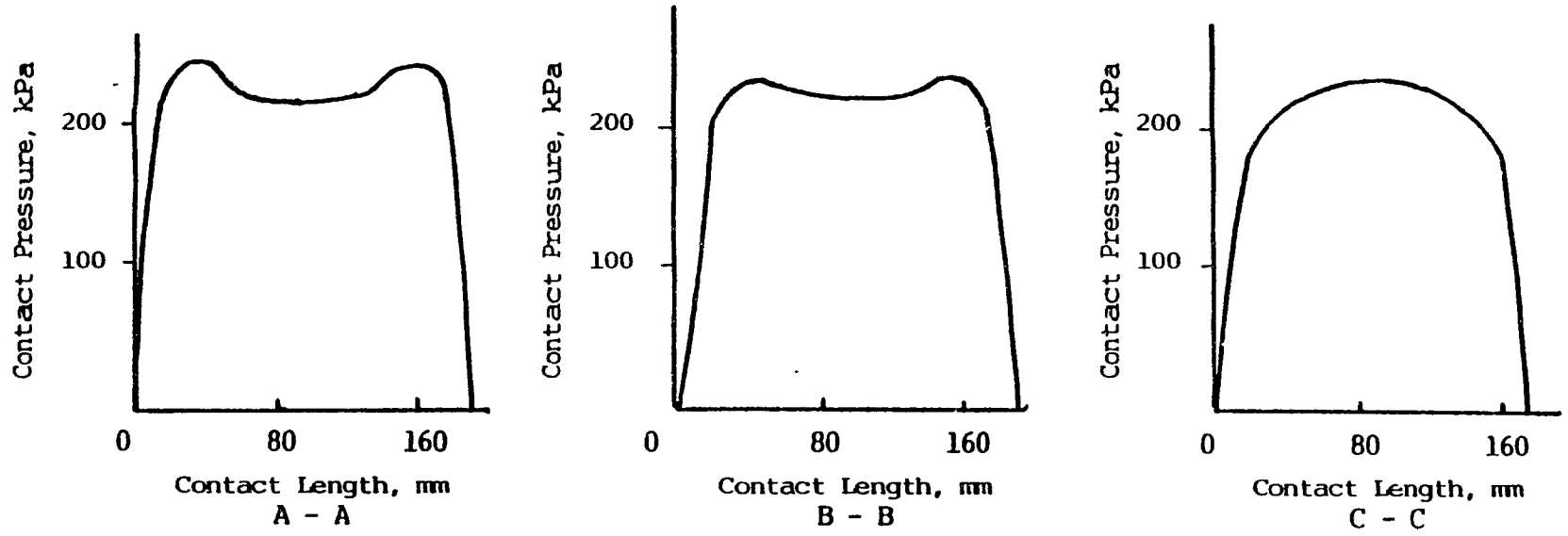
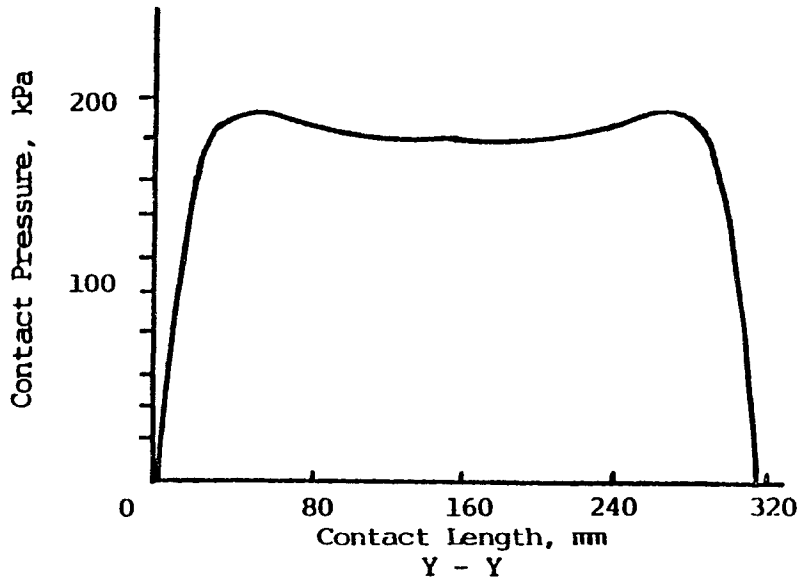


Fig. E.3a Isobars of Pressure Distribution Within the Footprint of GOODYEAR 7.00-16LT (treaded) in Sand





GOODYEAR 7.00 - 16 LT (treaded)
Sand
Inflation pressure = 34.5 kPa
Wheel load = 3.548 kN

Fig. E.3b Profiles of Pressure Distribution Within the Footprint of GOODYEAR 7.00-16LT (treaded) in Sand

GOODYEAR 7.00 - 16 LT (treaded)
Sand
Inflation pressure = 310.5 kPa
Wheel load = 3.548 kN
Average ground contact pressure = 73.5 kPa

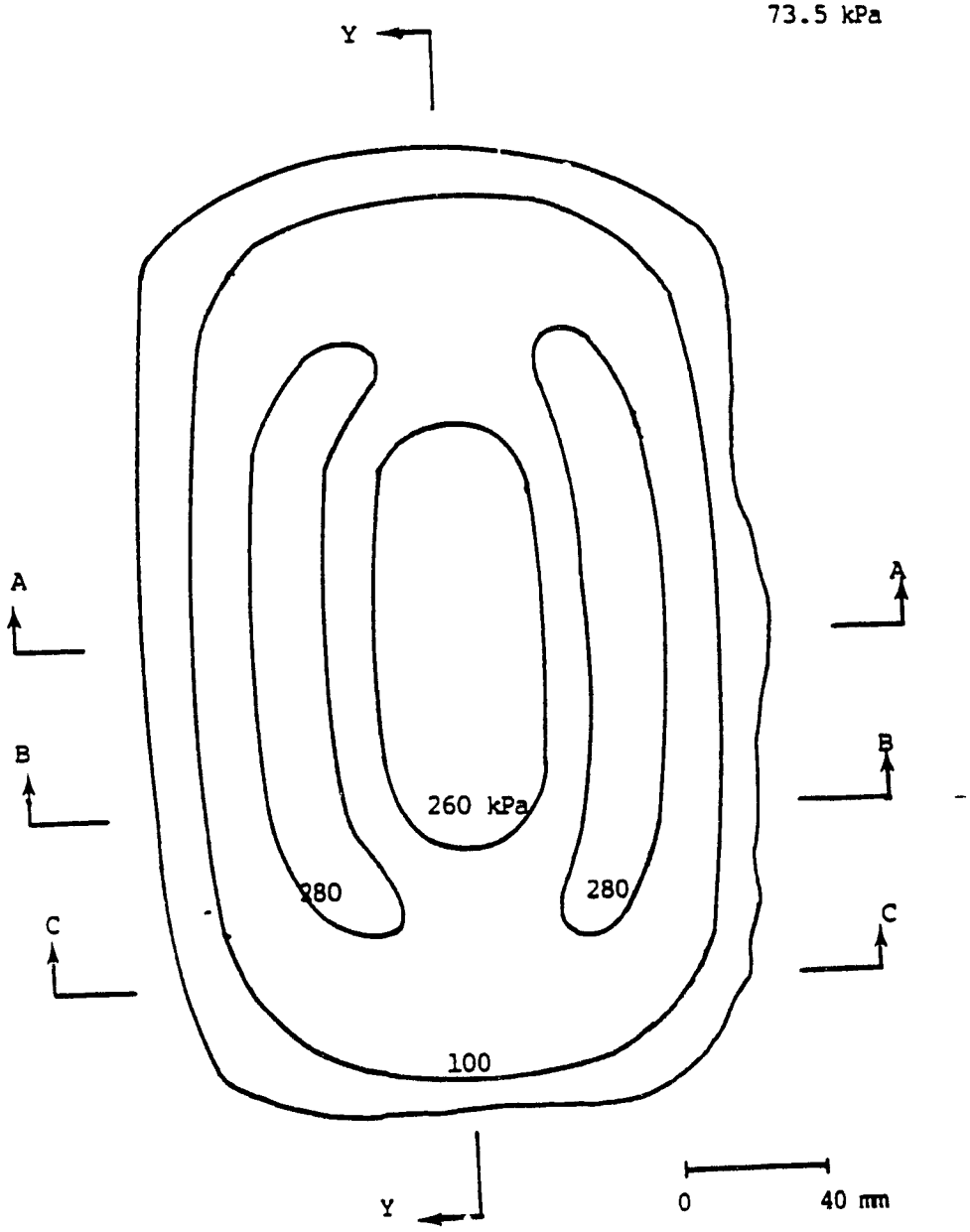


Fig. E.4a Isobars of Pressure Distribution Within the Footprint of GOODYEAR 7.00-16LT (treaded) in Sand

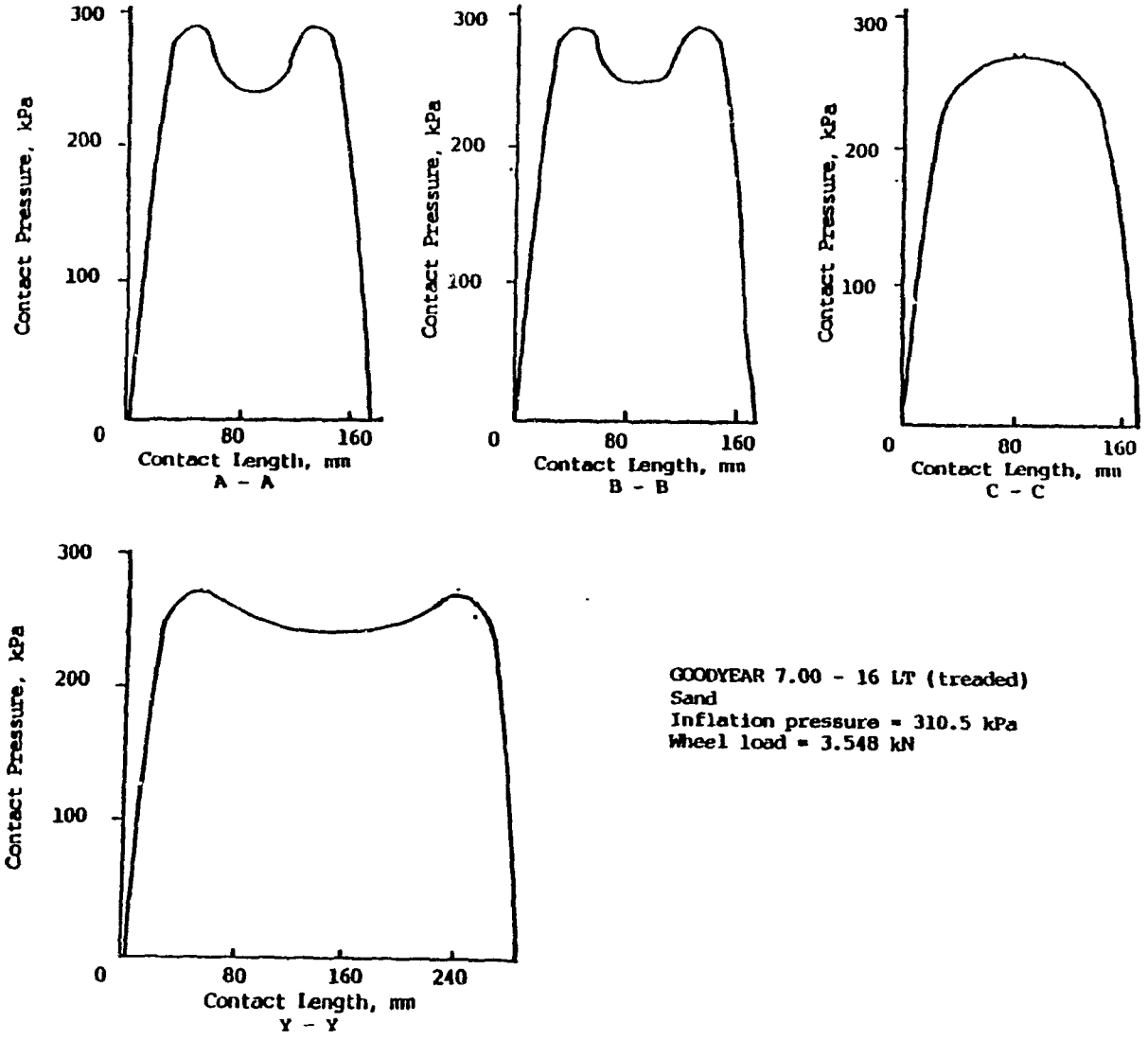


Fig. E.4b Profiles of Pressure Distribution Within the Footprint of GOODYEAR 7.00-16LT (treaded) in Sand

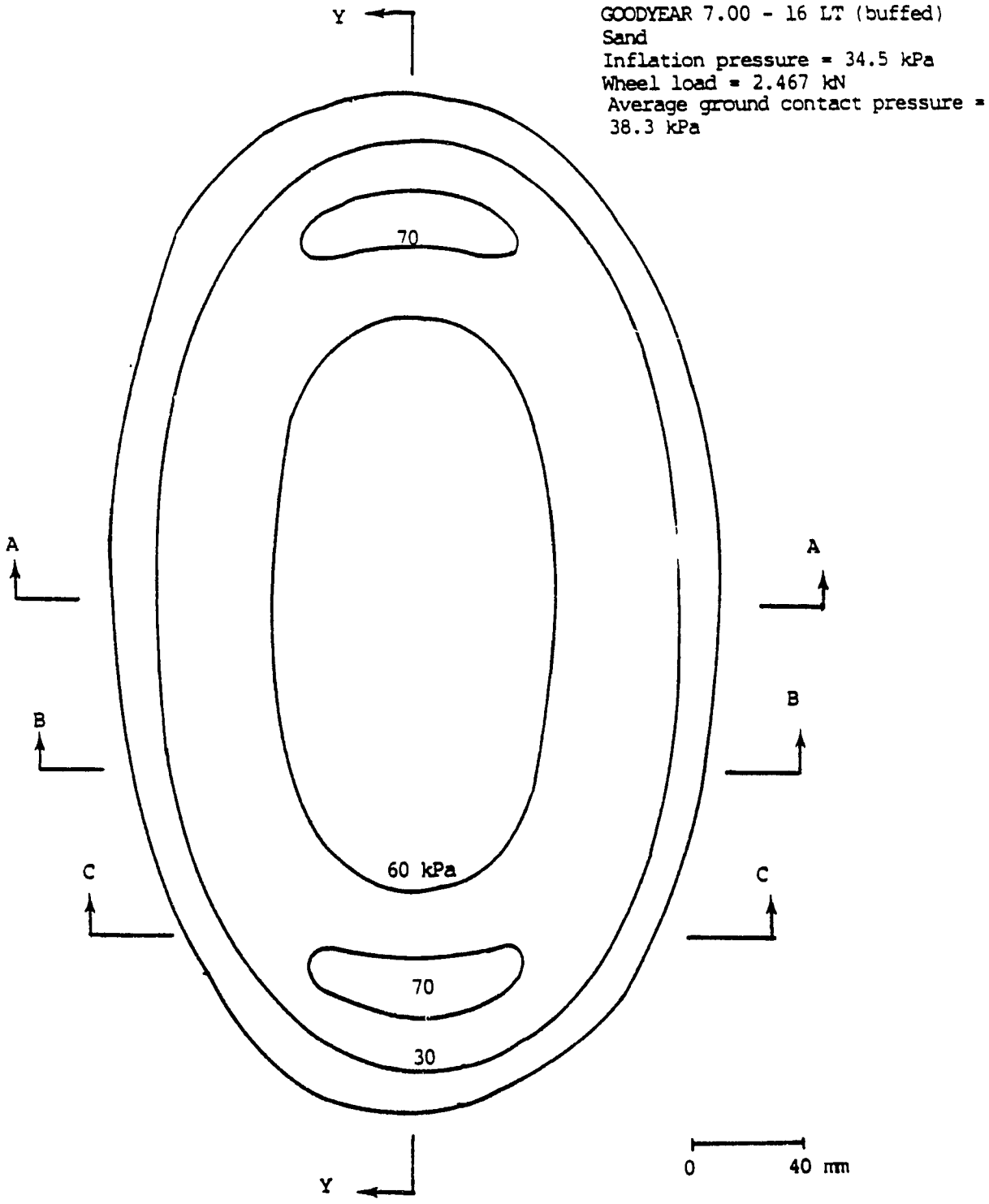
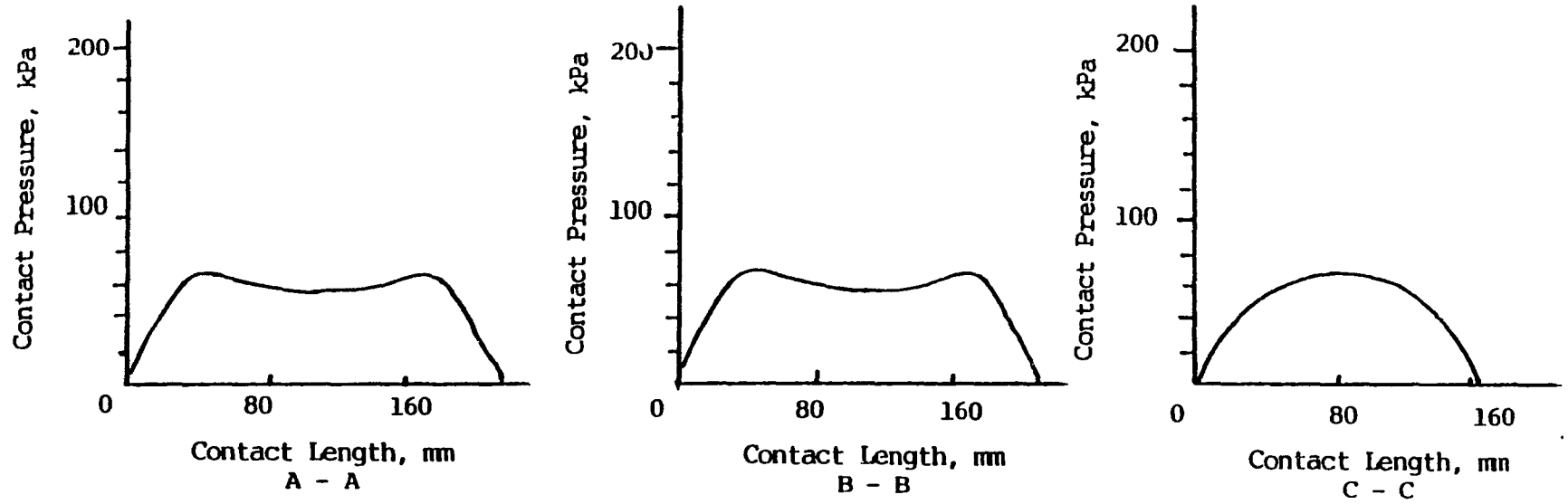
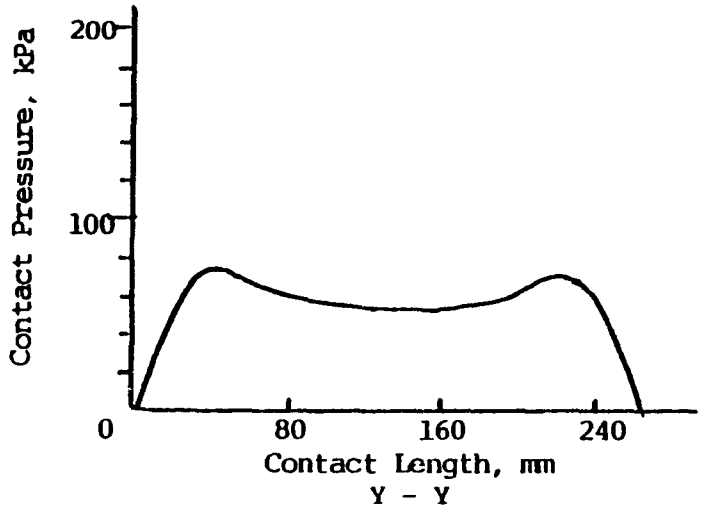


Fig. E.5a Isobars of Pressure Distribution Within the Footprint of GOODYEAR 7.00-16LT (buffed) in Sand





GOODYEAR 4.00 - 16 LT (buffed)
Sand
Inflation pressure =34.5 kPa
Wheel load = 2.467 kN

Fig. E.5b Profiles of Pressure Distribution Within the Footprint of GOODYEAR 7.00-16LT (buffed) in Sand

GOODYEAR 7.00 - 16 LT (buffed)
Sand
Inflation pressure = 310.5 kPa
Wheel load = 2.653 kN
Average ground contact pressure = 54.2 kPa

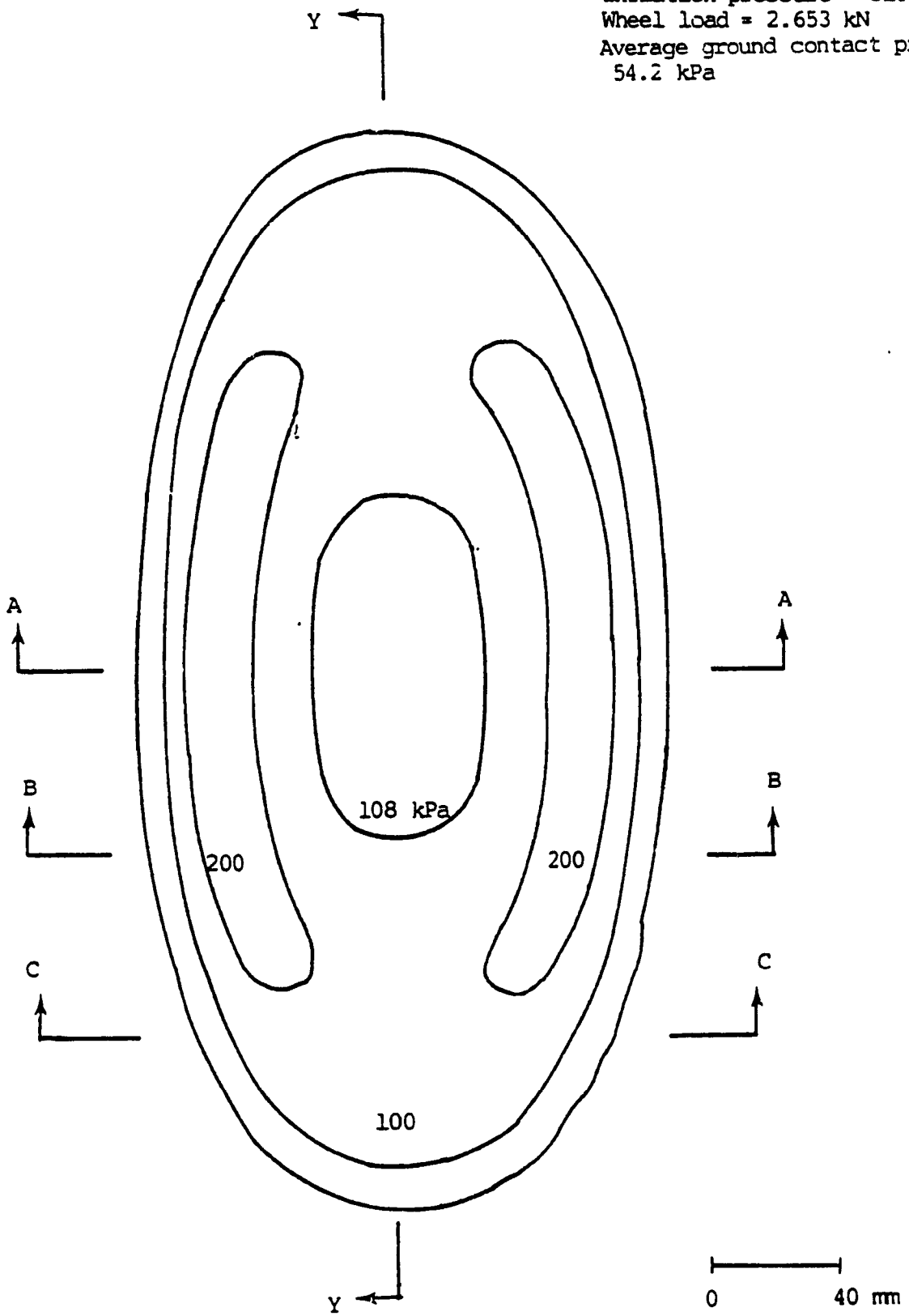


Fig. E.6a Isobars of Pressure Distribution Within the Footprint of GOODYEAR 7.00-16LT (buffed) in Sand

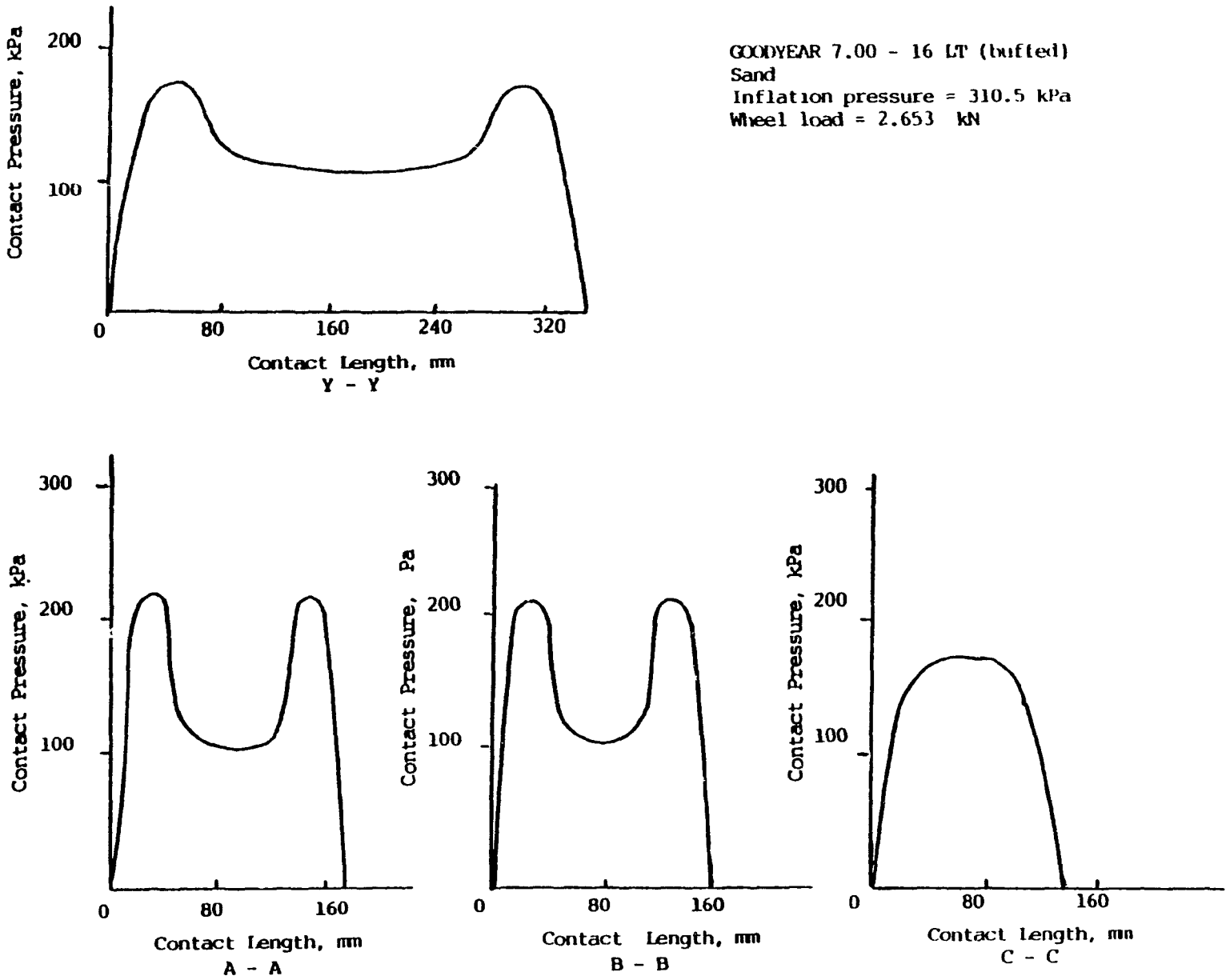


Fig. E.6 b Profiles of Pressure Distribution within the Footprint of GOODYEAR 7.00-16LT (buffed) in Sand

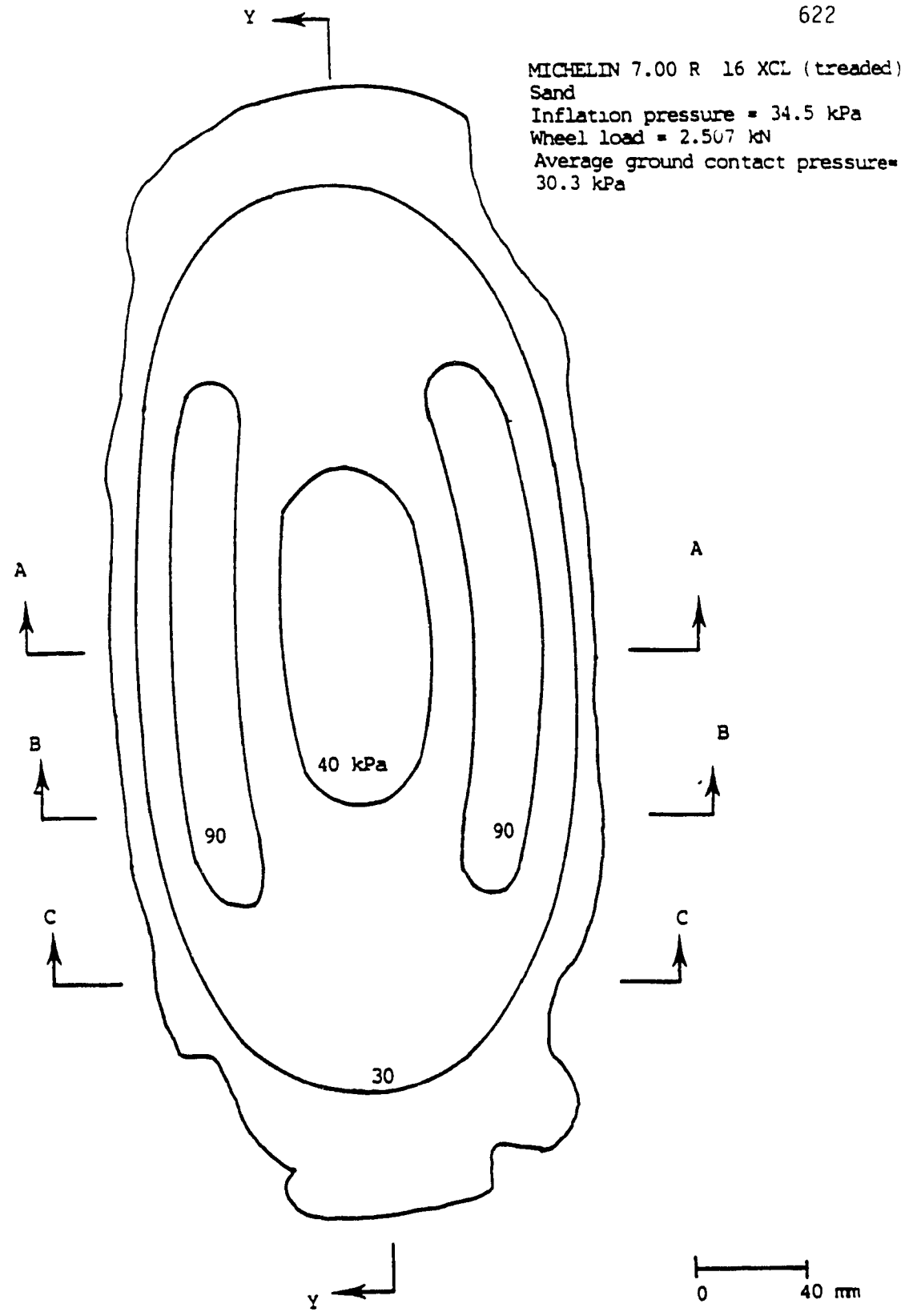


Fig. E.7a Isobars of Pressure Distribution Within the Footprint of MICHELIN 7.00R-16XCL (treaded) in Sand

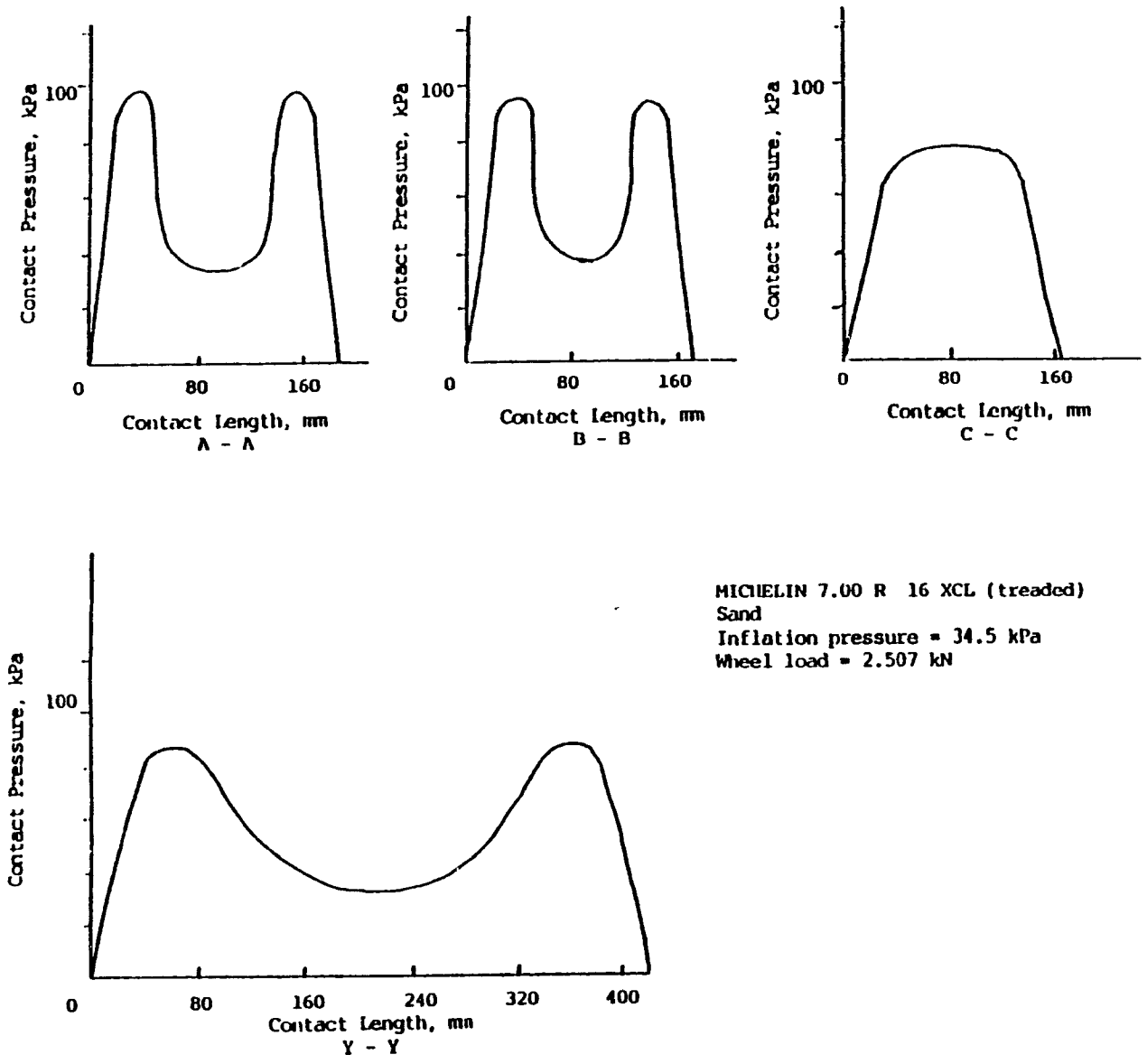


Fig. E.7b Profiles of Pressure Distribution Within the Footprint of MICHELIN 7.00R-16XCL (treaded) in Sand

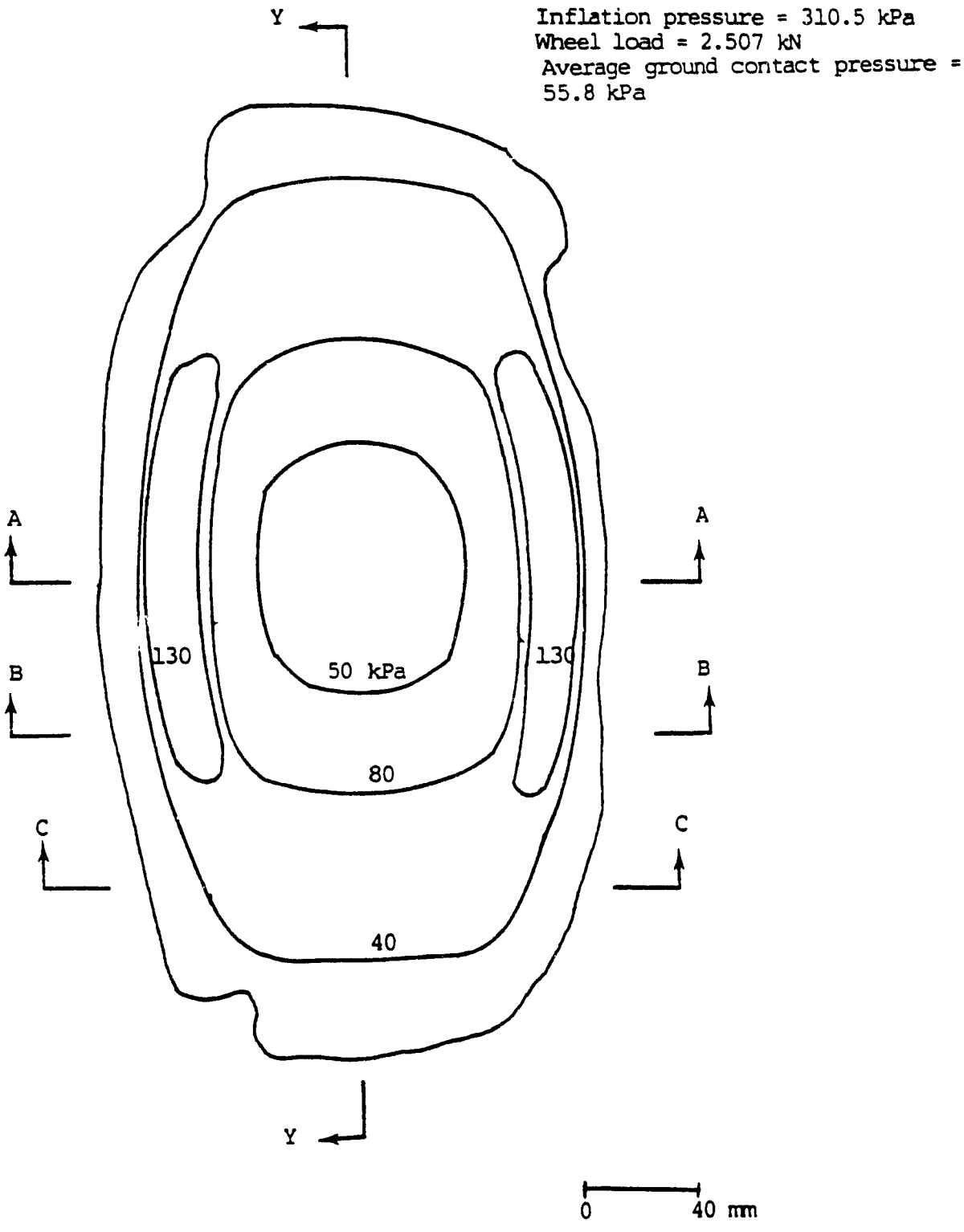


Fig. E.8a Isobars of Pressure Distribution Within the Footprint of MICHELIN 7.00R-16XCL (treaded) in Sand

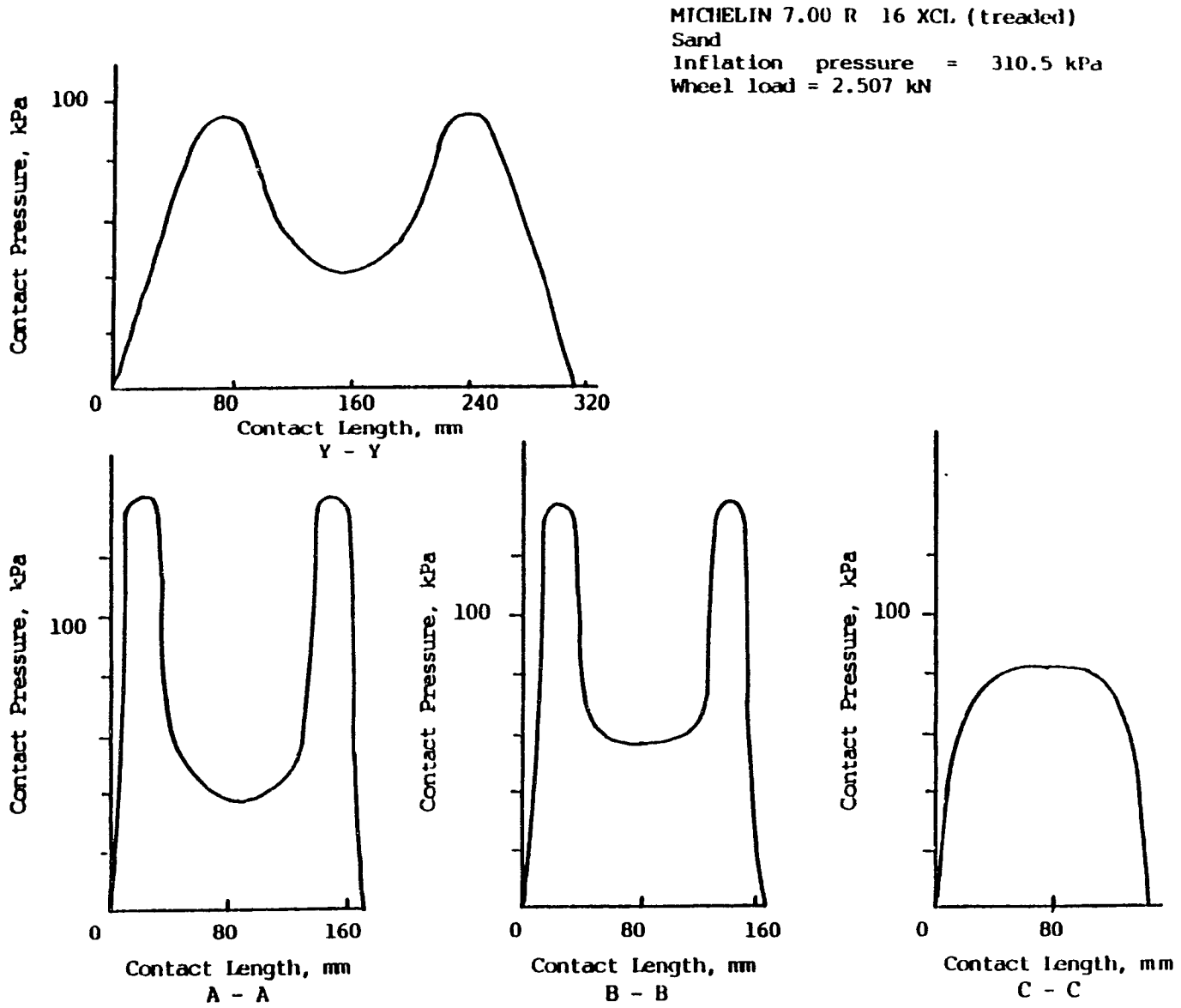


Fig. E.8b Profiles of Pressure Distribution Within the Footprint of MICHELIN 7.00R-16XCL (treaded) in Sand

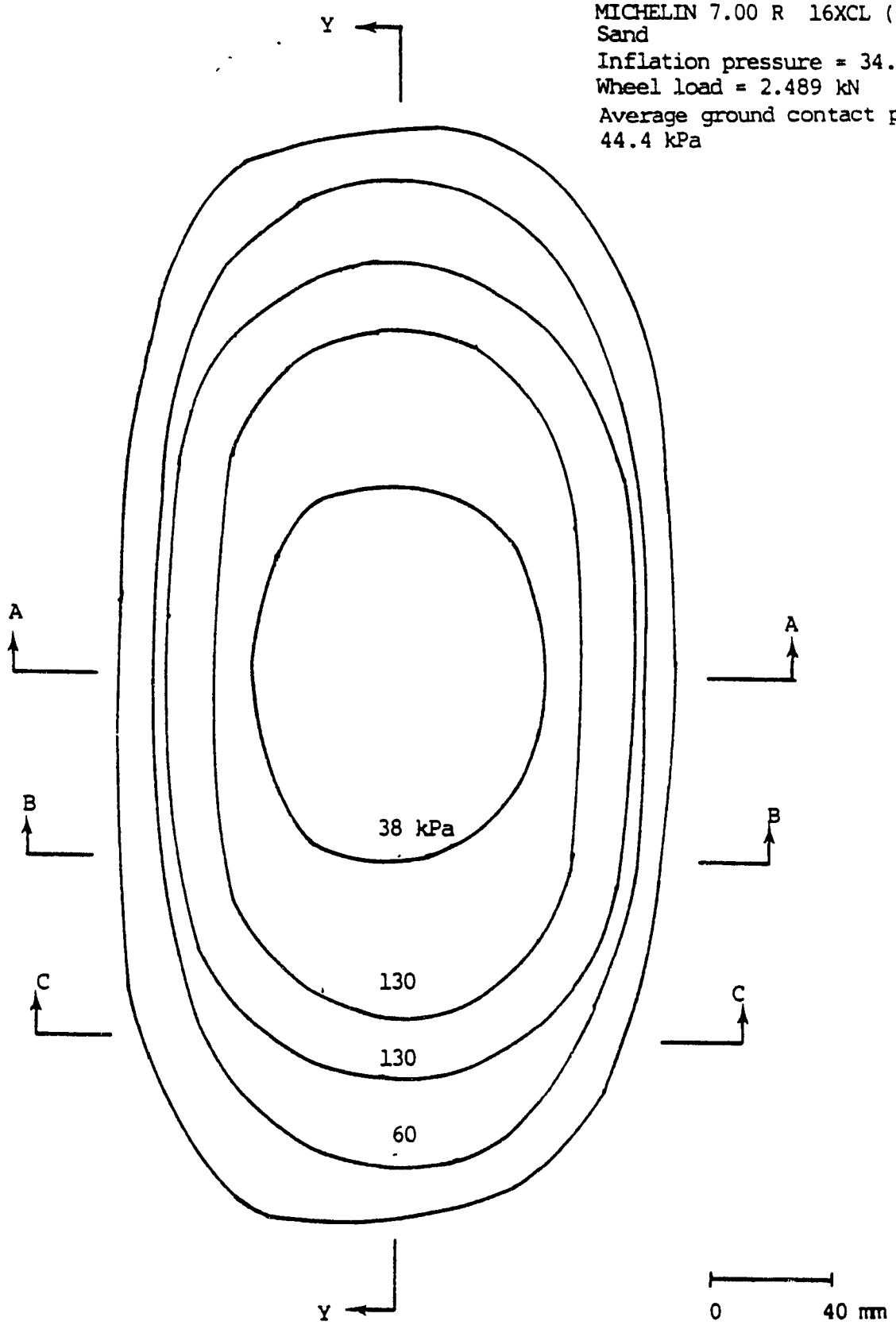


Fig. E.9a Isobars of Pressure Distribution Within the Footprint of MICHELIN 7.00-16XCL (buffed) in Sand

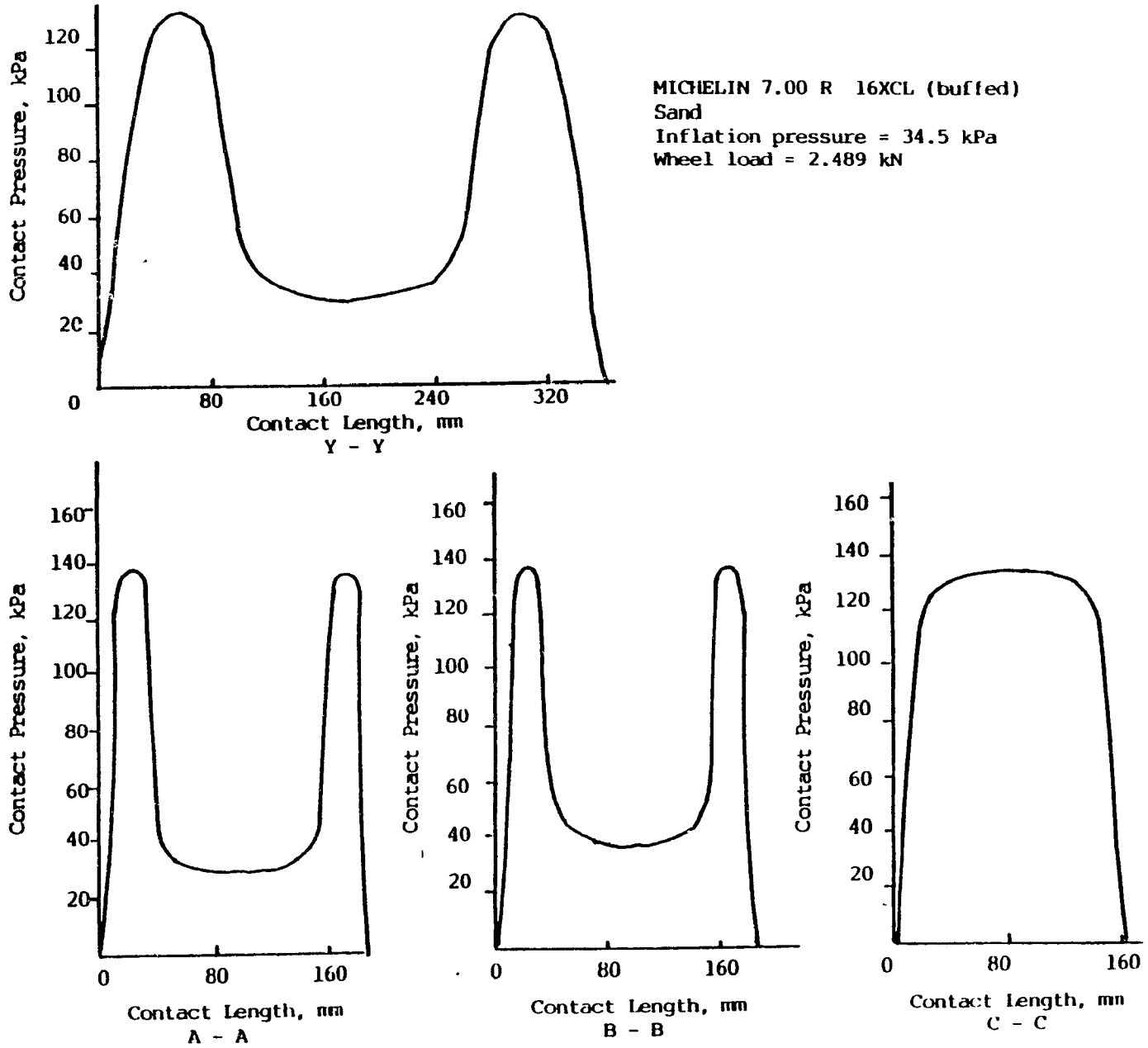


Fig. E.9b Profiles of Pressure Distribution Within the Footprint of MICHELIN 7.00R-16XCL (buffed) in Sand

MICHELIN 7.00 R 16 XCL (buffed)
SAND
Inflation pressure = 310.5 kPa
Wheel load = 2.676 kN

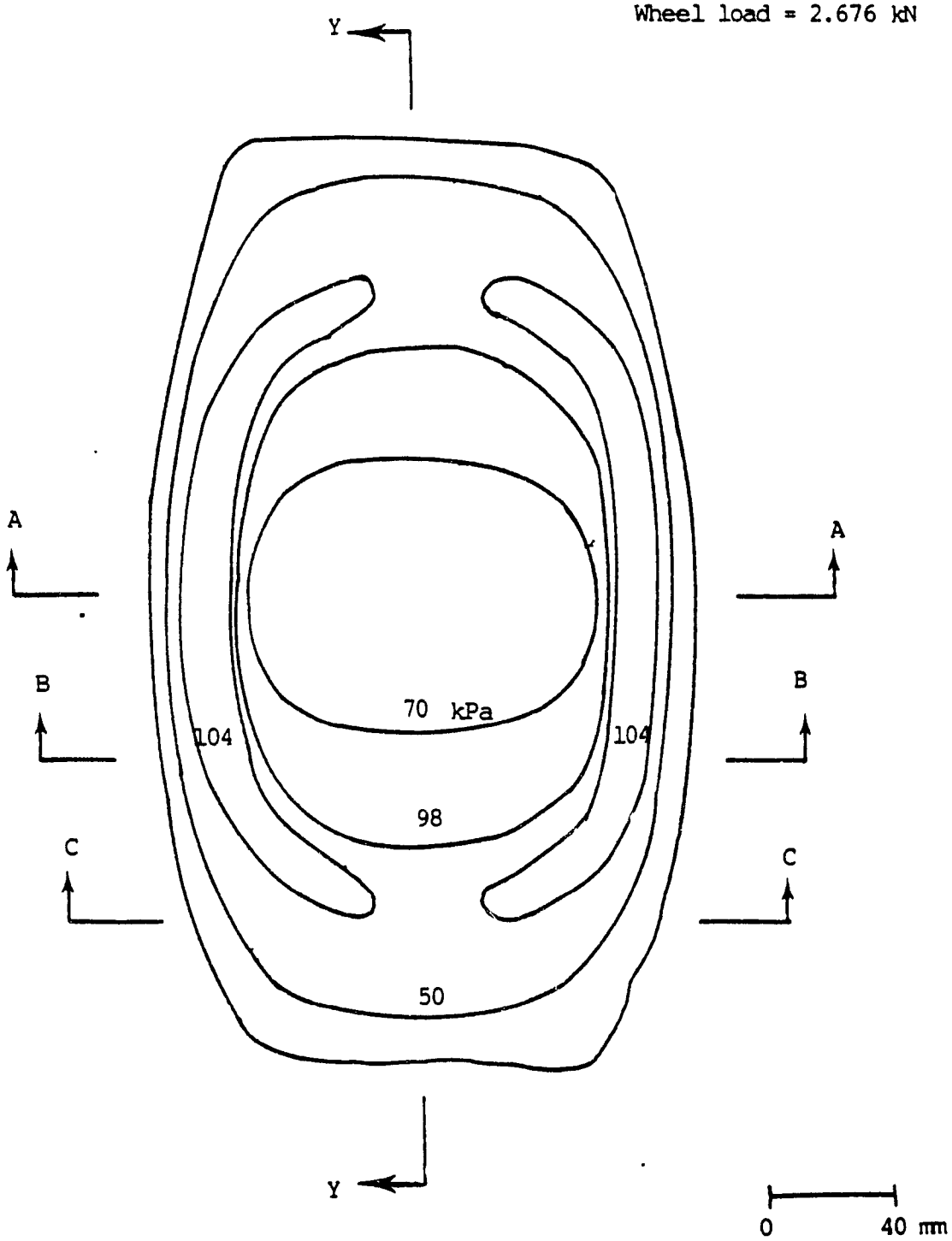


Fig. E.10a Isobars of Pressure Distribution Within the Footprint of MICHELIN 7.00R-16XCL (buffed) in Sand

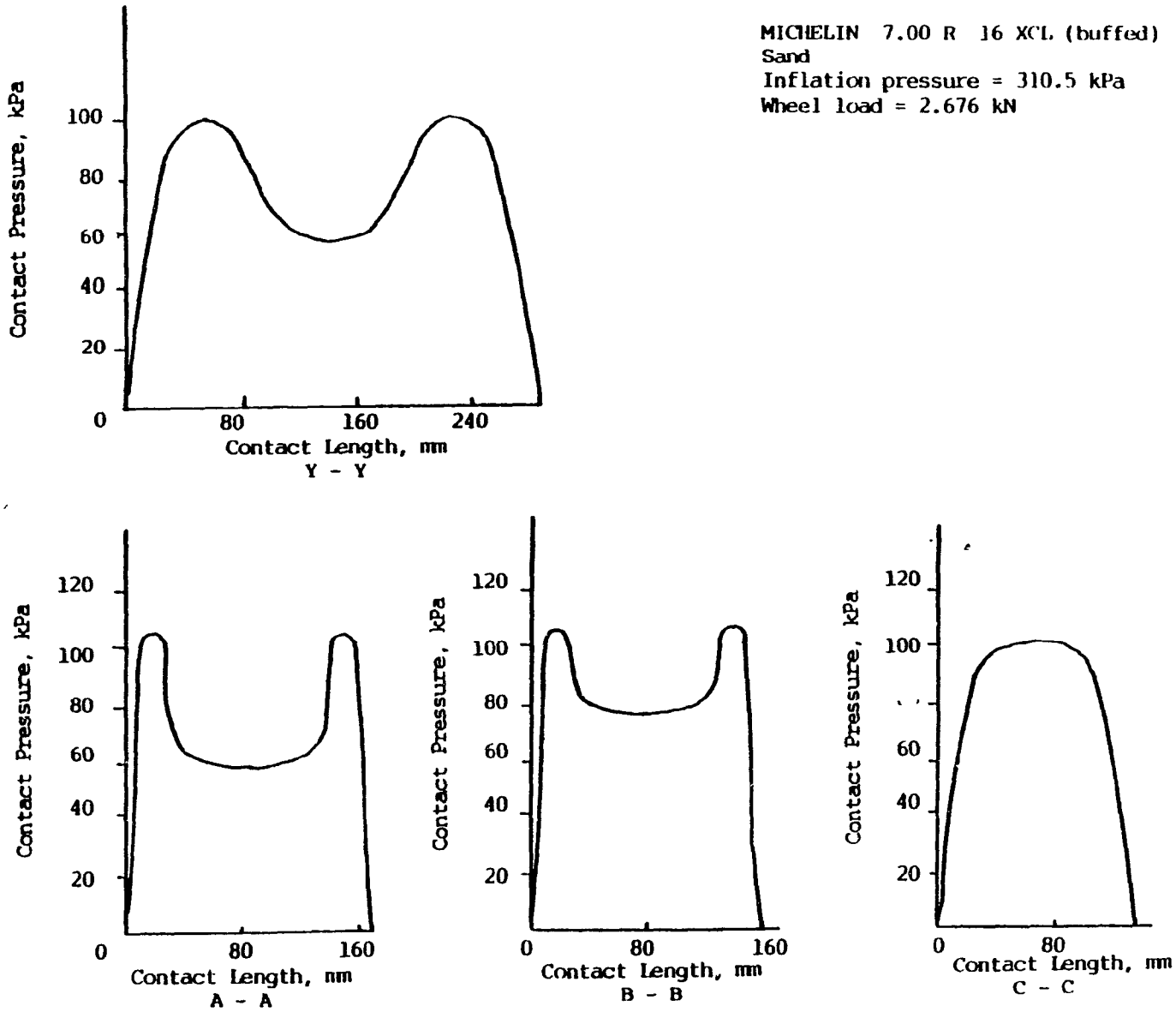


Fig. E.10b Profiles of Pressure Distribution Within the Footprint of MICHELIN 7.00R-16XCL (buffed) in Sand

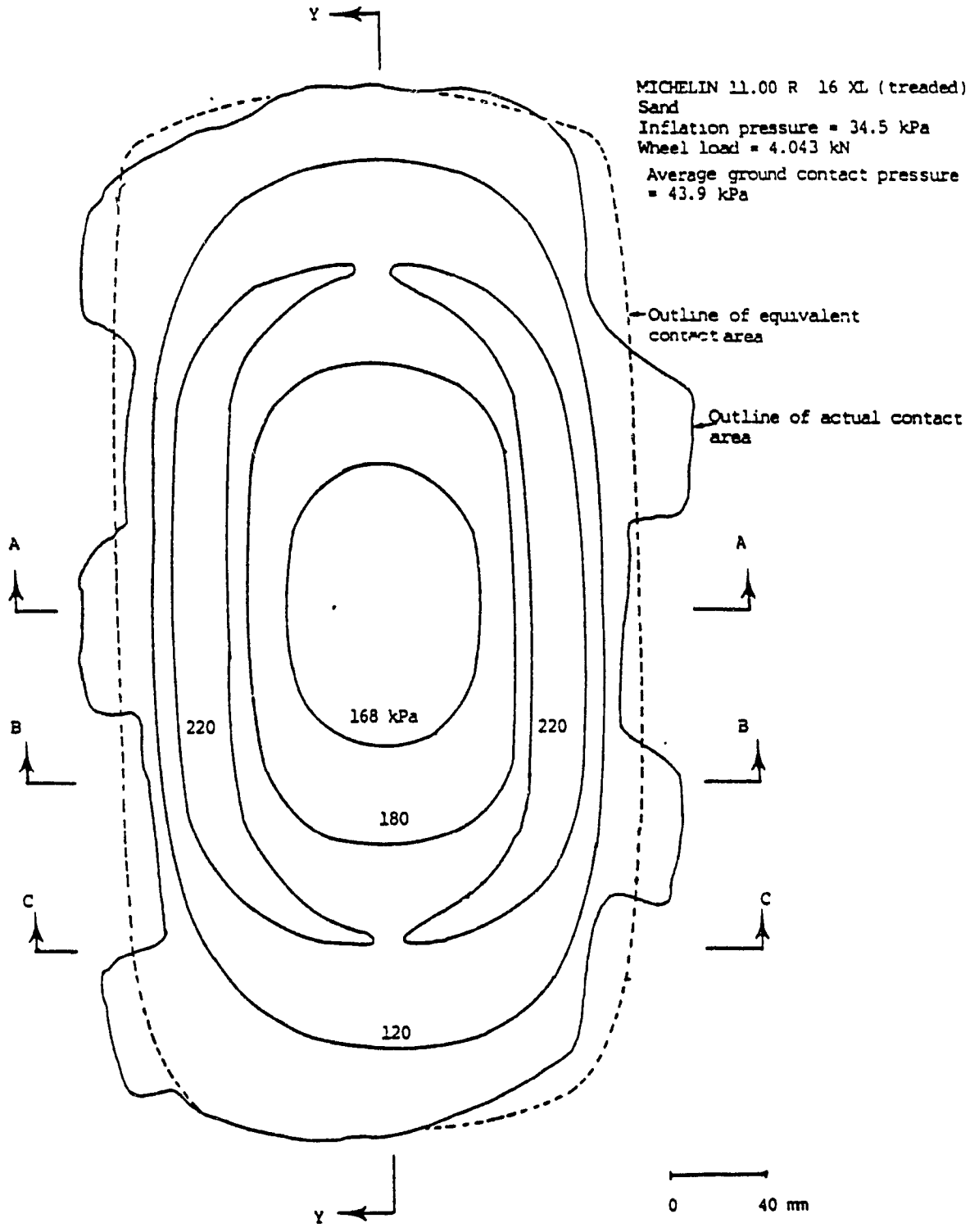


Fig. E.11a Isobars of Pressure Distribution Within the Footprint of MICHELIN 11.00R-16XL (treaded) in Sand

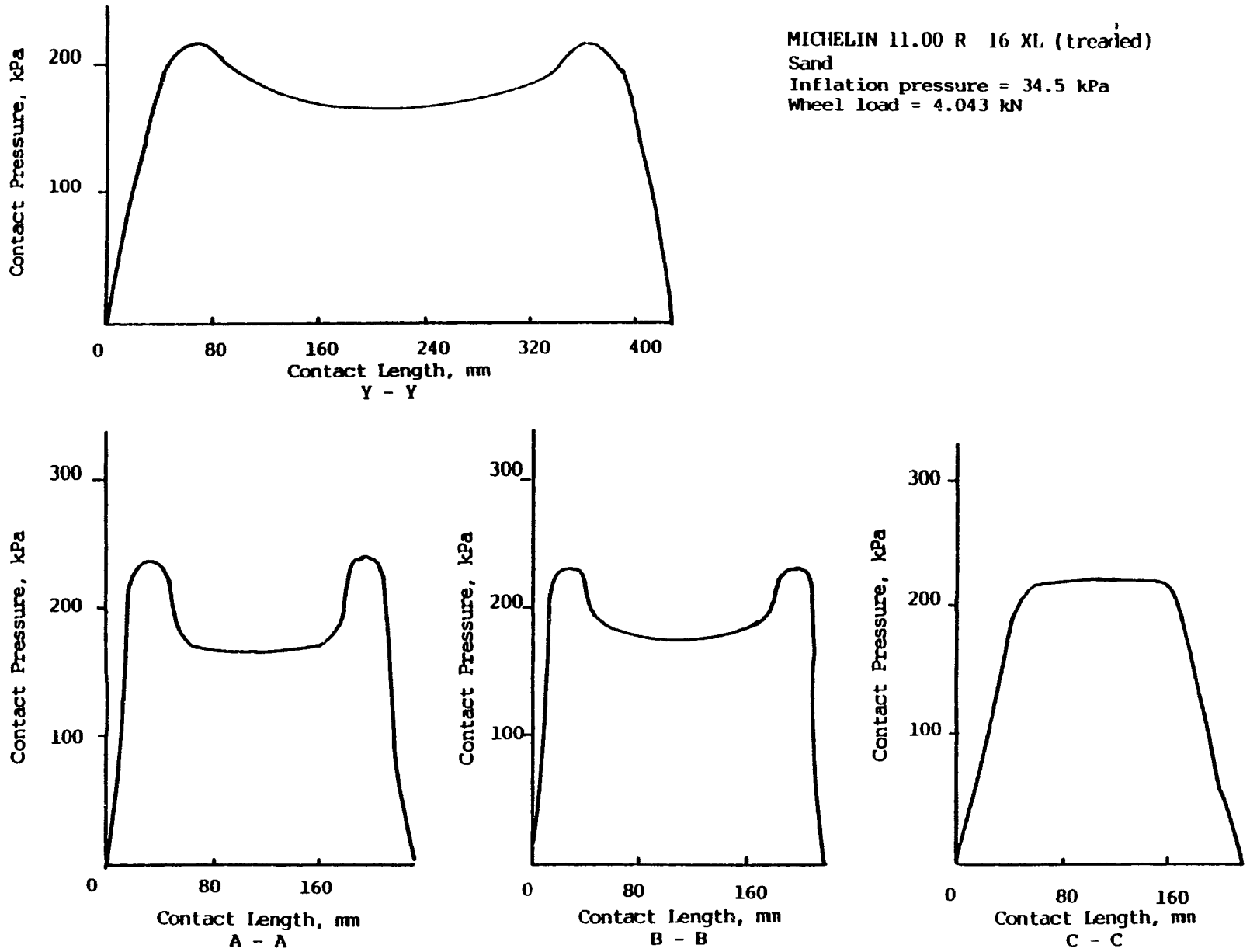


Fig. E.11b Profiles of Pressure Distribution Within the Footprint of MICHELIN 11.00R-16XL (treaded) in Sand

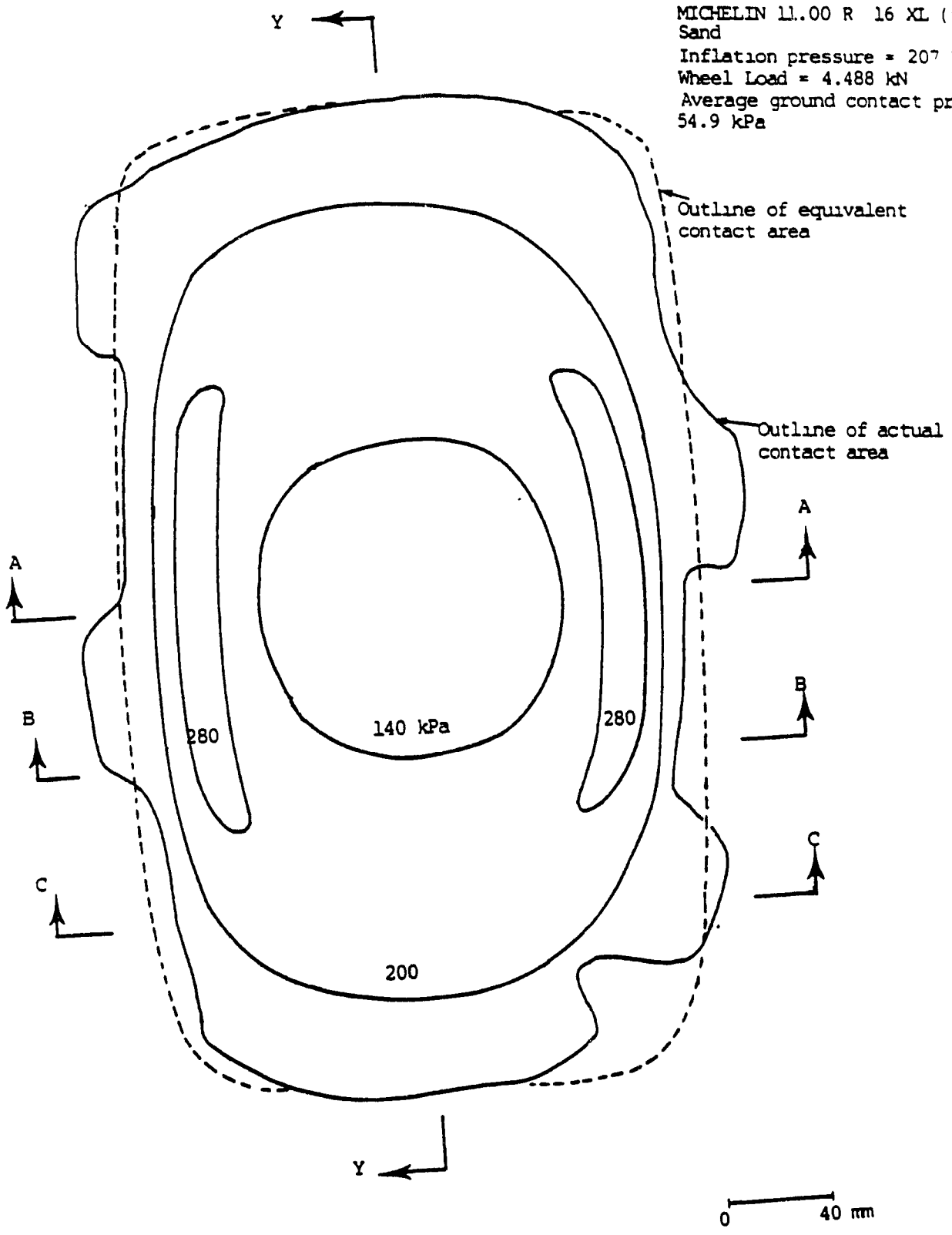


Fig. E.12a Isobars of Pressure Distribution Within the Footprint of MICHELIN 11.00R-16XL (treaded) in Sand

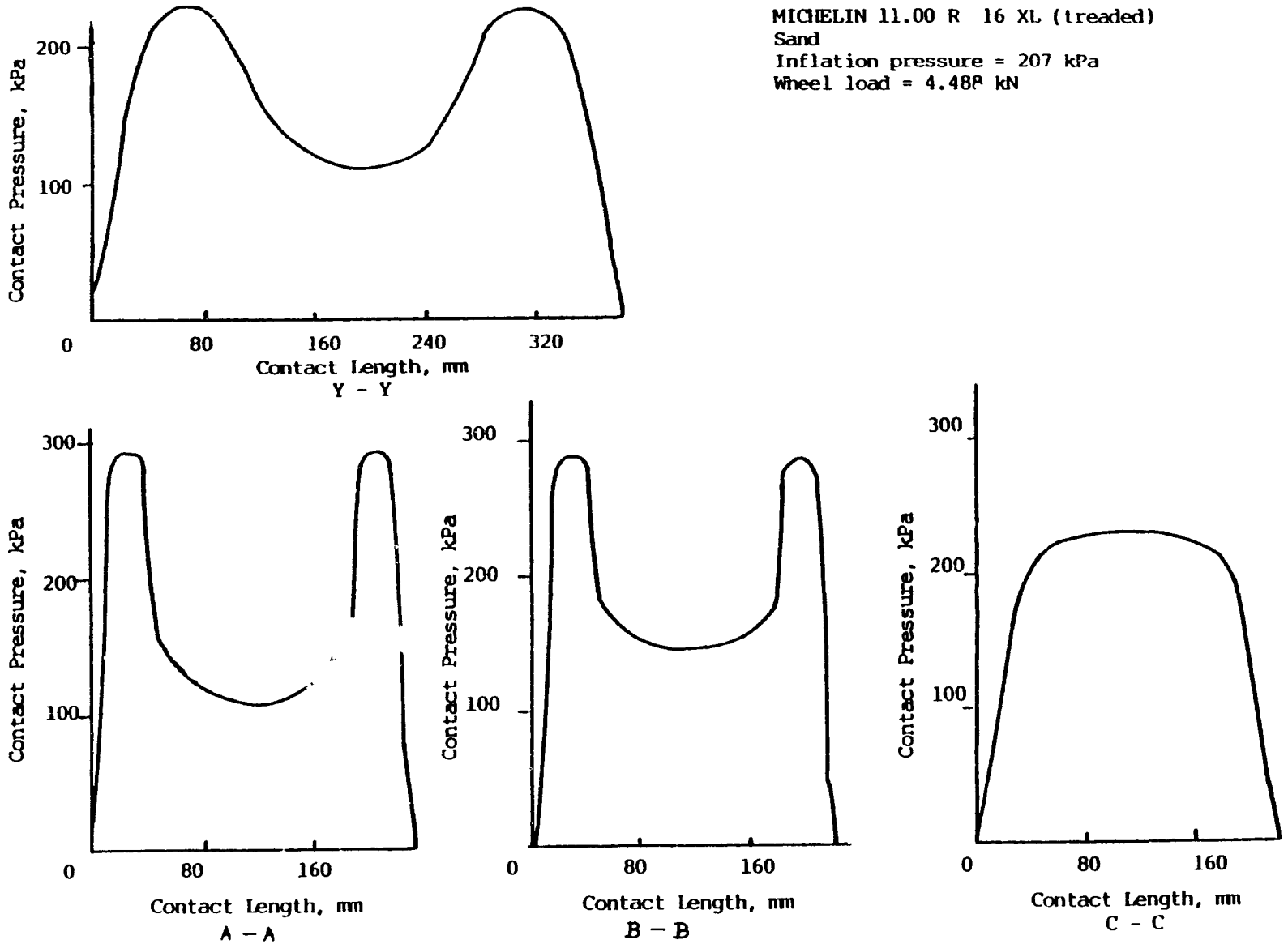


Fig. E.12b Profiles of Pressure Distribution Within the Footprint of MICHELIN 11.00R-16XL (treaded) in Sand

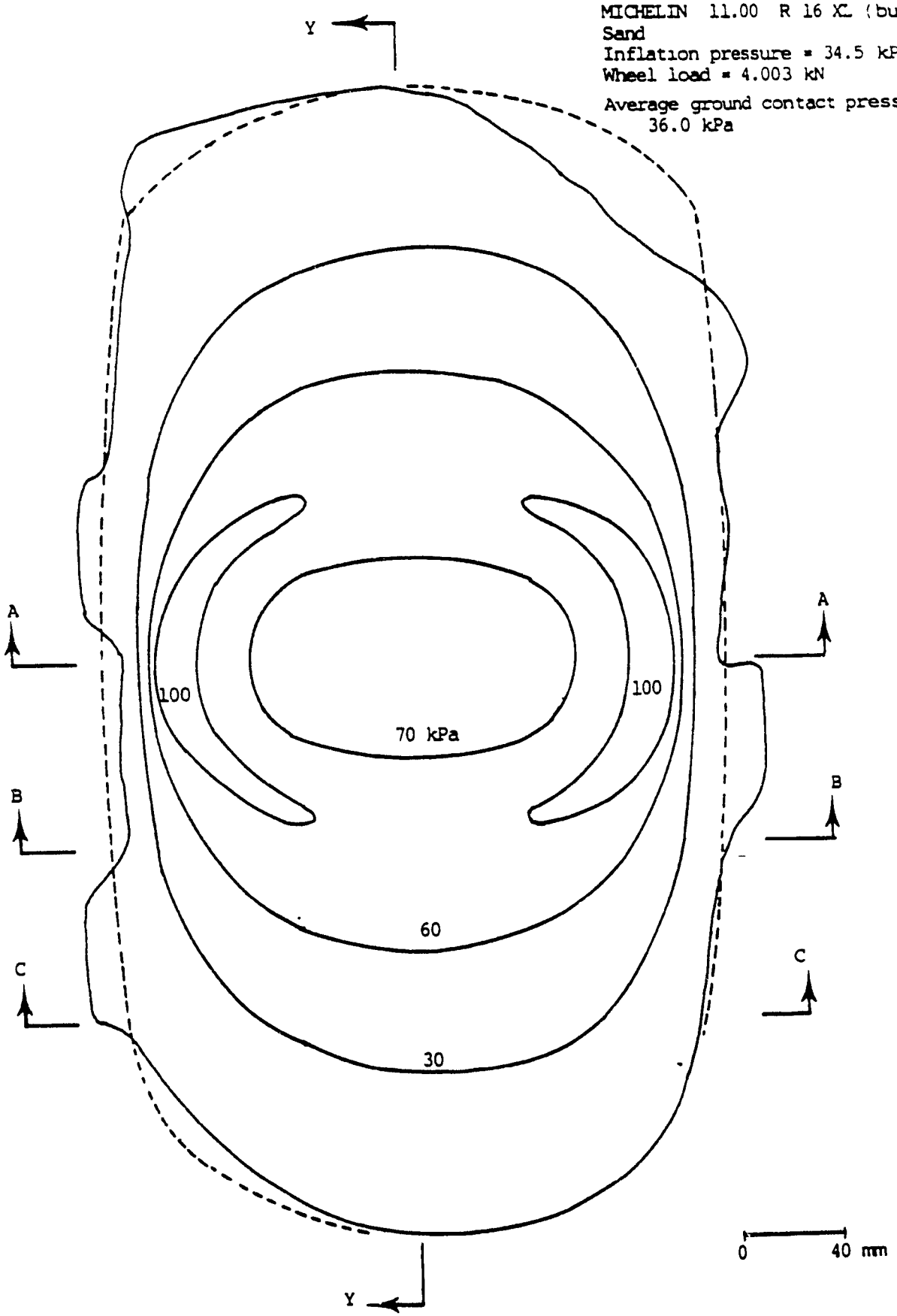


Fig. E.13a Isobars of Pressure Distribution Within the Footprint of MICHELIN 11.00R-16XL (buffed) in Sand

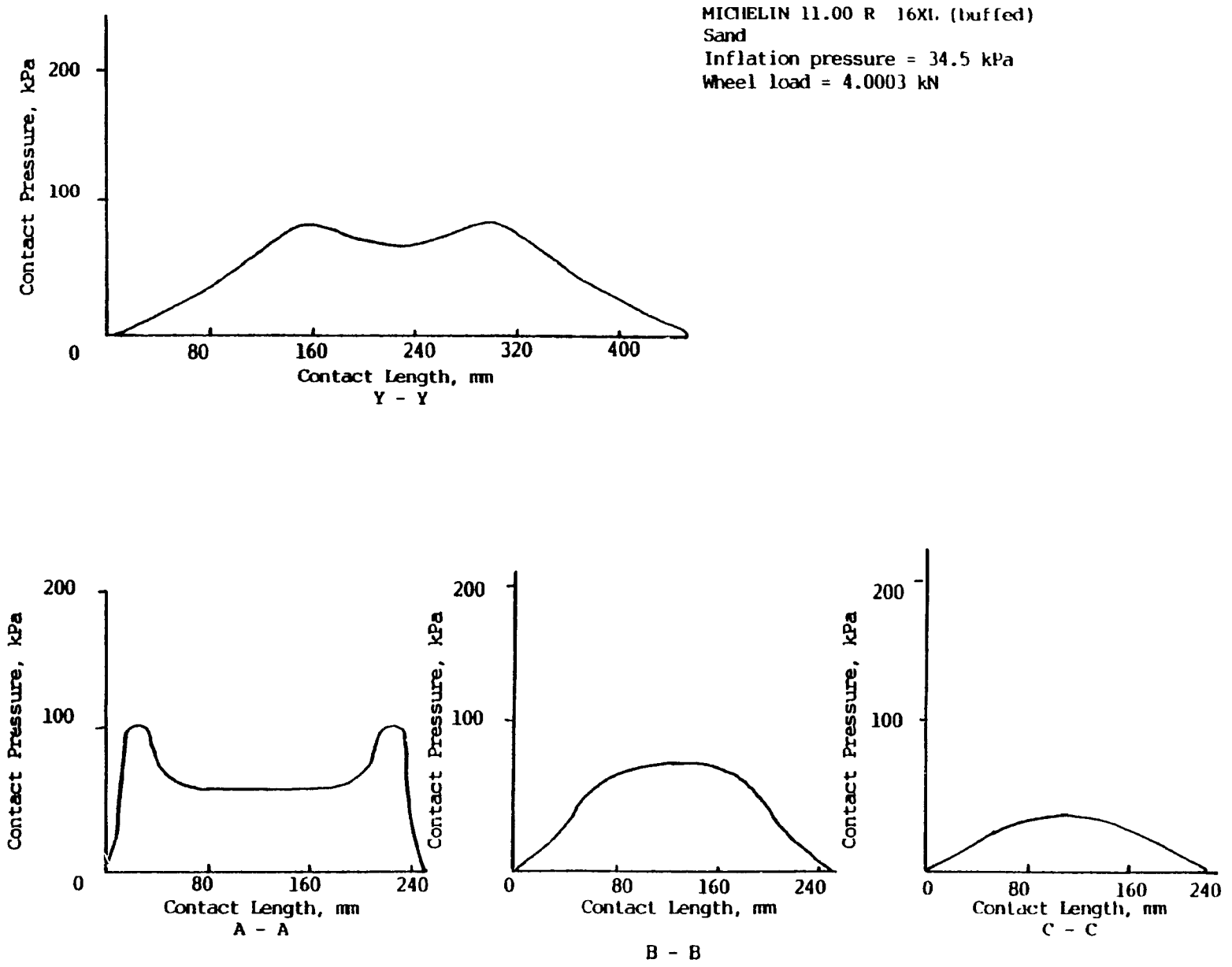


Fig. E.13b Profiles of Pressure Distribution Within the Footprint of MICHELIN 11.00R-16XL (buffed) in Sand

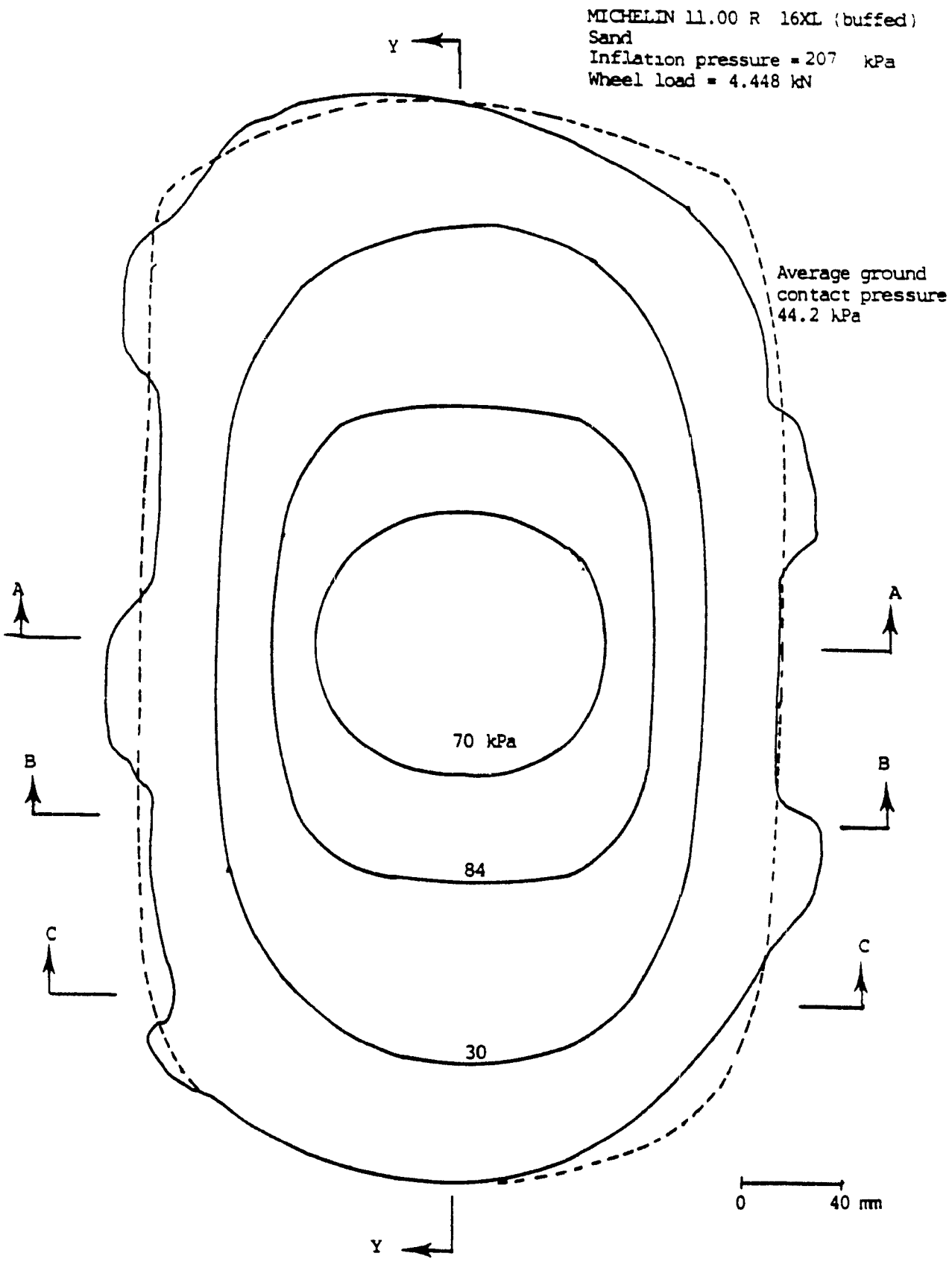
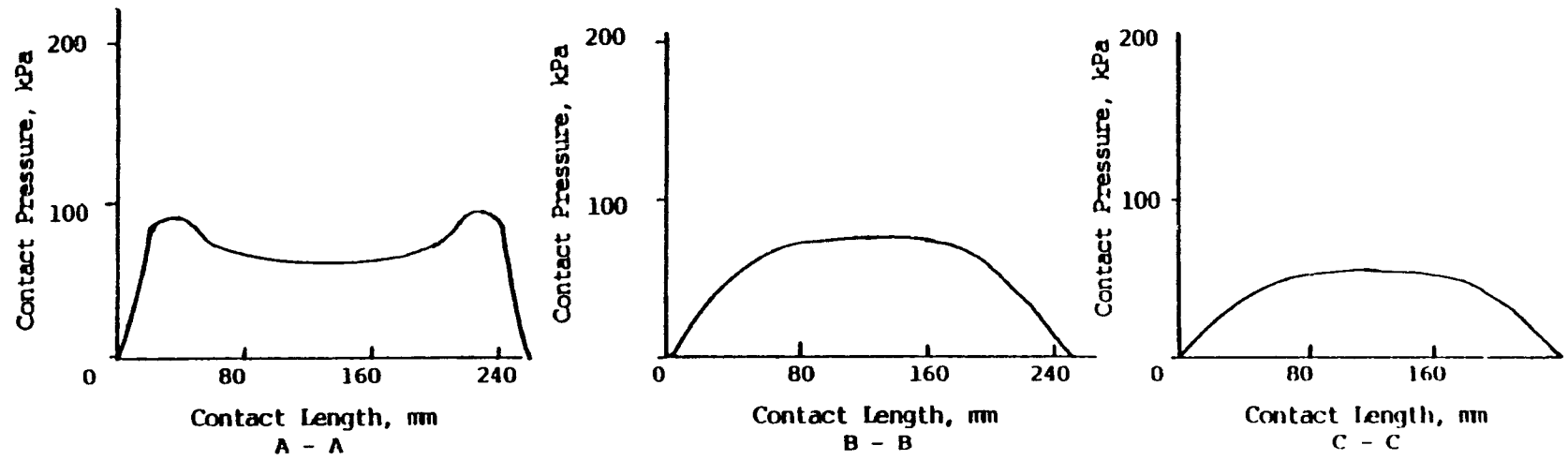


Fig. E.14a Isobars of Pressure Distribution Within the Footprint of MICHELIN 11.00R-16XL (buffed) in Sand



MICHELIN 11.00 R 16XL (buffed)
Sand
Inflation pressure = 207 kPa
Wheel load = 4.448 kN

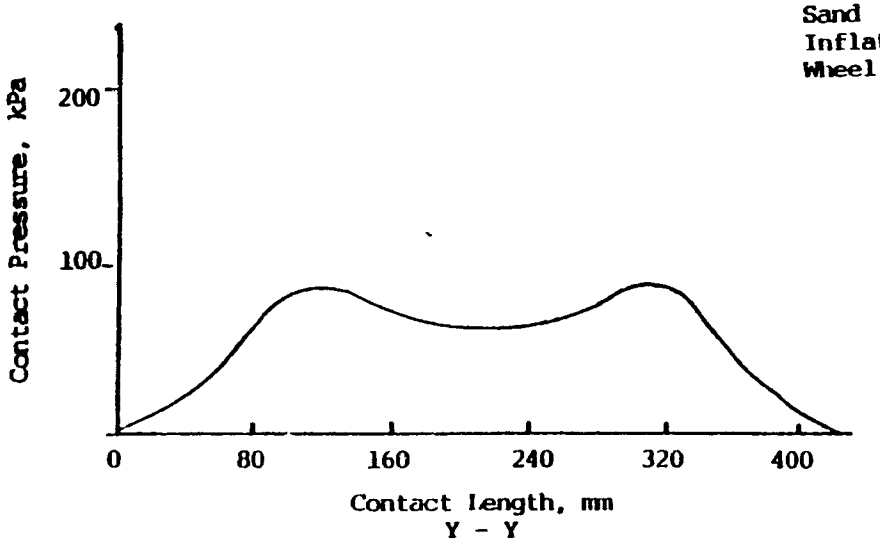


Fig. E.14b Profiles of Pressure Distribution Within the Footprint of MICHELIN 11.00R-16XL (buffed) in Sand

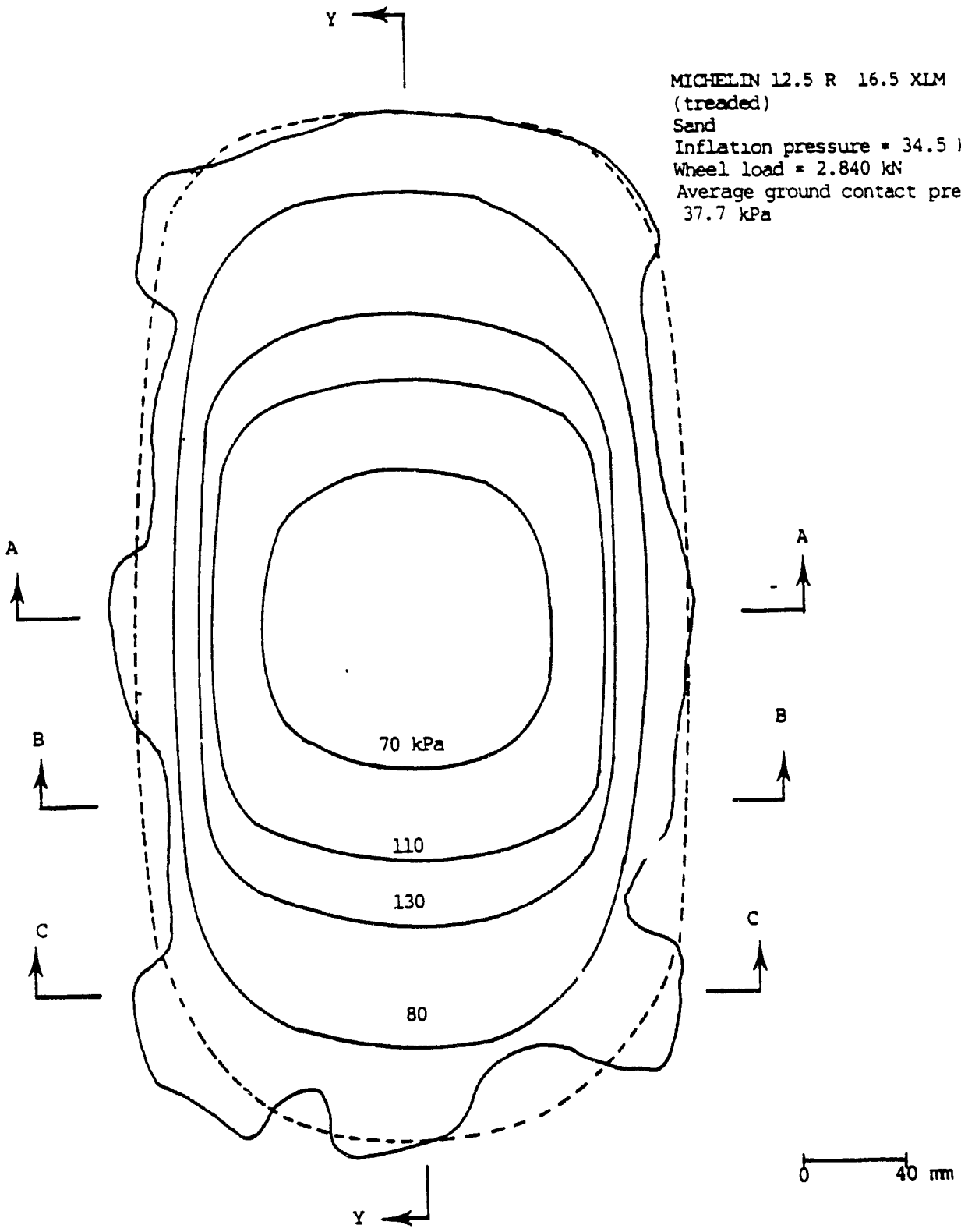


Fig. E.15a Isobars of Pressure Distribution Within the Footprint of MICHELIN 12.5R-16.5XLM (treaded) in Sand

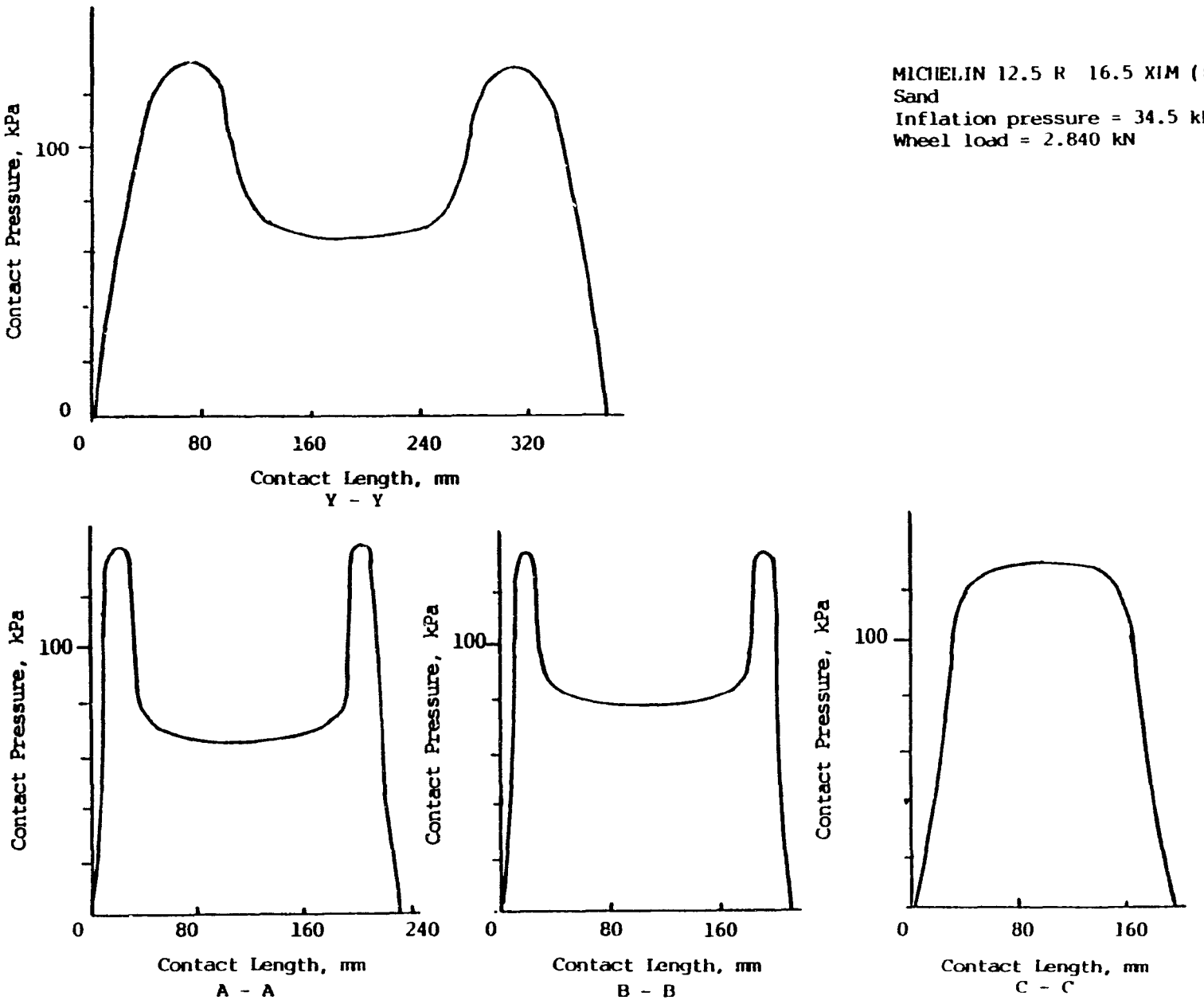


Fig. E.15b Profiles of Pressure Distribution Within the Footprint of MICHELIN 12.5R-16XLM (treaded) in Sand

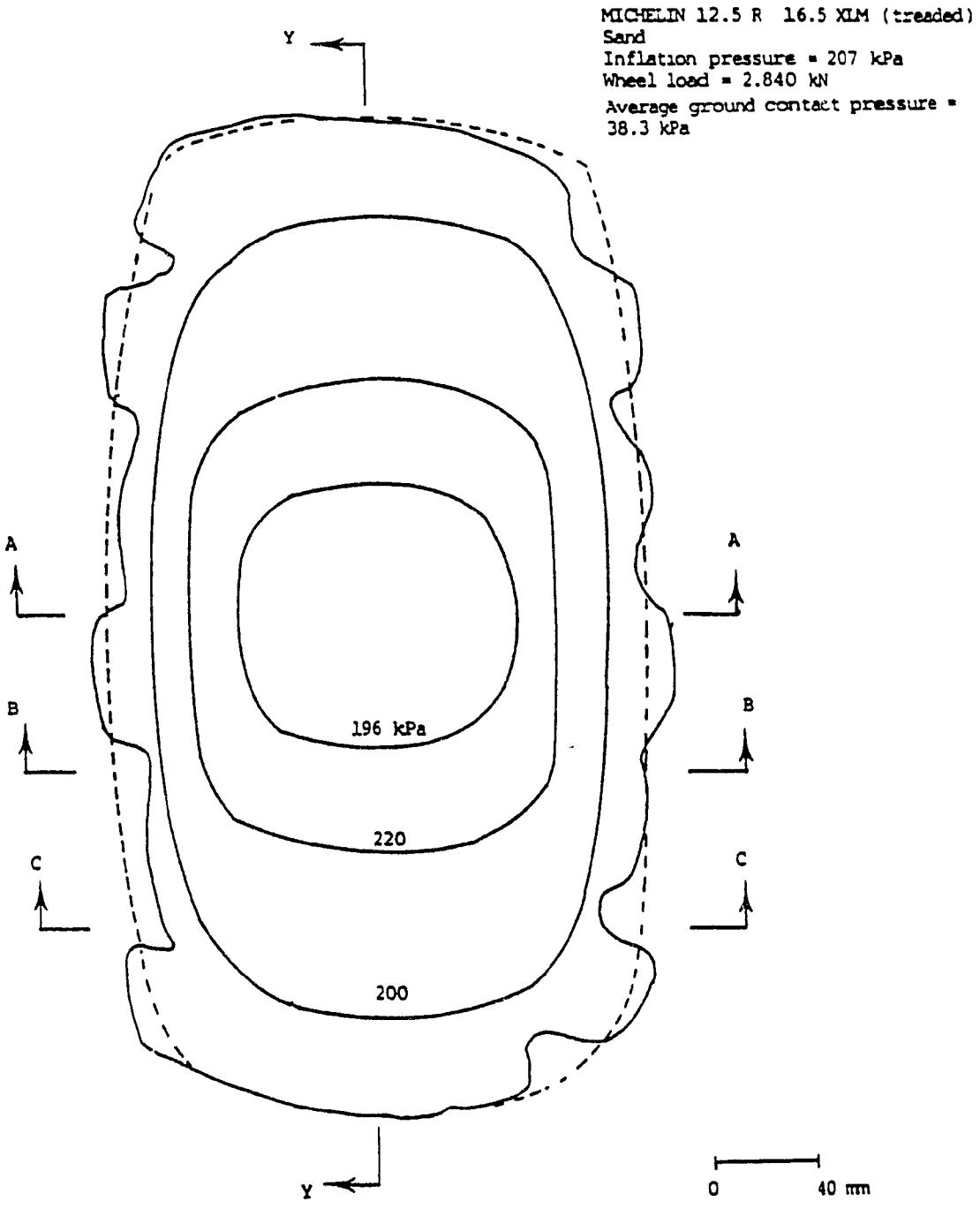


Fig. E.16a Isobars of Pressure Distribution Within the Footprint of MICHELIN 12.5R-16.5XLM (treaded) in Sand

MICHELIN 12.5 R 16.5 XIM (treaded)
Sand
Inflation pressure = 207 kPa
Wheel load = 2.840 kN

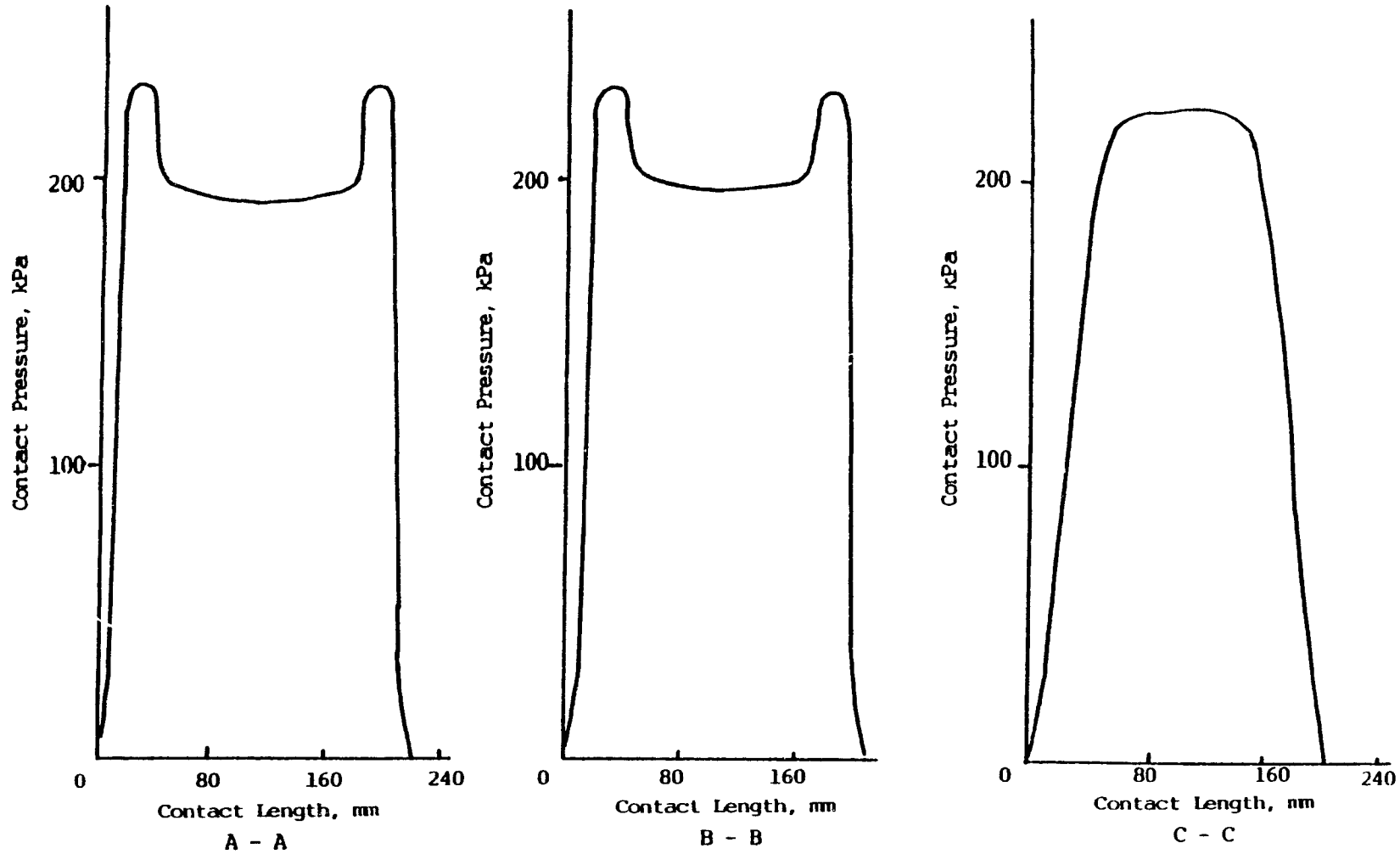


Fig. E.16b Profiles of Pressure Distribution Within the Footprint of MICHELIN 12.5R-16XLM (treaded) in Sand

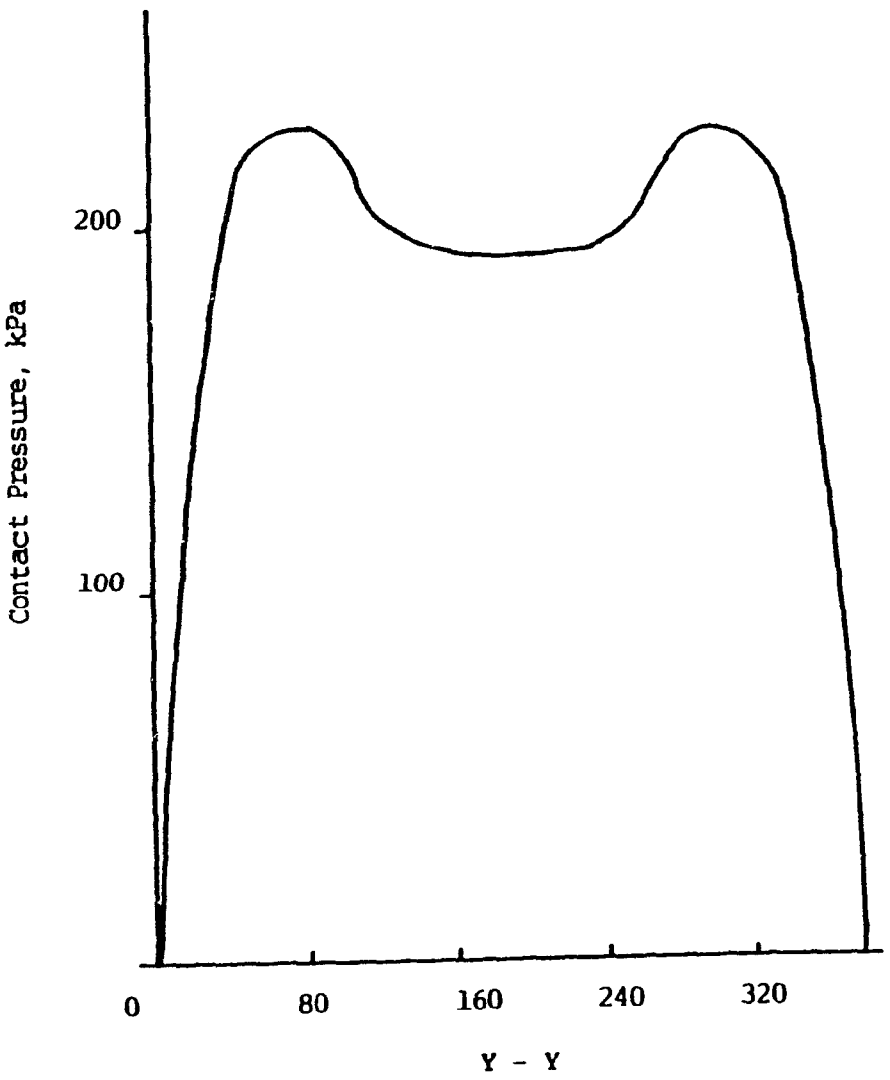


Fig. E.16c Profiles of Pressure Distribution Within the Footprint of MICHELIN 12.5R-16XLM (treaded) in Sand

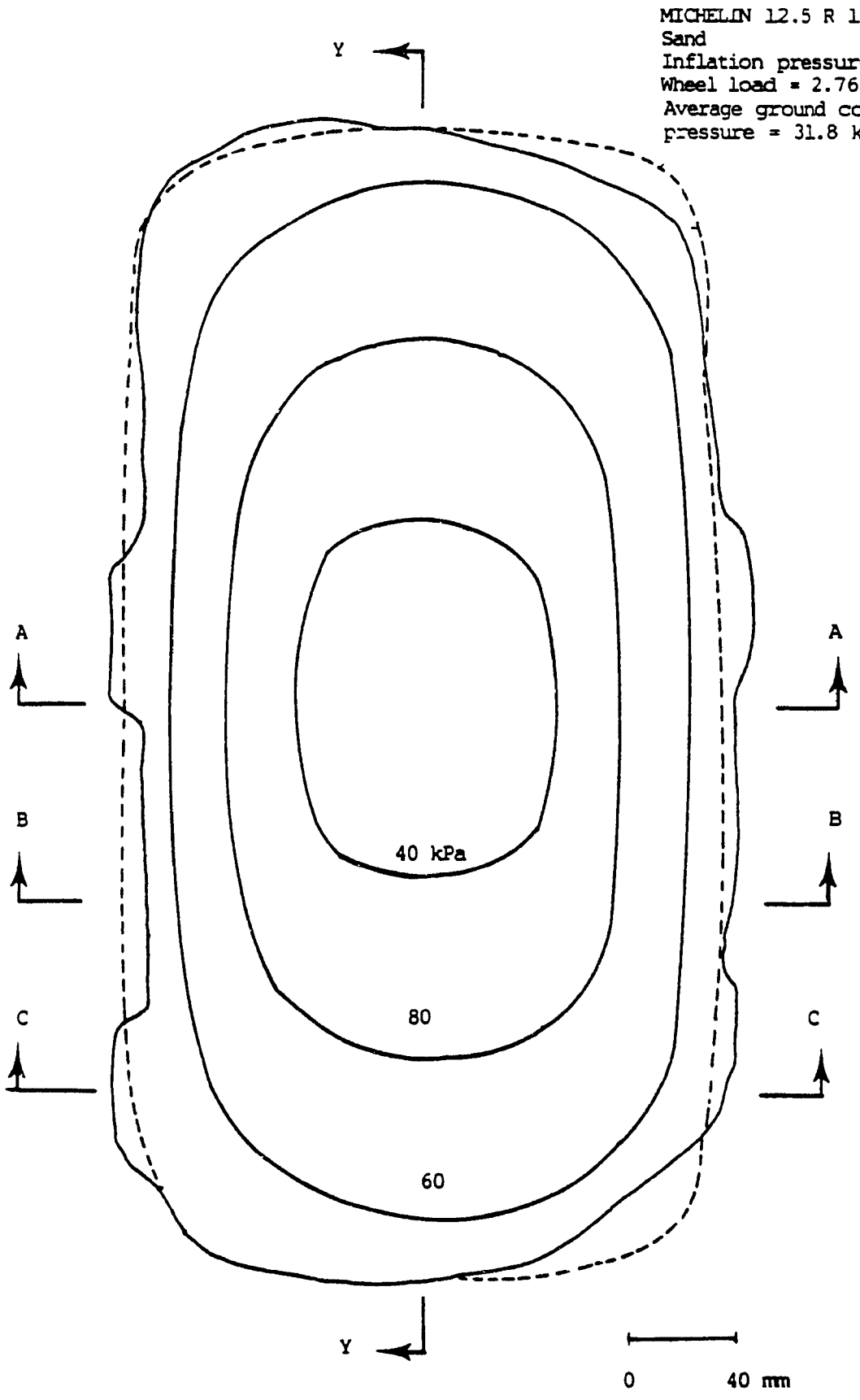


Fig. E.17a Isobars of Pressure Distribution Within the Footprint of MICHELIN 12.5R-16.5XLM (buffed) in Sand

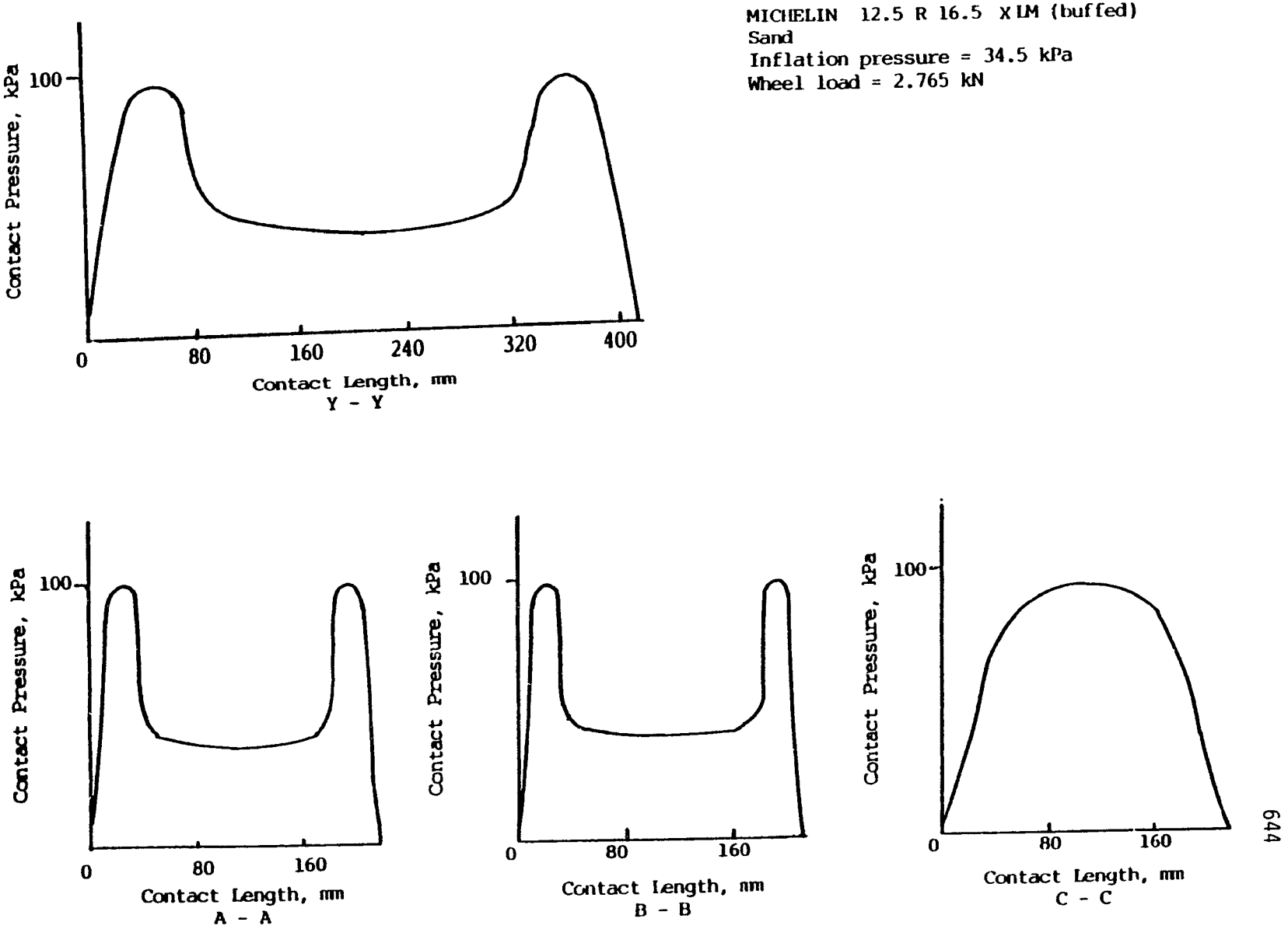


Fig. E.17b Profiles of Pressure Distribution Within the Footprint of MICHELIN 12.5R-16XLM (buffed) in Sand

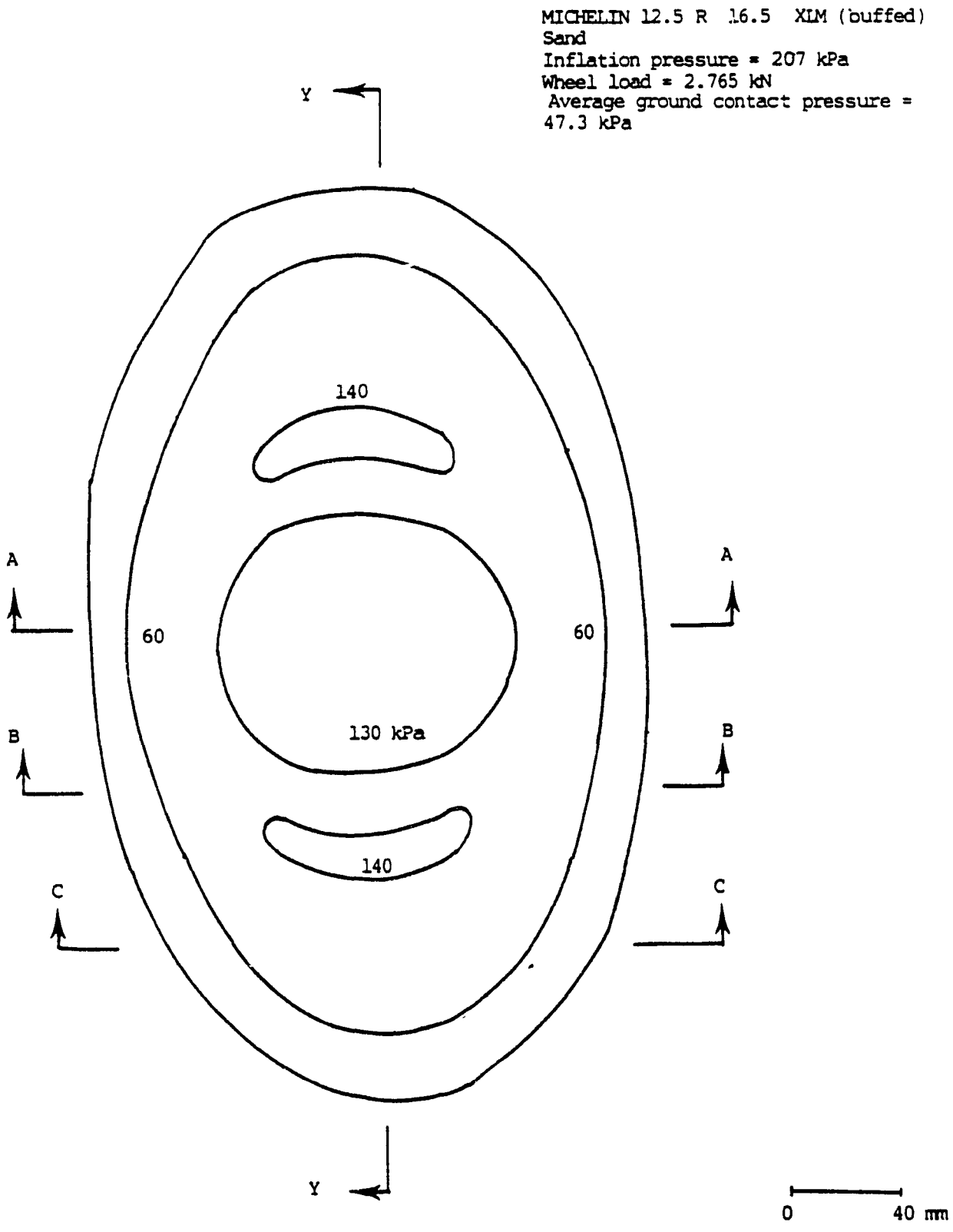


Fig. E.18a Isobars of Pressure Distribution Within the Footprint of MICHELIN 12.5R-16.5XLM (buffed) in Sand

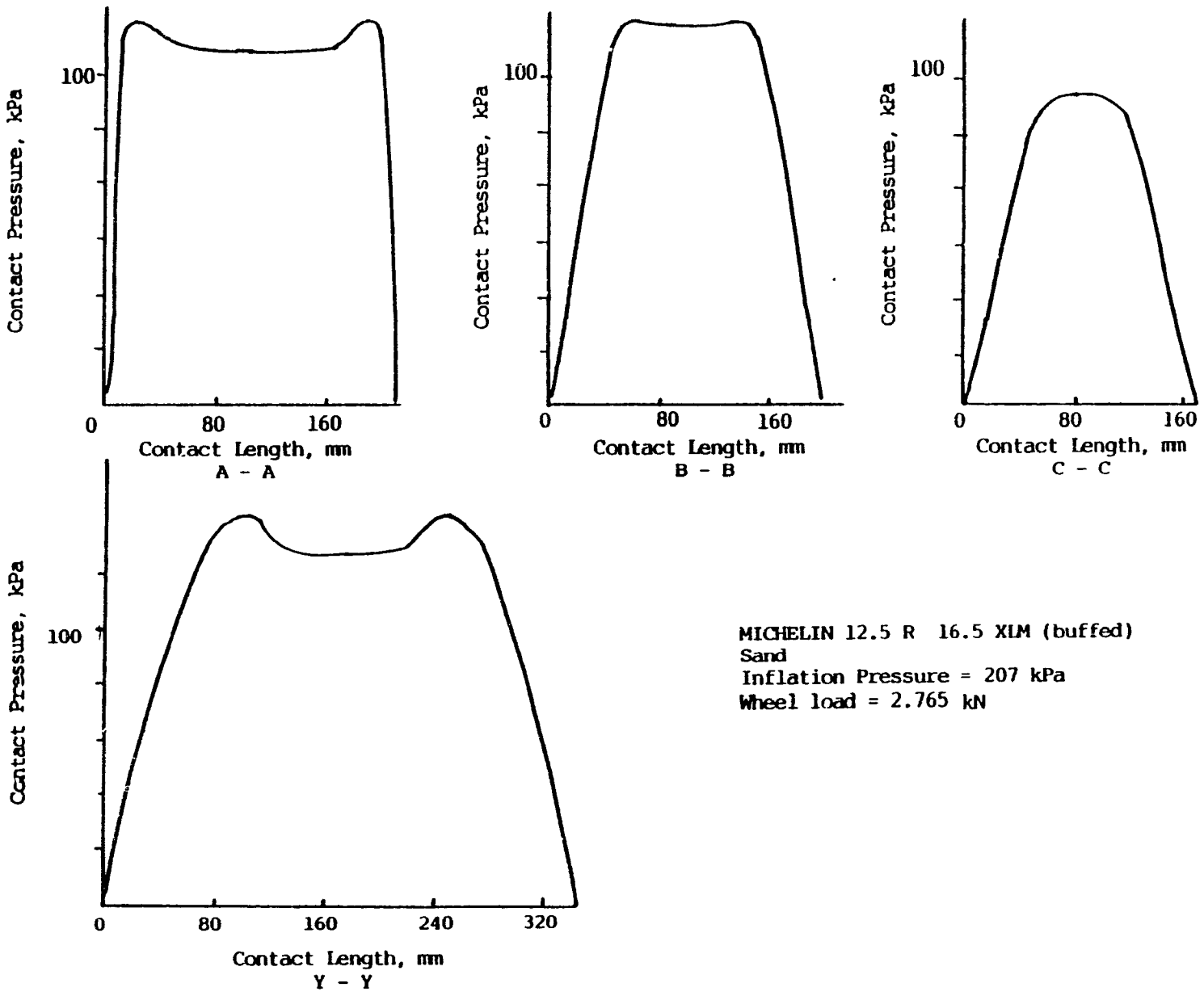


Fig. E.18b Profiles of Pressure Distribution Within the Footprint of MICHELIN 12.5R-16XLM (buffed) in Sand